

SEISMIC RESEARCH FOR HIGHWAY BRIDGES
(US-JAPAN PROGRAM)

Supported by
National Science Foundation
Grant Number CEE-8303659

Compiled by
John F. Fleming
Professor of Civil Engineering
University of Pittsburgh

DEPARTMENT OF CIVIL ENGINEERING
UNIVERSITY OF PITTSBURGH

JUNE 1984

Any opinions, findings, conclusions or recommendations expressed
in this publication are those of the author(s) and do not necessarily
reflect the views of the National Science Foundation.

REPRODUCED BY
NATIONAL TECHNICAL
INFORMATION SERVICE
U.S. DEPARTMENT OF COMMERCE
SPRINGFIELD, VA. 22161

REPORT DOCUMENTATION PAGE		1. REPORT NO. NSF/CEE-84034	2.	3. Recipient's Accession No. PB8 5 152148 /AS	
4. Title and Subtitle Seismic Research for Highway Bridges (US-Japan Program)				5. Report Date June 1984	
7. Author(s) J.F. Fleming				6.	
8. Performing Organization Name and Address University of Pittsburgh Department of Civil Engineering Pittsburgh, PA 15261				9. Performing Organization Rept. No.	
12. Sponsoring Organization Name and Address Directorate for Engineering (ENG) National Science Foundation 1800 G Street, N.W. Washington, DC 20550				10. Project/Task/Work Unit No.	
				11. Contract(C) or Grant(G) No. (C) (G) CEE8303659	
15. Supplementary Notes				13. Type of Report & Period Covered	
				14.	
18. Abstract (Limit: 200 words) Twenty-nine papers delivered at either the joint meetings of the United States-Japan Cooperative Program on Natural Resources Panel on Wind and Seismic Effects or the US-Japan Seminars on the Repair and Retrofit of Structures are presented. All papers address either the seismic design or evaluation of bridges. The papers focus on such topics as seismic resistant bridge design in California, specifications for the earthquake resistant design of Japanese high bridges, response of cable stayed bridges to static and dynamic loads, seismic vulnerability of prestressed concrete segmental bridges, behavior of concrete-filled steel tubes, repair and retrofit work on road bridge substructures, rehabilitation of road transportation networks damaged by earthquakes, and retrofitting bridges to increase their seismic resistance.					
17. Document Analysis a. Descriptors Earthquakes Earthquake resistant structures Dynamic structural analysis Bridges Loads (forces) Highways Highway bridges					
b. Identifiers/Open-Ended Terms Japan California J.F. Fleming, /PI					
c. COSATI Field/Group					
19. Availability Statement NTIS			20. Security Class (This Report)		21. No. of Pages 685
			20. Security Class (This Page)		22. Price

PREFACE

In 1971 the San Fernando earthquake in California demonstrated the inadequacy of many highway bridges to withstand the dynamic effects of seismic ground motion. The damage which occurred to bridges during this earthquake ranged from minor spalling of concrete on some structures to partial or total collapse of others. The repair cost for the freeway system was estimated at that time to be about 15 million dollars. The total cost was several times this number when the delays caused to individual businesses and the inconvenience to the public are also considered. Fortunately, there was no major threat to public safety, due to disruption of the transportation network, in this particular instance. However, this is a factor which must be considered, in any seismic event, since the access of emergency vehicles, to areas damaged by an earthquake, is vital. In the event of fires or large numbers of injuries, any delays in providing help can be disastrous.

The San Fernando earthquake represented a major turning point, in the United States, in the development of seismic design criteria for bridges. Considerable research has been performed since then on the seismic evaluation and design of highway bridges by a number of different investigators. At the same time, important research has also been performed in several other countries, particularly Japan. Unfortunately, there has been a serious lack of interaction between researchers in these countries with very little exchange of ideas or findings. If this research is to be of maximum value it must be properly disseminated. The purpose of this publication is to bring together into one volume a collection of papers prepared by prominent researchers in the United States and Japan. By reading these papers it should be possible to quickly become familiar with the present status of bridge research in these two countries. These papers have been obtained from two sources: the Proceedings of the Joint Meetings of the United States-Japan Cooperative Program on Natural Resources (UJNR) Panel on Wind and Seismic Effects; and the Proceedings of the US-Japan Seminars on the Repair and Retrofit of Structures.

The UJNR Panel Meetings are held yearly to discuss mutual topics of interest, dealing with wind and seismic effects, and to promote cooperative research efforts between the United States and Japan. The meetings have been alternated between locations in the United States and Japan, with the two most recent being the 15th Joint Meeting, which was held at the Public Works Research Institute in Tsukuba Japan in May 1983, and the 16th Joint Meeting, which was held at the National Bureau of Standards in Gaithersburg, Maryland in May 1984. The delegates to the meetings consist of the permanent panel members, who are representatives of various government agencies, and temporary members from both the academic and private industry sectors. A

TABLE OF CONTENTS

PREFACE.....	i
TABLE OF CONTENTS.....	iii
SEISMIC RESISTANT BRIDGE DESIGN IN CALIFORNIA.....	1
James H. Gates	
NEW SPECIFICATIONS FOR EARTHQUAKE RESISTANT DESIGN OF.....	15
JAPANESE HIGHWAY BRIDGES	
Eiichi Kuribayashi	
Toshio Iwasaki	
Osamu Ueda	
ANALYTICAL PROCEDURES FOR THE SEISMIC DESIGN OF HIGHWAY.....	39
BRIDGES	
R. A. Imbsen	
J. Penzien	
RESPONSE OF CABLE STAYED BRIDGES TO STATIC AND DYNAMIC LOADS...71	
John F. Fleming	
SEISMIC VULNERABILITY OF PRESTRESSED CONCRETE SEGMENTAL.....	97
BRIDGES	
Walter Podolny, Jr.	
BOX GIRDER BRIDGE HINGE RESTRAINER TEST PROGRAM.....	121
Lawrence G. Selna	
L. Javier Malvar	
MODEL EXPERIMENTS ON DYNAMIC BEHAVIOR OF REINFORCED CONCRETE..131	
BRIDGE PIER COLUMNS	
Toshio Iwasaki	
Ryoji Hagiwara	
Kinji Hasegawa	
Tatsuhiko Koyama	
Takeshi Yoshida	
BEHAVIOR OF CONCRETE FILLED STEEL TUBES.....	145
(PART 1, COMPRESSION MEMBERS)	
Nobuyuki Narita	
Shoichi Saeki	
Michio Kanai	
Toshio Ohshio	
BEHAVIOR OF CONCRETE FILLED STEEL TUBES.....	191
(PART 2, BENDING MEMBERS)	
N. Narita	
S. Saeki	
M. Kanai	

STUDIES IN THE REINFORCEMENT OF BRIDGE SEATS AGAINST.....	457
EARTHQUAKES	
Y. Shioi	
Y. Mitsuie	
T. Shimizu	
REPAIR AND RETROFIT WORKS FOR EXISTING HIGHWAY BRIDGES.....	509
Tatsuo Asama	
Yukitake Shioi	
Tadayuki Tazaki	
Hideya Asanuma	
EXAMPLES OF REPAIR AND RETROFIT WORK ON ROAD BRIDGE.....	549
SUBSTRUCTURES	
Hideya Asanuma	
REHABILITATION OF ROAD TRANSPORTATION NETWORKS DAMAGED BY.....	573
EARTHQUAKES	
Toshio Iwasaki	
Takeo Nakajima	
Katsushi Goto	
DEVELOPMENT OF SEISMIC REPAIR TECHNIQUES FOR REINFORCED.....	597
CONCRETE MEMBERS	
Masaya Hirosawa	
Shinsuke Nakata	
Tetsuo Goto	
Manabu Yoshimura	
Toshio Shiga	
Akenori Shibata	
Hiroshi Imai	
DEVELOPMENT OF RETROFIT GUIDELINES FOR HIGHWAY BRIDGES.....	613
James D. Cooper	
Richard V. Nutt	
Ronald L. Mayes	
RETROFITTING BRIDGES TO INCREASE THEIR SEISMIC RESISTANCE.....	629
Oris H. Degenkolb	
CONSIDERATIONS FOR RETROFITTING BRIDGES.....	635
Oris H. Degenkolb	
BRIDGE RETROFITTING DETAILS.....	651
Oris H. Degenkolb	
INSPECTION AND RETROFITTING FOR EARTHQUAKE RESISTANCE.....	667
VULNERABILITY OF HIGHWAY BRIDGES IN JAPAN	
Eiichi Kuribayashi	
Osamu Ueda	
Tadayuki Tazaki	

SEISMIC RESISTANT BRIDGE DESIGN IN CALIFORNIA

by
James H. Gates
Structural Mechanics Engineer
California Department of Transportation
Office of Structures Design

INTRODUCTION

The design of seismic resistant bridges in California made a dramatic turn in February, 1971. The heavy damage in San Fernando was unprecedented in the history of bridge design in California (4). In fact California had seen less than \$100,000 in earthquake damage to bridges in the 40 year history preceeding 1971. This earthquake created an increased effort to improve the evaluation and design of seismic resistant bridges. A comprehensive program was started immediately to evaluate and improve both the design specifications and details.

In 1973 a new criteria was implemented which considered the fault activity in California and the soils at the bridge site as well as the vibrational properties of the bridge itself (5,6). The California Department of Transportation criteria departed from the traditional seismic design criteria and presented for the first time:

- Site specific response spectra based on active faults in the region.
- Specified reductions for ductility and risk.
- Modular arrangement of variables for future adjustment.

In 1975, The California Department of Transportation criteria was modified and adopted by American Association of State Highway and Transportation Officials for national use in (8).

This paper will describe some of the developments in the design of seismic resistant bridges in the period since 1975. In addition to criteria developments, improved column and foundation design procedures, improved retrofit analysis procedures and the instrumentation of bridges for strong-motions will be discussed.

FACTORS CONSIDERED IN THE SEISMIC DESIGN CRITERIA

A primary requirement in the development of the criteria was to permit future flexibility. The criteria must be easily modified as new developments are made in earthquake engineering. Each component of the criteria was designed to represent the independent influence of a different discipline of earthquake engineering. The following factors, which affect the response of a structure to seismic forces, are included in the criteria:

The location of the bridge in relation to active faults.

The effect of a maximum credible earthquake on an active fault.

The dynamic responses of the bridge to the strong ground motion.

The reduction in force level for ductility and risk considerations.

The four components of the criteria (A, R, S and Z) are briefly defined as follows:

- A The peak rock acceleration, determined from seismological studies of fault activity and attenuation data gathered from historic events.
- R The acceleration spectra for rock based on actual recorded data.
- S The soil amplification factor, based on both computer studies and actual recorded data.
- Z The ductility and risk reduction factor, is based on observed damage plus computed and experimentally determined data.

The product of the first three factors (ARS) results in an elastic response spectra curve for the site that would result from a maximum credible event on the closest fault.

Division by the factor Z, after the distribution of the ARS forces, gives a design force for the portion of the structure under consideration. The factor Z is component dependant, thus the design force depends not only on the seismicity and site conditions, but on the structural component being designed.

RECENT CRITERIA DEVELOPMENTS

Recent criteria development for the design of seismic resistant bridge structures has been dominated by the Applied Technology Council project ATC-6. (13) This project, funded by the Federal Highway Administration and the National Science Foundation, was started in 1977 and was completed in 1981. The guidelines were developed to be applied the United States on a national basis and are the composite recommendations of a team of nationally recognized experts, composed of consulting engineers, university personnel, state bridge engineers and Federal representatives from throughout the United States. The guidelines contain several new concepts which are significant departures from previous design provisions :

- Four seismic performance categories are defined on the basis of expected acceleration levels at the bridge site, determined from a previously developed map (14).
- Different degrees of complexity and sophistication of seismic analysis and design are specified for each of the four seismic performance categories.
- Uncertainty in the direction of loading is accounted for by combining loads in two orthogonal directions by adding 30% of one direction loading to 100% of the loads in the other direction.
- Column spiral reinforcement in plastic hinge zones is specified based on work in New Zealand by the University of Canterbury (11).
- Bridge bent analysis is performed by the distribution of overstrength plastic moments in the bent.

The ATC-6 Seismic Design Guidelines (13), have been adopted by the American Association of State Highway and Transportation Officials as a guide specification, effective 1 March 1983. The guide specification may be utilized in lieu of the current American Association of State Highway and Transportation Officials Design Specifications for Highway Bridges for the seismic design of highway bridges in all parts of the United States and Puerto Rico.

The current California Department of Transportation seismic bridge criteria (1), is generally a modification of the Applied Technology recommendation (13). The California Department of Transportation has incorporated the reinforced concrete portions (including the distribution of plastic hinge moments) into their criteria but are retaining the seismic force level philosophy from previous versions of their criteria (5,6).

CALIFORNIA DEPARTMENT OF TRANSPORTATION FOUNDATION DESIGN

Both the ATC-6 criteria (13) and the current California Department of Transportation criteria (1) require the foundations to be designed to carry the plastic moment developed in the column. This moment is increased from the nominal value to obtain a realistic value for the actual moment developed.

The following excerpts from the California Department of Transportation criteria (1), show the major specifications utilized in the seismic design of the foundations.

EXCERPTS FROM SPECIFICATIONS (1)

1.2.20 - SEISMIC FORCES

...(F) Seismic Design of Bent and Pier Foundations.

Bent or pier foundations should be designed for the lesser of forces resulting from the seismic plastic hinging (Article 1.2.20(G)) or dead loads plus elastic ARS EQ forces. (Elastic ARS forces are unreduced for ductility and risk.)

Ultimate soil or pile capacity shall be used for resisting seismic foundation loads.

...(G)...(1) Moment

The column moment shall be the probable plastic moment as specified in Article 1.5.33(D).

1.4.6 - FOOTINGS

...(A)..... Bent and Pier footings shall be designed by the Load Factor design method.

...(D) (3) For Load Factor Design the strength reduction factor, ϕ , shall be as follows:

	Group Loads I through VI	Group VII (Seismic)
Soil bearing pressure	$\phi = 0.50$	$\phi = 1.00$
Pile capacity	$\phi = 0.75$	$\phi = 1.00$

...(G) (5) The minimum top flexural reinforcement for bent or pier footings shall be the greater of one half the bottom flexural reinforcement or #6 at 12 in each direction.

- ..(H)...The minimum shear reinforcement for column footings shall be vertical #5 bars at 12 inch spacing in each direction in a band between "d" of the footing from the column surface and 6 inches maximum from the column reinforcement. Shear bars shall be hooked around the top and bottom flexure reinforcement in the footing.
- ..(J) (7) The (column) bars shall be terminated in the footings with a standard hook. Lap splices shall not be used.

1.5.33 - COMPRESSION MEMBERS WITH OR WITHOUT FLEXURE

..(D) Probable Plastic Moment

The probable plastic moment is defined as the maximum moment which can be expected to actually develop in a well confined column section at yield.

For well confined sections with axial loads below P_b (P Balance) the probable plastic moment may be assumed to be 1.3 times the nominal moment. For loads above P_b , a more detailed analysis shall be performed.

SEISMIC RETROFIT OF BRIDGES

Current activities in the United States are two-fold. The California Department of Transportation has, since 1971 been involved in the retrofit of existing highway bridges. On a national level, the Federal Highway Administration is currently funding a research project with the Applied Technology Council to develop retrofit guidelines for bridges on a nationwide basis.

The California retrofit program began almost immediately after the 1971 San Fernando Earthquake. Projects which were under construction were modified where possible by contract change order to meet increased seismic requirements. This effort was extended to include bridges in the design phase.

The California Department of Transportation has identified about 1250 bridges (out of about 13,000) which are primarily deficient in seat width. These unrestrained joints represent the prime focus of the Departments retrofit program. To date about 750 of these bridges have been retrofit at a cost of \$27.5 million. Current budget allocations will permit completion of all 1250 bridges by 1990 at a total cost of \$60 million.

The average California retrofit project consists of the addition of steel restrainer cables at hinge and expansion joints to prevent spans from collapsing (3). It is expected that the potential for collapse can be minimized even though extensive damage is experienced.

The California design details for restrainer units have evolved to the point where reliable and economical systems are performing satisfactorily under service conditions in the field, although none have yet been tested by an actual earthquake.

Selection of structures for retrofit in California is currently based on a priority system (9). This system takes into account the expected accelerations at the site, the estimated cost to retrofit the structure, the cost of replacement in the event of loss, the length and availability of detours and the average daily traffic as well as other factors which reflect the importance of the bridge in the transportation system.

The Applied Technology Council retrofit project (ATC 6-2) is expected to be completed in 1983. The project objectives are to review the current retrofit methodologies being used worldwide and draft a set of guidelines for the retrofit of United States bridges. The project has defined the following scope:

- Provide a preliminary screening process for the initial selection of bridges to be retrofit.
- Provide a methodology to evaluate the seismic capacity of existing bridges.
- Provide a subjective criteria for the determination of retrofit details for existing bridges.
- Present examples of various retrofit measures.

SIMPLIFIED RETROFIT ANALYSIS

Current retrofit development in California is aimed at simplifying the analysis procedures to determine failure modes and retrofit requirements.

California has been developing a simplified restrainer analysis procedure which attempts to consider many of the non-linear features of multi-hinged bridges, such as expansion joint gaps and the impacting of the superstructure against the abutment fill. The procedure described on the following page describes a tentative analysis procedure which appears to have merit. The procedure is currently being tested on actual designs and should be formally implemented into the California design process in the very near future.

TENATIVE CALIFORNIA LONGITUDINAL RESTRAINER ANALYSIS PROCEDURE

1. Compute the maximum permissible restrainer deflection and compare with available seat width to verify seat capacity.
2. Assuming an unrestrained condition, compute the longitudinal seismic deflections of the superstructure moving away from the joint.
3. Determine the number of restrainers required to reduce the smallest superstructure deflection (from step 2) to the permissible restrainer deflection (from step 1).
4. Verify the deflections of the restrained system and revise the restrainer and/or column assumptions if required.
5. Repeat steps 1 to 4 if necessary until the restrained deflection is equal to the permissible restrainer deflection.

Simplified Restrainer Analysis -- Notes and Assumptions

- Assume one end of the restrainer is fixed and the mass of the superstructure is moving away from the joint.
- Two separate analyses are required to evaluate the restrainers at a particular joint, one for the superstructure on each side of the joint. The superstructure is assumed to be moving longitudinally away from the joint. Usually the lighter of the two superstructures will be the governing analysis, but if one segment is heavier and significantly stiffer it may require fewer restrainers. In this case the analysis which requires the fewer number of restrainers will govern.
- The longitudinal stiffness of the structure/restrainer system is computed by mobilizing the longitudinal stiffness of no more than one adjacent superstructure segment in addition to the longitudinal stiffness of the portion of superstructure under consideration.
- Consideration should be given to gaps in the system and a reduced stiffness assumed to model this effect.
- The stiffness of abutment soils should be considered if it is expected that the abutment can be mobilized as the superstructure moves toward the abutment.

AMBIENT VIBRATION TESTING OF BRIDGES

The Federal Highway Administration funded a 3.5 year research project (7), which was completed by The California Department of Transportation in 1982. The project recorded vibrational data on 57 typical bridges and compared these results with current elastic analysis procedures. This was the first time such a large sample of data was gathered for bridges.

This study was aimed primarily at obtaining a large amount of basic data on typical California bridges and correlating that with the current computer models being used by California bridge designers. All bridges currently instrumented to record strong-motions were included in this study.

System identification techniques were utilized to determine superstructure properties and boundary conditions for three of the bridges instrumented for strong-motions.

The bridges in this study were excited by wind and traffic with the maximum velocity on the structure in the range of 0.0001 - 0.01 in/sec. Application of the results to seismic analysis must be made with care because of the non-linearity of the bridge foundations.

SIGNIFICANT RESULTS

- The approximate fundamental frequency of an average bridge may be estimated using the charts presented in the report.
- For reinforced concrete bridges the moments of inertia of the superstructure were determined to vary as follows:
 - IX (Torsion) ----- Equal to the gross value.
 - IZ (Normal Bending) -- 40-60% of the gross value.
 - IY (Transv. Bending) - 60-80% of the gross value.
- For prestressed concrete bridges the moments of inertia of the superstructure were determined to vary as follows:
 - IX (Torsion) ----- 200% of the gross value.
 - IZ (Normal Bending) -- 120-140% of the gross value.
 - IY (Transv. Bending) - 100-120% of the gross value.
- The stiffness of skewed supports was not affected by the skew. The effect of increasing the stiffness of skewed column members to model out-of-plane bending was not seen.

STRONG MOTION INSTRUMENTATION

The California Department of Conservation, Division of Mines and Geology has been involved in the development of data on the characteristics of earthquake-generated strong motions for about ten years. A legislative statute brought the Division's Strong Motion Instrumentation Program into being on January 1, 1972. This statute gave the Division the role of procuring and installing strong motion instruments on representative structures (including bridges) and in various geologic environments throughout the state. The Statute has since been expanded (January 1, 1977), to mandate the instrument maintenance and record processing. The Division has been collecting data and archiving records since September 1976.

Funding for the California Strong Motion Instrumentation Program comes from a tax on building permits and currently amounts to about \$750,000 annually.

Current instrumentation consists of approximately 300 ground response stations, 56 building stations, 21 dam stations, 4 bridge stations and 1 tunnel station.

A catalog of strong motion records recovered by the Strong Motion Instrumentation Program up to January, 1982 (2), is available.

Three California bridges are currently instrumented under the program:

Meloland Road Overcrossing (El Centro area)

Route 154/101 Separation (Hollister area)

Painter Street Overcrossing (Eureka area)

Yincent Thomas Suspension Bridge (Los Angeles area)

The Meloland Road Overcrossing is a 2 span continuous reinforced concrete bridge over Interstate Route 8 located about 0.5 km southwest of the Imperial fault. The bridge is currently instrumented (5/83) to record 26 channels of data including 3 ground locations. (10, 12) The bridge was undamaged in the 15 Oct 79 Imperial earthquake but accelerations up to 0.5g were recorded on the bridge.

The following page contains information about the data recorded at the Meloland Road Overcrossing.

SIGNIFICANT RECORDS RECORDED AT MELOLAND RD. OC from (2)

TRIGGER DATE	D M G RECORD NUMBER	Max Acc (g) (On Structure)	Max Acc (g) (On Ground)
16 Mar 79	01336-C0164-79166.01	<.05	<.05
16 Mar 79	01336-C0165-79166.01	.12	<.05
unknown	01336-C0164-79290.01	<.05	<.05
unknown	01336-C0165-79290.01	.18	<.05
13 Oct 79	01336-C0164-79290.03	<.05	<.05
13 Oct 79	01336-C0165-79290.03	.08	<.05
15 Oct 79	01336-C0164-79290.04	.50	.44
15 Oct 79	01336-C0165-79290.04	.50	.38
15 Oct 79	01336-C0164-79290.05	.10	.09
15 Oct 79	01336-C0165-79290.05	.05	.09
15 Oct 79	01336-C0164-79290.06	.05	<.05
15 Oct 79	01336-C0165-79290.06	.09	<.05
15 Oct 79	01336-C0164-79290.07	.09	<.05
15 Oct 79	01336-C0165-79290.07	.05	<.05
14 Jan 80	01336-C0164-80015.03	<.05	<.05
14 Jan 80	01336-C0165-80015.03	.17	<.05
14 Jun 80	01336-C0164-80281.01	<.05	<.05
14 Jun 80	01336-C0165-80281.01	.13	<.05
01 Aug 80	01336-C0164-80281.03	<.05	<.05
01 Aug 80	01336-C0165-80281.03	.20	<.05
03 Nov 80	01336-C0164-81117.01	<.05	<.05
03 Nov 80	01336-C0165-81117.01	.22	<.05
05 Jun 81	01336-C0165-81322.01	.15	<.05

Notes-- Records C0164 and C0165 are 13 Channels each, they are tied together with common time and common trigger. A few instrument stalls occurred on the C0164 record during the 15 Oct 79 earthquake.

Magnetic tape and microfiche copies of the data recorded from the 15 Oct 79 Imperial Valley Earthquake are available for reproduction and handling costs.

Send to:

California Division of Mines and Geology
Office of Strong Motion Studies
2811 'O' Street
Sacramento, CA 95816
USA

FUTURE NEEDS AND DEVELOPMENTS

Design and Criteria

There is an increasing need for a simplified design technique for small bridges. Bridges in which the abutments play an important role in the response of the overall structure. The small two and three span bridge makes up about 75 to 80 percent of the total worldwide inventory of bridges. The development of both simplified design techniques and standardized, reliable abutment and bent details could greatly reduce earthquake damage in high seismic zones.

A unified criteria appears to be somewhat a reality, but there are a lot of unknowns and speculations in current versions. The non-linear effects of both the soils and the plastic hinging in columns should be explicitly addressed in the criteria rather than built in implicitly.

Retrofit

As bridges are being retrofit around the world to improve their seismic resistance, there is an increasing need to establish a data bank of retrofit case histories. This data could include information about any tests which were performed on the bridge as well as the costs of the retrofit.

Methods to evaluate the seismic resistance of existing bridges taking into consideration their age, structural configuration and vulnerable details need to be developed in order to facilitate the inventory of the thousands of existing bridges located on highly seismic areas.

Research and Testing

Full-scale testing is probably the only way to definitely answer questions about the ability of critical portions of the bridge to withstand heavy seismic attack. There is an urgent need to pool research money from a number of sources and develop a full-scale testing facility which can test a number of complete bridges to destruction. Even retrofit techniques could be evaluated at such a facility.

Better definition of the ground motions and force levels close to faults is needed to permit a more reliable estimation of the overall structural response.

The amount of out-of-phase displacement present over distances comparable to the length of a long bridge is currently unknown. Even more important is the design problem of dealing with these displacements once they become known.

REFERENCES

1. "Bridge Design Specifications Manual" Standard Specifications for Highway Bridges Adopted by the American Association of State Highway Bridges, Twelfth Edition, 1977. With Interim Bridge Specifications thru 1982, Washington, D.C., With revisions by The California Department of Transportation, Office of Structures Design, Sacramento, California, January, 1983.
2. "Catalog of Strong Motion Accelerograph Records Recovered by Office of Strong Motion Studies Before January 1, 1982", California Division of Mines and Geology, Special Report 154 (1982)
3. Degenkolb, O.H., "Retrofitting Bridges to Increase Their Seismic Resistance", Proceedings of the First Seminar on Repair and Retrofit of Structures. US/Japan Cooperative Earthquake Engineering Research Program. National Science Foundation, University of Michigan, Ann Arbor, Michigan, 1980, Vol 1, pp 109-114.
4. Fung, G., et al, "Field Investigation of Bridge Damage in the San Fernando Earthquake." Bridge Department, Division of Highways, California Department of Transportation, Sacramento, California, 1971.
5. Gates, James H., "California's Seismic Design Criteria for Bridges" Journal of The Structural Division, American Society of Civil Engineers. December, 1976. pp 2301-2313.
6. Gates, James H., "Factors Considered in the Development of the California Seismic Design Criteria for Bridges", Proceedings of a Workshop on Earthquake Resistance of Highway Bridges held on January 29-31, 1979. Applied Technology Council, Palo Alto, Ca 1979, pp 141-162.
7. Gates, James and Smith, Monte, "Verification Dynamic Modeling Methods by Prototype Excitation", Federal Highway Administration Report No. FHWA/CA/SD-82/07 (Nov., 1982)
8. "Interim Specifications, Bridges 1975," Subcommittee on Bridges and Structures. American Association of State Highway and Transportation Officials, Washington, D.C.
9. Mancarti, G.D., "New Concepts in Earthquake Retrofitting of Highway Bridges". Paper presented at Northwest Bridge Engineers Conference, Boise, Idaho, October, 1981.

10. McJunkin, R. and Ragsdale, J. "Compilation of Strong-Motion Records and Preliminary Data from the Imperial Valley Earthquake of 15 October 1979." California Division of Mines and Geology Preliminary Report 26 (1980)
11. Priestley, M.J.N. and Park, R., "Seismic Resistance of Reinforced Concrete Bridge Columns", California Seismic Design Criteria for Bridges", Proceedings of a Workshop on Earthquake Resistance of Highway Bridges held on January 29-31, 1979. Applied Technology Council, Palo Alto, Ca 1979, pp 253-283.
12. Rojahn, C., Ragsdale, J., Raggett, J. and Gates, J., "Main-Shock Strong Motion Records from the Meloland Road-Interstate Highway 8 Overcrossing (Imperial Valley Earthquake, Oct. 15, 1979)", U.S. Geological Survey Professional Paper 1254 pp 377-383 United States Government Printing Office, 1982.
13. "Seismic Design Guidelines for Highway Bridges", by Applied Technology Council, Palo Alto, Ca, Final Report, October 1981. Federal Highway Administration Report No. FHWA/RD-81/081
14. "Tentative Provisions for the Development of Seismic Regulations for Buildings", Applied Technology Council, (ATC-3). Palo Alto, Ca. 1978. National Bureau of Standards, Washington, DC Special Publication 510, National Science Foundation, Washington, DC Publication 78-8.

NEW SPECIFICATIONS FOR EARTHQUAKE-RESISTANT
DESIGN OF JAPANESE HIGHWAY BRIDGES

by

Eiichi Kuribayashi

Toshio Iwasaki

Osamu Ueda

ABSTRACT

This paper briefly discusses the history of seismic design provisions for highway bridges in Japan, and introduces the new specifications (Japan Road Association, 1980) for earthquake-resistant highway bridge design.

Preceding page blank

INTRODUCTION

Since the Kanto Earthquake of 1923 Japan has experienced a number of severe earthquakes, and the incidence of damage to highway bridges is considerable. Stemming from the damage caused by the Kanto Earthquake, seismic forces were first taken into account in highway bridges design in 1926. The seismic coefficient method in the practical design of structures was developed and introduced at that time. After experiencing severe damage during consecutive strong earthquakes, seismic regulations were reviewed and amended several times. In view of the damage caused by the Niigata Earthquake of 1964 the amended specifications for earthquake-resistant design of highway bridges were issued in 1971 by the Japan Road Association. Much work has been done to establish more rational seismic criteria for highway bridges. This includes recent advancements in earthquake engineering associated with bridges, the damage experience due to the Miyagi-ken-oki Earthquake of 1978, and the new specifications which were completed in March, 1980. This paper briefly describes the history of highway bridge seismic design codes in Japan, and introduces the new specifications (JRA, 1980) for highway bridge seismic design.

HISTORY OF EARTHQUAKE RESISTANT DESIGN PROVISIONS FOR HIGHWAY BRIDGES IN JAPAN

The Ministry of Home Affairs stipulated, in 1926, the "Specifications for Design of Road," which are parts of the "Road Laws." In the specifications, seismic forces were first taken into account in the design of highway bridges, since several highway bridges sustained substantial damage during the 1923 Kanto Earthquake. The specifications provided that highway bridges be designed using the seismic coefficient method, in which horizontal seismic coefficients were taken from 0.1 to 0.4. The values of the coefficients were dependent on areas and ground conditions. For bridges to be constructed in Tokyo and Yokohama, seismic coefficients of 0.3 or more were recommended. This seems due to the substantial damage to bridge structures in the areas during the Kanto Earthquake.

The Ministry of Home Affairs issued, in 1939, "Specifications for Design of Steel Highways," which took place of the earlier specifications. The new ones stipulated both a horizontal coefficient of 0.2 and a vertical coefficient of 0.1.

The specifications were revised again in 1964 by the Japan Road Association, with a commission from the Ministry of Construction. The revised specifications specified that

both a horizontal coefficient of 0.1 to 0.35 depending on areas and ground conditions, and a vertical coefficient of 0.1 shall be considered in the aseismic design.

In view of extensive damage to bridge structures from the 1964 Niigata Earthquake, the Japan Road Association, also with a commission from the Ministry of Construction, drew up in January 1971, comprehensive specifications [1,2] exclusively for earthquake-resistant design of highway bridges. In the 1971 specifications, two methods are provided for a seismic design. One is the conventional seismic coefficient method for rigid structures, where the horizontal coefficient ranges between 0.1 and 0.24 depending on areas, ground conditions, and importance. The other is the modified seismic coefficient which considers structural responses for comparatively flexible structures, where horizontal seismic coefficients vary from 0.05 to 0.3 depending on fundamental natural periods in addition to the three factors above.

During these years after the 1971 specifications were issued, technological advancements in bridge engineering and earthquake engineering have been remarkable. Especially comprehensive research works were executed in the New Aseismic Technology Development Project of the Ministry of Construction from 1972 through 1976. The results of the investigations achieved in this project were put into a unified form of provisions on earthquake resistant design for civil engineering structures and building structures, and "A Proposal for Earthquake Resistant Design Methods," was issued by the Ministry of Construction in March, 1977 [3,4]. Also, the Miyagi-ken-oki Earthquake of June 12, 1978 caused extensive damage to numerous bridges [5]. In view of the results of the above investigations and the damage features, the Japan Road Association amended the 1971 specifications and stipulated, in March 1980, new specifications for earthquake resistant design of highway bridges [6]. The new specifications became a part of "Specifications of Highway Bridges," which consist of five parts, Part I General Specifications (1972), Part II Steel Bridges (1972), Part III Concrete Bridges (1977), Part IV Substructures (1980), and Part V Earthquake Resistant Design. The new specifications (Part V Earthquake Resistant Design) will be outlined below. [6,7,8]

Further, characteristic criteria was proposed, between 1966 and 1968, tentatively for the aseismic design of highway bridges relating to specific projects administrated by the Japan Highway Public Corporation (JHPC), the Metropolitan Expressway Public Corporation (MEPC), the Hanshin Expressway Public Corporation (HEPC) and the Honsyu Shikoku Bridge

Authority (HSBA). The Japanese National Railways (JNR) stipulated in 1968, and revised in 1979, its own criteria for aseismic design of railway bridges.

Table 1 lists briefly this history of design loads (primarily seismic loads) for highway bridges in Japan. [9]

NEW SPECIFICATIONS (JRA-1980)

Outline

Efforts to revise the 1971 specifications into the form of Part V. of the Specifications for Highway Bridges have been underway by the Earthquake Resistant Design Subcommittee from 1977 to 1980, and the new specifications were issued in April, 1980. The contents of the new specifications are presented in Table 2. They apply to the design of highway bridges with span lengths not longer than 200 meters.

The specifications basically stipulate using seismic coefficient methods and provide two methods in determining design seismic coefficients. One is the conventional seismic coefficient method that applies to the design of relatively rigid structures. The other is the modified seismic coefficient method which considers structural responses that apply to the design of relatively flexible structures. Provisions on seismic motions in dynamic analysis, and seismic coefficient in ductility analysis, were newly introduced.

The principal features and improvements of the design methodology in the new specifications are described as follows:

Seismic Coefficient Method

(1) In the seismic coefficient method for relatively rigid structures, the horizontal design seismic coefficient (k_h) shall be determined by

$$k_h = v_1 \cdot v_2 \cdot v_3 \cdot k_0 \quad (1)$$

where k_h = horizontal design seismic coefficient,

k_0 = standard horizontal design seismic coefficient (= 0.2),

v_1 = seismic zone factor,

v_2 = ground condition factor,

v_3 = importance factor.

The values of v_1 , v_2 , and v_3 are shown in Tables 3, 4 and 5, respectively. The minimum values of k_h shall be taken as 0.1.

(2) The vertical design seismic coefficient may generally be considered as zero, except for special portions, such as bearing supports.

(3) The horizontal design seismic coefficient for structural parts, soils, and water below the ground surface may be considered as zero.

(4) Hydrodynamic pressures and earth pressures during earthquakes are specified in the specifications.

(5) Special attention is paid to very soft soil layers and soil layers vulnerable to liquefaction during earthquakes. The bearing capacities of these layers were either decreased or neglected in the design, in order to assure high earthquake-resistance for structures that are built in these layers.

(6) Special attention is also paid to the design of structural details, because of damage previously experienced on bridge structures. Provisions are specified for bearing supports and devices to prevent bridge girders from falling.

(7) Increases in allowable stresses of materials may be considered in the earthquake-resistant design, magnitudes of increases for various materials are specified in several related specifications.

The increasing rates are as follows:

concrete in reinforced concrete structures:	50%
reinforcements in reinforced concrete structures:	50%
structural steel for superstructures:	70%
structural steel for substructures:	50%
concrete in prestressed concrete structures subjected to compressive forces:	65%
foundation soils:	50%

Seismic Zoning Map

The newly developed seismic zoning map illustrated in Figure 1 was adopted. The map is based on the Proposal for Earthquake Resistant Design Methods [3,4] is intended to unify seismic zoning maps currently applied to civil engineering structures and buildings. Slight modifications were introduced to the proposed original map out of administrative considera-

tions. The values of v_i , are 1.0, 0.85 and 0.7 for A, B, and C zones, respectively, as shown in Table 3.

Classification of Ground Conditions

In the previous specifications, the classification of ground conditions was determined in accordance with geological conditions. However, since subsurface ground responses during earthquakes would generally be more largely affected by the predominant period of the ground, it is considered more reasonable to classify grounds into groups in terms of the period of the ground. Consequently in the new specifications, the ground conditions are classified into four groups according to Table 4, in which the characteristic value of ground, T_g , is stipulated to be principally calculated by the following equation:

$$T_g = \sum_i \frac{4H_i}{V_{si}} \quad (2)$$

where T_g = Characteristic value of ground (second)

H_i = Thickness of i -th subsoil layer (m)

V_{si} = Shear wave velocity of i -th subsoil layer at low strain (around 10^{-4} percent)

As for shear wave velocities, it is recommended that it be directly measured through site investigation. Shear wave velocities may be assumed from N -values of standard penetration tests by

$$V_s = \begin{cases} 100 N^{1/3} & (1 < N < 25) \text{ for cohesive soils} \\ 80 N^{1/3} & (1 < N < 50) \text{ for sandy soils} \end{cases} \quad (3)$$

The baserock for calculation of Eq. (2) is stipulated to take on the soil layer that has a shear wave velocity at low strain equal to 280 m/sec or higher and is not underlaid by materials having significantly lower shear wave velocities.

The characteristic value T_g implies a natural period of subsurface ground at low strain levels. The classification of T_g shown in Table 3 was proposed from numerical seismic analyses of various types of subsurface grounds. Such analyses revealed that the natural period T_s of subsurface ground at high strain levels which would be expected to occur during strong earthquakes can be approximately obtained by the following equation.

$$T_s = 1.25 T_g \quad (4)$$

It was also found that ground conditions could be adequately classified into four groups by taking T_g as $T_g < 0.25$ seconds, $0.25 < T_g < 0.5$ seconds; $0.5 < T_g < 0.75$ seconds and $T_g > 0.75$ seconds. The characteristic values T_g presented in Table 4 were thus obtained by substituting the above mentioned T_g into Eq. (4).

Figure 2 is one of representative results of analyses showing a relationship between the characteristic values T_g and the thickness of soil deposits. It is apparent from the result that the classification of ground conditions determined by the characteristic value T_g as shown in Table 4 can also be approximately estimated by the thicknesses of alluvial and diluvial layers. It is therefore recommended to use this relation to classify the ground condition when T_g cannot be obtained.

Figure 3 shows a comparison of the ground classifications which were provided in the 1971 specifications and in the new specifications. It is understood from the results that some ground areas which are evaluated as Groups 1 and 2 in the current specifications turn into Groups 2 and 3, respectively, in the new specifications.

Liquefaction of Sandy Soil Layers

In the 1971 specifications, it was stipulated that saturated sandy soil layers that are within 10 meters of the actual ground surface, and that have a standard penetration test N-value less than 10, a coefficient of uniformity less than 6, and also a D_{20} -value on the grain size accumulation curve between 0.04 mm and 0.5 mm, shall have a high potential for liquefaction during earthquakes, and that bearing capacities of these layers shall be neglected in design.

After the Niigata Earthquake, comprehensive studies were conducted to assess the vulnerability of saturated sandy soils. Based on these studies, the provisions for liquefaction are improved in the new specifications as follows:

(1) Sandy Soil Layers Needed to be Checked for Liquefaction -- Saturated alluvial sandy layers which have a water table within 10 meters from the ground surface, and have D_{50} -values on the grain size accumulation curve between 0.02 and 2.0 mm, are vulnerable to liquefaction for the depth between 0 and 20 m, and liquefaction potential of these layers shall be estimated according to item (2).

(2) Estimation of Liquefaction -- For those soil layers which are judged to be vulnerable for liquefaction, liquefaction potential shall be checked based on liquefaction resistance factor, F_L , defined by the following equation.

$$F_L = \frac{R}{L} \quad (5)$$

where F_L = liquefaction resistance factor

R = resistance of soil elements to dynamic loads, and

$$R = R_1 + R_2 \quad (6)$$

R_1 and R_2 shall be determined in accordance with Figures 6 and 7, respectively.

L = dynamic loads to soil elements induced by earthquake motion

$$L = r_d k_s \frac{\sigma_v}{\sigma_v'} \quad (7)$$

$$r_d = 1.0 - 0.015z \quad (8)$$

z = depth from the actual ground surface (m)

k_s = seismic coefficient for evaluation of liquefaction, and shall be determined by the following equation:

$$k_s = v_1 \cdot v_2 \cdot v_3 \cdot k_{s0} \quad (9)$$

v_1, v_2, v_3 = seismic zone factor, ground condition factor, and importance factor, provided in Tables 3, 4 and 5, respectively.

$$k_{s0} = 0.15$$

σ_v = total overburden pressure (kg/cm^2)

σ_v' = effective overburden pressure at the static condition (kg/cm^2)

Soil layers having a liquefaction resistance factor F_L smaller than 1.0 shall be judged to liquefy during earthquakes. Figures 4 and 5 are graphic illustrations of the first term R_1 and the second term R_2 represented in the following equations, which were proposed based upon the results of laboratory dynamic triaxial tests on soil specimens taken from several sites in Japan [10,11].

$$R = \begin{cases} 0.0882 \sqrt{\frac{N}{\sigma'_v + 0.7}} + 0.19 & (0.02 \text{ mm} < D_{50} < 0.05 \text{ mm}) \\ 0.0882 \sqrt{\frac{N}{\sigma'_v + 0.7}} + 0.225 \log_{10} \left(\frac{0.35}{D_{50}} \right) & (0.05 \text{ mm} < D_{50} < 0.6 \text{ mm}) \\ 0.0882 \sqrt{\frac{N}{\sigma'_v + 0.7}} - 0.05 & (0.6 \text{ mm} < D_{50} < 2.0 \text{ mm}) \end{cases}$$

(3) Treatment of Soil Layers which were Judged to Liquefy -- For those soil layers which are judged to liquefy by the above estimation and are within 20 meters of the actual ground surface, bearing capacities and other soil constants shall be either neglected or reduced in the seismic design by multiplying the original bearing capacities by reduction factors D_E which are determined in accordance with F_L -values and tabulated in Table 6.

Modified Seismic Coefficient Method

In the 1971 specifications, the modified seismic coefficient method was provided to apply to bridges which have flexible piers and fundamental periods longer than 0.5 seconds, such as those with piers taller than 25 meters above the ground surface. Accounting for seismic responses, magnification factors (β) for the modified seismic coefficient method were stipulated. However, it has been pointed out that fundamental natural periods sometimes exceed 0.5 seconds even for those bridges with piers lower than 25 meters above the ground surface. Using experimental data on the relationship between fundamental natural periods and pier heights, it is modified in the new specifications so that the modified seismic coefficient method shall apply to bridges which have flexible piers and long fundamental periods, such as those with piers higher than 15 meters above the ground surface.

In addition to the above change, the following two modifications were also introduced:

(1) The magnification factors (β) are modified as shown in Table 7 and Figure 6 so as to avoid a sudden change of β -value at a period of 0.5 seconds.

(2) In the 1971 specifications, the effects of subsoil conditions were not considered in estimating fundamental natural periods. Since the effects of subsoils would be predominant in calculating fundamental natural periods, especially for bridges with short piers, it is stipulated in the new specifications that the effects of subsoils shall be taken into account for those bridges which are constructed in the soft ground. It is recommended that the fundamental natural period for the individual system consisting of each substructure

and the part of superstructures supported by it be estimated using the following equation.

$$T = 2.01 \sqrt{\delta} \quad (11)$$

where T = Fundamental natural period in seconds of the system consisting of a substructure and the section of the superstructures supported by it.

δ = Maximum horizontal displacement (in meters) of the pier when subjected to the dead weight of the section of superstructure supported by the substructure and also to 80 percent of the dead weight of the substructure above the ground surface assumed in earthquake resistant design.

Seismic Motions in Dynamic Analysis

In the 1971 specifications, it is stipulated that dynamic earthquake response analyses shall be adopted for those bridges for which detailed investigations are required. In the new specifications, an article is introduced concerning the seismic motions to be utilized in dynamic response analyses. The principal provisions are as follows:

(1) Dynamic response analyses may apply to those bridges which are designed either by the seismic coefficient method or the modified seismic coefficient method, in order to investigate precisely the earthquake resistivity of bridges in terms of ductilities and maximum bearing capabilities. Dynamic analyses are needed for those bridges having structural systems which are significantly different from those assumed in the seismic coefficient method or the modified seismic coefficient method, those bridges having new structural types for which the experience of damage accumulated from past earthquakes cannot be adequately extended, those bridges which are constructed on extremely soft soil deposits and are expected to deform considerably during earthquakes, and those bridges for which detailed investigations on requirements of ductility of structures are needed.

(2) Two types of dynamic earthquake response analyses, i.e., response spectrum analyses and time history analyses can be used.

(3) Input motions used for the time history analyses shall be selected from strong-motion acceleration records which consider the dynamic characteristics of bridges and the characteristics of the records.

In determining input seismic motions, two procedures are proposed. One is to estimate expected intensities at the site based on the life-time of the bridge and the recurrence period of earthquake events. Another procedure is to estimate the expected ground motions by assuming the locations and the magnitudes of specific earthquakes around the site. In the second, ground motions can be evaluated either by the theory of seismic gaps or the statistics of the past historical earthquakes. It is also recommended that the input seismic motions be selected according to the objectives of the earthquake response analyses. It states that bridges shall maintain their functions for those motions which are expected to occur two or three times during the bridge lifetime, and they shall survive those motions which are expected to occur once, or rarely, at the site.

(4) In utilizing seismic ground motions recorded on soft soil deposits which have appreciably different ground conditions compared to those at a planned construction site, it is recommended such effects be taken into account in the analyses. For such purposes, earthquake response analyses based on the baserock motions are recommended.

(5) Input earthquake response spectra used for the response spectrum analyses shall be determined using the response spectra calculated from strong-motion accelerations. In an appendix to the new specifications, the results of statistical analyses of strong-motion acceleration records are presented. Some of the representative earthquake response spectra and relations between maximum horizontal accelerations and epicentral distances are presented in Figures 7 and 8, respectively [12].

Seismic Coefficient in Ductility Analysis

In order to avoid brittle failure during earthquakes, it is extremely important that reinforced concrete structures have adequate ductility. A provision that stipulates the seismic coefficient used for the design of reinforced concrete piers with ductility is introduced. It stipulates that the seismic coefficient in ductility analysis shall be determined using the following equation.

$$k_{hd} = v_4 \cdot k_h \quad (12)$$

where k_{hd} = seismic coefficient in ductility analysis

v_4 = structural characteristics factor (greater than 1.3)

k_h = horizontal design seismic coefficient provided in Eq. (1).

Table 8 shows maximum ductilities of ordinary RC bridge piers which were analytically determined to account for deformation due to bending of piers and deformation of reinforcement pulled out from footings, in which the critical strains of concrete were assumed as 0.35 percent. It can be recognized from these results that the maximum ductilities of bridge piers normally designed by the seismic coefficient method can be taken as approximately 6. However, since values for maximum ductilities are derived from analytical calculations for a half cycle loading, it is considered desirable to take maximum design ductilities to be smaller than 6. Considering the fact that concrete pier ductility decreases significantly under alternately repeated loading conditions [13], one third of the values tabulated in Table 8, which lead to about 2, is recommended as the ductility factor for design purposes.

CONCLUSIONS

Earthquake resistant highway bridge design criteria in Japan is briefly described with emphasis given to improvements and modifications in the new specifications (JRA-1980). In view of the history of the earthquake resistant design of highway bridges, it is considered necessary to concentrate a comprehensive investigation on the following subjects in the future..

(1) Analysis of the Effects of Soil-Structure Interactions

Bridge construction on deep, soft soil deposits has increased recently. From the evidence of past, extensive earthquake damage, it is well recognized that the influence of surrounding subsurface soils are very important for the seismic responses of substructures, especially for substructures which are embedded in deep soft ground. Consequently, considerable interest has been focused on the soil-structure interaction effects on such structures by model experiments and theoretical analyses. However, very limited research has been undertaken to investigate the seismic response of actual substructures during strong seismic excitations. Investigations of the effects of soil-structure interaction which utilize strong-motion records obtained at actual bridges are encouraged. For this purpose, it is recommended that strong motion observations, especially simultaneous observations of both the bridges and the surrounding subsurface grounds, be extended.

(2) Analysis of Seismic Behavior of Substructures in Liquefied Soil Layers

Due to the comprehensive research conducted after the 1964 Niigata Earthquake, determining the vulnerability of saturated sandy deposits and judging in situ liquefaction potential became both possible and practical. However, further investigation of the seismic behavior of substructures in liquefied layers is needed, as is the development of suitable earthquake resistant design procedures for bridges under such conditions.

(3) Experiments on Ductilities of Bridge Piers

Seismic damage to bridges were most commonly caused by pier and foundation failures. It is, therefore, extremely important to prevent brittle failure to substructures. Up to the present, only very limited experimental studies have been conducted on the hysteretic behavior of bridge piers under cyclic loading. Such a lack of data on the hysteretic response of piers is one of the major obstacles to introducing limit design to bridges to account for the ductility of members. It is recommended that extensive efforts be devoted to accumulating such experimental data.

(4) Design Details of Bearing Supports and Connections

For providing highway bridges with adequate resistance to seismic disturbances, it is very important to give special attention to the design details of connections between superstructures and substructures, to preventing girder fall, and to avoid severe damage which is caused by bearing support failures.

REFERENCES

- [1] Japan Road Association, "Specifications for Earthquake Resistant Design of Highway Bridges," 1971.
- [2] Kawakami, K., Kuribayashi, E., Iwasaki, T. and Iida, Y., "On Specifications for Earthquake Resistant Design of Highway Bridges," (January, 1971), 7th Joint Meeting, U.S.-Japan Panel of Wind and Seismic Effects, UJNR, Tokyo, 1975.
- [3] Ministry of Construction, "A Proposal for Earthquake Resistant Design Methods," 1977 (In Japanese).
- [4] Nakano, K. and Ohashi, M., "A Proposal for Earthquake Resistant Design Methods," 9th Joint Meeting, U.S.-Japan Panel on Wind and Seismic Effects, UJNR, Tokyo, 1977.
- [5] Okubo, T. and Iwasaki, T., "Summary of Experimental and Analytical Seismic Research Recently Performed on Highway Bridges," Workshop on Research Needs of Seismic Problems Related to Bridges, Palo Alto, California, USA, 1979.
- [6] Japan Road Association, "Specifications for Highway Bridges," Part V, Earthquake Resistant Design, 1980 (In Japanese).
- [7] Ohashi, M., Kuribayashi, E., Iwasaki, T., and Kawashima, K., "An Overview of the State of the Practice in Earthquake Resistant Design of Highway Bridges in Japan," Workshop on Research Needs on Seismic Problems Related to Bridges, Palo Alto, California, USA, 1979.
- [8] Kuribayashi, E., Iwasaki, T., "Progress Report on Research Work in Bridge Earthquake Engineering at the Public Works Research Institute, Japan," Seventh World Conference on Earthquake Conference, Istanbul, Turkey, 1980 (to be presented).
- [9] Iwasaki, T., Penzien, J., and Clough, R. W., "Literature Survey - Seismic Effects on Highway Bridges," EERC Report No. 72-11, University of California, Berkeley, 1972.
- [10] Ohashi, M., Iwasaki, T., Tatsuoka, F. and Tokida, K., "A Practical Procedure for Assessing Earthquake-Induced Liquefaction of Sandy Deposits," 10th Joint Meeting, U.S.-Japan Panel on Wind and Seismic Effects, UJNR, Washington, D.C., 1978.
- [11] Iwasaki, T., Tatsuoka, F., Tokida, K. and Yasuda, S., "A Practical Method for Assessing Soil Liquefaction Potential Based on Case Studies at Various Sites in Japan," Second International Conference on Microzonation for Safer Construction Research and Application, San Francisco, 1978.
- [12] Iwasaki, T., Katayama, T., Kawashima, K. and Saeki, M., "Statistical Analysis of Strong-Motion Acceleration Records Obtained in Japan," 2nd International Conference on Microzonation for Safer Construction Research and Application, San Francisco, 1978.
- [13] Osaka, Y. and Ohta, M., "Experimental Study on the Behavior of Reinforced Concrete Bridge Piers under Seismic Alternating Load," A.I.C.A.P.-C.E.P. Symposium on Structural Concrete under Seismic Actions, Rome, 1979.

Table 1 History of Design Loads for Highway Bridges in Japan
(Primarily Seismic Loads)

Year	Name of Regulations	Design Live Loads				Impact Loads	Seismic Loads k: Horizontal Seismic Coefficient	Other Seismic Regulations (k: seismic coef.)	Major Earthquake
		Class	Truck Roller Structure	Loops	Uniform Loads				
1) 1886	Order No. 13 Ministry of Home Affairs (MHA)				U-454 kg/m	-	not considered		(M7) after Eika Shogun (1871)
2) 1906	Order MHA		B-12.6 t S-12.7		U-400 400 kg/m (carriage way) U-270 400 kg/m (footway)	-	not considered		
3) 1919	Road Laws MHA		B-12.6 t T-11.2 t S-10 t		Same as 2)	-	not considered		
4) 1926	Specifications for Design of Roads, Road Laws, MHA	1st 2nd 3rd	T-12 t T-6 t T-4 t		U-400 kg/m U-500 kg/m U-500 kg/m	-	considered Seismic Coefficient Method k=0.15-0.4 depending on location and ground condition (k20.3 advised in Tokyo, Tohshama)	1926 Building Law (k20.3) 1950. Kansai's Seismic Map.	1923 Kanto (M7.9)
5) 1939	Specifications for Design of Steel High- way Bridges, MHA	1st 2nd	T-13 t T-9 t		U-500 kg/m U-400 kg/m	-	considered Seismic Coefficient Method k _h =0.2, k _v =0.1	1950. New Building Law (k=0.2, k _h 10m increase 0.01 per an increase of 1m above 10m)	1945 Nankai (M6.1) 1948. Fukuji (M7.3) 1952. Tohachi- oki (M6.2)
6) 1956 (and 1964)	Revision of Specifi- cations for Design of Steel HIGHWAY Bridges, JRA	1st 2nd	T-20 t T-14 t		- -	L=20 (St/m) L=14 (3.3t/m)	considered Seismic Coefficient Method k=0.1+0.35 depending on location and ground conditions		
7) 1966 to 1971	Specifications for Design of Substructures of Highway Bridges, JRA				Same as 6)		same k as 6) Detailed calculation methods	1964. High- rise Building (M45e) k=(0.1m+0.36) /T(T-period) (0.05k20.2)	1964. Nifuge (M7.5)
8) 1968* (and 1970)	Design Standards, JNFC				Same as 6)		Design Code for High- rise Bridges. (Increase in k with the height of the piers)	1965. Report of JSCE on Civil Eng of Engineering Structures.	
9) 1967*	Specifications for Earthquake Resistant Design of Honshu-Shikoku Bridges, JSCE		Special Live Loads and Impact Loads for Suspension Bridges are Considered				Modified Seismic Co- efficient Method (Basic Coef. k=0.2)	1966. Report of JSCE on Earthquake- Resistant Design of Substructures of Railway Bridges.	1968. Tohachi- oki (M7.9)
10) 1967*	Specifications for Earthquake-Resistant Design of Metropolitan Expressway Public Corporation, MEPC				Same as 6)		Seismic Coef. Method k=0.2+0.3		
11) 1968*	Asseismic Design Standards, MEPC				Same as 6)		Seismic Coef. Method k=0.2+0.20		
12) 1971	Specifications for Earthquake-Resistant Design of Highway Bridges, JRA				Same as 6)		Seismic Coef. Method k=0.1+0.24 (Rigid) Modified SCH. k=0.05+0.3 (Flexible)	1977. A Proposal for Earthquake Resistant Design Methods (MDC)	1978. Niyugiku- Oki (M7.4)
13) 1980	Part V Earthquake Resistant Design, Specifications for Highway Bridges (New Specifications), JRA				Same as 6)		Seismic Coef. Method k=0.1+0.24 (Rigid) Modified SCH. k=0.05+0.3 (Flexible) Earthquake Response Analysis (Very Flexible Bridges)	1979. New Specifi- cations for Earth- quake-Resistant Design of Railway Facilities	

* Specifications from 8) to 11) are for highway bridges related to special large projects.

Reproduced from
best available copy.



Table 2 Contents of Part V Earthquake Resistant Design, Specifications for Highway Bridges [Japan Road Association, 1980]

Contents	Same As the Previous Spec. (1971)	Modified		Newly Introduced
		Slightly	Completely	
Chapter 1	General	○		
	1.1 Scope	○		
Chapter 2	1.2 Definitions of Terms			
	Basic Principles for Earthquake Resistant Design		○	
Chapter 3	Loads and Conditions in Earthquake Resistant Design	○		
	3.1 General	○		
	3.2 Seismic Effects			
	3.3 Seismic Forces Transmitted from Superstructures to Substructures		○	
	3.4 Earth Pressures during Earthquakes		○	
	3.5 Hydrodynamic Pressures during Earthquakes	○		
	3.6 Classification of Ground Conditions in Earthquake Resistant Design		○	
	3.7 Soil Layers Whose Bearing Capacities are Reduced in Earthquake Resistant Design			○
	3.8 Ground Surface Assumed in Earthquake Resistant Design			○
Chapter 4	Design Seismic Coefficient		○	
	4.1 General		○	
	4.2 Design Seismic Coefficient in the Seismic Coefficient Method	○		
	4.3 Factors for Modifying the Standard Horizontal Design Seismic Coefficient		○	
	4.4 Design Seismic Coefficient in the Modified Seismic Coefficient Method Considering Structural Response			○
	4.5 Earthquake Motions in the Earthquake Response Analyses			○
Chapter 5	4.6 Design Seismic Coefficient Accounting of Ductilities			○
	General Provisions for Design of Structural Details		○	
	5.1 General		○	
	5.2 Devices for Preventing Superstructures from Falling		○	
	5.3 Vertical Seismic Forces for Design of Connections between Superstructures and Substructures	○		
	5.4 Methods for Transmitting Seismic Forces at Connections between Superstructures and Substructures		○	
Appendices	5.5 Devices Expected for Decreasing Seismic Forces	○		
	I. References on Liquefaction			○
	II. Examples of Classification of Ground Conditions			○
	III. Example of Estimation of Design Horizontal Seismic Coefficient	○		
	IV. References on Earthquake Motions in the Earthquake Response Analyses			○
	V. Example of Calculating Natural Periods Utilized in the Modified Seismic Coefficient Method			○
	VI. Example of Calculating Ductilities			○
	VII. Major Related Provisions Concerning Earthquake Resistant Design		○	
	VIII. Detailed Practices			○
	IX. References			○

Table 3 Seismic Zone Factor v_1 for Highway Bridges

Zone ¹⁾	Value of v_1
A	1.00
B	0.85
C	0.70

Note: 1) Zones A, B and C are illustrated in Fig. 1.

Table 4 Classification of Ground Conditions and Value of v_2

Group	Characteristic Value T_g (second)	Value of v_2
1	$T_g < 0.2$	0.9
2	$0.2 \leq T_g < 0.4$	1.0
3	$0.4 \leq T_g < 0.6$	1.1
4	$0.6 \leq T_g$	1.2

Table 5 Importance Factor v_3 for General Highway Bridges

Group	Definitions	Value of v_3
1	Bridges on expressway (limited-access highways), general national highways and principal prefectural highways. Important Bridges on general prefectural highways and municipal highways.	1.0
2	Other than the above	0.8

Note: The value of v_3 may be increased up to 1.10 for special cases in Group 1.

Table 6 F_L - D_E Relation

F_L	Depth, Z(m)	Reduction Factor, D_E
$F_L \leq 0.6$	$Z \leq 10$	0
	$10 < Z \leq 20$	1/3
$0.6 < F_L \leq 0.8$	$Z \leq 10$	1/3
	$10 < Z \leq 20$	2/3
$0.8 < F_L \leq 1.0$	$Z \leq 10$	2/3
	$10 < Z \leq 20$	1
$1.0 < F_L$	-	1

Table 7 Magnification Factor β for Modified Seismic Coefficient Method

G. C.	β -value			
Group 1	$\beta = 2T$	$\beta = 1.25$	$\beta = 1.40/T$	$\beta = 0.50$
	$0.5 \leq T \leq 0.625$	$0.625 \leq T \leq 1.12$	$1.12 \leq T \leq 2.8$	$T \geq 2.8$
Group 2	$\beta = 2T$	$\beta = 1.25$	$\beta = 1.75/T$	$\beta = 0.50$
	$0.5 \leq T \leq 0.625$	$0.625 \leq T \leq 1.4$	$1.4 \leq T \leq 3.5$	$T \geq 3.5$
Group 3	$\beta = 2T$	$\beta = 1.25$	$\beta = 2.10/T$	$\beta = 0.50$
	$0.5 \leq T \leq 0.625$	$0.625 \leq T \leq 1.68$	$1.68 \leq T \leq 4.2$	$T \geq 4.2$
Group 4	$\beta = 2T$	$\beta = 1.25$	$\beta = 2.50/T$	$\beta = 0.50$
	$0.5 \leq T \leq 0.625$	$0.625 \leq T \leq 2.0$	$2.0 \leq T \leq 5.0$	$T \geq 5.0$

Table 8 Maximum Ductilities from the Analyses of RC Bridge Piers

Section	Maximum Ductility	Number of Piers Examined
Circle-Shaped Column	6.4 ~ 8.1	6 Specimens
Hollowed-Circle Shaped Column	5.8 ~ 6.8	6 Specimens
2-Rectangular Column	Longitudinal	5.6 ~ 10.5
	Transverse	5.7 ~ 8.6
Oval-Shaped Column	Longitudinal	5.3 ~ 7.3

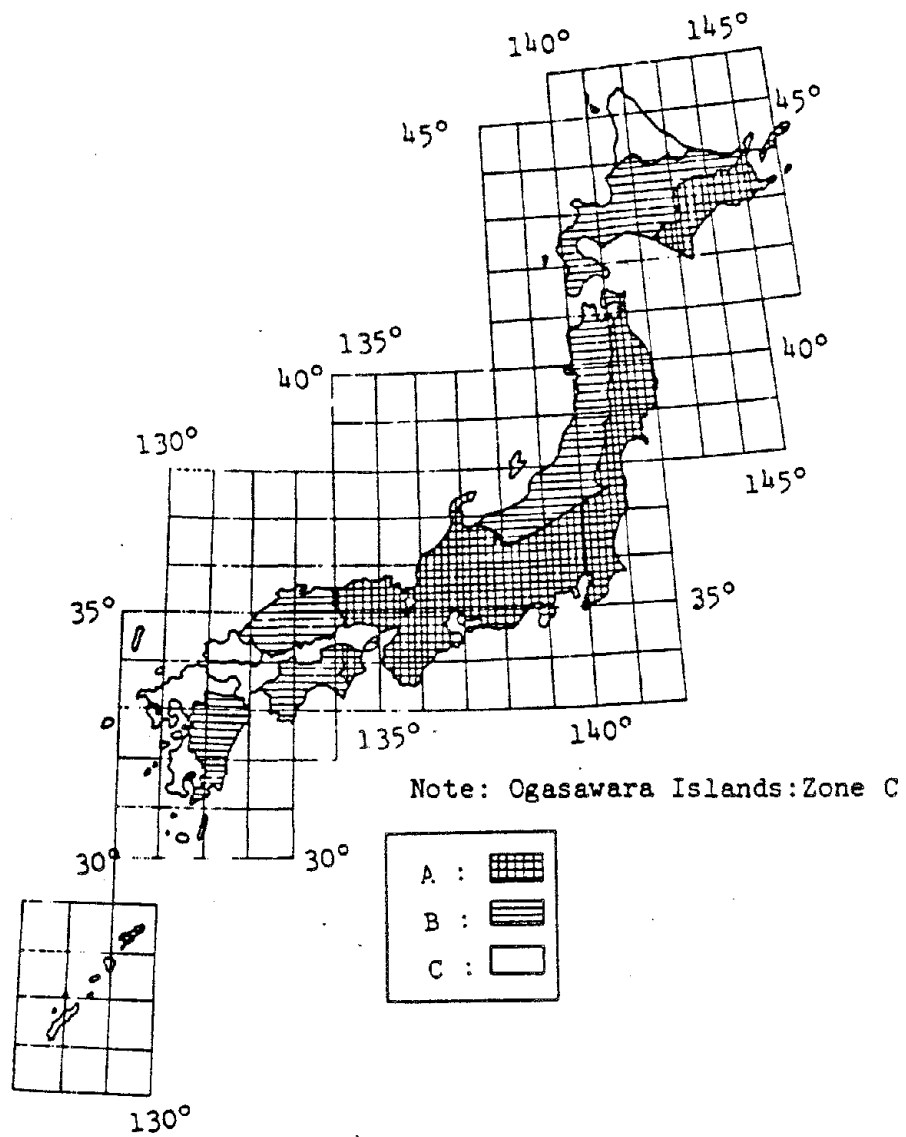


Fig. 1 Seismic Zoning Map
(New Specifications)

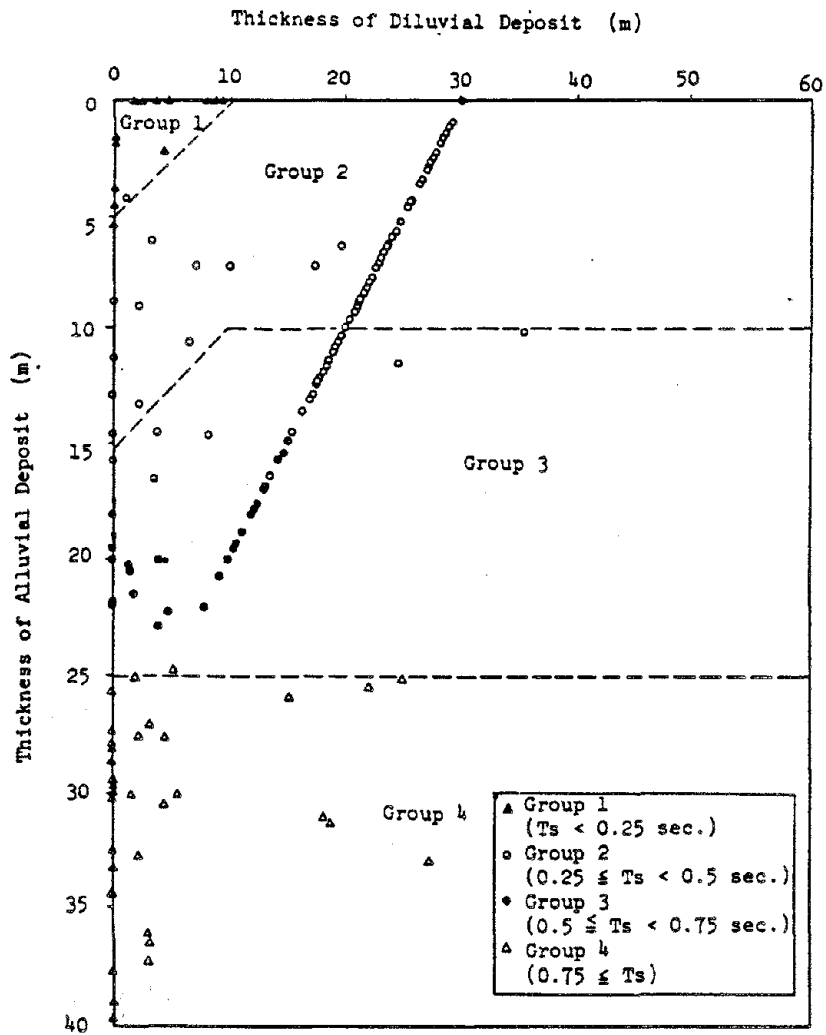


Fig. 2 Classification of Ground Conditions in Terms of Thicknesses of Alluvial and Diluvial Soil Layers

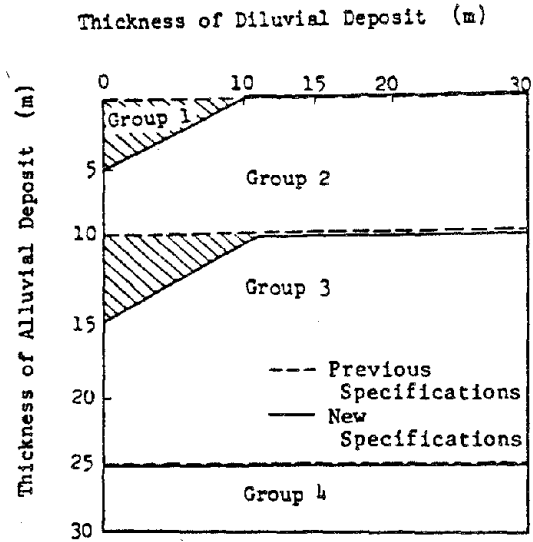


Fig. 3 Comparison of Ground Conditions Provided in Previous and New Specifications

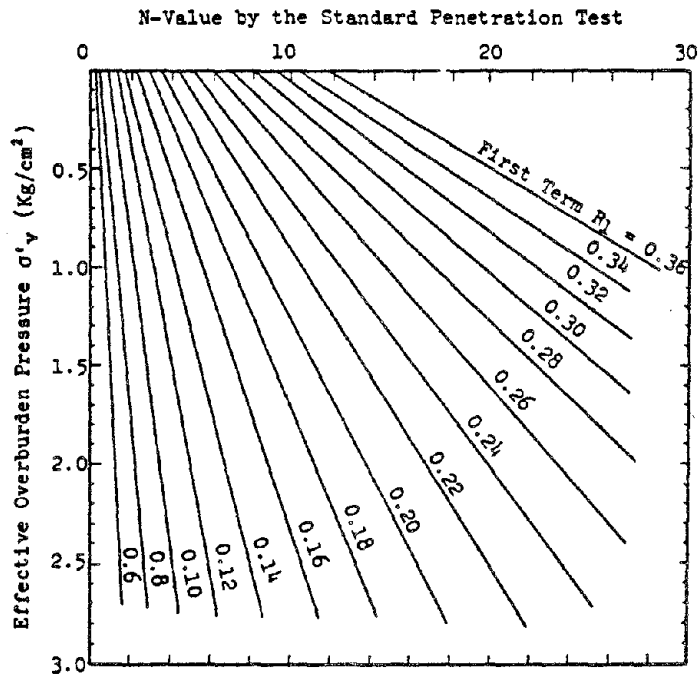


Fig. 4 R₁-Value (First Term of Resistance R)

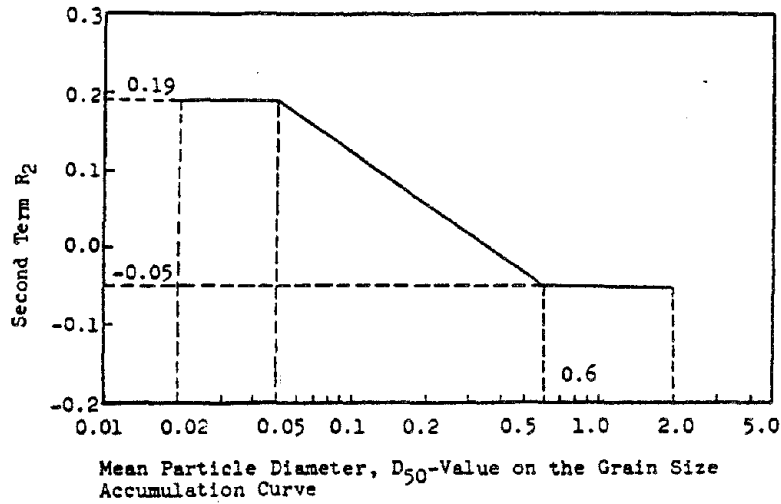


Fig. 5 R_2 -Value (Second Term of Resistance R)

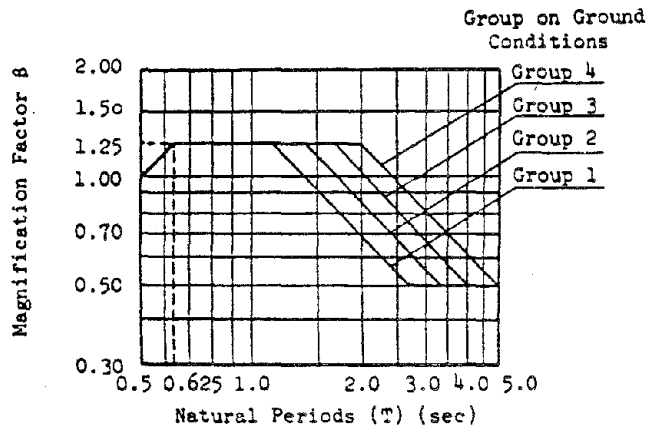
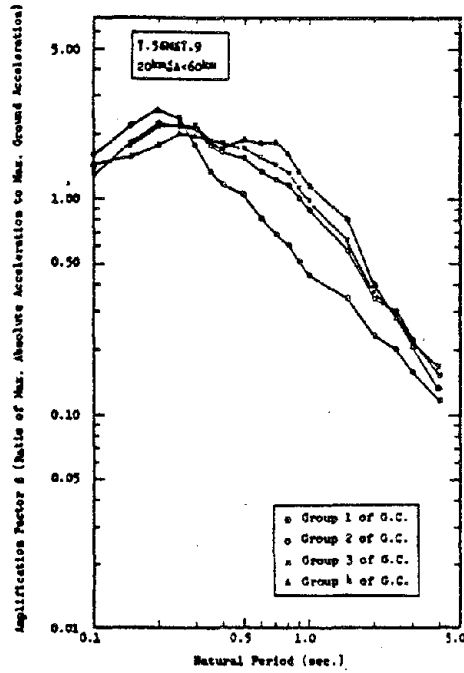
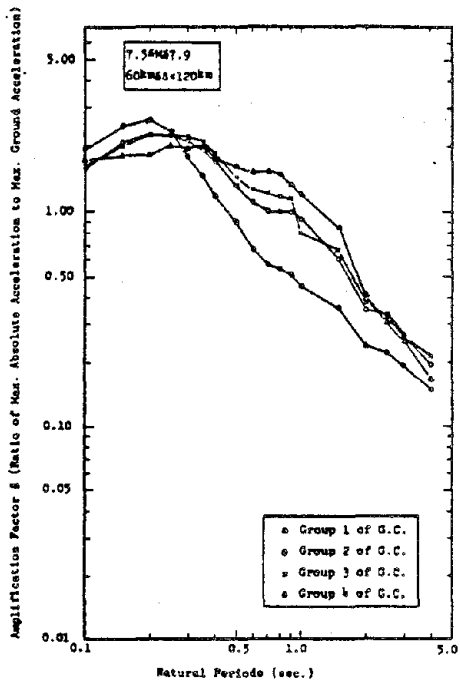


Fig. 6 Magnification Factor for the Modified Seismic Coefficient Method (New Specifications)

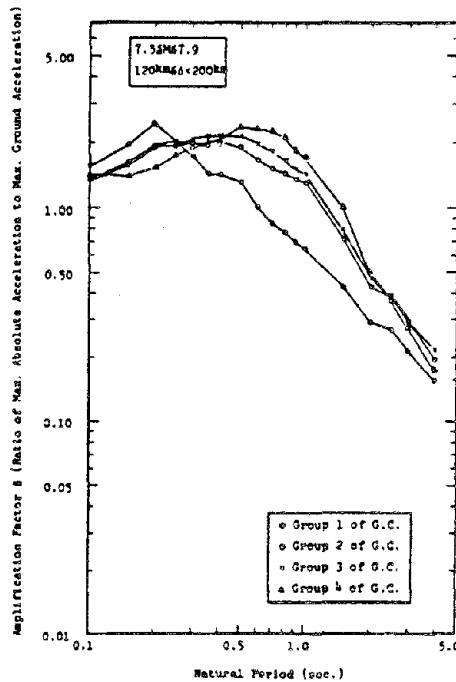
Fig. 7 Response Spectrum Curves β in case of $7.5 \leq M \leq 7.9$



(a) $20\text{km} \leq \text{Epicentral Distance} \leq 60\text{km}$

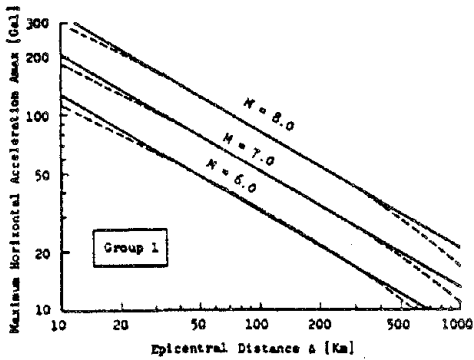


(b) $60\text{km} \leq \text{Epicentral Distance} \leq 120\text{km}$

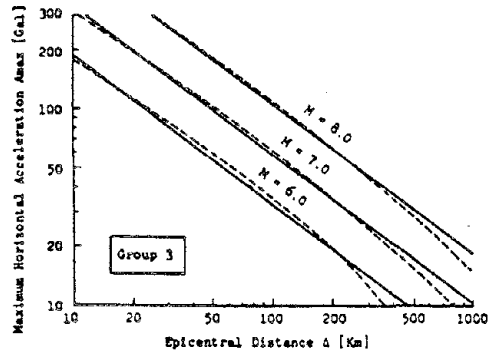


(c) $120\text{km} \leq \text{Epicentral Distance} \leq 200\text{km}$

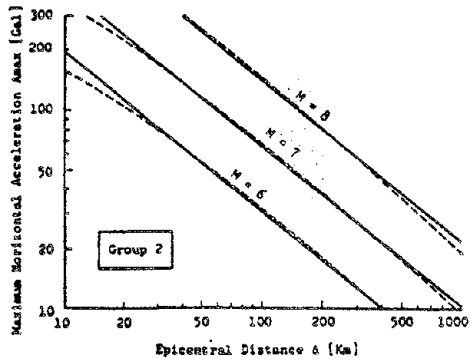
Fig. 8 Relationship Between Maximum Horizontal Acceleration (A_{max}) and Epicentral Distance (Δ) Obtained by Statistical Analyses of Strong-Motion Acceleration Records



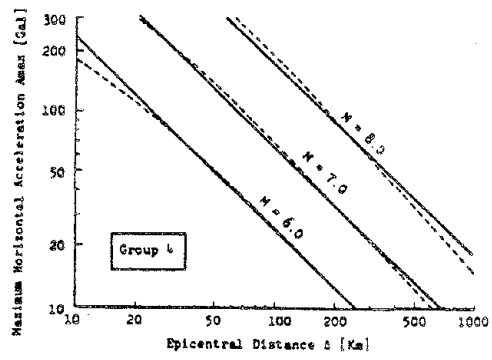
(a) Group 1



(c) Group 3



(b) Group 2



(d) Group 4

ANALYTICAL PROCEDURES USED FOR THE
SEISMIC DESIGN OF HIGHWAY BRIDGES

by

R. A. Imbsen
Engineering Computer Corporation

and

J. Penzien
University of California, Berkeley

1.0 INTRODUCTION

During the past decade, the government and engineering communities have increased their efforts to further the state-of-the-art relating to the seismic design of highway bridges. Most of the renewed interest in this subject was generated by the many spectacular bridge failures during the 1971 San Fernando, California earthquake. Many of the recent advancements in the state-of-the-art, however, have taken place so rapidly that they have not yet been implemented into design practice. This is especially true in geographical areas other than the west coast of the United States.

One of the most complicated tasks a bridge engineer is faced with in applying the latest principles of seismic design is the dynamic analysis of the structural system. This is a problem facing most bridge designers today, whether they use the current AASHTO (American Association of State Highway and Transportation Officials) design specifications [1] or the newly adopted ATC-6 Seismic Design Guidelines for Highway Bridges [2]. The introduction of structural dynamics to the bridge design process requires that bridge designers learn both the basic principles in dynamics and how to use computer programs having dynamics analysis capabilities. This also implies introductory training in the art of mathematical modeling.

Because of the new concepts introduced in the AASHTO and ATC-6 design specifications, a continuing effort is needed to train practicing bridge engineers in the latest principles of seismic design of highway bridges. This training must encourage immediate implementation of these principles and tools. In addition, it must stimulate the interest of the profession as a whole, thus broadening the base from which even further advancements in seismic design can be made.

Although the application of structural dynamics to the bridge engineering field is somewhat in its infancy, it has become apparent that certain types of bridges may be idealized so as to be more easily analyzed mathematically. Penzien and Imbsen developed the Single Mode Spectral Method (SMSM), presented in the ATC-6 guidelines, in an effort to simplify the task of implementing structural dynamics within the field of bridge engineering [3].

The SMSM is used to calculate the seismic design forces of a bridge that can be characterized as having its major dynamic response in a single mode of vibration. This method, although quite rigorous, reduces a complex dynamics analysis to the performance of just two statics analyses. The first static analysis is conducted to obtain the structure period, the second to apply inertial forces consistent with the displaced shape.

The SMSM, as formulated, can be applied to many types of bridges, including bridges with either continuous or discontinuous superstructures. Boundary conditions at the abutments and piers can be modeled to include the effects of the foundation. A bridge engineer can readily apply the SMSM by using hand calculations and conventional static structural analysis procedures. For the more complex bridges in the higher seismic zones, the seismic design guidelines recommend the Multimode Spectral Method (MMSM), which is a response spectrum analysis.

The computer program, SEISAB (SEISMic Analysis of Bridges), currently funded by the National Science Foundation, was developed by Imbsen et. al [4,5] specifically to help bridge designers conduct seismic analyses. The SEISAB program has both SMSM and MMSM capabilities. In addition, elastic time-history analysis capabilities have been recently incorporated into the program, allowing the designer to conduct more detailed analyses or correlation studies in which the structure remains within the elastic range. With a minimum amount of input data, this program can generate a structural model for a dynamic analysis of almost every type of deck-girder bridge.

2.0 SINGLE DEGREE OF FREEDOM MODELING OF A CONTINUOUS SYSTEM

Bridges are generally continuous systems made up of many components, each having distributed mass and elasticity, contributing to the overall response of the system. The response displacement of continuous systems, such as the one in Figure 1a, can be shown at any point in time to be a linear combination of the individual modes of vibration. Restricting the number of modes to one and recognizing that the true vibration shape is unknown results in the following displacement approximation for transverse displacements:

$$\begin{aligned}
 v(x,t) &= v_S(x)v(t) \\
 &= v_S(x)A\sin(\omega t - \phi)
 \end{aligned}
 \tag{1}$$

where $v_S(x)$ is the assumed vibration shape, $v(t)$ is a generalized coordinate representing the amplitude, 'A' is an arbitrary scaling factor and ω is the circular frequency. Since the true mode shape is unknown, the best approximation to it should be obtained.

The process of selecting the closest possible approximation of the shape function, such as the one shown in Figure 1b, can be facilitated by taking advantage of the fact that the free vibration displacements result from inertial forces. Since inertial forces are proportional to the mass distribution, a transverse distributed load proportional to the mass should produce a good approximation of the true mode shape. Because the mass is usually distributed uniformly in bridge decks, application of a uniformly distributed load, p_0 , shown in Figure 1c, will displace the bridge deck into the approximate shape of the mode. This method of obtaining an approximating shape results in $v_S(x)$ being consistent with the support condition and intermediate expansion joints in the deck.

2.1 DETERMINING THE PERIOD OF THE ASSUMED MODE SHAPE

The vibration period associated with the assumed mode shape can be determined by using Rayleigh's Method. Rayleigh's Method consists of equating the maximum strain energy with the maximum kinetic energy. The maximum strain energy is the stored internal energy resulting from the application of the load p_0 . The maximum strain energy is equal to the work done on the system in displacing the bridge deck into the displaced shape, $v_S(x)$, which can be expressed mathematically as

$$W_E = \frac{1}{2} \int_0^L p_0 v_S(x) dx = \frac{p_0}{2} \alpha
 \tag{2}$$

where,

$$\alpha = \int_0^L v_S(x) dx
 \tag{3}$$

The kinetic energy, K , is expressed as

$$\begin{aligned}
 K &= \frac{1}{2} \int_0^L m(x) \left[\dot{v}(x, t) \right]^2 dx \\
 &= \frac{1}{2} \int_0^L m(x) \left[\omega \cos(\omega t - \phi) v_S(x) \right]^2 dx \\
 &= \frac{\omega^2}{2g} \cos^2(\omega t - \phi) \int_0^L w(x) \left[v_S(x) \right]^2 dx \quad 4
 \end{aligned}$$

while $w(x)$ is the weight distribution along the deck. Equation 4 will be at its maximum when $\cos^2(\omega t - \phi)$ is equal to one (1), or

$$K_{\max} = \frac{\omega^2}{2g} \int_0^L w(x) \left[v_S(x) \right]^2 dx = \frac{\omega^2}{2g} \gamma \quad 5$$

where,

$$\gamma = \int_0^L w(x) \left[v_S(x) \right]^2 dx \quad 6$$

Equating Equation 2 and Equation 6 and noting that, $T = 2\pi / \omega$, results in:

$$T = 2\pi \sqrt{\frac{\alpha}{P_0 \alpha g}} \quad 7$$

2.2 PSEUDO INERTIAL LOADING

The maximum value of $v(t)$ can be obtained by applying the response spectrum method. The equation of motion for a continuous system approximated by a single generalized coordinate is found by using Hamilton's principle, which states that the first variation of $(K-V)$, where K is the kinetic energy and V is the strain energy, plus the first variation of all non-conservative forces, W_{nc} , is equal to zero (0). Mathematically, calculating the first variation of:

$$I = \int_{t_1}^{t_2} (K-V) dt + \int_{t_1}^{t_2} W_{nc} dt \quad 8$$

will produce the equation of motion. It can be shown [6] that calculating the first variation of Equation 8 will result in

$$m \ddot{v}(t) + c \dot{v}(t) + k v(t) - p_{eff}^*(t) = 0 \quad 9$$

where,

$$m^* = \int_0^L m(x) [v_S(x)]^2 dx \quad 10$$

$$c^* = \int_0^L c(x) [v_S(x)]^2 dx \quad 11$$

$$k^* = \int_0^L E^* I^*(x) \left[\frac{\partial^2 v_S(x)}{\partial x^2} \right]^2 dx \quad 12$$

$$p_{eff}^* = -\ddot{v}_g(x,t) \int_0^L m(x) v_S(x) dx \quad 13$$

$E^* I^*(x)$ is the equivalent bending stiffness of the deck and $\ddot{v}_g(x,t)$ is the horizontal ground acceleration. Dividing Equation 9 by m^* , noting that c^*/m^* is $2\xi\omega$, k^*/m^* is ω^2 , and defining:

$$\beta = \int_0^L w(x)v_S(x)dx \quad 14$$

results in:

$$\ddot{v}(t) + 2\xi \dot{v}(t) + \omega^2 v(t) = -\ddot{v}_g(x,t) \frac{\beta}{\gamma} \quad 15$$

Using the standard response spectrum method with a desired acceleration spectrum, noting that $S_d = S_a/\omega^2$ and given that $C_S = S_a/g$, $v(t)_{\max}$ is calculated by the following equation

$$|v(t)|_{\max} = \frac{\beta C_S g}{\gamma \omega^2} \quad 16$$

Substituting Equation 16 into Equation 1, $v(x,t)$ becomes:

$$v(x,t)_{\max} = \frac{\beta C_S g}{\gamma \omega^2} v_S(x) \quad 17$$

Equation 17 defines the maximum spectral displacements of all points on the bridge deck due to an assumed acceleration spectrum. The pseudo inertial load, \bar{F}_I , which is associated with this displacement and which approximates the inertial effects, is found by noting that $S_a = \omega^2 S_d = \omega^2 v(x,t)_{\max}$:

$$\begin{aligned} \bar{F}_I &= m(x)a \\ &= m(x)S_a \\ &= m(x)\omega^2 S_d \\ &= m(x)\omega^2 v(x,t)_{\max} \end{aligned}$$

$$= \frac{C_S \beta w(x)}{\gamma} v_S(x) \quad 18$$

The inertial load defined by Equation 18 is then applied to the deck as a uniformly transverse distributed load, as shown in Figure 1d, and the resulting static forces become the pseudo seismic forces.

2.3 PROCEDURE

Step 1

Apply a uniformly distributed load, p_0 , transversely to the bridge deck and calculate the displacements of the deck. The displacements will define $v_S(x)$.

Step 2

Using $v_S(x)$, calculate α , γ and β using Equations 3, 6 and 14, respectively.

Step 3

Calculate the period of the approximating vibration shape by using Equation 7.

Step 4

Select an acceleration spectrum with damping ratio, ξ , and compute the dimensionless seismic coefficient, C_S , associated with the period calculated in Step 3. Use C_S to compute the pseudo inertial load by using Equation 18.

Step 5

Apply the pseudo inertial loading transversely to the bridge deck and compute the displacements and forces for design.

2.4 SINGLE MODE-RESPONSE SPECTRUM COMPARISONS

The applicability of the SMSM is demonstrated by analyzing a bridge with two different sets of constraints at the abutments for seismic forces in the transverse direction. The results obtained by using the SMSM are compared to results obtained by using the MMSM. Response spectrum results are presented both for a single transverse mode and for more than one transverse mode. The number of transverse modes included in the analysis of each bridge is noted.

The computer program SEISAB was used to perform both the SMSM and the MMSM. The program fits cubic splines through the displaced nodes on the superstructure in order to solve the various integrals in the SMSM. In addition, the equivalent nodal forces resulting from the application of the pseudo inertial loading are obtained through use of the cubic splines. See Appendix A for details of how to use cubic splines in the SMSM.

2.5.1 Test Case 1 - South Turlock Overcrossing

The South Turlock Overcrossing, a two-span, single-column bent bridge, is shown in Figure 2. Both abutments allow longitudinal superstructure movement but not transverse movement. The SMSM coefficients, obtained by evaluating Equations 3, 6 and 14, are shown with other pertinent data in Table 1.

2.5.2 Test Case 2 - South Turlock Overcrossing with Abutment Foundation Springs

The bridge analyzed in Test Case 1 is again analyzed, but this test takes into consideration the soil flexibility at the abutments in the transverse direction. Spring coefficients of 1.0×10^4 kips/ft are applied at each abutment. Table 2 shows the comparisons between the SMSM and the MMSM.

3.0 A TOOL FOR IMPLEMENTING SEISMIC ANALYSIS PROCEDURES

The SMSM will yield good approximations for the seismic design displacements and forces as long as the bridge derives most of its dynamic response from the assumed mode shape. As noted, this requirement will be satisfied for many bridges. Bridges that receive their dynamic response from several modes of vibration must be analyzed by the MMSM or some other method that retains more than one mode. The MMSM is the most popular method used today because of practical and economic considerations. Unfortunately, most computer programs that implement the MMSM are cumbersome to use because of their input requirements.

The need for a computer program with MMSM capabilities written specifically for bridge designers resulted in the development of SEISAB. A complete, lumped parameter structural model is generated with only a few free-form input commands. The use of SEISAB will be illustrated by performing a response spectrum analysis on a six-span curved bridge. An ATC-6 acceleration spectrum will be used for the dynamic loading.

3.1 DESCRIPTION OF THE BRIDGE

A sketch of the reinforced concrete box girder bridge is shown in Figure 3a. The prismatic superstructure is continuous with the exception of Span 3 which contains an intermediate hinge. The hinge is outfitted with earthquake restrainer units to provide longitudinal restraint. Shear keys at the hinge provide transverse restraint between the two superstructure sections.

The seat-type abutments are radially oriented with transverse abutment-to-superstructure shear connections and longitudinal restraint provided by restrainer units. The radially-oriented single column bents are founded on pile groups.

3.2 MODELING AND PROGRAM INPUT DETAILS

To perform the response spectrum analysis, the physical model of the bridge requires a mathematical representation. As is conventionally done, the SEISAB program models bridges by lumping properties at discrete locations along the superstructure and columns, as shown in Figure 3b. The correct ordering for the input data blocks in SEISAB is shown in Figure 4.

3.2.1 Initiating a Response Spectrum Analysis

The user directs SEISAB to perform a response spectrum analysis by specifying a single command in the SEISAB Data Block. In addition, the number of intermediate node points to be used on the superstructure and columns (i.e., the degree of accuracy of the analysis) may be specified. Because of the curved geometry, coupling effects will be experienced and the default number of three (3) nodes on the superstructure will be increased to four (4).

The input in the SEISAB Data Block is shown below:

```
SEISAB 'RESPONSE SPECTRUM ANALYSIS, 6-SPAN CURVED BRIDGE'
RESPONSE SPECTRUM
SUPERSTRUCTURE JOINTS 4
```

3.2.2 Describing the Horizontal Geometry

To develop the most accurate model, the location of the bridge centerline must be correct. This information is supplied to SEISAB in the ALIGNMENT Data Block. Alignment information may be taken directly from bridge plans and used as input to SEISAB. The alignment of the bridge is shown in Figure 5 and the input for the ALIGNMENT Data Block is shown below:

```
ALIGNMENT
C              INITIAL REFERENCE POINT INFORMATION
STATION       100 + 0.0
COORDINATES   N 500.0 E 250.0
BEARING       N 0 E
C              CURVE INFORMATION
BC            10000.0
RADIUS        R 600.0
BEARING       N 66 16 20 E
```

3.2.3 Superstructure

The stiffness and mass characteristics of the superstructure are obtained from its cross-sectional properties, which are included in Figure 3a. The spans are prismatic, so only the properties of Span 1 are input. The torsional moment of inertia is calculated by using expressions based on thin-walled enclosed regions.

The input to SEISAB for the superstructure is shown below:

```
SPANS
LENGTHS      100.0, 143.0, 3*117.0, 100.0
AREAS        86.0          $ PROPERTY GENERATION WILL BE
I11          862.0        $ USED FOR SPANS 2-6. ALSO,
I22          13000.0     $ PROGRAM DEFAULTS WILL BE USED
I33          360.0       $ FOR THE MODULUS AND DENSITY.
```

3.2.4 Defining the Structural Members

One time-saving feature of SEISAB is that any structural member that can appear at more than one location in the bridge is described once in the DESCRIBE Data Block and then placed at the appropriate locations. The structural members in the six-span bridge that need to be defined are the bent columns and the longitudinal restrainers. Because the five columns are identical in cross-section, only one need be defined.

The input in the DESCRIBE Data Block is shown below:

```

DESCRIBE
C
COLUMN 'TYPE 1' "TYPICAL PRISMATIC COLUMN"
SEGMENTS 1
AREA 33.0
I11 146.0
I22 73.0 $ PROGRAM DEFAULTS WILL BE USED FOR THE
I33 143.0 $ MODULUS AND DENSITY
C
RESTRAINER 'TYPE 1' "GALV. H.S. ROD"
LENGTH 5.0
AREA 3.068E-03
E 2.010E+06
C
RESTRAINER 'TYPE 2' "GALV. STEEL CABLE"
LENGTH 20.0 $ PROGRAM DEFAULTS WILL BE USED FOR THE
AREA 0.01 $ MODULUS

```

3.2.5 Abutment Information

The modeling of the two abutments is accomplished through the ABUTMENT Data Block. Both the abutment and the longitudinal restrainers are shown in Figure 6a. The connectivity between the superstructure and the abutment will be assumed to offer translation constraint in the transverse and vertical directions and rotational constraint about a horizontal axis perpendicular to the centerline of the abutment. The shear keys will provide the translational constraint and the width of the superstructure will provide the torsional constraint.

The input in the ABUTMENT Data Block is shown below:

```

ABUTMENT STATION 100 + 0.0
ELEVATION 152.5 155.5
WIDTH NORMAL 35.0 $ GENERATION IS USED FOR ABUT 7
RESTRAINER NORMAL LAYOUT 'TYPE 1' 8.0, 8.0 'TYPE 1' AT 1,7

```

3.2.6 Bent Information

The number, type and spacing of bent columns are specified in the BENT Data Block. In addition, the user may also input the type of connectivity to the superstructure, the column end conditions and the locations of restrainers.

The bridge under consideration has only single-column bents with the columns oriented radially to the superstructure. The column end conditions are fixed at both ends.

Many program defaults in the BENT Data Block have been utilized for this bridge. The required input is shown below:

```

BENT
ELEVATION TOP  153.0, 153.5, 154.0, 154.5, 155.0
HEIGHT        25.0  $ HEIGHTS GENERATED FOR OTHER BENTS
COLUMN 'TYPE 1' AT 2 3 4 5 6

```

3.2.7 Foundation Information

Modeling the connection of the columns and abutments to the foundation may be accomplished either by assuming complete fixity or by allowing for a flexible support. Complete fixity is a program default and allowing movement of the column bottoms and/or abutments is done by modelling soil as uncoupled springs. The soil springs are input in the FOUNDATION Data Block.

The direction of the springs, shown in Figure 6b, is normal and tangential to the centerline of the bent. The specific values for the spring constants are also shown in Figure 6b.

The input in the FOUNDATION Data Block is shown below:

```

FOUNDATION
AT BENT  2 3 4 5 6
KF1  4.084E+08
KF2  4.084E+08
KM1  2.704E+10
KM2  1.292E+10
KM3  2.220E+10

```

3.2.8 Span Hinge Information

Discontinuities in the superstructure between bents (expansion joints) are input in the HINGE Data Block. The mathematical modeling of the expansion joint or hinge is done by using a special zero-length element that has the unique property of being able to release the moment along the centerline of the hinge. Translational connectivity is specified for a horizontal axis perpendicular to the centerline of the superstructure at the location of the hinge. In addition, longitudinal restrainers may be placed across the hinge.

The expansion joint in the bridge under consideration is shown in Figure 6c. The joint has transverse shear keys; thus the transverse force condition is input as fixed. Longitudinally, the only restraint offered is that of the restrainers. The width of the bridge is sufficient for transmitting torsional moment across the hinge.

The input in the HINGE Data Block is shown below:

HINGE
 AT 3 102.00 \$ HINGE IS IN SPAN 3; 102 FT FROM BEGIN.
 WIDTH NORMAL 33.5
 TRANSVERSE FIXED
 REST NORMAL LAYOUT 'TYPE 2' 4.5,4.0,4.0,4.5 'TYPE 2 AT 1

3.2.9 Earthquake Information

The last data block, the LOADINGS Data Block, specifies information about the loads applied to the bridge. The required loading for a response spectrum analysis is an acceleration spectrum. The program has the ATC-6 spectra stored away; therefore, because the default does not apply here, the only input needed to define the acceleration spectrum is the soil type. Soil Type 3 (30 ft. or more of soft-to-medium stiff clays) is present at the bridge site.

Two loading cases are desired: one along an axis connecting the two abutments (in a chord or longitudinal direction), the other transverse to that axis. Because these two loading cases are required by ATC-6, they are included in SEISAB as a program default and no input is needed.

The input to the LOADINGS Data Block is shown below:

```
LOADINGS
  RESPONSE SPECTRUM
  SOIL TYPE III
```

3.2.10 Termination of the Input File

The input file is completed by specifying the word 'finish' as the last piece of input:

```
FINISH
```

3.2.11 Summary

The complete input data file that directs SEISAB to perform a response spectrum analysis using the ATC-6 acceleration spectra on a six-span curved bridge is shown below, in Figure 7.

4.0 CURRENT RESEARCH ON SEISMIC ANALYSIS OF BRIDGES

Two of the current projects funded by the Federal Highway Administration that were initiated to improve seismic analyses of bridges include: (1) Evaluation of Improvement of Energy Absorption Characteristics of Bridges Under Seismic Conditions, and (2) Improved Mathematical Idealizations to Include Foundation Effects on Seismic Response of Highway Bridges. As part of the first project, Imbsen and Penzien extended the computer program NEABS (Nonlinear Earthquake Analysis of Bridge Systems) [8,9,10]

to include the ability to model energy-absorbing devices at intermediate expansion joints and strain-hardening effects on yielding, reinforced concrete columns. As part of the second project, Liu and Penzien continued to enhance NEABS by including the specification of a compliance function at the boundaries that includes the effects of radiation damping and the stiffness of the foundation. As a result, more detailed correlation studies can be conducted by using the NEABS capability to accurately model the dynamic characteristics of a bridge subjected to seismic excitations large enough to cause yielding of the component members. This capability is needed to assess newly developed strategies for seismic resistance.

5.0 CONCLUSIONS

Previous efforts to implement seismic design of bridges by Imbsen et. al., [7] indicated that there was a need to develop simplified methodologies and computer programs to assist the designer in this task. An initial pilot workshop was given to a group of experienced bridge engineers from the California Department of Transportation on SEISAB. The overwhelming acceptance of the proposed methodology and the computer program SEISAB by these seasoned engineers indicates that the developed methodology will assist in implementing the newly developed ATC-6 seismic design guidelines for bridges.

Development of these methodologies would not be possible without the continued research at the Universities to develop new analytical procedures and verify the developed procedures by physical testing.

6.0 REFERENCES

1. Standard Specifications for Highway Bridges, Twelfth Edition, 1977, American Association of State Highway and Transportation Officials.
2. Applied Technology Council, "Seismic Design Guidelines for Highway Bridges," Report No. ATC-6, Berkeley, California, October, 1981.
3. Penzien, J. and Imbsen, R., "Seismic Analysis of Bridges by a Single Mode Spectral Approach," Proceedings Advances in Earthquake Engineering, Continuing Education in Engineering, University of California, Berkeley, June, 1980.
4. Imbsen, R. A., et al., "SEISAB-I User Manual," Engineering Computer Corporation, October, 1982.

5. Imbsen, R. A., Kaliakin, V. N., and Lea, J., "SEISAB-I Example Problems," Engineering Computer Corporation, October, 1982.
6. Clough, R. W., and Penzien, J., Dynamics of Structures, McGraw-Hill, 1975.
7. Imbsen, R. A., Nutt, R. V., and Gates, J., "Seismic Design of Highway Bridges-Workshop Manual," Report No. FHWA-IP-81-2, U.S. Department of Transportation, Federal Highway Administration, January, 1982.
8. Tseng, W. S., and Penzien, J., "Analytical Investigations of the Seismic Response of Long Multiple Span Highway Bridges," Report No. EERC 73-12, Earthquake Engineering Research Center, University of California, Berkeley, June, 1973.
9. Penzien, J., Imbsen, R. A., and Liu, W. D., "NEABS User Instructions," Earthquake Engineering Research Center, University of California, Berkeley, May, 1982.
10. Kawashima, K., and Penzien, J., "Correlative Investigations on Theoretical and Experimental Dynamic Behavior of a Nodal Bridge Structures," Report No. EERC 76-26, Earthquake Engineering Research Center, University of California, Berkeley, July, 1976.

Appendix A

SINGLE MODE SPECTRAL METHOD USING CUBIC SPLINES

The Single Mode Spectral Method (SMSM) requires the evaluation of three (3) integrals and the computation of equivalent nodal forces resulting from an application of a pseudo inertial loading. The integrands of the integrals contain an expression for the displaced shape of the superstructure caused by the application of a uniformly distributed transverse and longitudinal load on the superstructure. The expression for the displaced shape may be obtained by several methods, but one very convenient method is to fit a cubic spline between each superstructure node point. The result of using cubic splines is that the integrals may be obtained in a closed-form solution without using numerical integration. In addition, the splines provide a smooth representation of the displaced shape.

The procedure for fitting cubic splines through the displaced superstructure node points begins by obtaining the normal displacement at each node point. The normal displacement at Node n in Figure A.1a is given by:

$$v_S(x'=x'_n) = -x_n \cos \theta_n + z_n \sin \theta_n \quad \text{A.1}$$

where X_n and Z_n are the global displacements of Node n and ϕ_n is the angle the normal at Node n makes with the negative Z -axis. Equation A.1 is applied to the $N+1$ node points that define the superstructure.

The general form of a cubic spline is given by:

$$S_n(x') = A_n + B_n h_n + C_n h_n^2 + D_n h_n^3 \quad \text{A.2}$$

where,

$$h_n = (x' - x'_n)$$

and x' is the arclength coordinate of the beginning of the n th cubic spline. The coefficients, A_n through D_n , are calculated by solving a system of equations obtained from cubic spline theory. Spline n is defined between x'_n and x'_{n+1} . Thus the displaced superstructure is divided into N cubic splines.

The SMSM coefficients may be evaluated after the spline coefficients, A_n through D_n , have been determined. The SMSM coefficient, α , is calculated by:

$$\begin{aligned} \alpha &= \int_0^L v_S(x') dx' \\ &= \sum_{n=1}^N \int_{x'_n}^{x'_{n+1}} \left[A_n + B_n h_n + C_n h_n^2 + D_n h_n^3 \right] dx' \\ &= \sum_{n=1}^N \left[A_n (x'_{n+1} - x'_n) + \frac{B_n}{2} (x'_{n+1} - x'_n)^2 + \frac{C_n}{3} (x'_{n+1} - x'_n)^3 + \frac{D_n}{4} (x'_{n+1} - x'_n)^4 \right] \text{A.3} \end{aligned}$$

The SMSM coefficient, β , is calculated by:

$$\begin{aligned} \beta &= \int_0^L w(x') v_S(x') dx' \\ &= \sum_{n=1}^N \sum_{m=1}^M w_m \int_{x'_m}^{x'_{m+1}} \left[A_n + B_n (x' - x'_n) + C_n (x' - x'_n)^2 + D_n (x' - x'_n)^3 \right] dx' \\ &= \sum_{n=1}^N \sum_{m=1}^M w_m \left\{ A_n (x'_{m+1} - x'_m) + \frac{B_n}{2} \left[(x'_{m+1} - x'_n)^2 - (x'_m - x'_n)^2 \right] \right. \\ &\quad \left. + \frac{C_n}{3} \left[(x'_{m+1} - x'_n)^3 - (x'_m - x'_n)^3 \right] + \frac{D_n}{4} \left[(x'_{m+1} - x'_n)^4 - (x'_m - x'_n)^4 \right] \right\} \text{A.4} \end{aligned}$$

where, $w(x')$ is the weight per unit length along the superstructure between x'_n and x'_{n+1} . Since $w(x')$ may vary along the superstructure, the integral must be divided into M parts where M is the number of different values of $w(x')$ between the two end points defining the spline.

The SMSM coefficient, γ , is calculated with an expression similar to Equation A.3, except that the splines are fitted to the square of the nodal displacements. The period of the assumed vibration shape is calculated by using Equation 7:

$$T = 2\pi \sqrt{\frac{\alpha}{P_0 g}} \quad \text{A.5}$$

The equivalent nodal loads resulting from applying the pseudo inertial load, \bar{F}_I , defined by Equation 18, may be calculated by considering the potential energy, Γ , of the inertial load:

$$\begin{aligned} \Gamma &= \int_{x'_n}^{x'_{n+1}} \bar{F}_I^n(x') \hat{w}(x') dx' \\ &= \frac{\beta C_s L}{\gamma} \sum_{m=1}^M w_m \int_{s_m}^{s_{m+1}} \left[A_n + B_n L s + C_n L^2 s^2 + D_n L^3 s^3 \right] \sum_{k=1}^4 M_k^*(s) \hat{w}_k ds \quad \text{A.6} \end{aligned}$$

$$s_m = \frac{x'_m - x'_n}{x'_{n+1} - x'_n} \quad s_{m+1} = \frac{x'_{m+1} - x'_n}{x'_{n+1} - x'_n} \quad L = (x'_{n+1} - x'_n)$$

where, $\hat{w}(x')$ is the transverse displacement approximation for a superstructure element and is given by (in a local variable, s):

$$\hat{w}(s) = \sum_{k=1}^4 M_k^*(s) \hat{w}_k \quad \text{A.7}$$

$$M_1^* = (1-3s^2+2s)$$

$$M_2^* = -(s^3-2s^2+s)*(x'_{n+1}-x'_n)$$

$$M_3^* = (3s^2-2s^3)$$

$$M_4^* = -(s^3-s^2)*(x'_{n+1}-x'_n)$$

$$0 \leq s \leq 1$$

The local variable s , is related to the variable x' by:

$$x' = (1-s)x'_n + sx'_{n+1} \quad \text{A.8}$$

and

$$dx' = (x'_{n+1}-x'_n)ds = Lds \quad \text{A.9}$$

See Figure A.1b for the definitions of the local displacements, \hat{w} . The equivalent nodal loads resulting from applying \bar{F}_I over a given superstructure element are defined in Figure A.2 and are obtained by calculating the partial derivative of Equation A.6 with respect to the node point unknowns, \hat{w} . Thus,

$$\frac{\partial \Gamma}{\partial \hat{w}_k}, \quad k = 1, 4$$

A.10

The resulting expressions for F_1 through F_4 are

$$\begin{aligned}
 F_1 = \frac{\partial \Gamma}{\partial \hat{w}_1} &= \frac{\beta C_S L}{\gamma} \sum_{m=1}^M w_m \left[A_n (s_{m+1} - s_m) + \frac{B_n L}{2} (s_{m+1}^2 - s_m^2) \right. \\
 &+ \frac{K_1}{3} (s_{m+1}^3 - s_m^3) + \frac{K_2}{4} (s_{m+1}^4 - s_m^4) \\
 &+ \frac{K_3}{5} (s_{m+1}^5 - s_m^5) + \frac{K_4}{6} (s_{m+1}^6 - s_m^6) \\
 &\left. + \frac{K_5}{7} (s_{m+1}^7 - s_m^7) \right]
 \end{aligned}$$

A.11

$$\begin{aligned}
 F_2 = \frac{\partial \Gamma}{\partial \hat{w}_2} &= \frac{\beta C_S L^2}{\gamma} \sum_{m=1}^M w_m \left[-\frac{A_n}{2} (s_{m+1}^2 - s_m^2) + \frac{K_6}{3} (s_{m+1}^3 - s_m^3) \right. \\
 &+ \frac{K_7}{4} (s_{m+1}^4 - s_m^4) + \frac{K_8}{5} (s_{m+1}^5 - s_m^5) + \frac{K_9}{6} (s_{m+1}^6 - s_m^6) \\
 &\left. - \frac{D_n L^3}{7} (s_{m+1}^7 - s_m^7) \right]
 \end{aligned}$$

A.12

$$\begin{aligned}
F_3 = \frac{\partial \Gamma}{\partial \hat{w}_3} &= \frac{\beta C_S L}{\gamma} \sum_{m=1}^M \left[A_n (s_{m+1}^3 - s_m^3) + \frac{K_{10}}{4} (s_{m+1}^4 - s_m^4) \right. \\
&\quad \left. + \frac{K_{11}}{5} (s_{m+1}^5 - s_m^5) + \frac{K_{12}}{6} (s_{m+1}^6 - s_m^6) - \frac{2D_n L^3}{7} (s_{m+1}^7 - s_m^7) \right] \quad A.13
\end{aligned}$$

$$\begin{aligned}
F_4 = \frac{\partial \Gamma}{\partial \hat{w}_4} &= \frac{\beta C_S L^2}{\gamma} \sum_{m=1}^M w_m \left[\frac{A_n}{3} (s_{m+1}^3 - s_m^3) + \frac{K_{13}}{4} (s_{m+1}^4 - s_m^4) \right. \\
&\quad \left. + \frac{K_{14}}{5} (s_{m+1}^5 - s_m^5) + \frac{K_{15}}{6} (s_{m+1}^6 - s_m^6) - \frac{D_n L^3}{7} (s_{m+1}^7 - s_m^7) \right] \quad A.14
\end{aligned}$$

where,

$$K_1 = C_n L^2 - 3A_n$$

$$K_6 = 2A_n - B_n L$$

$$K_2 = D_n L^3 - 3B_n L + 2A_n$$

$$K_7 = 2B_n L - A_n - C_n L^2$$

$$K_3 = 2B_n L - 3C_n L^2$$

$$K_8 = 2C_n L^2 - B_n L - D_n L^3$$

$$K_4 = 2C_n L^2 - 3D_n L^3$$

$$K_9 = 2D_n L^3 - C_n L^2$$

$$K_5 = 2D_n L^3$$

$$K_{10} = 3B_n L - 2A_n$$

$$K_{11} = 3C_n L^2 - 2B_n L$$

$$K_{14} = C_n L^2 - B_n L$$

$$K_{12} = 3D_n L^3 - 2C_n L^2$$

$$K_{15} = D_n L^3 - C_n L^2$$

$$K_{13} = B_n L - A_n$$

The equivalent nodal loads defined in Equations A.11 - A.14 are applied to each superstructure element. The resulting displacements and forces caused by these equivalent nodal loads are the pseudo seismic quantities needed for design.

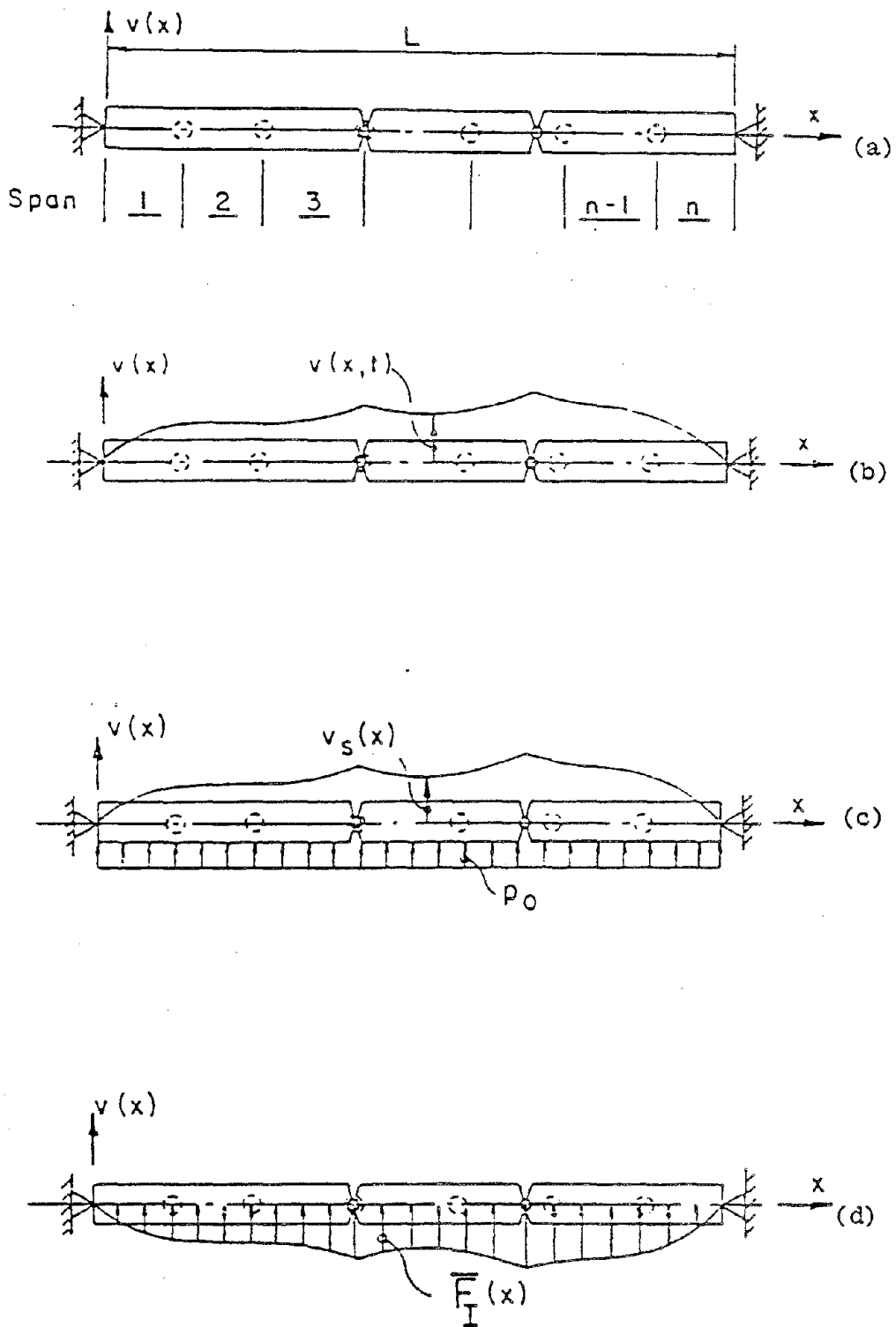
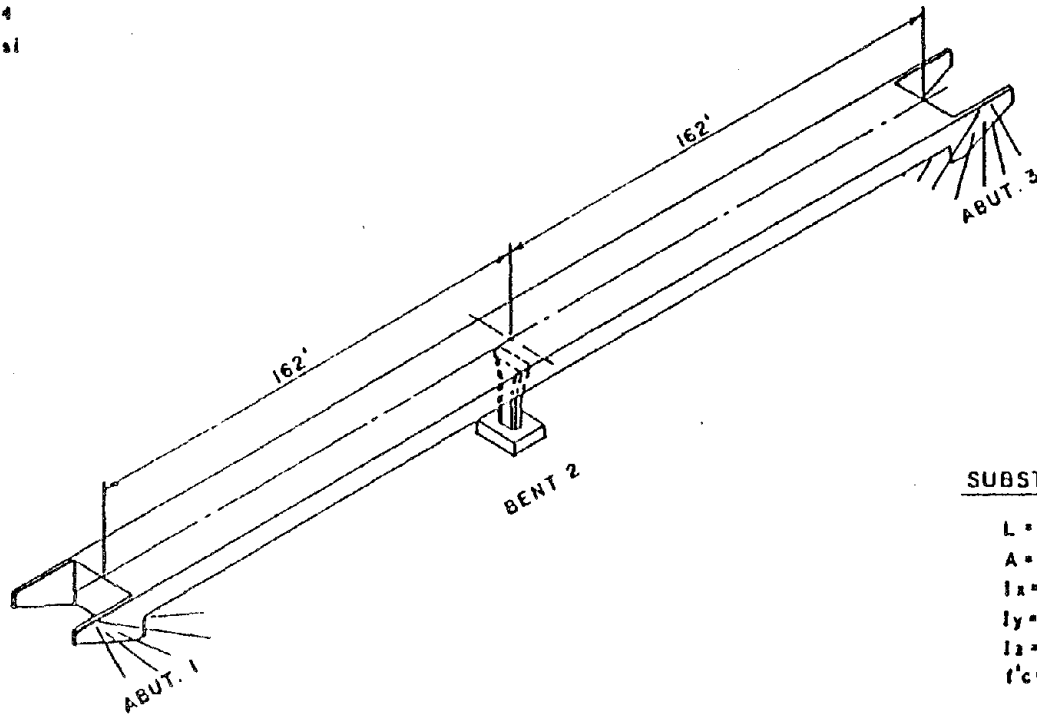


FIGURE 1 - a) Typical Bridge Configuration, b) Displacement Function, c) Mode Shape Due to Uniform Static Loading, d) Pseudo Inertial Loading

SUPERSTRUCTURE

L = 324 ft.
A_x = 42.3 ft.²
I_x = 546 ft.⁴
I_y = 1909 ft.⁴
I_z = 260 ft.⁴
f'c = 3250 psi



SUBSTRUCTURE

L = 25 ft.
A = 20 ft.²
I_x = 42 ft.⁴
I_y = 42 ft.⁴
I_z = 27 ft.⁴
f'c = 3250 psi

FIGURE 2 - SOUTH TURLOCK OVERCROSSING

Location	Displs. Due to p (Y(x))	Pseudo Inertial Loading - F	Forces Due to F	RESPONSE SPECTRUM		NORMALIZED TRANSVERSE DISPLACEMENTS		
				1st Trans. Mode	3 Trans. Modes - RMS	Uniform Load - p	Inertial Load - F	1st Trans. Mode Shape
Abutment 1	0.0 ft	0.0 kip/ft	278 kips	287 kips	291 kips	0.0	0.0	0.0
Span 1-1/4	0.0122	1.562				0.524	0.499	0.488
Span 1-1/2	0.0203	5.968				0.873	0.846	0.839
Span 1-3/4	0.0233	6.841				1.000	0.992	0.989
Bent 2	0.0232	6.811	1045	1134	1134	0.968	1.000	1.000
Span 2-1/4	0.0233	6.841				1.000	0.922	0.989
Span 2-1/2	0.0203	5.968				0.873	0.846	0.839
Span 2-3/4	0.0122	1.582				0.524	0.494	0.488
Abutment 3	0.0	0.0	278	287	291	0.0	0.0	0.0

$$\alpha = 5.460 \text{ ft}^2$$

$$\beta = 34.644 \text{ kip}\cdot\text{ft}^2$$

$$\gamma = 0.749 \text{ kip}\cdot\text{ft}^3$$

$$T_{\text{SMSM}} = 0.41 \text{ sec}$$

$$(T_{\text{MMSM}} = 0.4021 \text{ sec})$$

TABLE 1

Location	Displs. Due to p (Y(x))	Pseudo Inertial Loading - F	Forces Due to F	RESPONSE SPECTRUM		NORMALIZED TRANSVERSE DISPLACEMENTS		
				1st Trans. Mode	3 Trans. Modes - RMS	Uniform Load - p	Inertial Load - F	1st Trans. Mode Shape
Abutment 1	0.00707 ft	2.066 kip/ft	355 kips	381 kips	349 kips	0.286	0.221	0.281
Span 1-1/4	0.01701	4.971				0.688	0.636	0.616
Span 1-1/2	0.02316	6.768				0.937	0.911	0.900
Span 1-3/4	0.02472	7.224				1.000	1.000	1.000
Bent 2	0.02015	7.857	1136	1255	1254	0.977	0.968	0.993
Span 2-1/4	0.02472	7.224				1.000	1.000	1.000
Span 2-1/2	0.02316	6.768				0.937	0.911	0.900
Span 2-3/4	0.01701	4.971				0.688	0.636	0.616
Abutment 3	0.00707	2.066	355	381	349	0.286	0.221	0.281

$$\alpha = 6.600 \text{ ft}^2$$

$$\beta = 41.877 \text{ kip}\cdot\text{ft}^2$$

$$\gamma = 0.9093 \text{ kip}\cdot\text{ft}^3$$

$$T_{\text{SMSM}} = 0.411 \text{ sec}$$

$$(T_{\text{MMSM}} = 0.4117 \text{ sec})$$

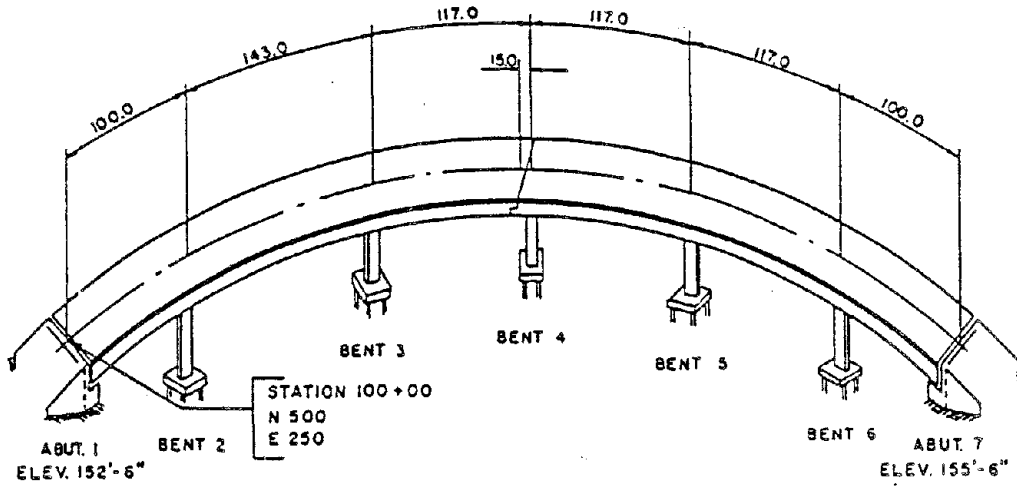
TABLE 2

SUPERSTRUCTURE PROPERTIES

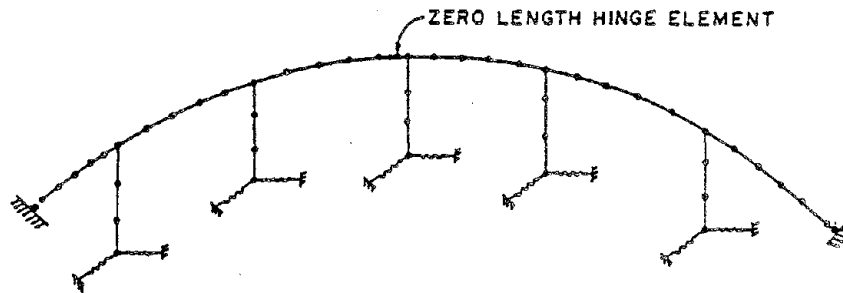
L = 694.0 ft
 A = 86.0 ft²
 I₁₋₁ = 862.0 ft⁴
 I₂₋₂ = 13000.0 ft⁴
 I₃₋₃ = 360.0 ft⁴
 R = 600 ft

SUBSTRUCTURE PROPERTIES

L = 25.0 ft
 A = 33.0 ft²
 I₁₋₁ = 146.0 ft⁴
 I₂₋₂ = 73.0 ft⁴
 I₃₋₃ = 143.0 ft⁴



(a)



(b)

FIGURE 3 - a) Physical Model, and b) Mathematical Model

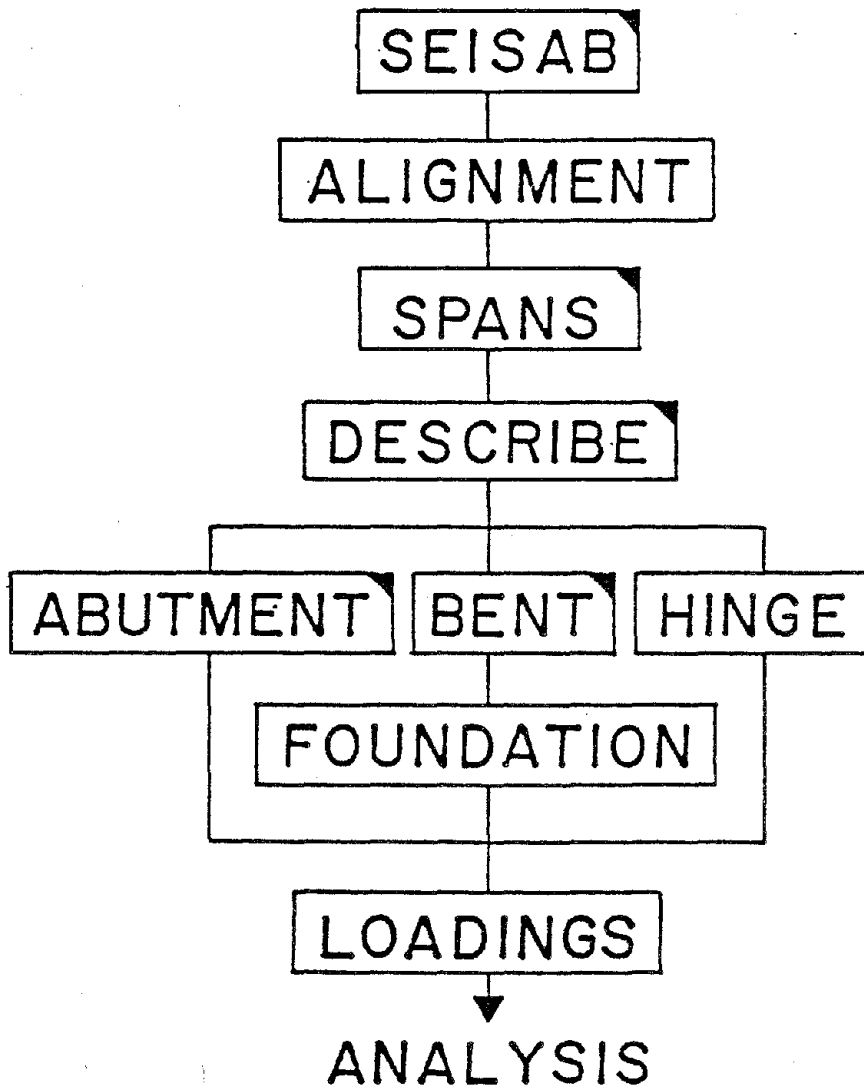


FIGURE 4 - Correct Ordering of Input Data Blocks in SEISAB

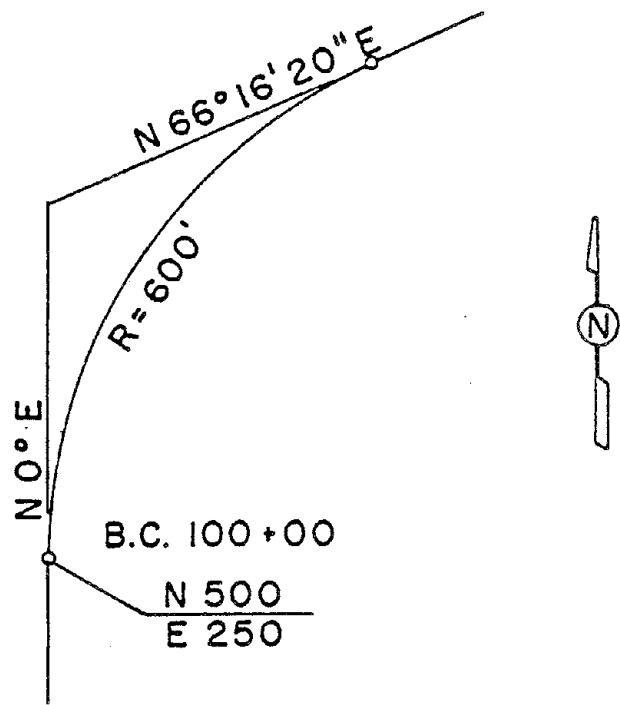
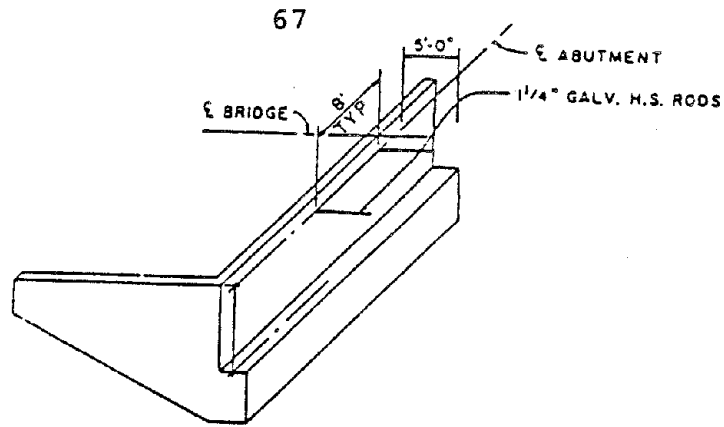
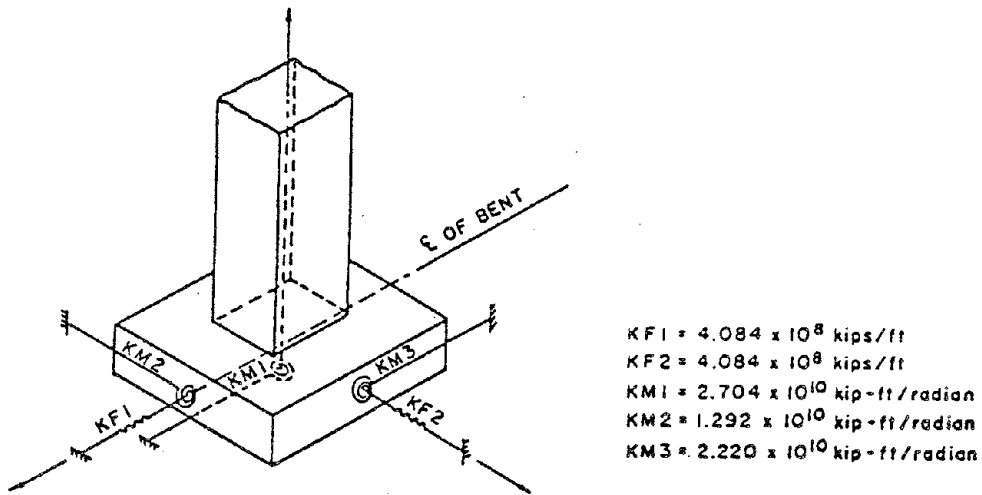


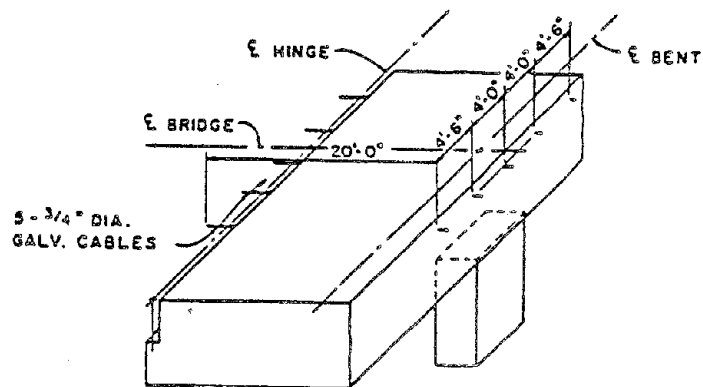
FIGURE 5 - Horizontal Alignment



(a)



(b)



(c)

FIGURE 6 - a) Abutment Details, b) Bent Foundation Spring Details, and c) Expansion Joint Details

```

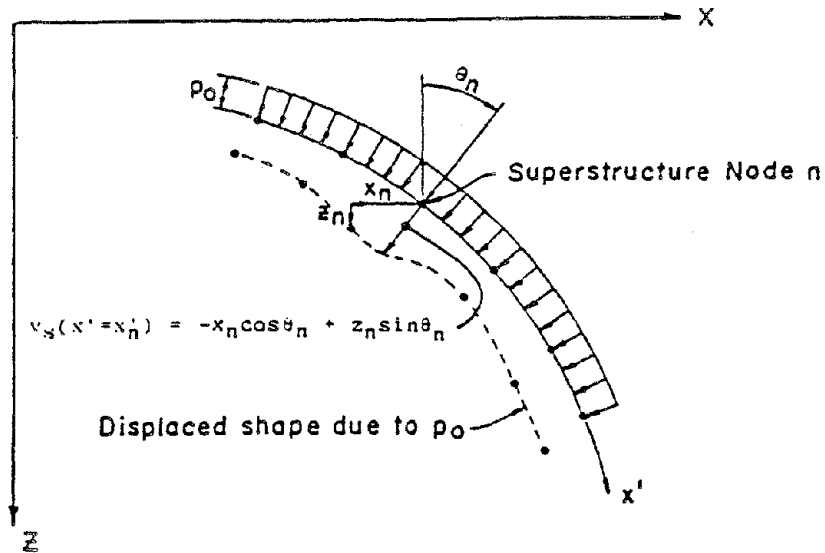
C
C ----- SEISAB DATA BLOCK -----
C
SEISAB 'RESPONSE SPECTRUM ANALYSIS, 4-SPAN BRIDGE'
RESPONSE SPECTRUM
SUPERSTRUCTURE JOINTS 4
C
C ----- ALIGNMENT DATA BLOCK -----
C
ALIGNMENT
C
INITIAL REFERENCE POINT INFORMATION
STATION      100 + 0.0
COORDINATES  N 500.0 E 250.0
BEARING      N 0 E
C
CURVE INFORMATION
BC          10000.0
RADIUS      R 400.0
BEARING     N 46 16 20 E
C
C ----- SPAN DATA BLOCK -----
C
SPANS
LENGTHS     100.0, 143.0, 3*117.0, 100.0
AREAS       86.0           $ PROPERTY GENERATION WILL BE
I11         862.0           $ USED FOR SPANS 2-6. ALSO,
I22         13000.0        $ PROGRAM DEFAULTS WILL BE USED
I33         360.0           $ FOR THE MODULUS AND DENSITY.
C
C ----- DESCRIBE DATA BLOCK -----
C
DESCRIBE
C
COLUMN 'TYPE 1' 'TYPICAL PRISMATIC COLUMN'
SEGMENTS 1
AREA      33.0
I11      146.0
I22      73.0   $ PROGRAM DEFAULTS WILL BE USED FOR THE
I33      143.0   $ MODULUS AND DENSITY
C
RESTRAINER 'TYPE 1' 'GALV. H.S. ROD'
LENGTH     5.0
AREA       3.068E-03
E          2.010E+06
C
RESTRAINER 'TYPE 2' 'GALV. STEEL CABLE'
LENGTH     20.0   $ PROGRAM DEFAULTS WILL BE USED FOR THE
AREA       0.01   $ MODULUS
C
C ----- ABUTMENT DATA BLOCK -----
C
ABUTMENT STATION 100 + 0.0
ELEVATION        152.5 155.5
WIDTH NORMAL     35.0   $ GENERATION IS USED FOR ABUT 7
RESTRAINER NORMAL LAYOUT 'TYPE 1' 8.0, 8.0 'TYPE 1' AT 1,7
C
C ----- BENT DATA BLOCK -----
C
BENT
ELEVATION TOP    153.0, 153.5, 154.0, 154.5, 155.0
HEIGHT           25.0   $ HEIGHTS GENERATED FOR OTHER BENTS
COLUMN 'TYPE 1' AT 2 3 4 5 6
C
C ----- FOUNDATION DATA BLOCK -----
C
FOUNDATION
AT BENT 2 3 4 5 6
KF1 4.084E+08
KF2 4.084E+08
KM1 2.704E+10
KM2 1.292E+10
KM3 2.220E+10
C
C ----- HINGE DATA BLOCK -----
C
HINGE
AT 3 102.00   $ HINGE IS IN SPAN 3; 102 FT FROM BEGIN.
WIDTH NORMAL 33.5
TRANSVERSE FIXED
REST NORMAL LAYOUT 'TYPE 2' 4.5,4.0,4.0,4.5 'TYPE 2 AT 1
C
C ----- LOADINGS DATA BLOCK -----
C
LOADINGS
RESPONSE SPECTRUM
SOIL TYPE III
C
FINISH

```

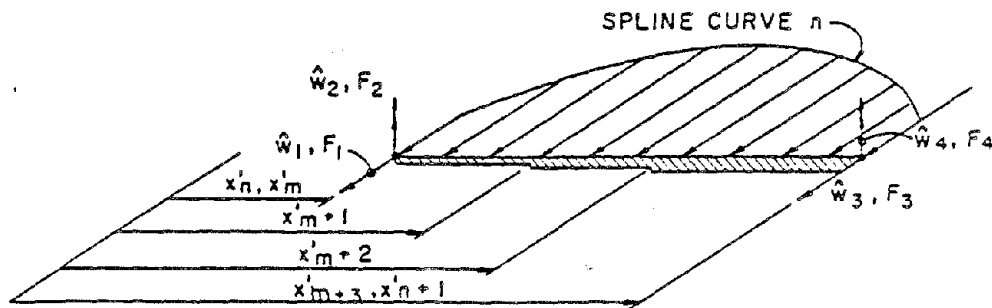
Reproduced from
best available copy.



FIGURE 7 - Complete Input for the Example Problem



(a)



(b)

FIGURE A.1 - a) Obtaining Normal Displacements of Superstructure Nodes, and b) Definitions of Local Displacement Approximations and Integration Limits for a Non-prismatic Superstructure Element

RESPONSE OF CABLE STAYED BRIDGES
TO
STATIC AND DYNAMIC LOADS

John F. Fleming
Department of Civil Engineering
University of Pittsburgh
Pittsburgh, Pennsylvania 15261

ABSTRACT

The static and dynamic response of cable stayed bridges is discussed. Several sources of nonlinear behavior are considered. Analyses of a number of different bridge geometries has shown that a cable stayed bridge can be analyzed as a linear system under the action of static and dynamic live loads. Nonlinear behavior should be considered, however, in computing the stiffness of the structure in the dead load deformed position.

INTRODUCTION

In a cable stayed bridge the roadway is supported by inclined cables which are attached to tall towers. One of the main differences encountered in their analysis and design, compared to more conventional structures, such as continuous girder bridges or rectangular framed buildings, is the possibility of nonlinear behavior under static and dynamic design loads. Most design engineers lack experience in dealing with nonlinear systems and therefore might be hesitant to undertake the task of designing a structure of this type. The purpose of this paper is to discuss the response of cable stayed bridges to static and dynamic loading to establish techniques which are applicable for their analysis.

NONLINEAR STATIC ANALYSIS

The displacements for a linear structural system can be easily computed by solving the set of linear simultaneous stiffness equations

$$[K]\{D\} = \{W\} \quad (1)$$

in which $[K]$ is a matrix containing the stiffness influence coefficients for the structure, $\{D\}$ are the joint displacements and $\{W\}$ are the applied joint loads. The terms in the matrix $[K]$ can be computed by summing the stiffnesses of the individual members at each joint in the structure. The terms in $[K]$ are constants which do not change as the structure deforms.

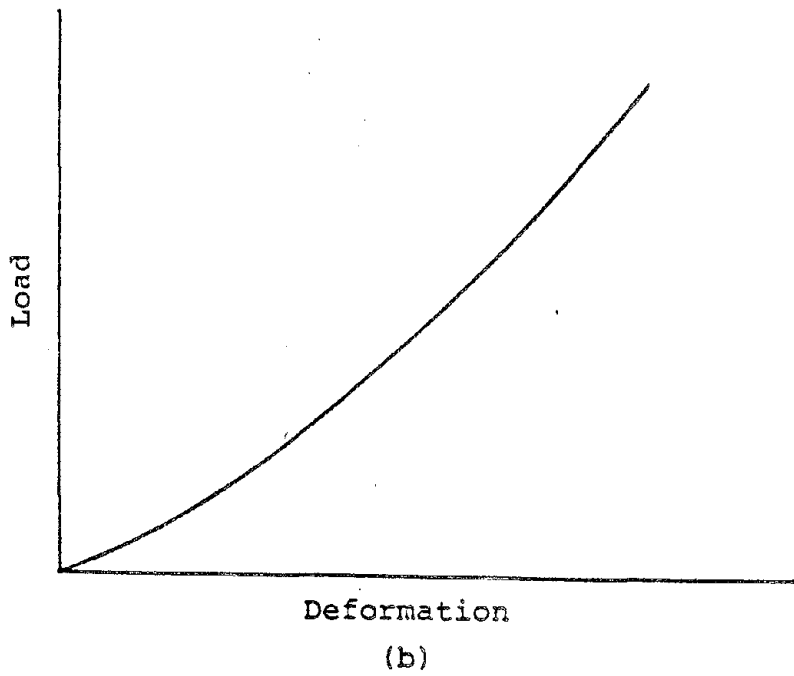
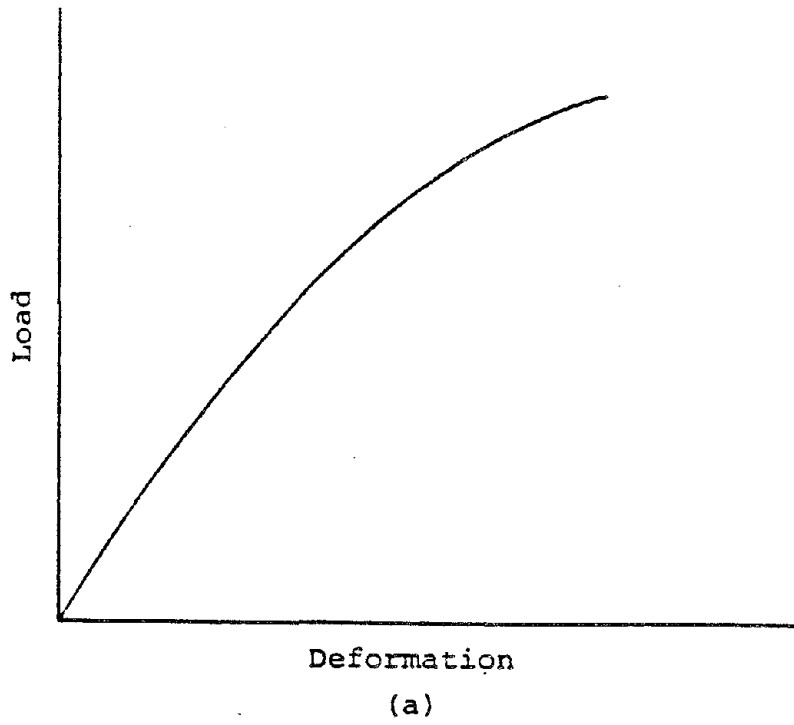
For a nonlinear structural system the stiffness of the structure changes as the structure deforms, therefore, the terms in the matrix $[K]$ change as the load is applied. This greatly complicates the analysis of the system since it is usually not feasible to algebraically solve the set of nonlinear simultaneous stiffness equations corresponding to Equation (1). For most structures it is necessary to resort to some sort of numerical solution to determine the displacements.

There are basically two ways in which the stiffness of a nonlinear system may vary with displacement, as shown in Figure 1. Figure 1a corresponds to a situation in which the overall stiffness of the structure decreases with increasing deformation, while Figure 1b represents the opposite case where the stiffness increases. It will be shown later that the overall behavior of a cable stayed bridge corresponds to this second case.

Several approaches may be used to obtain a numerical solution for the static displacements and stresses in a general nonlinear structural system. Two procedures which are well suited for application to complex multi-degree of freedom systems are an Incremental Approach and an Iterative Approach. In an Incremental Approach the total load is applied in small increments, assuming that the stiffness of the system remains constant during the application of each load increment. The displacements and member end loads which occur during the application of the first load increment are computed using the initial tangent stiffness of the undeformed structure. The stiffness of the structure is then recomputed using the member end loads and deformations corresponding to the deformed shape of the structure at the end of the load increment. This new stiffness is then used to compute the displacement increments which occur during the next load increment. The general form of the equations, which must be solved during the application of load increment i , are

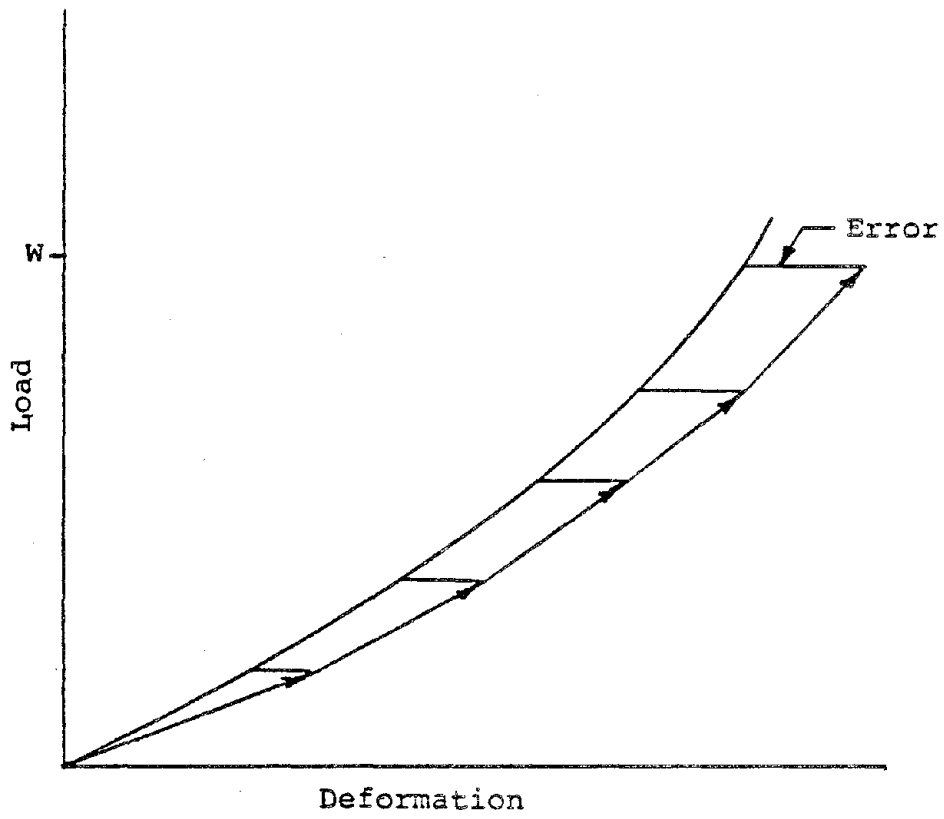
$$[K]_i \{\Delta D\}_i = \{\Delta W\}_i \quad (2)$$

in which $[K]_i$ is the stiffness matrix corresponding to the loading state at the beginning of the load increment, $\{\Delta D\}_i$ are the joint displacements which occur during the application of the load increment and $\{\Delta W\}_i$ are the joint load increments which are applied. The total displacements and member end loads at the end of the load increment are obtained by adding the values which occur during the load increment to the values at the beginning of the load increment. If the total load is applied in a sufficiently large number of increments, so that the change in stiffness over any load increment is relatively small, this approach can give an acceptable engineering solution. A graphical representation of this procedure is shown in Figure 2. It can be seen that the error accumulates for each step. If the total number of increments is sufficiently large, however, the accumulated error can be well within the limits of acceptable engineering accuracy.



Nonlinear Load-Deformation Relationship

Figure 1



Incremental Approach

Figure 2

In an Iterative Approach the total load is applied in one increment. The displacements are initially computed using the tangent stiffness of the undeformed structure, however, the stiffness is then recomputed corresponding to this deformed shape before the member end loads are computed. Since the final stiffness used to compute the member end loads differs from the initial stiffness used to compute the joint displacements, equilibrium will not be satisfied and unbalanced loads will exist at the joints. These unbalanced loads must next be applied as a new set of joint loads, with the corresponding change in displacements being computed using the stiffness corresponding to the new deformed position of the structure. The final solution can be obtained by iterating until the unbalanced loads at the end of a load cycle are smaller than an acceptable tolerance limit. A graphical representation of this procedure is shown in Figure 3. When the total load is applied during the first iteration cycle the displacements are computed using the initial tangent stiffness of the unloaded structure, as represented by the straight line extending from the origin to point A. These computed displacements actually correspond to loads on the true load-deformation curve denoted by point B. The unbalanced loads correspond to the distance AB. By reapplying these unbalanced loads and using the stiffness of the system in the deformed position, a new deflected position, denoted by point C, can be computed. By repeating this process a sufficient number of times, a solution may be obtained to any accuracy desired. This approach is very similar to the classical Newton-Raphson Method for solving nonlinear equations.

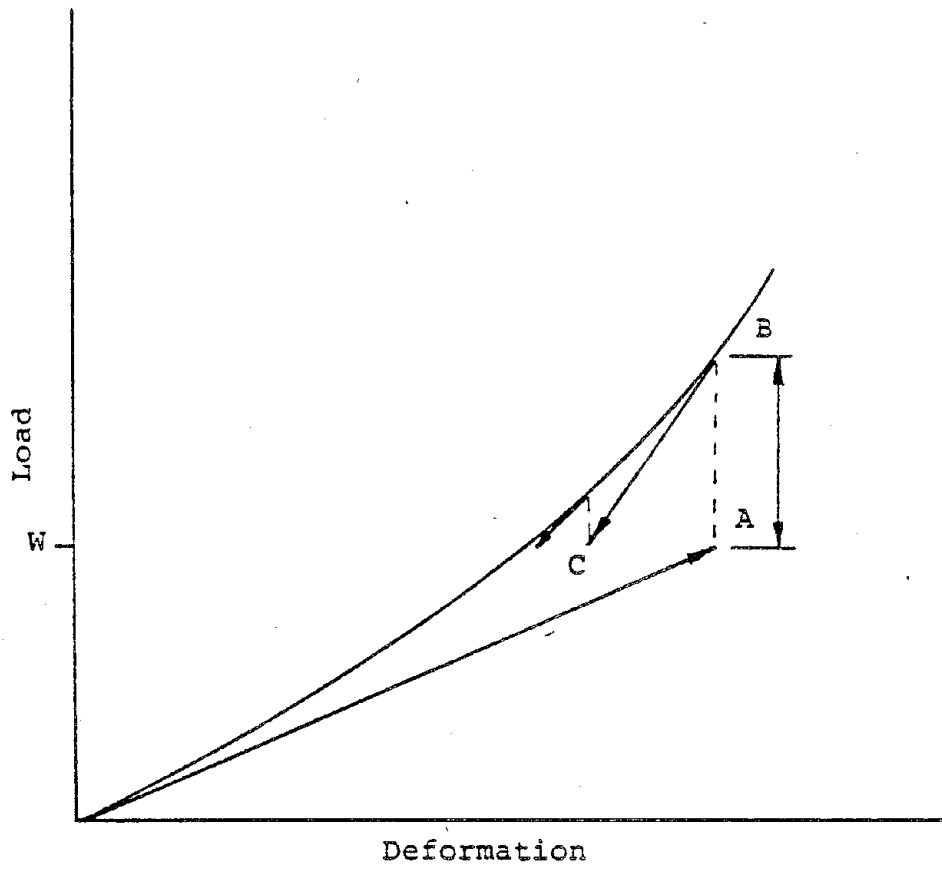
In the static analysis procedure used in this investigation a Combined Approach was used, in which the unbalanced loads were applied incrementally during each iteration cycle. This results in faster convergence.

Sources of Nonlinear Behavior:

Under normal design loads the material in a cable stayed bridge can be considered to remain elastic, however, the overall load-deformation relationship is nonlinear. Three primary sources of nonlinear behavior have been proposed by previous investigators. These are: the nonlinear sag tension relationship for the inclined cables; the interaction of the bending deformations and high axial forces in the towers and longitudinal deck members; and the overall changes in geometry which occur in the structure under normal design loads. All of these effects combine to result in the overall nonlinear behavior of the system.

Computation of Structural Stiffness:

In order to use the Combined Approach to compute the displacements and member end loads, it is necessary to compute the structure stiffness matrix, $[K]$, corresponding to the member



Iterative Approach

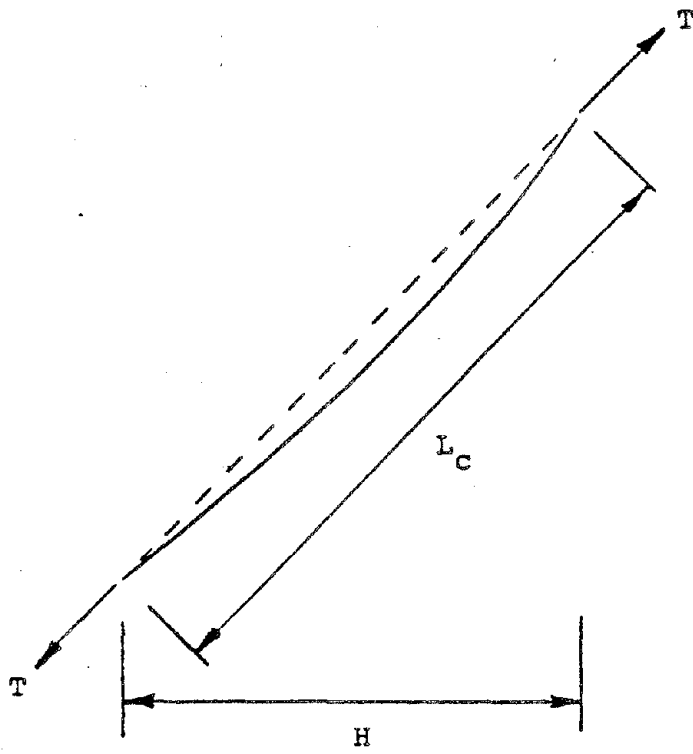
Figure 3

end loads and the deformed shape of the system after each load increment is applied. Since $[K]$, for any structural system, is obtained by adding the individual member stiffnesses at the joints, it is therefore necessary to express the stiffness of the individual cables and bending members in terms of the member end loads and the deformed shape of the structure.

Stiffness of Cables - When an axial tension force is applied to the ends of a cable, the ends will move relative to each other along the axis of the cable. For other types of tension members this relative movement is usually due entirely to the elongation of the member resulting from the strain in the material. For a cable the relative end movement is the result of three distinct actions in the cable. First, there is a change in strain in the cable material. This change in strain can be considered to vary linearly with stress in the cable material and is governed by the modulus of elasticity of the material. Second, there is a change in the sag of the cable, exclusive of material strain. This change in sag is strictly a geometric effect and is governed by the length of the cable, the weight of the cable and the tension force in the cable. The sagged shape of the cable is a catenary, for which equations are given in many elementary mechanics textbooks. This change in sag varies nonlinearly with the change in the tension force in the cable. Third, there is a rearrangement of the individual wires in the cable cross section under changing load. Part of this deformation, which is known as constructional stretch, is permanent. This permanent deformation is usually eliminated by the cable manufacturer by pre-stretching the cable to a load greater than the working load during the manufacturing process. The non-permanent part of this deformation can be compensated for by using a reduced effective modulus of elasticity of the cable material. For example, ASTM Specification A536 states that the effective modulus of elasticity for pre-stretched helical strand should be taken as 23 to 24 million pounds per square inch. The actual material modulus is approximately 29 million pounds per square inch. This equivalent modulus is assumed to be independent of the tension in the cable.

The total apparent change in length of a cable is a result of the sum of the three previously described effects. Therefore, since the sag varies nonlinearly with the axial tension force in the cable, the axial stiffness of the cable will also vary in a nonlinear manner. A convenient method for considering the nonlinearity in the inclined cables is to consider an equivalent straight chord member, as shown in Figure 4, with an equivalent modulus of elasticity which combines both of the effects of material and geometric deformations. An expression for this equivalent modulus, as derived by Ernst (1), is

$$E_{eq} = E_{ef} / \left[1 + \left[\frac{(wH)^2}{AE_{ef} l^2 T} \right] \right] \quad (3)$$



Inclined Cable Member

Figure 4

where E_{eq} is the equivalent modulus, E_{ef} is the effective modulus of the cable as described previously, w is the weight of the cable per unit length, H is the horizontal projected length of the cable, A is the cross section area and T is the cable tension. This equivalent modulus can be used to express the stiffness of any cable member, $[K_m]_c$, in the local member coordinate system shown in Figure 5, in the standard form

$$[K_m]_c = \begin{bmatrix} AE_{eq}/L_c & -AE_{eq}/L_c \\ -AE_{eq}/L_c & AE_{eq}/L_c \end{bmatrix} \quad (4)$$

where L_c is the chord length of the cable member.

Stiffness of Bending Members - For most structural systems the bending and axial deformations in the members can be considered to be independent. However, for flexible bending members subjected to high axial loads, the interaction of the bending and axial effects can have a significant effect upon the stiffness of the member. This interaction can be considered in the analysis of the system by modifying the stiffness of the member with factors known as stability functions (2,3). The stiffness of a typical three dimensional frame bending member, $[K_m]_b$, can be expressed as a 12 by 12 member stiffness matrix, in the local member coordinate system shown in Figure 6, in the form

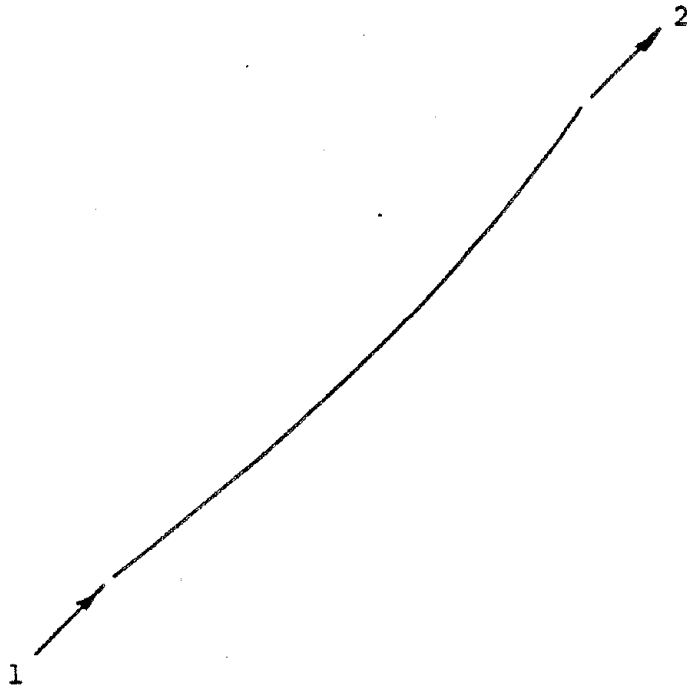
$$[K_m]_b = \begin{bmatrix} k(1,1) & k(1,2) & \dots & k(1,12) \\ k(2,1) & k(2,2) & \dots & k(2,12) \\ \cdot & \cdot & \cdot & \cdot \\ \cdot & \cdot & \cdot & \cdot \\ k(12,1) & k(12,2) & \dots & k(12,12) \end{bmatrix} \quad (5)$$

in which

$$k(1,1) = k(7,7) = -k(1,7) = -k(7,1) = S_5(AE/L) \quad (6a)$$

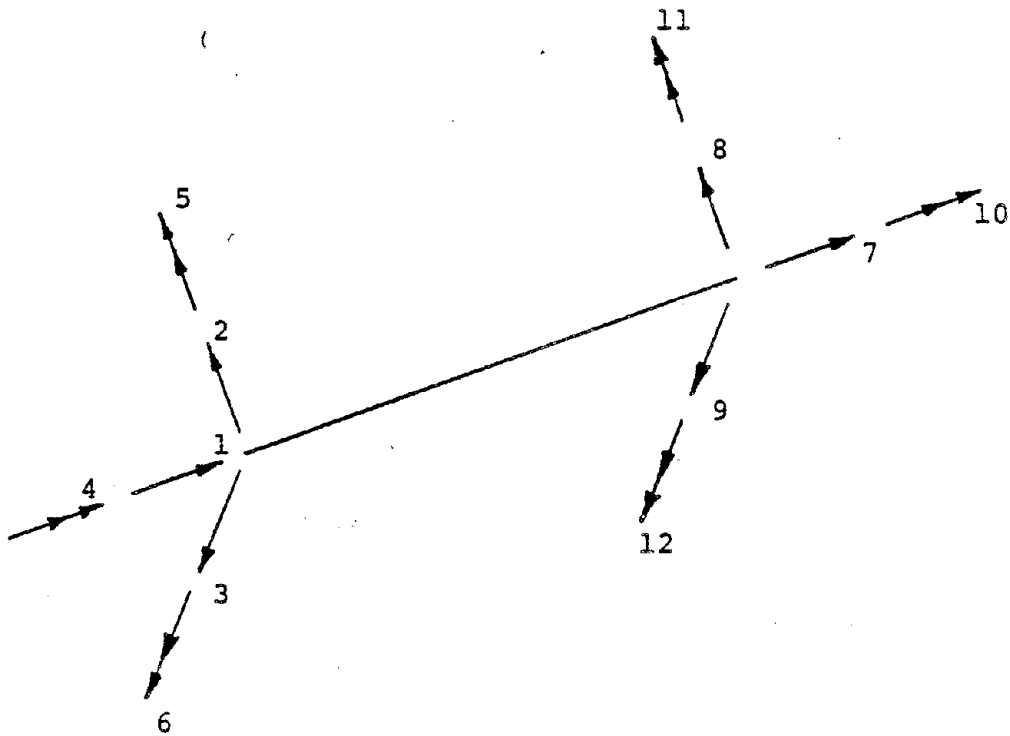
$$k(2,2) = k(8,8) = -k(2,8) = -k(8,2) = S_{1z}(12EI_z/L)^3 \quad (6b)$$

$$k(3,3) = k(9,9) = -k(3,9) = -k(9,3) = S_{1y}(12EI_y/L)^3 \quad (6c)$$



Local Cable Member Coordinate System

Figure 5



Local Bending Member Coordinate System

Figure 6

$$\begin{aligned} k(2,6) &= k(6,2) = k(2,12) = k(12,2) = -k(6,8) \\ &= -k(8,6) = -k(8,12) = -k(12,8) = S2z(6EIz/L)^2 \end{aligned} \quad (6d)$$

$$\begin{aligned} k(3,5) &= k(5,3) = k(3,11) = k(11,3) = -k(5,9) \\ &= -k(9,5) = -k(9,11) = -k(11,9) = S2y(6EIy/L)^2 \end{aligned} \quad (6e)$$

$$k(4,4) = k(10,10) = -k(4,10) = -k(10,4) = Gkt/L \quad (6f)$$

$$k(5,5) = k(11,11) = S3y(4EIy/L) \quad (6g)$$

$$k(6,6) = k(12,12) = S3z(4EIz/L) \quad (6h)$$

$$k(5,11) = k(11,5) = S4y(2EIy/L) \quad (6i)$$

$$k(6,12) = k(12,6) = S4z(2EIz/L) \quad (6j)$$

where E is the material modulus of elasticity, L is the member length, A is the cross section area, Iy and Iz are the moments of inertia of the cross section about the local principal y and z axes respectively, Kt is the torsional constant for the cross section and the quantities S1 through S5 are the stability functions.

The stability functions can be expressed in terms of the member axial force, P, and member end moments about the member y and z axes, as defined in Figure 7. For a compressive axial force, the stability functions S1z through S4z are

$$S1z = (QL)^3 \sin(QL)/12Rc \quad (7a)$$

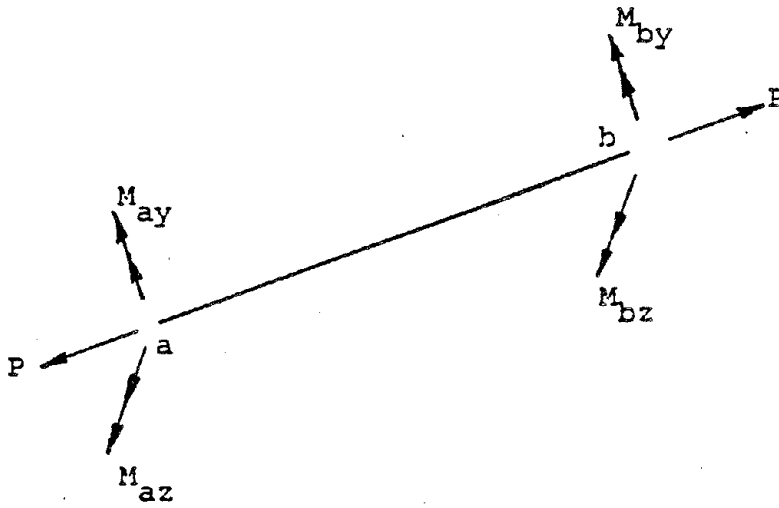
$$S2z = (QL)^2 [1-\cos(QL)]/6Rc \quad (7b)$$

$$S3z = (QL)[\sin(QL)-(QL)\cos(QL)]/4Rc \quad (7c)$$

$$S4z = (QL)[(QL)-\sin(QL)]/2Rc \quad (7d)$$

where

$$Q = (P/EIz)^{1/2} \quad (8)$$



Bending Member End Loads

Figure 7

$$R_c = 2 - 2\cos(QL) - (QL)\sin(QL) \quad (9)$$

while, for a tensile axial force

$$S_{1z} = (QL)^3 \sinh(QL) / 12R_t \quad (10a)$$

$$S_{2z} = (QL)^2 [\cosh(QL) - 1] / 6R_t \quad (10b)$$

$$S_{3z} = (QL)[(QL)\cosh(QL) - \sinh(QL)] / 4R_t \quad (10c)$$

$$S_{4z} = (QL)[\sinh(QL) - (QL)] / 2R_t \quad (10d)$$

where

$$R_t = 2 - 2\cosh(QL) + (QL)\sinh(QL) \quad (11)$$

and Q is the same as defined previously in Equation (8). The stability functions S_{1y} through S_{4y} can be determined in the same manner by merely replacing I_z by I_y in Equations (7) through (11).

For a compressive axial force the stability function S_5 can be expressed as

$$S_5 = 1 / [1 + EA(R_{cmy} + R_{cmz}) / 4P L^3] \quad (12)$$

where

$$R_{cm} = (QL)^2 (M_a + M_b) [\cot(QL) + (QL)\operatorname{cosec}(QL)] - 2(M_a + M_b) + (M_a M_b) [1 + (QL)\cot(QL)] [2(QL)\operatorname{cosec}(QL)] \quad (13)$$

while, for a tensile axial force

$$S_5 = 1 / [1 - EA(R_{tmy} + R_{tmz}) / 4P L^3] \quad (14)$$

where

$$R_{tm} = (QL) \frac{(M_a + M_b)^2}{2} [\coth(QL) + (QL) \operatorname{cosech}(QL)] - 2(M_a + M_b) + (M_a M_b) [1 + (QL) \coth(QL)] [2(QL) \operatorname{cosech}(QL)] \quad (15)$$

To compute R_{cmy} from Equation (13) the moments M_{ay} and M_{by} should be used and Q should be computed from Equation (8) using the moment of inertia I_y . To compute R_{cmz} the moments M_{az} and M_{bz} should be used and Q should be computed using I_z . The values of R_{tmy} and R_{tmz} can be computed from Equation (15) by the same procedure.

Computer Program:

A computer program which uses the analysis procedure just described has been developed on the University of Pittsburgh DEC PDP-10 Computer System for analyzing three dimensional cable stayed bridge structures under static dead and live load and user specified initial cable tensions. A combined incremental and iterative approach, as described previously, is used to reduce the unbalanced loads in the system to an acceptable user specified level. The stiffness matrix for the system is recomputed at the beginning of each load increment in order to account for the nonlinear behavior of the system. Extensive studies, using mathematical models representing several actual or proposed bridges, have shown that it is usually sufficient to divide the unbalanced load into three increments during the first iteration cycle and then to apply the remaining unbalanced load in one increment for each succeeding cycle. The program has been developed so that the user can specify the number of load increments to be used. (A listing of the FORTRAN source program is available, to anyone requesting it. No facilities are available for supplying the program on tape.)

NONLINEAR DYNAMIC ANALYSIS

The equations of motion for a lumped mass system, subjected to a set of concentrated dynamic loads, can be written in the form

$$[M]\{A\} + [C]\{V\} + [K]\{D\} = \{W(t)\} \quad (16)$$

where $[M]$, $[C]$ and $[K]$ are the mass matrix, the viscous damping matrix and the stiffness matrix of the system; $\{D\}$, $\{V\}$ and $\{A\}$ are the displacements, the velocities and the accelerations corresponding to each dynamic degree of freedom at the mass points; and $\{W(t)\}$ are the externally applied dynamic loads. If the variation of the loads is known with time, the displacements

can be computed by solving the set of differential equations represented by Equation (16). It will be found, however, that for most dynamic loads, such as wind or seismic action, which are considered in the design of bridge structures, it is not feasible to obtain an algebraic solution for the displacements. In a cable stayed bridge the solution is further complicated by the changing stiffness of the structure, as described previously, thus resulting in a variation of the stiffness matrix $[K]$ as the structure deforms. The only practical approach is to use a numerical approach to obtain a solution to the equations of motion.

Many different numerical procedures have been presented in the literature. Several popular methods, which have been shown to give acceptable results for the solution of structural dynamics problems, are: the Average Acceleration Method (4); the Newmark Beta Method (5); and the Wilson Theta Method (6). Each of these is a single step forward procedure, therefore, the change in stiffness of the structure can be easily considered by recomputing the stiffness matrix $[K]$ corresponding to the deformed shape of the system at the beginning of each time step during the solution process.

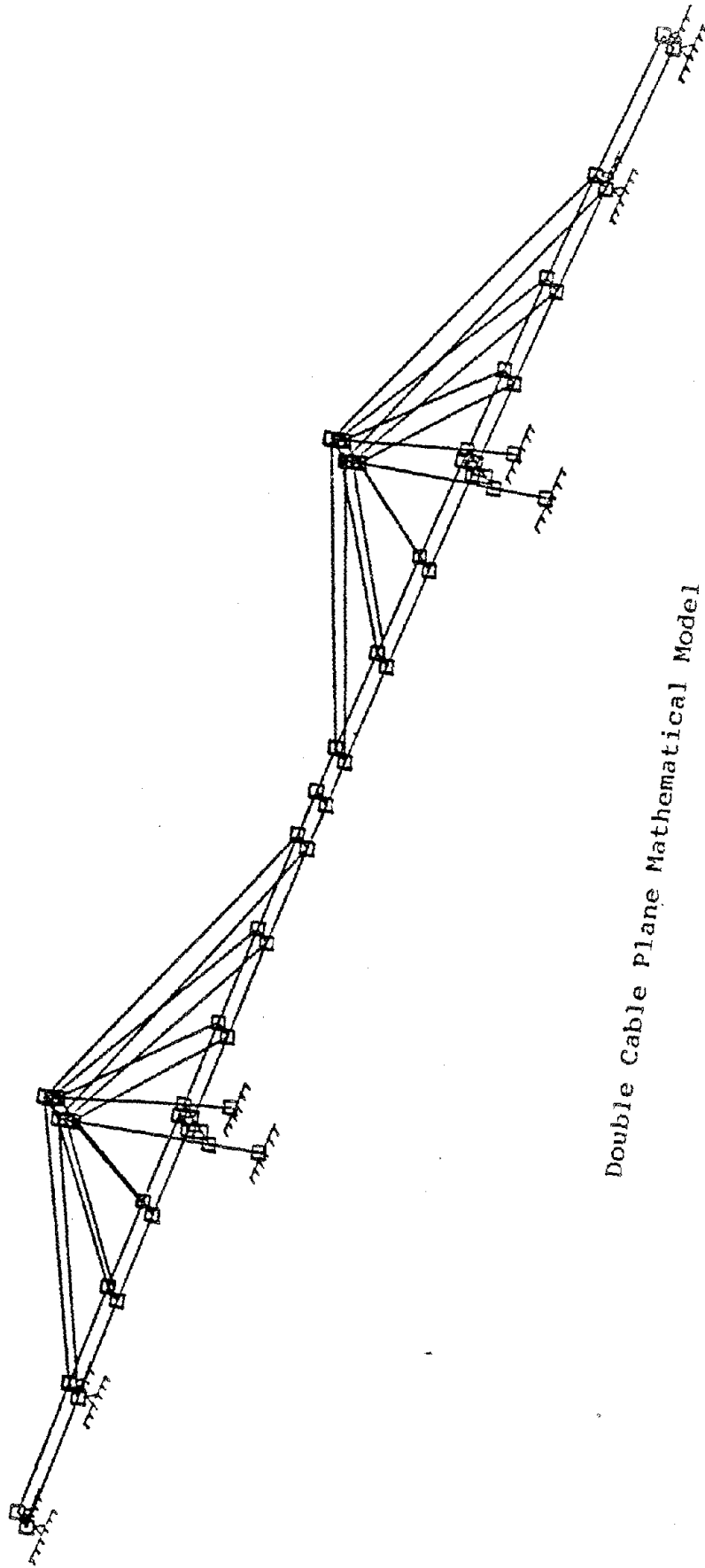
STATIC BEHAVIOR

As described previously, three primary sources of nonlinear behavior have been proposed by previous investigators for cable stayed bridge structures. In order to investigate the importance of each of these, a number of static analyses have been performed, for several mathematical models with properties similar to actual or proposed bridges. A typical mathematical model, in which the cables are in two parallel planes on either side of the roadway, is shown in Figure 8. Various geometries for the cables and towers were studied. Several cases were also considered in which the cables were in a single plane in the center of the roadway.

Effect of Geometry Change:

For most structural systems it can be assumed that the geometry changes which occur, due to the applied loads on the structure, are small and therefore the original unloaded geometry can be used to compute the member lengths, member slopes, moment arms and other geometric quantities used in the analysis. In a cable stayed bridge the displacements under normal design loads can be large, therefore, the question arises whether the changes in geometry can have a significant effect upon the structural behavior.

The effect of the changes in geometry were incorporated in the analysis by revising the geometry of the mathematical model after each load increment was applied. The structural stiffness was then recomputed using the revised geometry. The structure



Double Cable Plane Mathematical Model

Figure 8

was considered to be subjected to a uniform deck load and a set of initial cable tensions. A wide range of initial cable tensions and deck loads were investigated. Figures 9 and 10 show the results of two typical sets of analyses for the mathematical model shown in Figure 8. Figure 9 shows the variation of the normalized vertical deflection at center span with the uniform deck load, while Figure 10 shows the variation of the normalized horizontal deflection component, along the longitudinal axis of the bridge, at the top of one of the towers. The solid lines show the results obtained when the effect of the change in geometry is neglected while the dashed lines include the geometry change. For both sets of analyses the cables were assumed to be tensioned initially to their full design values, and the uniform deck load was considered to range from essentially zero to a value corresponding to five times the full dead load of the structure. This load is much larger than any loading which might be expected under normal operating conditions since, for long span bridges, the majority of the design load is usually the dead load of the structure. The results of these particular analyses, and other analyses performed on mathematical models representing other bridges, indicate that the effect of the change in geometry of the structure is small, for normal design loads, and can be neglected without significantly affecting the computed behavior of the structure.

Effect of Axial-Bending Interaction:

The effects of the change in the stiffness of the bending members in the structure, due to axial-bending interaction, were incorporated in the analysis by introducing stability functions into the individual member stiffness matrices, as described previously. A number of analyses were performed, for several different mathematical models, for a wide range of deck loads. For all cases considered, the computed stability functions varied by less than three percent from a value of 1.0, and for most cases the variation was less than one percent. A value of 1.0 for the stability functions corresponds to no change in the stiffness. It can therefore be concluded that even though the longitudinal deck members and towers are subjected simultaneously to high axial forces and bending moments, the effect of the interaction of these quantities upon the overall stiffness of the structure is small. In order to simplify any future analyses their effect can be safely neglected.

Effect of Nonlinear Cable Stiffness:

The final nonlinear effect to be considered is the overall change in stiffness of the structure due to the variation of the stiffness of the cables as the tensions in the cables change under the applied load. Figure 11 shows the variation of the normalized vertical deflection at center span with the uniform deck load for the mathematical model shown in Figure 8. The individual curves correspond to different values of the initial

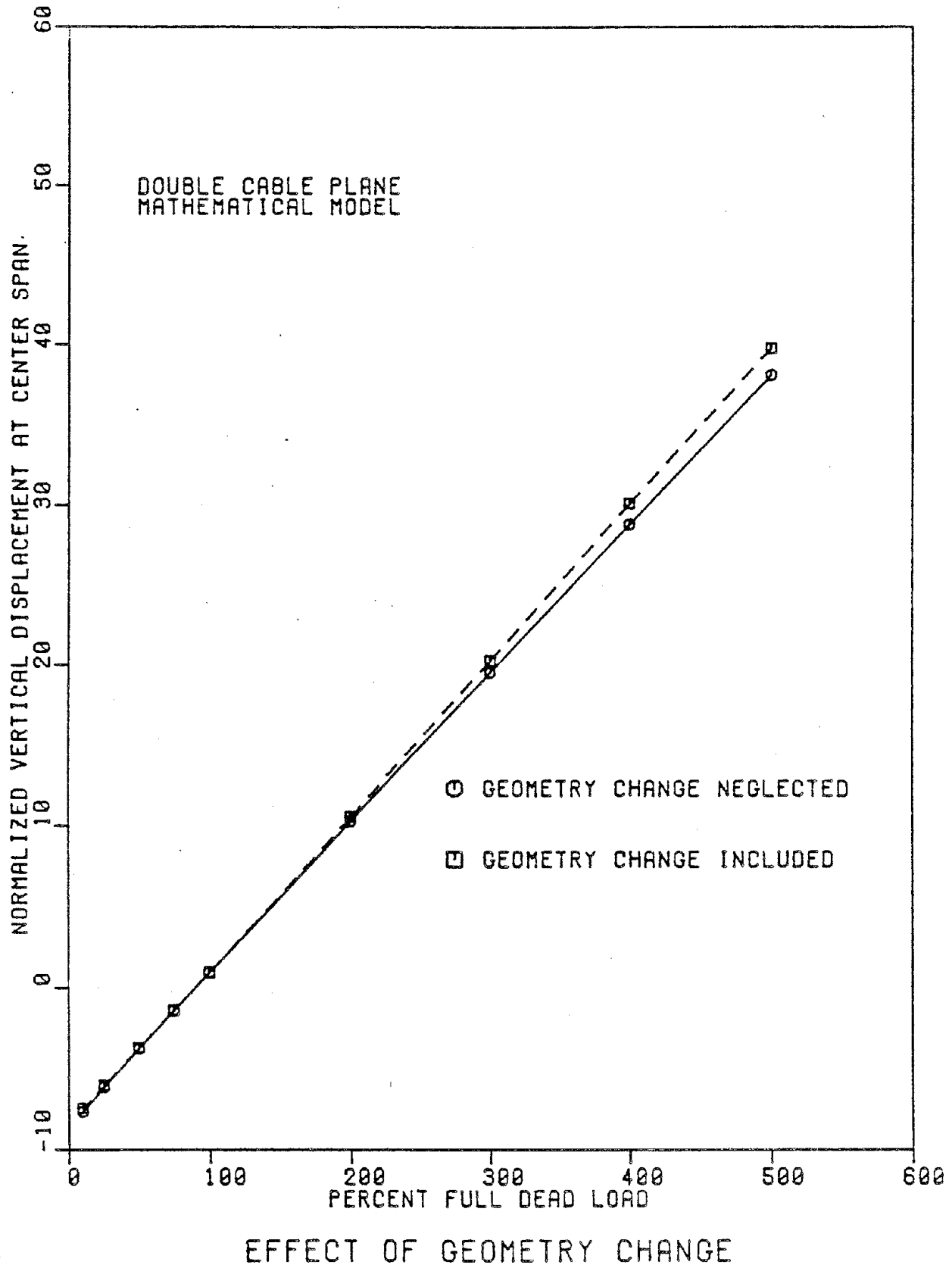


FIGURE 9

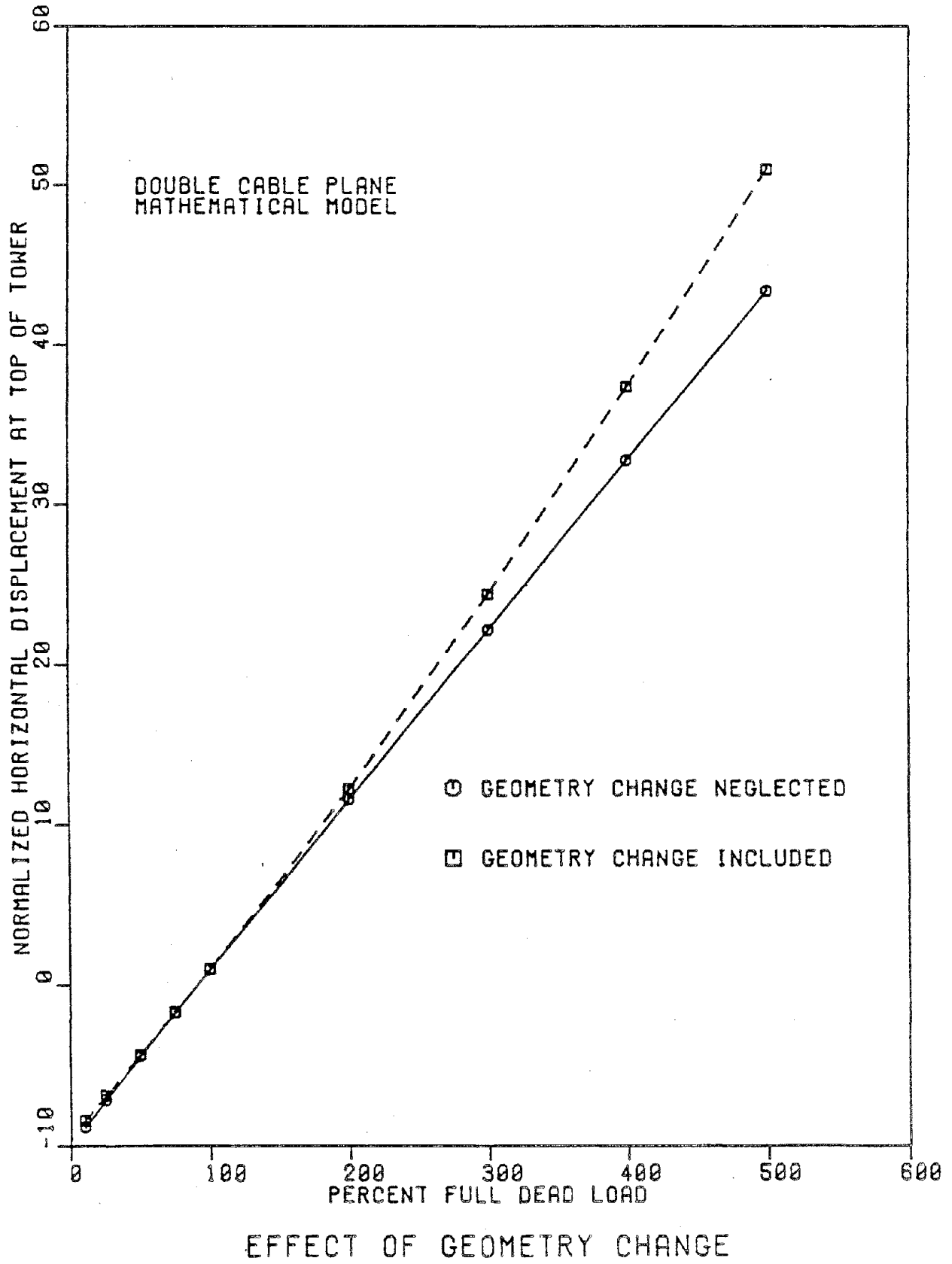
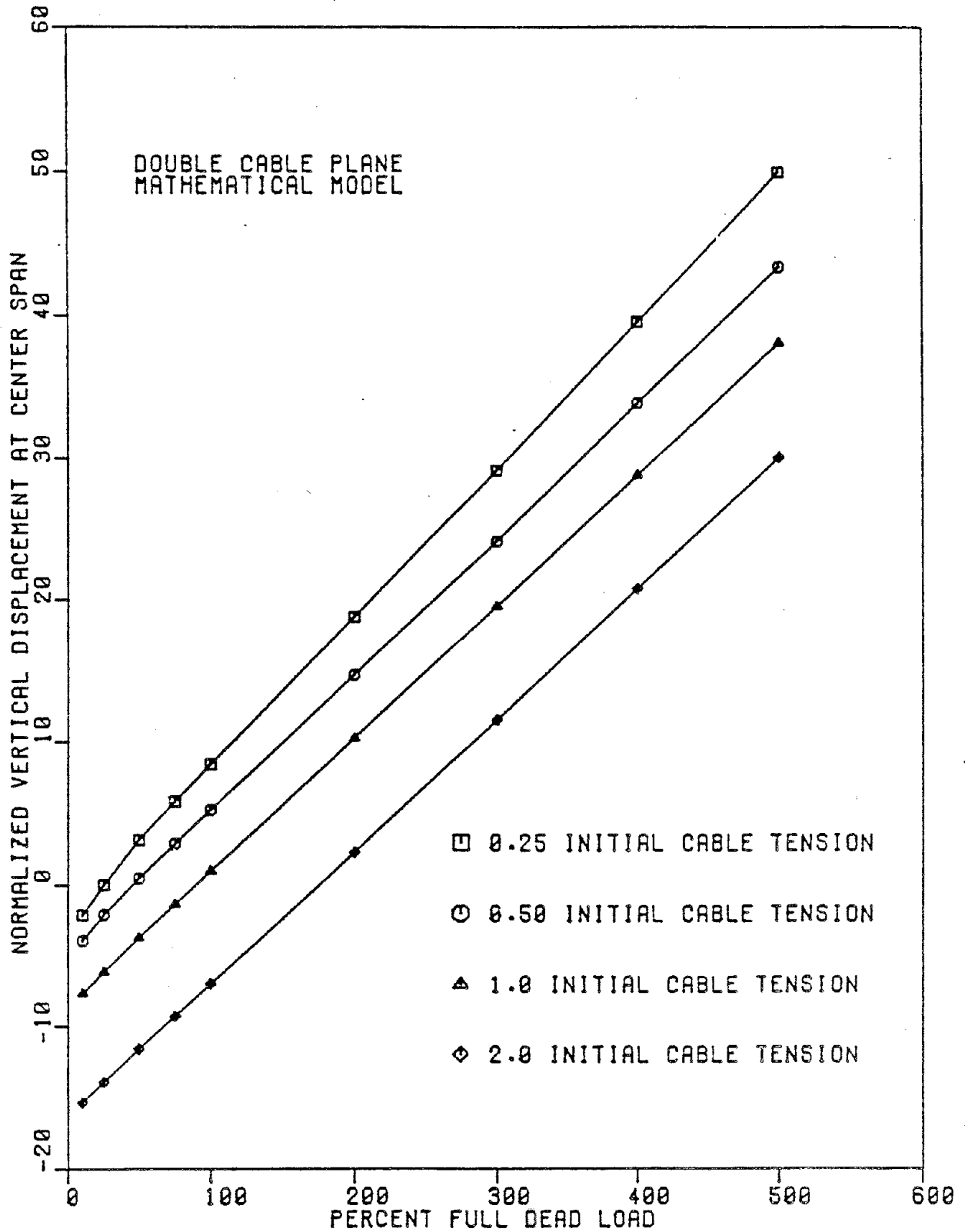


FIGURE 10



EFFECT OF CABLE NON-LINEARITY

FIGURE 11

cable tensions, ranging from 0.25 to 2.0 times the full design values for each cable.

These curves show that the load-displacement relationship is nonlinear for low values of the uniform deck load, however, as the load is increased, the relationship becomes more linear. For loads equal to the full dead load or greater, the relationship is essentially linear for all initial cable tensions considered. The nonlinear effect also decreases as the initial cable tension is increased. Similar results were obtained for the other mathematical models which were considered in the investigation for other computed quantities, such as: the horizontal displacement at the top of the towers; the moment in the deck or the towers; and the final cable tensions (7).

DYNAMIC BEHAVIOR

In order to investigate the dynamic behavior of cable stayed bridges, time history analyses were performed for several different dynamic loadings (8,9). One of the loadings was that caused by the ground motion due to the vertical component of the May 18, 1940 El Centro, California earthquake. The purpose of these time history analyses was not to investigate the level of stress produced in the structure, but rather to investigate the degree of nonlinear behavior. It was assumed that the material in the bridge remained elastic during the dynamic response.

The mathematical model considered for the time history analyses was a single load bearing plane of a bridge with a geometry similar to that shown previously in Figure 8. The mass of the structure was assumed to be lumped at 22 node points. Only translational degrees of freedom were considered. The structure was assumed to start at rest in the dead load deformed position with stiffness corresponding to this loaded state.

Three types of analyses were performed, which consisted of the following combinations of static and dynamic analysis: linear static analysis to compute the structure stiffness in the static dead load deformed position and linear dynamic analysis, in which the stiffness is assumed to remain constant, hereafter denoted as Linear-Linear; nonlinear static analysis and linear dynamic analysis, hereafter denoted as Nonlinear-Linear; and nonlinear static analysis and nonlinear dynamic analysis, in which the stiffness is recomputed corresponding to the deformed shape of the structure at the beginning of each dynamic time step, hereafter denoted as Nonlinear-Nonlinear. The combination of linear static analysis and nonlinear dynamic analysis was not considered.

Figure 12 shows the variation of the undamped vertical displacement of the deck at center span, for the three types of analyses just described, for the El Centro ground motion. It can be seen that the Nonlinear-Linear and Nonlinear-Nonlinear analyses give almost identical results, which vary considerably

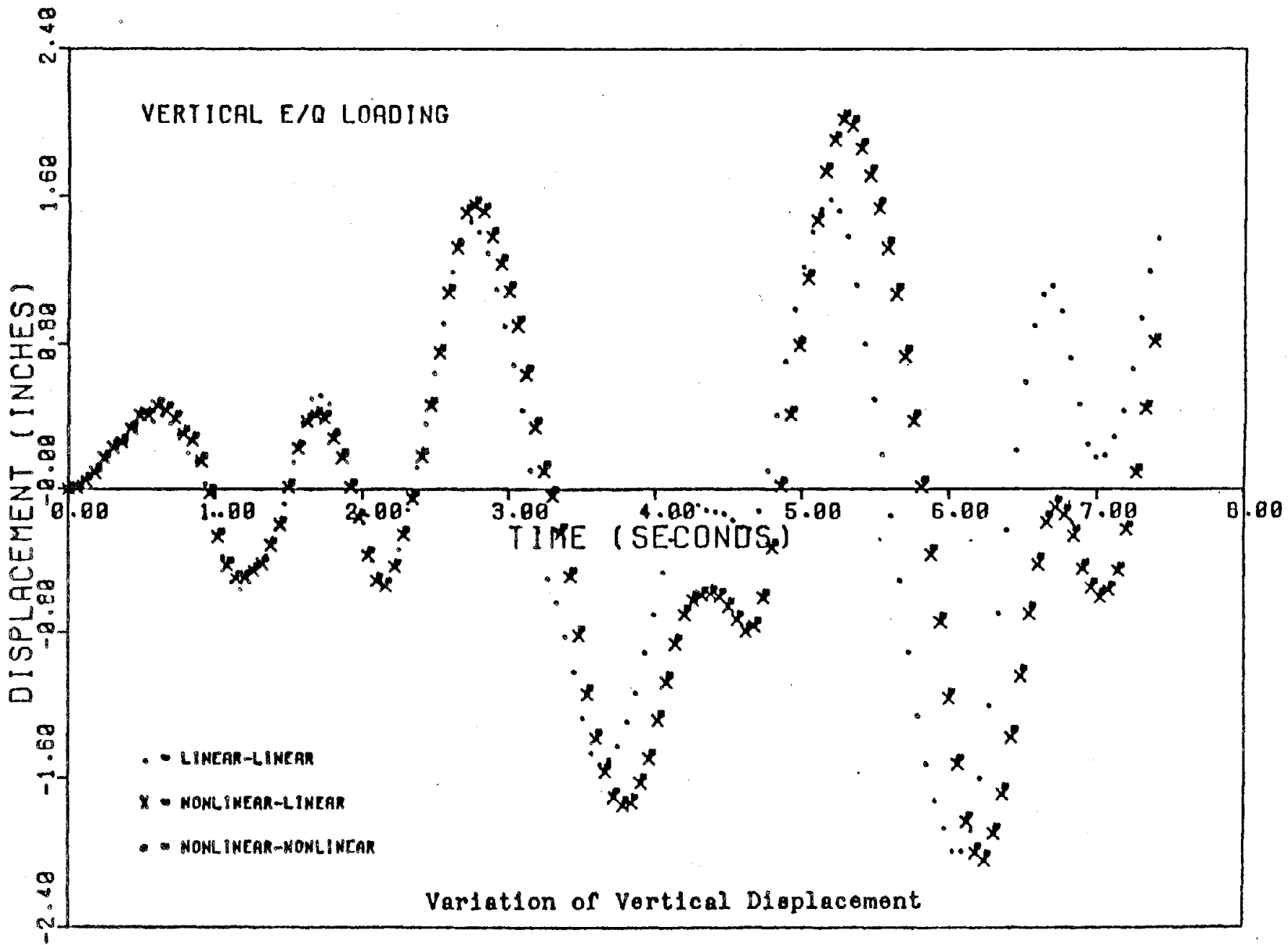


FIGURE 12

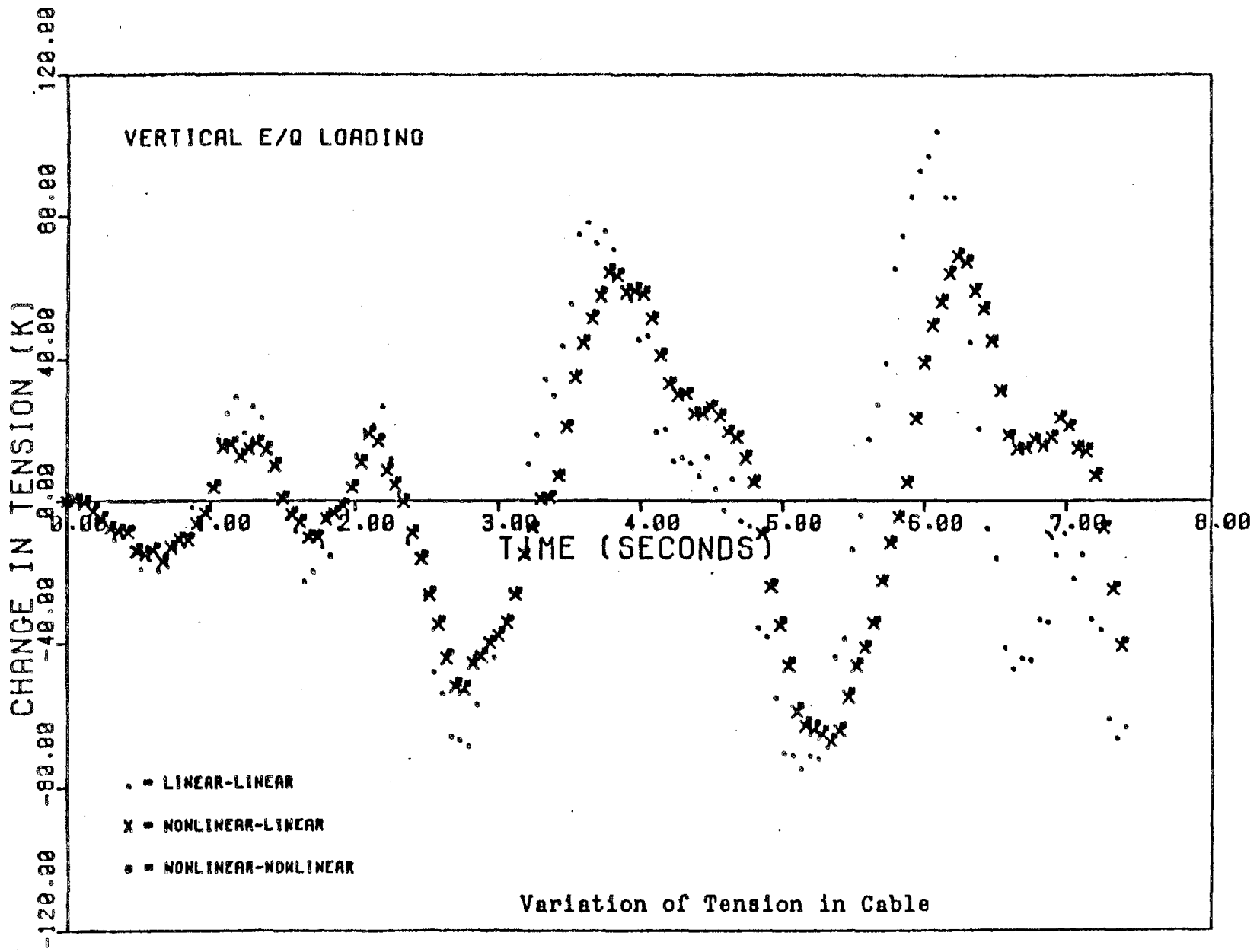


FIGURE 13

from the Linear-Linear analysis. Similar results were obtained for the variation of the tension in one of the cables as shown in Figure 13. The results of these analyses, and several other analyses which were performed for both a simulated dynamic wind loading and a moving traffic load (8), indicate that although a nonlinear static analysis is required to obtain the stiffness of the structure in the dead load deformed position, a linear dynamic analysis will suffice starting at this position. This conclusion agrees with the results described previously for the static analyses.

CONCLUSIONS

The results of the static and dynamic analyses, which have been described, lead to the conclusion that a cable stayed bridge structure does behave in a nonlinear manner for low loads, however, after the full dead load deformed position has been reached, the structure can be considered to behave linearly. Therefore, the stiffness of the structure, which is represented by the slope of the curves shown in Figure 11, can be considered to be constant for static or dynamic live loads. This means that linear analysis techniques, such as influence lines for static loads and the response spectrum method for dynamic loads, are applicable to this type of structure, starting at the dead load deformed position. However, if an accurate solution is to be achieved, the nonlinear behavior of the structure under the initial dead load should be considered to arrive at the correct stiffness to be used in the linear analysis.

ACKNOWLEDGEMENTS

The investigation reported here was sponsored in part by National Science Foundation Grant No. PFR-7923023 to the University of Pittsburgh with John F. Fleming as Principal Investigator. Acknowledgement is also given to Ms. Diane Kokoski (10) and Mr. Joseph Zenk (11) who helped perform some of the analyses presented here while working as Research Assistants at the University of Pittsburgh.

REFERENCES

1. Ernst, J.H., "Der E-Modul von Seilen unter Berucksichtigung des Durchanges", Der Bauingenieur, February 1965
2. Harrison, H.B., "Computer Methods in Structural Analysis", Prentice Hall Publishers, 1973
3. Livesley, R.K. and Zellner, W., "Stability Functions for Structural Frameworks", Manchester University Press, 1956

4. Fleming, J.F. and Romualdi, J.P., "A General Procedure for Calculating Dynamic Response Due to Impulsive Loads", Journal of the Franklin Institute, Vol 275, No 2, February 1963
5. Newmark, N.M., "A Method of Computation for Structural Dynamics", Proceedings of the American Society of Civil Engineers, Vol 85, No EM3, July 1959
6. Wilson, E.H., "A Computer Program for the Analysis of Underground Structures", SESM Report 68-1, Department of Civil Engineering, University of California, Berkeley, 1968
7. Fabian, R.A., "Behavior of Cable Stayed Bridges and Techniques for Their Analysis", M.S. Thesis, Department of Civil Engineering, University of Pittsburgh, 1980
8. Egeseli, E.A., "The Nonlinear Dynamic Response of a Cable Stayed Girder Bridge to Various Loadings", Ph.D. Dissertation, Department of Civil Engineering, University of Pittsburgh, 1975
9. Fleming, J.F. and Egeseli, E.A., "Dynamic Behavior of a Cable Stayed Bridge", Journal of Earthquake Engineering and Structural Dynamics, Vol 8, No 1, 1980
10. Kokoski, D.L., "Three Dimensional Nonlinear Analysis of Cable Stayed Bridge Structures", M.S. Thesis, Department of Civil Engineering, University of Pittsburgh, 1979
11. Zenk, J.D., "Static and Dynamic Analysis of Cable Stayed Bridges", M.S. Thesis, Department of Civil Engineering, University of Pittsburgh, 1983

SEISMIC VULNERABILITY OF
PRESTRESSED CONCRETE SEGMENTAL BRIDGES

by

Walter Podolny, Jr.
Bridge Division
Office of Engineering
Federal Highway Administration
Washington, D.C.

ABSTRACT

For the most part, in the United States, prestressed concrete segmental bridges have been constructed in zones of zero or low seismic vulnerability. However, this method of constructing bridges is now being considered in zones of medium to high seismic activity. This then raises the question of how bridges constructed in this manner behave or respond to dynamic loads generated during a seismic event.

We are aware of only one segmental bridge that has been subjected to a seismic event. This was the Incienso Bridge during the 1976 Guatemala Earthquake. Although this bridge did not suffer any distress as a result of the 7.5 Richter Magnitude event, there are nevertheless concerns as to the potential for damage or failure resulting from dynamic earthquake loads.

With regard to the performance of segmental bridges during a seismic event, this paper raises concerns relative to segment joints, anchorage details, bond transmission length, external tendons, redundancy and pull-out of horizontally curved tendons. The intent of this paper is to point out research needs to alleviate engineering design concerns.

Key Words: Bridge, prestressed concrete, segmental construction, joints, anchorages, horizontal curvature, vertical curvature, external tendons.

Introduction

Prestressed concrete segmental bridge construction began in 1950 in Germany when Ulrich Finsterwalder applied the cast-in-place, balanced cantilever method to a bridge crossing the Lahn River at Balduinstein. Wide acceptance of this system of constructing bridges was rapidly gained in Germany, after construction of a bridge crossing the Rhine River at Worms in 1952. Concurrently, precast segmental construction was evolving during this period. The first major application of match-cast, precast, segmental construction was the construction of the Choisy-le-Roi Bridge crossing the Seine River south of Paris, France. These concepts have been refined and have spread from Germany and France to many other countries throughout the world, including Japan and the United States.

Within approximately the last ten years, this method of constructing bridges has gained acceptance in the United States and there are currently over 150 such bridges that are completed, under construction or in design. For the most part, in the United States, segmental bridges have been constructed in zero or low seismic vulnerability areas. However, this method of constructing bridges is now being considered in areas of medium to high areas of seismic activity.

This then raises the question of how bridges constructed in this manner behave and respond to dynamic loads generated during a seismic event. To the author's knowledge, the only segmental bridge, thus far, to experience a seismic event was the Incienso Bridge during the 1976 Guatemala Earthquake¹ which was a Richter Magnitude of 7.5, Figure 1. The three main spans were twin segmental, precast, prestressed concrete box girders with spans of 203, 400 and 203 feet (62, 122 and 62 m) constructed by the balanced cantilever method. Total deck width is 82 feet (25 m). The main span is supported on reinforced concrete piers 262 feet (80 m) and 230 feet (70 m) in height. Although there was evidence of some minor distress in the prestressed I-girder approach spans, the three main segmental spans suffered no visible damage. Perhaps our Japanese colleagues can provide us with their

experience and/or data regarding the response and behavior of this type of bridge to a seismic event, if any exist.

Segment Joints

Aside from the global response of the structure, the local behavior at the segment joints is of interest. The capacity of a joint to resist shear and flexural stresses is a function of the prestressing force normal to the joint, development of friction on the joint face and the presence or absence of shear keys.

The joints in cast-in-place segmental construction are similar to a construction joint in conventional cast-in-place on falsework construction. The joint face has a roughened surface, to a depth of 3/8 inch (10 mm), to provide an interlock with the next segment to be cast and in addition to the prestress tendons, conventional reinforcement crosses the joint.

Joints for precast segments are match-cast and thus have no conventional reinforcement across the joint, only the prestress tendons cross the joint. For shear transfer, as well as for alignment purposes, there are two options, either a large single key or a small multiple-key arrangement, Figure 2. In addition, the joint may contain an epoxy adhesive between the faces of the joint. Occasionally, no epoxy is specified in the joints between the segments; that is, the design is based on a dry joint. This means that there must be permanent compression along the plane of the joint, i.e., no tension. These joint planes must be checked to insure that they are non-sliding.

This requirement of non-sliding is expressed by the criterion

$$T/N \leq 0.3$$

where T denotes the shear force in the section and N the normal force. The coefficient of friction of concrete on concrete is assumed to be a minimum of 0.6 which provides a factor of safety in excess of 2 for sliding in the above equation.

From a design point of view, it would be of interest to have a comparative evaluation of the various joint configurations, with regard to the dynamic forces

imparted during an earthquake, as to ductility, shear capacity, slip or displacement in the joint, and if the joints open-up, is there a impacting of the segments on each side of a joint that will cause degradation of the joint. In other words, the behavioral characteristics and failure modes.

Post-tensioning anchorages

Contemporary segmental bridge construction utilizes a blister detail for the anchorage of post-tensioning tendons, Figure 3. In most instances the blisters are located at the juncture of a flange and web. In some cases a tendon anchorage may be located at some intermediate point between the webs or flanges and may then be an isolated blister block or a continuous buttress between the webs or flanges.

The curved tendon not only produces a uniform radial pressure but also a longitudinal and transverse component with respect to the flange or web. The longitudinal component not only produces tension in the web or flange behind the blister but also a moment by virtue of its eccentricity with the centerline of the web or flange. The stresses in the blister and in the flange or web in the vicinity of a blister are complex and require careful evaluation. Again the concern to be expressed for these details is if the blister will have a tendency to pull-out or rip away from the flange or web as a result of dynamic loading produced during an earthquake event.

External tendons

In recent years, external post-tensioning tendons in conjunction with the span-by-span method of segmental construction has been utilized for bridge construction in the United States. A typical installation is illustrated in Figure 4. The tendon profile is similar to that of pretensioned I-girders with two harping or hold-down points. Each tendon is one span in length and anchored into the segment diaphragm located at each pier. Adjacent span tendons are overlapped at the pier diaphragms to provide continuity.

There are many advantages to this method of construction. Since the tendon

is external to the cross section and located inside the cell of the box; there is reduced congestion in the webs of the box, reduction of web thickness, reduced fabrication time and manpower, all of which translate to an economic advantage. There is also a relatively high rate of erection with this method. On one project, with 135 foot (41 m) spans, an average rate of erection was one span per day.

However, the structure must be designed such as to be serviceable with minimal damage after an earthquake. This then raises a number of concerns. Is there a potential for resonance between the external tendons and the superstructure? There is also the question of redundancy under seismic loading. If the pier diaphragms or tendon anchorages were to fail as a result of seismic loading the prestressing would be lost with a subsequent collapse of the structure.

To alleviate, to some extent, these concerns the following measures have been suggested for incorporation into a recent design of this type located in a seismic area:

- tendons be continuous for a two span length and staggered such that there is at least one continuous tendon (per web) at each pier diaphragm, Figure 5.
- the horizontal portion of each tendon profile is encased in concrete in a subsequent construction operation after tensioning, Figure 6.
- conventional reinforcement is placed in the tendon encasing concrete such that it is continuous across the segment joints, Figure 6.
- provisions are made for future additional tendons to be placed in each span, Figure 5.

Thus, the assumptions are as follows:

- the bottom straight tendons bonded to the cross section for the full span length remain fully effective for their total length.
- partially bonded tendons anchored in the pier diaphragm lose their

prestressing force in the inclined unbonded portion of the profile and are only effective in areas where bond may develop, i.e., the horizontal portion of the profile that is encased in concrete.

- the inclined portion of the tendon profile that is continuous at the pier would be considered effective.

It is hoped that research on this problem would at least touch upon the following:

- is the concern valid.
- if so, are the above precautions adequate and sufficient.
- if not, what other requirements are necessary to make this construction method acceptable.
- bond transmission length of large multi-strand tendons when the anchors are lost (not all of the individual strands are encapsulated in the grout).
- are there any other areas of concern regarding this system when subjected to seismic loading.

Vertically curved tendons in soffit flanges

Tendons for continuity or positive moment prestress in segmental bridges may not, or even should not, always be located in the fillet between web and bottom flange. They may be located in the bottom flange proper. When a variable-depth member is used, the bottom flange has a curvature in the vertical plane, which must be followed by the prestress tendons. Unless careful consideration is given to that fact at the concept and detailed design stages, difficulties are likely to develop; this is indicated in Figure 7, which shows the free-body diagrams of stresses in the bottom flange due to the curvature. Curvature of a tendon induces a downward radial load, which must be resisted by transverse bending of the bottom flange between the webs.²

Longitudinal compressive stresses in the bottom flange similarly induce an upward radial reaction in the flange, counteracting at least in part the effect of the tendons. Unfortunately, when the full live load and variable effects, such

as thermal gradients, are applied to the superstructure, the longitudinal stresses vanish and consequently the partial negation of the effect of tendon curvature is lost. Therefore, the effect of tendon curvature adds fully to the dead-load stresses of the concrete flange. The corresponding flexural stresses are four to five times greater than the effect due to dead load only, and if sufficient reinforcement is not provided for this effect, heavy cracking is to be expected and possibly failure.

Given this situation for static loading, what is the potential for tendon pull-out and/or bottom flange failure resulting from inertia forces if there is a seismically induced vertical mode of oscillation.

Tendon pull-out in horizontally curved girders

A problem has occurred relatively recently with small radius horizontally curved, post-tensioned concrete box girder bridges. It concerns the lateral force produced in the webs by the tensioning of horizontally curved longitudinal tendons.

As an example; a continuous, cast-in-place, post-tensioned concrete box girder consisted of three spans of 176, 234 and 176 feet (53.6, 71.3 and 53.6 m) with slightly over half of the eastern 176 foot (53.6 m) span aligned on a horizontal curve with a 250 foot (76 m) radius, Figure 8. In cross section the bridge is a two cell box, Figure 9. The bridge was post-tensioned with 12 draped tendons, which were continuous throughout the entire length of the structure. Four bundled tendons were placed in each web and all tendons were jacked from both ends at the abutments.

Failure occurred during prestressing operations when the 12th and last tendon, located in the north web along the inside of the curve, was near its full prestress. A loud noise, described as a "bang," was heard and all four tendons in that web broke away from the web for almost the entire length of the curved east span, tearing the curved reinforced web along the profile of the tendons, Figure 10. Two days later, the east quarter-span length of tendons broke out of the concrete web, again making a loud noise.

An immediate inspection of the structure indicated that the horizontally curved tendons, exerting a radial horizontal pressure, had overloaded the reinforced concrete webs. This overload had caused the concrete to fail, allowing the tendons to straighten-out and pull away from the webs. Additional observations indicated that the tendons continued to pull away from the webs, and the failure progressed to the abutment and pier.

In this structure there was a combination of relatively sharp curvature, thin concrete cover over the tendons and the bundling of a number of large size tendons close together. This failure is somewhat unique in that the problem would not have surfaced in the case of flatter curvature, thicker concrete cover over the tendons, or adequate spreading of the tendons into individual ducts as versus bundled ducts.

The analysis of this type of failure and suggested design methodology and details for this type of static loading are presented in Appendix A.^{3,4,5} The question to be raised in this case is similar to that presented above for vertically curved tendons. Will the dynamic loading imparted during an earthquake intensify the radial pressure produced by a horizontally curved tendon? As the superstructure oscillates laterally as a result of the earthquake input will there be a potential pull-out failure of the tendons?

Summary

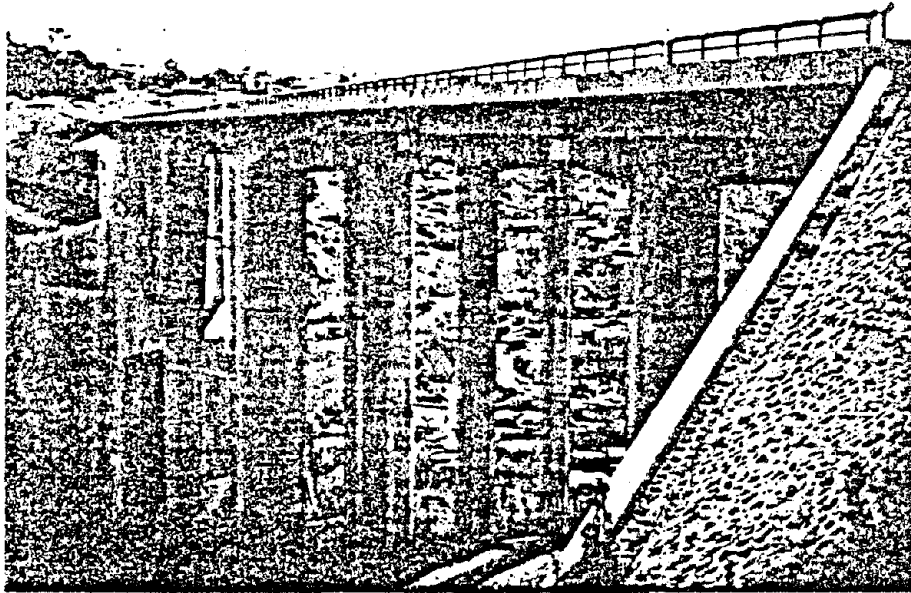
The author has presented a number of design concerns for prestressed concrete segmental bridges as they relate to potential failures from dynamically induced loading produced by an earthquake event. In some cases these concerns are equally applicable to prestressed concrete bridges constructed by more conventional methods. The intent in presenting these concerns is to hopefully generate interest in researching these concerns to determine if they are valid, and if so, to determine what procedures and methods are required to alleviate these concerns.

References

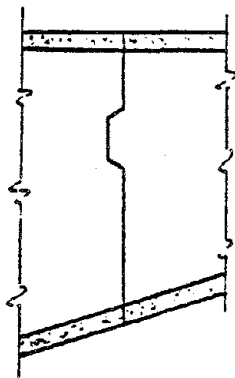
1. Cooper, James D., "Bridge and Highway Damage Resulting from the 1976 Guatemala

Earthquake," Report No. FHWA-RD-76-148, May 1976, Federal Highway Administration, Washington, D.C.

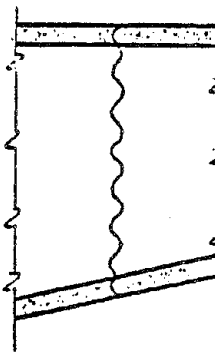
2. Podolny, Walter Jr. and Muller, Jean M., "Construction and Design of Prestressed Concrete Segmental Bridges," John Wiley & Sons, New York, 1982.
3. "Las Lomas Bridge - Causes of Structural Failure," Report to Department of the Army, San Francisco District Corps of Engineers, T. Y. Lin International, August 1979.
4. "Kapiolani Interchange On-Ramp Project No. I-H1-1(157):24," Design Review: Interim Report to Department of Transportation, State of Hawaii, T. Y. Lin International, April 1982.
5. Memo to Designers, "Curved Post-Tensioned Bridges," 11-31, November 1982, California Department of Transportation.



Inciense Bridge, Guatemala
Figure 1



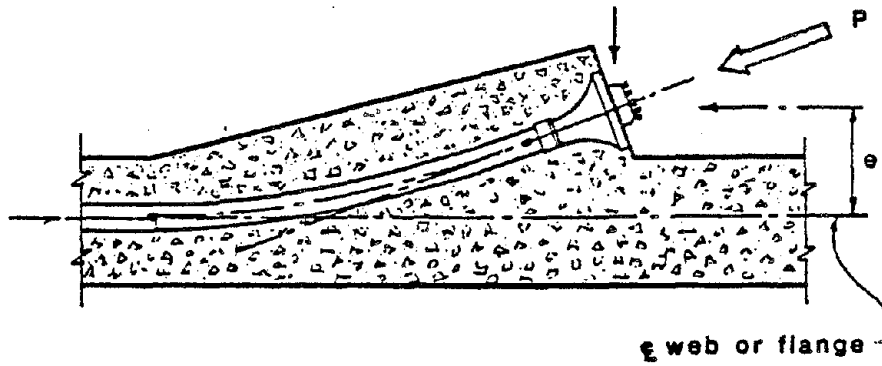
single large key



multiple small keys

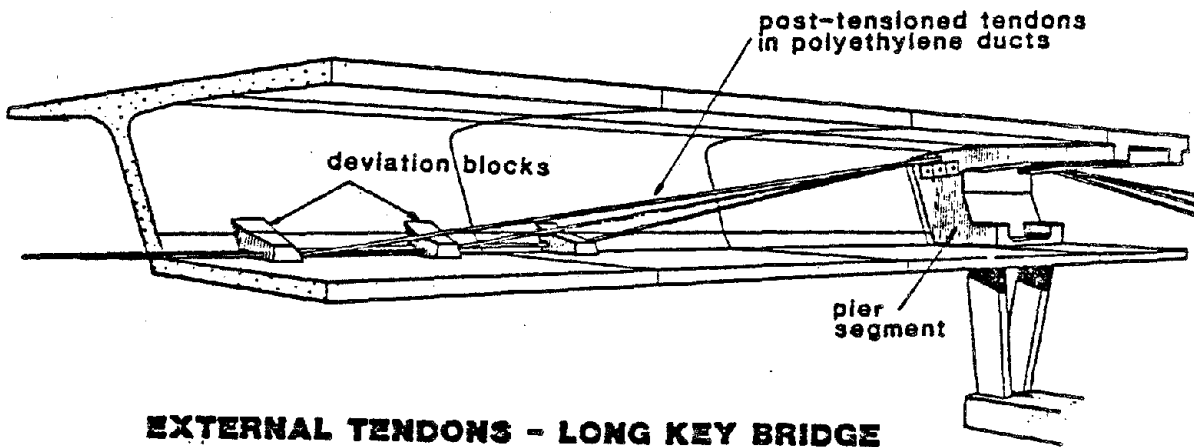
SHEAR KEYS

Figure 2



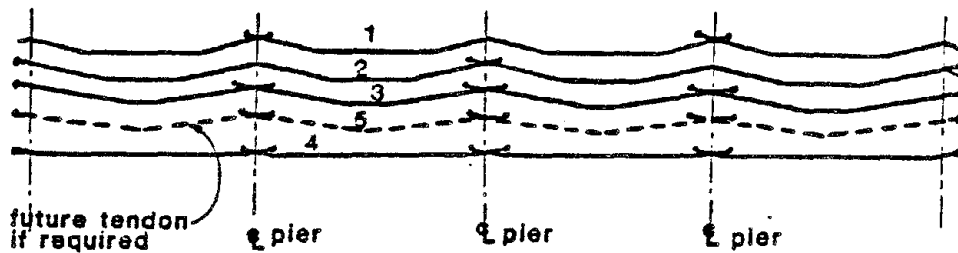
ANCHORAGE BLISTER

Figure 3



EXTERNAL TENDONS - LONG KEY BRIDGE

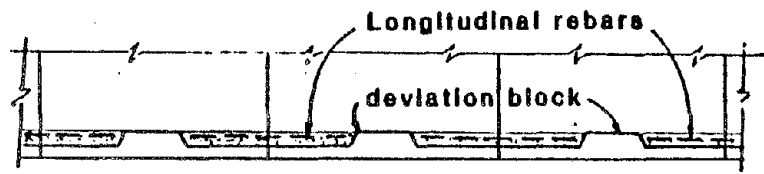
Figure 4



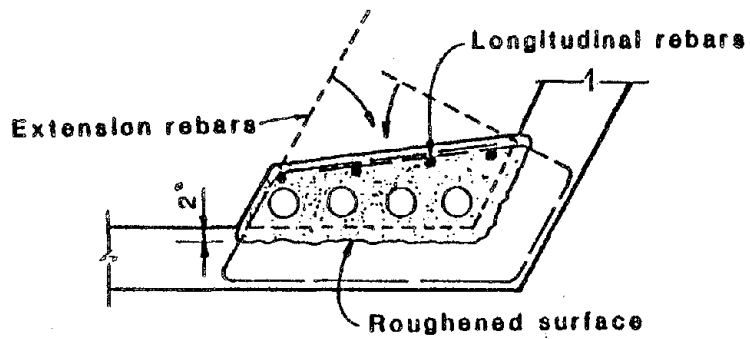
TYPICAL SCHEMATIC P.T. LAYOUT

(PER WEB)

Figure 5



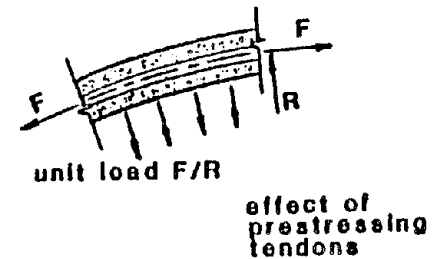
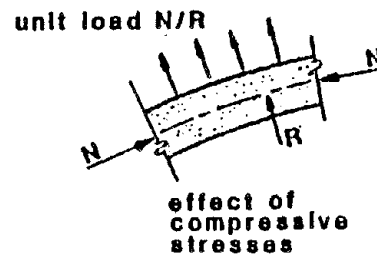
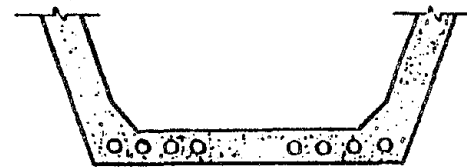
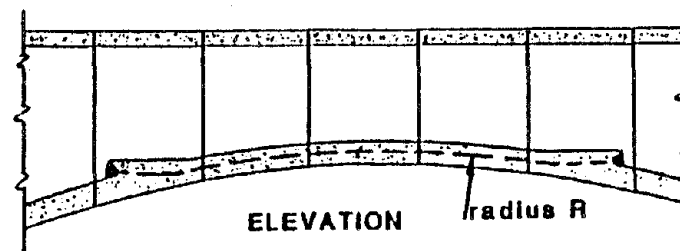
ELEVATION



SECTION

CAST-IN-PLACE ENCASING CONCRETE

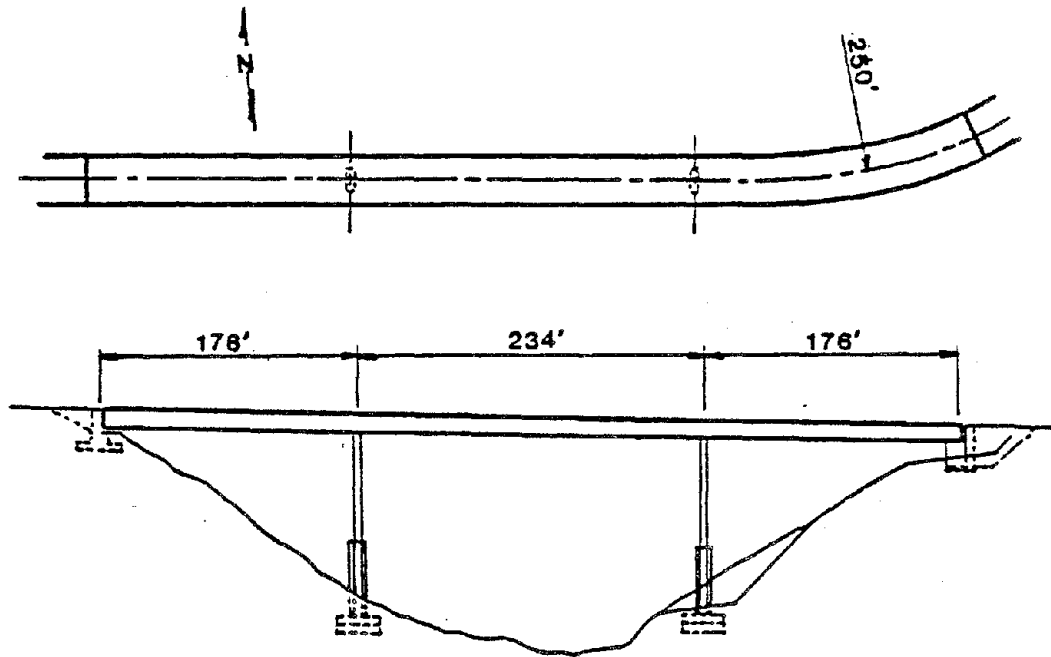
Figure 6



FREE BODY DIAGRAM

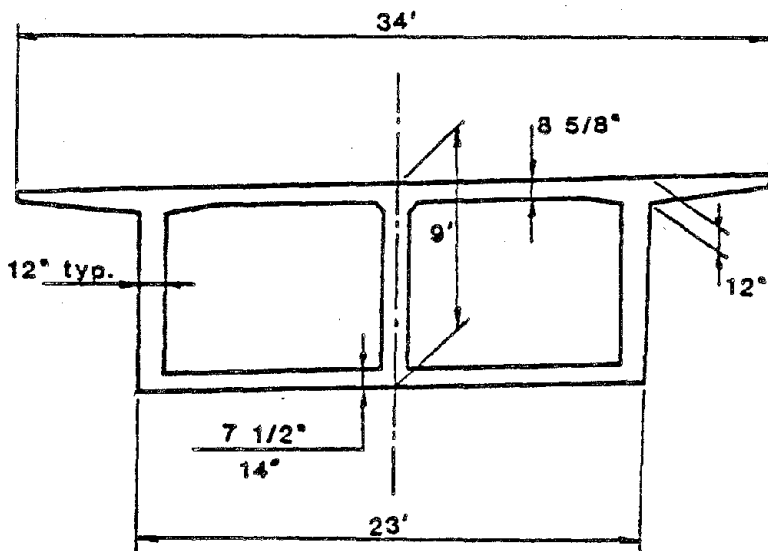
VERTICALLY CURVED TENDON

Figure 7



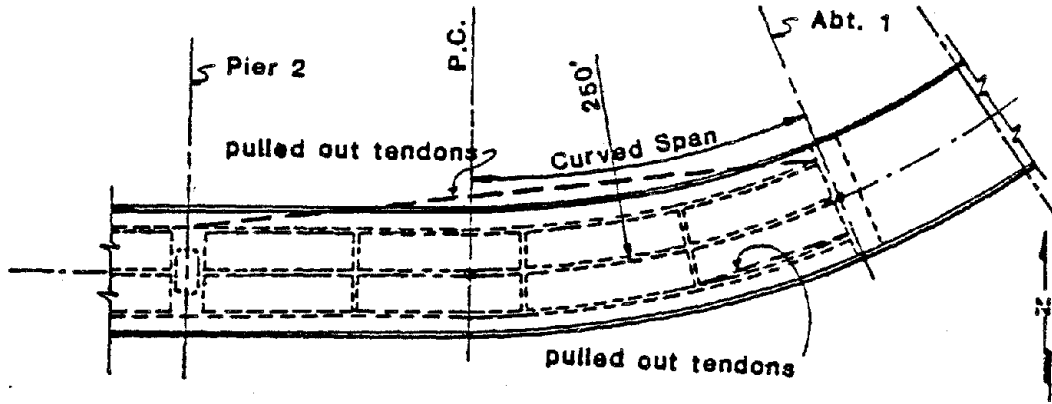
BRIDGE ELEVATION AND PLAN

Figure 8



TYPICAL CROSS SECTION

Figure 9



Partial Plan



ZONES OF WEB FAILURE

Figure 10

APPENDIX A
ANALYSIS OF
TENDON PULLOUT IN HORIZONTALLY CURVED,
POST-TENSIONED, BOX GIRDER BRIDGES

The analysis of tendon pull-out in horizontally curved post-tensioned girders can be divided into three separate actions which need to be considered in design, Figure A-1.

1. The global or overall girder action of the bridge together with its supporting piers and abutments.
2. Regional beam action of each web supported at the top and bottom flanges as a beam.
3. Local slab action of the concrete cover over the tendons.

It is important from both the analysis and the design point of view to look into all three of these actions and their effect on both the concrete and the reinforcing steel in the webs of the boxes.

Global girder action should consist of a three dimensional analysis performed for that part of the bridge under consideration as a whole. That is, between expansion joints or other discontinuities and encompassing the curved portion of the structure taking into account the loads from adjoining spans acting at the tips of cantilevers (hinge joints in a span).

One point about the global action of the girder is the restraining effect of the piers, and the bridge bearings. A curved bridge tends to shrink along certain directions, depending on the flexibility of the piers while the movement of the bearings may be restrained to take place along a different direction, thus secondary moments in the horizontal direction may be produced in the girder. From experience gained in the investigation of two such failures it has been determined that such stresses are not a major factor. Thus, it is believed that the global action, for both of the structures investigated, had only minor effects

on the failures experienced, and were not quantitatively considered.

Regional beam action considers each web as a beam supported at the top and bottom flanges, Figure A-2. This beam is acted upon by the radial force from the tendons. The radial tendon force produces shear and bending in the web, as it spans vertically. The bending moment and shear in the web are also influenced by the fact that the web concrete is under longitudinal compression from tendon prestress. This precompression has an arching effect which partly counteracts the radial force from the tendons, thus reducing the bending moment produced by the tendon force. In other words, the tendency to push radially inward by the curved tendons is counteracted to some degree by the tendency to push radially outward by the concrete.

This is shown schematically in Figure A-3. This condition of equilibrium is often taken for granted so that the local and regional effects of these forces are not normally calculated, in spite of the fact that they may be far from being balanced, depending on degree of curvature and amount of prestress tendon pressure locally or regionally. The inward pressure from the tendons is often much higher than the outward radial arch pressure from the concrete. Such a force imbalance has been resisted without failure in thousands of structures that have been constructed, although some of them may be on the verge of failure and not detected.

The stirrups in the beams are designed, as usual, to resist the vertical web shear at the ultimate range. Generally, the webs of the box do not crack under normal loadings and the stirrups are seldom called into action. On the other hand, at ultimate load, where the beam webs do crack, then the stirrups are called into full action. At that time the stirrups may or may not have excess capacity to serve as the beam flexure reinforcement for the web in the vertical direction. It appears that the stirrups should be provided to take ultimate web shear first and to resist the web-beam action in addition. In one structure, where #5 stirrups at 12 inch centers were provided, they were overstressed in beam action alone, even

without their service as shear stirrups.

Local slab action is probably the most important item that actually caused the failure in both of the structure failures investigated. The local slab action can be studied in different ways, Figure A-4. First, consider the cover as a slab two inches thick (reinforced with #5 bars along the inside face only) acting as a two-span continuous beam with a central support furnished by the concrete between the two sets of bundled tendons, as shown on the left in Figure A-4. This can be analyzed as a plain concrete beam acting in shear and in flexure. However, there is a tendency for concrete to shrink against the more rigid ducts. As a result, the tensile strength of the concrete can be entirely lost, both in the support area between bundled tendons and maybe in the two inch slab itself. Since it is not considered good practice to design plain concrete to take tension, this analysis has very little meaning.

The second analysis, shown to the right in Figure A-4, assumes that the concrete has cracked and is unable to supply tension for the support area between the bundled tendons. If this is the case, the slab will act as a single span fixed at the ends, however, the reinforcement is in one plane on the inside face only. This can offer very little resistance to the radial force from the tendons, both in bending and in shear. The stresses are exceedingly high. An extraordinarily high percentage of reinforcing steel would be required to resist such moments. Unfortunately the tendons were tied to the stirrups on the inside of the curvature, thus the stirrup reinforcement is in position next to the tendon ducts such that it does not function to resist positive moment produced by the radial forces. Thus, the concrete cover essentially is a plain concrete slab and its resistance is nil.

The order of magnitude of the stress produced by the three causes discussed, when compared to the allowable stresses in concrete or its reinforcement is approximately as follows:

- | | |
|---|------------|
| 1. for global secondary horizontal stress | 1 to 10% |
| 2. for regional bending stress | 5 to 50% |
| 3. and for local slab bending stresses | 10 to 300% |

Of course, every case is different and could fall outside of these ranges. But the percentages cited give an approximate order of magnitude.

Another important factor is the bundling of the large tendons. It appears that bundled tendons should not be used for horizontally curved bridges with a radius under 700 feet, unless proper design considerations are implemented.

It therefore appears that, for both failures investigated, the local slab action was the primary cause of failure, but the regional beam action could have been a contributory cause, and could by itself have overstressed some of the stirrups, even if not to the point of failure. The global action had a relatively small effect upon these failures.

In design of curved post-tensioned concrete box girders the designer must consider the lateral prestress force. In recognition of this problem the California Department of Transportation (CALTRANS) has prepared and implemented design guides. They have prepared charts and details to be used as a check of girder webs for containment of tendons and adequate stirrup reinforcement to resist flexural bending.

As an example, assume that the design of the girder requires a prestress jacking force (P_j) of 2900 kips per web, a radius of curvature (R) of 300 feet and a vertical inside height of web (h_c) of 6.83 feet. By dividing the jacking force (P_j) by the radius (R), a lateral prestress force (F) of 9.67 kips per foot is obtained. The first step is to enter the chart, Figure A-5, with this value (F) on the horizontal axis of the graph and traveling vertically upward until the ordinate (h_c) of web height is reached. The chart then indicates that a web thickness of 12 inches, #5 stirrups at 9 inch spacing, and tendon placement detail "A" as opposed to a "standard detail" is required. A similar set of curves, Figure A-6,

has been prepared for #6 stirrups. In cases that specify final prestress force (P_f) rather than jacking force (P_j), it may be assumed that P_j is equal to 1.25 P_f . Up to a value of lateral prestress force pressure (F) of 7.2 kips per foot, indicated by the vertical dashed line, the charts indicate a "standard" tendon placement, at this value and higher, detail "A" is required.

The "standard detail" indicated at the left of Figure A-7, as the name implies, is a standard detail for bundled tendons. Detail "A", at the right of Figure A-7, indicates that the tendons are stacked vertically and placed against the outside stirrup with respect to curvature. This is done to provide a greater thickness for local slab action and to put the inside stirrup in a position to participate as active reinforcement in the slab action.

Further, tendon detail "A" requires #4 ties between the stirrups and adjacent to the bundled tendons and a hoop around the bundled tendon hooked to the outside stirrup, Figure A-8. This then mobilizes the outboard stirrup and the central concrete area behind the inboard stirrup in participating in resisting the pull-out of the tendons.

The application of these guides are based upon the following assumptions:

1. The girder web is assumed to be a beam with a length equal to the clear distance between top and bottom flanges.
2. The lateral prestress force is assumed acting at mid-height of the web.
3. The moment is calculated by simple beam formula reduced 20 percent for continuity between web and flanges with a 1.0 load factor applied.
4. The shear and bending stresses in the web stirrups are additive.

However, for the purpose of these design aids the stirrups are considered capable of handling these stresses independently for the following reasons:

- a) The ultimate moment is calculated for the maximum condition of

the lateral prestress force (F) acting at mid-height of the web span. This occurs at only two points in a span due to tendon drape

- b) The jacking force (P_j) is used in the calculations of ultimate moment, and at the time P_j is applied, the structure is supported on falsework. When the falsework is removed and vertical shear forces act, the prestressing force has been reduced by losses.

It appears that these details should be incorporated in the design of horizontally curved post-tensioned girders which have a radius of approximately 700 feet or less.

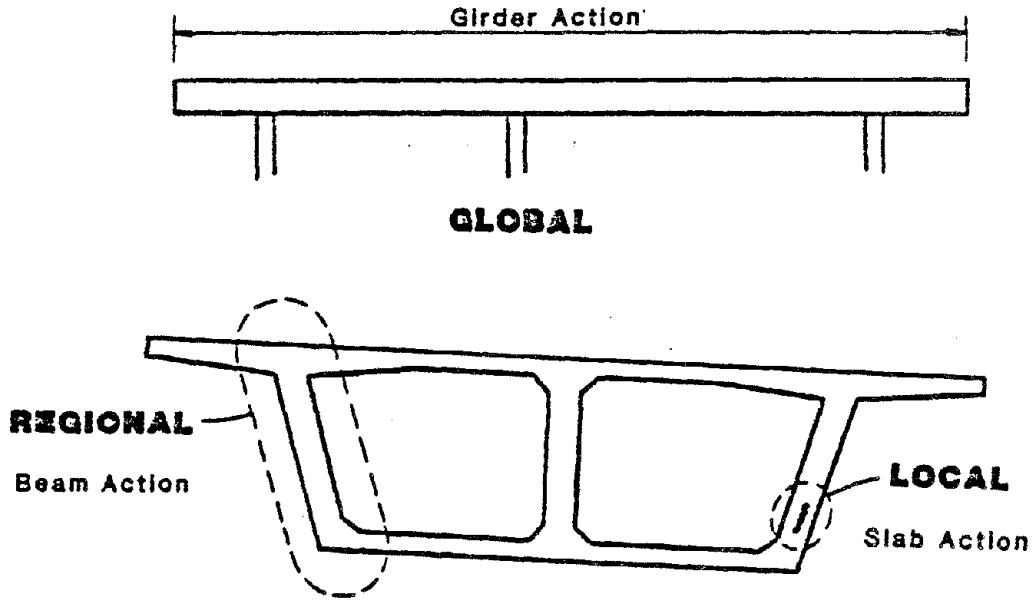
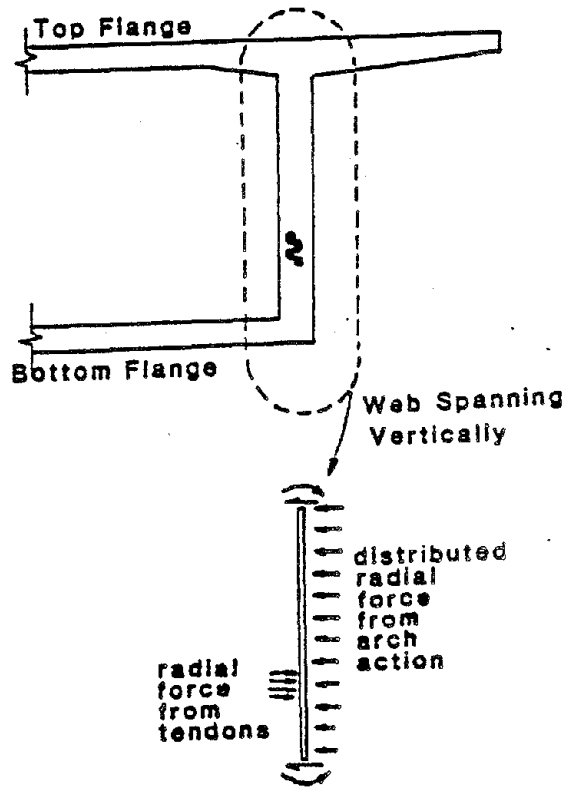
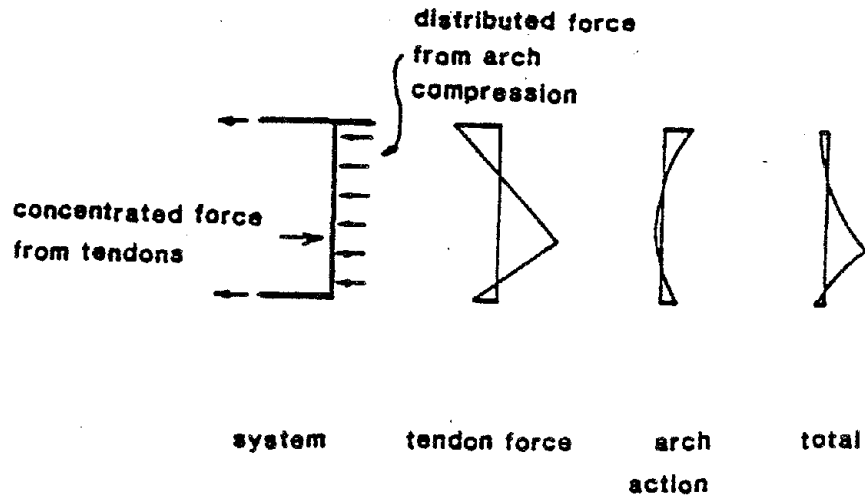


Figure A-1



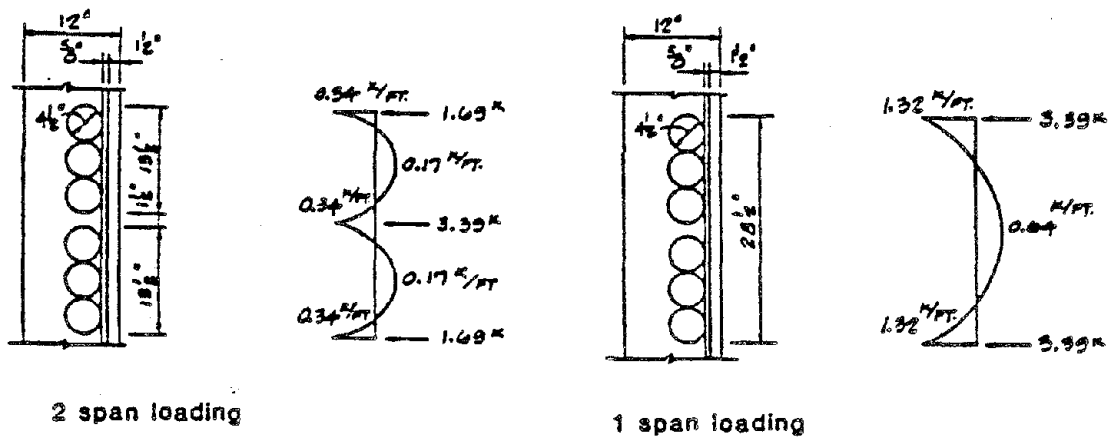
VERTICAL SPAN OF WEB

Figure A-2



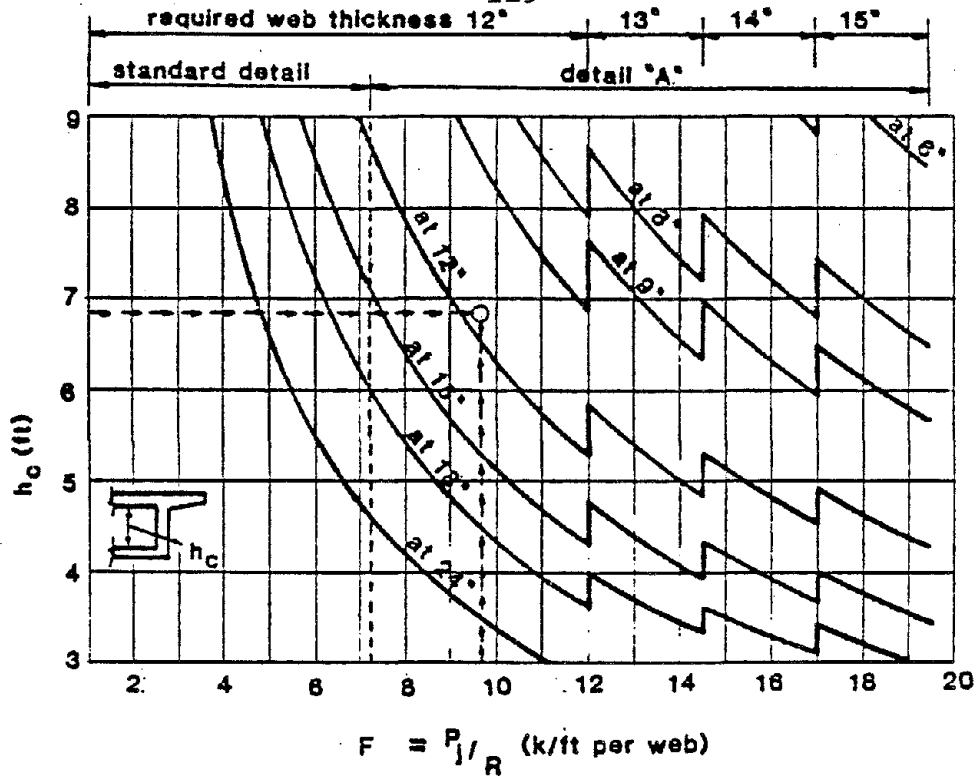
MOMENTS IN VERTICAL SPAN OF WEB

Figure A-3



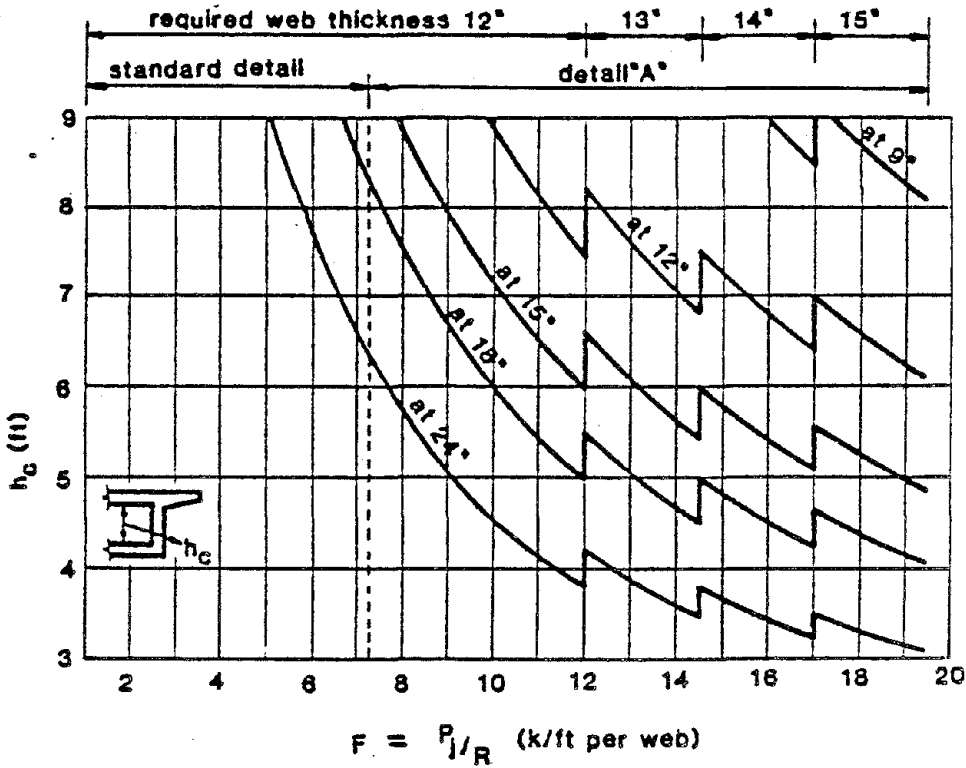
SLAB ACTION

Figure A-4



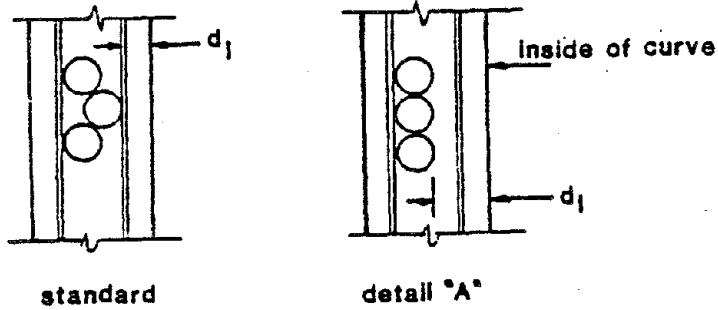
#6 STIRRUPS

Figure A-5



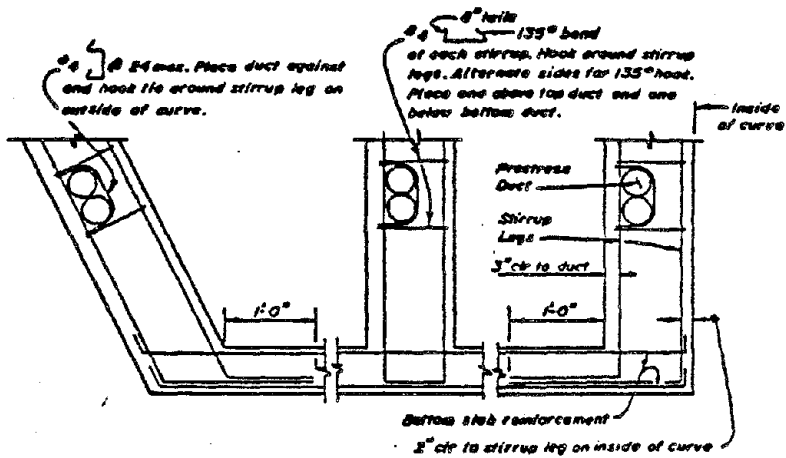
#6 STIRRUPS

Figure A-6



TENDON PLACEMENT DETAILS

Figure A-7



TENDON PLACEMENT DETAIL "A"

Figure A-8

BOX GIRDER BRIDGE HINGE RESTRAINER
TEST PROGRAM

Lawrence G. Selna¹
L. Javier Malvar²

SUMMARY

Full scale structural testing of bridge components with earthquake inputs has been missing from experimental research programs in the USA. Facilities that are required must be substantial, but they can be developed at University and National Laboratories. Bridge structural components have geometric size and strength capabilities that are comparable in magnitude with full scale building components.

A structural test facility which accommodates full scale bridge component specimens has been constructed at UCLA. The initial experiments conducted using the facility focus on testing the restrainers which are used to retrofit box girder highway bridges. The restrainers are installed so that hinge separation is prevented during earthquakes.

INTRODUCTION

Background

Post-earthquake investigations of box girder highway bridges after the 1971 San Fernando Earthquake (Ref. 1) showed that the decks pulled apart at the hinge and bearing seat locations. In 1980, two box girder spans of the Fields Landing Overhead near Eureka, California dropped when the hinge seats opened during the Trinidad-Offshore Earthquake (Ref. 2).

By the end of 1982 a significant amount of bridge strengthening or retrofitting had been performed by the State of California, Department of Transportation (CALTRANS). The unrestrained joint seats represent the prime focus of the CALTRANS retrofit program (Ref. 3). Six hundred ninety bridges out of 1240 identified as deficient had joint restrainers installed by that time.

Two types of longitudinal restrainers used for retrofitting are favored by CALTRANS bridge engineers (Ref. 4): 1) the Type C1 Hinge Restrainer consists of 7-3/4"φ galvanized cables, bearing plates, and drum, and 2) the restrainer bar is a 1 1/2"φ high strength steel rod satisfying ASTM A-722 (Ref. 5). Both types of hinge restrainers are under investigation in experimental test programs (Ref. 6,7).

-
1. Professor, Department of Civil Engineering, University of California, Los Angeles, California, USA
 2. Research Assistant, Department of Civil Engineering, University of California, Los Angeles, California, USA

The structural configuration of the hinge region of a box girder bridge is shown in Fig. 1. The box girder bridge is hollow and so it is possible for workmen to enter existing construction for installation of the restrainers. A cable installation is shown in Figs. 1 and 2. A rectangular cross section called a bolster (Ref. 8) is added to thicken the hinge diaphragm (Fig. 1) so that punching shear failures are avoided.

A retrofitted hinge seat subjected to an opening displacement experiences a complicated distribution of stresses in the bolster, hinge diaphragm, webs, soffit slab, and deck slab that are adjacent to the restrainer. The restrainer carries a tension force which causes it to lengthen. As the opening displacement becomes larger and the tension forces increase then there is an increased likelihood of failure. CALTRANS bridge engineers have selected the restrainer properties so that the failure is likely to occur in the restrainer instead of the hinge diaphragm or adjacent components.

Soon after the 1971 San Fernando Earthquake it was decided (Ref. 9) that longitudinal hinge restrainers should be capable of resisting a minimum force equal to 25% of the weight of the lighter segment joined. Bridge designs at the time were based on working stresses. The reduction of force in the restrainers due to shears carried in the piers was neglected in the design procedure.

When load factor design methods are used almost identical results are obtained using 33% of the dead load (Ref. 6). Recently, CALTRANS bridge design specifications (Ref. 10) have adopted use of the actual ground acceleration at the site with a minimum 35% value. The loads based on the controlling acceleration are applied to the bridge structure allowing the columns to carry their share. Restrainers are designed to carry the remaining forces at the joints.

The longitudinal restrainer design force values were established more from judgement than from analysis. Dynamic analyses using linear and non-linear mathematical models have been performed (Ref. 11) on curved bridges fitted with hinge restrainers, but there is some question concerning the veracity of the results. The computer representations of the longitudinal force-deflection properties of restrained hinge seats has not been verified by experimental testing. Structural dynamic analysis computer programs use the hinge seat force-deflection properties so that the effect of the retrofitted hinge seat is represented in the model. If the computer representation of the force-deflection were confirmed then designers would have greater confidence when using the structural dynamic idealization of the bridge. The required longitudinal restrainer design force in terms of dead load percentage could be established with a verified force-deflection relation, and then used in subsequent bridge designs.

Objective

The objective of the present paper is to discuss the box girder bridge restrainer test program. The development of the testing facilities, equipment, and specimens at UCLA is emphasized.

FACILITIES AND EQUIPMENT

Reaction Frame

A reinforced concrete reaction or loading frame composed of a test bed and two reaction blocks is capable of resisting 1500 kips (6666 kN) and is depicted in Figs. 1 and 2. A bridge specimen's anchor bars are shown protruding through the west reaction block of the loading frame in Fig. 3. Alternating tension-compression forces up to 1500 kips (6666 kN) can be applied to full scale bridge components. The 4 ft (1.22 m) thick reaction blocks have numerous 3 in. (7.6 cm) diameter pipe passages used for tension anchors which restrain the actuators and components to be tested. The 32 ft (9.75 m) clear distance between the reaction blocks permit static and dynamic structural testing of components up to 22 ft (6.71 m) in length.

The test bed section of the reaction frame extends 4 ft. (1.22 m) below grade. At the location of the reaction blocks the test bed is thickened to 6 ft (1.82 m) to provide sufficient anchorage distance for the vertically oriented flexure reinforcement in the reaction blocks. The test bed is extended 5 ft (1.52 m) outside of the reaction blocks so that the longitudinal reinforcement of the test bed is sufficiently anchored.

Twenty-one "tie-downs", positioned in a 3 x 7 grid with 4 ft (1.22 m) intervals in both directions, are embedded in the test bed between the reaction blocks. A 4 in x 8 in (10.2 cm x 20.3 cm) rectangular cross section shaft extends 4 ft (1.22 m) deep into the bed. The shaft then enlarges to a 12 in (30.5 cm) diameter and extends 15 in (38.1 cm) deeper to a total depth of 63 in (160.0 cm). The top of the shaft is at grade level while the top of the cavity is located below the test bed reinforcement. The "tie-downs" are used to hold actuators which in turn impart vertical and horizontal shears to specimens. For example, a specimen with one end anchored to the east reaction block can have its other end subjected to two components of shear in addition to an axial force component generated by an actuator affixed to the west reaction block.

The test bed and reaction blocks were constructed as a class project by undergraduate and graduate engineering students of the School of Engineering and Applied Science, University of California, Los Angeles between October 1982 and June 1983. Excavation necessary for the test bed was performed by a private contractor.

Grade 60 reinforcing steel is used throughout the installation. Top and bottom reinforcement in the test bed consists of 18 - #14 bars at both elevations. Three 50 ft long cages with 70 - #4 stirrup ties and 10 or 11 - #14 bars in each cage were fabricated above grade. Before lowering the cages into the test bed the tie-down forms were installed between the longitudinal bars from below.

The flexure reinforcement for each reaction block consists of 36 - #9 "U" bars with the tails pointing downward. The "U" bar tails penetrate through the horizontal #14 bars of the test bed. Horizontal cross ties are used for shear reinforcement and for prevention of buckling of the

#9 U flexure bars. Vertical shear reinforcement is also placed in the reaction block. Transverse horizontal #9 bars are also placed on the wide faces of the reaction blocks so that concentrated forces are distributed to the #9 "U" bars.

The concrete was placed in two separate pours: 1) 100 yd³ of 7.5 scy stone concrete was cast against excavation for the test bed, and 2) 20 yd³ of 7 scy concrete with superplasticizer donated by Conrock, Inc., Los Angeles, was cast in forms for the reaction blocks. Both concretes reached 28 day compressive strengths in excess of 5000 psi.

Actuators and Controllers

One 18 in (45.7 cm) diameter by 12 in (30.5 cm) stroke actuator and two 12 in (30.5 cm) diameter by 24 in (61.0 cm) stroke actuators are used in the testing. They are controlled by Moog servovalves and controllers. A 5 HP pump drives the system with a maximum speed of 1 in/min (2.54 cm/min).

SPECIMENS

Bridge Test Components

The hinge region of a box girder bridge in service is duplicated by the components which are constructed for testing. All structural properties that are used by CALTRANS (Ref. 10) including dimensions and material properties are matched during the construction of the bridge components for testing.

The dimensions used in old construction are the same for most bridges. Only the cross section depth is changed for different span lengths. The thicknesses used in the test components are as follows: 1) webs or stems - 12 in (30.5 cm); 2) hinge diaphragm - 10 in and 25 in (25.4 cm and 63.5 cm); 3) bolster - 9 in (22.9 cm); 4) soffit slab - 5.5 in (14.0 cm); and 5) deck slab - 7.5 in (19.1 cm). The bridge component length dimension on each side of the hinge is 10 ft (3.05 m) making a total length of bridge that is represented equal to 20 ft (6.10 m). The bridge component width used in the test is 10 ft (3.05 m) which is equivalent to the distance between webs or stems of an actual bridge. The height of the test component is 4 ft (1.22 m). All except the height dimension are standardized box girder bridge dimensions.

The concrete proportions used in the bridge test components follow the CALTRANS specifications in force during the 1950-1970 period, i.e. the cement content is 6 sacks per cubic yard, 1½ in (3.81 cm) is the max aggregate size, and the design slump is 4 in (10.2 cm). The design f'_c is 3250 psi (22.39 MP). The concrete is placed in three separate pours in accord with CALTRANS procedure as follows: 1) soffit slab, stems, and hinge diaphragm, 2) deck slab, and 3) bolster. The same forms are used for the east and west test components.

Grade 60 reinforcement is used in the tested components. The reinforcement configuration is shown in Fig. 4. For the cable restrainer test

20 - #14 bars are used to anchor the west bridge component to the reaction block (Fig. 3). The anchor bars are necessary because of the projected 750 kip (3,333 kN) cable strength. A similar number is used to join the east bridge test component to the actuators (Figs. 1 and 2). The large anchor bars are spread outward to the stems in the hinge region so that only the standard reinforcement (Refs. 4,8,10) of the hinge diaphragm and bolster remain at that location (Fig. 4). Therefore an accurate experimental representation of the hinge diaphragm is obtained.

Type C1 Hinge Restrainer

The Type C1 Hinge Restrainer (Ref. 4) consists of 7 - 3/4 in (1.91 cm) ϕ cables which lash the hinge diaphragms together (Figs. 1 and 2). The seven cables are anchored on the face of the west bolster, pass through both hinge diaphragms, wrap around a drum located on the face of the east bolster, pass back through the second hole, and are anchored again on the west bolster. The cables are swaged to 1 in (2.54 cm) studs which pass through a plate for the anchorage.

Restrainer Bars

Two 1.25 in (3.18 cm) restraints are installed through both hinge diaphragms at two transverse locations. The ends of the bars are threaded for anchorage nuts.

TESTING ARRANGEMENT

The test arrangement is indicated in Figs. 1 and 2. The west test component is fixed to the west reaction block by the anchor bars which have the ends threaded. The bars pass through the reaction block and are held with washers and nuts. The east test component rolls on solid steel round stock. The rounds bear on steel strip rails embedded in the test bed and the east bridge test component so that frictionless motion occurs. The strip rails were leveled (Fig. 5) so that gravity does not affect measured test results.

The completed hinge seat and adjoining east and west bridge components are shown in Fig. 6. The anchor bars of the west component can be seen protruding through the reaction block.

Servo-controlled actuators are mounted to the east reaction block (Fig. 7). Steel fittings join the actuators to the anchor bars of the east test component so that the test component is moved by the jacks. Load cells are used to measure the jacking force. Three LVDT's are mounted across the hinge joint in order to measure and assist in controlling the opening displacement. The experiment is conducted so that the displacement history of the opening is controlled at all times.

CALIBRATION

Displacement transducers are easily calibrated using dial gages, but the force calibration is difficult. The 750 kip (3,333 kN) forces which are present during the test to failure require the use of heavy steel

shafts which connect the jacks to the east component of the specimen. One 5 in (10.2 cm) and two 4 in (12.7 cm) diameter shafts used for pulling also serve as load cells. The load cells are calibrated while installed but the specimen is left unloaded during the calibration. A temporary reaction system consisting of 4 calibrated 2½ in diameter rods and pipe joining two "strongbacks" mounted behind the pulling yoke (Fig. 7) has been prepared. The jacks and shaft pull against the yoke which is anchored by the "strongbacks". The 5 in diameter pipe and 24 in WF beams used in the temporary reaction system are shown in Fig. 8. After the calibration is completed the temporary reaction system is removed and the cable restrainer is installed in the specimen for testing.

CONCLUSION

The testing program for reinforced concrete box girder hinge restrainers is underway in the Department of Civil Engineering at the University of California, Los Angeles. Full scale box girder bridge test components and prototype restrainers used in the CALTRANS earthquake retrofit program are subjected to cyclic loadings which represent seismic inputs.

A reaction frame capable of accommodating the large dimensions and forces of the bridge test components and restrainers has been constructed. The reaction blocks and test bed of the reaction frame can impart three dimensional force distributions to full scale bridge components to be tested.

ACKNOWLEDGMENTS

The bridge testing program is possible because of the help and cooperation supplied by many groups and individuals.

Funding was provided by National Science Foundation Grant CEE-8207543 and State of California, Department of Transportation Research Technical Agreement Number RTA 13945.

Technical guidance for the work was given freely by CALTRANS bridge engineers Oris Degenkolb, Ray Zelinski, and James Gates of the Office of Structures Design.

The Engineering Shops of the School of Engineering and Applied Science at UCLA have contributed substantially to the program through the production of parts, purchasing of supplies, and operation of the construction crane. Mr. Joseph Becker has made the work go forward because of his energy. Mr. John Langholff has contributed machining and welding skills to the project.

Mr. Dean White of Conrock, Inc. of Los Angeles has supplied vital information on concrete properties to the project and on several occasions visited and worked at the test site. Guy F. Atkinson Company has loaned a concrete bucket to the project so that concrete placement is feasible.

Senior engineering students earned laboratory credit while working on the project during academic quarter periods. The students are David Bek, Charles Suszko, Scott Pickles, Sandor Hasznos, Susan Helmstetter, John

Mayall, David Flattum, Richard Steeb, Jameel Akhrass, Thomas Hickey, Julian De La Torre, Robert Troy, Duane Ashton, and Richard Bernard. Their contributions are appreciated.

REFERENCES

1. Murphy, L.M. (Coord.), "San Fernando, California, Earthquake of February 9, 1971," v. II Utilities Transportation, and Sociological Aspects, Supt. of Doc., USGPO, Wash., D.C. 20402.
2. Imbsen, R., "Trinidad-Offshore California Earthquake, Structural Damage to Bridges, November 8, 1980," EERI Newsletter, EERI, Berkeley, CA, 2/81.
3. "ATC-12 Comparison of United States and New Zealand Seismic Design Practices for Highway Bridges," Applied Technology Council, Palo Alto, CA, August 1982.
4. MEMO TO DESIGNERS: Number 21-18, "Hinge and Bearing Restrainers," Office of Structures Design, CALTRANS, Sacramento, CA.
5. 1982 Annual Book of ASTM Standards, Part 4, ASTM A722-75, "Uncoated High-Strength Steel Bar for Prestressing Concrete," ASTM, Philadelphia, PA.
6. Selna, L.G., "Seismic Testing of Full Scale Box Girder Bridge Hinge Cable Restrainers," NSF Project Number CEE-8207543, NSF, Washington, D.C.
7. Selna, L.G., "Seismic Testing of Full Scale Box Girder Bridge Hinge Seats Retrofit with Restrainer Bars," State of California, Department of Transportation Research Technical Agreement Number RTA 13945-G13798.
8. Degenkolb, O., Concrete Box Girder Bridges, Iowa State University Press, Ames, Iowa, 1977.
9. Degenkolb, O., "Retrofitting of Existing Highway Bridges Subject to Seismic Loading - Practical Considerations," Proceedings of a Workshop on Earthquake Resistance of Highway Bridges, ATC 6-1 Report, Palo Alto, CA, 1979.
10. Bridge Design Specifications, Section 1.2.20, CALTRANS, Sacramento, CA, October 1981.
11. Imbsen, R., Nutt, R., and Penzien, J., "An Investigation of the Effectiveness of Existing Bridge Design Methodology in Providing Adequate Structural Resistance to Seismic Disturbances, Phase VI: Seismic Response of Bridges - Case Studies," Report No. FHWA-RD-78-157, Federal Highway Administration, Office of R&D, Wash., D.C. 20590, October 1978.

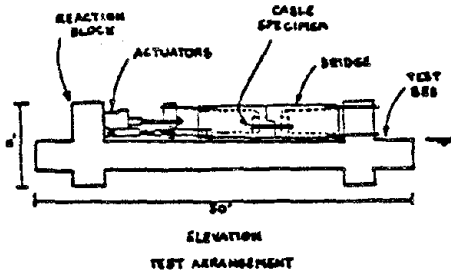


Fig. 1 - Elevation View of Bridge and Reaction Frame

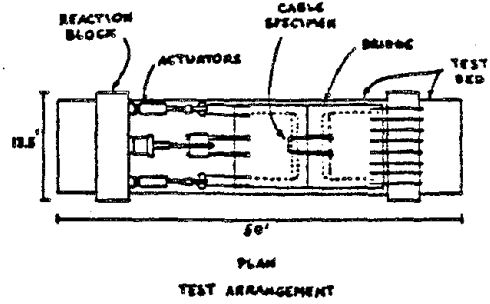


Fig. 2 - Plan View of Bridge and Reaction Frame

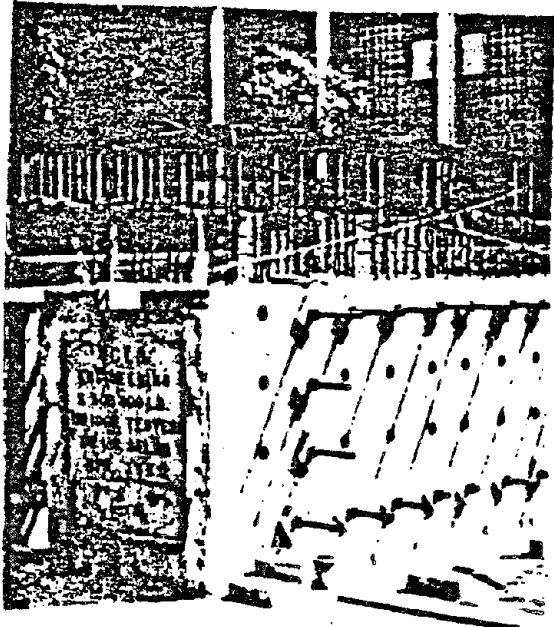


Fig. 3 - Bridge Component Installed in Reaction Frame

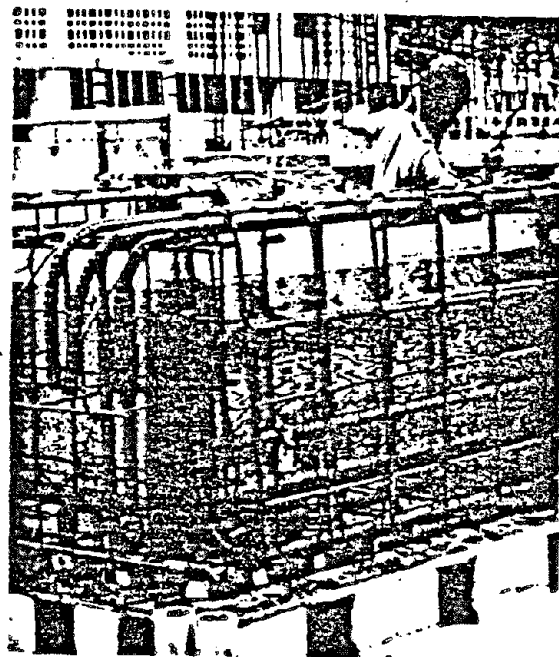


Fig. 4 - Reinforcement for Box Girder Hinge Component

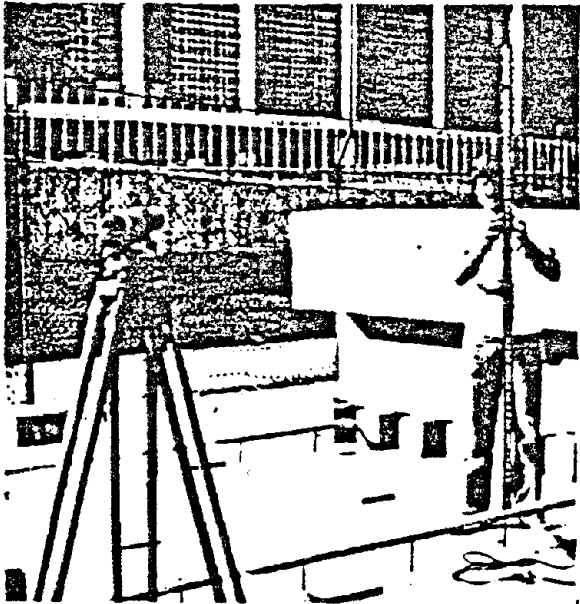


Fig. 5 - Strip Rails for
East Bridge Component
Are Levelled

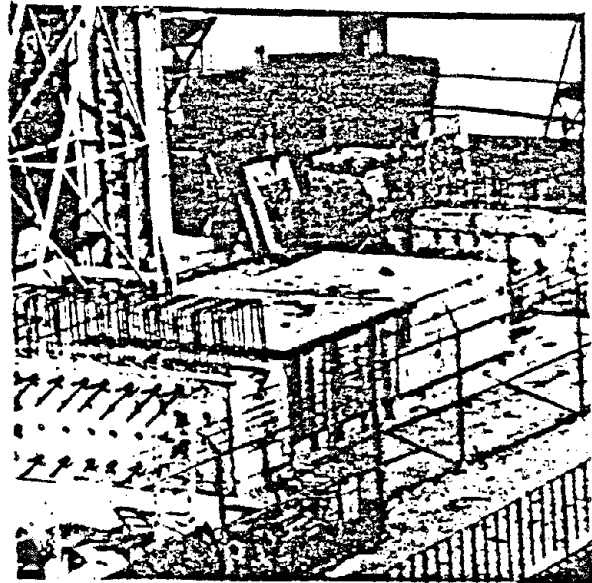


Fig. 6 - Completed Hinge
Seat and Adjacent
Components

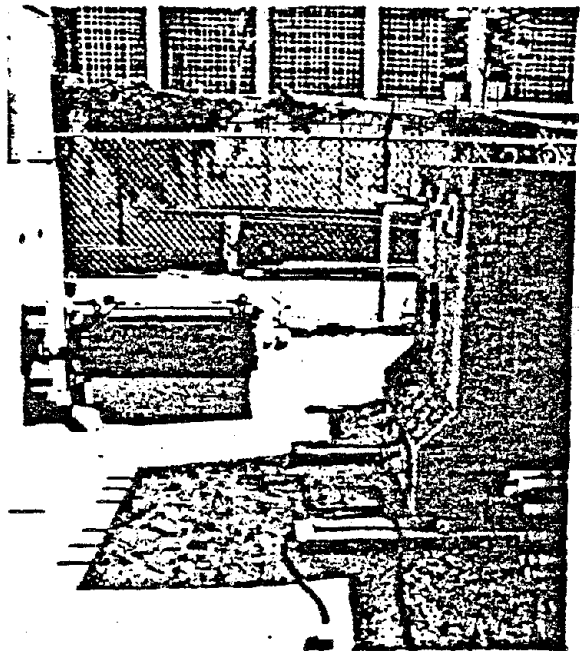


Fig. 7 - 12 in Diameter
Actuator Mounted on
East Reaction Block
and Pulling Yoke Attached
to Specimen

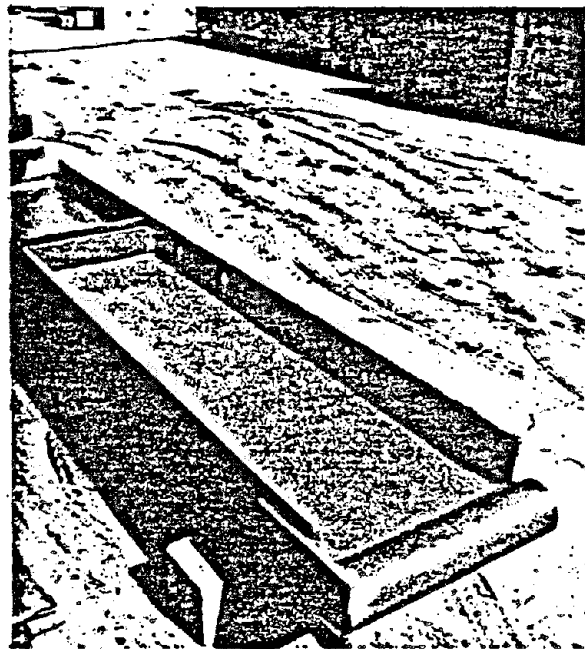
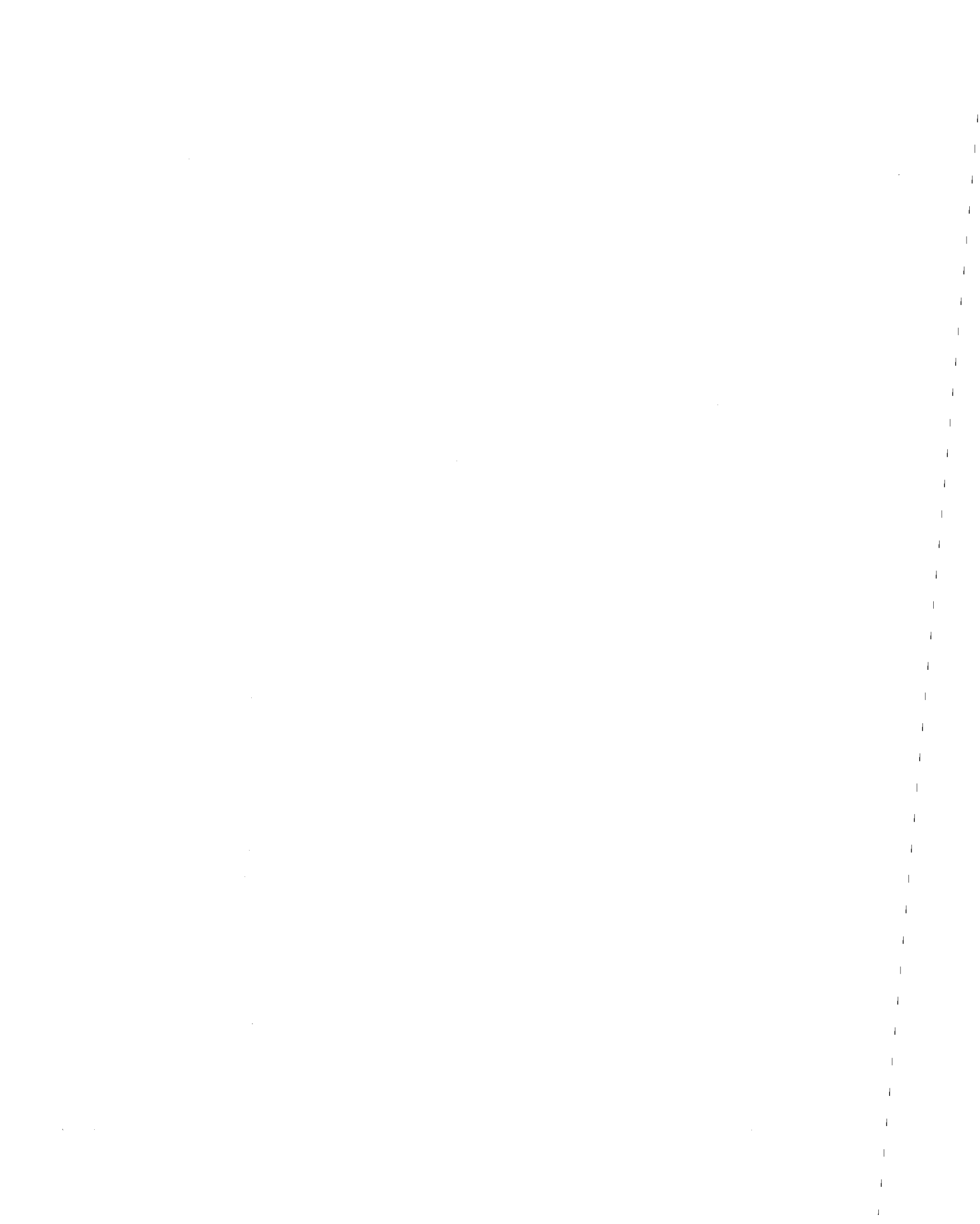


Fig. 8 - "Strongback" Beam
and 5 in (12.7 cm) D
Pipe Used in Force
Calibration



**MODEL EXPERIMENTS ON DYNAMIC BEHAVIOR
OF REINFORCED CONCRETE BRIDGE PIER COLUMNS**

By

Toshio Iwasaki, Dr. Eng., Head
Ryoji Hagiwara, Research Engineer
Kinji Hasegawa, Research Engineer
Tatsuhiko Koyama, Research Assistant
Takeshi Yoshida, Research Assistant
Earthquake Engineering Division
Earthquake Disaster Prevention Department
Public Works Research Institute
Ministry of Construction

ABSTRACT

An experimental research program on dynamic behavior of reinforced concrete bridge pier columns using the dynamic structural experimental facility at the Earthquake Engineering Laboratory of the Public Works Research Institute started in 1981. Following preliminary tests conducted in 1981, reversed cyclic loading tests of reinforced concrete bridge pier column models with different longitudinal reinforcement ratios were performed in 1982.

The length scale ratio of the models to the prototype for a Japanese typical bridge pier column was taken about 1/5. The longitudinal reinforcement ratios of the three types of model were $P_g = 1.79\%$, 0.87% , and 0.48% . Reversed cyclic displacements of ten cycles with an amplitude of $n\delta_y$ (δ_y : yield displacement, $n = 1, 2, 3, 4, 5, \dots$) were applied to the top of the column. The loading was static and dynamic (sinusoidal waves with a velocity amplitude of 25 cm/sec). The models were flexurally failed with concrete crush and longitudinal reinforcement cut at the bottom of the column. Displacement ductility factors μ (= ultimate displacement/yield displacement) of the three types of column were about $\mu = 4$ for $P_g = 1.79\%$ (tensile reinforcement ratio: $P_t = 1.02\%$), $\mu = 7$ for $P_g = 0.87\%$, ($P_t = 0.50\%$), and $\mu = 10$ for $P_g = 0.48\%$ ($P_t = 0.27\%$). The ductility factor increased as the longitudinal reinforcement ratio decreased.

1. OUTLINE OF THE EXPERIMENT

The setting of the specimen and actuator is shown in Fig. 1.1.

1.1 Specimens

Specimens of typical reinforced bridge pier column models used in the experiment are shown in Fig. 1.2. The scale of the specimens was about 1/5 of the prototype bridge pier column. Dimensions of the specimen columns were height of 2.4m, cross section of 0.4m × 0.8m, and shear-span ratio h/d of 6.9 (h = column height = 2.4m, d = effective depth of the section in the loading direction = 0.35m).

Three types of specimen with a longitudinal reinforcement ratio of $P_L = 1.79\%$ ($P_T = 1.02\%$, Type A), $P_L = 0.87\%$ ($P_T = 0.50\%$, Type B), and $P_L = 0.48\%$ ($P_T = 0.27\%$, Type C) as shown in Table 1.1 and Fig. 1.3 were considered in the experiment. The tensile reinforcement ratio of most bridge pier columns in Japan ranges from 0.25% to 1.0%. Type B column represents a common bridge pier column. Type A column represents a high-longitudinal reinforcement ratio bridge pier column, and Type C column does a low-longitudinal reinforcement ratio column.

1.2 Measuring

Measuring items are listed in Table 1.2. Lateral loads at the column top and lateral displacements at the top and middle of the column were measured. Uplift and sinking (rotation) of the column were measured at the column bottom where a plastic hinge was to be formed. Strains of longitudinal reinforcements and hoops were measured at the bottom of the column. In the case of static loading test, peak and residual crack widths were measured. In the case of dynamic loading test, accelerations were measured at the top of the column to estimate inertia forces for the modification of measured lateral loads.(Fig. 1.4).

1.3 Loading

Static and dynamic lateral loads were applied at the top of the column by an actuator. load of superstructures acts on a bridge pier column, the axial load was not applied to the 125mm of the maximum stroke, and ± 1 m/sec of the maximum velocity with a frequency range of DC-30 cycle/sec.

The loading history is shown in Fig. 1.5. Up to the yield of the column, the load was increased step by step (10 steps). After the yield of the column, 10-cycle displacements with an amplitude of δy (yield displacement), $2\delta y$, $3\delta y$, $4\delta y$, $5\delta y$, were applied. In the case of dynamic loading test, the input motion was sinusoidal waves, and the loading velocity amplitude was 25 cm/sec. Though an axial stress of 5 Kg/cm² — 20 Kg/cm² by the dead load of superstructures acts on a bridge pier column, the axial load was not applied to the specimen column in the experiment.

2. TEST RESULTS

2.1 Results of the Material Test

Results of the material test are shown in Table 2.1 and Table 2.2.

2.2 Failure Mode

Failure modes of the columns by the dynamic loading are shown in Fig. 2.1. The figures show the state of the column after the 10th-cycle ($n = 10$) loading of each step. The failure modes of the columns by the static and dynamic loading were similar. The development of a failure was as follows:

Type A: horizontal crack → diagonal crack (at $3\delta y$) → cover concrete spalling (at $4\delta y$) → longitudinal reinforcement cut (at $4.5\delta y$, finally two reinforcements were cut at $4.5\delta y$)

Type B: horizontal crack → diagonal crack (at $5\delta y$) → cover concrete spalling (at $6\delta y$) → longitudinal reinforcement cut (at $7\delta y$, finally two reinforcements were cut at $7\delta y$)

Type C: horizontal crack → separation between the column and footing (partial cover concrete spalling) → longitudinal reinforcement cut (at $9\delta y$, finally four reinforcements were cut at $10\delta y$).

The damage (diagonal crack, cover concrete spalling, longitudinal reinforcement cut) developed at the bottom of the columns. In the low-longitudinal reinforcement ratio column (Type C), significant diagonal cracks and cover concrete spalling did not occur.

Until the spalling of cover concrete (crushing of concrete) following diagonal cracks, Type A and Type B columns held strength larger than the yield load. After the cover concrete spalling, longitudinal reinforcements were cut and the column strength decreased remarkably. Type C columns held strength larger than the yield load until the cut of longitudinal reinforcements following the separation between the column and footing. After the cut of longitudinal reinforcements, the column strength decreased remarkably.

Cover concrete spalling occurred in a region of $1.5D$ for Type A columns and that of D for Type B columns, where D is the column width (40 cm) in the loading direction, above the column bottom. In Type C columns, cover concrete spalling occurred partially at the column bottom. The cover concrete spalling region (plastic hinge region) got wider as the longitudinal reinforcement ratio increased.

2.3 Strength and Ductility

Load-displacement envelope curves obtained by the static and dynamic loading tests are shown in Fig. 2.2. Performance of the columns is shown in Table 2.3 and Fig. 2.3.

The higher the longitudinal reinforcement ratio was, the larger the yield load, ultimate load (maximum load), yield displacement, and ultimate energy were. The ultimate load was 10 — 30% larger than the yield load. Displacement ductility factors μ ($= \delta u / \delta y$) were about 4 for Type A columns, 7 for Type B columns, and 10 for Type C columns. The lower the

longitudinal reinforcement ratio was, the larger the displacement ductility factor was.

Though the results of the static and dynamic loading tests were almost the same, the ultimate load, ultimate displacement, displacement ductility factor, and ultimate energy in the dynamic loading test were slightly larger than those in the static loading test. The difference between the dynamic and static ultimate loads was 5% for Type A column, 5% for Type B column, and 4% for Type C column of the static value. That between the dynamic and static ultimate displacements and displacement ductility factors was 14% for Type A column, 8% for Type B column, and 0% for Type C column of the static value. That between the dynamic and static ultimate energies was 19% for Type A column, 12% for Type B column, and 2% for Type C column of the static value. Effects of the loading velocity were larger when the longitudinal reinforcement ratio was high.

2.4 Rotation at the Bottom of the Column

Column rotations by the damage concentration and extension of longitudinal reinforcements at the column bottom were measured in the loading tests. Fig. 2.4 shows column top displacements by the rotation at the bottom of the column. In the loading tests of Type A and Type B columns, bending deflections of the column were dominant before the yield of the column. After the yield of the column, the displacement by the rotation became large and was about 40% of the total column top displacement at δ_y and 70% of that after $2\delta_y$. In the loading test of Type C column, most of the total column top displacement (about 80%) was by the rotation.

2.5 Hysteretic Damping

Hysteretic damping constants obtained from the load-displacement hysteresis loops are shown in Fig. 2.5. The damping constants of Type A and Type B columns at the first-cycle ($n = 1$) loading were about 0.05 at δ_y and 0.2 after $2\delta_y$. That of Type C column was about 0.1 at δ_y , 0.15 at $2\delta_y$, and 0.2 after $3\delta_y$. Though the damping constants in the dynamic loading test were generally larger than those in the static loading test, there was little difference between them.

3. CONCLUSIONS

The following results were obtained by the reversed cyclic loading test of reinforced concrete bridge pier column models with different longitudinal reinforcement ratios.

- (1) Damage to a general reinforced concrete bridge pier column develops at the column bottom as follows:

horizontal crack — diagonal crack — cover concrete spalling — longitudinal reinforcement cut

The column holds the strength larger than the yield load until the cover concrete spalling (crushing of concrete) occurs. In the case of a low-longitudinal reinforcement

ratio (tensile longitudinal reinforcement ratio $P_t \leq$ about 0.25%) column, significant diagonal cracks and cover concrete spalling do not occur.

- (2) Displacement ductility factors μ ($= \delta u / \delta y$) of the columns were $\mu = 4$ for the longitudinal reinforcement ratio $P_g = 1.79\%$ (tensile reinforcement ratio $P_t = 1.02\%$), $\mu = 7$ for $P_g = 0.87\%$ ($P_t = 0.50\%$), and $\mu = 10$ for $P_g = 0.48\%$ ($P_t = 0.27\%$) in the experiment. The ductility factor of a reinforced concrete bridge pier column increases as the longitudinal reinforcement ratio decreases. The plastic hinge region (cover concrete spalling region) of the columns were 1.5D for $P_g = 1.79\%$, D for $P_g = 0.87\%$, and partial for $P_g = 0.48\%$, where D is the column width in the loading direction, above the column bottom in the experiment. The plastic hinge region of a reinforced concrete bridge pier column increases as the longitudinal reinforcement ratio increases.
- (3) Though the results of static and dynamic loading tests were similar, the ultimate strength (maximum strength), ultimate displacement, ductility factor, and ultimate energy in the dynamic loading were slightly larger than those in the static loading. Effects of the loading velocity increased as the longitudinal reinforcement ratio increased in the experiment.
- (4) Bending deflections are predominant in the deformation of a reinforced concrete bridge pier column when the damage is small. After the yield of longitudinal reinforcements at the column bottom, the rotation of the column increases by the damage concentration and extension of longitudinal reinforcements at the column bottom. Column top displacements by the rotation were about 40% of the total displacement at δy and 70 – 80% of that at larger displacements in the experiment.
- (5) Hysteretic damping constants of a reinforced concrete bridge pier column were estimated as $h = 0.05 - 0.10$ at δy and $h \approx 0.20$ at larger displacements.

REFERENCES

- 1) Kuribayashi, E., Uyeda, O., Hagiwara, R., Shibata, M., Koyama, T., "Reversed Cyclic Loading Test of Bridge Pier Models", Technical Memorandum of PWRI No. 1801, October, 1981.
- 2) Kuribayashi, E., Iwasaki, T., Hadate, T., Hagiwara, R., "Experimental Studies on Seismic Behavior of Structural Members Using a Dynamic Structural Testing Facility at PWRI", The 14th Joint Meeting of U.S. – Japan Panel on Wind and Seismic Effects, UJNR, May, 1982.
- 3) Iwasaki, T., Hagiwara, R., Koyama, T., "Dynamic Behavior of a Reinforced Concrete Bridge Pier Subjected to Cyclic Loadings", The Sixth Japan Earthquake Engineering Symposium, October, 1982 pp. 785 - 792.

- 4) Mutsuyoshi, H., Machida, A., "Dynamic Properties of Reinforced Concrete Piers", The Sixth Japan Earthquake Engineering Symposium, October, 1982, pp. 793 - 800.
- 5) Ohta, M., "Earthquake Resistant Design Method of Reinforced Concrete Bridge Pier Single Columns", Technical Memorandum of PWRI No. 1513, July, 1979.

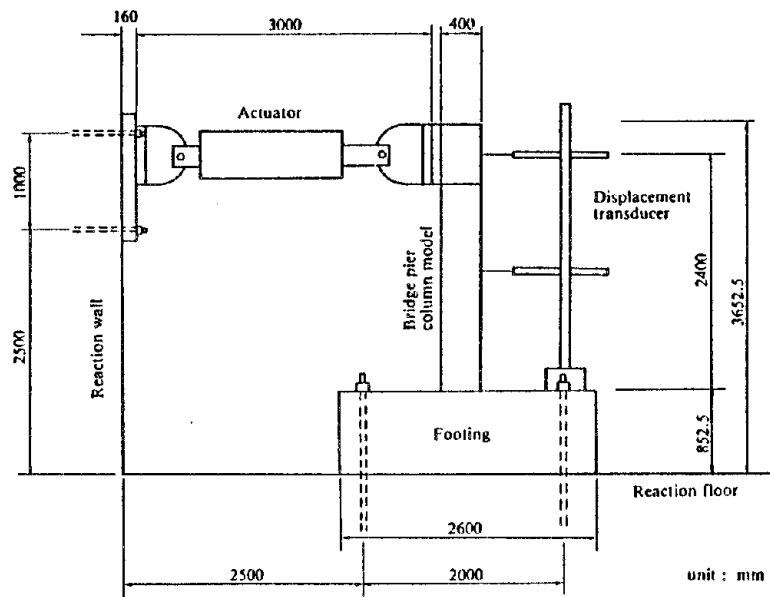


Fig. 1.1 Setting of the Specimen and Actuator

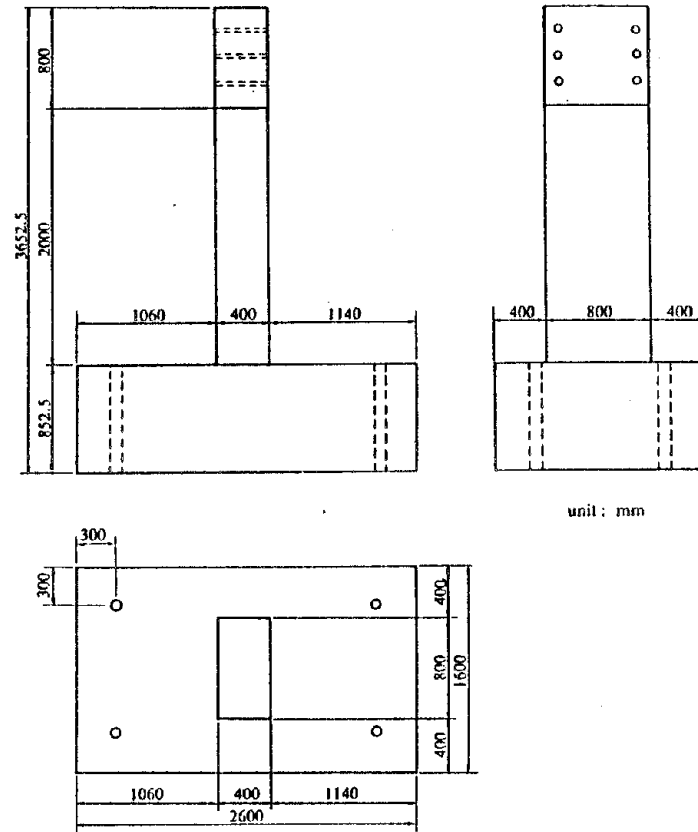


Fig. 1.2 Dimension of the Specimen

Table 1.1 Specimen Types

	Type A	Type B	Type C
Longitudinal reinforcement ratio (SD30) ρ_g	1.79% (D19)	0.87% (D16)	0.48% (D13)
Hoop ratio ρ_w	0.08%	0.08%	0.08%
Spacing of hoop (SR24, $\phi 9$)	20cm	20cm	20cm

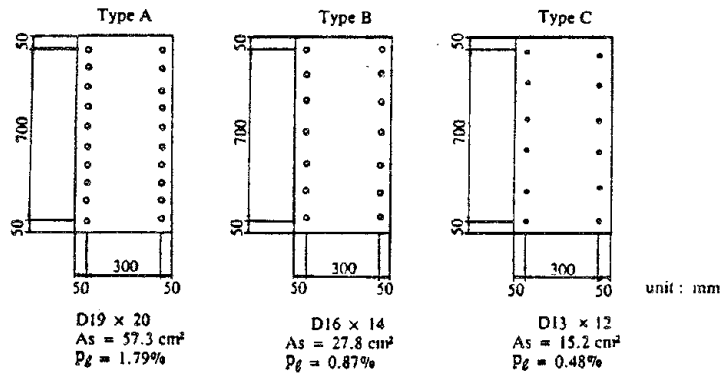


Fig. 1.3 Column Cross-Section of the Specimen

Table 1.2 Measuring Items

Actuator	Load	1 point
	Displacement	1 point
Column	Top displacement	1 point
	Middle displacement	1 point
	Uplift and sinking at the bottom	4 points
	Top acceleration (dynamic loading test)	1 point
	Crack width (static loading test)	
Longitudinal Reinforcement	Strain at the bottom of the column	4 points
	Strain in the footing	6 points
Hoop	Strain near the bottom of the column	4 points

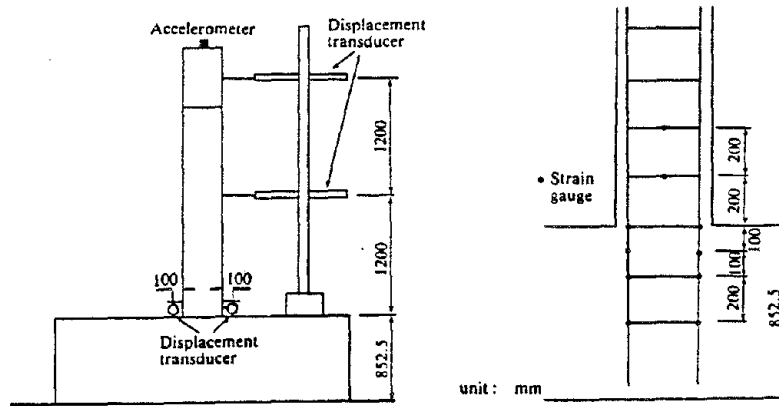


Fig. 1.4 Setting of Instruments

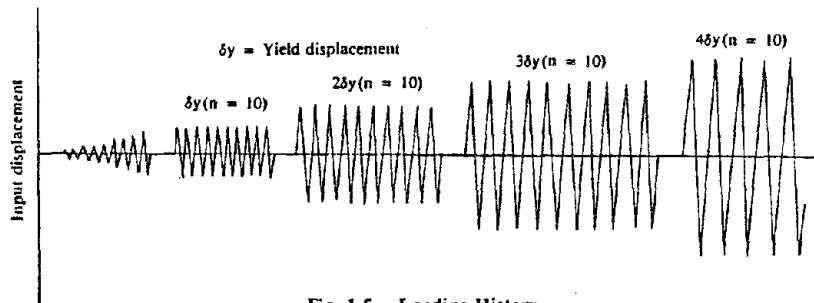


Fig. 1.5 Loading History

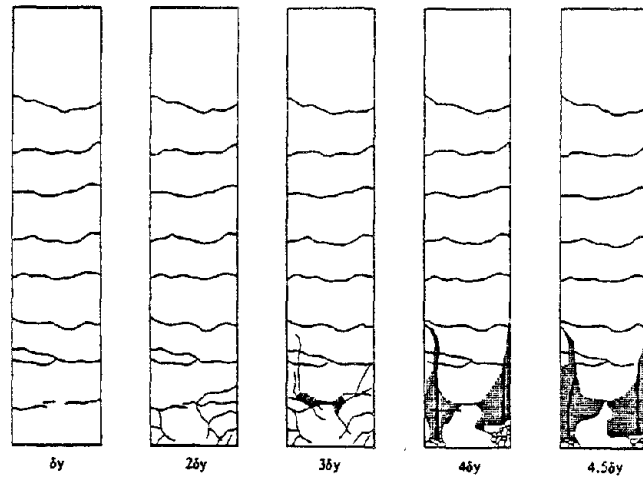
Table 2.1 Compressive Strength of Concrete

Specimen for the static loading test	290kg/cm ²
Specimen for the dynamic loading test	258kg/cm ²

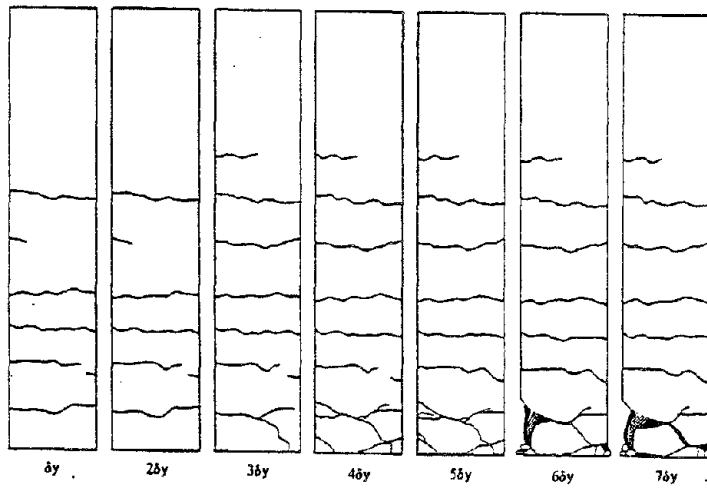
Table 2.2 Yield Point of Reinforcement

Longitudinal Reinforcement (SD30)	D19 (Type A : $p_g = 1.79\%$)	3,804kg/cm ² ($\epsilon_{sy} = 1,811 \times 10^{-4}$)
	D16 (Type B : $p_g = 0.87\%$)	3,625kg/cm ² ($\epsilon_{sy} = 1,726 \times 10^{-4}$)
	D13 (Type C : $p_g = 0.48\%$)	3,701kg/cm ² ($\epsilon_{sy} = 1,762 \times 10^{-4}$)
Hoop (SR24) $\phi 9$		3,302kg/cm ² ($\epsilon_{sy} = 1,572 \times 10^{-4}$)

Type A
($P_g = 1.79\%$)



Type B
($P_g = 0.87\%$)



Type C
($P_g = 0.48\%$)

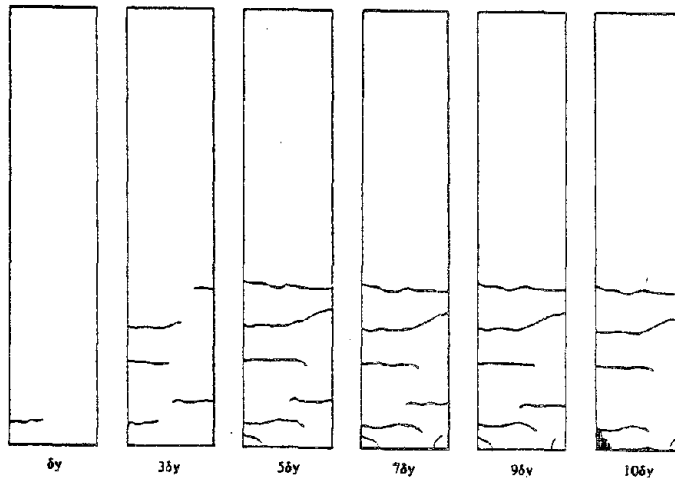
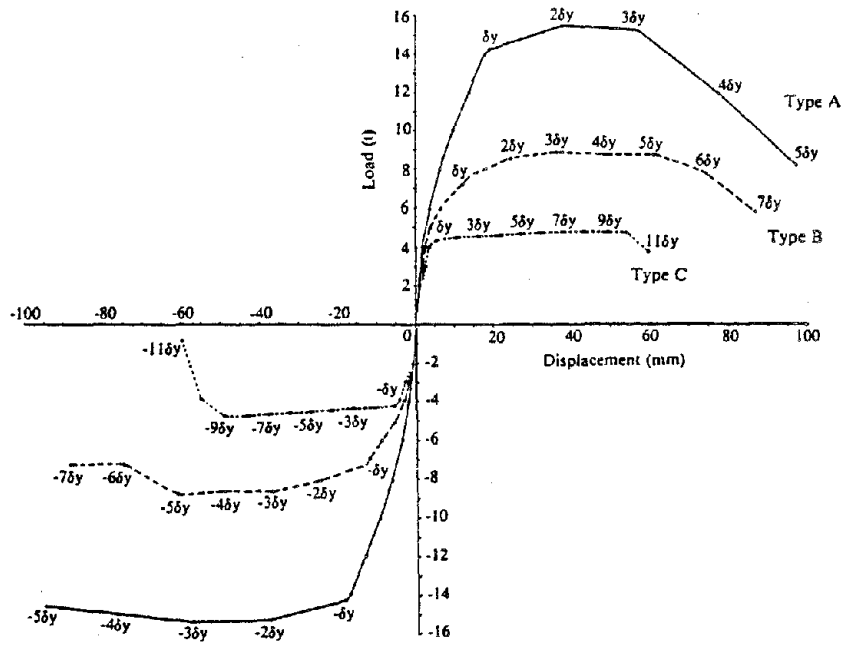
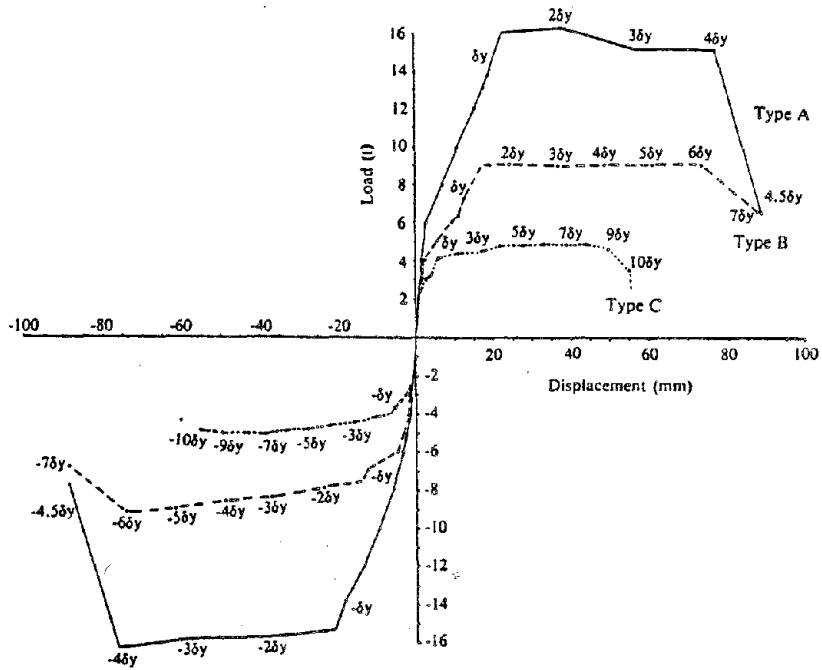


Fig. 2.1 Failure Mode (Dynamic Loading Test)



Static Loading Test



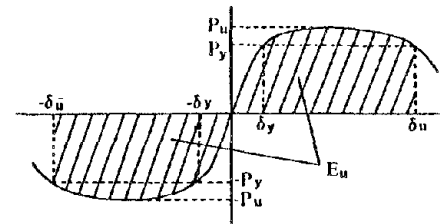
Dynamic Loading Test

Fig. 2.2 Load-Displacement Envelope Curve

Table 2.3 Performance of the Columns

	Static Loading Test			Dynamic Loading Test		
	Type A	Type B	Type C	Type A	Type B	Type C
Yield load P_y (t)	14.3	7.1	4.3	13.8	7.1	3.9
Ultimate load P_u^* (t)	15.4	8.8	4.8	16.2	9.2	5.0
R_u/P_y	1.08	1.24	1.12	1.17	1.30	1.28
Yield displacement δ_y (mm)	19.0	12.2	5.4	19.0	12.2	5.4
Ultimate displacement δ_u^{**} (mm)	69	80	55	79	86	55
δ_u/δ_y	3.6	6.6	10.2	4.2	7.0	10.2
Ultimate energy E_u^{***} (tm)	1.87	1.25	0.49	2.22	1.40	0.50

Notes: * P_u : Maximum load on the load-displacement envelope curve
 ** δ_u : Column top displacement when the load decreases to the yield load
 *** $E_u = \int_0^{\delta_u} P(\delta) d\delta + \int_0^{\delta_y} P(\delta) d\delta$



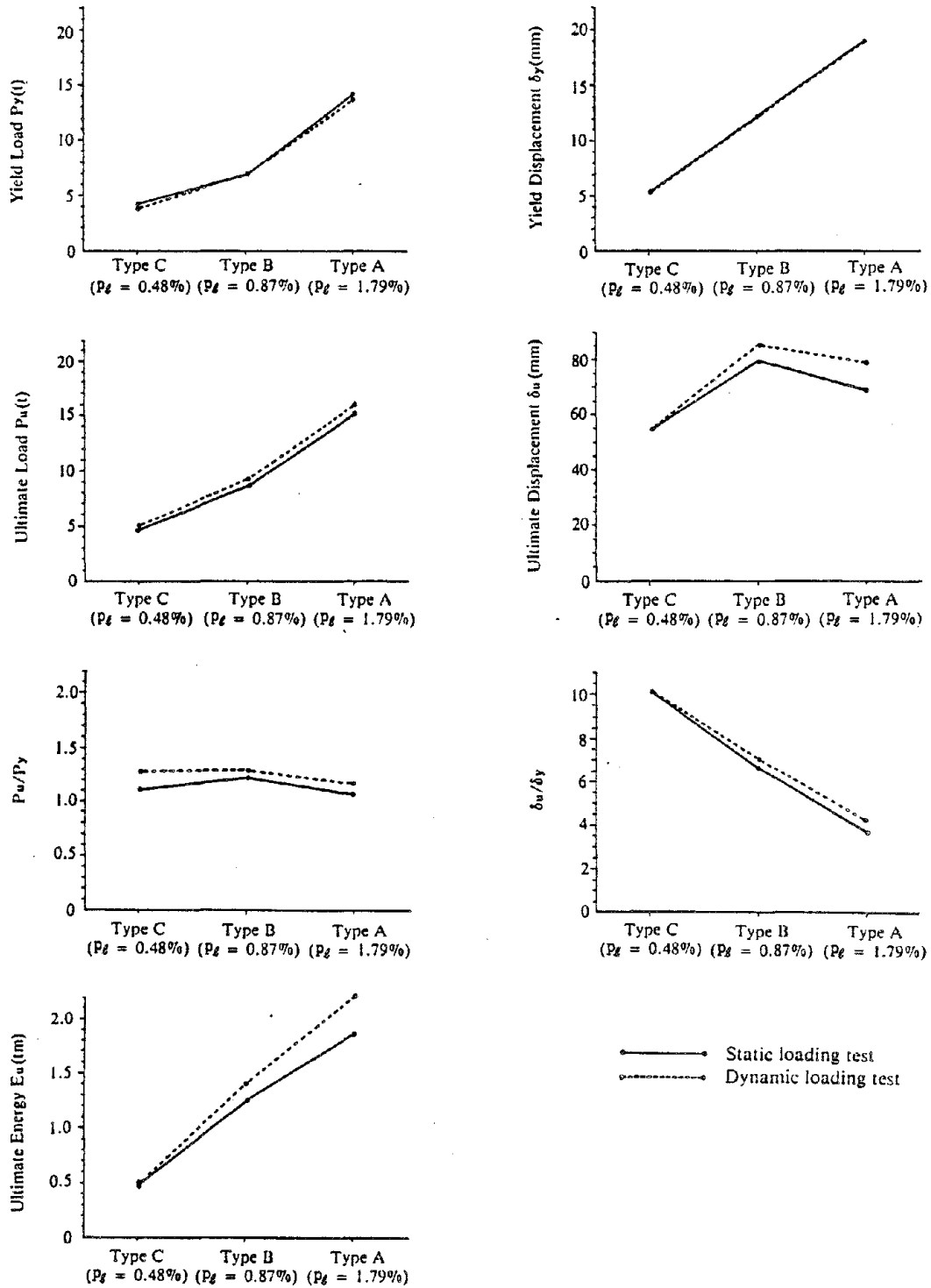


Fig. 2.3 Performance of the Columns

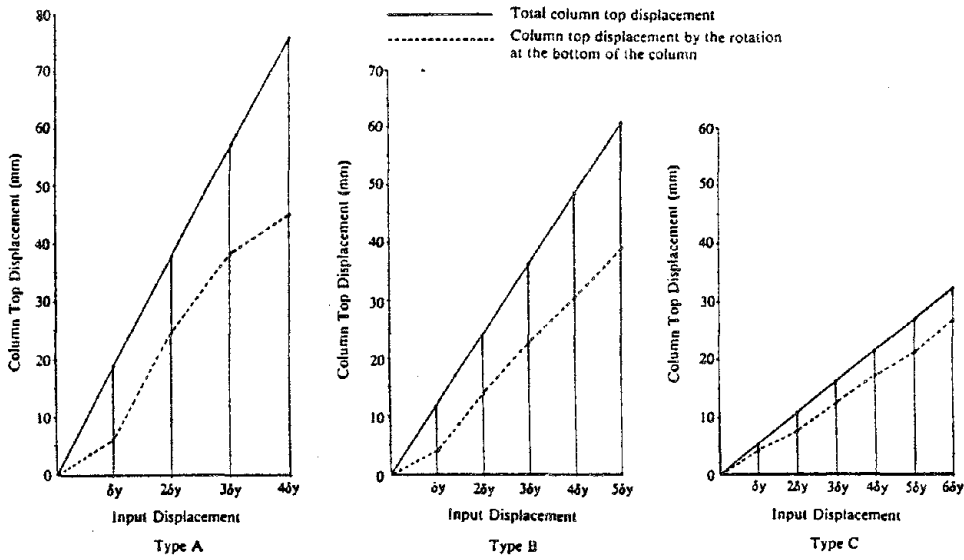


Fig. 2.4 Column Top Displacement by the Rotation at the Bottom of the Column (Dynamic Loading Test)

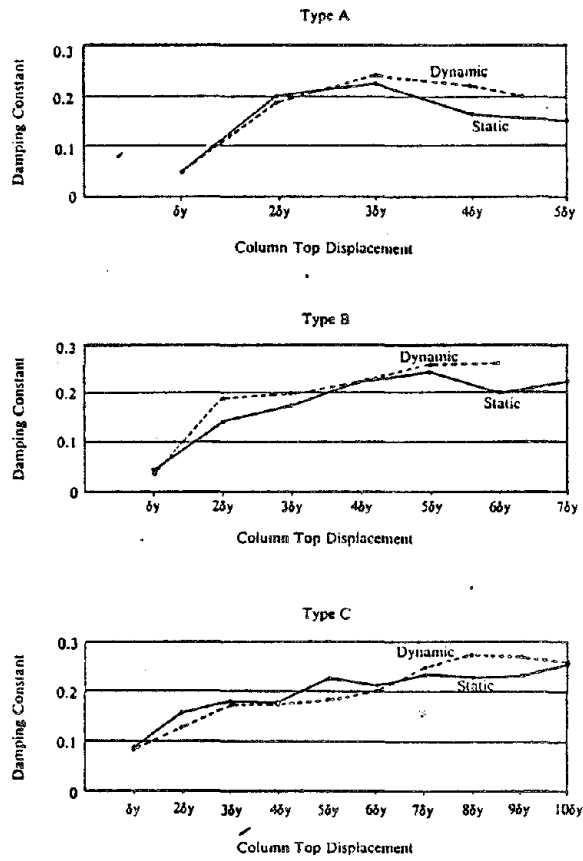


Fig. 2.5 Hysteretic Damping Constant Obtained from the Hysteresis Loops (n = 1)

BEHAVIOR OF CONCRETE-FILLED
STEEL TUBES

(Part-1, Compression Members)

FEB, 1982

Bridge Division
Ministry of Construction
Public Works Research Institute

P R E F A C E

In our country, bridge piers are subjected to strong motions due to earthquake. Furthermore, size of bridge piers are strictly limited in metropolitan highways and in monorails. High ductility and high resistance is, therefore, required for bridge piers in Japan. In this regard, use of concrete-filled steel tubes is examined.

Steel Tubes have pretty high resistance; however, steel tubes are liable to yield local buckling and to lose ductility after yielding local buckling. Concrete piers with adequate reinforcing have good ductility; however, they are large-sized. Concrete-filled steel tubes are thin steel tubes with concrete and shear connectors in the tubes. When they are subjected to a strong motion, concrete prevents the local buckling of thin steel tubes, steel tubes giving adequate reinforcing to the concrete. Therefore, even small-sized concrete-filled steel tubes have excellent ductility and resistance.

Sometimes, concrete-filled steel tubes were used for bridge piers or building members. However, they were used just to increase the rigidity of the members or to stiffen the steel tubes, and they were not designed as composite structures. In our report, concrete-filled steel tubes are regarded as composite structures to expect higher resistance and ductility. At present, many problems are not settled to design concrete-filled steel tubes as composite structures, such as provisions for shear connectors, plate thickness and so on. In the report, these problems are examined in detail, based on the results of full-size tests, and design recommendations are presented.

The following reports are coming in series.

- Part I Compression Members
- Part II Long Columns
- Part III Bending Members
- Part IV Beam Columns

The study is carried out by the following members of the Public Works Research Institute.

Nobuyuki Narita;	Director, Structure and Bridge Department
Shoichi Saeki;	Head, Bridge Division
Michio Kanai;	Research Engineer, Bridge Division
Toshio Ohshio;	Engineer, Bridge Division

CHAPTER - 1 INTRODUCTION

Bridge piers should be designed to resist earthquakes which are expected during the lifetime of the structures. However, we cannot but say that it is waste of national budget to construct the bridge piers which can resist the severest earthquake. In this regard, the concept of "minimum total cost" should be introduced.

On the other hand, admitting the above, brittle structures which may cause disasters due to the collapse of the structures should be avoided as far as possible. Ductile structures, which will not collapse even in the strongest earthquake, yielding some local failures, is desirable for bridge piers. For example, Fig. 1 (a) shows the ductile structures, Fig. 1 (b) showing the brittle structures. Ductile structures may yield some local failures, but they will not lose resistance even in the region of large deformation.

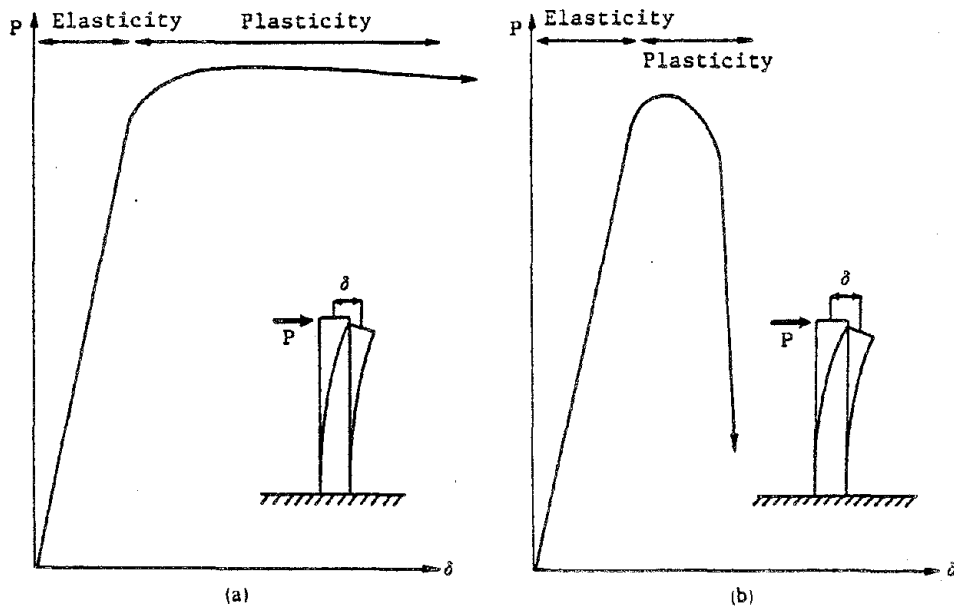


Fig. 1 Ductile and Brittle Structures

Steel tubes are ductile or brittle depending on the Diameter - Thickness ratio (D/t). Thin steel tubes are economical in the elastic design, but they are usually brittle. Thick steel tubes are usually ductile, but they are not economical in the elastic design. Therefore, it is very difficult to determine the adequate D/t value for bridge pier design.

In this regard, behavior of composite concrete-filled steel tubes is excellent. Concrete prevents the local buckling of thin steel tubes, steel tubes giving adequate reinforcing to the concrete. Therefore, concrete-filled steel tubes have excellent resistance and ductility. However, we do not have good design specifications to design the concrete-filled steel tubes as composite structures. In the following chapters, the behavior of the concrete-filled steel tubes is examined in detail based on the full-size tests with 3000 ton testing machine of the P.W.R.I. . In this report, the test results of the short compression members are described.

CHAPTER - 2 DESIGN PROBLEMS OF CONCRETE-FILLED STEEL TUBES

As described in the Preface, concrete-filled steel tubes are sometimes used for bridge piers and building members; however, they are used to give the rigidity to the members or to stiffen the local buckling of the steel tubes. Higher economy can be expected by designing the concrete-filled steel tubes as steel-concrete composite structures. In this regard, the following problems should be settled.

1. When steel and concrete are both elastic, Poisson's ratio of the concrete (about $1/6$) is much smaller than that of the steel (about 0.3). Therefore, under axial compression, concrete and steel will separate from each other in a cross section (Fig. 2). When steel and concrete are connected by studs or something, steel will be subjected to compression for hoop direction. On the other hand, when steel and concrete are not connected, the both will behave independently, and they will not be composite structures. So, how to give enough bond between steel and concrete is a important problem. Natural bond may not be enough and studs may be required.

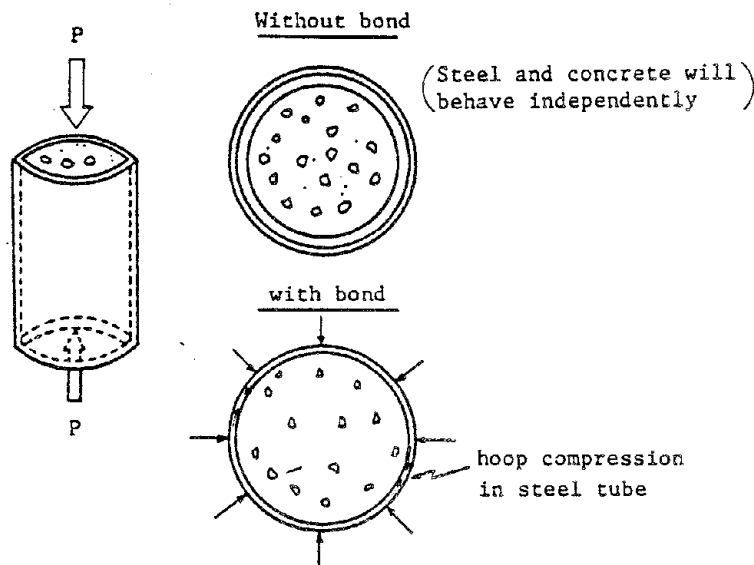


Fig. 2 Behavior in Elasticity

2. When steel and concrete are plastic, Poisson's ratio of the concrete increases to about 0.5 which is much larger than that of the steel. Therefore, steel tube will be subjected to tension for hoop direction. At this time, steel and concrete will behave together without the bond, and high resistance and ductility is expected. These effects should be examined.

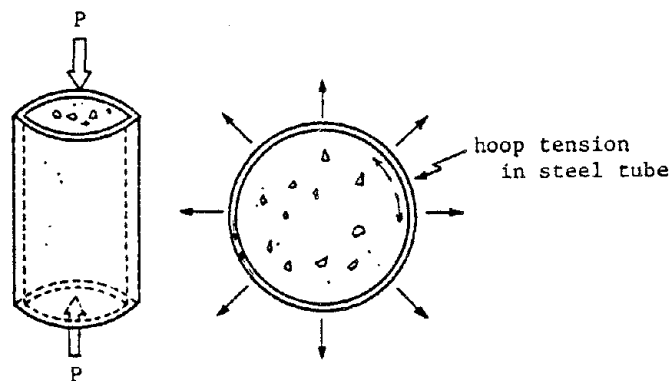


Fig. 3 Behavior in Plasticity

3. The behavior described above is affected by many factors such as plate thickness, concrete strength, steel strength, arrangement of studs and many others. These relations should be cleared up and design specifications should be provided.

In this report, the above problems are examined. Meanwhile, the following problems should be further settled to give complete design specifications. These will be described in the coming reports in series.

4. Under bending, concrete will be subjected to tension, and may yield cracking. Resistance and rigidity of concrete-filled steel tubes under bending should be, therefore, examined. At the same time, arrangement of shear connectors should be examined.

5. Under repeated loadings, the resistance of concrete-filled steel tubes may decrease, due to the extension of cracking, the accumulation of plastic strain, the stress concentration due to studs and so on. Furthermore, the bond between concrete and steel may be lost. These should be examined in detail.

6. The resistance of long columns composed of concrete-filled steel tubes should be examined. The evaluation of slenderness ratio is pretty complicated in composite structures.

CHAPTER - 3 OUTLINE OF THE TESTS

In the compression tests, ten full-size specimens were fabricated. We needed full-size specimens in order to provide studs inside the steel tubes, and also to examine the bond problem in detail. The configuration of the specimens are shown in Fig. 4, the specifications being shown in Table 1.

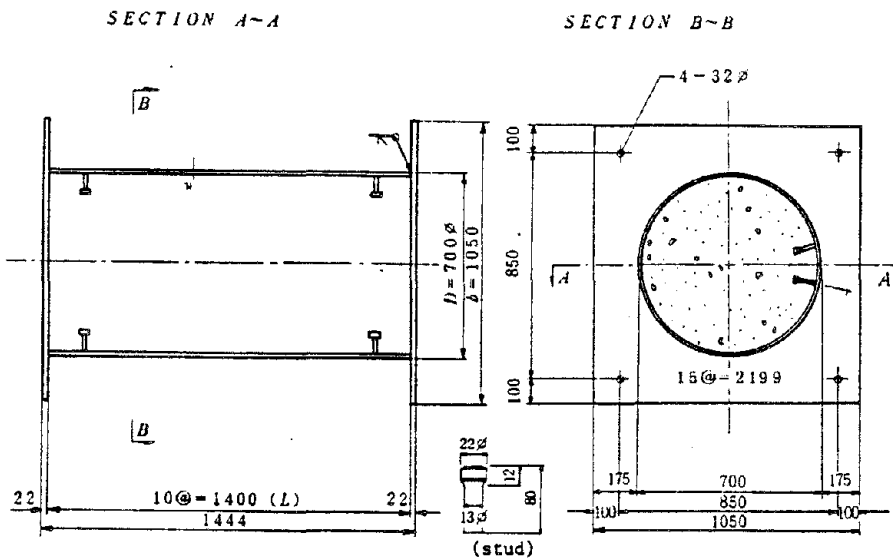


Fig. 4 Configuration of Test Specimen

Table 1. Specifications for The Test Specimens

No.	Diameter x plate thickness	Concrete	Stud	Yield strength of steel	Concrete strength	Remarks
A-1	700 x 6	without	without	4600	254	for cyclic loading
A-2	" x 8	"	"	4720	"	
A-3	" x 8	"	"	"	"	
A-4	" x 12	"	"	4000	"	
B-1	700 x 6	with	with	4600	"	for cyclic loading
B-2	" x 8	"	"	4720	"	
B-3	" x 8	"	"	"	"	
B-4	" x 12	"	"	4000	"	
B-5	" x 8	"	without	4720	"	
B-6	" x 8	"	with	"	410	

Steel plate material is SM 50Y, which has nominal yield strength of 3600 kg/cm². Tensile strength of the material was tested by test pieces taken from bent up steel tubes. The results are shown in Table 2.

Table 2. Yield Strength of Steel

Size	Yield strength (kg/cm ²)	Breaking strength (kg/cm ²)	Elongation (%)
φ 700 x 6	4570	5700	23.4
	4620	5750	23.0
	4630	5670	22.1
average	4600	5700	22.8
φ 700 x 8	4720	5650	25.8
	4720	5660	26.0
	4720	5620	25.7
average	4720	5640	25.8
φ 700 x 12	4000	5710	22.4
	4030	5770	22.1
	3970	5770	21.6
average	4000	5750	22.0
nominal	3700 up	5000 ~ 6200	15 up

The steel tubes are bent up as shown in Photo 1, and welded from inside and outside as shown in Photo 2 and Photo 3. The welding was carried out as shown in Fig. 5 and Table 3. The studs were welded by a stud-gun, as shown in Photo 4.

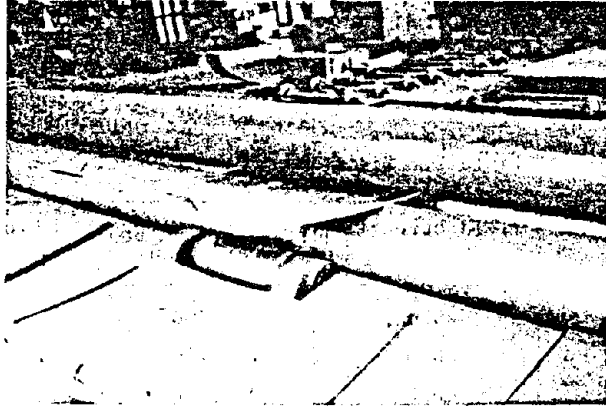


Photo-1. Bending Process of Steel Tubes

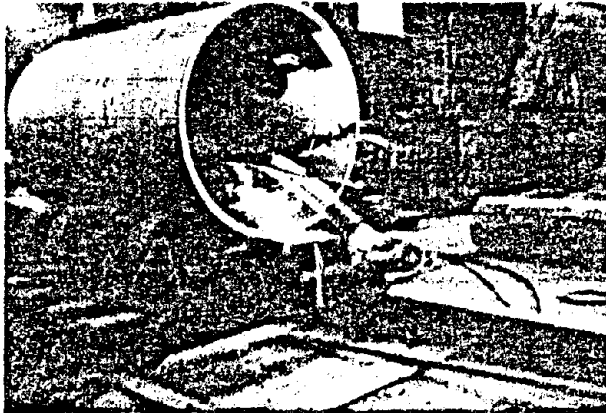


Photo-2. Welding (Inside)

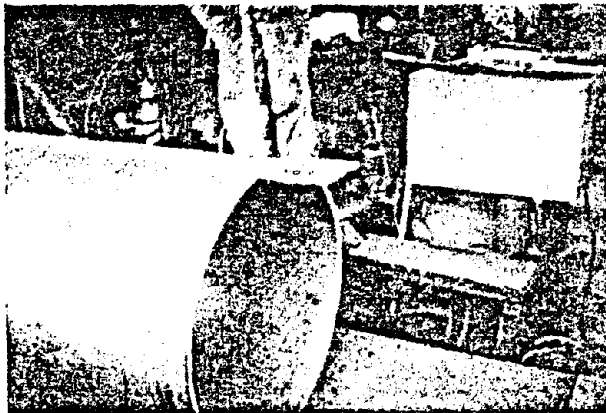
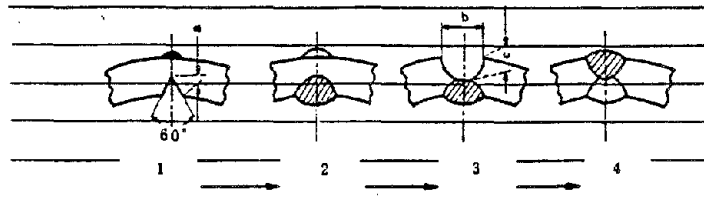


Photo-3. Welding (Outside)



Dimensions

Plate thickness	a	b	c
12	3	10	5
8	2	8	3
6	2	-	-

Fig. 5 Welding Process

Table. 3 Specifications for Welding

Plate thickness	Place	I	V	Velocity
12 (mm)	Inside	560 ^A	38 ^V	37 ^{cm/mm}
	Outside	580	36	30
8	Inside	430	35	50
	Outside	580	38	45
6	Inside	370	32	85
	Outside	580	36	60

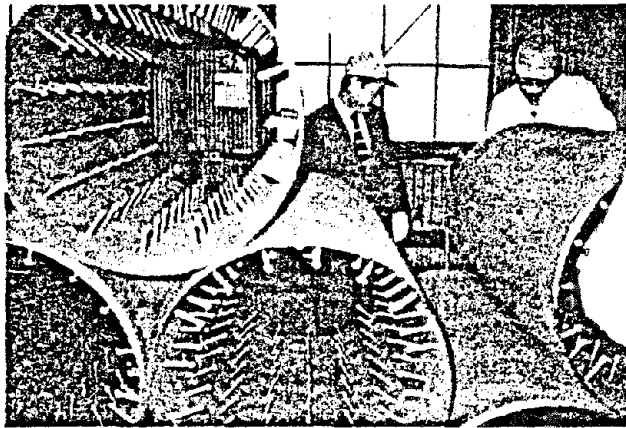


Photo-4. Stud Welding

Table 4. Specifications for Concrete

Nominal	Unit	Water	Cement	Fine aggregate	Coarse aggregate
$\sigma = 210\text{kg/cm}^2$	1 m ³	152kg	249kg	826kg	1110kg
$\sigma = 400\text{kg/cm}^2$	1 m ³	151kg	357kg	650kg	1179kg

Concrete Strength

Nominal	(1)	(2)	(3)	Average
210	241	247	247	245
400	438	436	429	434

The specifications for the concrete and the concrete strength are shown in Table 4. After casting the concrete, the concrete will yield shrinkage, which will prevent uniform loading of the specimen. Therefore, non-shrinkage mortar was casted at the top and the bottom of the specimen three weeks after casting the concrete, and then top and bottom plates were welded to the specimen. Both top and bottom plates were ground up by facing machines in order to obtain uniform loading. (Photo 5 - Photo 7)

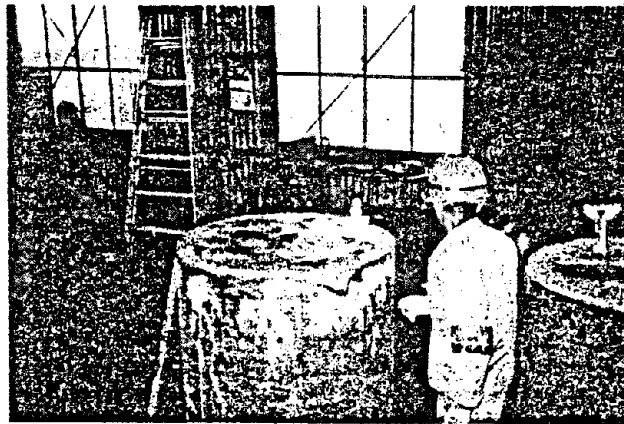


Photo-5. Mortar Casting



Photo-6. Bottom and Top Plate

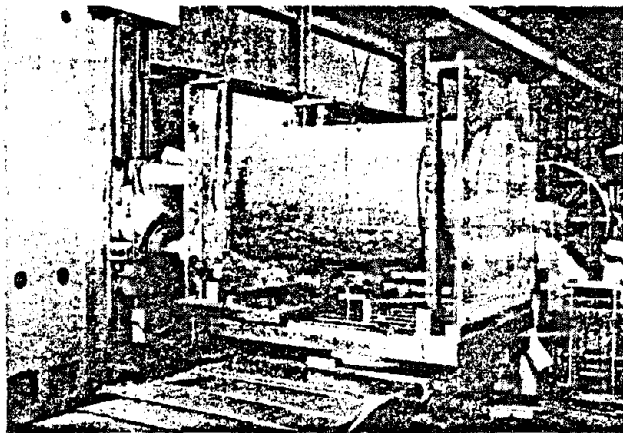


Photo-7. Grinding of Top and Bottom Plate

Specimens A-1 to A-4 are steel tube specimens without concrete in them. A-3 is same as A-2, but it is for cyclic loading.

Specimens B-1 to B-6 are concrete-filled steel tubes. B-1 to B-4 are the same ones as A-1 to A-4 respectively, except for the concrete and the studs in them. B-5 is originally same as B-2, but it is not provided with studs. B-6 is also same as B-2, but it has high strength concrete in it.

In the tests, total deformation, strain of the steel tubes (128 points) and out-of-plane deflection of the steel tubes (52 points) were measured by automatic computer system. Fig. 6 shows the strain gauges, Fig. 7 showing the measurement of out-of-plane deflection. Photo 8 shows the testing machine and the measurement system.

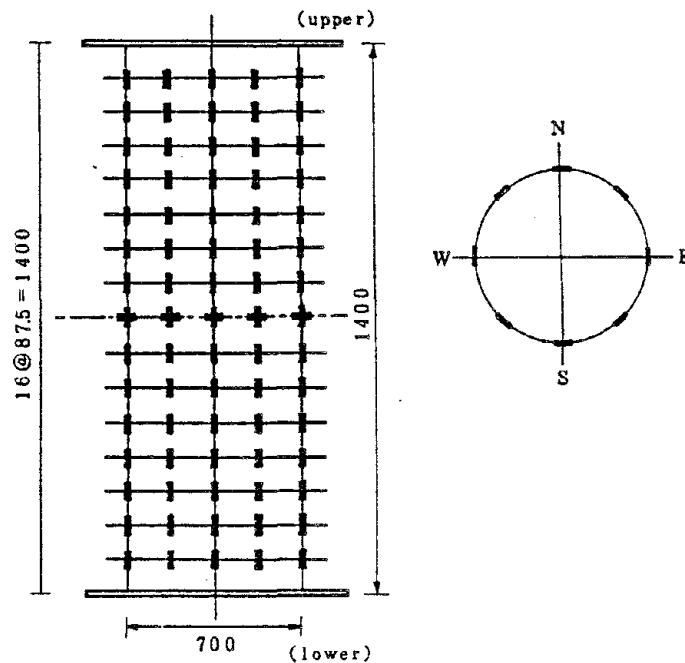


Fig. 6 Measurement of Strain

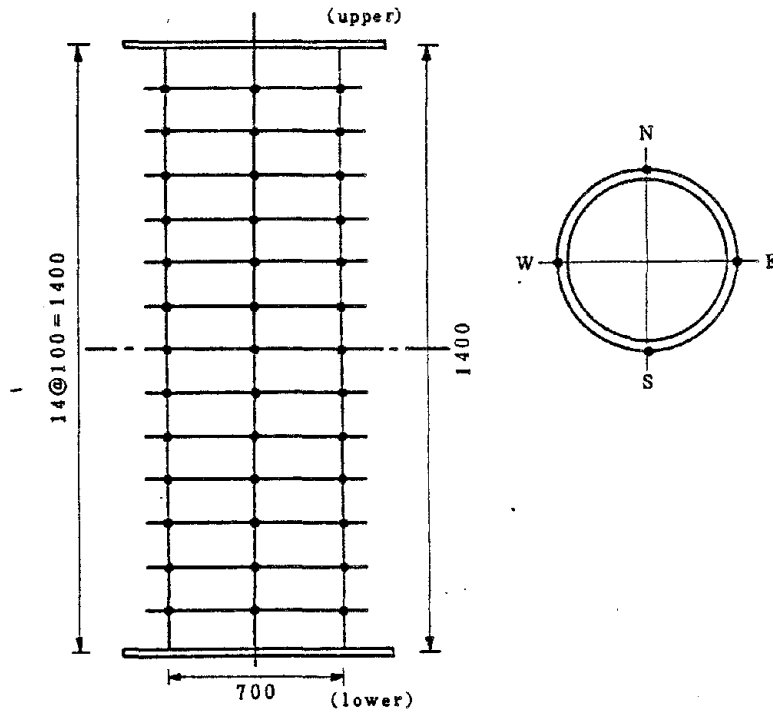


Fig. 7 Measurement of Out-of-Plane Deflection

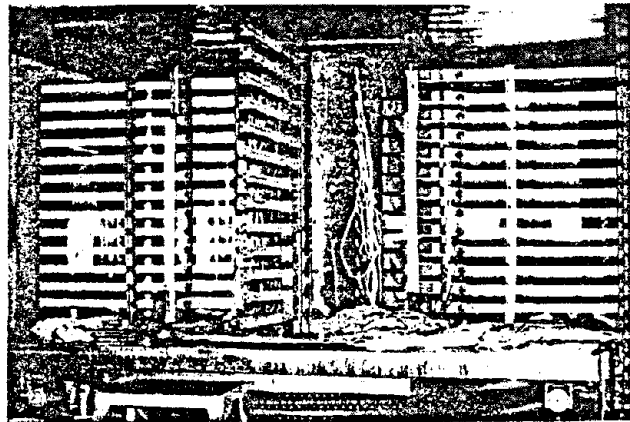


Photo-8. Measurement of Out-of-Plane Deflection

CHAPTER - 4 TEST RESULTS AND ANALYSIS

4.1 Resistance of concrete-filled steel tubes

The theoretical values and the test results of the resistance of the specimens are listed in Table 5, where,

Table 5. Theoretical and Experimental Resistance

No.	Experimental Resistance	Theoretical Resistance					Experimental Sc+Sb	Experimental Sc+Sy
		Sc(t)	Sb(t)	Sy(t)	Sc+Sb(t)	Sc+Sy(t)		
A-1	540	-	567	602	567	602	0.95	0.90
A-2	753	-	786	821	786	821	0.96	0.92
A-3	760	-	786	821	786	821	0.97	0.93
A-4	1087	-	1010	1037	1010	1037	1.07	1.05
B-1	1509	911	567	602	1478	1513	1.02	1.00
B-2	1730	900	786	821	1686	1721	1.03	1.01
B-3	1722	900	786	821	1686	1721	1.02	1.00
B-4	2230	879	1010	1037	1889	1916	1.18	1.16
B-5	1694	900	786	821	1686	1721	1.00	1.10
B-6	2663	1595	786	821	2381	2416	1.12	1.10

Sc ; resistance of the concrete, obtained from the cylinder test result of the concrete.

Sb ; resistance of the steel tube, obtained from the local buckling strength of the steel tube. Effects of residual stresses and initial defections are considered in the following Donnell-Wan equations.

$$\sigma_{cr} = \sigma_y (N - \sqrt{N^2 - \sigma_{cl} / \sigma_y}) \dots\dots\dots (1)$$

in which,

σ_{cr} ; local buckling strength, where effects of initial imperfections are considered.

σ_y ; yield strength of the steel

σ_{cl} ; elastic local buckling strength of the steel tube,
which is obtained from

$$\sigma_{cl} = \frac{E}{\sqrt{3(1-\nu^2)}} \frac{t}{R}$$

E, ν ; Modulus of elasticity and Poisson's ratio of the steel.

R, t ; radius and plate thickness of the steel tube.

N ; constant obtained from

$$N = \frac{1}{2} \left(1 + \frac{\sigma_{cl}}{\sigma_y} + \frac{U \cdot E}{2\sigma_y} \right)$$

U ; measure of initial imperfections.

$U = 0.001$ is recommended in the Highway Bridge Specifications in Japan.

S_y ; resistance of the steel tube, obtained from the yield strength of the steel.

As shown in Table 5, the resistance of the specimen A-1 to A-4 is sometimes lower than the theoretical values (S_b), because the effects of initial imperfections is significant in the thin plate steel tubes.

The followings three cases can be considered about the theoretical resistance of the specimens B-1 to B-6.

Case 1 ; When the steel tube and the concrete behave independently, the resistance will be $S_c + S_b$.

Case 2 ; When they are connected together, the concrete will prevent the local buckling of the steel tube, then the resistance will be $S_c + S_y$.

Case 3 ; When the concrete is confined by the hoop tension of the steel tube in plastic region, the concrete strength will be higher than the cylinder strength, then, the resistance will be higher than $S_c + S_y$.

Table 5 shows that the resistance of the specimens B-1 to B-3 is about the same as $S_c + S_y$, because even in these thin-plate specimens, local buckling is prevented by the concrete. The resistance of the specimen B-4 is higher than $S_c + S_y$, because the thick steel tube confine the concrete and the concrete strength is higher than the cylinder strength. Therefore, the resistance of the Case 2 is expected in the thin plate concrete-filled steel tubes, the resistance of Case 3 being expected in the thick plate ones.

On the other hand, the resistance of B-5 is smaller than that of B-2, and it is nearly same as the resistance of Case 1, where the steel tube and the concrete behave independently. Studs may be, therefore, needed to expect the resistance of Case 2.

Finally, the resistance of the specimen B-6 is much higher than $S_c + S_y$, that is, the resistance of Case 3 is obtained. The steel tube of B-6 is same as that of B-2, so, it is rather thin plate. Actually, the resistance of B-2 was that of Case 2.

Therefore, the status of the concrete is another important factor in estimating the total resistance. That is, in B-2 specimen, the concrete was broken into small blocks in plastic region, but the high strength concrete of B-6 specimen was not broken even in plastic region. This is why high resistance was obtained in B-6 specimens. Therefore, high-strength or high-quality concrete is needed to expect the resistance of Case 3.

4.2 Ductility of concrete-filled steel tubes

The ductility of the specimens can be examined by load-deformation curves, which are shown in Fig. 8 to Fig. 17.

Fig. 8 to Fig. 10 show that the thin plate steel tubes have small ductility, and lose strength after attaining the maximum strength, Photo 9 shows the local buckling of A-2 specimen which cause the loss of ductility. Fig. 11 shows that the thick plate steel tube has good ductility. Thick plate steel tube will not yield local buckling as shown in Photo 10.

Fig. 12 to Fig. 17 shows that even thin plate concrete-filled steel tubes have good ductility.

Furthermore, the ductility is not lost in repeated loadings. Therefore, concrete-filled steel tubes are good for bridge piers as far as compression members are concerned. Even B-5 specimen without studs shows good ductility.

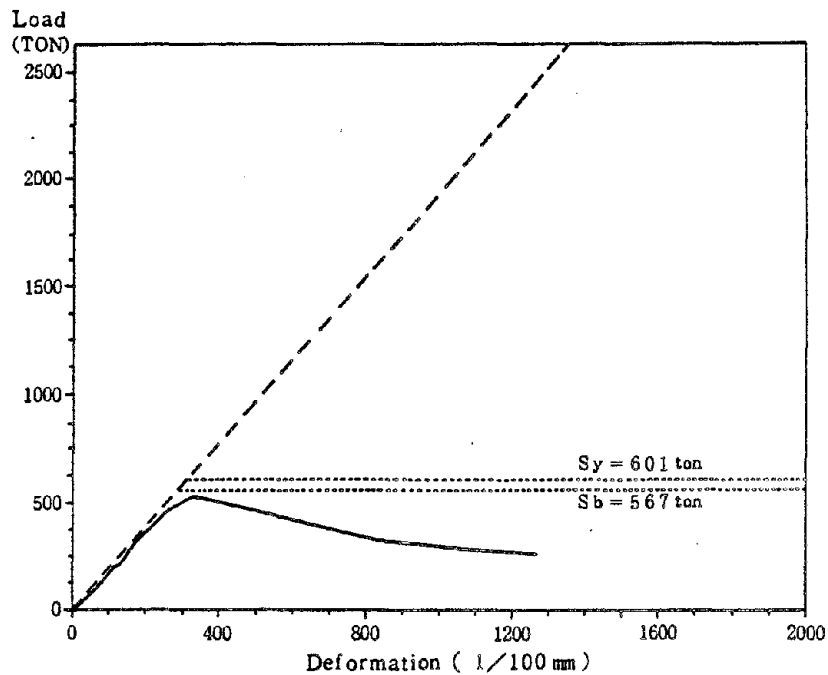


Fig. 8 Load-Deformation Curve (A - 1)

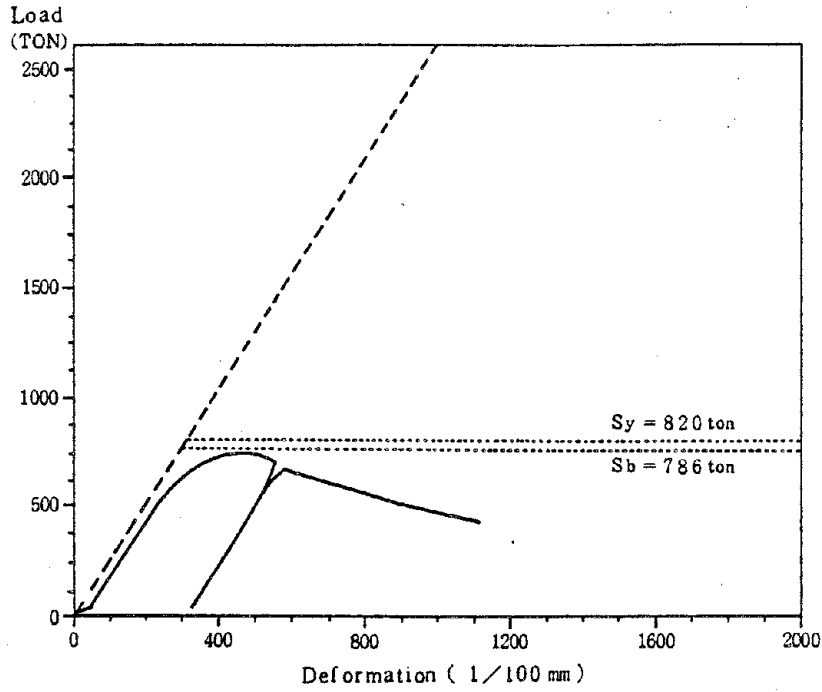


Fig. 9 Load - Deformation Curve (A - 2)

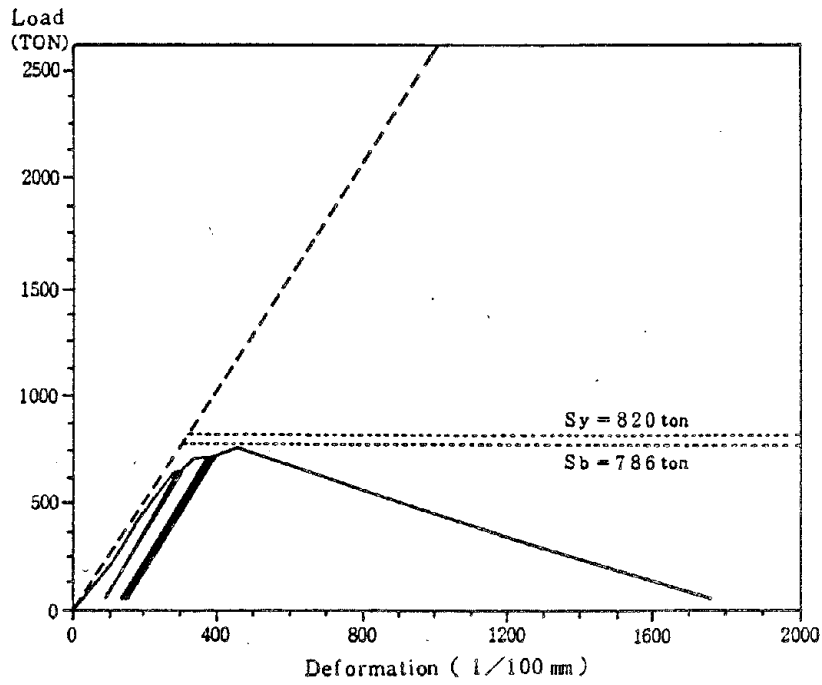


Fig. 10 Load - Deformation Curve (A - 3)

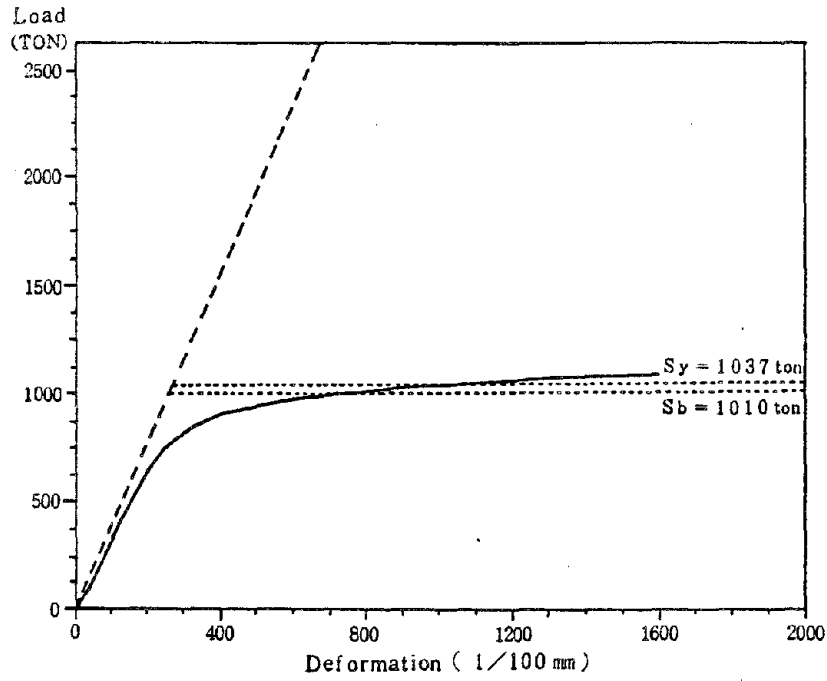


Fig. 11 Load - Deformation Curve (A - 4)

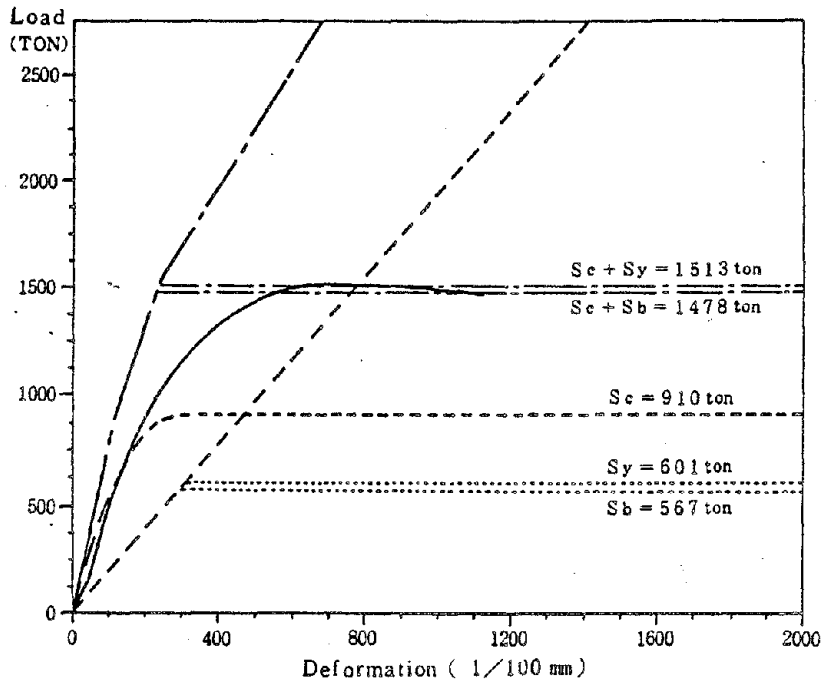


Fig. 12 Load - Deformation Curve (B - 1)

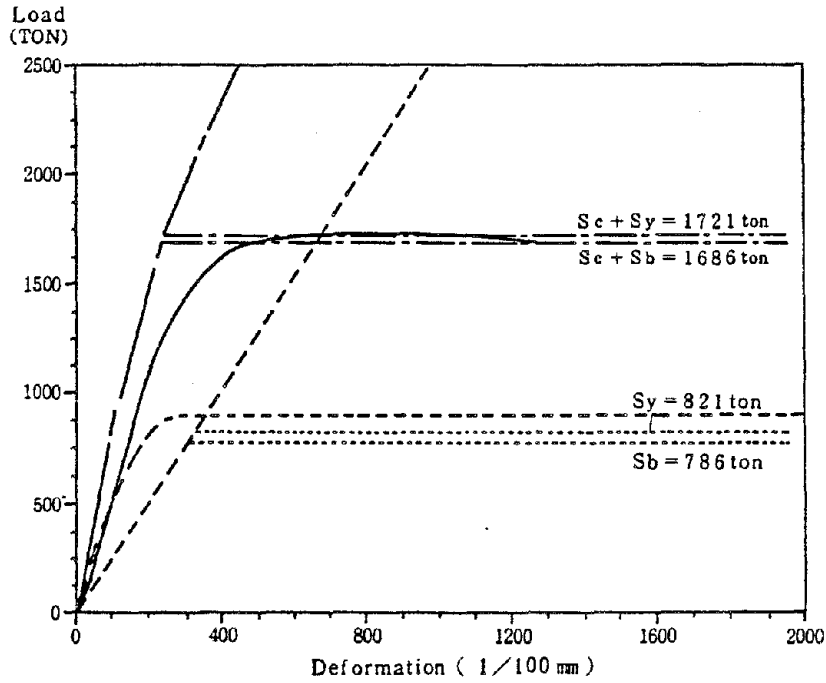


Fig. 13 Load - Deformation Curve (B - 2)

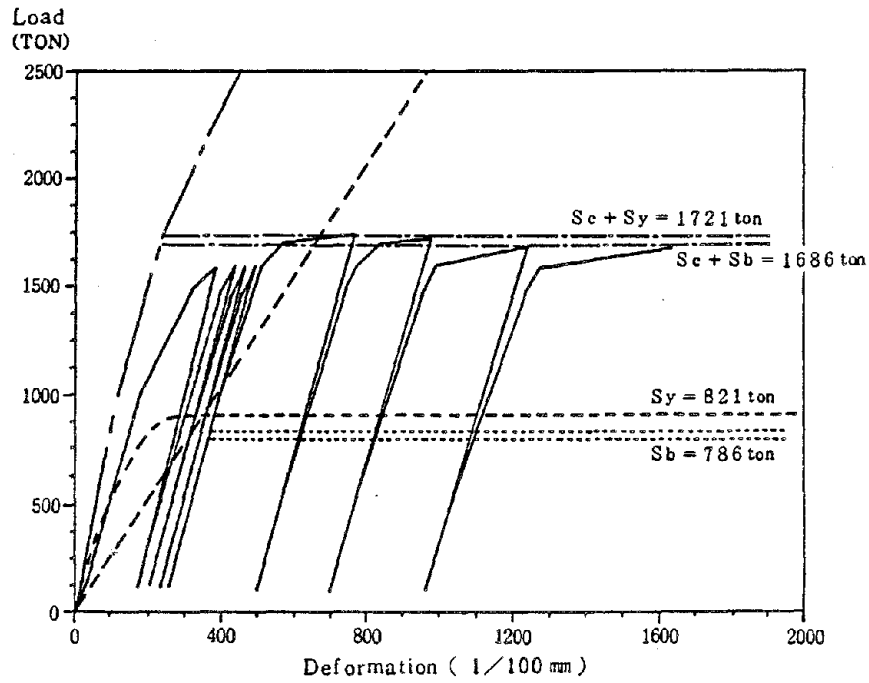


Fig. 14 Load - Deformation Curve (B - 3)

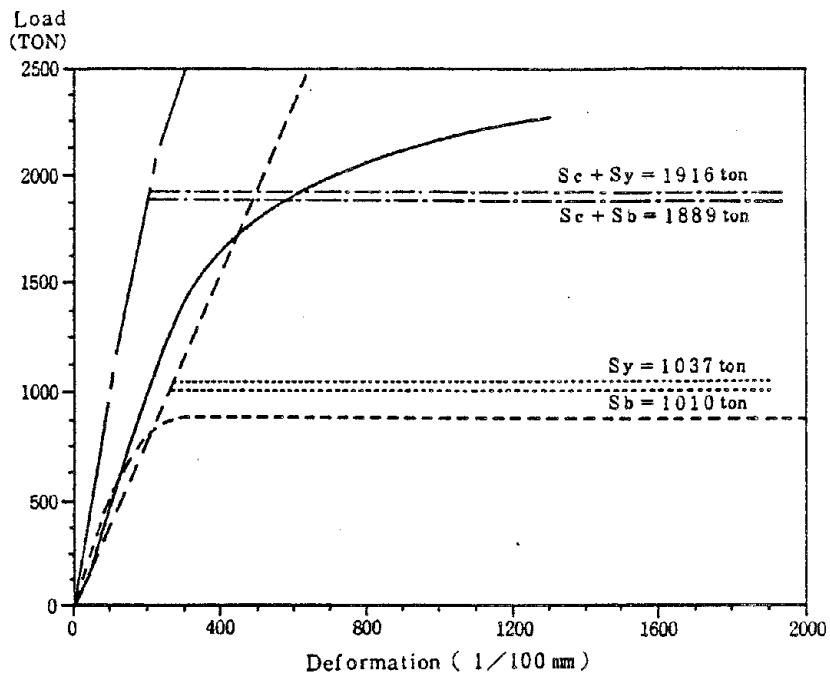


Fig. 15 Load - Deformation Curve (B - 4)

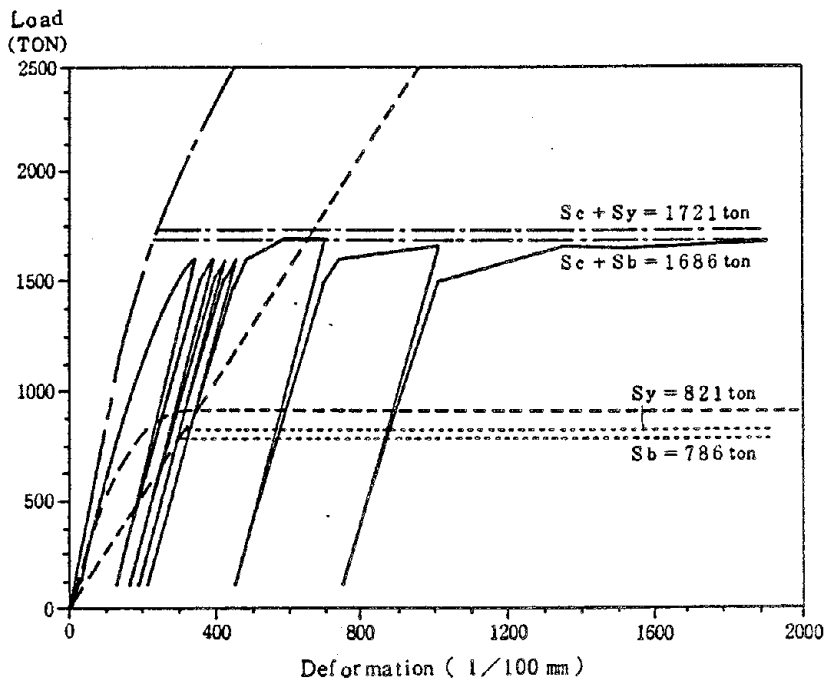


Fig. 16 Load - Deformation Curve (B - 5)

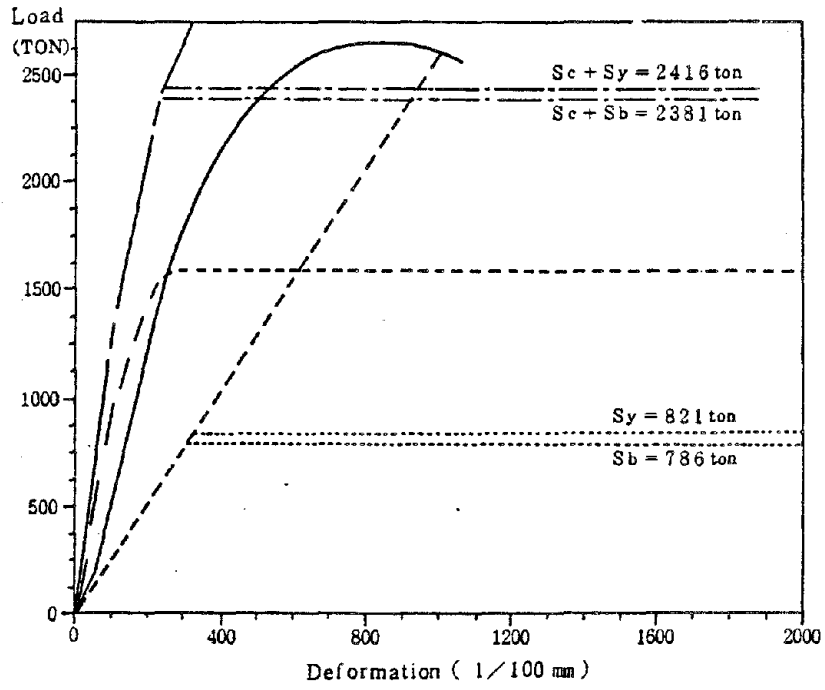


Fig. 17 Load-Deformation Curve (B - 6)

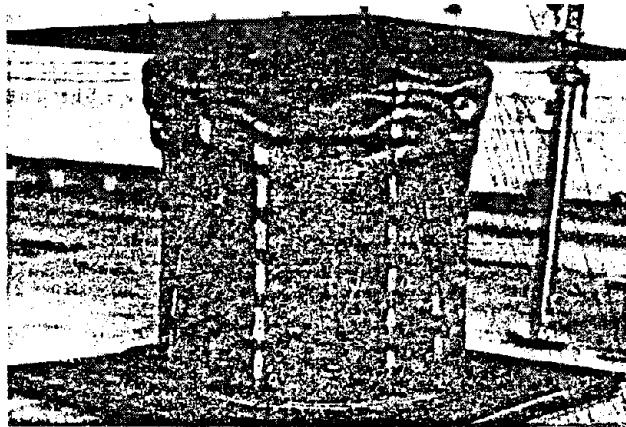


Photo-9. Specimen A - 2 After Loading

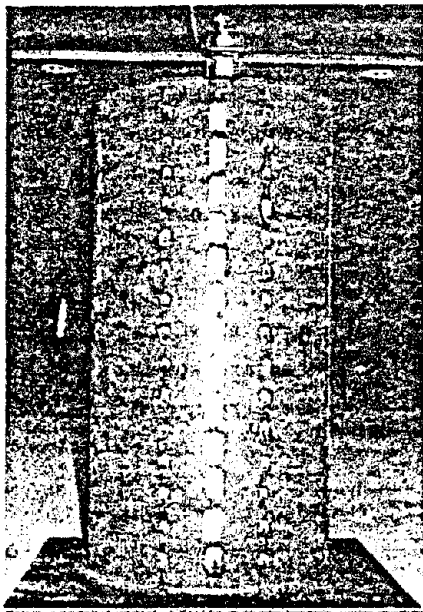


Photo-10. Specimen A - 4 After Loading

Photo 11 shows the B-2 specimen after loading. Concrete-filled steel tubes are also subject to local buckling as shown in the photo, however, even in the plastic region the local buckling did not spread out, and the specimen did not lose the resistance. Photo 12 shows the B-3 specimen which was loaded to large-deformation region. At that time, pipe diameter was widened significantly at the center due to the hoop tension force. But, it did not lose the resistance. Therefore, as far as hoop tension action is expected, concrete-filled steel tubes will keep their ductility.

In the previous section, it was described that high strength concrete was required to expect the resistance of Case 3. It depends on whether the concrete is broken or not. Photo 13 shows the concrete after loading, where no local buckling of the steel tube is observed. Photo 14 shows the concrete where local buckling is observed. In the Photo 14, the concrete is broken in small blocks. It is reasonable to conclude that, if the concrete is strong enough, the concrete will not be broken even

in the plastic region, and therefore, the resistance of Case 3 can be expected, while if the concrete is not strong enough, the concrete will be broken into small blocks in plastic region, and at that time, the resistance of Case 3 cannot be expected, the hoop tension not being enough. Actually, specimen B-6 did not yield any local buckling, and showed the resistance of Case 3 (Photo 15).

In the load-deformation curves shown in Fig. 12 to Fig. 17, the rigidity of the specimens are somewhat lower than the theoretical rigidity, where stress-strain curve of the concrete is supposed as follows.

$$\sigma = \sigma_{ck} \frac{\epsilon}{0.002} \left(2 - \frac{\epsilon}{0.002} \right) \quad 0 \leq \epsilon \leq 0.002 \quad \dots (2)$$

In the equation, the ratio of the modulus of elasticity is 8.5 at $\epsilon = 0$, which may be reasonable for the concrete.

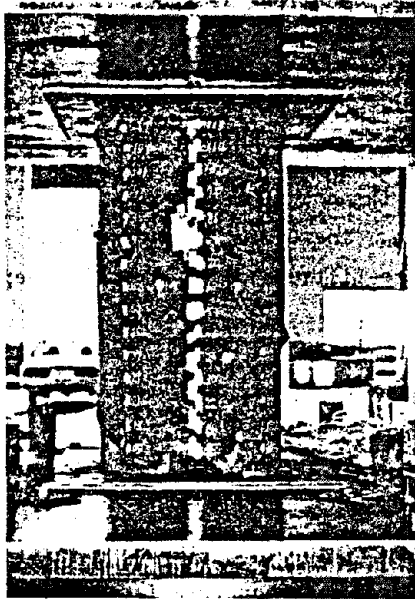


Photo-11.
Specimen B-2 After Loading

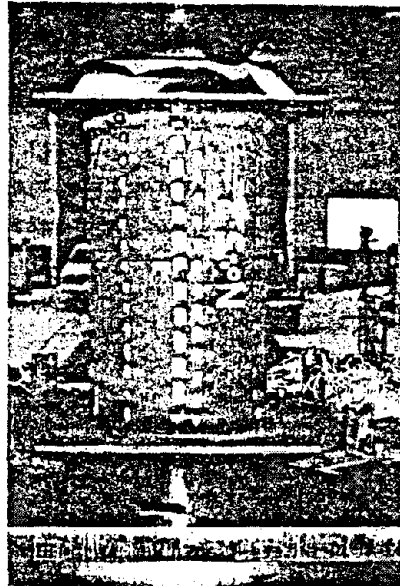


Photo-12.
Specimen B-3 After Loading



Photo-13.
Concrete After Loading

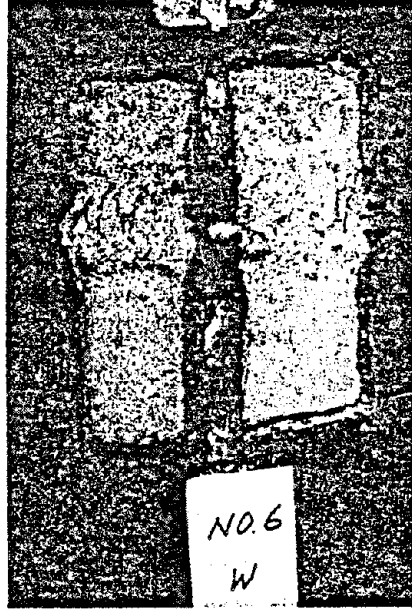


Photo-14.
Concrete After Loading

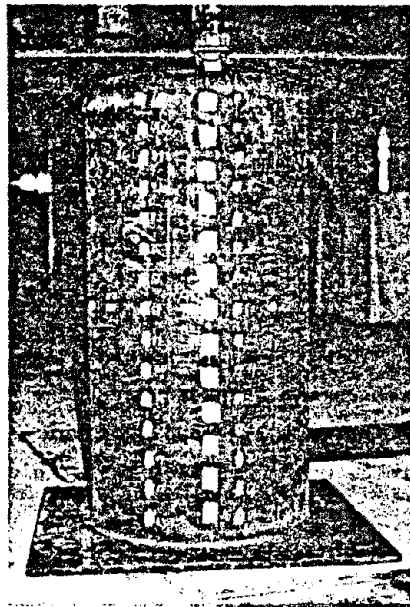


Photo-15. Speimen B - 6 After Loading

The followings can be considered to explain the above.

1. The residual stresses due to the studs may bring about lower rigidity. Actually, specimen B-5, which has no stud, shows pretty high rigidity.
2. It is reported that the quality of the concrete cast and cured in the airtight condition in a pipe is not so good. Therefore, the rigidity of the concrete itself might have been lower than expected.

4.3 Behavior of longitudinal strain

Fig. 18 to Fig. 27 shows the behavior of the longitudinal strains of the specimens. All the strains were measured at the surface of the steel tubes. The figures show the strains where local buckling was observed. Therefore, local buckling behavior can be observed from the figures.

Fig. 18 to Fig. 20 show that the local buckling of the specimens is pretty elastic, because they are thin plate steel tubes, while Fig. 21 shows that A-4 specimen did not yield local buckling and showed only elasto-plastic behavior.

Fig. 22 to Fig. 27 shows a little disturbance of the strains which may be caused by residual stresses due to studs. They also show that the rigidity of the specimens is somewhat lower than the theoretical values, which was described in the previous section. But, besides these, no special problem can be observed. The residual stresses due to studs may cause fatigue problems if subjected to highly cyclic loadings, but as far as bridge piers are concerned, we can neglect the problem.

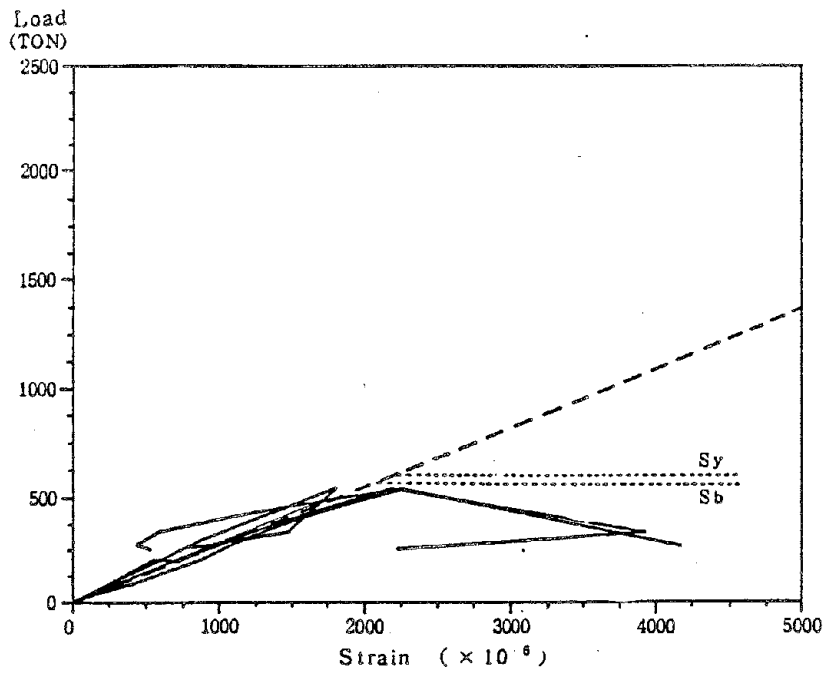


Fig. 18 Load - Strain Curve (A - 1)

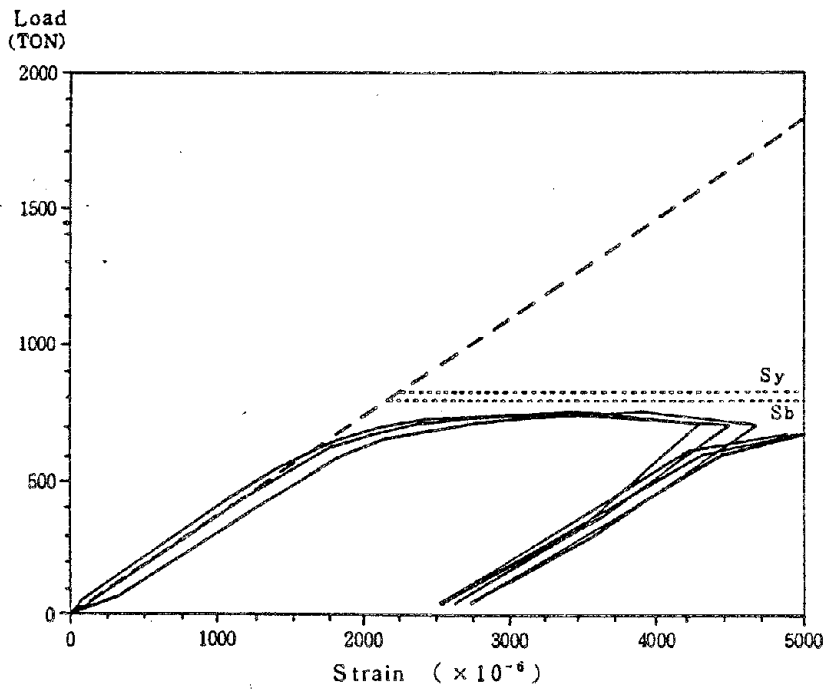


Fig. 19 Load - Strain Curve (A - 2)

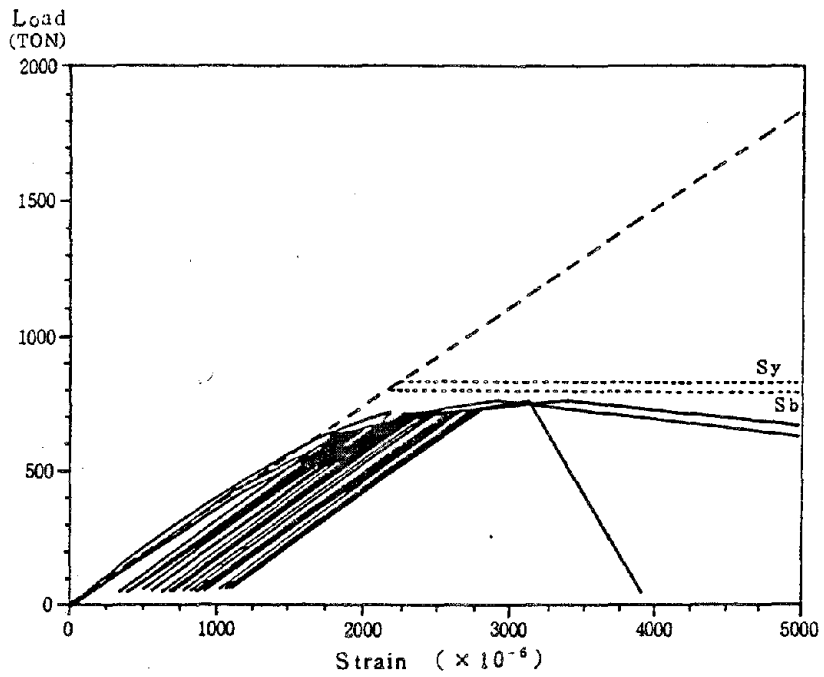


Fig. 20 Load - Strain Curve (A - 3)

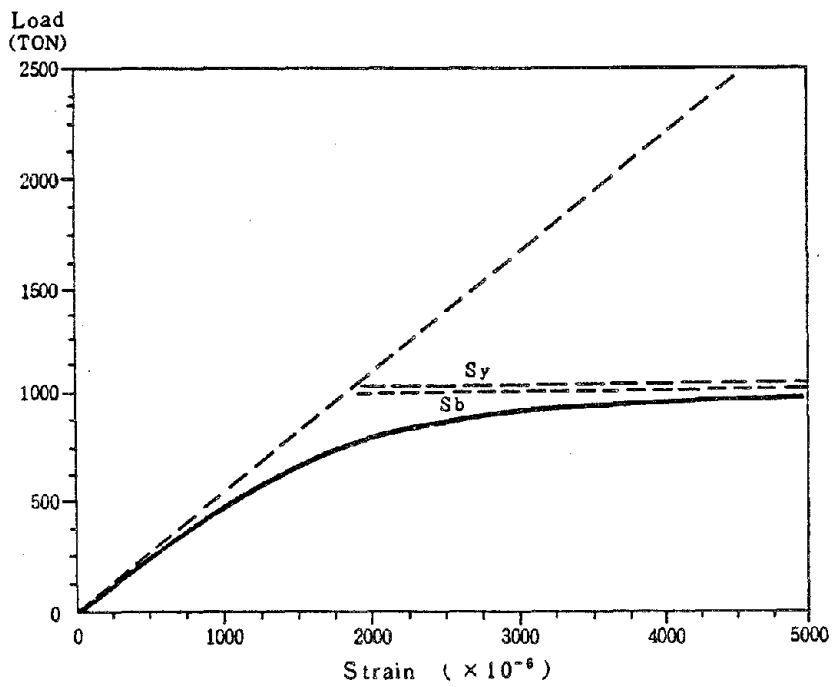


Fig. 21 Load - Strain Curve (A - 4)

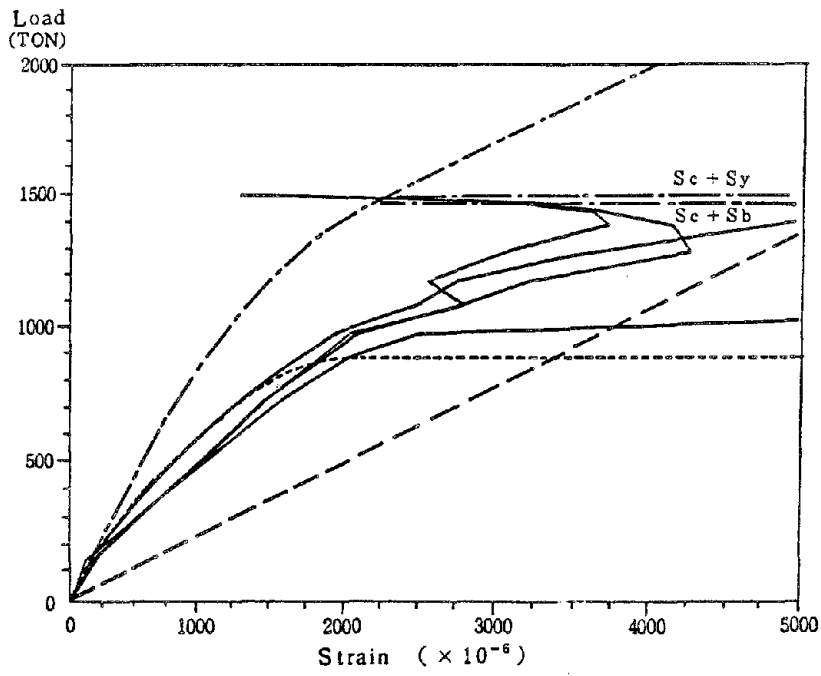


Fig. 22 Load - Strain Curve (B - 1)

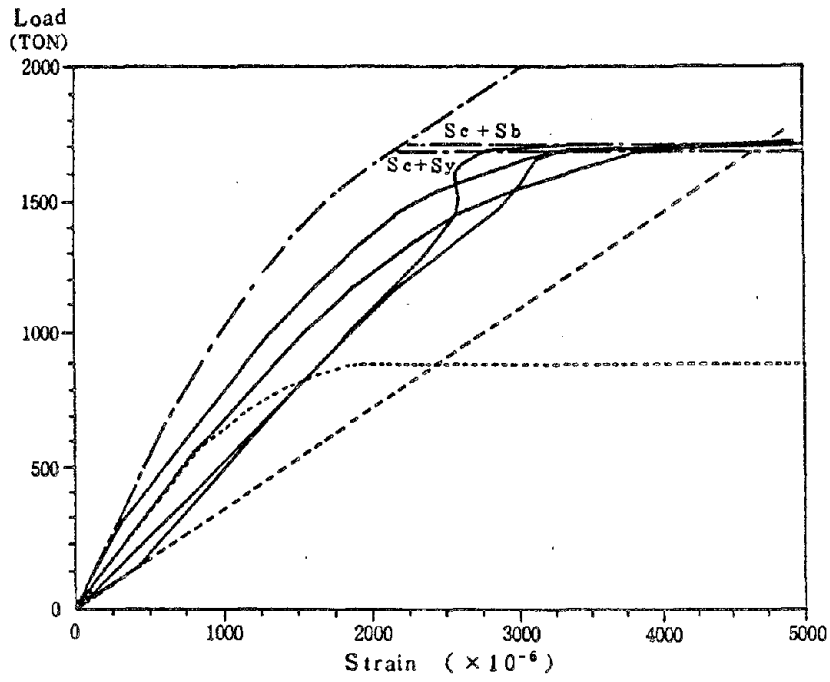


Fig. 23 Load - Strain Curve (B - 2)

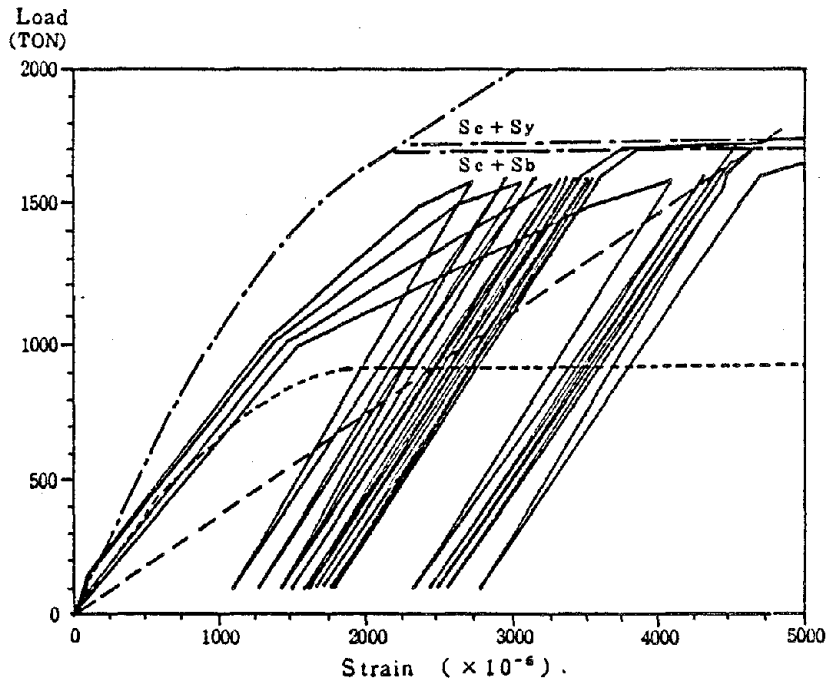


Fig. 24 Load - Strain Curve (B - 3)

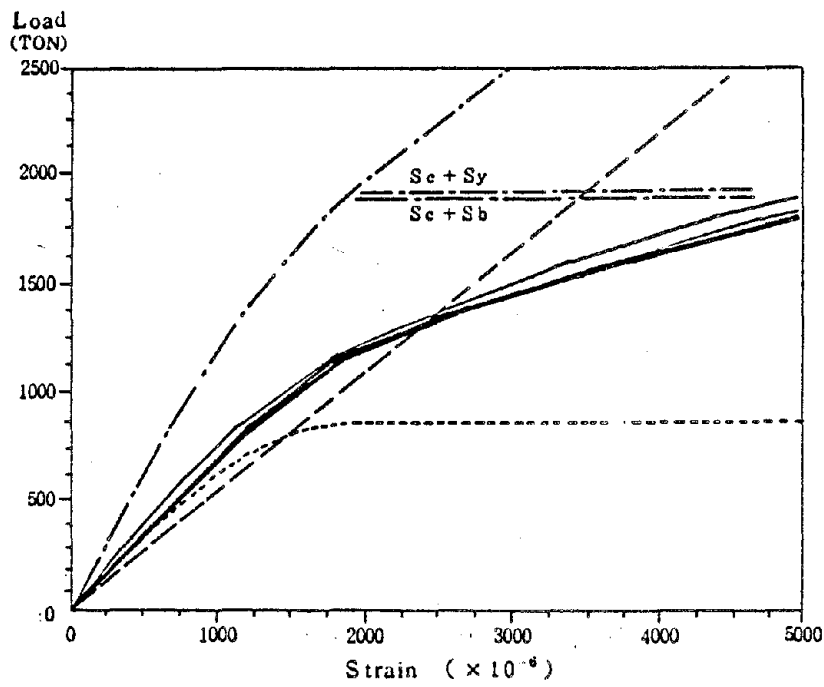


Fig. 25 Load - Strain Curve (B - 4)

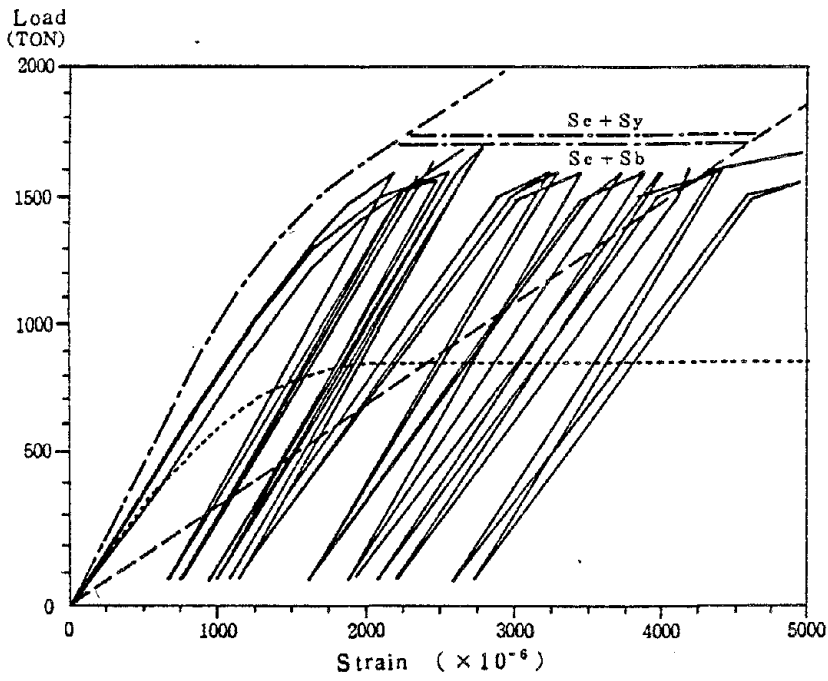


Fig. 26 Load - Strain Curve (B - 5)

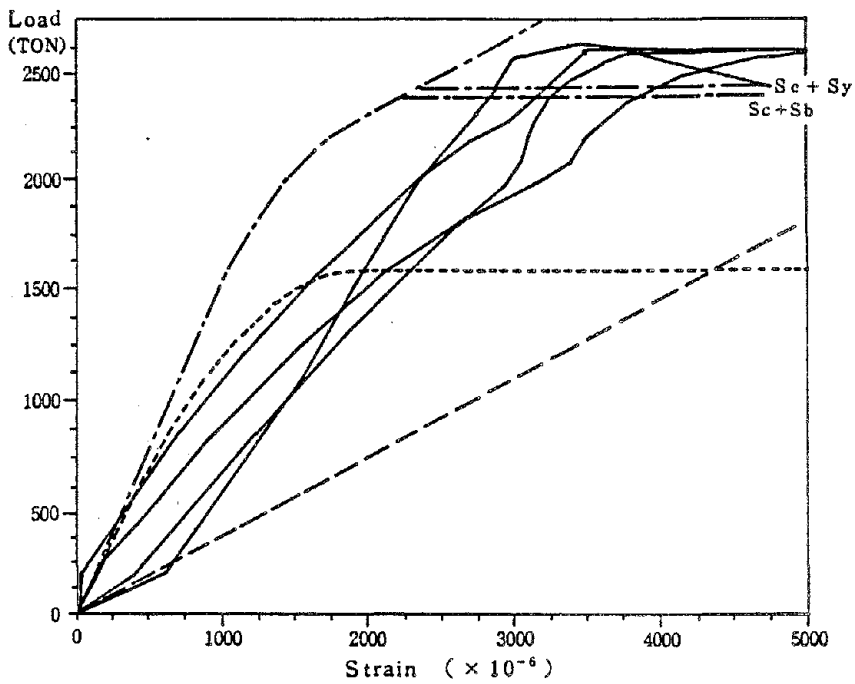


Fig. 27 Load - Strain Curve (B - 6)

4.4 Behavior of hoop stain

As described in Chapter 2, the concrete and the steel tube of a concrete-filled steel tube will separate from each other in elastic region. Regarding the problem, the following theoretical solution can be obtained.

First, when the steel and the concrete behave independently, the hoop stains of the steel tube and the concrete is expressed by the following formulas.

$$\epsilon_{hs} = -\nu_s \cdot \epsilon_x \quad \dots\dots\dots (3)$$

$$\epsilon_{hc} = -\nu_c \cdot \epsilon_x \quad \dots\dots\dots (4)$$

where, ϵ_x means longitudinal strain, and ν_s and ν_c means the Poisson's ratio of the steel and concrete respectively.

When they are connected together by the bond stress σ_{co} , the hoop strain of the steel is expressed by the followings (fig. 28).

$$\epsilon_{hs} = -\left(\nu_s \epsilon_x + \frac{\sigma_{co} \cdot R}{E_s \cdot t}\right) \quad \dots\dots\dots (5)$$

where, R and t is the radius and the thickness of the steel tube. The hoop strain of the concrete is

$$\epsilon_{hc} = -\left(\nu_c \cdot \epsilon_x - \frac{(1 - \nu_c) \sigma_{co}}{E_c}\right) \quad \dots\dots\dots (6)$$

If the concrete and the steel behave together, ϵ_{hs} must be equal to ϵ_{hc} . Therefore, σ_{co} can be expressed as follows.

$$\sigma_{co} = \frac{\nu_c - \nu_s}{\left[\frac{R}{t} / E_s + (1 - \nu_c) / E_c\right]} \epsilon_x \quad \dots\dots\dots (7)$$

and ϵ_{hs} can be expressed as

$$\epsilon_{hs} = -\epsilon_x \left(\nu_s - \frac{\nu_s - \nu_c}{[1 + (1 - \nu_c) \frac{t \cdot E_s}{R \cdot E_c}]} \right) \dots\dots\dots (8)$$

Now, to examine the behavior of the concrete-filled steel tubes, Where the maximum resistance is attained, let's assume that $E_s/E_c = 15.0$. Assuming that $\sigma_y = 4000 \text{ kg/cm}^2$, the required bond stress is expressed as follows.

$$\sigma_{co} = \frac{533}{R/t + 12.5} \text{ (kg/cm}^2\text{)} \dots\dots\dots (9)$$

and the hoop stain is expressed as follows, assuming that $E_s/E_c = 7.0$ in this case

$$\epsilon_{hs} = \left(0.3 - \frac{2}{15[1 + 5.83(t/R)]} \right) \epsilon_x \dots\dots\dots (10)$$

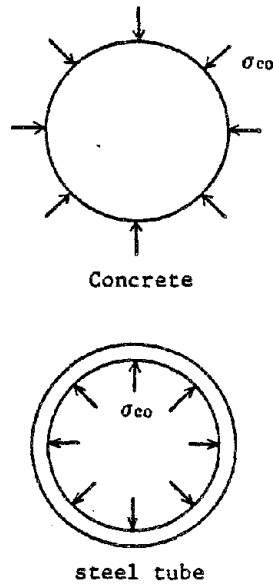


Fig. 28 Bond Stress

If the concrete and the steel behave independently, the hoop strain will be expressed by equ.(3), and if they behave together, the hoop strain will be expressed by equ.(10), the required bond stress being expressed by equ.(9).

When the bond is kept, the Poisson's ratio of the specimen is not 0.3, but $\left(0.3 - \frac{2}{15 [1 + 5.83 (R/t)]} \right)$.

So, let's call this as modified Poisson's ratio. In Table 6, the bond stress σ_{co} and the modified Poisson's ratio is listed.

Fig. 29 to Fig. 38 show the behavior of hoop strains. In the figures, the theoretical curves obtained from equ.(3) and equ.(10) are also shown. The hoop strains of the specimens A-1 to A-4 are just same as the theoretical curves. The hoop strains of the specimen B-1 to B-4 and B-6 are same as the theoretical values, obtained from modified Poisson's ratio, however; the hoop strains of the specimen B-5 is rather like the theoretical values, obtained from Poisson's ratio of 0.3. Therefore, it is concluded that the natural bond between concrete and steel is not enough to connect them together, and without studs, the concrete and the steel will behave independently, while they will behave together with adequate studs. Therefore, studs may be required to design the concrete-filled steel tubes as composite structures.

Table 6. Modified Poisson's Ratio
of the Specimens

Specimen	B - 1	B - 2 B - 3 B - 5 B - 6	B - 4
R/t	58.3	43.8	29.9
σ_{co} (kg/cm ²)	7.5	9.5	12.8
Modified Poisson's Ratio	0.179	0.182	0.189

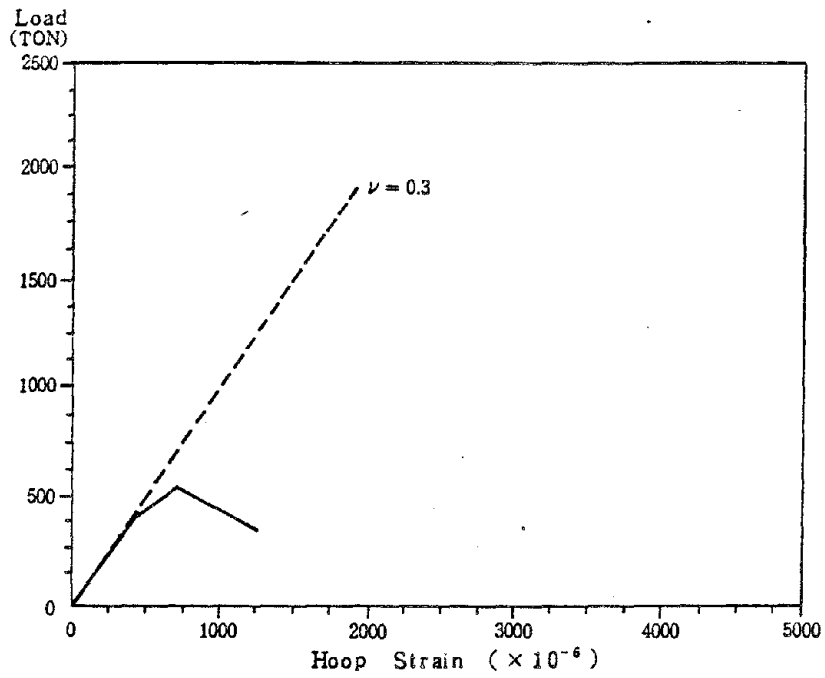


Fig. 29 Load-Hoop Strain Curve (A - 1)

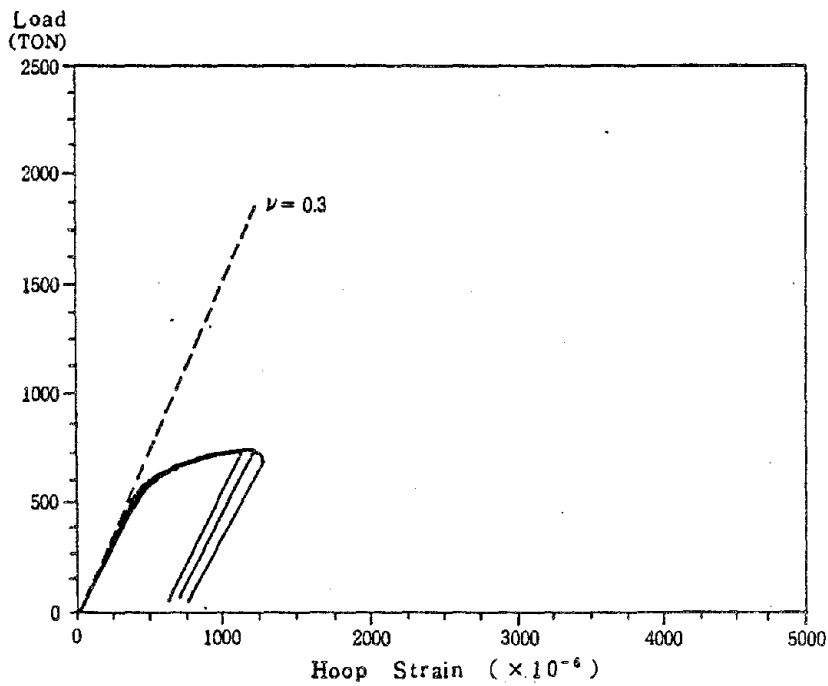


Fig. 30 Load-Hoop Strain Curve (A - 2)

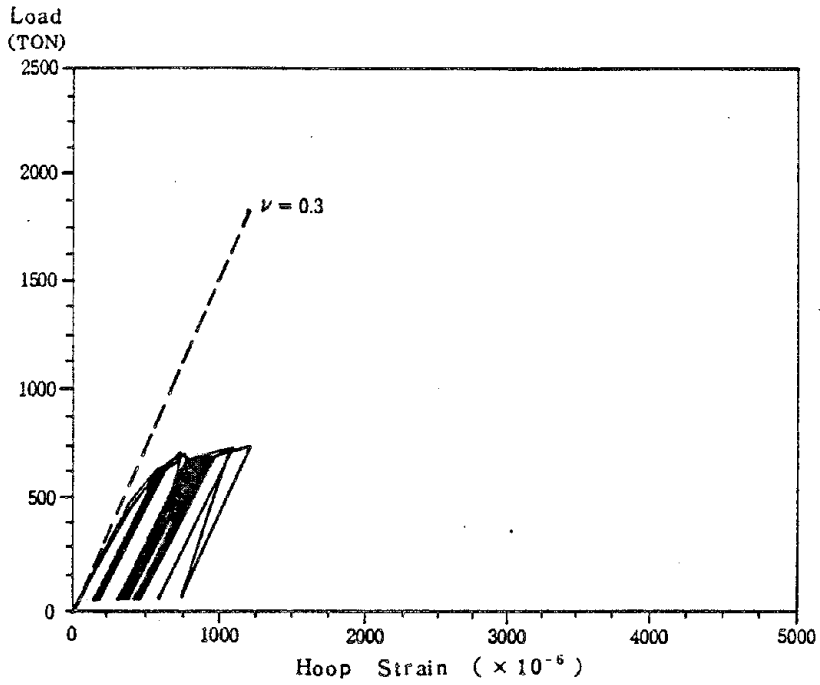


Fig. 31 Load - Hoop Strain Curve (A - 3)

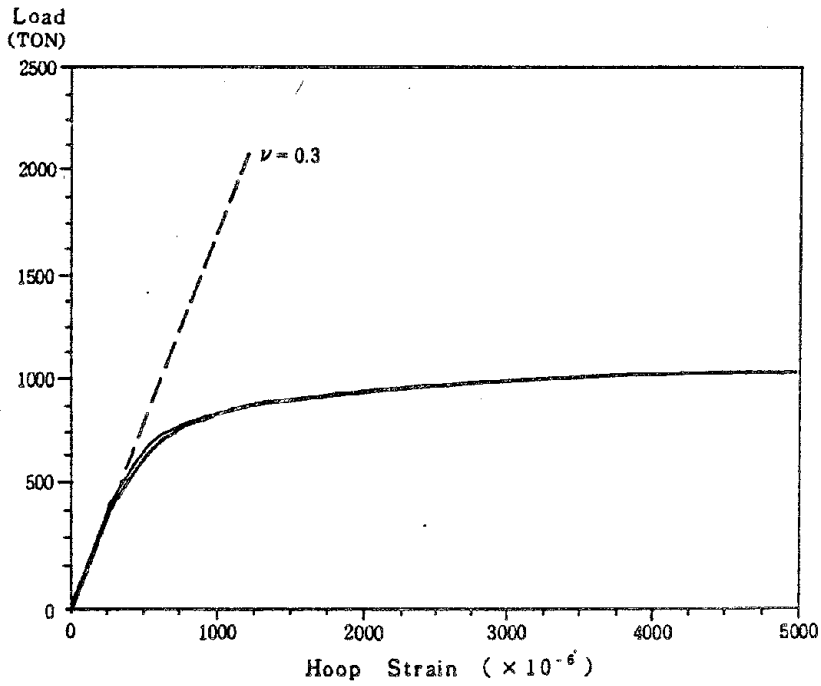


Fig. 32 Load - Hoop Strain Curve (A - 4)

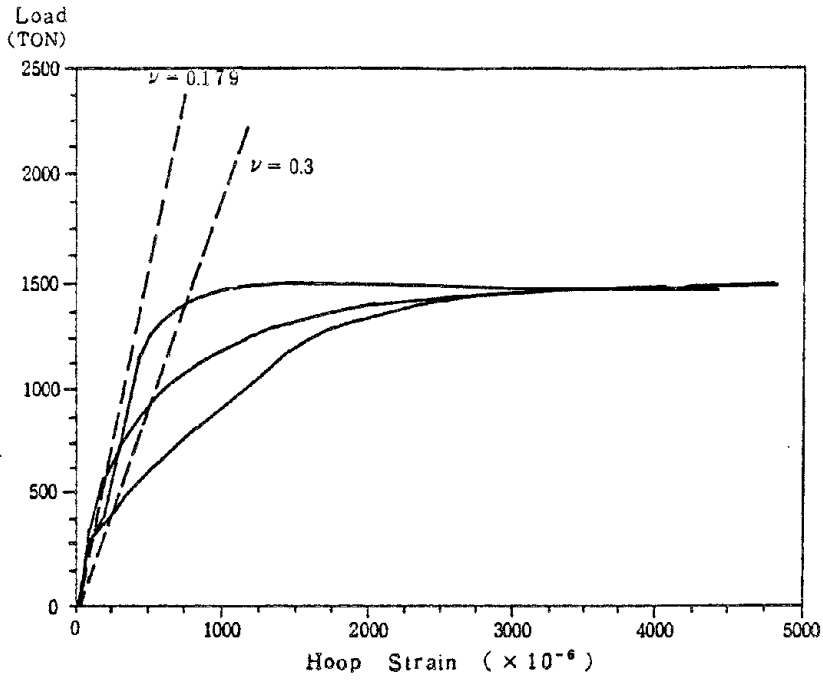


Fig. 33 Load - Hoop Strain Curve (B - 1)

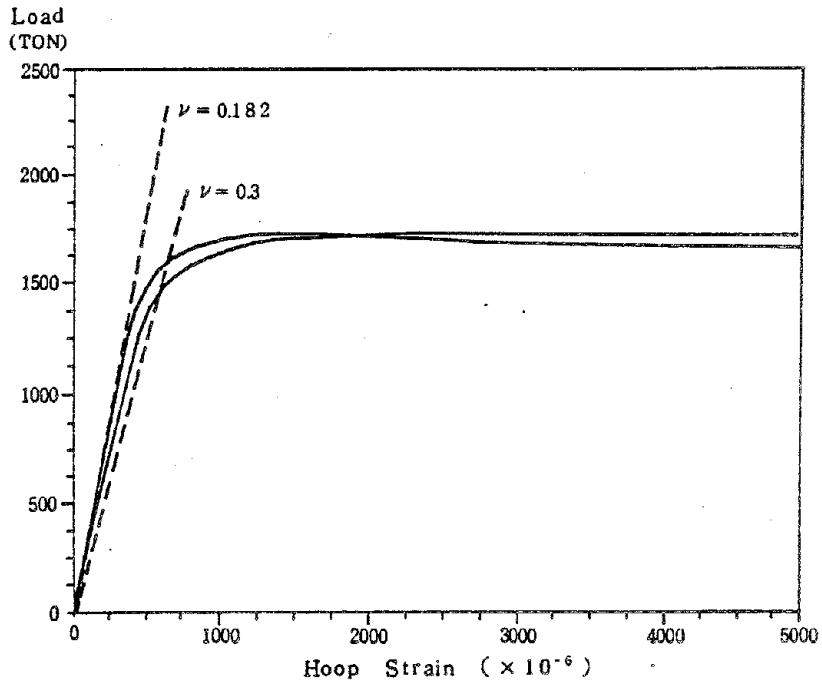


Fig. 34 Load - Hoop Strain Curve (B - 2)

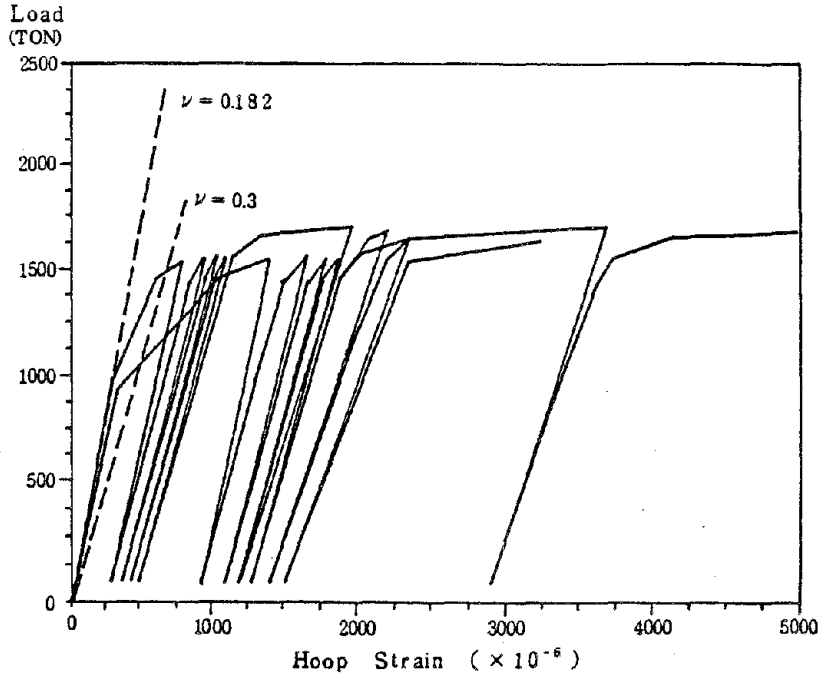


Fig. 35 Load - Hoop Strain Curve (B - 3)

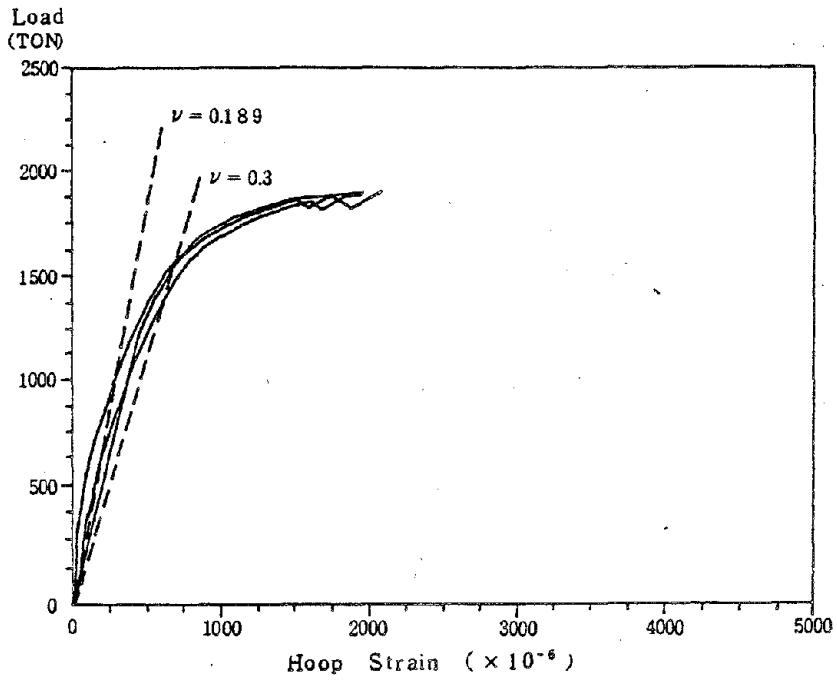


Fig. 36 Load - Hoop Strain Curve (B - 4)

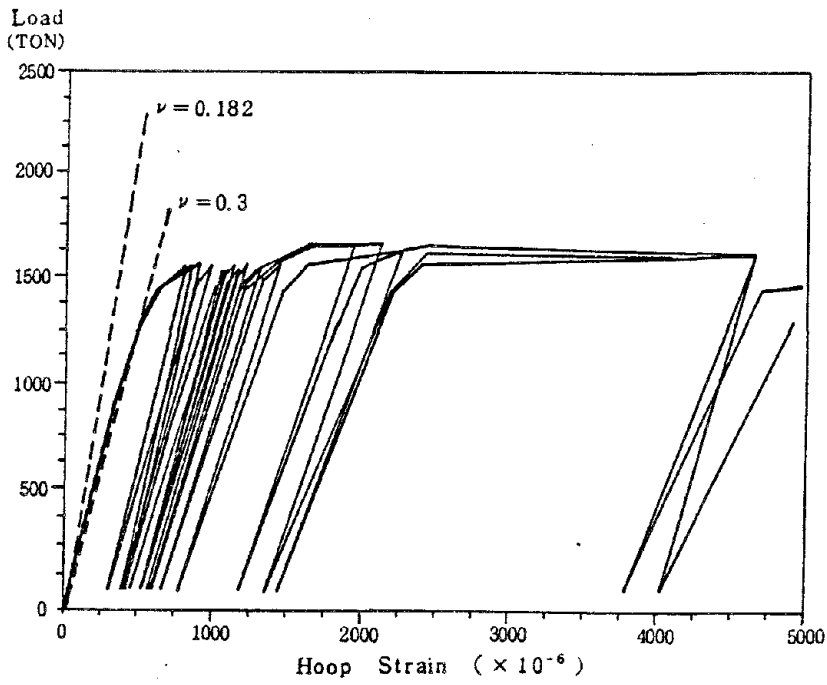


Fig. 37 Load-Hoop Strain Curve (B - 5)

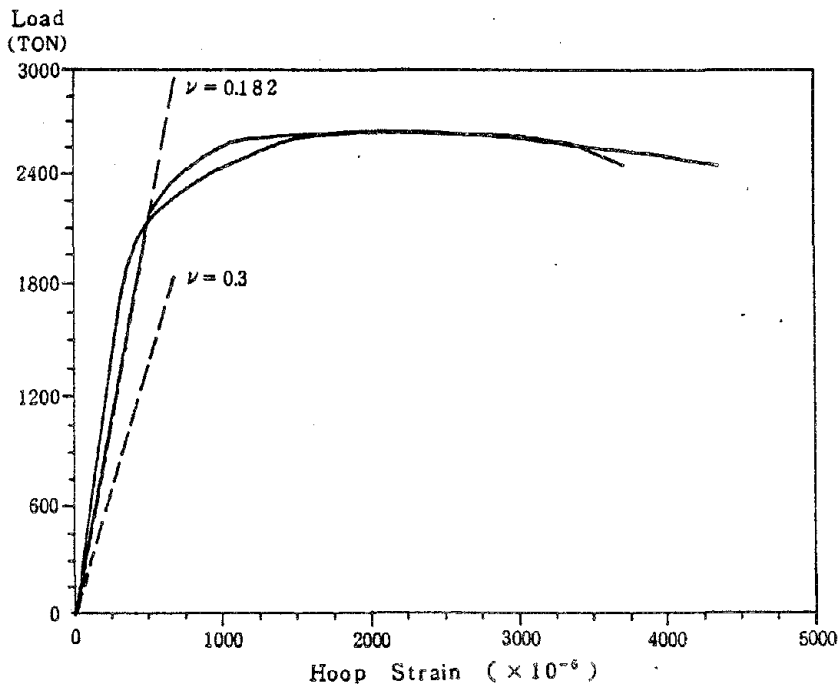


Fig. 38 Load-Hoop Strain Curve (B - 6)

CHAPTER - 5 CONCLUSION

The followings may be concluded about the behavior of concrete-filled steel tubes under compression.

- (1) When studs are provided, the sum of the steel yield strength and the concrete cylinder strength can be, at least, expected irrespective of the steel plate thickness and the concrete strength. When thicker plate is used, or high strength concrete is used, higher resistance can be expected because of the hoop tension action of steel tubes.

On the other hand, when studs are not provided, the resistance of concrete-filled steel tubes will be the sum of the buckling strength of the steel tubes and the concrete cylinder strength, because they behave independently.

- (2) Concrete-filled steel tubes have good ductility, while steel tubes themselves have usually small ductility. Steel tubes of the concrete-filled steel tubes will yield local buckling and the concrete inside will be broken if the plate is not thick, or if the concrete is not strong, but it will not impair the resistance and the ductility significantly. But in this case, hoop tension effect cannot be expected.
- (3) Judging from the hoop strain behavior, concrete-filled steel tubes without studs cannot be designed as composite structures. Adequate studs may be required for composite concrete-filled steel tubes.

References

1. Tomie, M., et al, "Design Problems of Concrete-filled Steel Tubes"
Column No. 73, 1979.7
2. Tomie, M., et al, "State-of-the-art of Concrete-filled Steel Tubes"
Concrete Engineer, Vol. 13, No. 2, 3, 1975
3. Kishida, H., et al, "Bending Strength of Concrete-filled Steel Tubes"
JSSC, Vol. 15, No. 164
4. Oki, T., et al, "Concrete-filled Steel Tubes in Compression"
Journal of the Japan Society for Architectural
Engineers, Vol. 69, 1961
5. Saito, J., et al, "Concrete-filled Steel Tubes with Low Strength
Mortar", Report of Ohbayashigumi, Vol. 9, 1974
6. "Specification for Concrete-filled Steel Tubes" Japan Society for
Architectural Engineers 1980.2 .
7. L.H. DONNELL, C.C. WAN ; "Effect of imperfections on Buckling of
Thin Cylinders and Columns Under Axial
Compression", JOURNAL OF APPLIED
MECHANICS, 1950.3 .
8. N.J. GARDNER, E.R. JACOBSON ; "Structural Behavior of Concrete
Filled Steel Tubes", ACI JOURNAL,
1967.7 .
9. P.K. Neogi, H.K. Sen, J.C. Chapman ; "Concrete-filled Tubular Steel
Columns under Eccentric Loading",
THE STRUCTURAL ENGINEER, No.5,
Vol. 47, 1969.5 .

10. C.G. SCHILLING ; Buckling Strength of Circular Tubes, ASCE,
Vol. 91, No. ST.5, 1965
11. Yamada, M., "Experimental Study on the Concrete-filled Steel Tubes"
Journal of the Japan Society for Architectural
Engineers, Vol. 103, 1964.10 .
12. Oki, T., "Concrete-filled Steel Tubes under Eccentric Loading"
Journal of the Japan Society for Architectural Engineers,
1965.9 .

BEHAVIOR OF CONCRETE-FILLED STEEL TUBES

(PART 2; BENDING MEMBERS)

by

N. Narita*, S. Saeki** and M. Kanai***

ABSTRACT

Concrete-filled Steel Tubes are suitable for bridge piers, because of their high resistance and good ductility. However, design specifications for concrete-filled steel tubes are not well established, because their behavior is pretty complicated.

Last year, we reported about the behavior of concrete-filled steel tubes subjected to compression. In this report, the behavior of concrete-filled steel tubes subjected to bending is discussed in detail. The conclusions are as follows:

1. The resistance of concrete-filled steel tubes subjected to bending will be more than the full-plastic bending moment due to the hoop-tension action of the steel tubes, on condition that the natural bond between the steel tubes and the concrete is secured.
2. The steel tubes and the concrete of concrete-filled steel tubes may separate from each other, when enough amount of shear connectors are not provided.

1. INTRODUCTION

Last year, the behavior of concrete-filled steel tubes was discussed under compression. High resistance and good ductility of concrete-filled steel tubes were observed, because the local buckling of the steel tubes was prevented and the concrete is triaxially compressed due to the hoop tension action of the steel tubes. However, shear connectors are sometimes needed to secure the composite action of the concrete-filled steel tubes.

In this report, the behavior of concrete-filled steel tubes under bending is discussed. Although the concrete-filled steel tubes are not expected to be used as beams, bending tests are effective to know the behavior of beam-columns. The beam-column tests are expected to be made next year.

* Director, Planning and Research Adm. Dep., P.W.R.I.

** Head, Bridge Division, P.W.R.I.

*** Research Engineer, Bridge Division, P.W.R.I.

2. OUTLINE OF THE TESTS

Six specimens were tested, the dimensions of which are shown in Table 1. Specimens A-1 to A-3 have diaphragms which are designed to satisfy the Highway Bridge Specifications in Japan. The shearing forces between the steel tubes and the concrete can be shared with diaphragms. A-1 has 16 studs in every 15 cm section, which transmit the shearing forces and prevent the local buckling of the tube. A-2 has no stud, the shearing forces are transmitted by the natural bond of the steel tubes and the concrete. A-3 has grease between the steel tubes and the concrete, which will remove the natural bond.

Specimens B-1 to B-3 have no diaphragms, B-1 has enough studs to transmit the shearing forces and to prevent the separation of the steel tube and the concrete in elasticity. The separation occurs because the Poisson's ratio of concrete is smaller than that of the steel tubes in elasticity. B-2 has studs only to secure the transmission of the shearing forces. B-3 has no studs, the shearing force being transmitted by the natural bond only.

The test was performed using 3000 ton testing machine of the P.W.R.I.. The strain of the steel tubes and of the concrete, and the deformation were measured in the test (Photo-1,2).

3. RESISTANCE

The Load-Deformation curves of the specimens are shown in Fig. 3 - Fig. 8. The theoretical curves are also shown, supposing gross section, net section (reinforced concrete theory), and steel section are effective. The loadings corresponding to the full-plastic bending moment (P_p), and to the tensile yielding of the steel tube (P_{syt}) are also shown in the Figures. Concrete-filled steel tubes will not collapse even if the yielding of the materials are observed, therefore, the resistance of the concrete-filled steel tubes can not be evaluated by reinforced concrete theory. In this report, full-plastic bending moment is used as a measure to evaluate the resistance. The tensile yielding of the steel tubes are indicated to show the beginning of plasticity.

The full-plastic moment is evaluated supposing the following conditions.

- 1) Stress distribution is shown in Fig. 9, because local buckling of the tubes and shearing failure of the concrete is prevented.
- 2) The steel tube and the concrete will confine each other strictly.

3) The hoop tension action of the steel tube and the triaxial compression of the concrete are not considered.

4) The thickness of the tube is much smaller than the radius.

Then, the full-plastic moment (M_p) is evaluated as follows. First, the location of neutral axis (d) is obtained by solving the follows.

$$(1 + 4 \cdot \frac{t}{r} \cdot \frac{\sigma_{sy}}{\sigma_{ck}}) \cdot (\frac{\pi}{2} - \alpha) + \sin \alpha \cdot \cos \alpha = \frac{\pi}{2} \quad \dots\dots\dots(1)$$

$$d = r \cdot \cos \alpha \quad \dots\dots\dots(2)$$

Then the M_p is obtained by the follows.

$$M_p = M_c + M_{sc} + M_{st} \quad \dots\dots\dots(3)$$

where, M_c indicates the bending moment due to the concrete and can be estimated as,

$$M_c = A_c \cdot Y_c \cdot \sigma_{ck} \quad \dots\dots\dots(4)$$

where A_c , Y_c are given by

if $\alpha \geq \pi/4$

$$A_c = r^2 (\alpha - \sin \alpha \cdot \cos \alpha) \quad \dots\dots\dots(5)$$

$$Y_c = r \left(\frac{2 \sin^3 \alpha}{3(\alpha - \sin \alpha \cdot \cos \alpha)} - \cos \alpha \right) \quad \dots\dots\dots(6)$$

if $\alpha < \pi/4$

$$A_c = \frac{2}{3} r^2 \alpha^3 (1 - 0,2\alpha^2 + 0,019\alpha^4) \quad \dots\dots\dots(7)$$

$$Y_c = 0,2R\alpha^2 (1 - 0,0619\alpha^2 + 0,0027\alpha^4) \quad \dots\dots\dots(8)$$

and M_{sc} and M_{st} denotes the bending moment of steel tubes in compression and in tension, which can be evaluated as follows.

$$M_{sc} = A_{sc} \cdot Y_{sc} \cdot \sigma_y \quad \dots\dots\dots(9)$$

$$A_{sc} = 2 \cdot \alpha \cdot t \cdot r \quad \dots\dots\dots(10)$$

$$Y_{sc} = r \left(\frac{\sin \alpha}{\alpha} - \cos \alpha \right) \quad \dots\dots\dots(11)$$

$$M_{st} = A_{st} + Y_{st} \cdot \sigma_y \quad \dots\dots\dots(12)$$

$$A_{st} = 2 \cdot \alpha' \cdot t \cdot r \quad \dots\dots\dots(13)$$

$$Y_{st} = r \left(\frac{\sin \alpha'}{\alpha} - \cos \alpha' \right) \quad \dots\dots\dots(14)$$

Now, the following behavior of the specimens is observed from the Figures, except for specimen A - 3.

- 1) Gross section is effective at the first state of loadings, but after that net section (obtained from reinforced concrete theory) is effective due to the cracking of the concrete in tension.
- 2) Even after the yielding of the materials, the load bearing capacity of the specimens increases steadily, finally exceeding the full-plastic bending moment due to the triaxial compression of the concrete.
- 3) High ductility can be expected.

While in specimen A - 3, the full-plastic moment cannot be expected and poor ductility was observed because the natural bond of the steel tube and the concrete was removed.

Therefore, as far as the resistance of the beams is concerned, high resistance and good ductility is secured by the natural bond between the steel tube and the concrete, and studs are not needed. However, the resistance will be reduced significantly when natural bond is impaired.

After the loading, local buckling of the steel tube and cracking of the concrete were observed at the center span of the beam (Photo-3,4). However, even after yielding local buckling, the resistance of the beam is secured, because of the hoop tension action of the steel tubes. The concrete in tension has many cracks (Photo-5).

4. STRAIN OF CONCRETE

Typical behavior of the strain of the concrete (specimen A - 1) is shown in Fig. 10. At the loading of 60 tons (about 2/5 of the maximum loading), the strain of concrete in compression can be estimated conservatively by reinforced concrete theory. Of course, the strain of the concrete in tension can be disturbed by the cracking.

At the loading of 150 tons, measured strains exceeds the theoretical values because of the yielding of the steel and the concrete. However, the location of neutral axis may be estimated by reinforced concrete theory.

Therefore, the strain of concrete-filled steel tubes before yielding

can be evaluated conservatively by reinforced concrete theory, whereas the strain after yielding is pretty complicated. The resistance of the concrete-filled steel tubes should be evaluated by plastic theory.

5. STRAIN OF STEEL TUBE

The strains of the steel tubes in compression at the center span of the beam is shown in Fig. 11 to Fig. 16. The strain in the right side is compressive axial strain, the strain in the left side being hoop tension strain. Two theoretical curves for the hoop tension strain are shown in the Figures. Supposing that the steel tube and the concrete will behave independently without bond, the strain is given by

$$\epsilon_h = \nu_s \cdot \epsilon_x \quad \dots\dots\dots(15)$$

where ϵ_h denotes the hoop tension strain, ϵ_x is the axial strain and ν_s is the Poisson's ratio of the steel tube. While supposing that the steel tube and the concrete will behave together, the strain will be given by

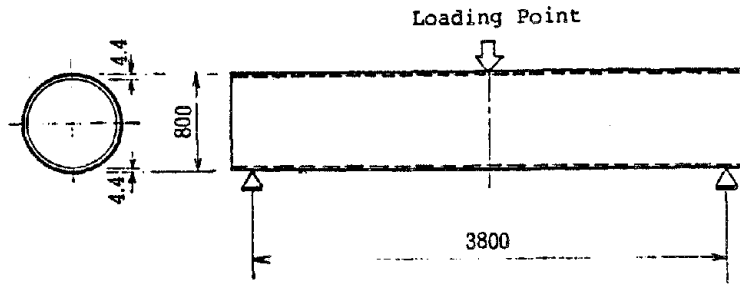
$$\epsilon_h = - \left(\nu_s - \frac{\nu_s - \nu_c}{1 + (1 - \nu_c) \frac{t \cdot E_s}{R \cdot E_c}} \right) \epsilon_x \quad \dots\dots\dots(16)$$

Now, the hoop strain of the specimen A - 1 shows that the strain follows the curve (16), where the bond between the steel tubes and the concrete is supposed, and the steel tube and the concrete behave together, because of the studs between them. However, the strain of A - 2 and A - 3 shows that the bond is not enough. Similarly, B - 1 has enough studs to secure the composite action of the steel tube and the concrete, whereas the strains of B - 2, B - 3 indicates that the studs in B - 2 and the natural bond of B - 3 are not enough for the steel tubes and the concrete to behave together. As discussed earlier, even the specimens A - 2, B - 2 and B - 3 has high resistance and good ductility; however, the behavior is doubtful when subjected to repeated loadings, because the steel tube and the concrete do not behave together in elasticity. More research works are required in this regard.

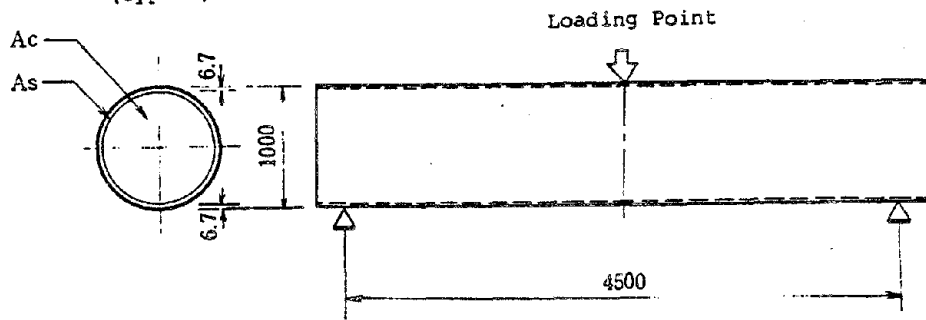
Table-1 Dimensions of the Specimens

specimen	material	stud	t (mm)	A _c (cm ²)	A _s (cm ²)	σ _{ck} (kg/cm ²)	σ _{sy} (kg/cm ²)
A-1	S S 41	with	4.4	4916	41	284	2800
A-2	S S 41	without	4.4	4916	41	284	2800
A-3	S S 41	grease	4.4	4916	41	284	2800
B-1	SM50Y	with(768)	6.8	7642	212	249	4540
B-2	SM50Y	with(288)	6.6	7648	206	247	4400
B-3	SM50Y	without	6.7	7645	209	247	4490

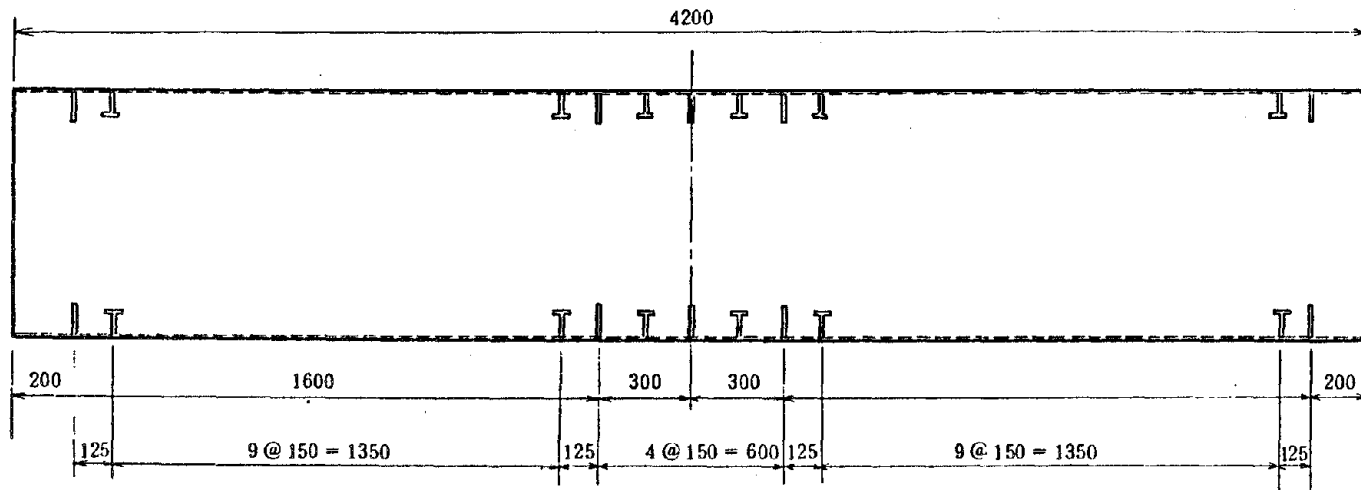
(Type A)



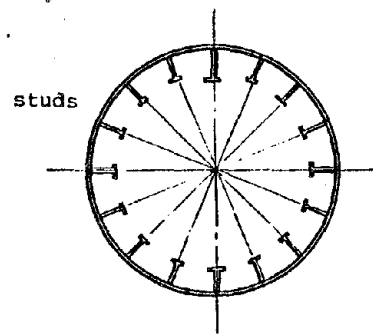
(Type B)



(in mm)



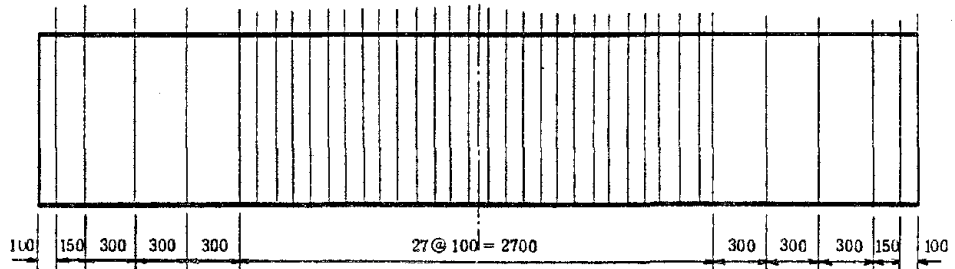
(in mm)



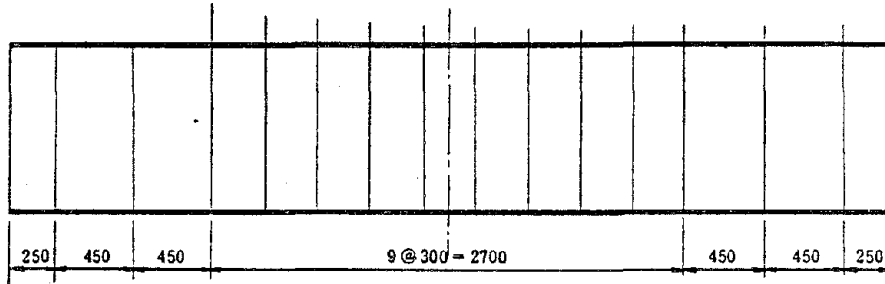
** Only A-1 has studs

Fig.-1 A-type Specimens

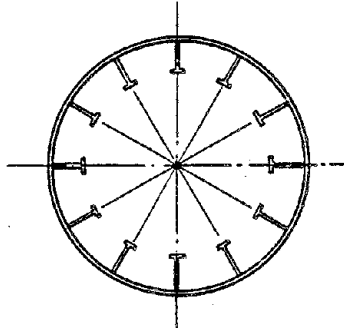
(Location of studs in B-1)



(Location of studs in B-2)



(Cross Section of B-1)



(Cross Section of B-2)

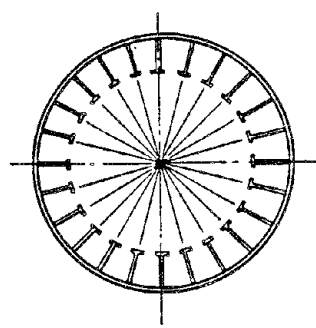


Fig.-2 B-type Specimens

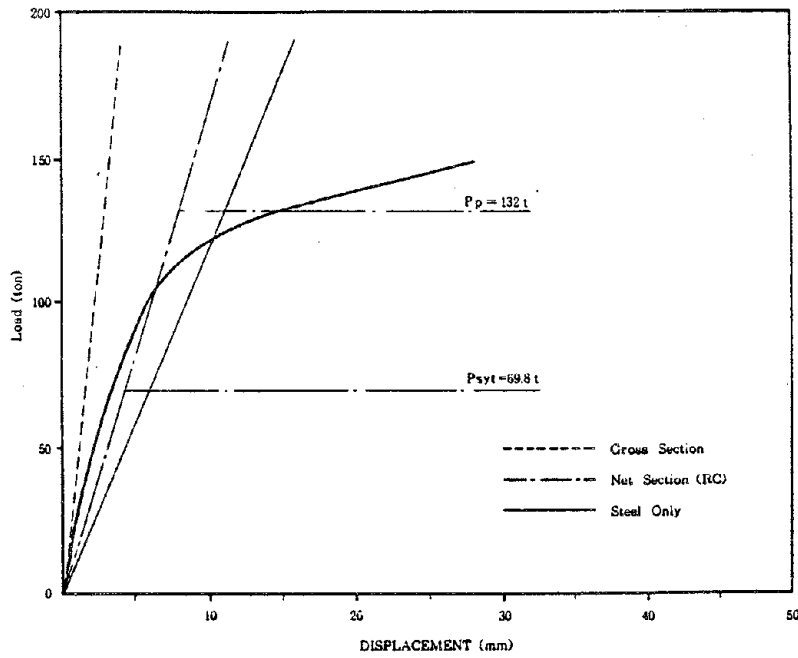


Fig.-3 Load-Deformation Curves (A-1)

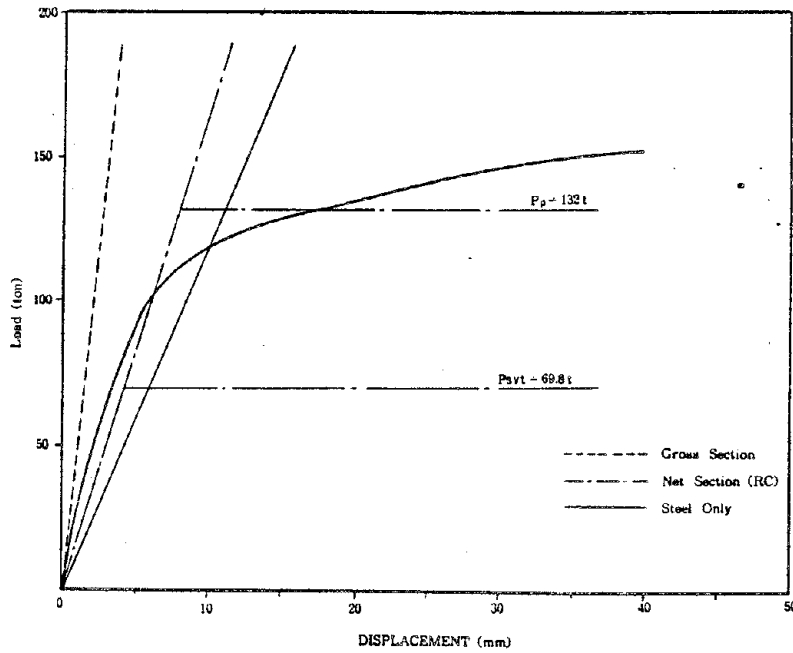


Fig.-4 Load-Deformation Curves (A-2)

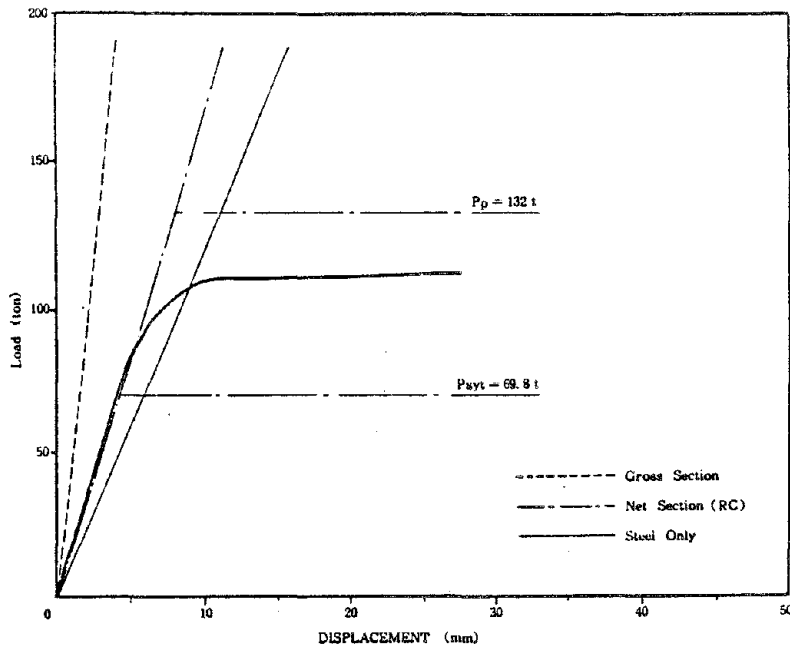


Fig.-5 Load-Deformation Curves (A-3)

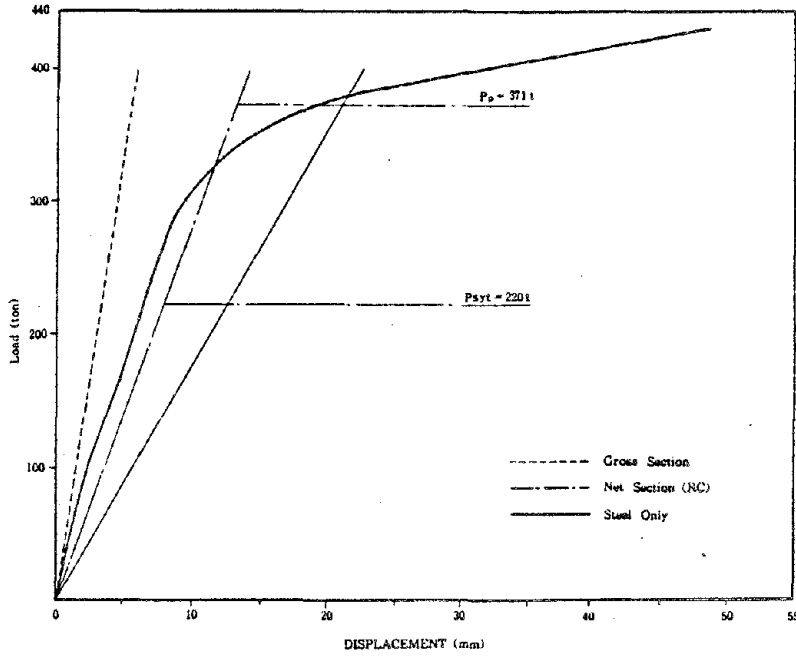


Fig.-6 Load-Deformation Curves (B-1)

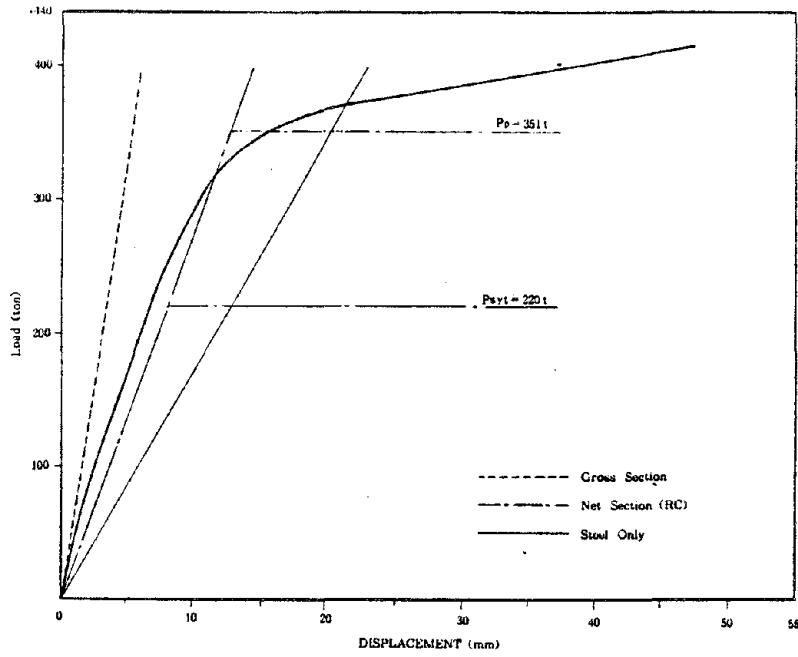


Fig.-7 Load-Deformation Curves (B-2)

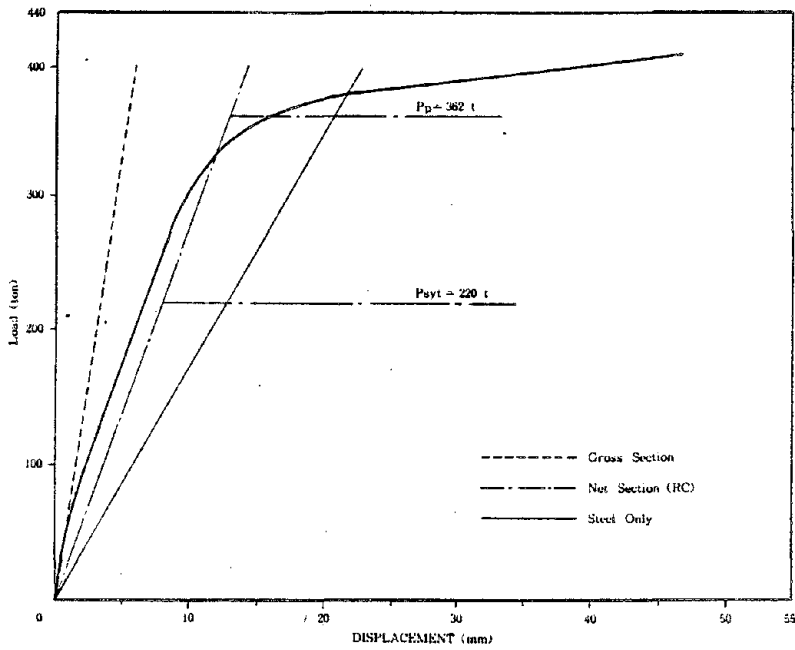


Fig.-8 Load-Deformation Curves (B-3)

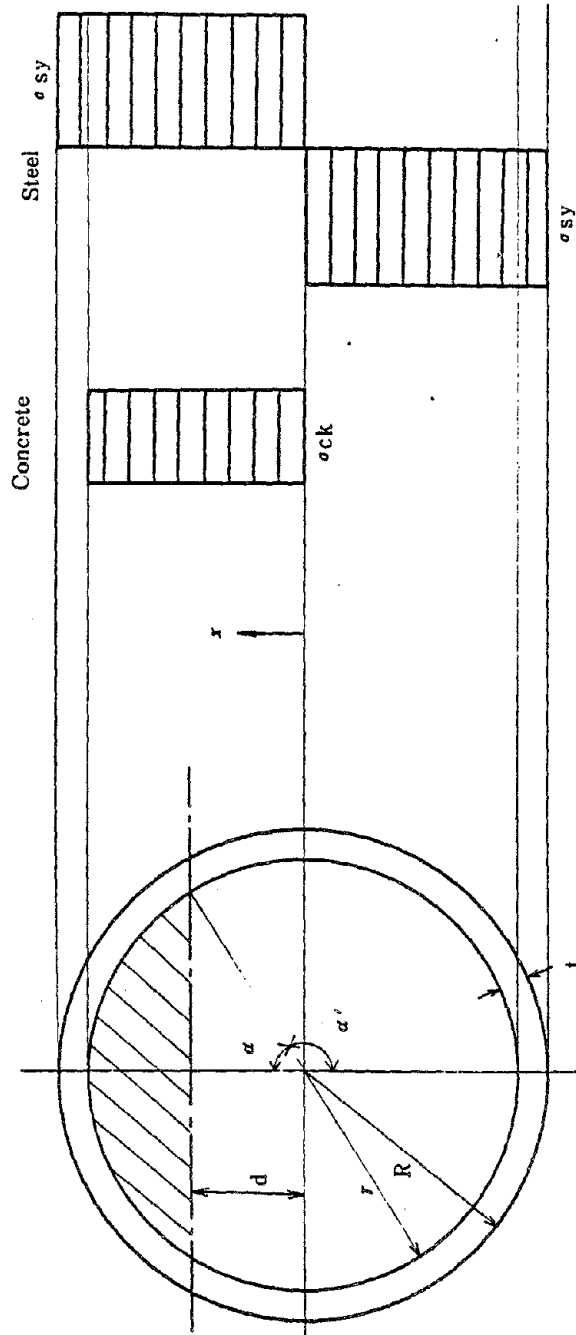


Fig.-9 Full-Plastic Bending Moment

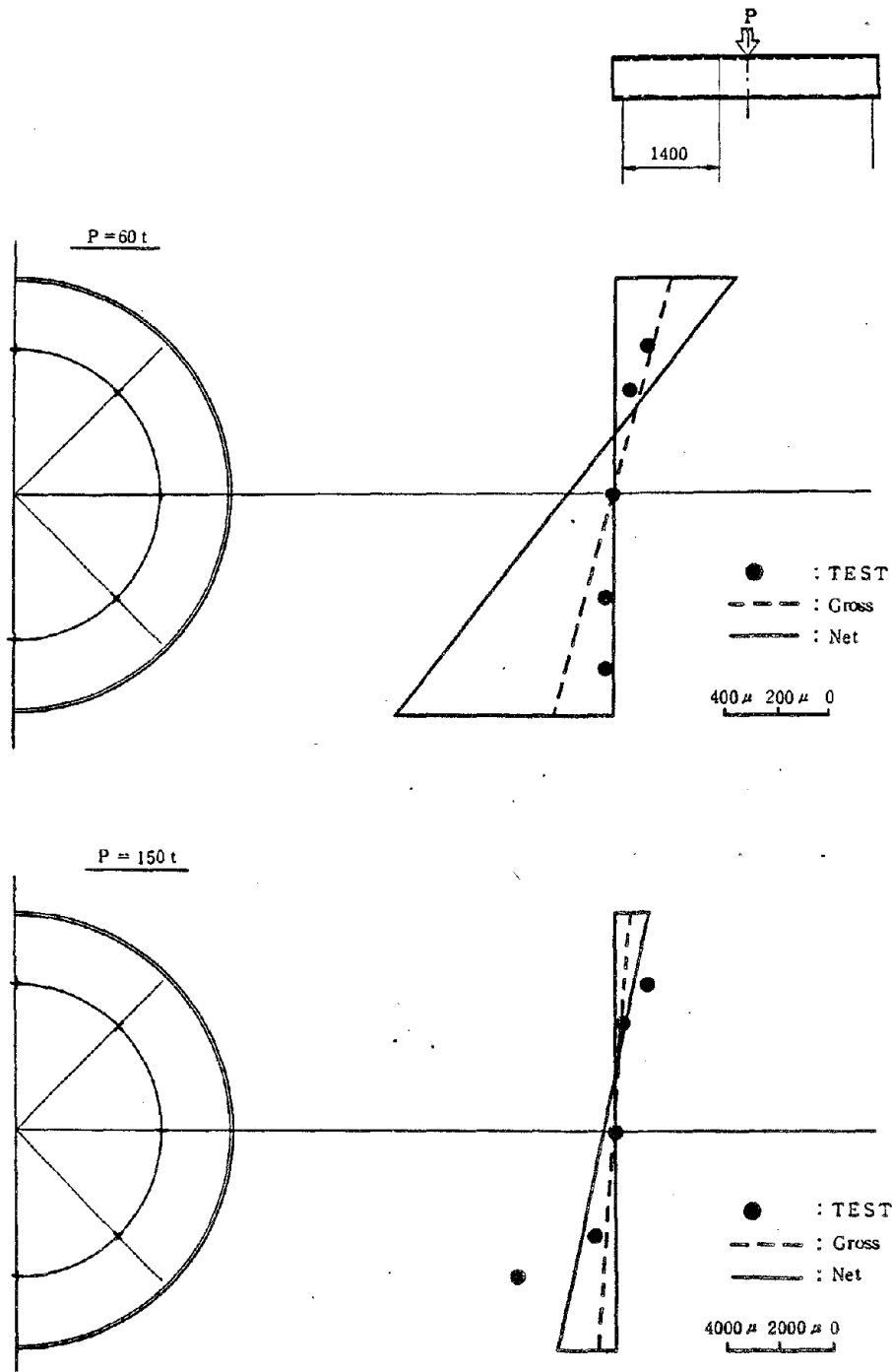


Fig.-10 Strain of Concrete (A-1)

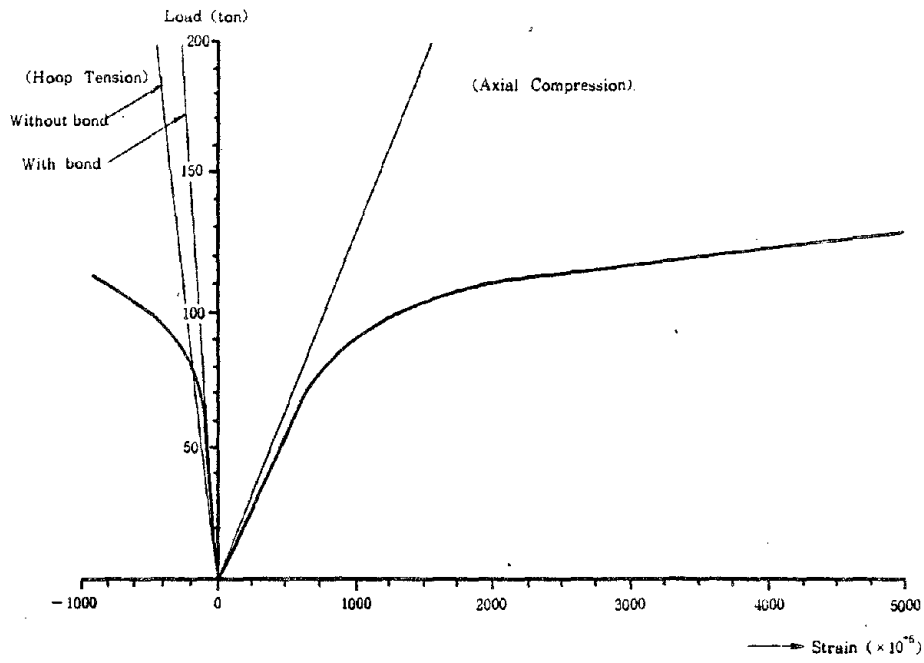


Fig.-11 Strain of Steel Tube (A-1)

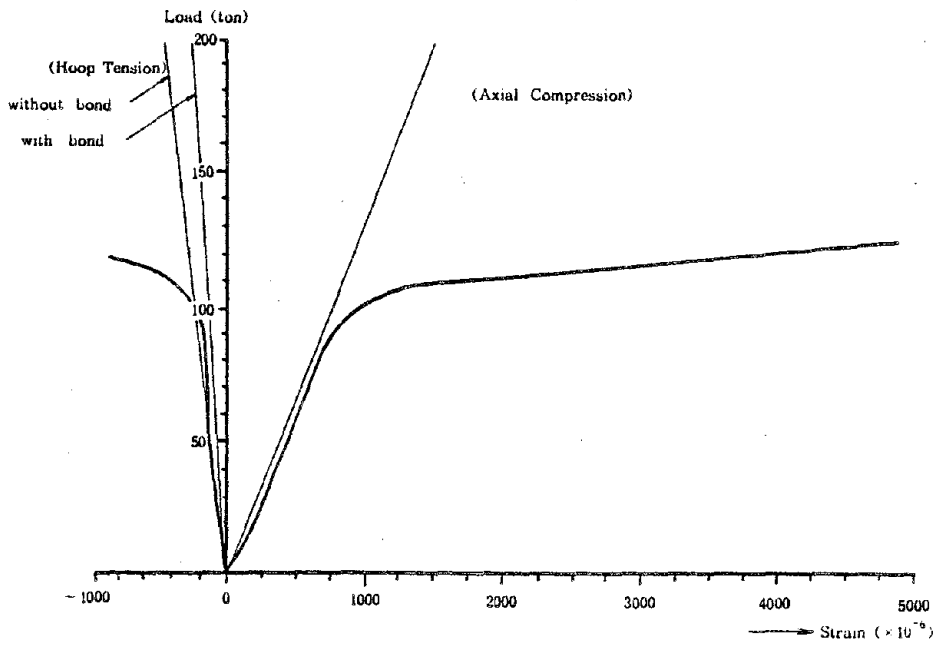


Fig.-12 Strain of Steel Tube (A-2)

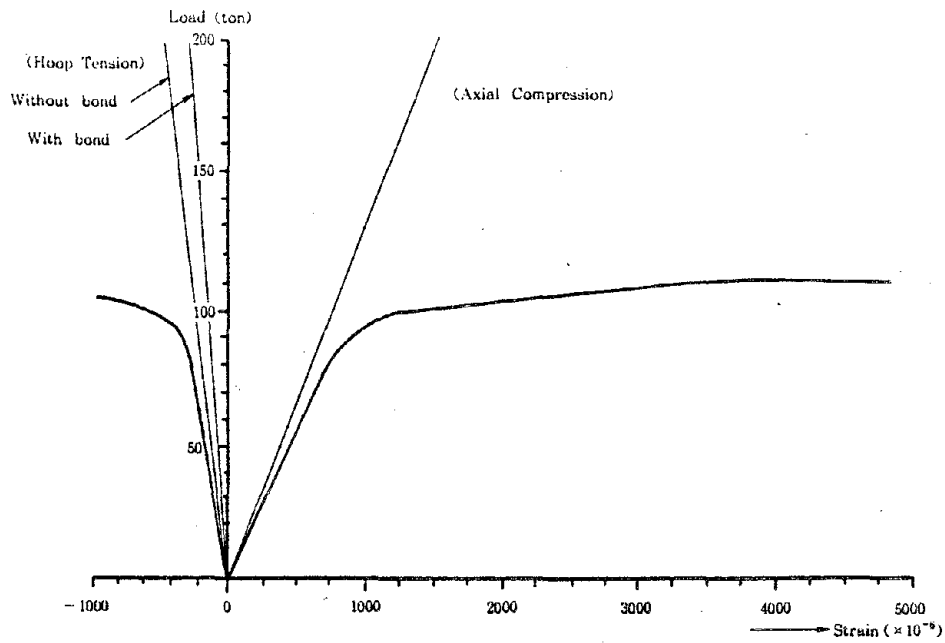


Fig.-13 Strain of Steel Tube (A-3)

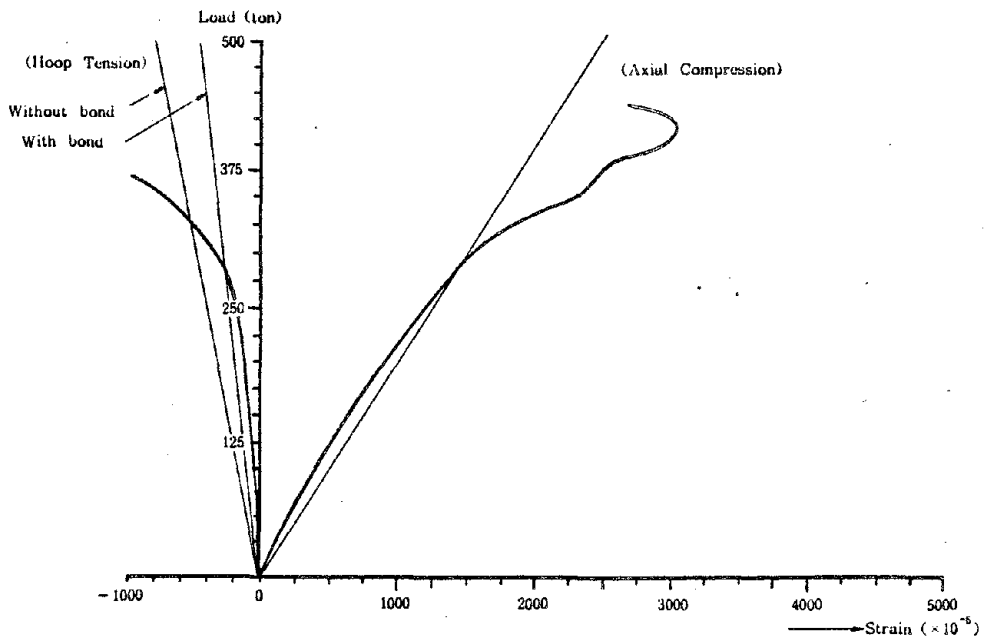


Fig.-14 Strain of Steel Tube (B-1)

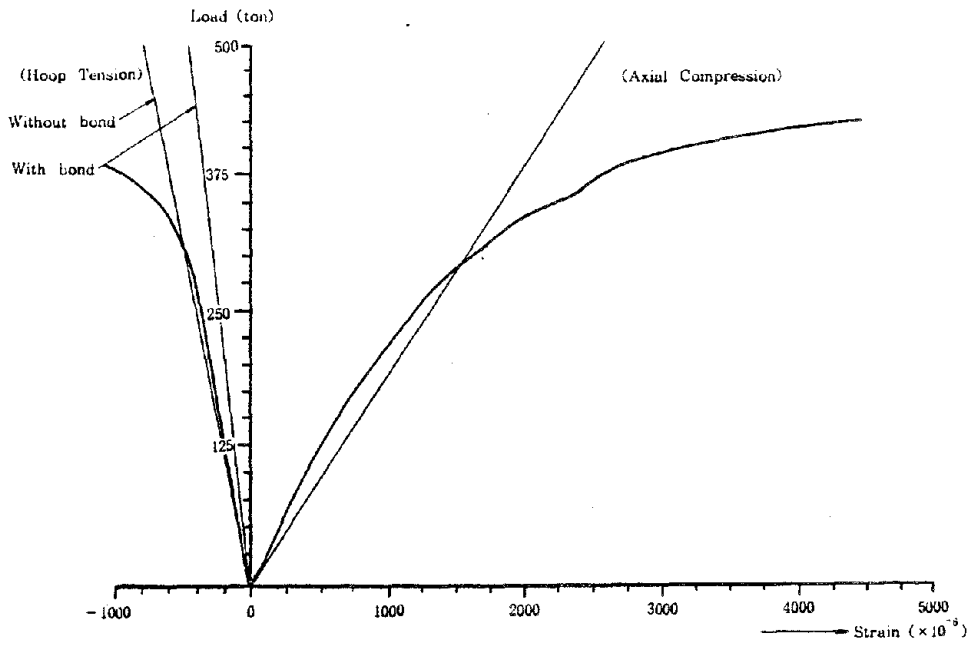


Fig.-15 Strain of Steel Tube (B-2)

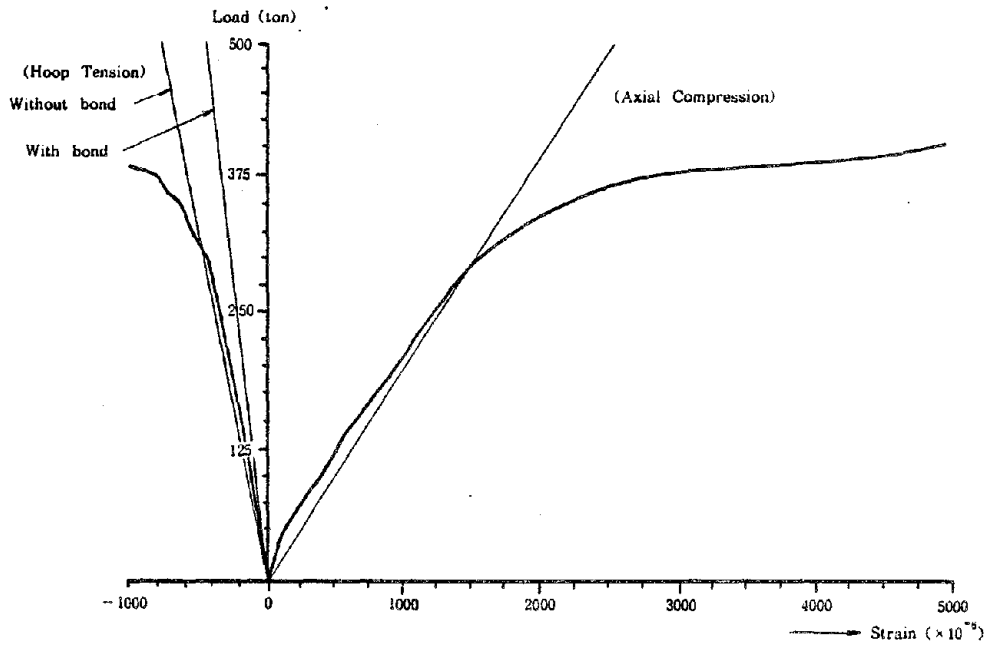


Fig.-16 Strain of Steel Tube (B-3)

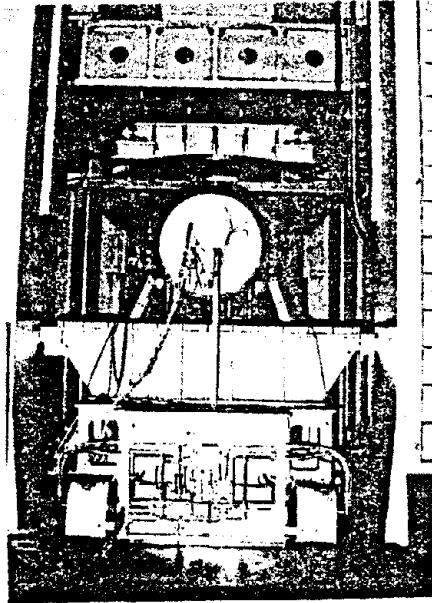


Photo-1 Loading Test

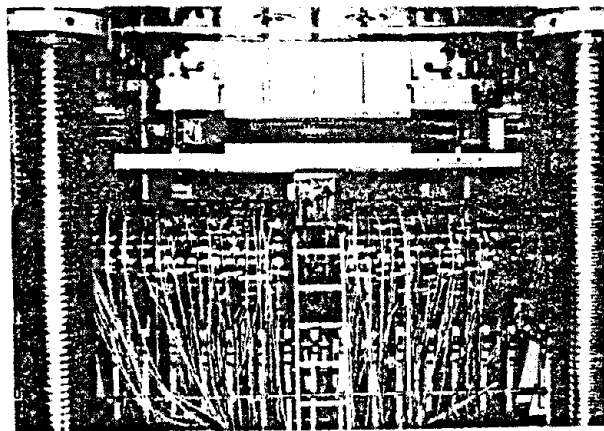


Photo-2 Loading Test



Photo-3 After Loading
(Compression Side near Center Span)

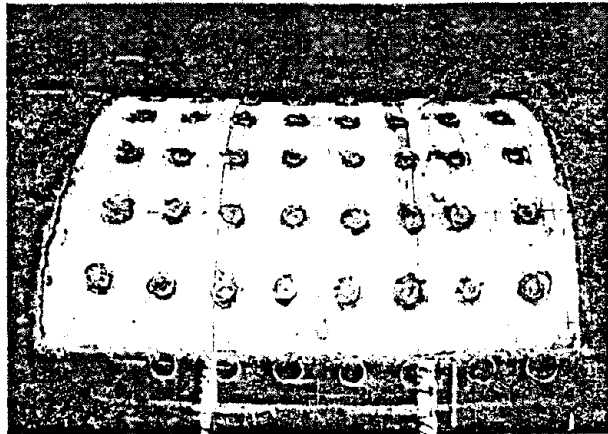


Photo-4 After Loading
(Compression Side near Center Span)

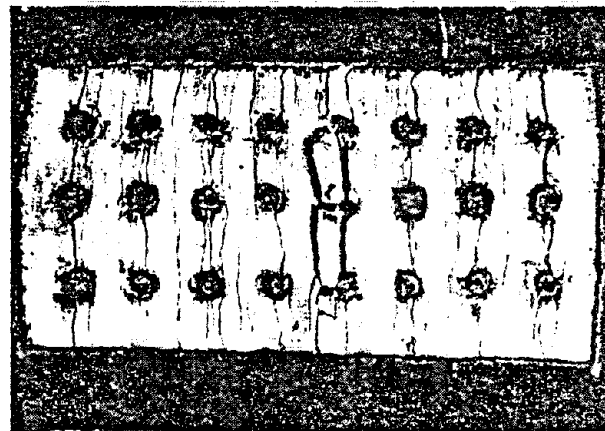


Photo-5 After Loading
(Tension Side near Center Span)

BEHAVIOR OF CONCRETE-FILLED STEEL TUBES
(PART 3; BEAM-COLUMN MEMBERS)

by

S.Saeki*, K.Minosaku**, A.Takizawa***

ABSTRACT

We reported the outline of test results of concrete-filled steel tube about compression and bending members respectively at 14-th and 15-th UJNR Joint Meetings.

In this report, we continuously describe the outline of test results of beam-column members.

Principal conclusions of this report are as follows.

- 1) The concrete-filled steel tubes have high capacity and good toughness. It is proved that the ultimate capacity of beam-column is nearly equal to the full-plastic bending moment independent of the concrete strength and the thickness of steel tube.
- 2) On the other hand, it is proved that the flexural rigidity of concrete-filled steel tubes should be taken account of the only flexural rigidity of steel tube in calculating the horizontal displacement, because the concrete and the steel tube do not behave together under the axially load.

1. INTRODUCTION

From the results of former two tests, it can be said that the concrete-filled steel tubes have fully toughness due to the composite action between the concrete and the steel tube, and do not lose high capacity even when a large displacement produces.

This test is carried out to clear up the fact whether the concrete-filled steel tubes have such high capacity and good toughness as beam-column members.

Main purposes of this test are as follows.

- 1) In case of beam-column members, the second-order bending moment must be considered. Calculating the second-order

* Head, Bridge Division, P.W.R.I.

** Research Engineer, Bridge Division, P.W.R.I.

*** Research Assistant Engineer, Bridge Division, P.W.R.I.

bending moment, the horizontal displacement has to be calculated. The method to calculate the flexural rigidity must be established, which the condition of concrete and the composite degree between the concrete and the steel tube are taken into consideration.

- 2) From the former test on compression members, it is ascertained that the concrete separates from the steel tube due to the difference of Poisson's ratio of two in the elastic region. Therefore, it is feared that the concrete-filled steel tubes as beam-column members would behave like the built-up beam and lose their merits as composite structures, when the bending moment subjects on them under the axially load.

For these reasons, the behavior of concrete-filled steel tubes as beam-column members must be made clear up experimentally.

2. OUTLINE OF TESTS

1) SPECIMENS

Four specimens, type-A to type-D shown in Fig.-2 and Table-1 were fabricated for tests. All specimens were same in diameter, 700mm, and in height, 3500mm.

Type-A, type-B and type-C have 6mm in the thickness of steel tube and 271kg/cm, 341kg/cm, 436kg/cm in the concrete strength respectively.

These specimens were set to investigate the influence of the concrete strength on the behavior of concrete-filled steel tubes. The concrete strength of type-D was much the same as that of type-A and the thickness of steel tube of type-D was set 12mm in order to investigate how the difference of the thickness of steel tube influences on the behavior.

Shear connectors such as studs were not provided for all specimens between the concrete and the steel tube. And also specimens were stiffened with double panels in order to fix the test machine by bolts.

2) METHOD OF TESTS

Tests were carried out by using Large Structural Members Bi-axial Test Machine of P.W.R.I..

The loading process was composed of the only axially loading and the bi-axially loading. In the only axially loading, specimens were set at the fixed position of the machine not to produce the eccentric load. And then the axially load was increased till 700ton as 50ton in the pitch of the load. Photo-1 shows the condition of specimens.

In the bi-axially loading, the horizontal load was increased till the load when bending cracks produce in part of the tension side of the fixed edge. Continuously, the repetitive loading was carried out at ten times, which the load was 0ton to the cracking load. After that, the load was increased till the ultimate load.

3) METHOD OF MESUREMENTS

In tests, 2 directional strain guages on a surface of the compression side of steel tube and 1 directional strain guages on a surface of the tension side were put on to mesure strains of steel tubes at every loading steps as shown in Fig.-3. And also mould guages were set inside the concrete of the compression side, the center of cross section and the tension side as shown in Fig.-4.

Foremore, displacements in the vertical direction and the horizontal direction were mesured at positions shown in the same figure.

3. SUMMARY OF TEST RESULTS

1) PROPERTY AS COMPRESSION MEMBERS

Fig.-5 shows the relationships between the load and the displacement in the vertical direction of each specimen.

As shown in the same figure, all specimens show proportional load and displacement relationships till 700ton. The theoretical displacements of each specimen versus 700ton in the vertical load shown in Fig.-5 are got, taking account of the ratio of Young's modulus between the concrete and the steel tube. In the calculation, Young's modulus of concrete is determined by the specified cylinder test. All mesured

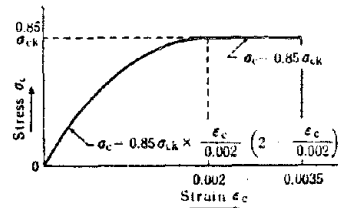
values are larger than theoretical values in comparison with two values.

In each type, theoretical values of type-A and type-B are about forty per cent larger than measured values and about twenty per cent larger in type-C and type-D.

The difference of Young's modulus of concrete between the concrete for the cylinder test and actual concrete may be considered as the reason.

Fig.-6 to Fig.-9 show the relationships between the vertical load and the axial strain of steel tube, and between the vertical load and the circumferential strain of steel tube, and between the vertical load and the axial strain of concrete, and also theoretical lines of the axial strain versus the vertical load. Theoretical lines are based on the following assumptions.

- (1) The relationship specified by the Highway Bridge Specification of Japan is used as the stress and strain curve of concrete. (reference on Fig.-1)



- (2) The relationship of stress and strain of steel tube is linear. Young's modulus are set from the material test.

Fig. - 1 Stress-strain curve of concrete

- (3) The strain distribution in cross section follows the rule of plane preservation.

$$N = E_s \epsilon A_s + 0.85 \sigma_{ck} \frac{\epsilon}{0.002} \left(2 - \frac{\epsilon}{0.002} \right) A_c \dots\dots\dots (1)$$

where,

- N; vertical load
- ε; axial strain
- E_s; Young's modulus of steel tube
- σ_{ck}; concrete strength
- A_s; cross sectional area of steel tube
- A_c; cross sectional area of concrete

In Fig.-6 to Fig.-9, two theoretical lines between the

circumferential strain of steel tube and the vertical load are indicated. One is got by the assumption of no bond between the concrete and the steel tube, and the other is got by the assumption of enough bond.

In case of no bond, the circumferential strain can be calculated by the following equation.

$$\epsilon_h = -\nu_s \cdot \epsilon_x \quad \dots\dots\dots (2)$$

where,

- ϵ_h ; circumferential strain
- ν_s ; Poisson's ratio of steel tube (0.3)
- ϵ_x ; axial strain

On the other hand, in case of enough bond, the circumferential strain is as follows.

$$\epsilon_h = - \left(\nu_s - \frac{\nu_s - \nu_c}{1 + (1 - \nu_c) \frac{t E_s}{R E_c}} \right) \epsilon_x \quad \dots\dots\dots (3)$$

where,

- t ; thickness of steel tube
- R ; radius of steel tube
- ν_c ; Poisson's ratio of concrete
- E_s, E_c ; Young's modulus of steel tube, concrete

From Fig.-6 to Fig.-9, the following results are obtained as compression members of concrete-filled steel tubes.

- (1) The relationship between the vertical load and the axial strain calculated by equation-(1) appears again measured values sufficiently. However, as shown in type-B and type-C, the theoretical values obtained by equation-(1) give small axial strains when the concrete and the steel tube independently resist against the vertical load.
- (2) About the circumferential strain of steel tube, the measured values of type-A and type-D may agree well with

the theoretical values obtained by equation-(3) based on the assumption that enough bond is secured. Alternatively, the measured values of type-B and type-C approach the theoretical lines for no bond. The difference of concrete strength between type-A,D and type-B,C may lead to the results, And a cast of concrete and a curing method of concrete and a curing days or concrete may be influential on this results. Further, a bond of type-B,C may be small due to a shrinkage of concrete.

- (3) In comparison with the relationship between the vertical load and the axial strain, and between the vertical load and the circumferential strain, when the steel tube and the concrete resist against the vertical load individually, measured values separate the previous theoretical lines obtained by equation-(1).

3. PROPERTY AS BEAM-COLUMN MEMBERS

As mentioned in the beginning of this report, it is proved that the concrete-filled steel tubes have high capacity and good toughness in case of beam-column members.

Photo-2 and photo-3 show type-D during the loading and after the loading, and photo-4 shows the situation of local buckling of steel tube. Foremore, the state of concrete in the compression side and the tension side are respectively shown in photo-5 and photo-6.

As shown in these photos, a local buckling of steel tube and a crush and a crack of concrete produce. However the capacity dose not drop down even in the plastic region and indicates enough toughness as described later due to the composite action between the concrete and the steel tube.

Fig.-10 to Fig.-13 show the relationships between the load and the displacement in the horizontal direction.

These figures indicate that all specimens may almost hold the load corresponding to the full plastic bending moment (P_p).

In these figures, the measured loads and the calculated loads when bending cracks produce in the tension side of the fixed edge are indicated. Foremore, the loads when the yield

of steel tube produces in the compression side of the fixed edge. It is assumed that bending cracks produce when the tension stress of concrete becomes 30kg/cm . And also, two theoretical lines which express the relationships between the load and the displacement in the horizontal direction are indicated. One is based on the assumption that whole section is effective, taking account of the ratio of Young's modulus as above mentioned. The other is based on the assumption that the only steel tube resist against the bending moment.

From these figures, the relationships between the load and the displacement in the horizontal direction are linear till the load when the yield of steel tube produces in the compression side of the fixed edge. Afterward, it is proved that the displacements have the tendency which are getting larger.

About the flexural rigidity of specimens, when the thickness of steel tube is thin, that is, in case of type-A, type-B and type-C, the flexural rigidity of concrete contributes to whole flexural rigidity under small horizontal load, but the ratio of Young's modulus should be taken a larger value quantitatively. When the thickness is thick, this tendency is remarkable. The flexural rigidity of concrete cannot be expected, because the experimental lines nearly equal to the theoretical lines based on the assumption that the only steel tube is effective.

On the other hand, it is proved that the horizontal displacements under the horizontal loads corresponding to the full-plastic bending moment nearly equal to the theoretical displacements, supposing that the only flexural rigidity of steel tube is effective.

Fig.-14 to Fig.-17 show the relationships between the horizontal load and the axial strain, between the horizontal load and the circumferential strain of steel tube, and between the horizontal load and the axial strain of concrete.

In these figures, two theoretical lines which express the relationships between the circumferential strain and the horizontal load are drawn as above mentioned. One is based on

the assumption that the steel tube and the concrete behave individually, the other is based on the assumption that the steel tube and the concrete behave together. The strains corresponding to O_{ton} in the horizontal load indicate the strains after the only axial loading. From these figures, it is proved that all specimens have similar load and strain relationships.

Mesured circumferential strains of steel tube nearly equal to the theoretical lines, supposing that the concrete and the steel tube behave independently. And the axial strains are gradually getting larger from the load when the yield of steel tube produces in the compression side of the fixed edge.

4. FUTURE RESEARCH PROGRAM

From this test and former two tests, it could be well known how the concrete-filled steel tubes behave.

From now on, the following items must be clear up in order to apply the concrete-filled steel tubes to actual structures.

(1) BEAM-COLUMN MEMBERS

The behavior of concrete-filled steel tube under the repetitive load.

(2) CONNECTOR

The structural detailing and connectors which can effectively transmit high capacity and good toughness of concrete-filled steel tubes to beam-members.

Table. - 1 Specification of Specimens

TYPE	Dia- meter (mm)	Thick- ness of Steel Tube (mm)	Height (mm) (Span Length)	Steel	Yield Strength of Steel (kg/cm ²)	Concrete Strength (kg/cm ²)	Young's Modulus of Concrete (kg/cm ²)
A	700	6	3500 (2920)	SM50Y	4400	271	2.59×10^5
B	700	6	3500 (2920)	SM50Y	4400	341	2.77×10^5
C	700	6	3500 (2920)	SM50Y	4400	436	3.01×10^5
D	700	12	3500 (2920)	SM50Y	4000	264	2.57×10^5

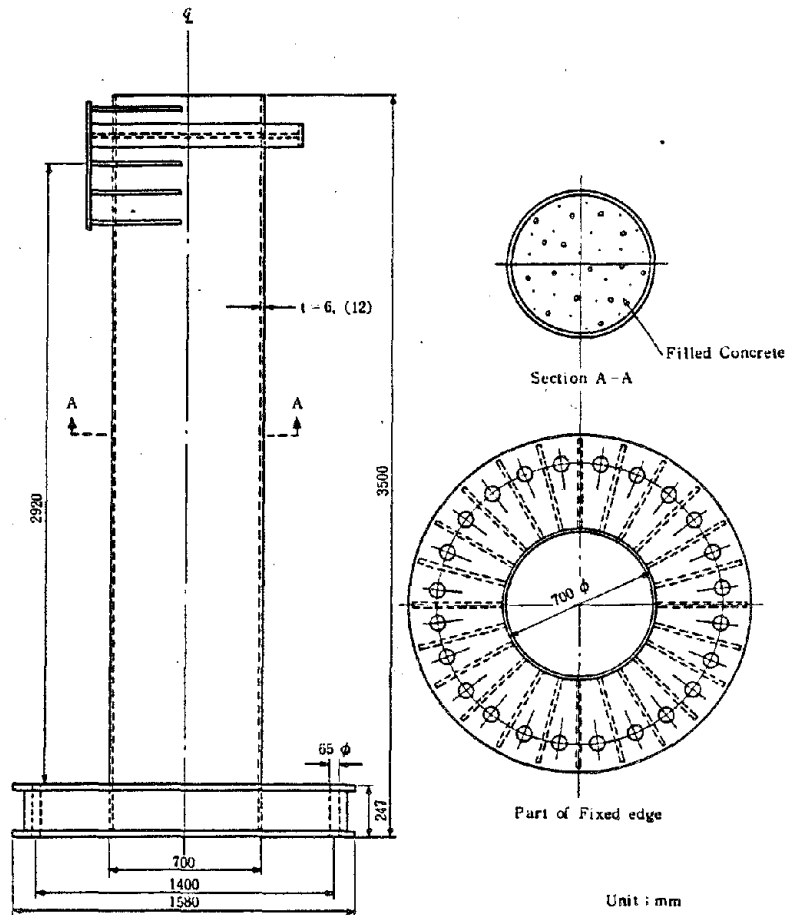


Fig.-2 Configuration of Specimen

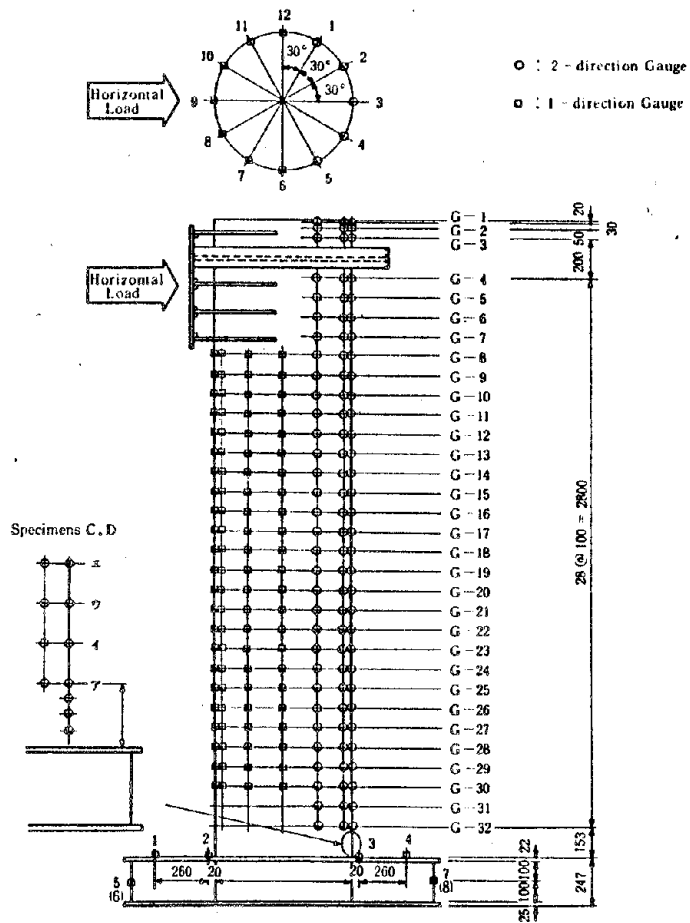


Fig.-3 Position of Strain Gauge on Steel Tube

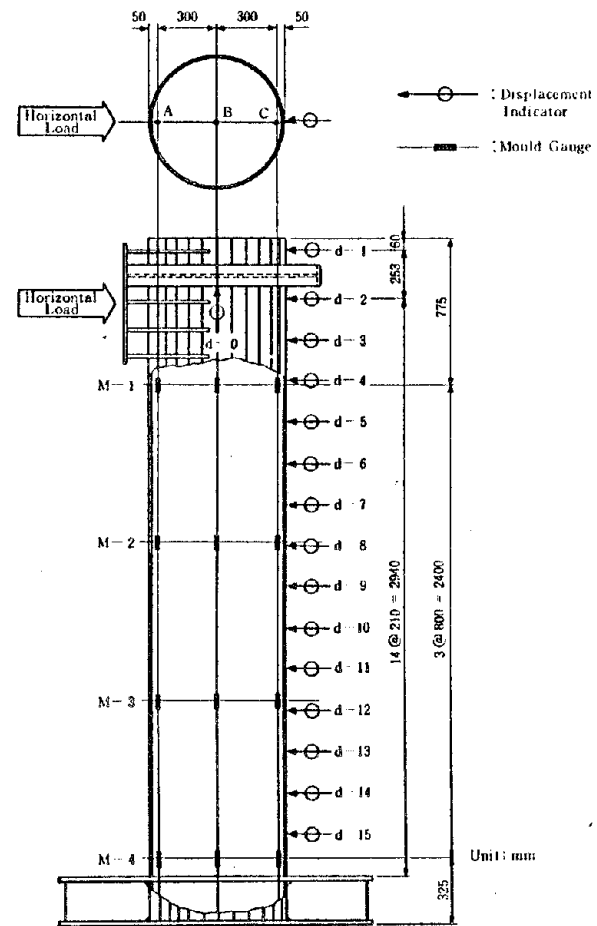


Fig.-4 Position of Mould Gauge of Concrete and Displacement Measurement

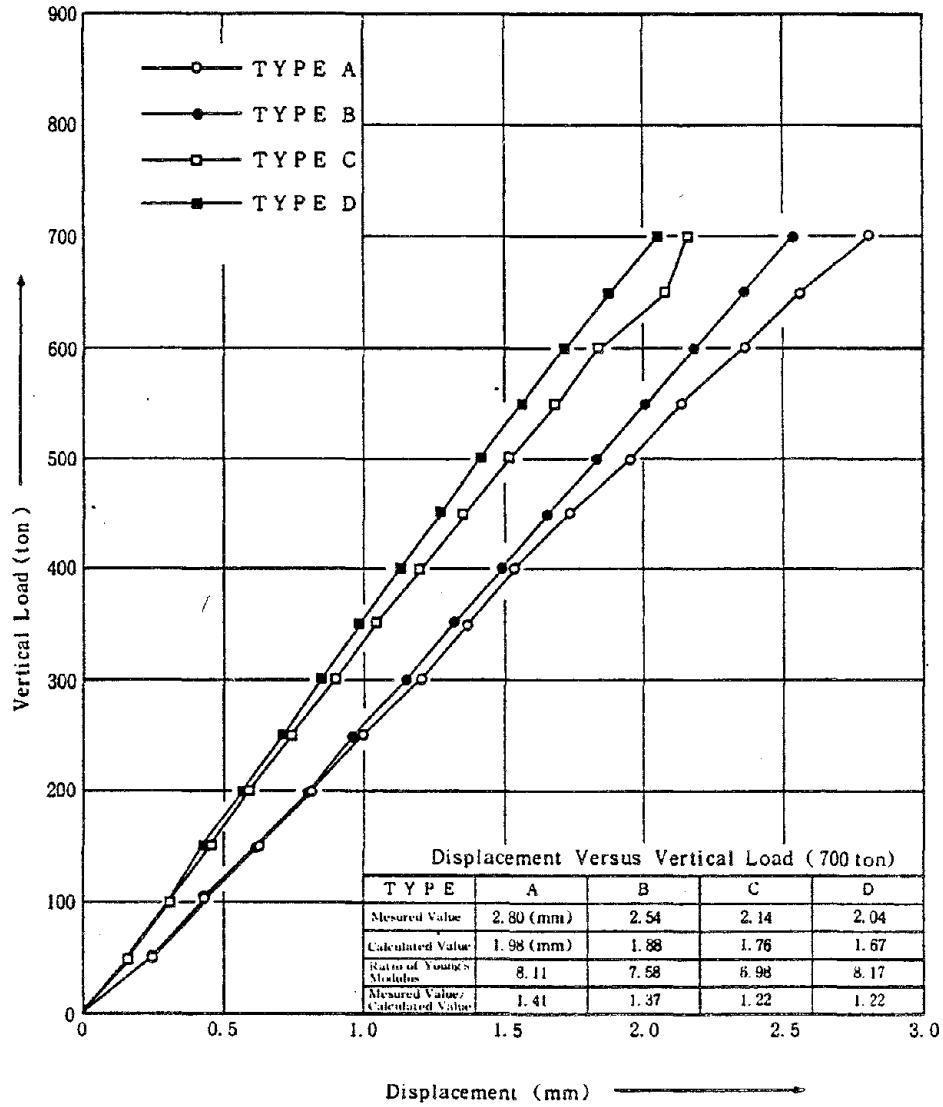


Fig.-5 Vertical Load-Displacement

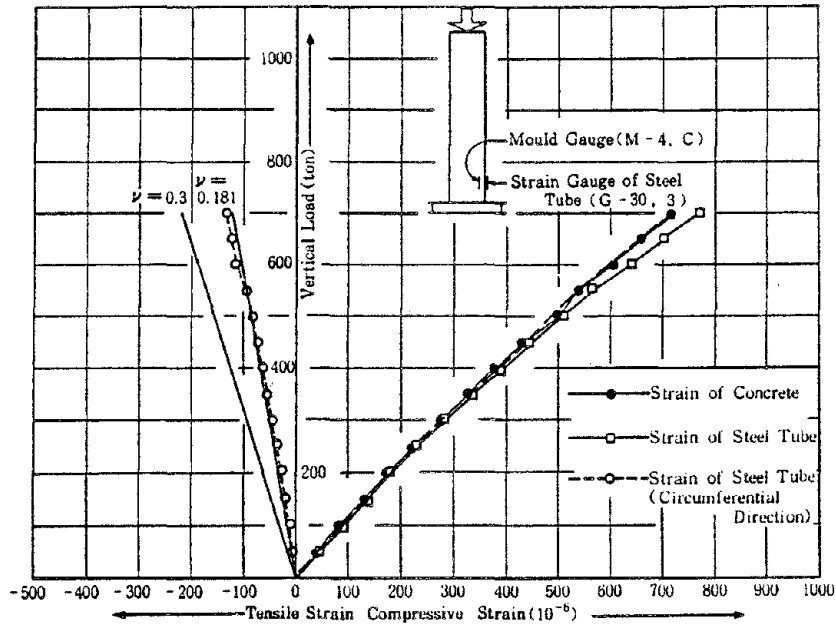


Fig.-6 Vertical Load-Strain (Type-A)

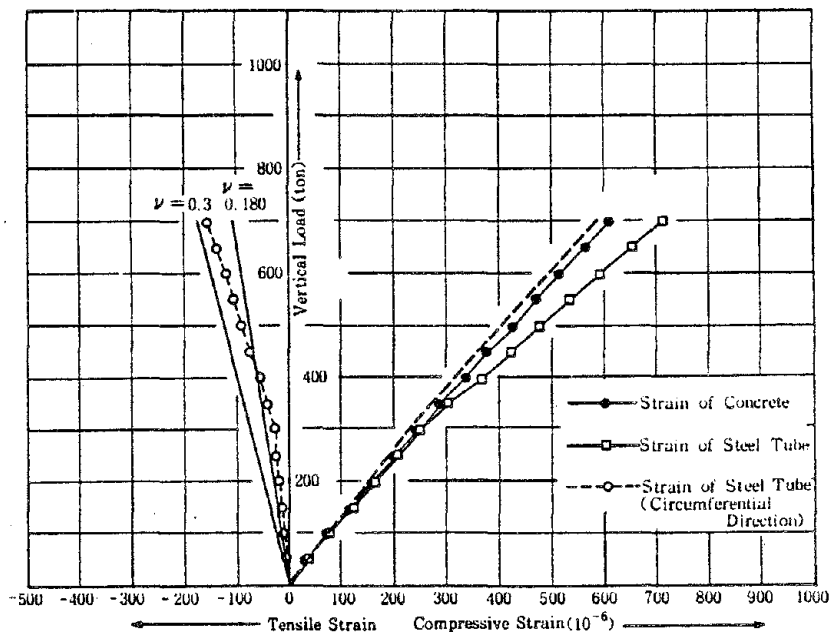


Fig.-7 Vertical Load-Strain (Type-B)

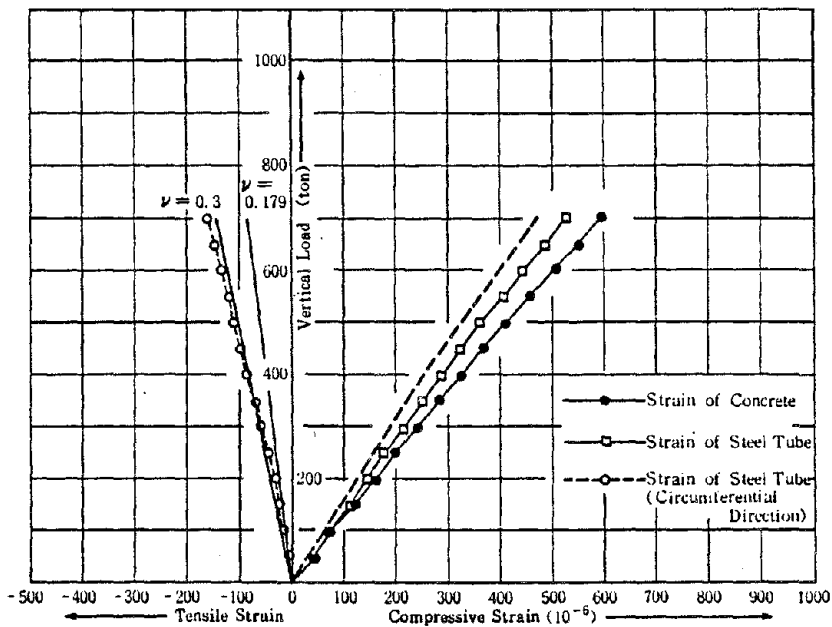


Fig.-8 Vertical Load-Strain (Type-C)

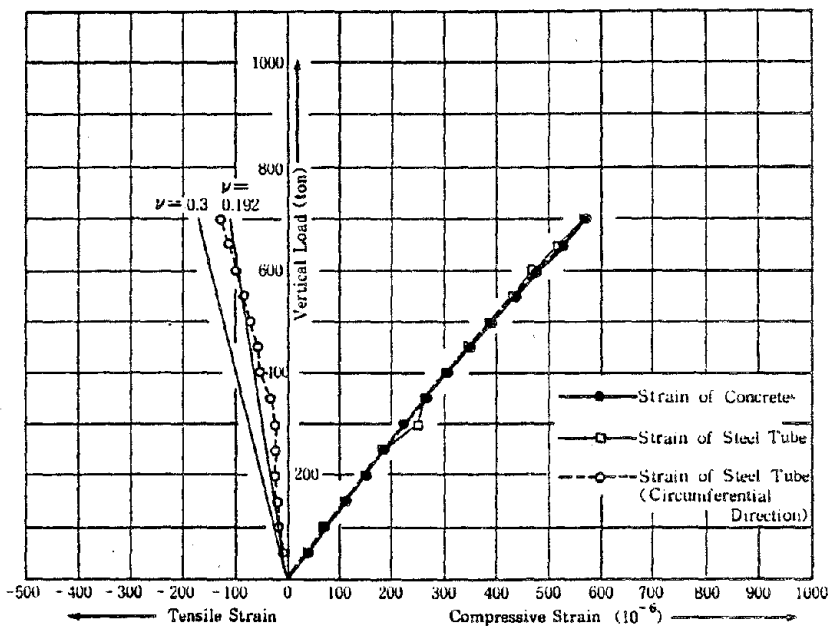


Fig.-9 Vertical Load-Strain (Type-D)

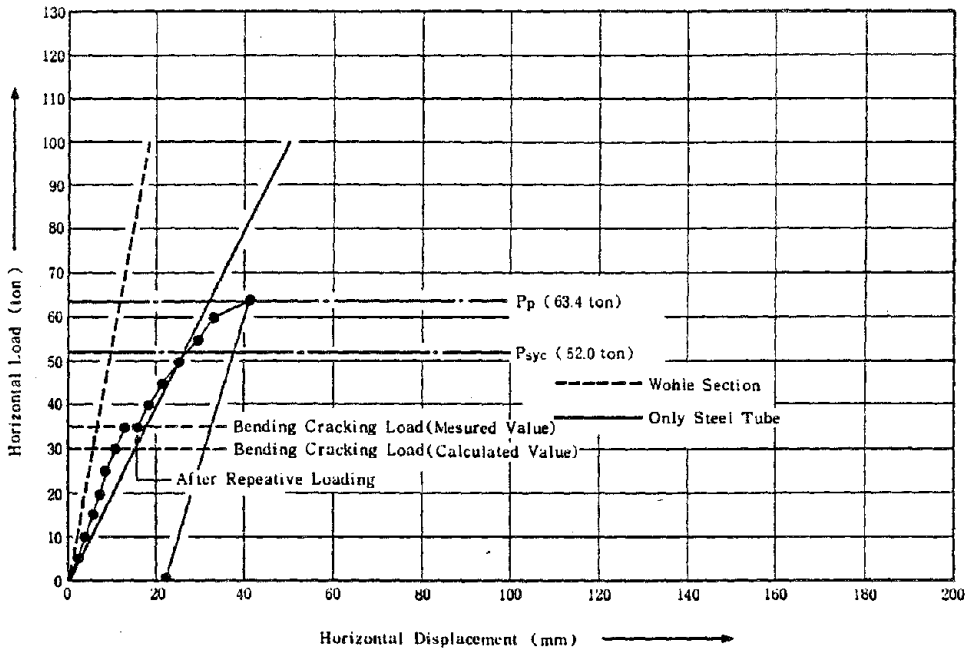


Fig. -10 Horizontal Load-Displacement (Type-A)

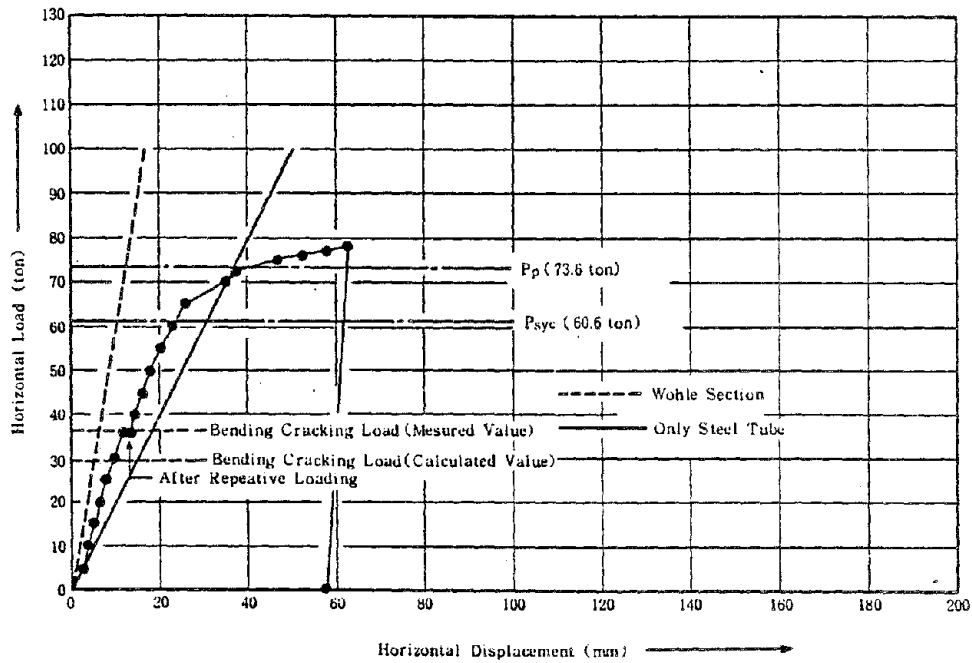


Fig. -11 Horizontal Load-Displacement (Type-B)

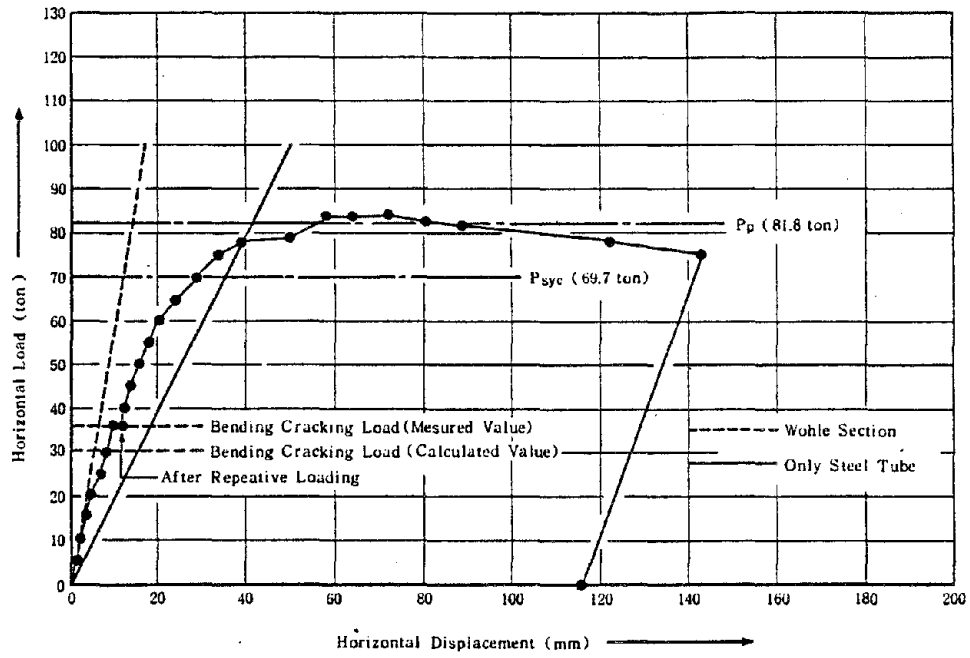


Fig. - 12 Horizontal Load - Displacement (Type - C)

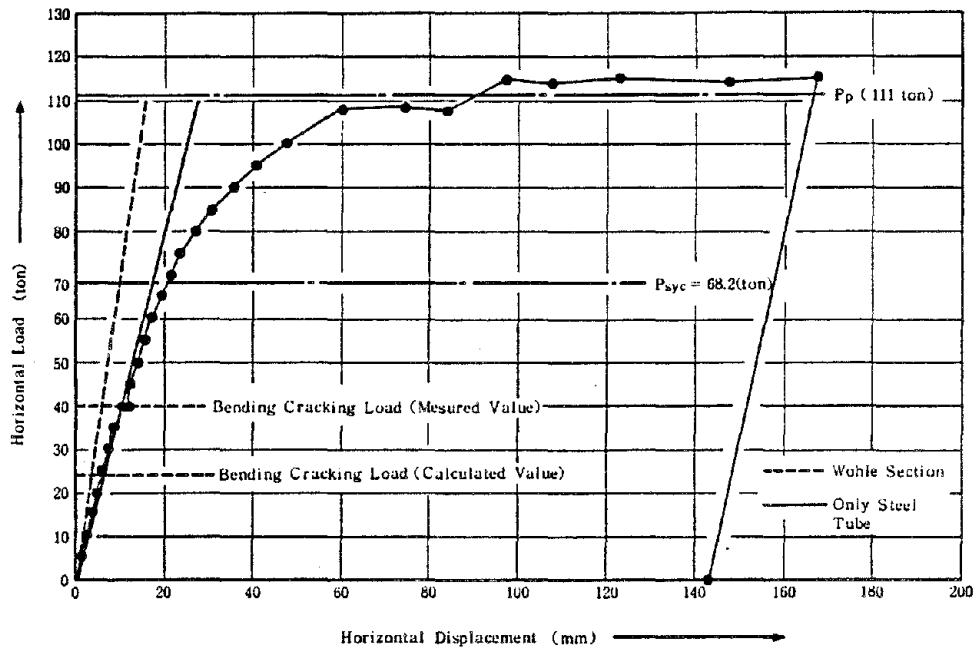


Fig. - 13 Horizontal Load - Displacement (Type - D)

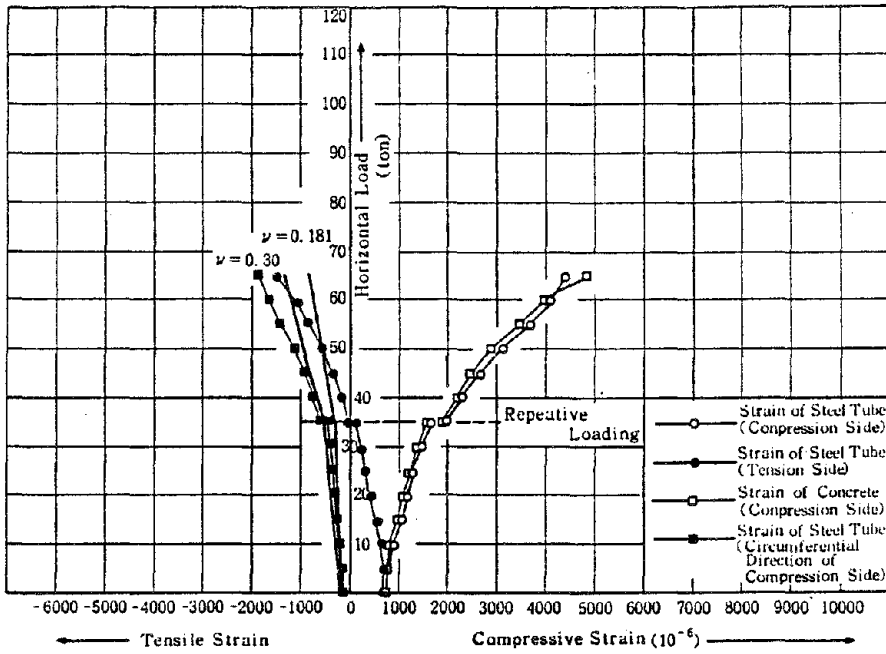


Fig. -14 Horizontal Load - Strain

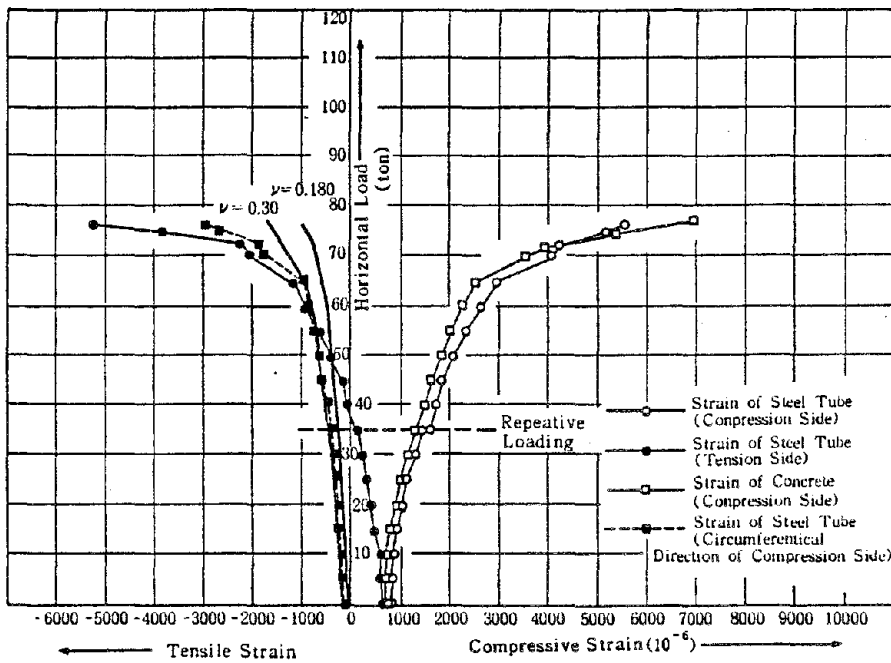


Fig. -15 Horizontal Load - Strain

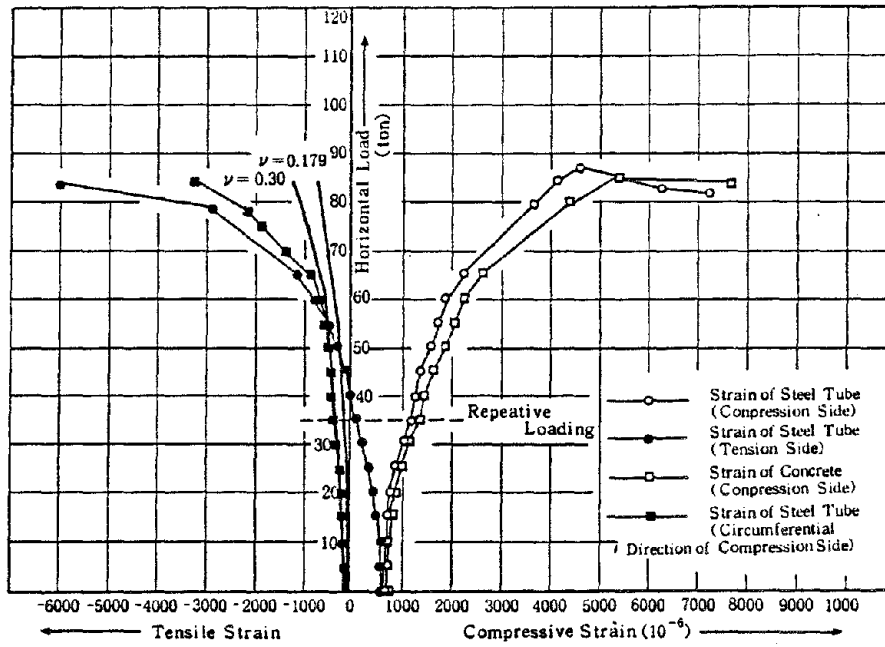


Fig. -16 Horizontal Load - Strain

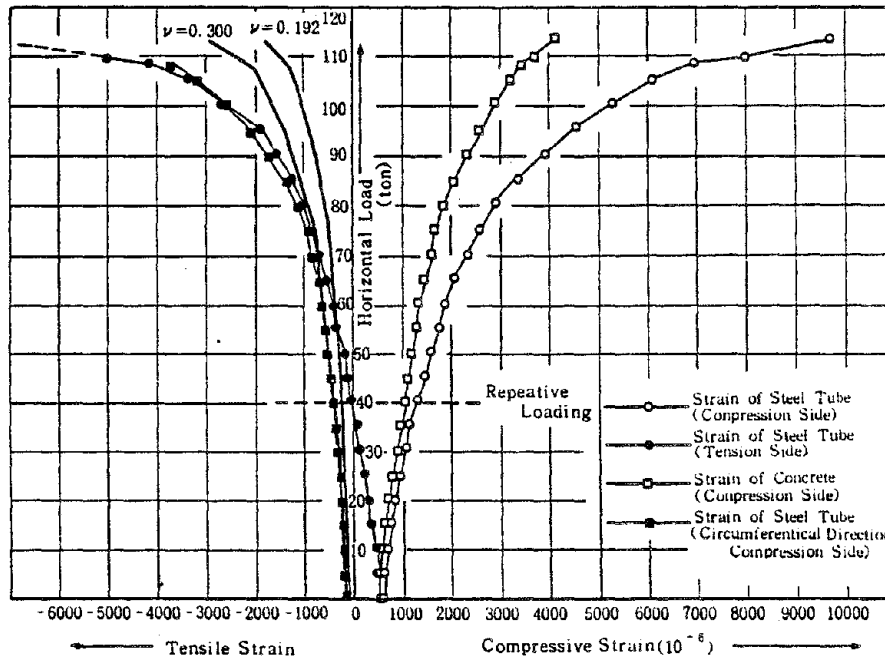



Fig. -17 Horizontal Load - Strain

Reproduced from
best available copy. 

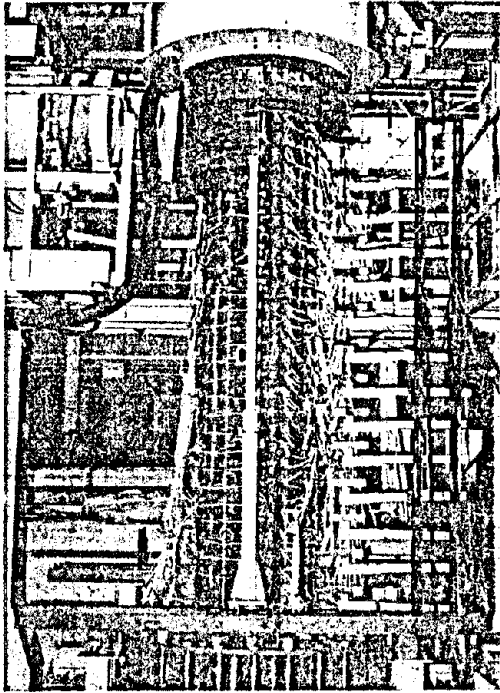


Photo-1 Specimen before Loading

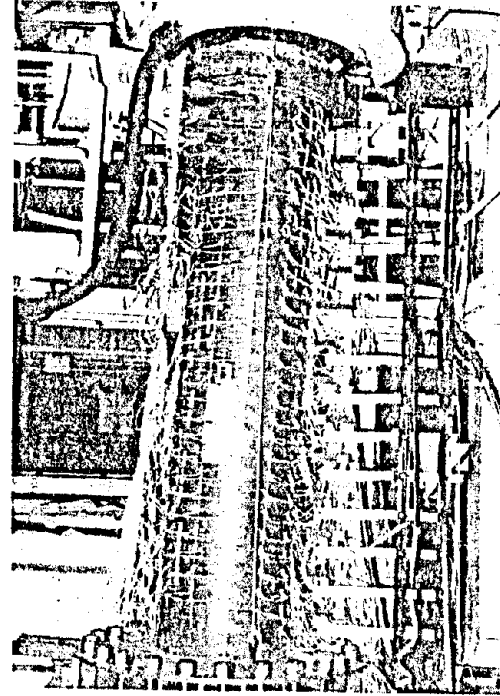


Photo-2 Specimen during Loading

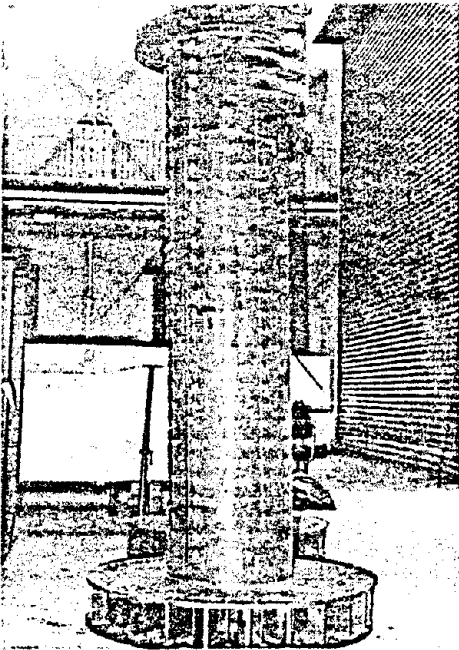


Photo-3 Specimen after Loading

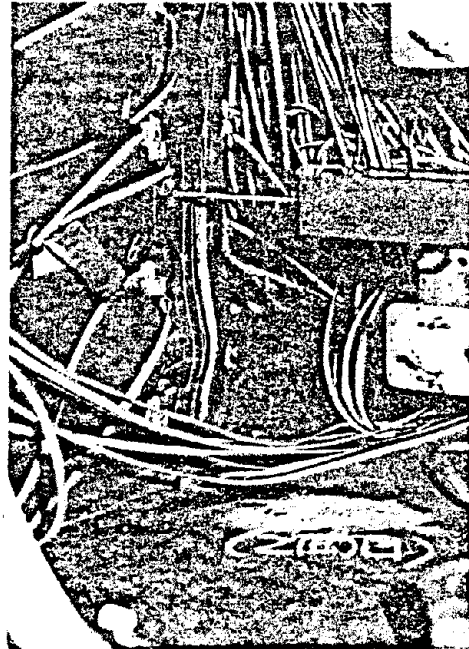


Photo-4 Local Buckling of Steel Tube



Photo-5 Crush of Concrete after Loading

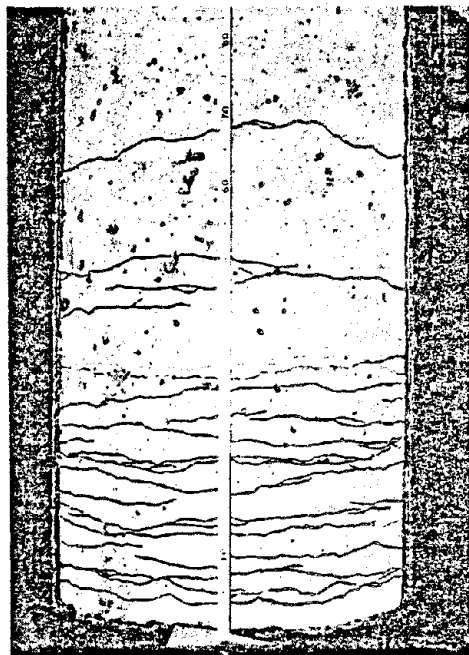


Photo-6 Crack of Concrete after Loading

SEISMIC RESPONSE ANALYSIS OF THE ITAJIMA BRIDGE
THROUGH USE OF STRONG MOTION ACCELERATION RECORDS

Masamitsu Ohashi

Toshio Iwasaki

Kazuhiko Kawashima

Public Works Research Institute

Ministry of Construction

ABSTRACT

In analyzing the seismic behavior of highway bridges constructed on soft soil deposits, it is important to take into account soil-structure interaction effects. In this paper, the seismic response of a bridge pier-foundation is analyzed from earthquake acceleration records taken simultaneously from the pier crest and the ground surface near the bridge. Four motions were used in the analysis, i.e., two were induced by two earthquakes with magnitudes of 7.5 and 6.6, and two by their aftershocks. In the former two earthquakes, the maximum accelerations were 186 and 441 gals on the ground surface, and 306 and 213 gals on the pier top. Analyses of frequency characteristics of the motions showed that the predominant frequencies of the pier-foundation were always almost identical to the fundamental natural frequency of the subsoil. Analytical models were formulated to calculate the seismic response of the pier-foundation assuming the subsoil and pier-foundation to be a shear column model with an equivalent linear shear modulus and an elastically supported beam on the subsoil, respectively. Bedrock motions were computed from the measured ground surface motions and then applied to the bedrock of the analytical model. The seismic responses of the pier-foundation were thus calculated and compared with the measured records and produced a good agreement.

KEYWORDS: Bridge-pier foundations; bridge seismology; earthquake frequency characteristics; ground surface accelerations; foundation structure response.

INTRODUCTION

In the past, numerous highway bridges have suffered extensive damage due to strong motion earthquakes. Seismic damage to bridges consisting of simply supported girders or trusses rested on massive piers and abutments were commonly caused by foundation failures resulting from excessive ground deformations and/or loss of stability and bearing capacity of the foundation soils. As a direct result, the substructures often tilted, settled, or sometimes overturned, and these large displacements of the supports caused relative shifting of the superstructures, induced failures of the bearing supports, and even caused dislodging of the spans from their supports.

It has been well recognized from these evidences that the influences of surrounding sub-surface ground are very important for the seismic responses of foundations deeply embedded in the ground, and considerable interests were concentrated on the soil-structure interaction effects of such structures through model experiments and theoretical analyses. However very limited researches have been undertaken in studying seismic responses of actual foundations during high intensity seismic excitations since little data have been available for such purposes. This investigation presents the results of observation of seismic motions on a bridge pier and on the ground surface nearby with high accelerations which were measured during four earthquakes, and also correlates the pier motions measured with the pier motions analyzed using the ground surface acceleration records.

STRUCTURAL AND SITE CONDITIONS OF THE BRIDGE

The Itajima Bridge studied is a five-span simply-supported plate girder bridge as shown in Figure 1. The strong-motion acceleration observations have been conducted since 1966 at a crest of one of the piers and on the free field ground surface located about 400 m apart from the pier. Two SMAC-B2 type accelerographs are set at both sites to measure accelerations in the longitudinal, transverse and vertical directions of the bridge axis.

Ground surveys were performed at both sites and information on soil profile, N-value of standard penetration test, and shear wave velocities were obtained. Figure 2 shows the soil profiles and N-values at both sites. It is recognized from the results that the ground conditions are essentially the same between the two sites, i.e., the soil profiles consist of upper soft alluvium loam to fine sand formations with the averaged N-value of approximately

7 and lower stiff diluvium gravel formations with the averaged N-values of 30 or more. The shear wave velocities of the upper and lower formations were estimated to be approximately 130 and 480 m/sec, respectively. Figure 3 shows the geological structures around the Itajima Bridge. The stiff diluvial gravel formations are recognized to be underlain by mesozoic cretaceous formation. According to Figures 2 and 3 it can be recognized that the ground conditions are continuous and almost identical between the two sites. The gravel formations were assumed to be the bedrock at the sites in calculating seismic responses of the ground and foundation in the following paragraph.

ANALYSES OF STRONG-MOTION ACCELERATION RECORDS

Strong-Motion Acceleration Records

Four simultaneous strong-motion acceleration records have been obtained at the Itajima Bridge as summarized in Table 1 which were induced by four earthquakes, i.e., main and after shocks of both the Hyuganada Earthquake of April 1, 1968 and the Bungosuido Earthquake of August 6, 1968, which are designated herein as A, B, C and D Earthquakes, respectively. Figures 4, 5, 6 and 7 show the acceleration records thus obtained in the longitudinal and transverse directions of the bridge axis. In the D-Earthquake, accelerations on the pier could not be recorded, unfortunately, and only the maximum value of acceleration was obtained. It should be noted here that although the seismic response accelerations developed at the pier crest were very high, superstructures and foundations of the Itajima Bridge suffered no structural damages through any of these four earthquakes.

Figure 8 represents amplifications of maximum accelerations between the ground surface and the crest of the pier. It can be recognized from this result that the amplifications of maximum accelerations are very much different between the Hyuganada Earthquake (A- and B-Earthquakes) and the Bungosuido Earthquake (C- and D-Earthquakes), i.e., the amplification factors are in the range of 1.1 - 1.7 in the case of A- and B-Earthquakes, whereas they are in the range of 0.4 - 0.6 in the C- and D-Earthquakes. The frequency characteristics of the motions were then investigated. Predominant frequencies of the records are summarized in Table 2, based on the power spectra presented in Figure 9.

Characteristics of Ground Motions

Based on Figure 9 and Table 2, it can be understood that the ground motions induced during the A-Earthquake have the predominant frequencies of 1.5 Hz and 4.5 Hz in the longitudinal motion, and 1.3 Hz and 4.0 Hz in the transverse motion. The frequencies of 1.5 Hz and 1.3 Hz are the most predominant ones whereas the frequencies of 4.5 Hz and 4.0 Hz are the secondary predominant ones. The ratio between the most predominant frequency f_1 and secondly predominant frequency f_2 are approximately 3.0 in both longitudinal and transverse motions. The geological situation at the site consists of two formations with significantly different stiffnesses, i.e., alluvium loam & silt formation and diluvium gravel formation. In such case that subsoils with shear wave velocity V_s and thickness H are rested horizontally on the stiff formation, the natural period T_n of the subsoils can be estimated by Eq. 1 for the n -th mode of shear vibration.

$$T_n = \frac{1}{2n-1} \cdot \frac{4H}{V_s} \quad (1)$$

The ratio between T_1 and T_2 (T_1/T_2) are always evaluated as 3.0 in such case, which well explains the characteristics of ground motions developed during the A-Earthquake. It can be understood therefore that the predominant frequencies observed in the ground motions would represent the fundamental and second natural frequencies of the subsoils. Since there are not any predominant frequencies beyond 1.3 & 1.5 Hz and 4.0 & 4.5 Hz in the ground motions, it is considered that the incident motions in the bedrock themselves have these frequencies as their predominant frequencies.

According to the ground condition presented in Figure 2, the fundamental natural period T_1 of the subsurface ground at the free field observatory can be estimated by Eq. 2 taking the diluvium gravel formation as bedrock.

$$T_1 = \sum_1 \frac{4H_i}{V_{si}} = 4 \left(\frac{4}{107} + \frac{4}{125} + \frac{5}{145} + \frac{3.5}{125} \right) = 0.53 \text{ sec} \quad (2)$$

Consequently the fundamental natural frequency f_1 of subsurface ground is estimated as 1.9 Hz which is considered to be the natural frequency during low amplitude vibration. Assuming that the difference of fundamental natural frequency f_1 between 1.9 Hz derived by Eq. 2 and

the values shown in Table 2 depends on the strain dependence of soil modulus, the ratio of shear wave velocity which would be developed during the A-Earthquake V_{s1} and that during the low amplitude vibration V_{s0} would approximately be estimated as follows.

$$\frac{V_{s1}}{V_{s0}} = \frac{1.3 \text{ \textasciitilde } 1.5}{1.9} = 0.68 \text{ \textasciitilde } 0.79 \quad (3)$$

Consequently the ratio of soil stiffness during the A-Earthquake G_1 and that corresponding to low amplitude strain level G_0 can be estimated as follows.

$$\frac{G_1}{G_2} = \left(\frac{V_{s1}}{V_{s0}}\right)^2 = 0.46 \text{ \textasciitilde } 0.62 \quad (4)$$

According to laboratory experiments concerning the strain dependence of soil stiffnesses, such a reduction of soil stiffness is reasonable.

The explanation of ground motion characteristics for the A-Earthquake can also be applicable for the ground motions of the B- and C-Earthquakes, i.e., the ground motions of the B-Earthquake have predominant frequencies of 1.9 Hz and 5.1 Hz in the longitudinal motion, and 1.5 Hz and 4.9 Hz in the transverse motion, which shows that the ratios between two predominant frequencies are approximately 3.0 in both directions. The ground motions of the C-Earthquake have predominant frequencies of 1.4 Hz, 3.7 Hz, 4.2 Hz and 4.8 \textasciitilde } 5.2 Hz in both the longitudinal and transverse motions. Although there are many apparent predominant frequencies, it would be considered that the frequencies of 1.4 Hz and 4.3 Hz represents the fundamental and second mode frequencies, respectively, which again shows that the ratio between two predominant frequencies are approximately 3. The frequencies of 3.7 Hz and 4.8 \textasciitilde } 5.2 Hz are considered to be the predominant frequencies of the incident motions in the bedrock.

Characteristics of Pier Motions

It is understood from the power spectra of Figure 9 that in the A-Earthquake the most predominant frequencies of the pier motions are 1.5 Hz in the longitudinal direction and 1.3 Hz in the transverse direction, which are approximately equal to those of ground motions. Also all of the four acceleration records during the A-Earthquake are narrow banded waves with a single frequency predominant. It is also understood from Table 2 that in the B-Earthquake the predominant frequencies of the pier motion are approximately 1.6 Hz in the

transverse direction, which is very close to the predominant frequency of the ground motion of 1.5 Hz. In the longitudinal direction, however, the pier motion has several predominant frequencies. The most predominant one is approximately 1.8 Hz which is again very close to the predominant frequency of the ground motion of 1.9 Hz. As is the case of A-Earthquake, the acceleration records on the ground in both directions and the acceleration record on the pier top in the transverse direction are narrow banded waves with a single frequency predominant. On the other hand, the records during the C-Earthquake are somewhat different from those for the A- and B-Earthquakes described as above. The most predominant frequencies of the pier motions are approximately 1.4 Hz in both the longitudinal and transverse directions which are different from the most predominant frequencies of the ground motions, i.e., approximately 3.7 Hz in both directions. It should be noted here, however, that the ground motions have a predominant frequency close to the 1.4 Hz although they are not the most predominant.

It can be recognized from these results that the acceleration records of pier always contain the motions in the range of 1.3 - 1.8 Hz as the most predominant ones in both the longitudinal and transverse directions, which is considered to correspond to the lowest natural frequency of the subsurface ground. The frequency response functions were then computed between the pier motions and the ground motions as shown in Figure 10. It can be recognized from Figure 10 that amplifications of the frequency response functions are rather small for the range of frequency of 4 Hz or more because of low pass filter effects of the foundation. The amplifications vary almost evenly between 0.5 Hz and 4 Hz although the apparent natural frequency of the foundation is not evaluated.

It would be deduced from these considerations that the most predominant frequency that is always contained in the motions of the pier is significantly influenced by the lowest natural frequency of the subsurface ground so that the pier vibrates in accordance with the motion of the subsurface ground nearby.

Nonsteady Vibrations of Pier and Ground

In order to investigate the time dependence of predominant frequencies of the pier and ground motions, running power spectra were computed. One of the results is displayed in Figure 11 for the A-Earthquake. Based on the running power spectra changes of predominant frequencies of the motions in time domain were estimated as shown in Figure 12. For the

A- and C-Earthquakes, it can be observed that the frequencies are rather low at the main parts of the motion where a large amplitude of vibration occurred. For instance, in the case of the transverse motion of the A-Earthquake, the predominant frequency is approximately 2 Hz around 4 seconds in time. The predominant frequency then decreased to 1.3 Hz around 12 - 18 seconds, and again recovered to 1.7 Hz around 30 seconds. It should be noted here that the predominant frequency developed at the beginning and ending of the motions are very close to that estimated by Eq. 2 by employing the shear wave velocity of subsurface ground at low strain amplitude.

It should also be noted here that the time dependence of the predominant frequencies described as above are almost identically developed in both the pier and the ground motions. Such characteristics of the time dependence of motions suggest that the nonsteady responses of the foundation were not derived from degradation of the soil stiffness just around the foundation but were caused by the nonsteady responses of subsurface ground nearby.

SEISMIC ANALYSIS PROCEDURE OF FOUNDATION

A discrete analytical model as shown in Figure 13 was formulated to calculate earthquake responses of the pier foundation. The equation of motions of the system can be written as

$$(\underline{M}_p + \underline{M}_e) \ddot{\underline{u}}_p + \underline{C}_p \dot{\underline{u}}_p + \underline{K}_p \underline{u}_p + \underline{C}_e (\dot{\underline{u}}_p - \dot{\underline{u}}_g) + \underline{K}_e (\underline{u}_p - \underline{u}_g) = \underline{0} \quad (5)$$

where,

\underline{M}_p = mass matrix of the foundation

\underline{M}_e = mass matrix of surrounding soils

\underline{C}_p = damping matrix of the foundation

\underline{K}_p = stiffness matrix of the foundation

\underline{C}_e = damping matrix expressing radiational dampings

\underline{K}_e = stiffness matrix expressing springs between foundation and surrounding soils

$\underline{u}_p, \dot{\underline{u}}_p, \ddot{\underline{u}}_p$ = absolute displacement, velocity and acceleration vectors of foundation

$\underline{u}_g, \dot{\underline{u}}_g$ = absolute displacement and velocity vectors of subsurface ground

in which the subsurface ground motions of \underline{u}_g and $\dot{\underline{u}}_g$ are assumed to be specified. Denoting as

$$\begin{aligned}
 \underline{M} &= \underline{M}_p + \underline{M}_e \\
 \underline{C} &= \underline{C}_p + \underline{C}_e \\
 \underline{K} &= \underline{K}_p + \underline{K}_e
 \end{aligned}
 \tag{6}$$

Eq. 5 can be written as

$$\underline{M} \ddot{\underline{u}}_p + \underline{C} \dot{\underline{u}}_p + \underline{K} \underline{u}_p = \underline{C}_e \dot{\underline{u}}_g + \underline{K}_e \underline{u}_g
 \tag{7}$$

The vector \underline{u}_p can be conveniently decomposed into a quasi-static displacement vector \underline{u}_{ps} and a dynamic displacement vector \underline{u}_{pd} , i.e.,

$$\underline{u}_p = \underline{u}_{pd} + \underline{u}_{ps}
 \tag{8}$$

By definition of quasi-static displacement in the form as

$$\underline{K} \underline{u}_{ps} - \underline{K}_e \underline{u}_g = \underline{0}
 \tag{9}$$

\underline{u}_{ps} can be written as

$$\underline{u}_{ps} = \underline{K}^{-1} \underline{K}_e \underline{u}_g = \underline{K}_s \underline{u}_g
 \tag{10}$$

Substitution of Eqs. 8 and 9 into Eq. 7 gives

$$\underline{M} \ddot{\underline{u}}_{pd} + \underline{C} \dot{\underline{u}}_{pd} + \underline{K} \underline{u}_{pd} = \underline{M} \underline{K}_s \ddot{\underline{u}}_g + (\underline{C}_e - \underline{C} \underline{K}_s) \dot{\underline{u}}_g
 \tag{11}$$

Usually the damping term on the right hand side of Eq. 8 is less significant when compared with the inertia terms so that it can be dropped from the equation without introducing significant errors. Then Eq. 11 can be written as

$$\underline{M} \ddot{\underline{u}}_{pd} + \underline{C} \dot{\underline{u}}_{pd} + \underline{K} \underline{u}_{pd} = \underline{M} \underline{K}_s \dot{\underline{u}}_g
 \tag{12}$$

Eq. 12 can be solved by modal-superposition procedures provided that the damping matrix on the left hand side of the equation is assumed to be triangularized in the same manner as the mass and stiffness matrices in the form of the critical damping ratio.

CALCULATION OF PIER MOTIONS

The pier motions were computed by using the analytical procedure described in the preceding paragraph based on the measured ground motions for the A-, B-, and C-Earthquakes, and they were compared with the measured motions.

The bedrock motions were computed from the measured ground surface motions by the de-convolution procedure taking account of the strain dependence of the shear moduli and hysteretic damping ratio of the subsoils as shown in Figure 14. The subsoils and foundation were idealized by a one-dimensional shear column model with equivalent linear soil properties and one-dimensional elastic beam supported elastically by the surrounding subsoils, respectively. The weight of a girder supported by the pier was idealized as an additional mass lumped at the crest of pier. The lowest natural frequencies of the pier and surrounding subsoils thus estimated are shown in Table 3.

The response accelerations of pier were then calculated based on Eq. 12 by applying the bedrock motions at the bottom of the shear column model of subsoils. The comparative plots of both the theoretical and measured accelerations at the crest of pier are shown in Figures 15, 16 and 17 for the A-, B-, and C-Earthquakes, respectively. The damping ratios assumed in the analyses are shown in Table 3. It is recognized from the results that fairly good agreements are obtained for the motions in the A- and B-Earthquakes. However, the correlation for the motion in the C-Earthquake is appreciably less satisfactory and further precise investigations are needed to clarify the frequency characteristics of the foundation.

CONCLUSIONS

Based on the results presented, the following conclusions may be deduced:

- 1) Seismic responses of the deeply embedded foundation are significantly influenced by the effects of surrounding subsurface soils. The most predominant frequencies which are always contained in the motions of the pier crest are prescribed by the lowest natural frequency of the subsurface ground so that the pier foundation responses in accordance with the motion of the subsurface ground nearby.

- 2) The nonsteady responses developed on the pier foundation are almost identical with those observed on the ground surface, which suggest that the nonsteady responses of the pier

foundation are not derived from degradation of the soil stiffness just around the foundation but are primarily caused by nonsteady responses of the subsurface ground nearby.

3) Seismic response accelerations of the foundation can be calculated with fairly good accuracy by the analytical procedure presented herein from the free-field ground accelerations measured near the foundation for earthquakes which induce ground accelerations at the bridge site with the most predominant frequencies lower than the fundamental natural frequency of the foundation.

REFERENCES

- [1] Iwasaki, T., "Earthquake-Resistant Design of Bridges in Japan," Bulletin of Public Works Research Institute, Volume 29, Public Works Research Institute, Ministry of Construction, May 1973.
- [2] Kuribayashi, E. and Iwasaki, T., "Dynamic Properties of Highway Bridges," Fifth World Conference on Earthquake Engineering, Roma, December 1972.
- [3] Iwasaki, T., Wakabayashi, S., Kawashima, K. and Takagi, Y., "Strong-Motion Acceleration Records from Public Works in Japan (No. 3)," Technical Note of the Public Works Research Institute, No. 34, Public Works Research Institute, Ministry of Construction, 1978.
- [4] Yamahara, H., "Ground Motions During Earthquakes and the Input Loss of Earthquake Power to an Excitation of Buildings," Soils and Foundations, Vol. 10, No. 2, 1970.
- [5] Duke, C. M., et al., "Strong Motions and Site Conditions -- Hollywood," Bulletin of the Seismological Society of America, Vol. 60, No. 4, 1970.
- [6] Matsushima, Y., "Structure-Soil Interaction for Finite Element Hysteretically Damped Systems, Journal of Architectural Institute of Japan, No. 199, 1972.
- [7] Iwasaki, T. and Kawashima, K., "Seismic Analysis of Highway Bridge Utilizing Strong-Motion Acceleration Records," Proceedings of Second International Conference on Microzonation, San Francisco, California, USA, 1978.

Table 1 Strong Motion Acceleration Records at The Itajima Bridge

Earthquake No.	Earthquake	Date	Richter Magnitude	Epicentral Distance(km)	Maximum Acceleration (Gal)			
					Pier Motion		Ground Surface Motion	
					Longitudinal	Transverse	Longitudinal	Transverse
1	The Hyuganada Earthquake	1968.4.1.09:42	7.5	101	209	306	169	186
2	The Hyuganada Earthquake (Aftershock)	1968.4.1.16:13	6.3	99	38	66	34	42
3	The Bungosuido Earthquake	1968.8.6.01:17	6.6	11	199	231	441	353
4	The Bungosuido Earthquake (Aftershock)	1968.8.6.13:21	5.3	19	100	63	227	172

Table 2 Predominant Frequencies of Strong Motion Acceleration Records Measured on Pier Crest and Ground Nearby [Hz]

Earthquake No.	Earthquake	Longitudinal		Transverse	
		Ground	Pier Crest	Ground	Pier Crest
1	The Hyuganada Earthquake	1.5	1.5	1.3	1.3
2	The Hyuganada Earthquake (Aftershock)	1.9	1.8,2.0,2.3,3.7	1.5	1.6
3	The Bungosuido Earthquake	3.7	1.4	3.7,4.4	1.4
4	The Bungosuido Earthquake (Aftershock)	4.2	-	4.4	-

Table 3 Lowest Natural Frequencies and Damping Ratio Assumed in Seismic Analyses

Earthquake	Surrounding Ground		Caisson-Pier Foundation		Hystretic Damping Ratio of Subsoils(%)	Radiational Damping Ratio(%)
	1st	2nd	1st	2nd		
The Hyganada Earthquake (A-Earthquake)	1.6	4.9	2.8	7.8	10	20
The Hyuganada Earthquake (After Shock) (B-Earthquake)	1.9	5.7	3.1	8.3	5	20
The Bungosuido Earthquake (C-Earthquake)	1.6	4.7	2.7	7.7	8 - 12	20

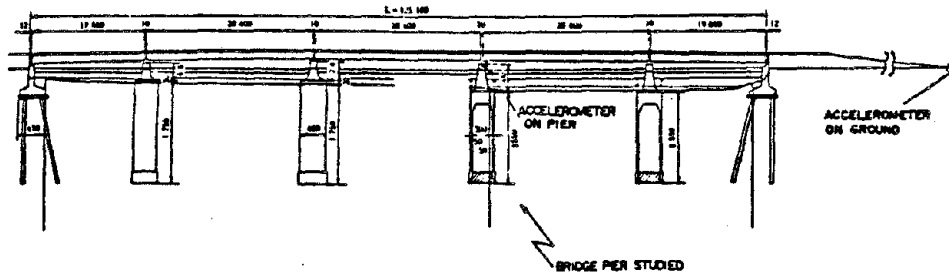


Fig. 1 General View of The Itajima Bridge

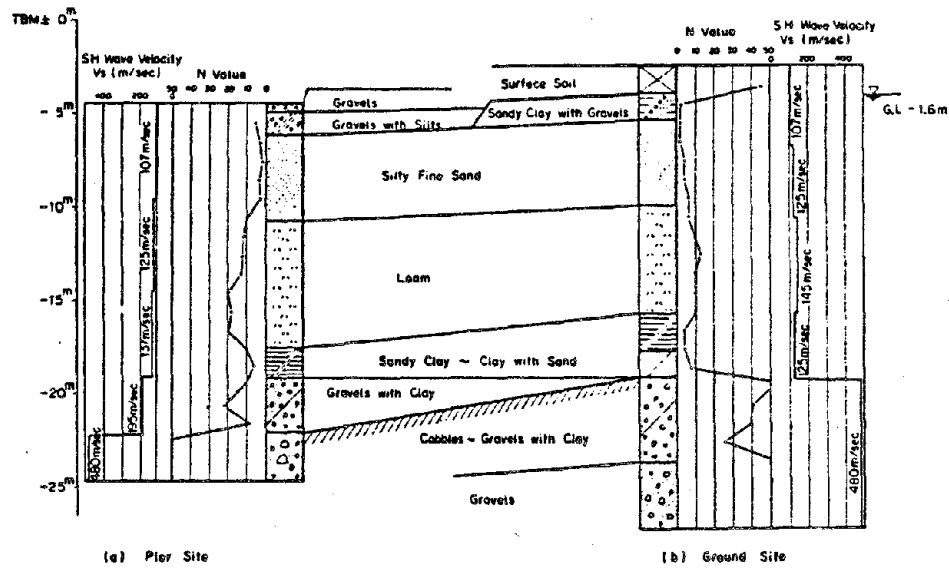


Fig. 2 Soil Profile at the Pier Site and Ground Observatory Site

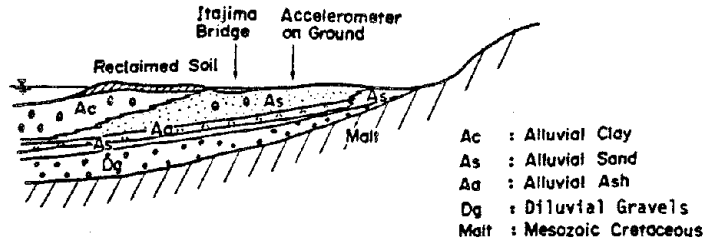


Fig. 3 Geological Condition Around The Itajima Bridge

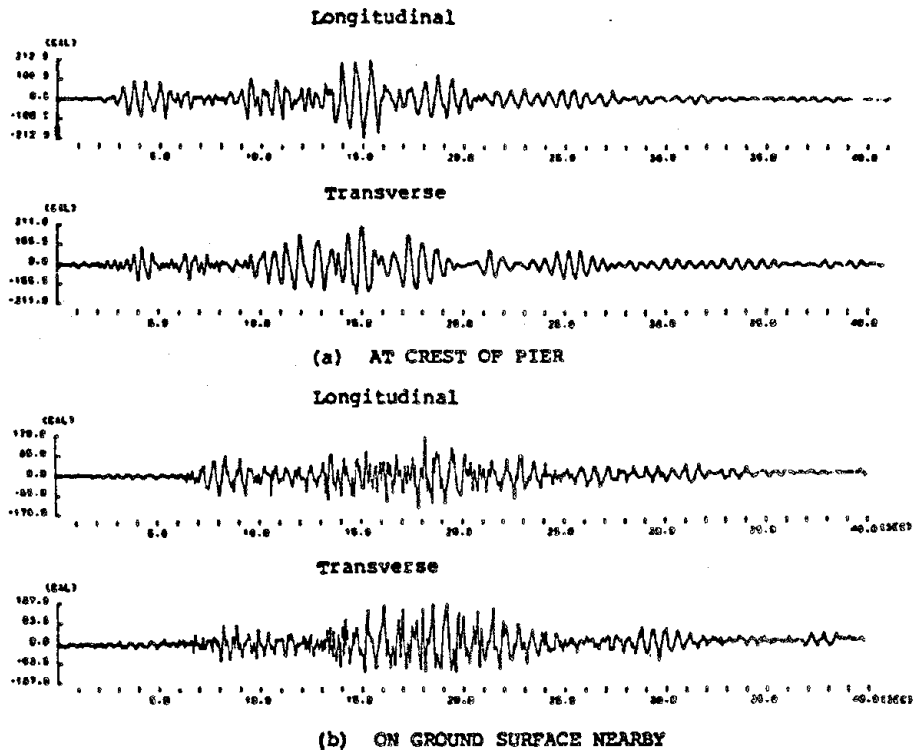


Fig. 4 Acceleration Records At the Itajima Bridge During the Hyuganada Earthquake of April 1, 1968 (A-Earthquake)

Fig. 5

Acceleration Records at the Itajima Bridge During An Aftershock of the Hyuganada Earthquake of April 1, 1968 (B-Earthquake)

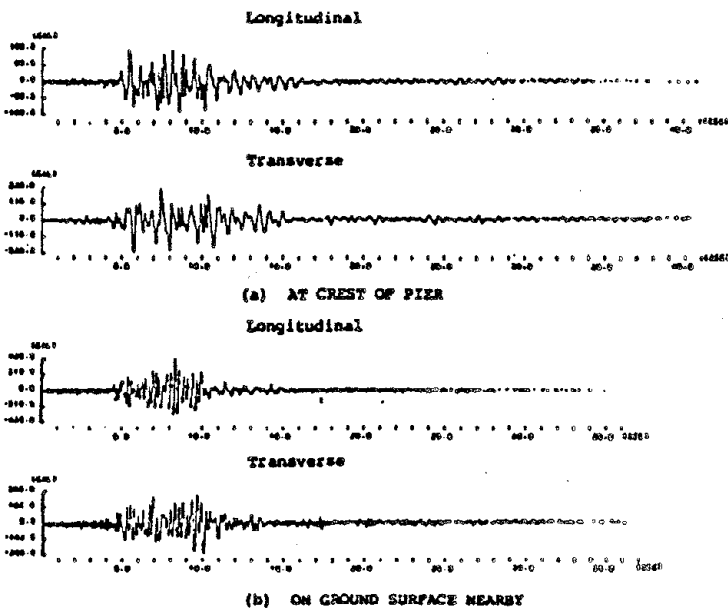
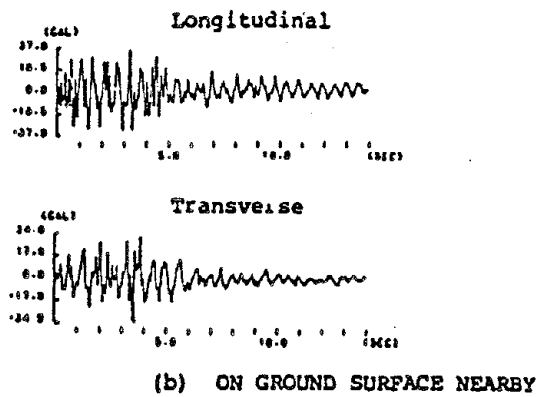
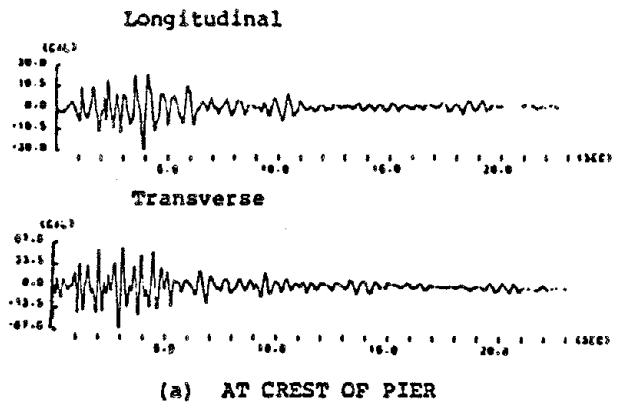
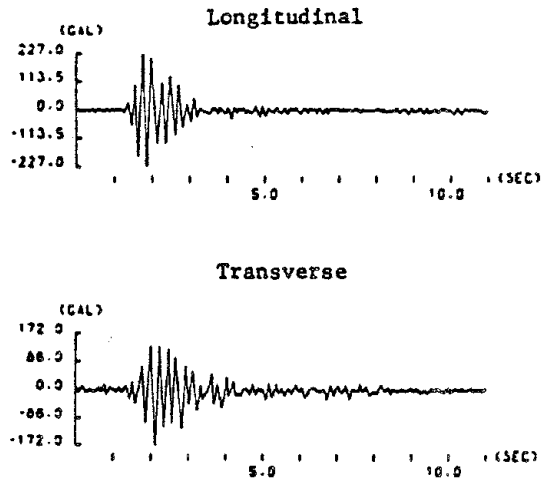


Fig. 6

Acceleration Records at the Itajima Bridge During the Bungosuido Earthquake of August 6, 1968 (C-Earthquake)



(a) ON GROUND SURFACE NEARBY

Fig. 7 Acceleration Records At The Itajima Bridge During An Aftershock of the Bungosuido Earthquake of August 6, 1968 (D-Earthquake)

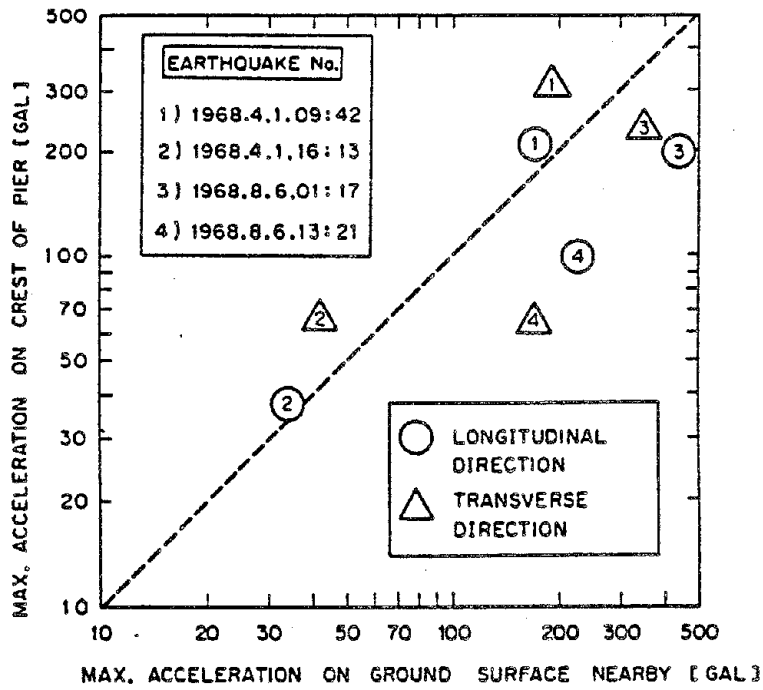
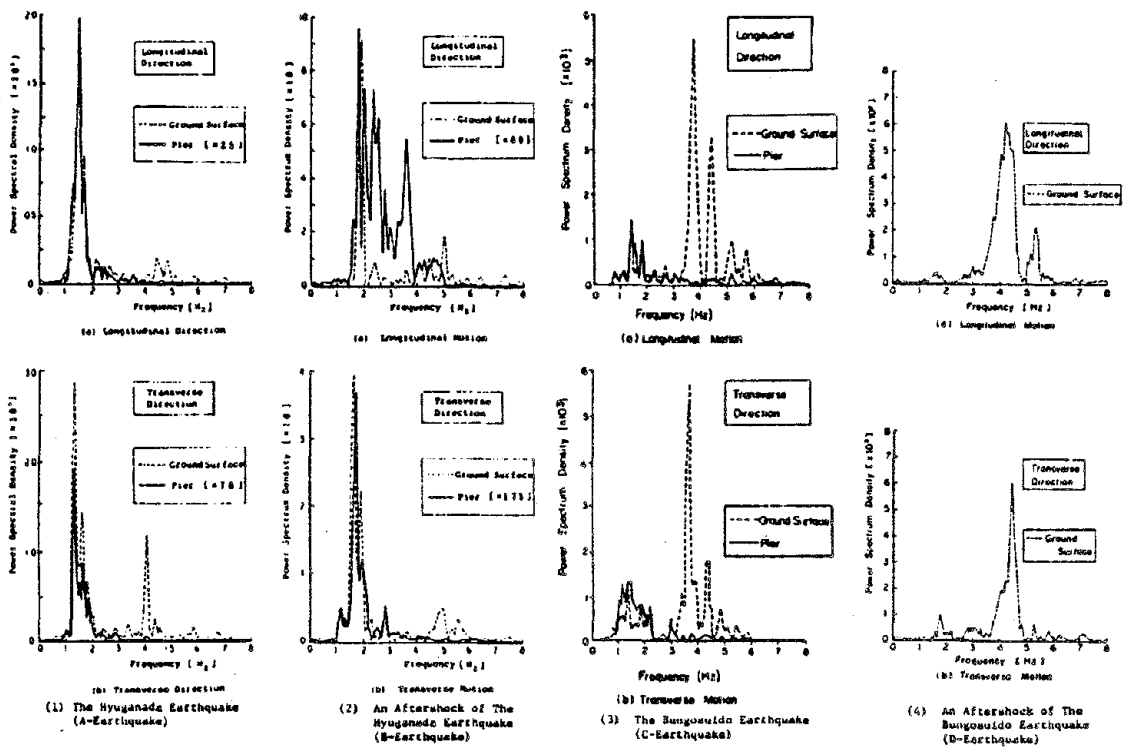
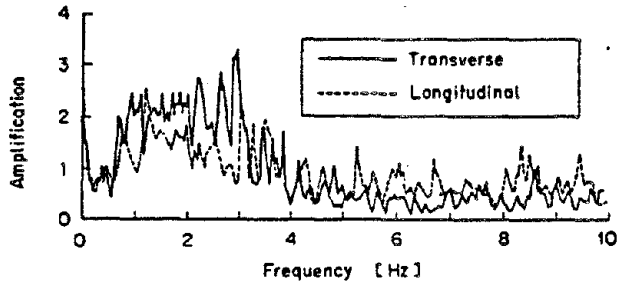


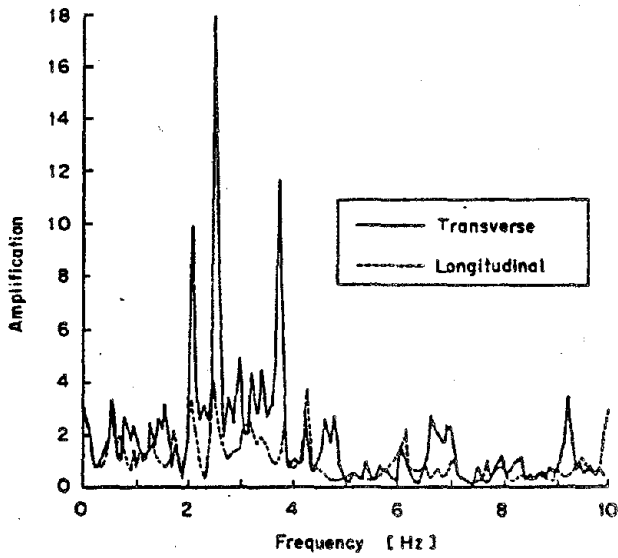
Fig. 8 Amplifications of Maximum Acceleration Between The Pier Crest and Ground Surface Nearby

Fig. 9 Power Spectra of Acceleration Records at the Itajima Bridge

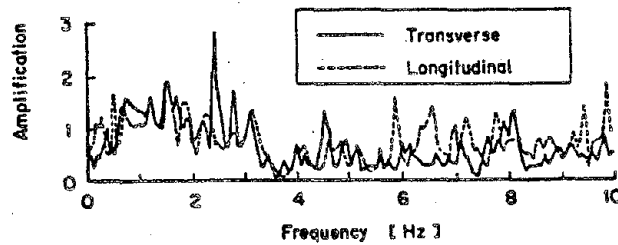




(a) The Hyuganada Earthquake (A-Earthquake)



(b) An Aftershock of The Hyuganada Earthquake (B-Earthquake)



(c) The Bungosuido Earthquake (C-Earthquake)

Fig. 10 Frequency Response Functions Determined by Measured Strong Motions Between Pier Crest and Ground Surface

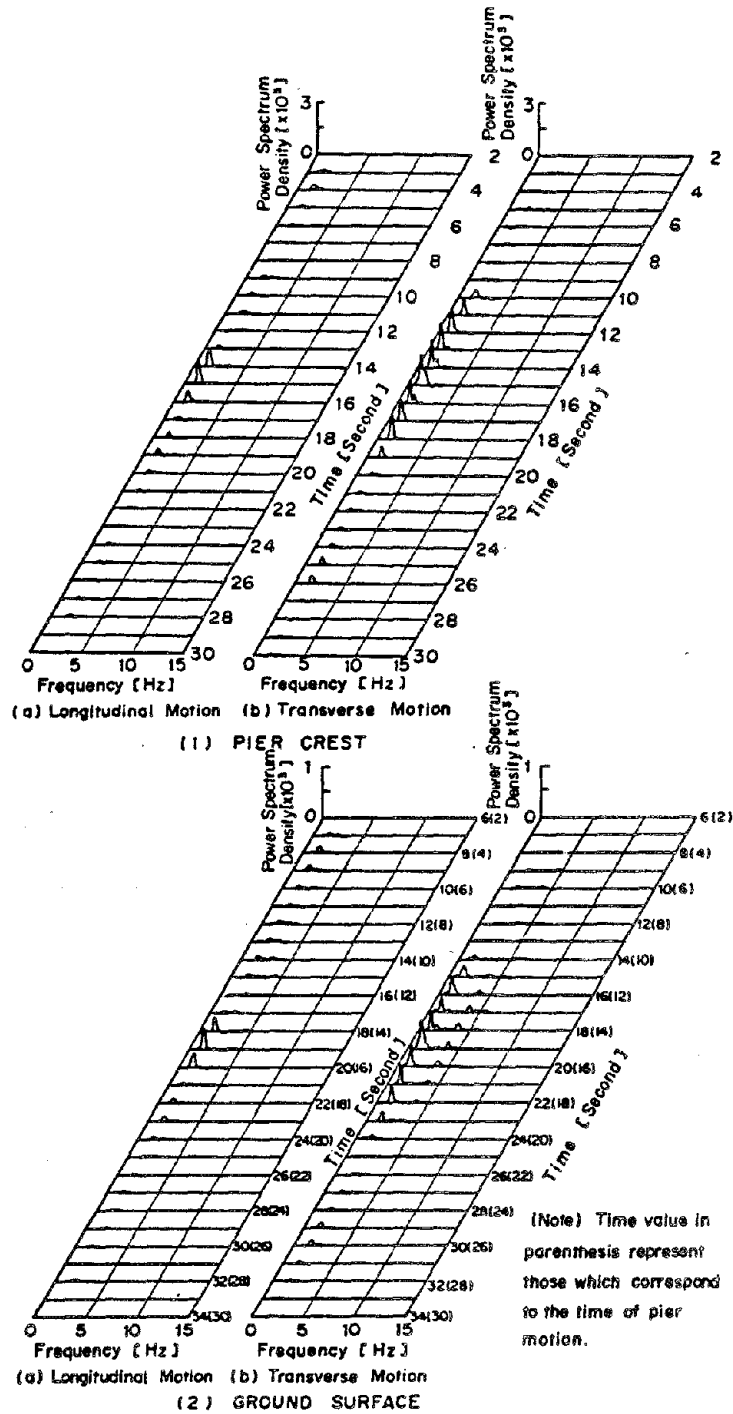
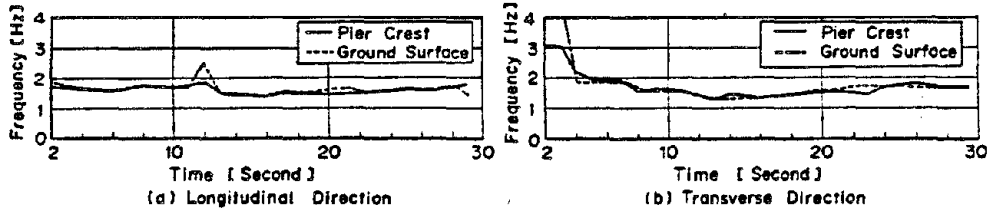
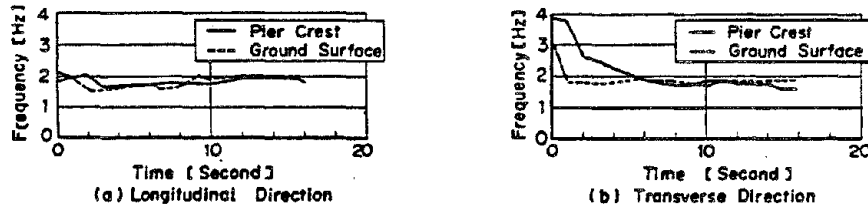


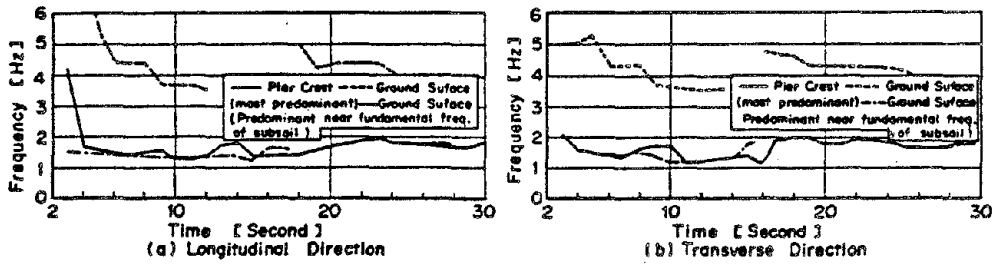
Fig. 11 Running Power Spectra of Strong Motions During The Hyuganada Earthquake (A-Earthquake)



(1) THE HYUGANADA EARTHQUAKE (A-Earthquake)



(2) AN AFTERSHOCK OF THE HYUGANADA EARTHQUAKE (B-Earthquake)



(3) THE BUNGOSUIDO EARTHQUAKE (C-Earthquake)

Fig. 12 Time Dependence of Predominant Frequencies of Pier and Ground Motions

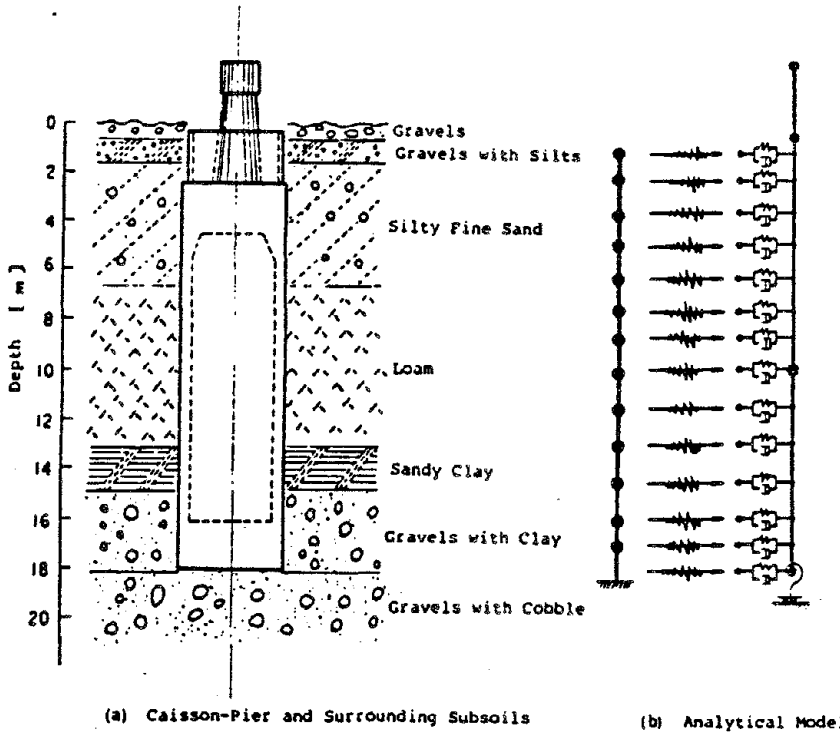


Fig. 13 Analytical Model of Subsoils and Foundation

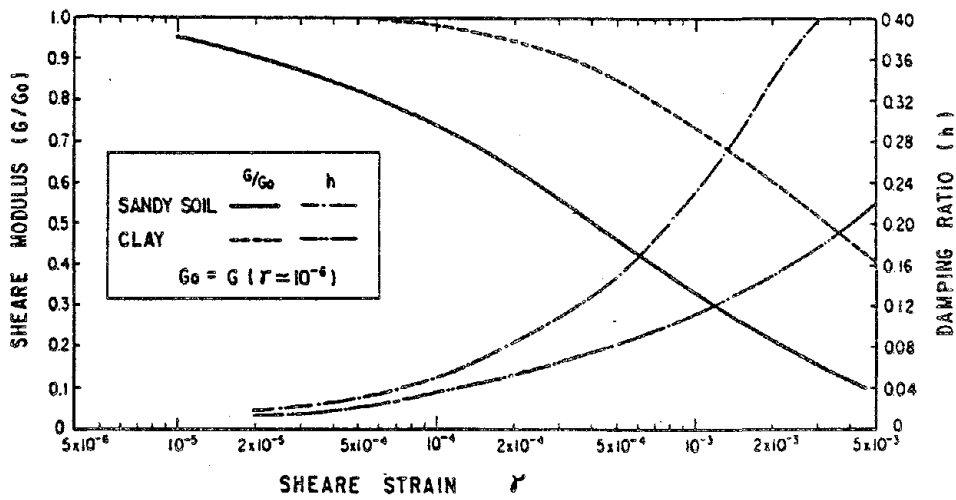
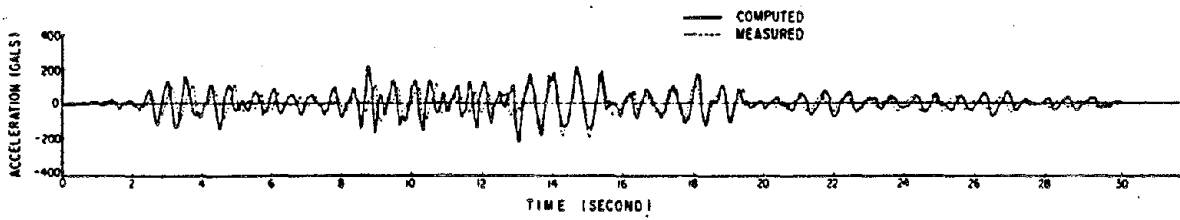
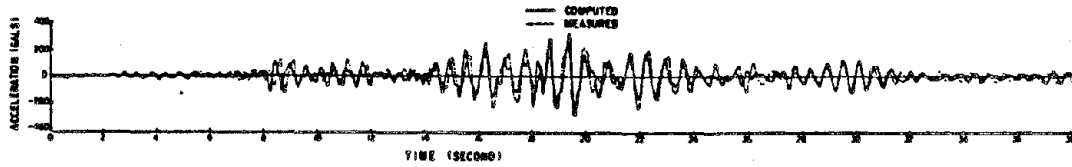


Fig. 14 Shear Strain Dependence of Shear Modulus and Hysteretic Damping Ratio Assumed in Seismic Analyses

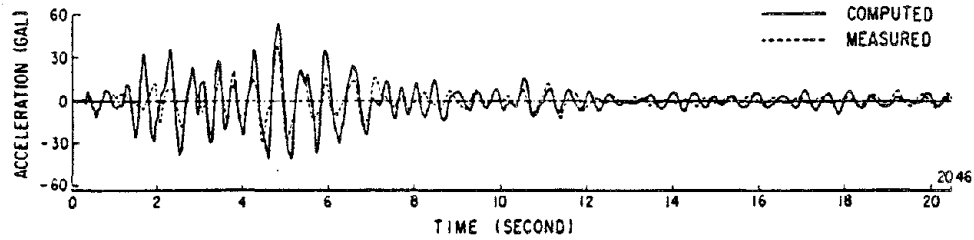


(a) Longitudinal Motion

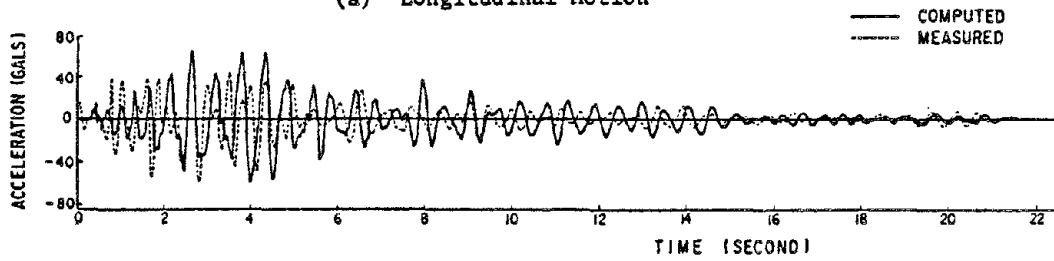


(b) Transverse Motion

Fig. 15 Correlation of Seismic Response Acceleration At the Pier Crest
(The Hyuganada Earthquake; A-Earthquake)



(a) Longitudinal Motion



(b) Transverse Motion

Fig. 16 Correlation of Seismic Response Acceleration At The Pier Crest
(An Aftershock of The Hyuganada Earthquake; B-Earthquake)

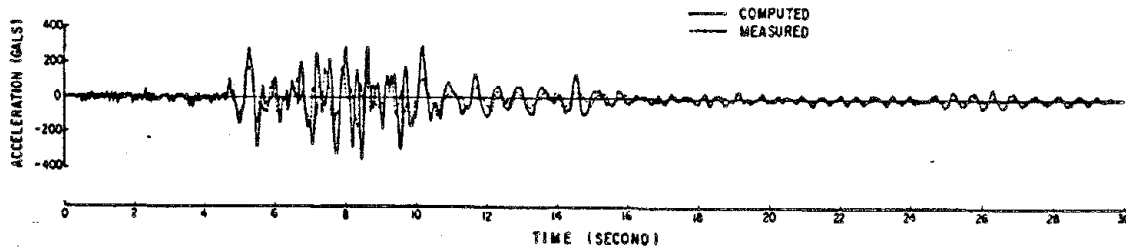


Fig. 17 Correlation of Seismic Response Acceleration At The Pier Crest
(The Bungosuido Earthquake; C-Earthquake)

REPORT OF THE INVESTIGATION ON EARTHQUAKE DAMAGE
TO SHIZUNAI BRIDGE

by

I II III
Nobuyuki NARITA, Misato MURAKAMI, Hideya ASANUMA

ABSTRACT

Shizunai Bridge is on national highway route 235 and spans the Shizunai River at Shizunai-cho in Hokkaido. It sustained tremendous damage during the Urakawaoki Earthquake which occurred on the 21st of March, 1982.

The damage to the other public facilities in the area was slight and only that to the Shizunai Bridge was severe, with the failure characteristics of the bridge piers being different from those of other reinforced concrete structures. The Ministry of Construction organized a group to investigate the earthquake damage on the Shizunai Bridge, and conducted research to determine the cause of the damage. This is the summary of its report.

1. INTRODUCTION

At 11:32, March 21st, 1982, a large-scale earthquake now known as the "1982 Urakawaoki Earthquake", occurred in the Pacific Ocean off Urakawacho, Hokkaido. According to the reports of the Meteorological Agency, the magnitude of the earthquake was 7.1 on the Richter Scale and 6 on the Japanese scale of 7. Its epicenter was located at $143^{\circ}36' \pm 01''$ E longitude, $42^{\circ}04' \pm 00''$ N latitude, and the depth of the seismic center was some 40km. The distance from Shizunai Bridge to the epicenter was about 30km. The maximum acceleration measured by strong motion accelerographs in Hokkaido is shown in Table-1.

A set of strong motion accelerographs had been installed at the depth of 2m and 40m in the ground adjacent to the Shizunai Bridge and measurements had been carried out for a long time. However, they had begun to malfunction and had consequently been removed for repairs four days before the earthquake. Therefore, measurement for the earthquake were not obtained for the site of the bridge. The closest observation spot to the epicenter was the Horoman Bridge about 40 km away. The maximum acceleration measured there was about 100gal. This bridge is about 60km

-
- I. Director, Planning Department, Public Works Research Institute,
Ministry of Construction, Tsukuba Science City, Ibaraki-ken, Japan
II. Director, Structure and Bridge Department, ditto
III. Head, Foundation Engineering Division, ditto

southeast of the Shizunai Bridge and opposite the bridge concerning Mitsuishi-cho, a center of aftershocks.

Deposits around the Horoman Bridge consist of a 10m deep alluvial layer with underlying bedrock. Although the ground subsurface differs from that of the Shizunai Bridge, the earthquake data for Horoman Bridge was used for the earthquake response analysis because of the proximity of this bridge to the epicenter. Fig-1 shows the records of the acceleration, velocity and displacement at the Horoman Bridge during the earthquake.

2. DAMAGE TO SHIZUNAI BRIDGE

Shizunai Bridge was constructed in 1972 at the mouth of the Shizunai River. It is a three-span continuous plate-girder bridge of 406.5m in total length. As to substructure, A-1 abutment has a pile foundation, piers P-1 to P-7 have caisson foundations, and both pier P-8 and abutment A-2 have spread ones. Fig-2 is a general view of the bridge.

Damage to the bridge during the Urakawaaki Earthquake was concentrated on the piers with that to the super structure being very slight. Almost all piers, with reinforced concrete columns of 2.2m in diameter, except P-1 and P-8 developed horizontal and/or diagonal cracks. In the case of piers P-2, P-3 and P-6, part of the concrete spalled, resulting in exposure of reinforcing bars. Since these cracks were mainly caused by the force acting transversely to the bridge axis, it can be assumed that a large earthquake force acted in this direction. Photographs 1 to 6 show the damage to the bridge piers.

After examining damage to the P-3 pier which suffered the heaviest damage, the failure is thought to have occurred as follows:

As a result of the large earthquake force acting transversely to the bridge axis, bending moment cracks first appeared on the columns. Next, the main reinforcement yielded, resulting in the development of the cracking, to be followed by buckling of the reinforcing bars and spalling of the concrete at the buckled portions. At this stage, and for some reason, the shearing resistance capacity decreased and cracks of a different nature gradually developed diagonally to the original ones, resulting in the final collapse along this shearing section. The concrete of the failure part of pier P-3 completely disintegrated into small blocks, and only the cage of main and hoop reinforcing bars prevented it from falling off.

3. OUTLINE OF THE INVESTIGATION

After an on-site inspection of the Shizunai Bridge was completed, the group to investigate the damage to the bridge established the following outline for the investigation in order to determine the factors which caused the damage. The following are the points which were to be clarified by the investigation.

- 1) Despite the comparatively strong seismic motion (of intensity 6 on the Japanese scale of 7), why was the Shizunai Bridge the only structure which sustained heavy damage?
- 2) Why were some piers so completely destroyed beyond mere cracking?
- 3) Why did the damage characteristics of the ten piers differ so much? In particular, why the damage to piers P-2, P-3 and P-6 especially heavy?
- 4) Were there any mistakes in the design and/or execution of the piers.

The group decided to pursue the following themes:

- 1) To execute soil exploration at the Shizunai Bridge site to learn the composition of deposits and various soil conditions for aseismic design.
- 2) To estimate the ground tremor for the base deposit beneath the Shizunai Bridge.
- 3) To conduct a dynamic response analysis.
- 4) To conduct experiments on a one-third scale model of the pier.
- 5) To conduct strength tests on samples of material from the damaged pier.

4. RESULTS OF SOIL EXPLORATION AND MATERIAL TESTS

(1) Soil Exploration

In-situ and laboratory soil tests were conducted in order to determine the input conditions for the dynamic response analysis and also to obtain fundamental informations regarding the liquefaction of the ground. A total of six borings were carried out to confirm the location of the base mudrock, while standard penetration tests, horizontal load tests in boreholes, seismic reflection survey and formation density logging were also executed. In addition, undisturbed specimens of the soil at pier P-2 were collected by a triple tube sampler and their laboratory tests were conducted to confirm the dynamic deformation characteristics

and the strength of the ground. Fig-3 shows the soil profile at Shizunai Bridge. Other boring data obtained before the construction are also shown in the figure. The test results are shown in Table-2, and the dynamic deformation characteristics measured by dynamic torsional shearing test are shown in Fig-4.

These data were used as the input data for the dynamic response analysis. Regarding the liquefaction of the ground, the number of shaking and the liquefaction resistance factor were obtained by means of tri-axial vibration test for both disturbed and undisturbed samples of the ground. The liquefaction resistance factor was calculated using these test results as shown in Table-3. It was found through these tests that there existed a possibility that liquefaction had occurred in the soil around the layers Ag-1 and Ag-2.

On the actual site, small traces of sand bursts were found in the Ag-1 layer, so we can say that small scale liquefaction had occurred in the Ag-1 layer. However, since the crown of every caisson rests below this layer, it can be said that the liquefaction of the Ag-1 layer did not have any adverse effect upon the stability of the foundation.

(2) Material Test

In order to confirm the quality of the reinforcing bars and the concrete used in the piers, tension and compression tests were conducted by using specimens of concrete core and reinforcing bar sampled from the damaged piers.

The tensile and yield strength of the main reinforcing bars were 3,450kg/cm² and 5,150kg/cm² respectively. The compressive strength of the concrete cores was 260kg/cm².

Consequently, the reinforcing bars and concrete of the piers were proved to have enough strength provided in for the specification. We can thus safely conclude that there were no problems resulting from the quality of the materials used.

5. EARTHQUAKE MOTION ESTIMATION AND DYNAMIC RESPONSE ANALYSIS

The shape of the seismic wave and the magnitude of the earthquake should always be given in advance as input data in a dynamic response analysis. However, in the case of the Shizunai Bridge, the set of strong motion accelerographs which had been installed in the ground nearby the

abutment had been removed for repairs several days before the earthquake resulting in there being no available records of the actual earthquake motion for the site of the Shizunai Bridge.

Therefore, the estimation of the maximum acceleration and the selection of the input wave shape were carried out on the spot after an extensive study of an analysis of the acceleration records for the Urakawaoki Earthquake, the statistically analyzed data of Japanese earthquakes as well as such observational information as the number of overturned tombstones in cemeteries near Shizunai Bridge. The maximum acceleration was estimated to be 300gal on the surface.

Concerning the input wave shape, the records for Horoman Bridge which has a foundation condition very similar to that of Shizunai Bridge in addition to being very close, were used. In addition, the Shizunai Bridge records for another earthquake which took place in the sea off Hokkaido in 1981 and having a magnitude of 7.1 on the Richter Scale were also used for the dynamic response analysis to form a basis for comparison. Fig-5 shows the input earthquake motions used for the analysis.

Since the results of the dynamic earthquake response analysis are reported in the theme II-19 of this panel, we will not deal with them here. The following are brief conclusions drawn from the analysis of the behaviour in the direction transverse to the bridge axis.

- 1) When the selected wave shape of the earthquake was applied to the ground with the maximum acceleration value of 300gal, strong acceleration with the value of more than 400gal occurs at the top of piers P-1 through P-6. Subsequently, some reinforcing bars are considered to have yielded due to the large bending moment. On the other hand, at the piers P-7, P-8 and abutment A-2 which are resting on a mudstone base rock, the maximum acceleration and horizontal displacement were relatively small. Where the piers P-1 through P-6 were constructed, the sustaining layer of mudstone is deep, and the predominant period of the ground is estimated at 0.5 to 0.7 seconds by the dynamic analysis. In the case of the ground where P-7 and P-8 are constructed, the bearing stratum is located at a relatively shallow place, and the predominant period is calculated to be about 0.2 seconds. The inherent period of the bridge was found to be 0.5 to 0.6 seconds by the dynamic analysis (for the 1st through 4th modes of vibration).

Therefore, it is obvious that the response was amplified because the inherent period of bridge was almost equal to the predominant period of the ground.

2) In case of a continuous bridge like Shizunai Bridge, a seismic force applied to pier tops in a transverse direction is not distributed proportionally to the dead load of the super structure. The ratio of the seismic force calculated by the dynamic analysis to that of the static design, is largest for piers P-3 and P-6 as shown in Fig-6, and this corresponds well to the actual failure situation of the Shizunai Bridge.

6. MODEL TESTS

Among many bridges, only the piers of the Shizunai Bridge especially the P-3 pier, sustained serious damage from the earthquake, so some doubts concerning the design or execution of the piers were held. To investigate this, model tests were conducted by using 1/3 typical specimens of the P-3 pier. Research items are as follows:

- 1) Whether the pier had enough strength against the design seismic force.
- 2) Whether the pier had enough deformation capacity against the design value.
- 3) Effects of hoop reinforcement on the strength of the column.
- 4) Effects of vertical seismic coefficient on the strength of the column.

Six typical specimens of the same main reinforcement ratio and material strength as the actual pier were prepared as illustrated in Fig-7. Details and characteristics of the actual pier and typical specimens are described in Table-4 as well. A two-directional loading apparatus as illustrated in Fig-8 was used for this test. Applying a specified vertical load, a test was conducted under the condition of reciprocally increased horizontal loads until the main reinforcement yielded. Once some main reinforcing bars yielded, the test was continued under the confined displacement condition until the specimen fractured. The results of the test are summarized as follow.

1) The fracture mode of specimens in the test is very similar to that of the actual P-3 pier as shown in Photograph-7. In case of these

model specimens, some main reinforcing bars yielded at the transition section of reinforcement at first when horizontal load increased to some extent, and cracks were produced. As the load increased still more, extending up to the axis of the column, these cracks turned into diagonal shearing cracks, until the column collapsed in the form of a brittle rupture.

2) Although the load-displacement relation in elastic zone and the yield strength in the model tests were the same as theoretical values, the difference between model tests and the theory became wider after the load exceeded the yield point. And finally, the value of the horizontal displacement measured at the loading spot turned out half the theoretical value for instance.

That is, the theoretical analysis based on bending rupture could explain actual rupture of the pier columns, but once main reinforcement yields, it becomes impossible to be applied. This fact shows that the rupture condition changed from bending rupture to a different rupture mode (it seems to be the shearing rupture mode) after the yield of main reinforcement.

3) With respect to the actual pier P-3, the bending moment for the main reinforcement to yield was about 1.4 times larger than that produced by the design seismic force at the upper reinforcement transition section. Therefore, it is supposed that a seismic load more than 1.4 times as large as the design value acted on the actual pier P-3.

4) Using an average ultimate shearing stress obtained from the experiments, the shearing strength of the actual pier was calculated to be 1.6 times as large as the design value. Therefore, from this point of view, a seismic force more than 1.6 times as large as the design value acted on the pier so as to break it in the mode of shearing rupture.

5) An additional model, details of which are almost the same other than the enough anchorage of main reinforcing bars, abiding by the "Specification for Highway Bridges, Part 4, Specification for Substructures (May 1980)", was tested. Results showed that the specimen did not break in a shearing fracture mode and that both the ultimate strength and ductility of the specimen were excellent compared to those having an insufficient anchorage length. (refer to Fig-9)

6) Two model specimens with half or twice the amount of hoop reinforcement as the pier P-3 were prepared and tested. Through the

tests, it was made clear that the amount of hoop reinforcement affects neither strength nor ductility of a pier. Results of another model test, that was carried out under a 20% increased vertical load condition, showed that the ultimate strength might increase to some extent while the capacity of deformation would decrease a little. Then, it may be deduced that the fluctuation of vertical seismic coefficient hardly affected the rupture mode of the pier. (refer to Fig-10)

7. CONCLUSION

When a reinforced concrete bridge pier sustains serious damage as seen on the Shizunai Bridge, there should exist several factors which cause the damage. And among these factors, one single factor may happen to be a both necessary and sufficient condition for the fracture, while another factor is really necessary but not sufficient. The latter one would become the sufficient condition when it acts simultaneously with some other factors.

As extensively reviewing results of the investigation, we have found out that there is no single factor that causes the fracture sufficiently by itself, but that the pier P-3 finally came to the serious fracture as a result of the combination of following factors.

1) On the piers which support movable bearings of a continuous girder bridge, the horizontal earthquake force in the transverse direction surpassed the designed values distributed proportionally to the vertical reaction due to dead load of the super structure.

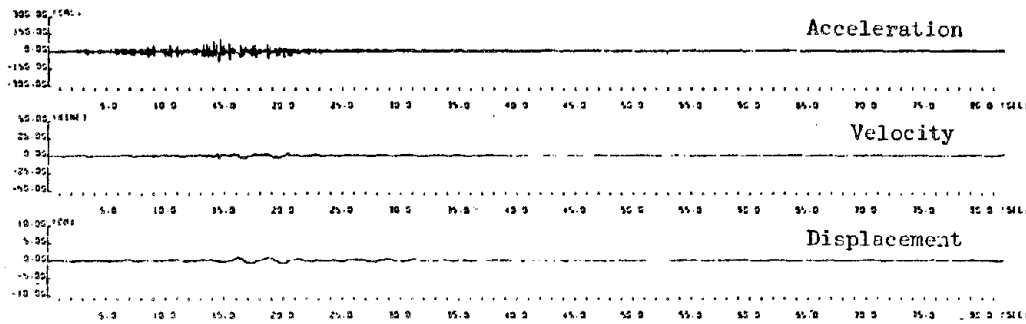
2) Since the predominant period of the ground was very similar to the inherent period of the bridge, the seismic response of the bridge was greatly amplified.

3) The shearing strength of a reinforced concrete member was so reduced in accordance with the occurrence of cracks, that the real shearing strength became relatively low compared with the original design one.

The reason we have reached concerning the pier fracture is as follows:

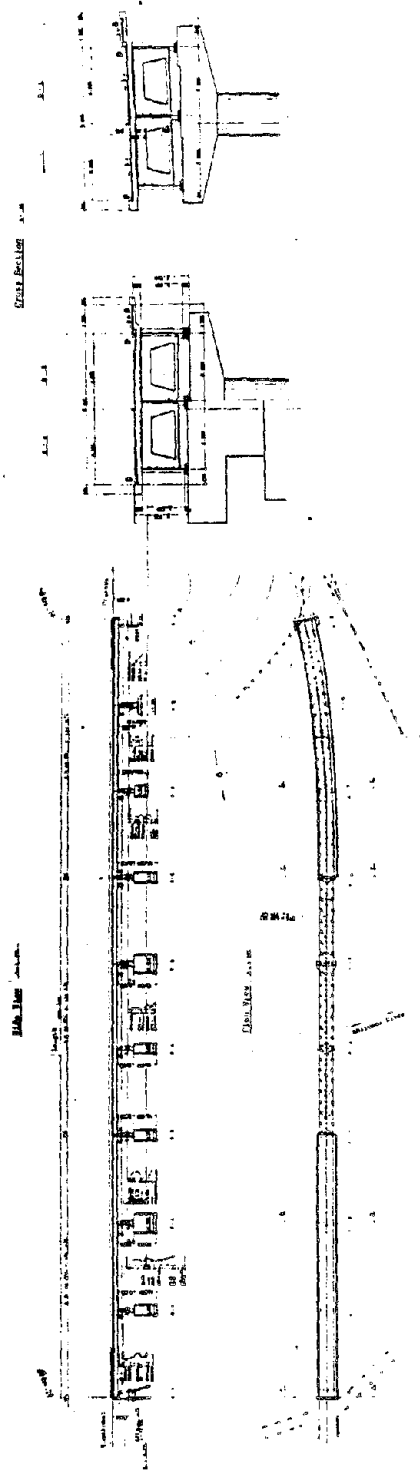
The horizontal seismic force applied to Shizunai Bridge transversely to its axis by the Urakawaoki Earthquake, had exceeded the design value (design seismic coefficient was 0.2) as a result of combined effect of the above 1) and 2) factors. Consequently, the main reinforcing bars

yielded at the upper reinforcement transition section, so that the bending cracks produced and developed around the section. As the cracks sufficiently progressed, the shearing strength of the concrete decreased. And, when the applied seismic force surpassed the shearing resistance of the pier, the brittle shearing rupture finally occurred.



Transverse to the Bridge Axis

Fig-1 Records of Acceleration, Velocity and Displacement (Horoman Br.)



Reproduced from
best available copy.

Fig-2 General View of Shizunai Bridge

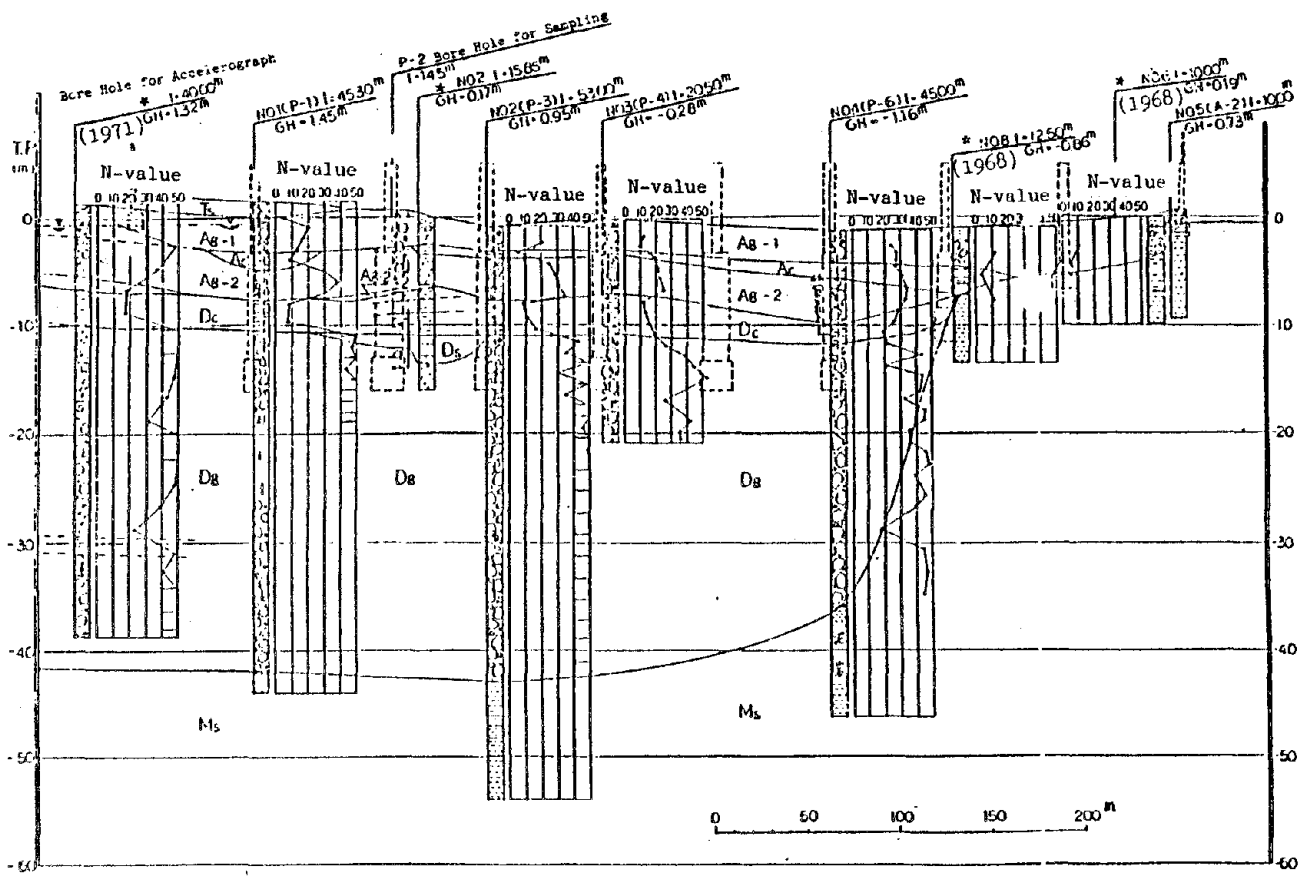


Fig-3 Soil Profile

* : Data before Construction

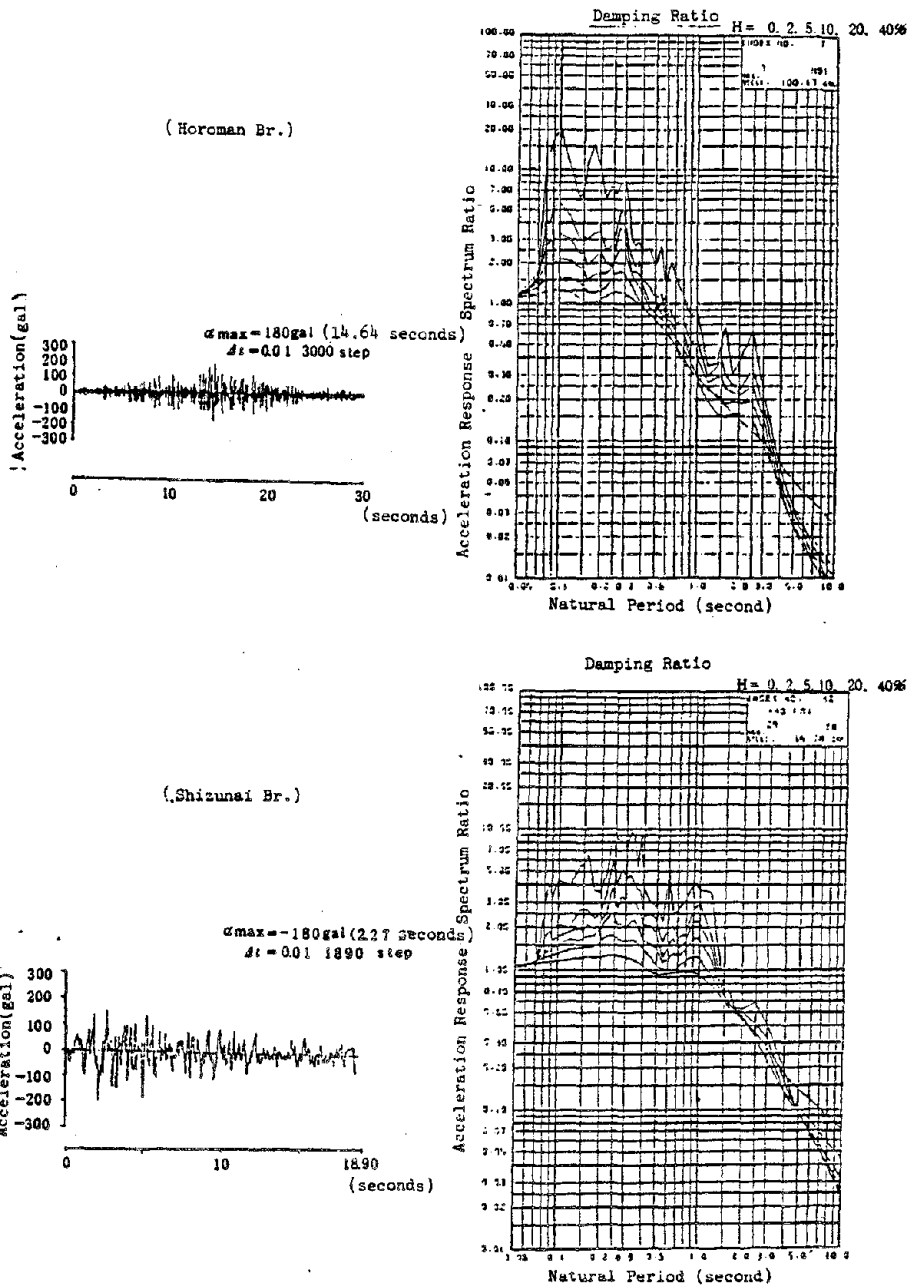
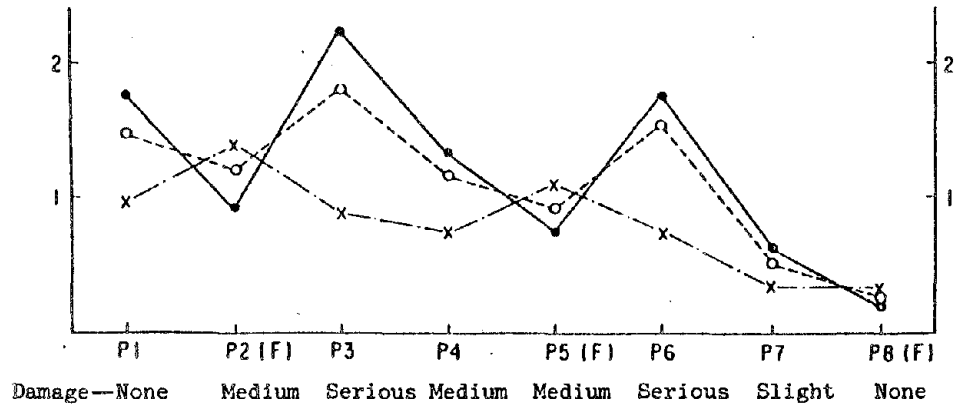


Fig-5 Input Earthquake Motion (Horoman Br. and Shizunai Br.)

(2)/(1)



(1) : Theoretical Value (Dynamic Analysis)

(2) : Design Value (Static Analysis)

●—● : Horizontal Force

○—○ : Bending Moment

x—x : Shearing Force

Note: On fixed shoes, design value is based on static longitudinal load.

Fig-6 Ratio of Dynamic Seismic Force to Static Seismic Force

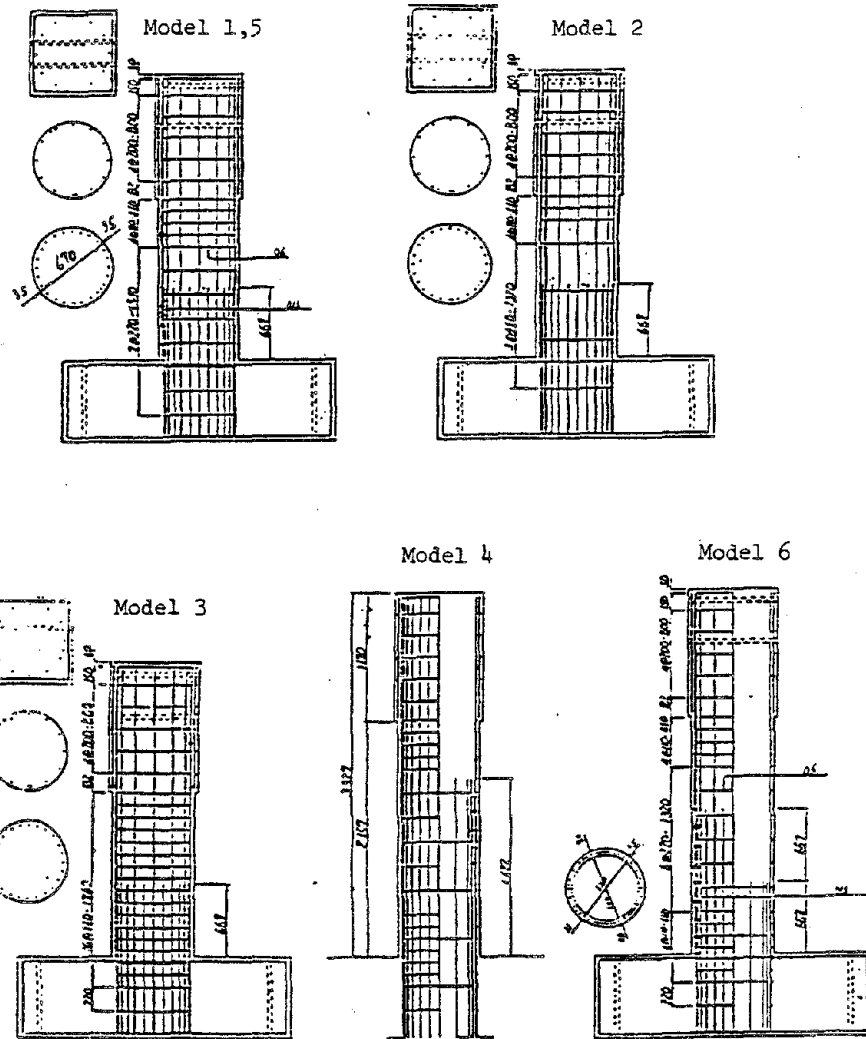


Fig-7 Reinforcement Arrangement of Specimens

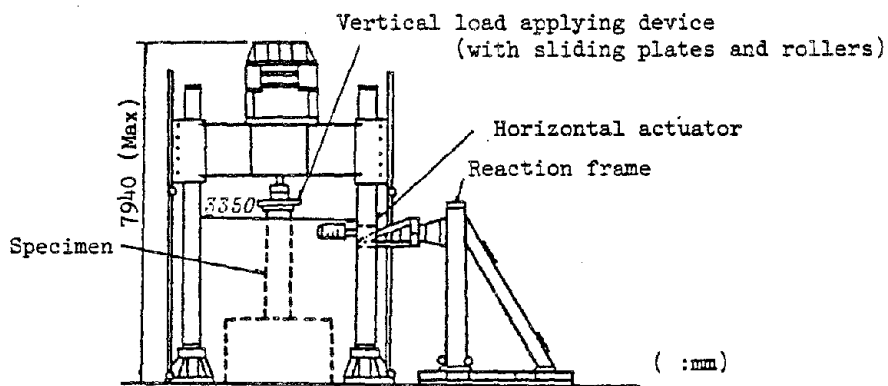


Fig-8 Testing Machine

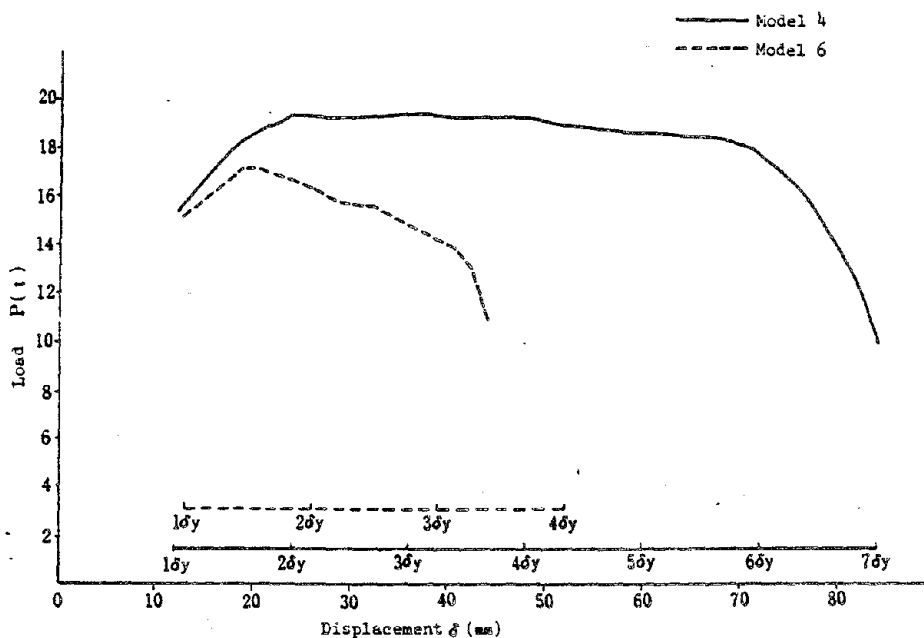


Fig-9 Load-Displacement Envelope Curves

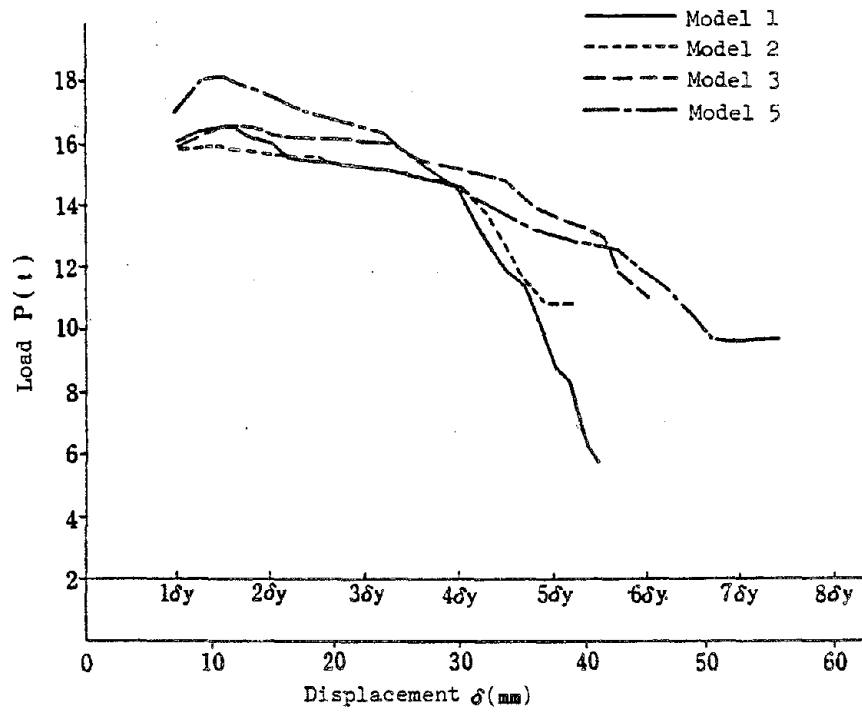


Fig-10 Load-Displacement Envelope Curves

Table - 1 Strong Motion Records of the Urakawaoki Earthquake

No.	Observed Point (on the ground surface)	Maximum Acceleration (gal)		Instrument Correction	Proprietor
		NS	EW		
1	Horoman Br.	95	100	after correction	Hokkaido Development Bureau
2	Hiroo Br.	266	209	"	"
3	Shimamatsuzawa Br.	121	108	"	"
4	Sapporo I. C Br.	250	299	"	"
5	Chiyoda Br.	74	84	"	"
6	Ishikari Estuary Br.	36	45	"	"
7	Nishikioka Br.	77	58	before correction	"
8	Tomakomai	79	93	after correction	"
9	Muroran	173	189	"	"
10	Tokachi Port	152	254	"	"
11	Hakodate	47	35	"	"
12	Hiroo Town Office	297	206	before correction	Building Research Institute
13	Otanoshige Br.	18	14	"	Hokkaido Development Bureau
14	Otaru Port	15	18	"	"
15	Niikappu Dam	24	27	"	Hokkaido Electric Power Company
16	Higashi Muroran	249	166	"	Japan National Railroads
17	Tomakomai	37	84	"	"
18	Chitose	36	48	"	"
19	Shinyubari	33	33	"	"

Table - 2 Test Results

Layer		Standard Penetration Test (Number of Blow)	Modulus of Deformation E_p (kg/cm ²)	ρ_t g/cm ³	V_p m/sec	V_s m/sec	$G \times 10^4$ kgf/cm ²	ν	$E \times 10^4$ kg/cm ²	$K \times 10^6$ kg/cm ²	Remarks
Alluvial Gravel Layer	Ag-1	20	90	2.20	1340	170	0.065	0.402	0.19	4.02	Possibility of liquefaction due to earthquake should be examined.
Alluvial Cohesive Soil Layer	Ac	8	50	1.79	1140	220	0.088	0.481	0.26	2.29	E_p was estimated by $E_p = 7N$
Alluvial Gravel Layer	Ag-2	30	210	2.20	1570	250	0.140	0.490	0.42	5.33	
Diluvial Cohesive Soil Layer	Dc	14	80	1.84	1450	200	0.075	0.490	0.22	3.73	Diluvial Sand (Ds) considered to be equivalent to Dc.
Diluvial Gravel Layer	Dg	> 40	290	2.27	2060	400	0.371	0.480	1.10	9.15	
Mudstone	Ms	> 50	450	2.03	2390	520	0.560	0.475	1.65	11.01	

Table - 3 Liquefaction Resistance Factor

Layer		Condition of Specimens	Depth(m)	Dynamic Load to Soil Elements induced by Earthquake Motion. L	Resistance of Soil Elements to Dynamic Load :R	Liquefaction Resistance Factor : $F_t = R/L$
Alluvial Gravel Layer -1	Ag-1	disturbed	1.35	1.96Ks	0.215	0.66
Alluvial Gravel Layer -2	Ag-2	disturbed	5.90	1.82Ks	0.270 (0.180)	0.90 (0.60)
Alluvial Gravel Layer -2	Ag-2	undisturbed	7.38	1.78Ks	0.310	1.06
Diluvial Cohesive Soil Layer	Dc	undisturbed	9.33	1.72Ks	0.355	1.25
Diluvial Sand Layer	Dc	undisturbed	11.95	1.64Ks	0.335	1.24

K_s (horizontal seismic coefficient on the ground surface)=0.165

Table - 4 Models of Test

Model	Height (m)	Cutting-off		Main Steel Bar		Hoop Steel Bar		Test Condition and Characteristics of Model, etc
			Position (m)	Amount of Steel Bars	Steel Bar Ratio(%)	Pitch(m)	Steel Bar Ratio(%)	
Prototype	9.08	Bottom of the Column	0	84-D25	1.12	D13 etc 300	0.038	
		1st Transition Section	2	56-D25	0.75			
		2nd Transition Section	4	28-D25	0.37			
1	2.36	Bottom of the Column	0	24-D13	0.71	D6 etc 220	0.039	Modified Model of scale 1/3 with the same steel ratio and column height considering buried part of the column. (Hoops with lap joint)
		1st Transition Section	0.667	12-D13	0.35			
2	2.36	Bottom of the Column	0	24-D13	0.71	D6 etc 440	0.019	Amount of hoops is half of Model-1.
		1st Transition Section	0.667	12-D13	0.35			
3	2.36	Bottom of the Column	0	24-D13	0.71	D6 etc 110	0.078	Amount of hoops is 2 times of Model-1.
		1st Transition Section	0.667	12-D13	0.35			
4	3.027	Bottom of the Column	0	36-D13	1.06	D6 etc 220	0.039	Modified Model of scale 1/3 with the same steel ratio and column height, but the location of cutting-off is $(d + 30\phi)$ higher than Model-1. (Hoops with hook)
		1st Transition Section	1.622	24-D13	0.71			
5	2.36	Bottom of the Column	0	24-D13	0.71	D6 etc 220	0.039	Axial force is 20% stronger than Model-1. (Using the same model as Model-1)
		1st Transition Section	0.667	12-D13	0.35			
6	3.027	Bottom of the Column	0	36-D13	1.06	D6 etc 220	0.039	1/3 scale model of the real pier.
		1st Transition Section	0.667	26-D13	0.71			
		2nd Transition Section	1.333	12-D13	0.35			

Material of test pieces:

concrete $\dots \sigma_c = 210 \text{ kg/cm}^2$
 Steel bar \dots SD35-D13, $\sigma_{sy} = 3,700 \text{ kg/cm}^2$
 for main steel bars, (SD30) D6 for hoops.

Note: Applied Vertical Load

Models except Model-5 \dots 44t
 Model-5 \dots 54.4t

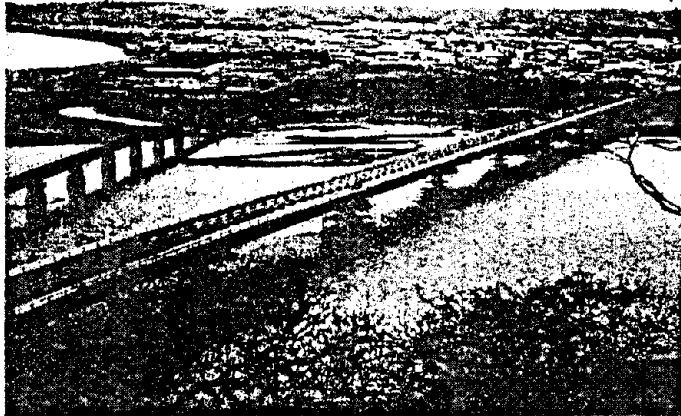


Photo-1 General View

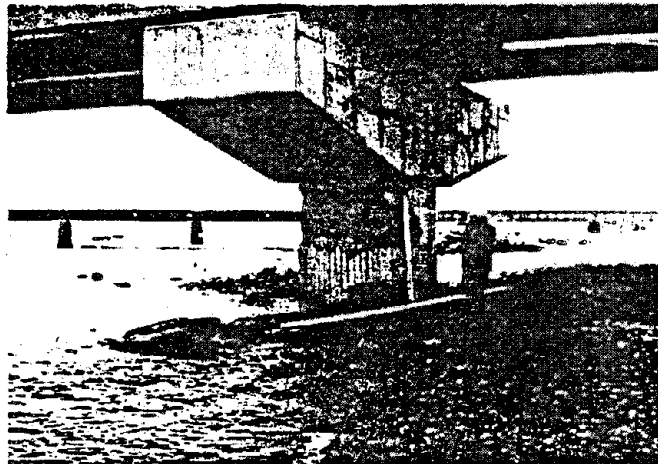


Photo-2 P-2

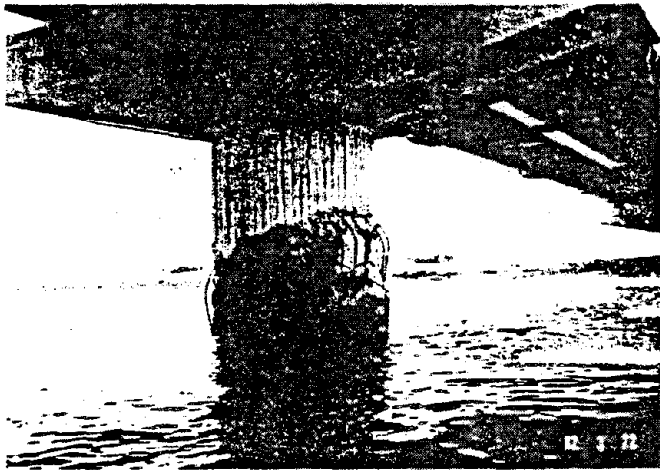


Photo-3 P-3

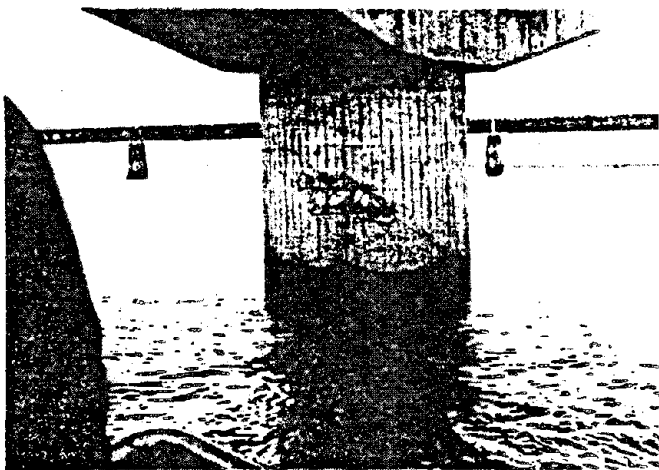


Photo-4 P-4

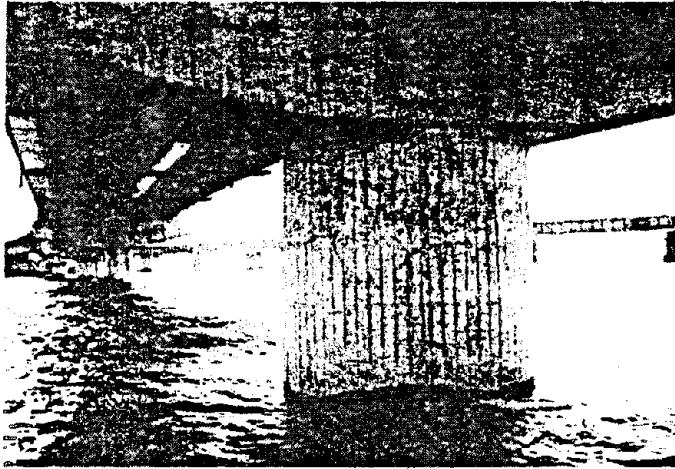


Photo-5 P-5

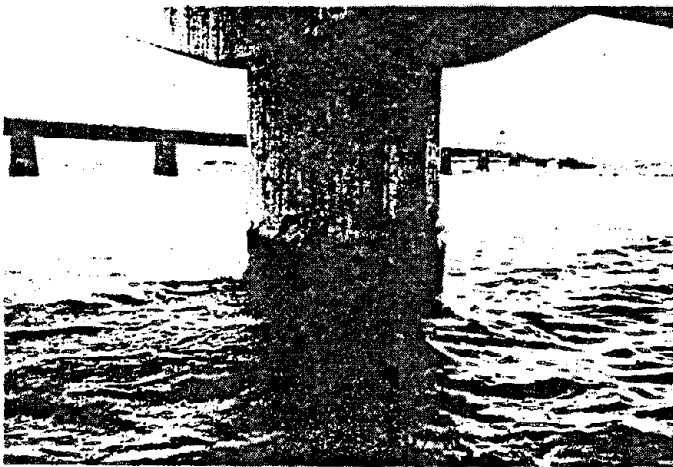


Photo-6 P-6

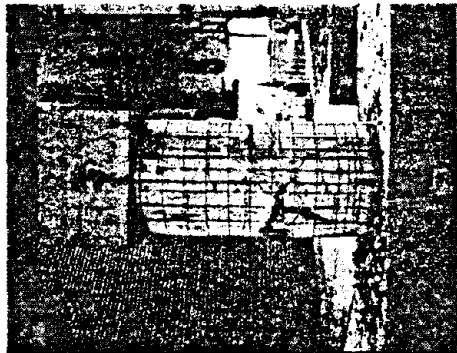


Photo-7 Comparison between P-3 and the Model



DYNAMIC RESPONSE ANALYSIS OF SHIZUNAI BRIDGE
DAMAGED BY THE URAKAWA-OKI EARTHQUAKE OF MARCH 21, 1982

By

Toshio Iwasaki, Dr. Eng., Head
Ryoji Hagiwara, Research Engineer
Earthquake Engineering Division
Earthquake Disaster Prevention Department
Public Works Research Institute, Ministry of Construction

ABSTRACT

On the morning of March 21, 1982, a severe earthquake of a magnitude of 7.1 on the Richter scale hit Urakawa-oki or off Urakawa, southern part of Hokkaido Island in Japan. It is reported by the Japan Meteorological Agency (JMA)¹⁾ that the hypocentral depth was 40km and the highest JMA seismic intensity was 6 at Urakawa town. Shizunai Bridge, located near the epicenter, sustained serious damages to 6 pier columns out of 8. Very heavy cracks occurred at 2 pier columns (Piers-3 and 6), and medium to minor cracks were observed at 4 pier columns (Piers-2, 4, 5, and 7).

This paper briefly describes an outline of the Urakawa-oki Earthquake, damage features of Shizunai Bridge, and results of a dynamic response analysis of Shizunai Bridge, which was conducted for investigating the causes of damages to the bridge.

Two different analytical models are employed for the dynamic analysis. The first is a model of the overall system involving the entire parts of the bridge, although the second is a model of Pier-3 which was most seriously injured. In the both cases, structural responses to seismic motions in the direction transverse to the bridge axis, are computed.

In an analysis for the overall model, two abutments, 8 piers, and 9-span girders are considered as a lumped mass-spring system. Surrounding soils above the bedrock are also included in the system, and non-linear characteristics of soils are considered. All of structural parts made of steel and reinforced concrete are assumed as elastic members. From the analysis for the overall model, it is concluded that responses (ratios of acting forces to design forces) of Piers-3 and 6 (supporting two ends of continuous girders) which sustained heavy damages are extensive comparing with those of the other piers, and that horizontal forces analyzed for Piers-3 and 6 are higher than 2 times their design horizontal forces, respectively.

Next, in the analysis of Pier-3 model, non-linear characteristics of the reinforced concrete pier column are considered. From the analysis, it is concluded that plastic state will extensively develop at a section of 4.0m above the bottom of the column, which well explains the actual behavior of Pier-3 during the earthquake.

1. OUTLINE OF THE URAKAWA-OKI EARTHQUAKE OF MARCH 21, 1982

From the report of the Japan Meteorological Agency (JMA)¹⁾, the characteristics of the earthquake are outlined as follows:

- 1) Date and Time : 11:32 am, March 21, 1982
- 2) Magnitude : 7.1 on the Richter scale
- 3) Epicenter : 20km off Urakawa
142°36' E, 42°4' N
- 4) Focal Depth : 40km
- 5) Seismic Intensities : 6 – Urakawa
(JMA scale) 4 – Tomakomai, Sapporo, Otaru, Iwamizawa, Hiroo, Kuchan, Obihiro
3 – Kushiro, Asahikawa, Muroran, Hakodate, Aomori, Morioka

Fig. 1 illustrates the epicenter and JMA seismic intensities at various locations. Fig. 2 is a detailed map showing the epicenter of the main shock, epicenters of numerous aftershocks, obtained from a densely instrumented network of Science Department of Hokkaido University.²⁾ From Fig. 2 it is seen that the epicenter (the center of the large octagon) is located off Mitsuishi about 15km west from Urakawa.

Strong-motion accelerographs recorded time histories of accelerations at several locations. The locations and peak ground accelerations are shown in Figs. 3 and 4. The greatest acceleration (about 300 gals) was triggered at Hiroo, about 60km east from the epicenter. At the surface of firm ground near Horoman Bridge located about 40km east from the epicenter, the peak acceleration was about 80 gals from a SMAC-B2 type accelerograph (the corrected value was about 100 gals).

An average value of peak accelerations at Sapporo city of epicentral distance of 150km was about 70 gals.

2. DAMAGE FEATURES OF SHIZUNAI BRIDGE

Pier columns of Shizunai Bridge located near the estuary of Shizunai River in Shizunai town, were seriously damaged.^{3),4)} It is seen from Fig. 2 that Shizunai Bridge is sited at the northern border in the focal area.

General views of Shizunai Bridge are illustrated in Fig. 5 and Photo 1. The bridge, completed in 1972, consists of 3 of 3-span continuous steel plate girders (9 spans totally), 2 abutments, and 8 piers.

Soil conditions at the bridge site are also shown in Fig. 5. Soil conditions at the bridge site are indicated in Fig. 5. Soft soils are rather deep at the right-bank side (Abutment-1 side) and the central parts. Soft soils are very shallow at the left-bank side (Abutment-2 side). A bedrock layer (mudston of tertiary era) is seen on the surface near the site of Abutment-2, and Pier-8 and Abutment-2 have spread foundations resting directly on the mudstone layer.

Four piers (Piers-1, 3, 4, and 6) have well foundations of diameter of 6 meters and depth

of 12 meters, two piers (Piers-2 and 5—fixed piers) have well foundations of diameter of 10 meters and embedment depth of 12 meters, one pier (Pier-7) has a well foundation of diameter of 6.5 meters and depth of 7 meters, and the final pier (Pier-8) has a spread foundation of 10 x 10 meters. Abutment-1 on the right bank has a pile foundation.

All of the eight piers have reinforced concrete circular columns of diameter of 2.2 meters and height of 8.1 meters. As for Piers-2 and 5 diameters become greater at lower sections.

Due to the Urakawa-oki Earthquake, two pier columns (Piers-3 and 6) sustained very heavy cracks. Especially Pier-3 was almost failed as seen from Photos. 2 and 3. Photo 4 shows a damage feature of Pier-6. The lower sections of the column under the water sustained diagonal cracks similar to those of Pier-3.

Photos. 5 and 6 indicate medium damages to Piers 2 and 4, respectively. Separations of concrete and cracks are seen at higher sections of the columns. Diagonal cracks are rather minor for Piers-5 and 6.

Photos 7 and 8 show minor damages to Piers-5 and 7, respectively. Horizontal and diagonal cracks are seen for Pier-5, and a horizontal crack is seen for Pier-7.

Quick repairing works for Piers-2, 3, and 6 completed by the middle of April, and the bridge temporarily reopened on April 15 for light traffic (lighter than 5 tons) with several restrictions such as a speed limit. It took six months to completely repair all the damages, and the bridge eventually reopened on October 1, 1982 for all vehicles without restrictions.

3. EARTHQUAKE RESPONSE ANALYSIS FOR THE OVERALL ELASTIC SYSTEM OF SHIZUNAI BRIDGE

3.1 Objectives

To obtain earthquake response of each part of structural members of Shizunai Bridge, a dynamic response analysis will be conducted for its overall system involving the superstructures, substructures, and surrounding soils. In the analysis structural members are assumed to be elastic, although the surrounding soils are assumed to have nonlinear characteristics. A principal aim of the analysis is to compare the differences of response values for the eight piers, and to grasp the causes of the difference of damage extents for the piers.

3.2 Input Seismic Motions at Bedrock

Two seismic bedrock motions were employed for the dynamic analysis. First one is the acceleration record (peak value being 100 gal in the longitudinal direction of the bridge axis) obtained on the ground surface at the site of Horoman Bridge (the epicentral distance of 36km) during the Urakawa-oki Earthquake of March 21, 1982. The second one is the acceleration record (peak value being 37 gal in the transverse direction to the bridge axis) obtained under the ground (40 meters below surface) at the site of Shizunai Bridge (the epicentral distance of 17km) during the Hokkaido Southern Coast Earthquake of January 23, 1982 (Magnitude of 7.1 and the focal depth of 130km). Fig. 6 (A) shows locations of the epicenters

of the two earthquakes and the two recording sites. The wave form and response spectrum curves of the second record (Shizunai Bridge record) are shown in Fig. 6 (B) and (C).

In the analysis accelerations are enlarged so that the peak surface motion become about 300 gal. The peak bedrock acceleration was adjusted to be 180 gals. A time interval is taken as 0.01 second in the analysis. Results of analysis for the Shizunai Bridge record will be described in the following sections.

3.3 Earthquake Response Analysis of the Grounds

A non-linear analytical computer program, named "NON-SOIL⁵⁾" (developed by the Ground Vibration Division, Public Works Research Institute, Ministry of Construction) using Ramberg - Osgood models, will be employed for the analysis of the grounds at the site of Shizunai Bridge.

The bedrock for the analysis is taken as the upper boundary of the Tertiary mudstone with the shear wave velocity of 520 m/sec. From the results of soil survey (measurement of P-wave and S-wave velocities) conducted by the Hokkaido Development Bureau, a flat bedrock line exist about 46 meters below the surface at the right bank (Abutment-1) side the to Pier-4. On the other hand, from Pier-6 to Abutment-2, the bedrock line goes up near the surface. At the left-bank (Abutment-2) side an outcrop of the bedrock appears on the surface.

In view of the above feature of the bedrock line, a seismic analysis will be conducted for grounds between Abutment-1 and Pier-7. Fig. 7 illustrates a classification of soil layers grounds between Abutment-1 and Pier-7. Fig. 7 illustrates a classification of soil layers considered in the analysis. In the figure, an analytical model for structural members is also shown. Table 1 tabulates shear wave velocities of these soil layers. In the analysis, shear moduli and hysteretic damping constants are determined as functions (non-linear characteristics) of strain levels, which are obtained from the results of dynamic torsional shear tests for soil specimens sampled insitu.

As a result of the analysis, Table 2 shows predominant periods of vibration at several ground points. Predominant periods for deeper soils at points between Abutment-1 and Pier-4 are about 0.7 to 1.0 sec, those for shallow soils at points of Piers-5 and 6 are about 0.5 sec, and that of very shallow soils at Pier-7 is about 0.2 sec. It is estimated that predominant periods at points of Pier-8 and Abutment-2 are around 0.2 sec.

Fig. 8 indicates a distribution of response accelerations of grounds, when an input motion of the Shizunai Bridge record is induced. The peak accelerations on the ground surface are 300 to 400 gal. The peak displacements on the ground surface (relative displacements to the bedrock) are found to be 4.8 cm at Abutment-1 site, 3.1 cm Pier-1 site, 3.3 cm at Pier-2 site, 2.6 cm at Piers-3 to 6 sites, and 0.5 cm at Pier-7 site. Furthermore, shear strains developed in grounds are rather large in the diluvial clayey soils (Dc-layer) at sites between Abutment-1 and Pier-6, and the peak strain level become about $(3.4 \text{ to } 4.9) \times 10^{-3}$. In this analysis, shear

moduli of soils become smaller for high shear strain, according to the results of laboratory soil test conducted for insitu soil specimens. Shear moduli for the shear levels described in the above are only 10 percent of the original value of shear moduli ($G_0 = \rho V_s^2$ for $\gamma = 10^{-6}$).

3.4 Earthquake Response Analysis of the Bridge

A response analysis for the overall system of Shizunai Bridge will be conducted in the transverse direction of the bridge axis, with use of a linear computer program "DAST-M" (developed by the Earthquake Engineering Division, Public Works Research Institute, Ministry of Construction), in which multiple-points motions given from the results of the analysis of the grounds (described in 3.3) can be considered as input motions to the bridge structural points, and a model for the overall system is shown in Fig. 7. As shown in Fig. 7, for the most piers the effects of grounds only below the top of the well foundations are considered. The effects of grounds above the top of the well foundations are also included for Piers-1 and 2, because of the rather deep embedment of soils near the two pier sites.

In modeling bearing supports connecting girders and pier crowns, rotations with respect to the longitudinal axis of the bridge and lateral displacements in the transverse direction will be assumed to be identical at the both ends of the connections. In other words, the conditions of the bearing supports will be completely fixed for the rotations with respect to the bridge axis and the transverse displacements.

On the other hand, rotations with respect to the vertical axis will be assumed fixed at the fixed bearing supports (Piers-2, 5 and 8), and free at the movable bearing supports (Piers-1, 3, 4, 6 and 7).

In the analysis, masses of girders, pier columns, and well foundations, torsional inertia of girders along the bridge axis, and rotational inertia of pier top beams along the bridge axis, are considered. An equivalent viscous damping ratio of 20 percent to critical is assumed, accounting for the various different damping effects.

From the eigenvalue analysis for the overall system shown in Fig. 7, the fundamental mode shape (first mode) is shown in Fig. 9. The fundamental natural period is about 0.6 sec, and the entire parts of the system move to the same direction. Bending deformations of pier columns prevail for the fundamental mode. The participation factor of the fundamental mode is most essential comparing with other modes.

Figs. 10 and 11 illustrate the distributions of peak response accelerations and peak response displacements, respectively, when Shizunai Bridge is subjected to the input motion of shizunai Bridge record already shown in Fig. 6 (the peak acceleration at the beserock is assumed 180 gals). Maximum response accelerations are observed at pier tops and girders between Pier-1 and Pier-6, and the peak value of acceleration is rather great (480 to 660 gal). Maximum response displacements (between 4.2 and 6.6 cm) (displacement of the pier top \approx 0.5 cm) are also large for the sites between Abutment - 1 and Pier-6.

Next, Fig. 12 (A)–(D) shows the distributions of peak bending moments for all pier columns. In the figure, design bending moments (M_D), bending moments to cause cracks (M_C), bending moments to cause yielding (M_Y) and ultimate bending moments (M_U) are illustrated, as well as peak response bending moments (M_{pi}) given for each pier from the dynamic analysis. It is seen from Fig. 12 that response bending moments (M_{pi}) are quite large ($M_p > M_U$) at Piers-3 and 6 which sustained very heavy cracks. Response bending moments at Piers-2, 5, 1, 4, and 7 are nextly large ($M_p > M_D$, and M_p are nearly equal to M_U at the section of cut-off of reinforcements). Response bending moments at Pier-8, however, are small ($M_p < M_D$).

Peak response shearing forces are higher than shearing strengths at Piers-1, 2, 3, 5, and 6, although response shearing forces are less than shearing strengths at Piers-4, 7, and 8.

Table 3 shows (A) comparison of design lateral forces and response lateral forces analyzed, (B) comparison of yielding bending moment (M_Y) and response bending moments analyzed, and (C) comparison of shearing strengths (S_u) at most dangerous sections and response shearing forces (S).

Ratios of response lateral forces to design lateral forces for Piers-3 and 6, are large being 2.6 and 2.4, respectively. The ratios for Piers-2, 4, 5, and 7 which sustained moderate to minor damages, are between 1.1 and 1.5. Although Pier-1 did not sustain any damage, the ratio is rather large being 1.9. Furthermore, the ratio for Pier-8 with no damage is very small (0.3).

Next, ratios of response bending moments to yielding bending moments are also large for Piers-3 and 6, and small for Pier-8. This tendency is identical to the case of lateral forces.

Furthermore, ratios of ratios of response shearing forces to shearing strengths are greater than 1.0 for Piers-1, 2, 3, 5, and 6, and less than 1.0 for Piers-4, 6, and 8.

4. EARTHQUAKE RESPONSE ANALYSIS FOR THE ELASTO-PLASTIC SYSTEM OF PIER-3

4.1 Objectives

As indicated in Chapter 2, it is supposed that Pier-3 behaved extensively beyond the elastic limit. In Chapter 3, elastic responses of the overall system of Shizunai Bridge are analyzed. In this Chapter, a detailed dynamic analysis will be performed for Pier-3, which sustained the heaviest damage among the eight piers, by considering non-linear characteristics of soils and reinforced concrete structures. The principal objective is to accurately grasp dynamic behavior (including behavior after the outbreak of cracking) of Pier-3 during the Urakawa-oki Earthquake.

4.2 Input Seismic Motions at Bedrock

Similarly to the analysis of the overall system described in 3, two seismic bedrock motions were employed, namely the Horoman Bridge Record (obtained during the Urakawa-oki Earthquake of March 21, 1982, and the Shizunai Bridge Record (obtained during the Hokkaido Southern Coast Earthquake of January 23, 1981). Time histories of the two acceler-

ation records were adjusted so that the peak bedrock acceleration = 180 gal, and the time interval = 0.002 sec. In the following, some results for the Shizunai Bridge Record will be described.

4.3 Analytical Model

For establishing an analytical model of Pier-3 of Shizunai Bridge, a number of different preliminary analyses were conducted. Fig. 13 illustrates a mathematical model eventually adopted for the analysis. The top mass of the model represents the mass of the superstructure (mass and moment of inertia of the girder of one-span length are taken). The effects of lateral rigidity and rotation rigidity of the superstructures are neglected, because the effects were found to be negligible from a preliminary analysis.

As for restoring forces of the pier column, a degrading tri-linear model (proposed by K. Muto⁷⁾), was employed, as shown in Fig. 14 which shows a relationship between bending moments and curvatures at any column sections. Fig. 16 displays the arrangements of reinforcing bars of some sections of the column of Pier-3. Also, skelton curves of bending moment-curvature relationships for the bottom section and the section 4.0 m above the bottom of the column are demonstrated in Fig. 16.

As for the model of surrounding soils, a weight of soils equal to 1,000 times the pier weight (sectional area of soils of 15,000 m²) was taken, so that motions of the pier do not affect those of soils. Equivalent shear moduli of soils were assumed to be equal to secant gradients of the skelton curves computed from the analysis shown in 3.3, in which a Remberg-Osgood model was adopted. A strain level (about 2×10^{-3} at most) of about 60 percent of the peak strain was taken for the cases.

As for damping effects, viscous damping (2 percent to critical) of the pier column, viscous damping of the foundation-soil-spring system (20 percent to critical), and hysteretic damping of the pier column and soils are considered.

4.4 Results of Analysis for Pier-3 Model

A result of a characteristic analysis (or an eigenvalue analysis) for the elastic stage of Pier-3 model is shown in Fig. 17. The fundamental mode shape is essentially the one of bending deformation of the pier column, and the natural period of the fundamental mode is 0.60 sec.

Fig. 18 illustrates a wave form of response ground acceleration, when subjected to an input bedrock motion of Shizunai Bridge Record with the peak acceleration of 180 gal. From this it is seen that the peak ground acceleration is 348 gal, and the number of repetition of motions with acceleration of 200 gal or higher, is about 10. The peak ground displacement was about 2.5 cm.

A distribution of peak acceleration along the vertical axis is shown by the solid line in Fig. 19. The dotted line in the figure represents a result of non-linear soil analysis described in 3.2. It is seen from this that the results coincide approximately. Response acceleration

spectrum curves for the ground motions computed from the above analysis are shown in Fig. 20. Response accelerations are comparatively high over the range of periods between 0.2 and 1.0 sec.

Nextly, responses of the pier structure are shown in Figs. 21 to 23. Peak values of response acceleration and displacement of the superstructure are 509 gal and 10.0 cm, respectively. The response displacement is larger (1.7 times) than the result for the overall system described in 3.4. It seems that this large displacement is due to the effects of plastic deformation of the pier column. Distributions of peak bending moments and peak shearing forces of the Pier-3 are shown in Figs. 24 and 25, respectively. These values are smaller than those obtained from the analysis for the overall elastic system described in 3.4. The response bending moments, however, are larger than yielding bending moments (M_y) at the sections of cut-off of reinforcing bars and the bottom sections. The response shearing forces are less (one half) than the shearing strengths. Table 3 tabulates peak response values of bending moments and shearing forces developed at three sections (bottom, 2.0 m, and 4.0 m above the bottom) of Pier-3.

Fig. 26 demonstrates the hysteretic curve of the relation between bending moment and curvature at the section (section of cut-off of reinforcements) of 4.0 m above the bottom where a plastic stage developed most extensively among others. Peak curvature value (or the ductility factor for curvature, μ_p) reaches to 5.0. In view of the actual damage which occurred at the section of 4.0 m above the column bottom, it is seen that the results explain very well the damage features. From the analysis, the peak displacement at the pier top is about 10 cm, which is equal to 2.2 times the yielding displacement ($\delta_y = 4.3$ cm). In other words, the ductility factor for displacement, μ_s becomes 2.2. It is estimated, however, from the damage features of the pier column and the results of laboratory experiments (for one-third scale models), that the actual ductility factor may have reached to 3 or higher. It can be concluded that the results of analysis indicate responses slightly lower than the actual values.

5. CONCLUSIONS

From the two different analyses on dynamic behavior of Shizunai Bridge damage during the Urakawa-oki Earthquake of March 21, 1982 (Richter Magnitude = 7.1), the following conclusions can be made:

- (1) It seems that during the Urakawa-oki Earthquake Shizunai Bridge sustained seismic forces much higher than the expected design forces. Especially for piers located in the right-bank side where deeper surface soft soils exist, responses were extensive. It will be noted that one of the causes of the damages to these piers was an coincidence of period of vibration between the predominant period of soils and the fundamental period of bridge structure for Piers-1 to 6. In order to improve seismic design procedures for bridge structures, it will be essential to consider the effects of dynamic interactions between bridge structure and surrounding soils.

- (2) From the results of an analysis for the overall system, ratios of response lateral forces to design lateral forces at the pier tops and ratios of response bending moments to yielding moments at weak sections of pier columns were computed.

Those ratios are extensively high for Piers-3 and 6 which sustained heavy damages during the Earthquake. The results of analysis approximately coincide with the damage features of pier columns except Pier-1.

- (3) Basing on the current specifications of seismic design of highway bridges⁸⁾, design lateral forces acting on piers which supports ends of continuous girders (such as Piers-3, 6 of Shizunai Bridge), become smaller than those acting on other piers. This is due to the fact that the current specifications require that design lateral forces are the product of the seismic coefficient and the dead weight of girders (or reactions) acting on piers, and that reactions are rather small on the ends of continuous girders.

For the dynamic analysis for the overall system, however, response lateral forces generated in Piers-3 and 6 (supporting the ends of continuous girders) are not necessarily small. Therefore, it seems that the ratios of response lateral forces to design lateral forces became greater for the Piers-3 and 6. This tendency might be one of the causes of heavy damages to the selective piers of Shizunai Bridge.

- (4) It is supposed that large lateral forces generated in the longitudinal direction as well as those in the transverse direction of the bridge axis, for Piers-2, 5, and 8 which are fixed in the longitudinal directions.
- (5) Ratios of response shearing forces to shearing strength become smaller than ratios of response bending moments to yielding moments. From this it is estimated that heavy damages to pier columns of Shizunai Bridge may be caused firstly by bending moments at the sections of cut-off of reinforcing bars, and secondly by shearing forces at the same sections where sectional areas became small due to preceeding bending failures. It seems that the shearing forces finally caused diagonal cracks and serious shear failures to Piers-3 and 6.
- (6) From another dynamic analysis for Pier-3 where non-linear characteristics of reinforced concrete were taken into consideration, it seems that reinforcing bars at the section of 4.0 m above the column bottom (cut-off section of bars) yielded. This fact coincides with the actual behavior of the bridge during the Urakawa-oki Earthquake.

It is pointed out that cut-off of reinforcing bars caused yielding of bars and poor ductility (or toughness) of the pier column. In order to avoid brittle failure of reinforced concrete columns, elongation of bars (cut-off of reinforcing bars) should be carefully considered.

6. ACKNOWLEDGMENTS

The dynamic analysis was conducted by the Earthquake Engineering Division, Public Works Research Institute, Ministry of Construction, with a commission of the Hokkaido

Development Bureau (HDB). The Investigation Committee on the Earthquake Damage to Shizunai Bridge (Chairman: Dr. N. Narita, Director, Planning and Research Administration Department, Public Works Research Institute) consisting of staff members of HDB, the Road Bureau of MOC, and PWRI, discussed and gave guidances for analysis conditions, detailed analysis procedures, and results of the analysis.

In-situ soil surveys after the Urakawa-oki Earthquake broke off, and acquisition of strong-motion records during the Earthquake were performed by HDB. Digitization of strong-motion records and their basic analysis were done by the Ground Vibration Division, PWRI.

The authors express their sincere appreciation to concerned staff members of the Hokkaido Development Bureau, the Road Bureau of the Ministry of Construction, and the Public Works Research Institute.

7. REFERENCES

- 1) Japan Meteorological Agency, "The Seismological Bulletin of the Japan Meteorological Agency for March, 1982," 1982.
- 2) Science Department of Hokkaido University, "Report of the Urakawa-oki Earthquake," March, 1982.
- 3) T. Yasue, Y. Sasaki, H. Asanuma, and T. Nakajima, "Prompt Report on Damages to Civil Engineering Structures due to the Urakawa-oki Earthquake," Journal of Civil Engineering (Doboku Gijutsu Shiryo), 24-7, July, 1982.
- 4) T. Yasue, T. Iwasaki, Y. Sasaki, H. Asanuma, and T. Nakajima, "Report of the Urakawa-oki Earthquake of March, 21, 1982," Proceedings of the 14th Joint Meeting, Panel on Wind and Seismic Effects, UJNR, (Washington, D.C., U.S.A., May 17-20, 1982), Published by PWRI, MOC, December 1982.
- 5) T. Iwasaki, F. Tatsuoka, and K. Kawashima, I. Morimoto, "An Analytical Investigation on the Effects of Non-Linear Characteristics of Soils on Seismic Response of Grounds," Memorandum of the Public Works Research Institute, No. 1582, March, 1980.
- 6) E. Kuribayashi, O. Ueda, and T. Hadate, "Seismic Response Analysis of A Submerged Tunnel Including Ventilation Towers," Memorandum of the Public Works Research Institute, No. 1578, March, 1980.
- 7) K. Muto, "Dynamic Analysis of Structures," Maruzen, January, 1977.
- 8) Japan Road Association, "Specifications of Highway Bridges and Commentaries, Part V Earthquake-Resistant Design," May, 1980.

Photo 1
View of Shizunai Bridge
from Right Bank
to Left Bank and to Downst-
ream, Pier-4 in foreground.

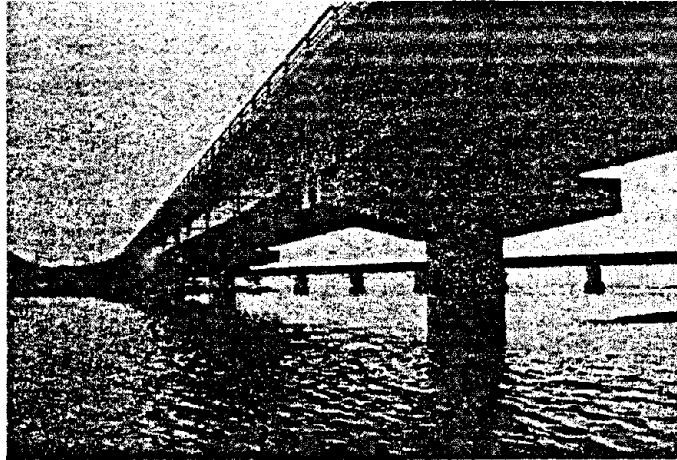


Photo 2
Damage to Pier-3
Shizunai Bridge, Seen
from Pier-2 site.

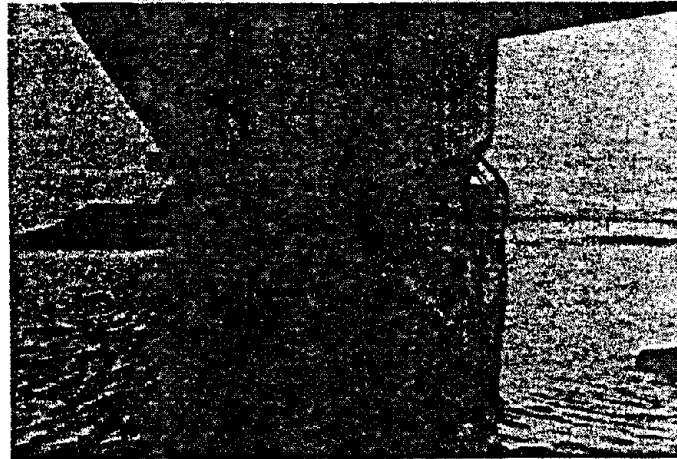


Photo 3
Closer View of
Failed Section of
Pier-3 of
Shizunai Bridge,
Seen from Downstream.
Note cut-off of bars.

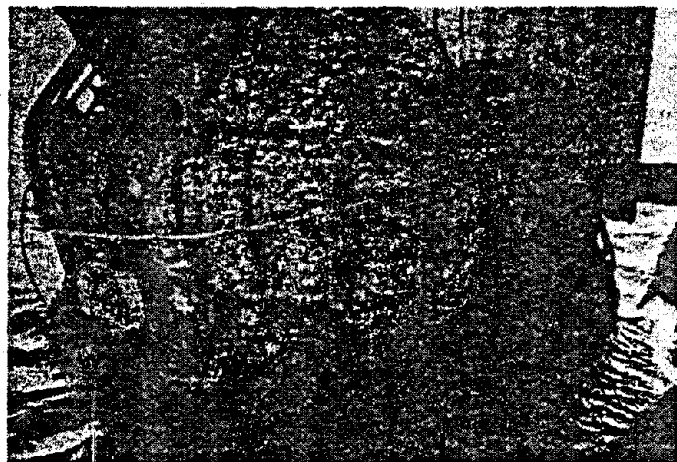


Photo 4
Damage to Pier-6 of
Shizunai Bridge,
Seen from Pier-7.

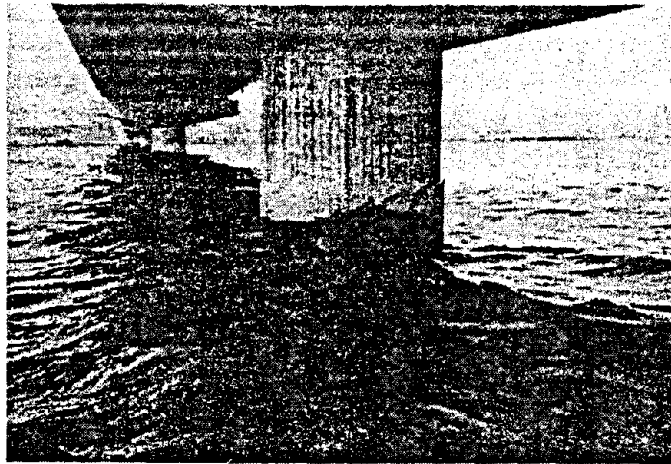


Photo 5
Damage to Pier-2 of
Shizunai Bridge,
Seen from Upstream of
Pier-1 side.

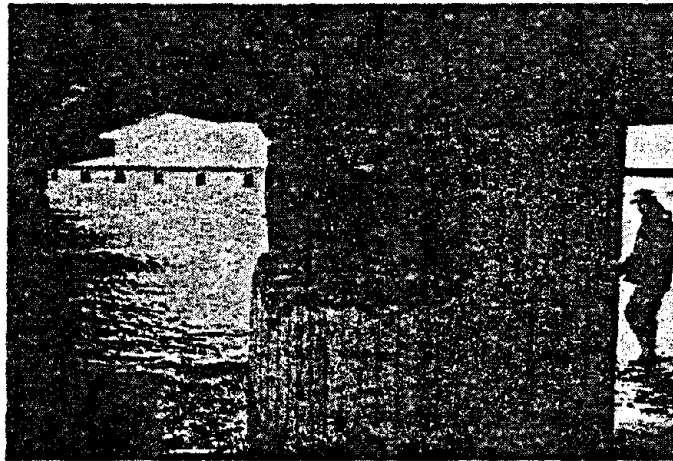


Photo 6
Damage to Pier-4 of
Shizunai Bridge.

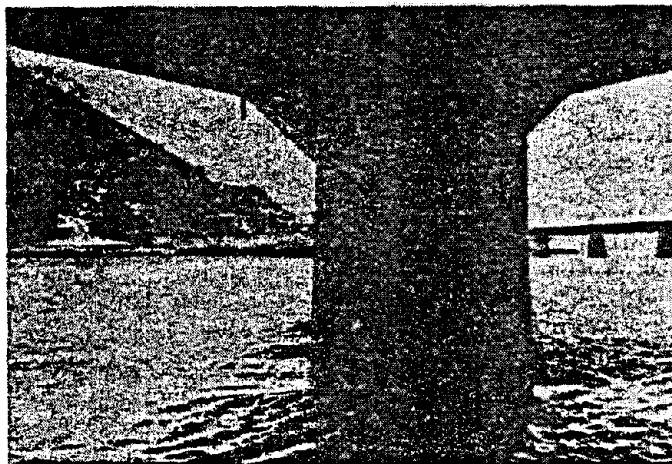


Photo 7
Damage to Pier-5 of
Shizunai Bridge,
Diagonal Cracking on
Downstream side.

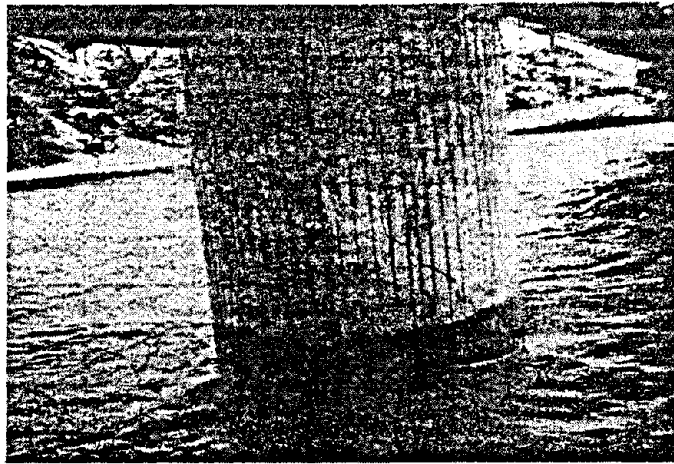


Photo 8
Damage to Pier-7 of
Shizunai Bridge,
Light Horizontal Cracking.

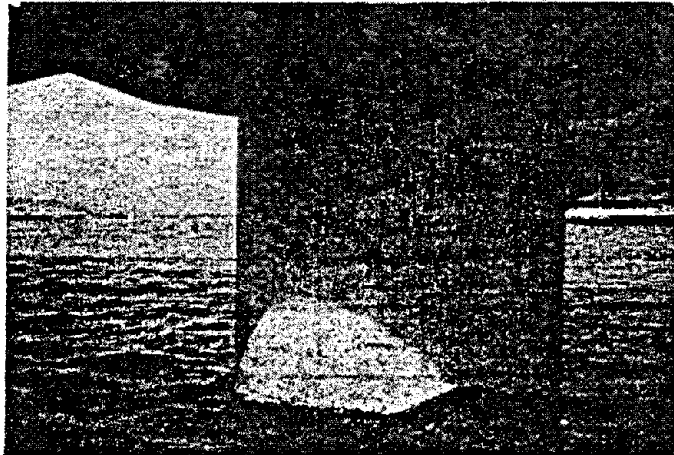


Table 1 Shear Wave Velocities of Soil Layers

Symbol of Soil Layers	Soil Classification	Shear Wave Velocities Measured (m/sec)
T _s	Top Soil	150
A _g -1	Alluvial Gravel (Upper)	170
A _c	Alluvial Clay	220
A _g -2	Alluvial Gravel (Lower)	250
D _c	Diluvial Clay	200
D _s	Diluvial Sand	200
D _g	Diluvial Gravel	400
M _s	Tertiary Mudstone	520

Note) See Fig.7 for depth of each soil layer

Table 2 Predominant Periods at Various Sites

Sites	A1	P1	P2	P3. P4	P5. P6	P7
Predominant Period (sec)	1.00	0.75	0.75	0.68	0.47	0.23

**Table 3. Result of Dynamic Analysis for Overall System of Shizunai Bridge
(In Transverse Direction to Bridge Axis)**

Forces	Piers	P ₁	P ₂	P ₃	P ₄	P ₅	P ₆	P ₇	P ₈	Remarks
(A) Lateral Force at Pier Top	(1) Design (t)	102	(277)	74	102	(277)	74	102	(277)	Values in (): Longitud. Direction
	(2) Analysis (t)	195	300	192	159	301	176	114	91	
	(2)/(1)	1.91	1.08	2.59	1.56	1.09	2.38	1.12	0.33	
(B) Bending Moment at Critical Section of Pier Column	Yielding Moment (t · m)	890	1,325	677	890	1,325	677	890	1,371	=1.57 A
	(2) Analysis (t·m)	1,512	1,891	1,628	1,386	1,796	1,506	906	539	
	(2)/(1)	1.70	1.43	2.40	1.56	1.36	2.22	1.02	0.39	
(C) Shearing Force at Critical Section of Pier Column	(1) Shearing Strength (t)	205	205	205	205	205	205	205	205	
	(2) Analysis (t)	221	327	220	183	326	217	132	103	
	(2)/(1)	1.08	1.60	1.07	0.89	1.59	1.06	0.64	0.50	

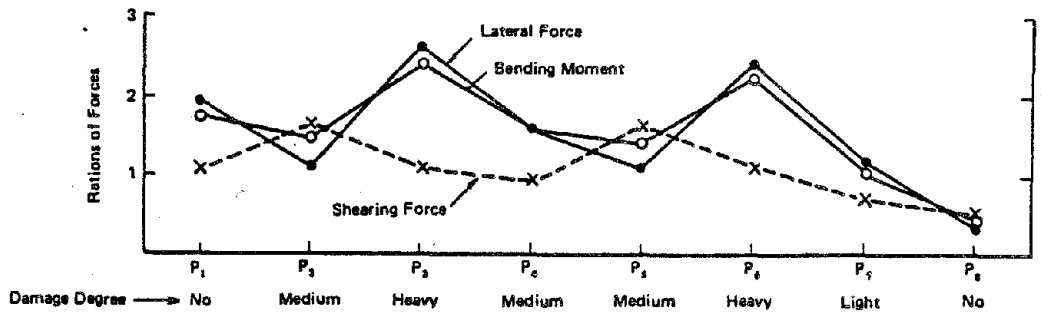


Table 4. Bending Moment and Curvature at Three Sections of Pier Column of Pier-3.

	Section	Column Bottom	2.0 m Above Column Bottom	4.0 m Above Column Bottom
Bending Moment	Yielding Moment (My)	1,200 (t·m)	960 (t·m)	677 (t·m)
	Peak Response Moment (M)	1,291 (t·m)	1,060 (t·m)	801 (t·m)
	M/My	1.08	1.10	1.18
Curvature	Yielding Curvature (ϕ_y)	12.6×10^{-6} (1/cm)	12.3×10^{-6} (1/cm)	11.8×10^{-6} (1/cm)
	Peak Response Curvature (ϕ)	21.9×10^{-6} (1/cm)	31.2×10^{-6} (1/cm)	59.0×10^{-6} (1/cm)
	ϕ/ϕ_y	1.73	2.54	4.98

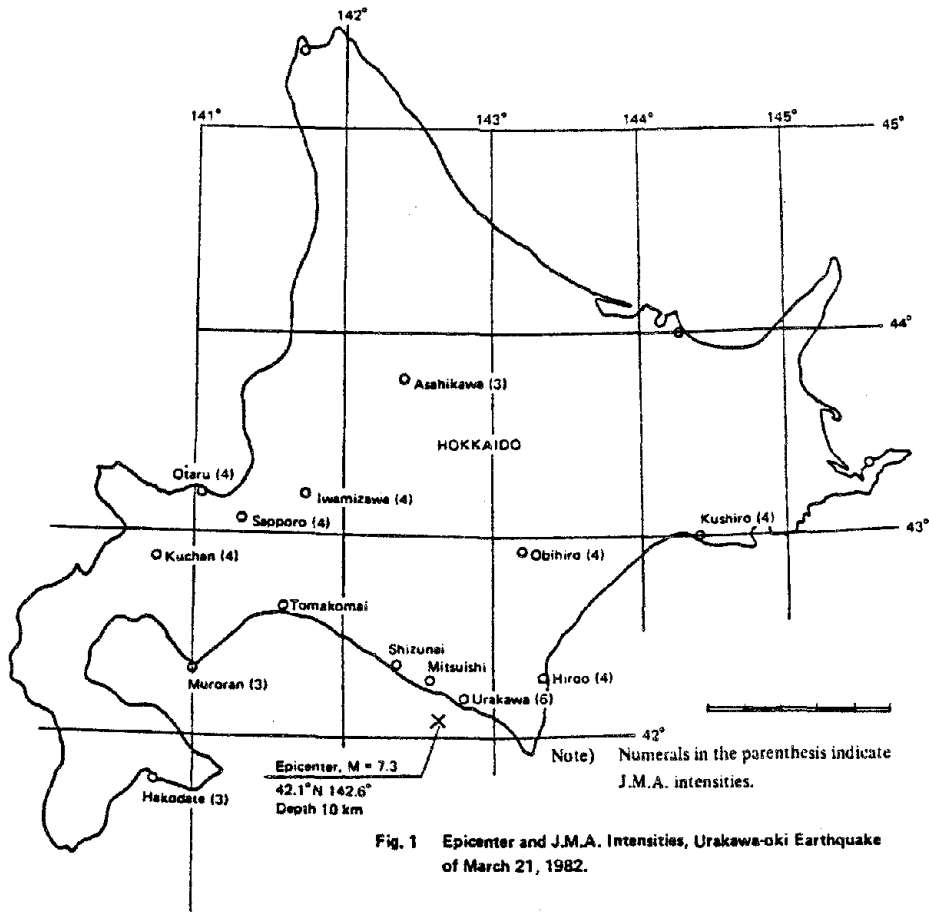


Fig. 1 Epicenter and J.M.A. Intensities, Urakawa-oki Earthquake of March 21, 1982.

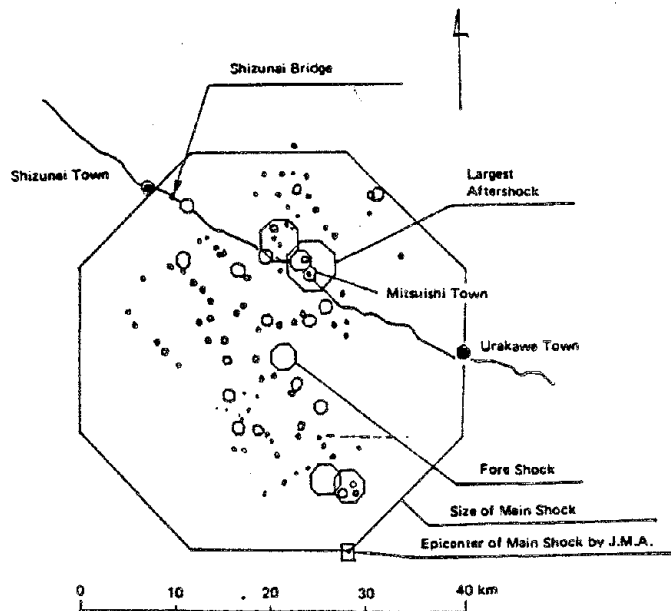


Fig. 2 Epicenters of Fore Shock, Main Shock and Numerous Aftershocks (After Science Department, Hokkaido Univ.)

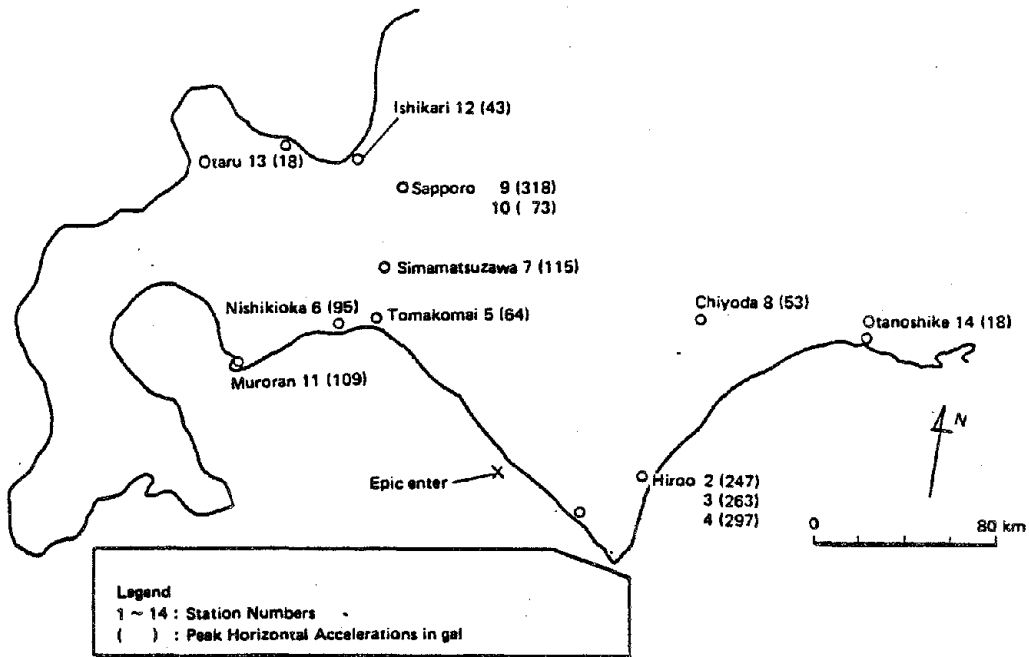


Fig. 3 Strong Motion Stations Recorded and Peak Horizontal Accelerations on Ground.

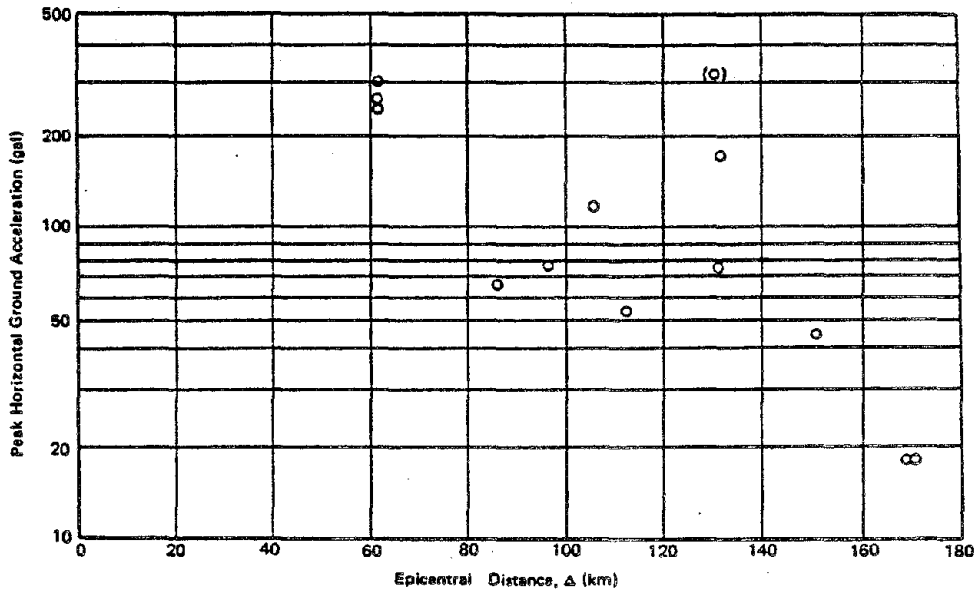


Fig. 4 Epicentral Distance Versus Peak Horizontal Ground Acceleration (Δ is measured from the center of octagon of Fig. 2).

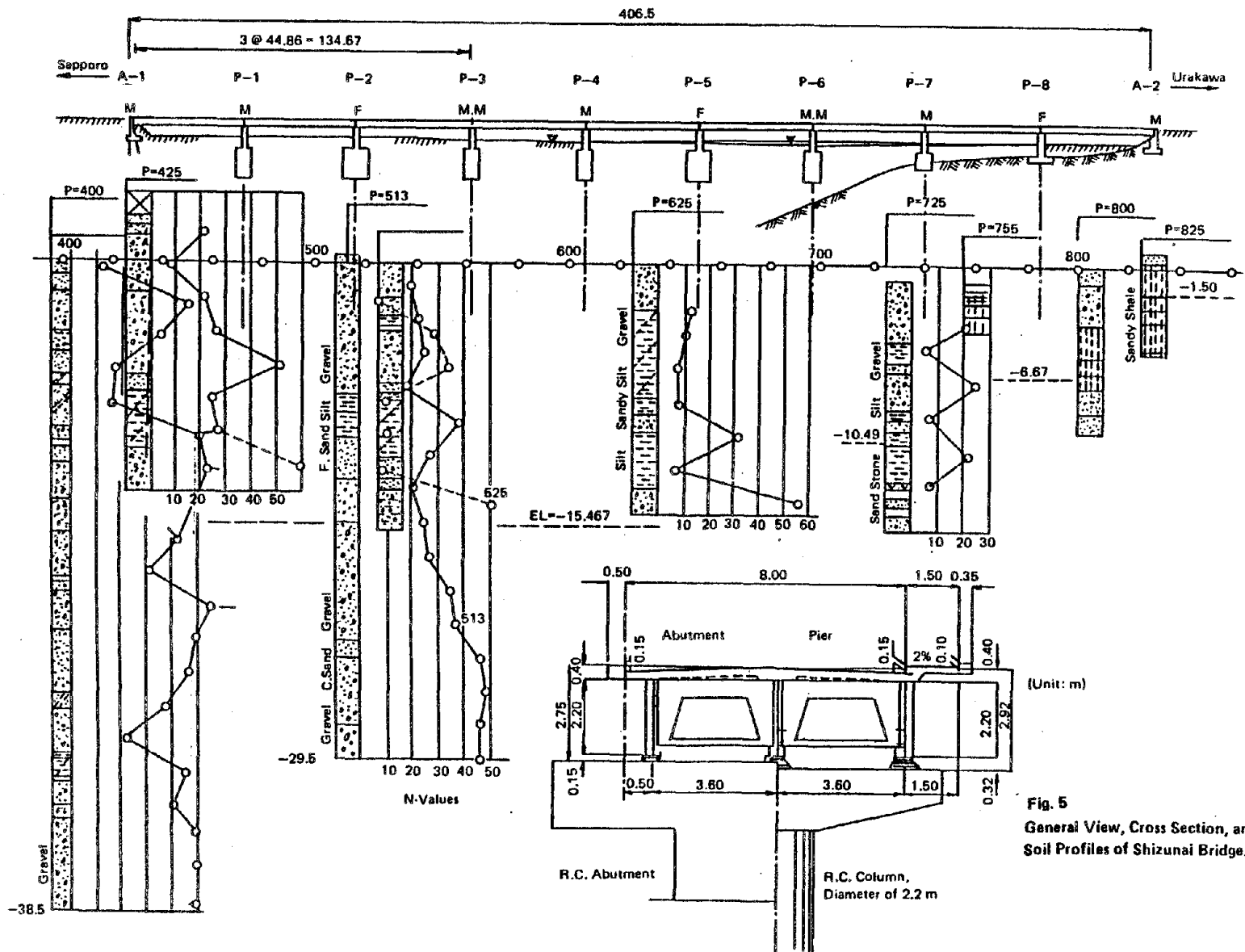
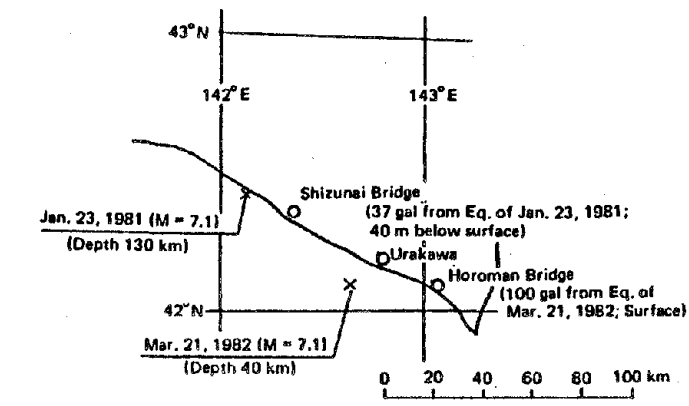
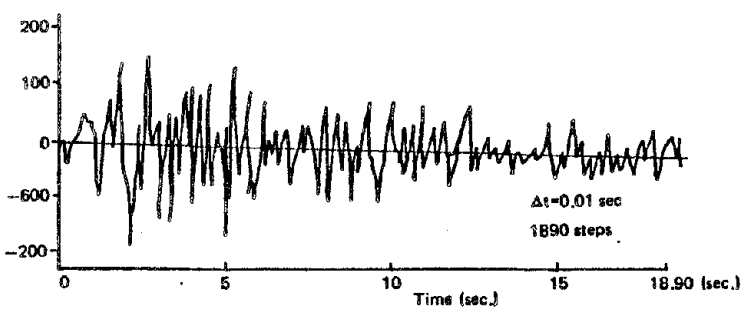


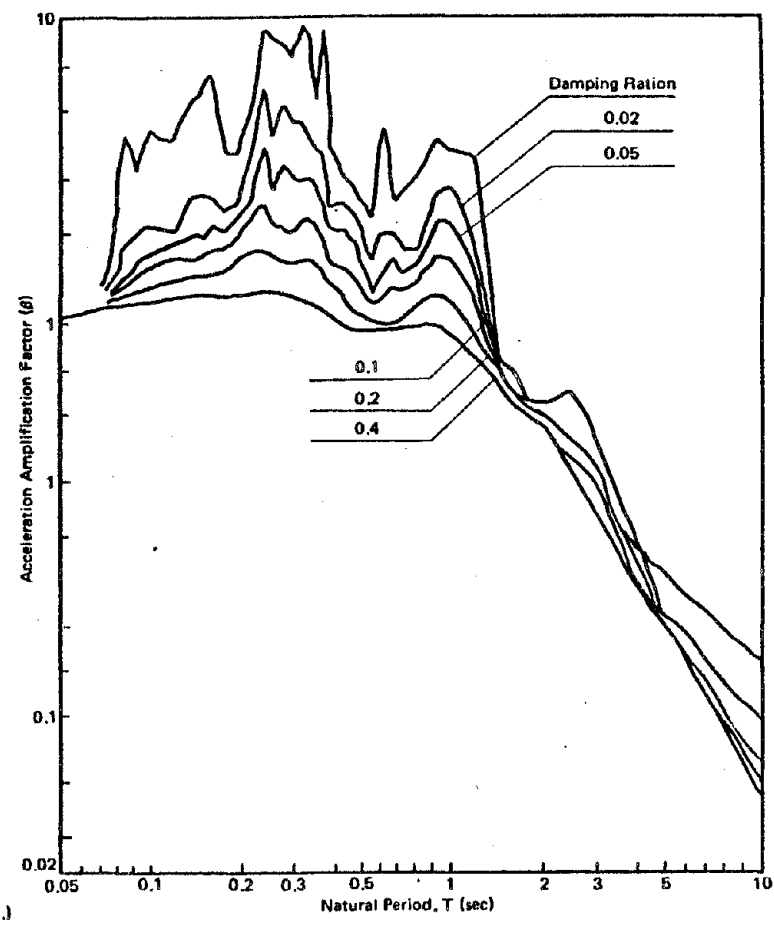
Fig. 5
General View, Cross Section, and
Soil Profiles of Shizunai Bridge.



(A) Locations of Epicenters of Two Earthquakes and Recording Sites.



(B) Time History of Shizunai Bridge Record
 (Jan. 23, 1981, Peak acceleration recorded=37 gal, Above wave is enlarged so that peak value=180 gal)



(C) Response Spectrum Curves.

Fig. 6 Shizunai Bridge Record and Response Spectrum Curves.

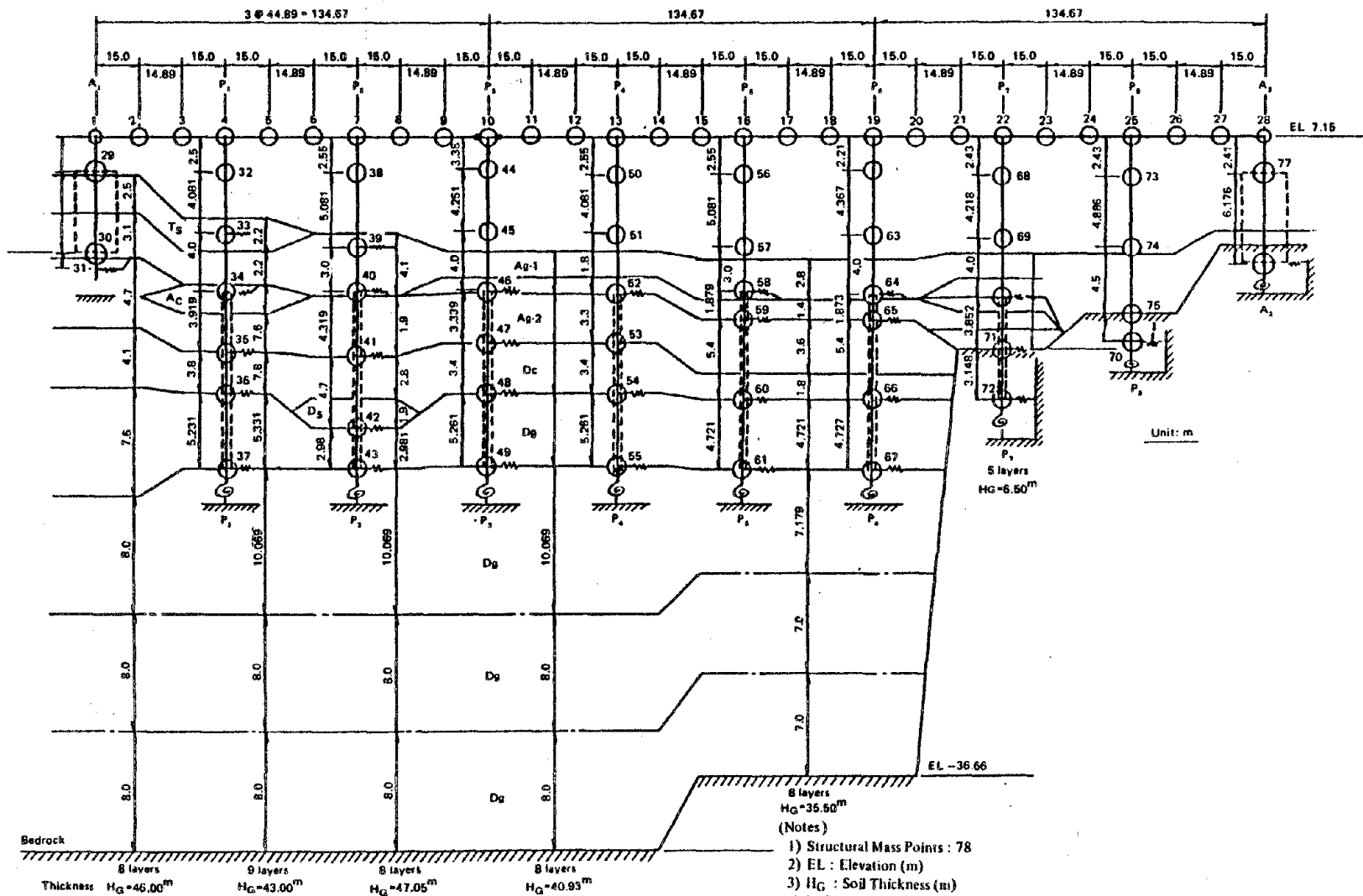


Fig. 7 Analytical Model of Overall System of Shizunai Bridge (In Transverse Direction).

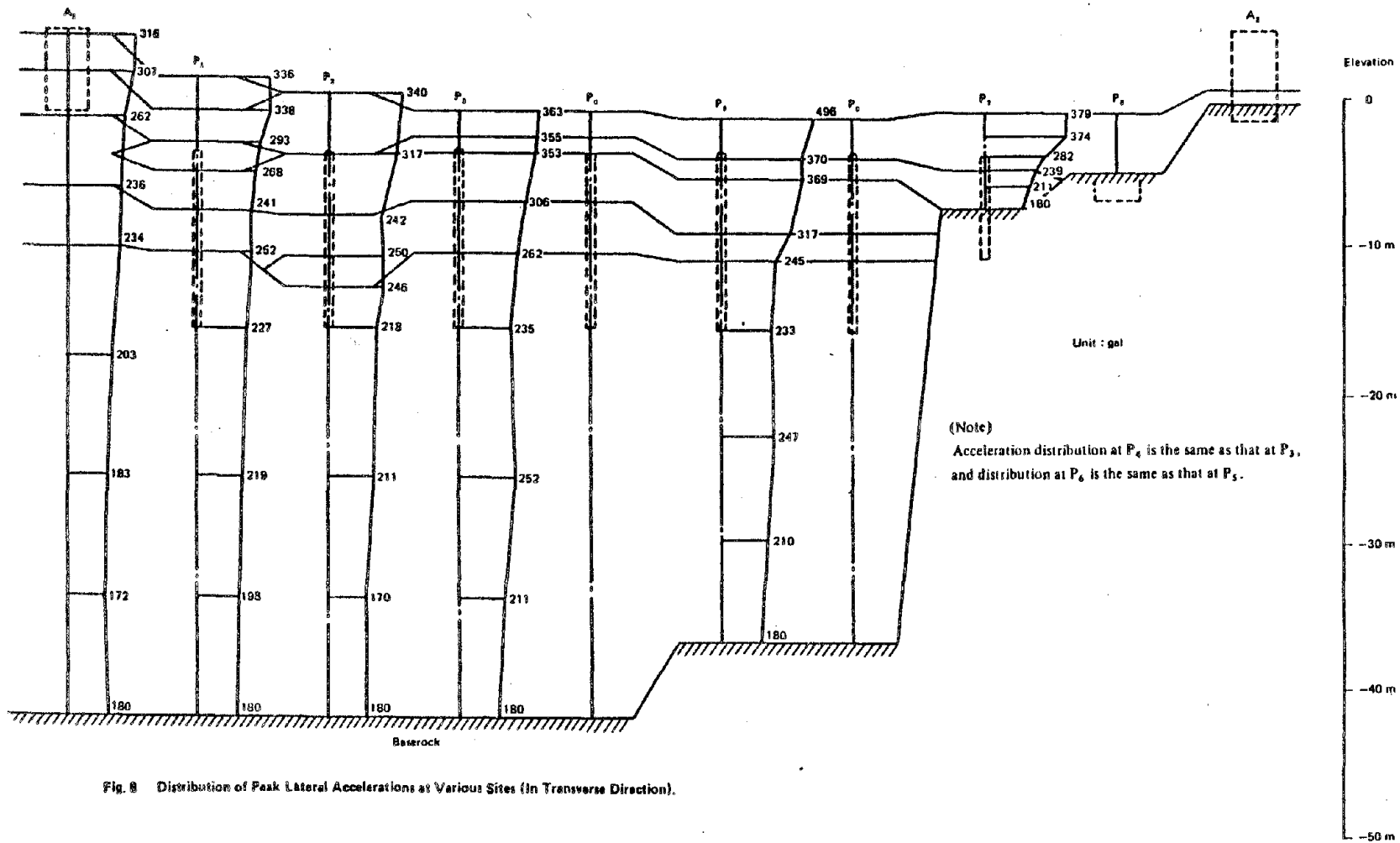


Fig. 8 Distribution of Peak Lateral Accelerations at Various Sites (In Transverse Direction).

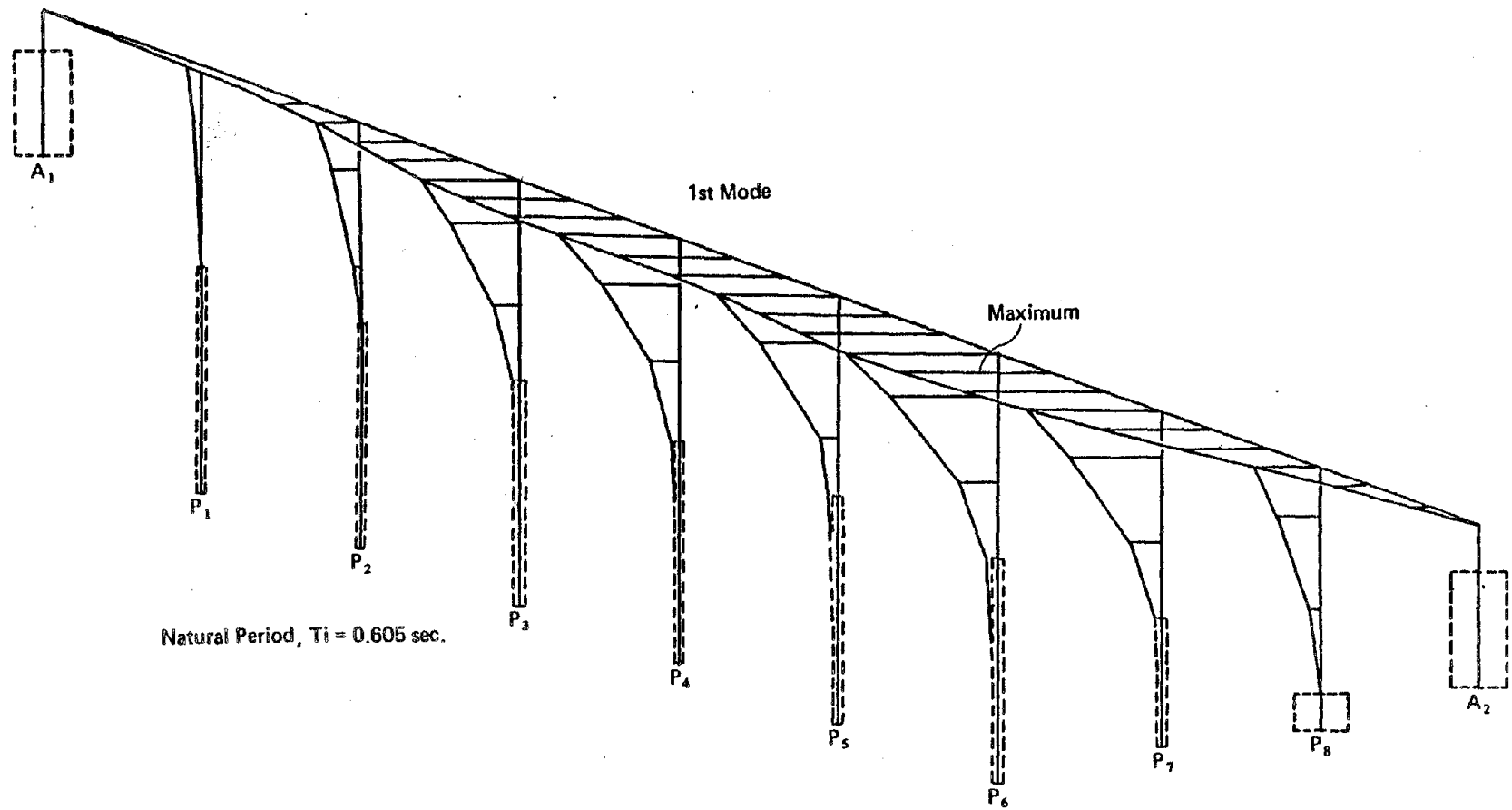


Fig. 9 Modal Shape of the 1st Mode for Overall System of Shizunai Bridge (In Transverse Direction).

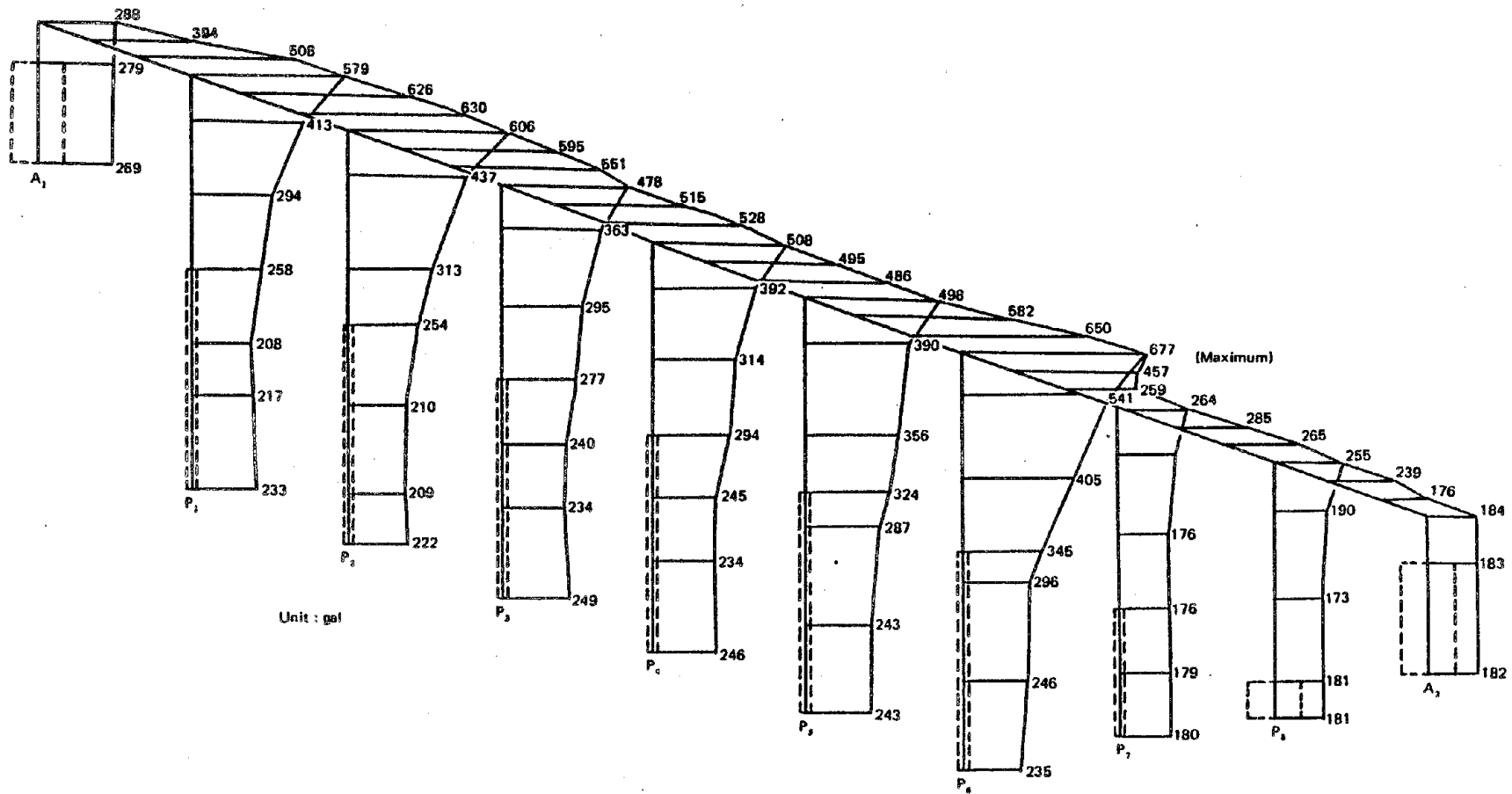


Fig. 10 Distribution of Peak Response Accelerations at Various Structural Points.
(in Transverse Direction)

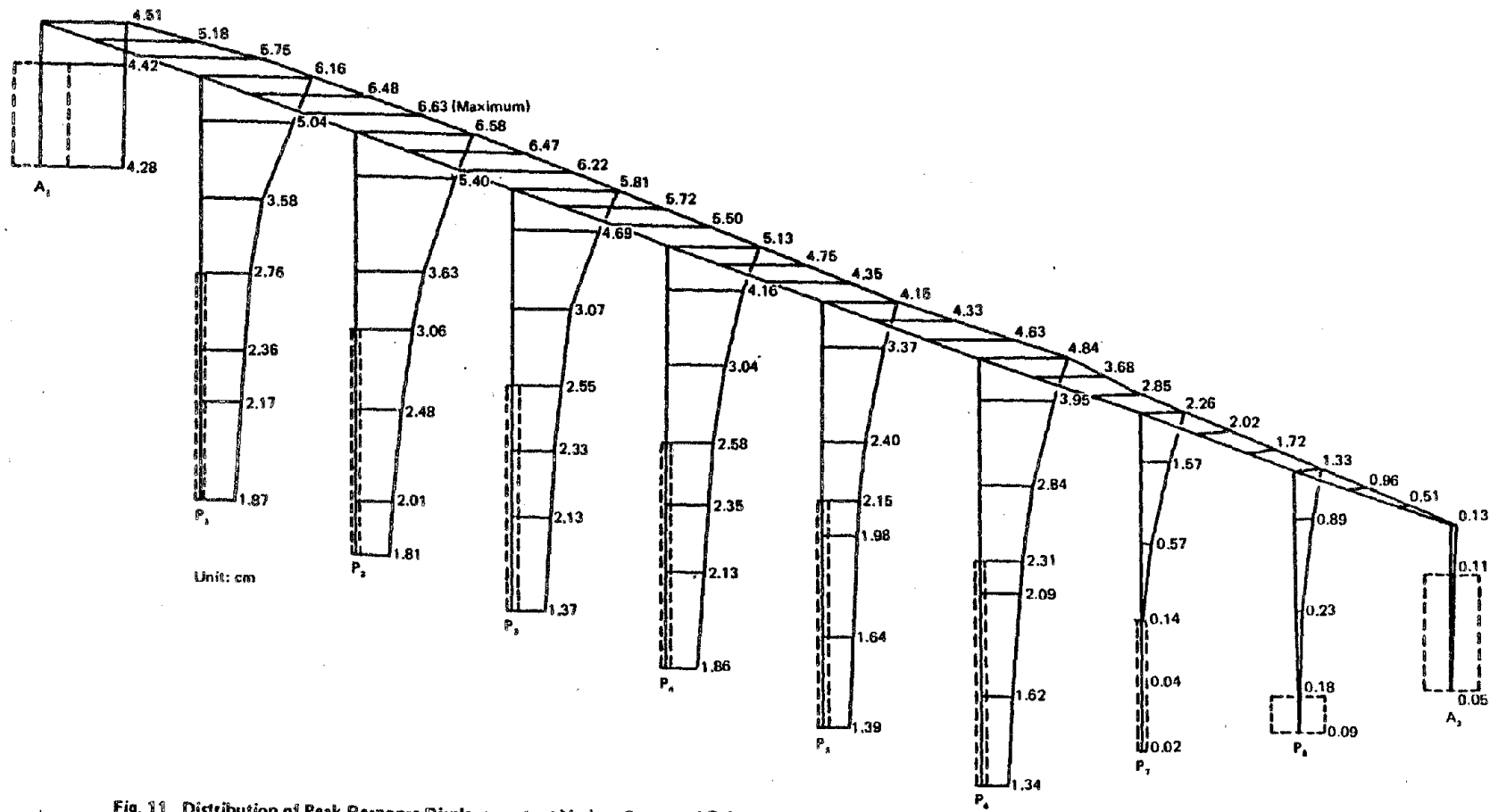


Fig. 11 Distribution of Peak Response Displacements at Various Structural Points. (In Transverse Direction)

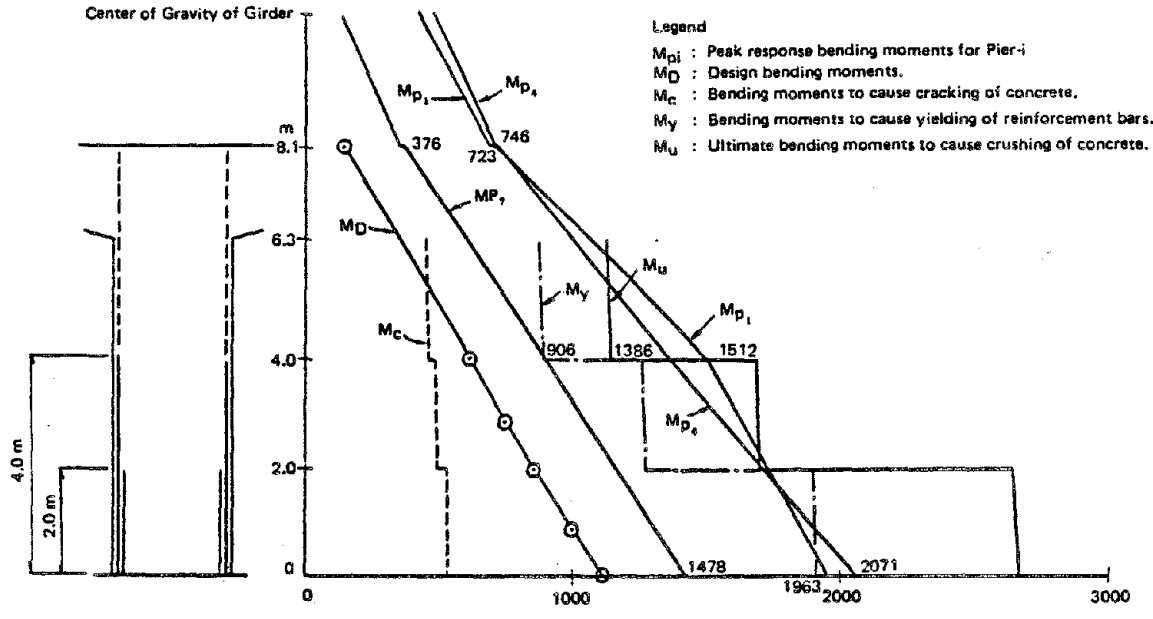


Fig. 12 (A) Distributions of Peak Bending Moments for Pier-1, Pier-6, and Pier-7. (In Transverse Direction)

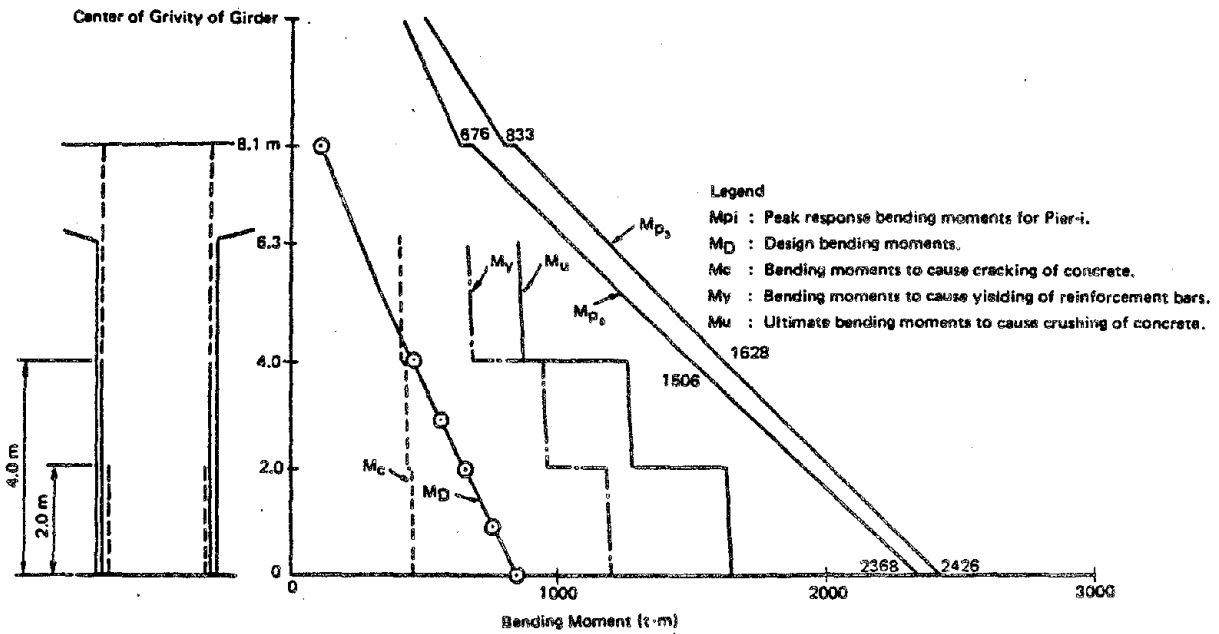


Fig. 12 (B) Distributions of Peak Bending Moments for Pier-3 and Pier-6. (In Transverse Direction)

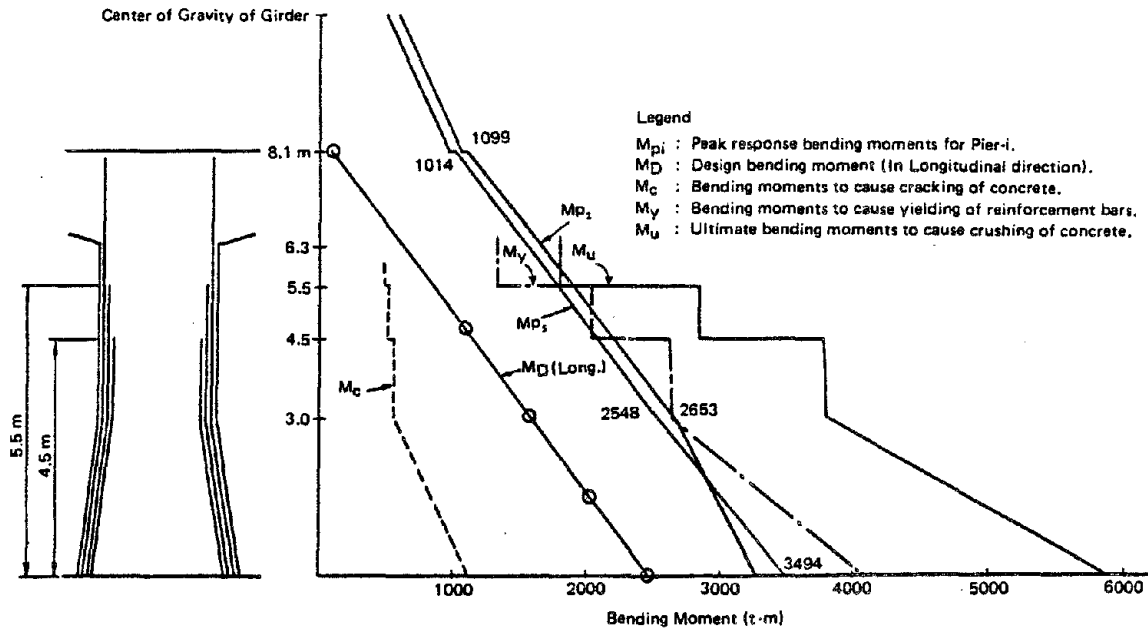


Fig. 12 (C) Distributions of Peak Bending Moments for Pier-2 and Pier-5.
(In Transverse Direction)

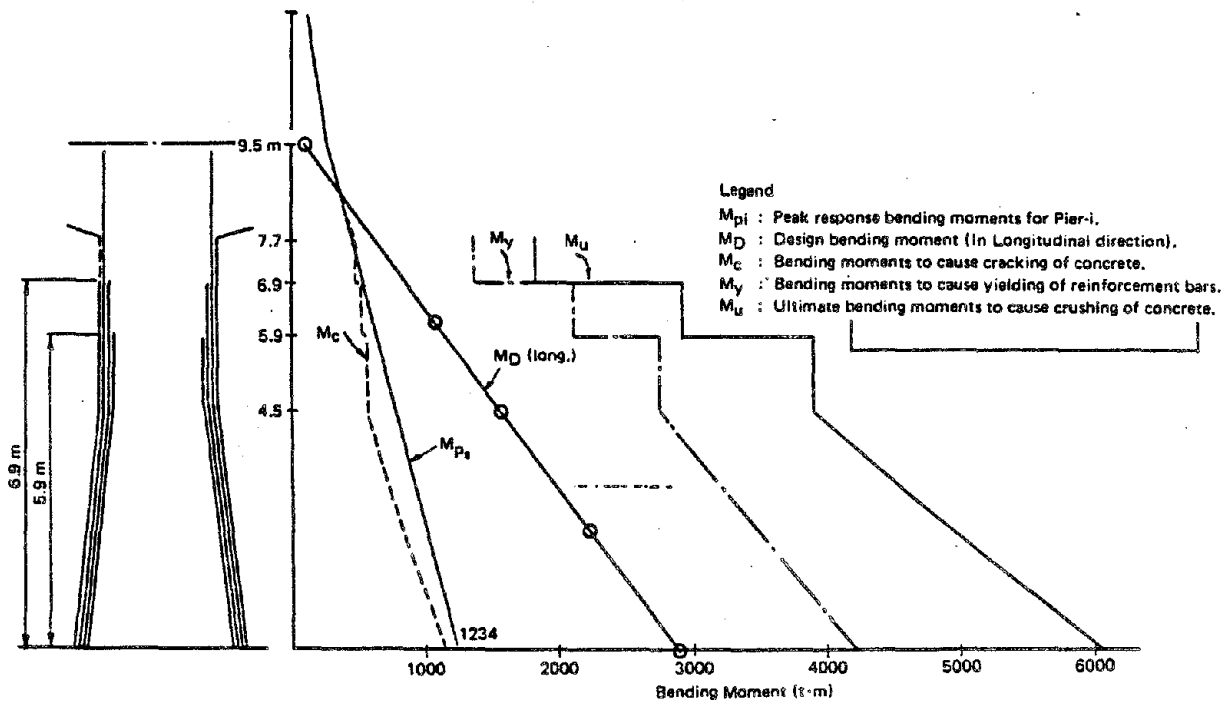


Fig. 12 (D) Distributions of Peak Bending Moments for Pier-8.
(In Transverse Direction)

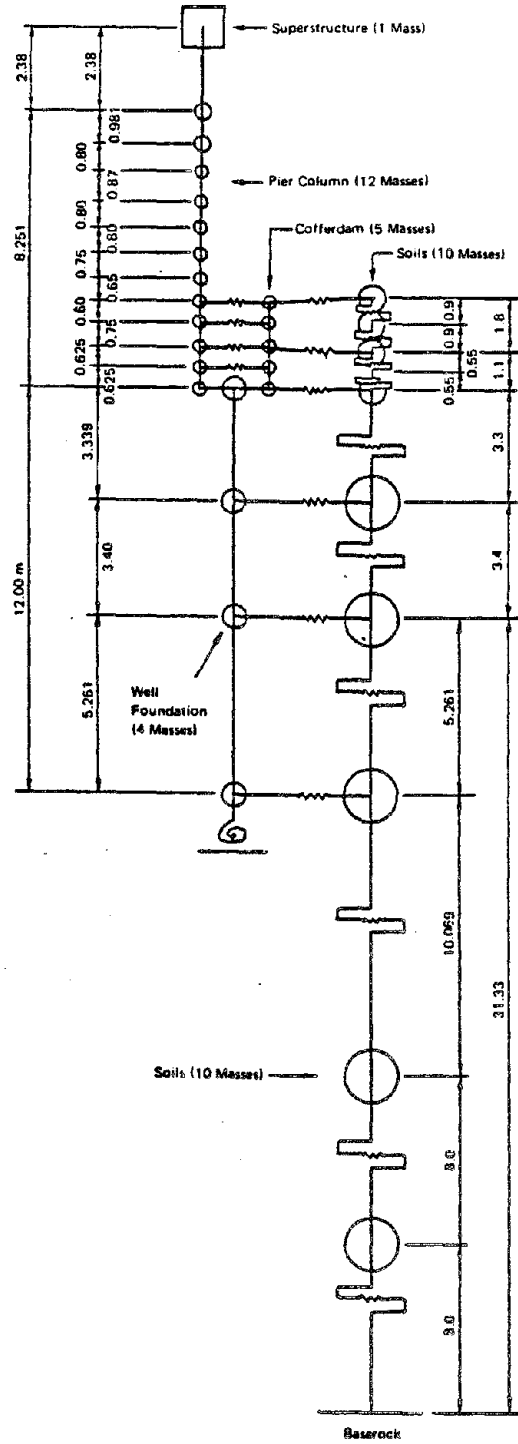
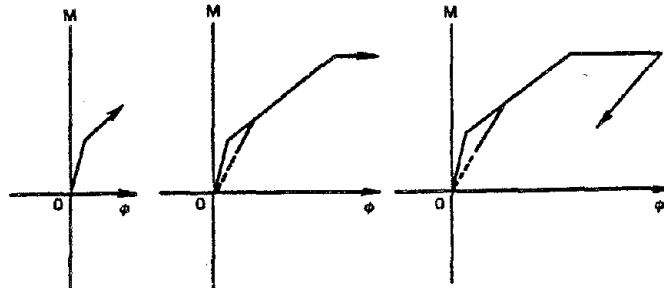
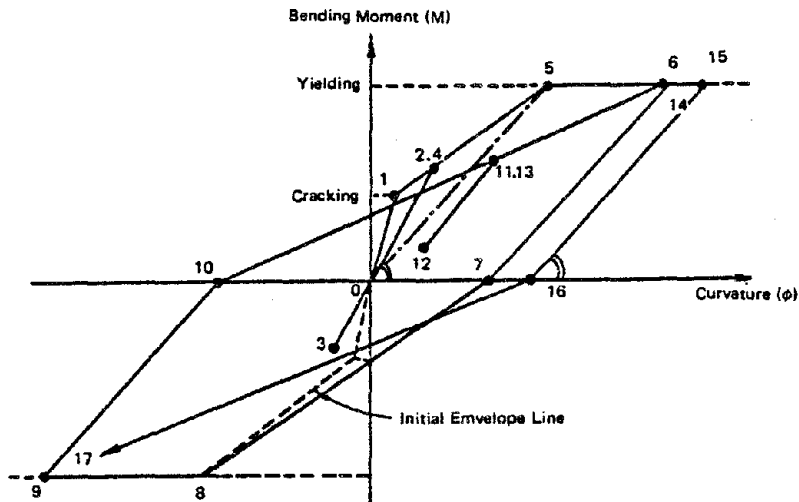


Fig. 13 Analytical Model of Pier-3 Non-Linear System.



Explanation of Muto's Degrading Tri-Linear System.

- 1) The skeleton curve is a degrading tri-linear one with corner points at cracking point (1) and yielding point (5).
- 2) The system is linear before cracking develops at point (5).
- 3) After cracking develops, the hysteresis curve goes along the second slope (initial envelope line). The curve goes toward the original point (0) from the maximum point, unless the curve reaches to the yielding point (5).
- 4) After the curve reaches to the yielding point (5), the curve goes along the third slope, and goes back on the line parallel to the line connecting the yielding point (5) and the original point (0), until the curve reaches to the abscissa (16). Next, the curve goes toward the farthest point (9) experienced. Points 1 to 17 in the above figure indicate an example of time history of the system.

Fig. 14 Muto's Degrading Tri-Linear System for the Bending Moment-Curvature Relation of Pier Column.

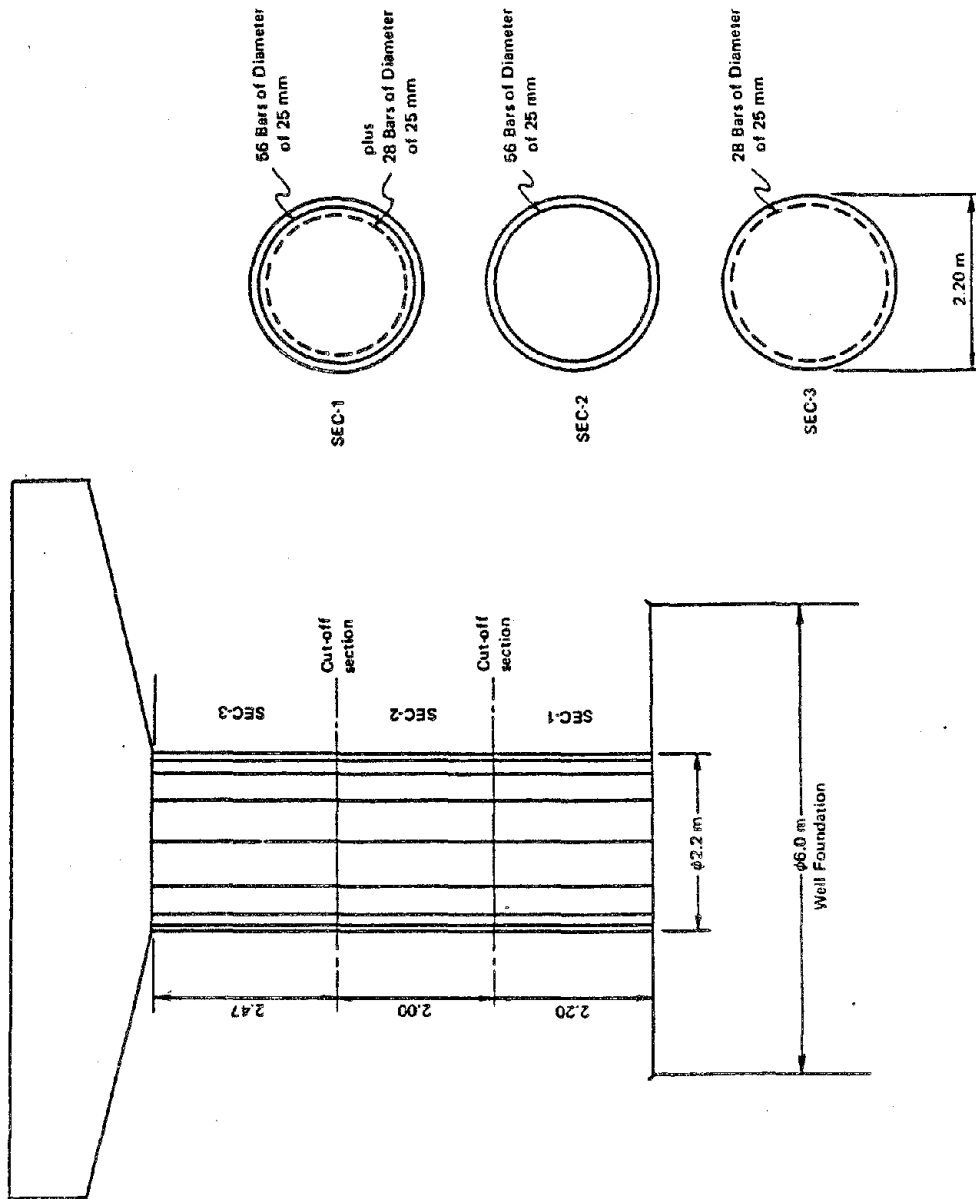


Fig. 15 Arrangement of Reinforcement Bars for Column of Pier-3.

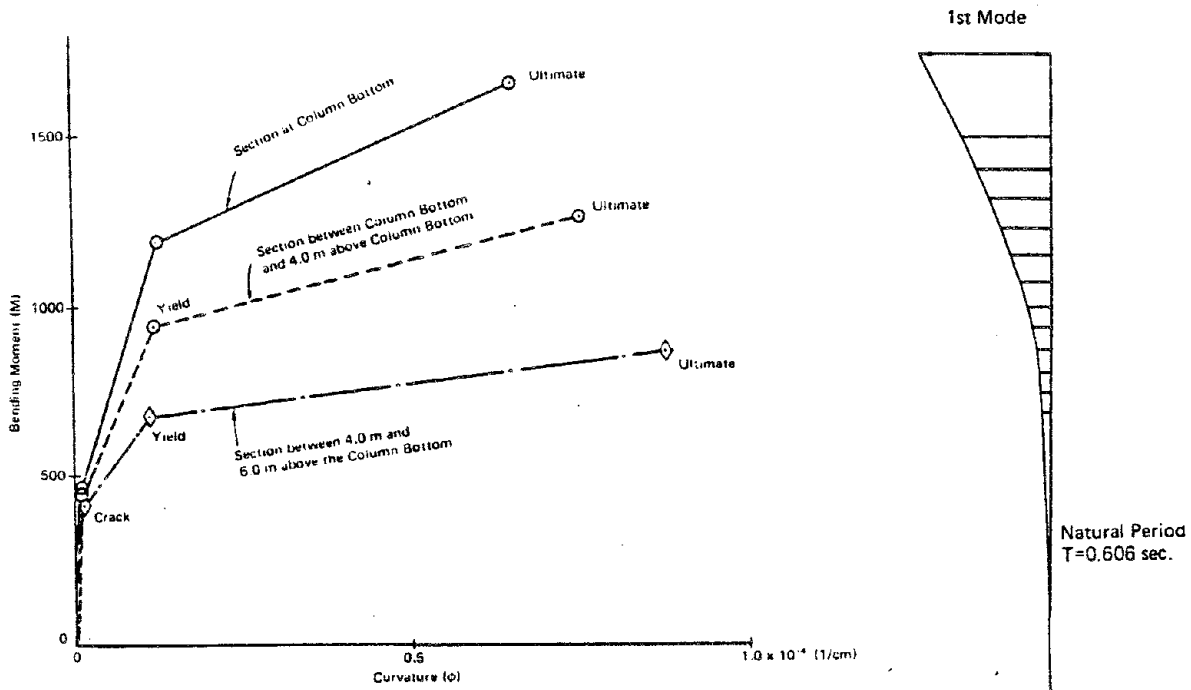


Fig. 16 Skeleton Curve of Bending Moment - Curvature Relation at Three Sections.

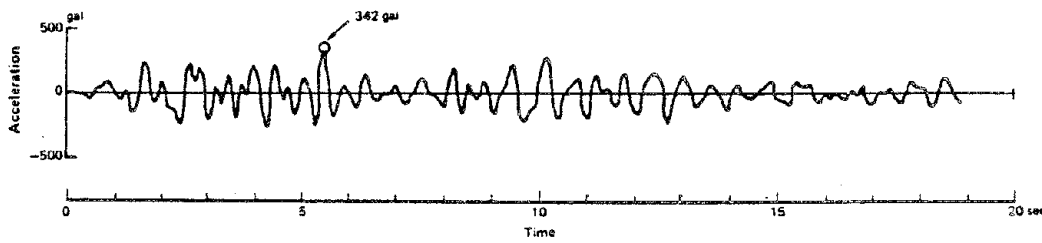


Fig. 18 Time History of Response Acceleration at Ground Surface.

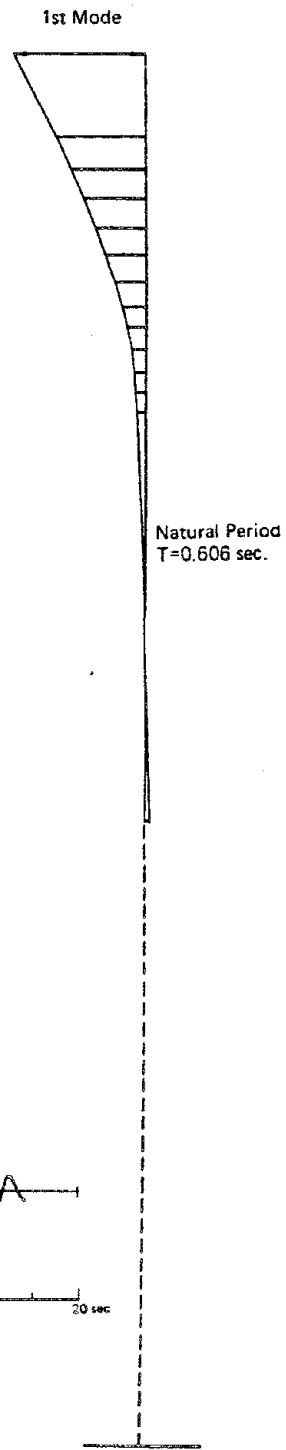


Fig. 17 Mode Shape of 1st Mode of Pier-3 System.

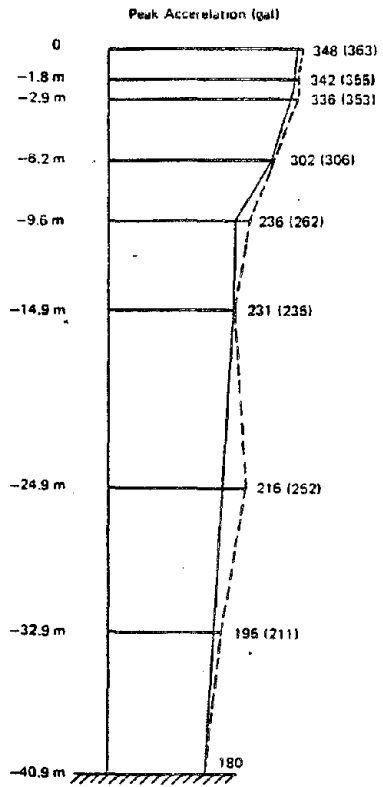


Fig. 19 Distribution of Peak Ground Accelerations.

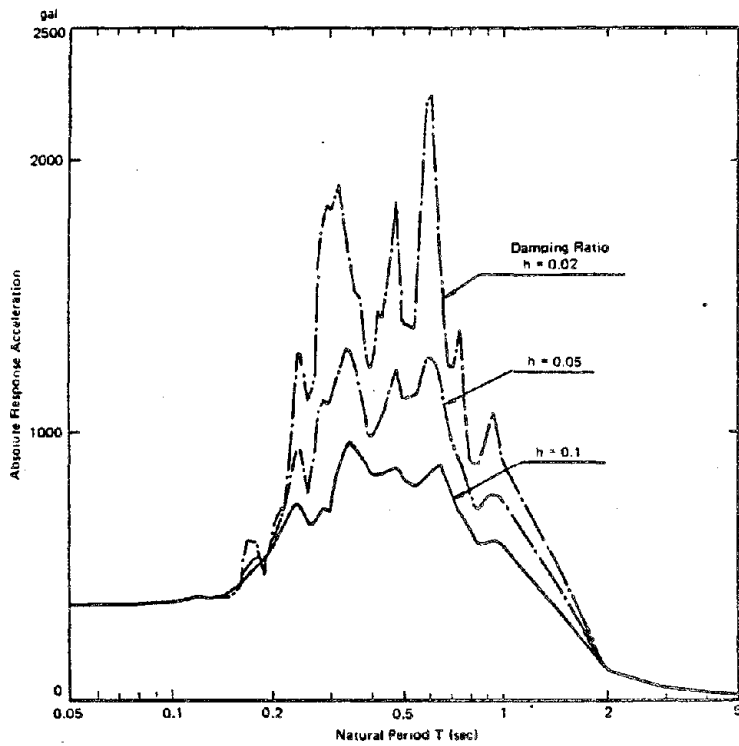


Fig. 20 Absolute Response Acceleration for the Ground Acceleration ($A_{max} = 348$ gal).

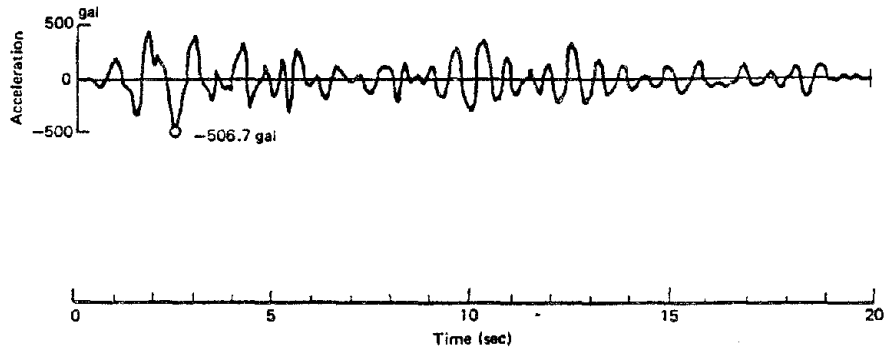


Fig. 21 Time History of Response Acceleration at Superstructure.

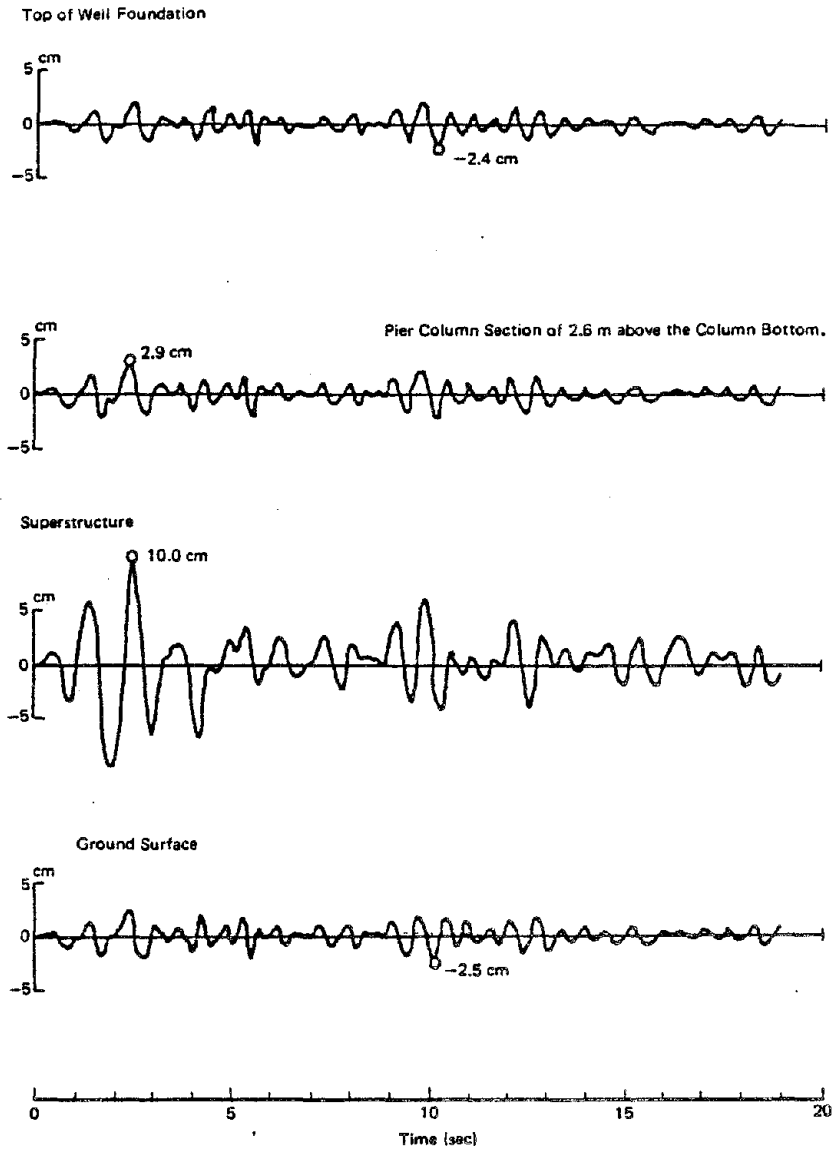


Fig. 22 Time History of Response Displacements at Four Points.

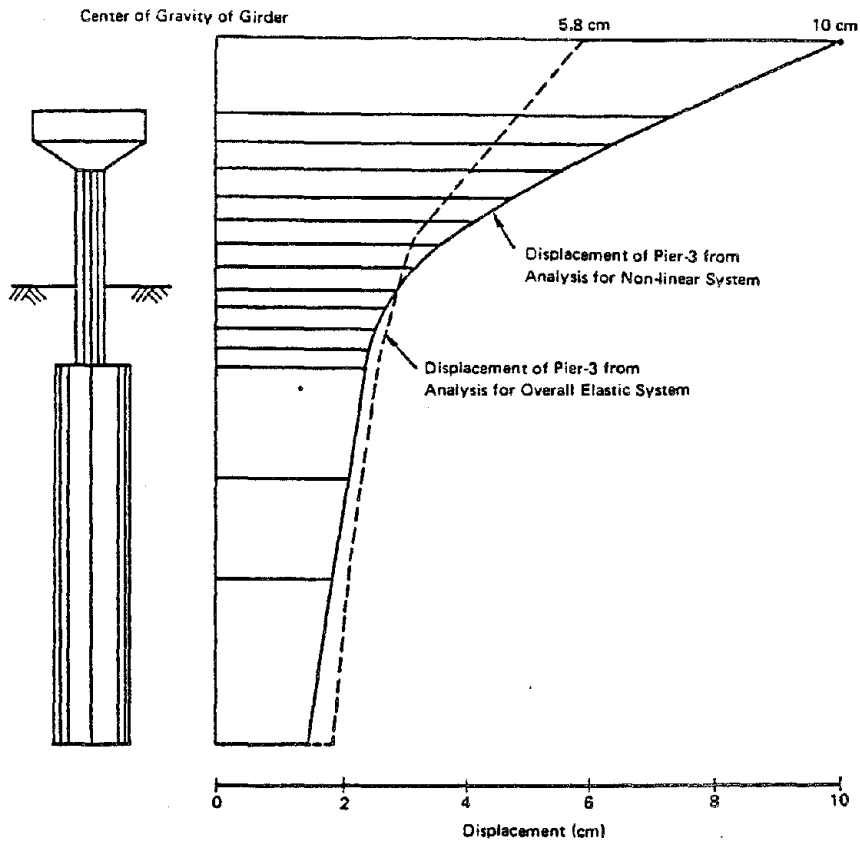


Fig. 23 Distribution of Peak Displacements.

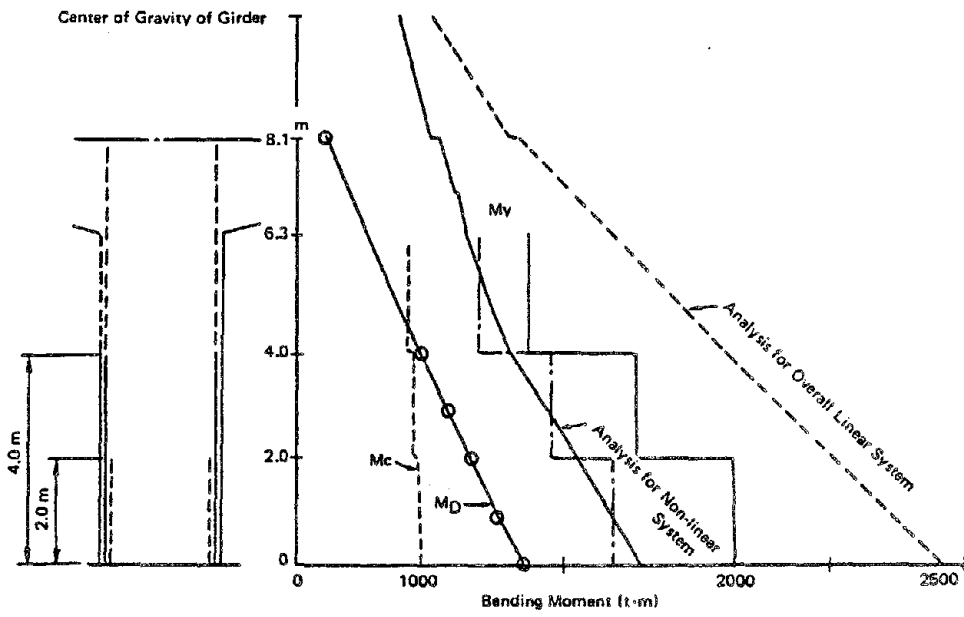


Fig. 24 Distribution of Bending Moment for Pier-3.

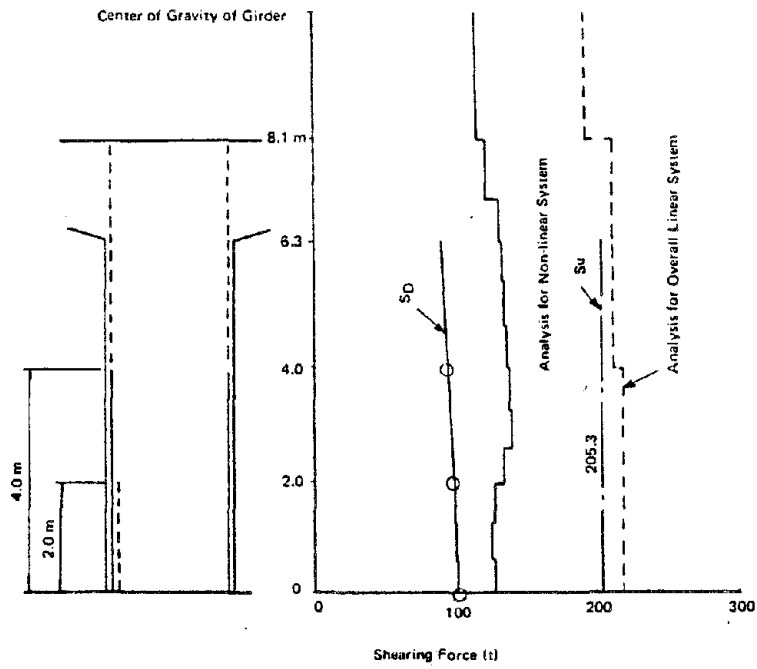


Fig. 25 Distribution of Shearing Force for Pier-3.

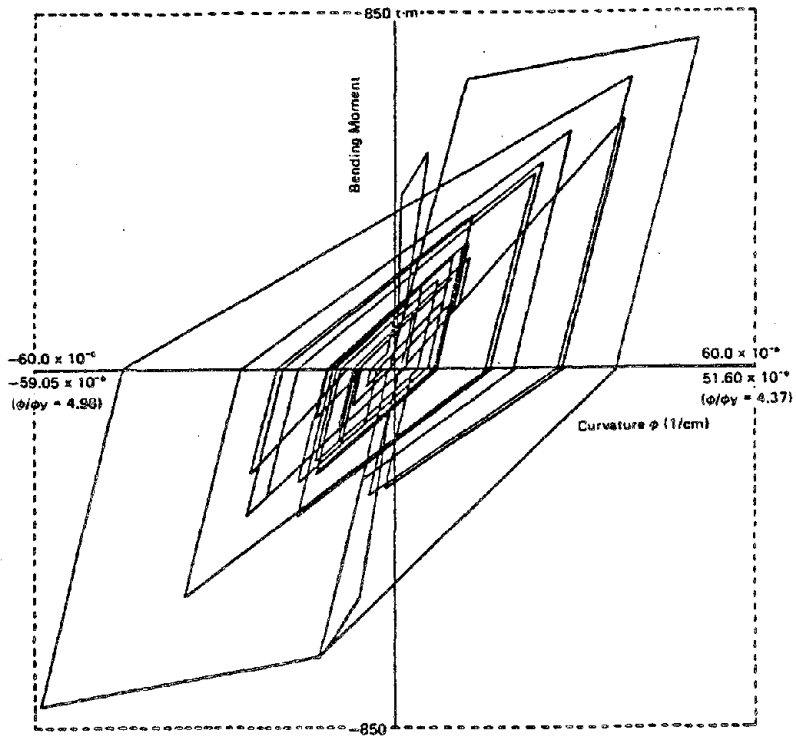


Fig. 26 Hysteretic Curve of $M-\phi$ Relation at Section of 4.0 m above Column Bottom.

DATA PROCESSING AND METHODOLOGIES FOR ASSESSING
SEISMIC RESPONSE CHARACTERISTICS OF
MELOLAND ROAD OVERPASS

By

S.D. Werner* and M.S. Agbabian†

ABSTRACT

The Meloland Road Overpass, a two-span reinforced concrete bridge located near El Centro, California, survived very strong shaking during the 1979 Imperial Valley Earthquake with virtually no damage. This shaking triggered an array of 26 strong motion accelerometers located on or near the bridge, providing the most extensive array of earthquake response measurements yet obtained for bridges in the United States. In view of this, a project is being implemented to evaluate these measured data, as a means for enhancing our understanding of the behavior and design of bridges in an earthquake environment. This paper describes new methodologies developed under this project to support this data evaluation effort, as well as special data digitization and processing operations necessitated by field recorder malfunctions.

* Associate, Agbabian Associates, El Segundo, California, USA

† President, Agbabian Associates, El Segundo, California, USA

INTRODUCTION

In October 1979, a magnitude 6.4 earthquake occurred along the Imperial fault just south of the United States-Mexico border and caused significant ground shaking throughout Southeastern California and Northcentral Mexico. This event, the Imperial Valley Earthquake, triggered numerous strong motion accelerometers, to provide an extensive set of strong motion measurements, particularly in the near field (Brady, 1980; McJunkin and Ragsdale, 1980; Porcella et al., 1982; and Brune et al., 1982).

Among the accelerograms recorded during this earthquake were those measured by an array of 26 transducers located on or near the Meloland Road Overpass - a two-span bridge structure located 0.5 km southwest of the causative fault (see Figure 1). This bridge (Figure 2) consists of a continuous reinforced-concrete three-cell box girder road deck on open-end diaphragm abutments and a reinforced-concrete single-column pier, all on timber piles. The two spans of the bridge, each 104 ft long, are not skewed and contain no joints or sliding details. The bridge was designed in 1968-69 by the California Department of Transportation (CALTRANS), using 1968 California Division of Highways design criteria (Degenkolb and Jurach, 1980; Rojan et al., 1982).

The Imperial Valley earthquake induced very intense shaking at the bridge, with peak horizontal and vertical accelerations along the road deck reaching levels of 0.51 g and 0.50 g respectively. Despite this, the bridge was virtually undamaged by the shaking, except for some evidence of small relative motion and separation at the abutment/backfill interface (Rojan et al., 1982). This can be contrasted with the New River bridges, northeast of El Centro, which were located further from the causative fault but nevertheless suffered extensive damage from the Imperial Valley earthquake motions.

The array of measurements obtained at the Meloland Road Overpass during the 1979 Imperial Valley earthquake represents the most extensive set of strong motion data yet obtained for bridges in the United States. In view of this, these data provide a means for gaining important insights into the behavior of bridges during earthquakes, and for addressing the following key questions.

- a. What new insights for enhancing future seismic design provisions for bridges can be obtained from examination of this extensive array of strong motion measurements?
- b. What configurational characteristics of the Meloland Road Overpass caused it to survive its very strong motion with no damage?

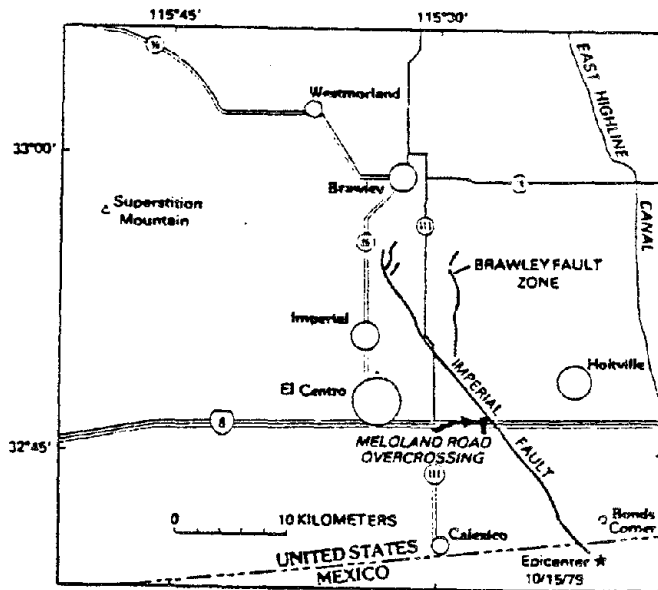


FIGURE 1. LOCATION OF MELOLAND ROAD OVERPASS

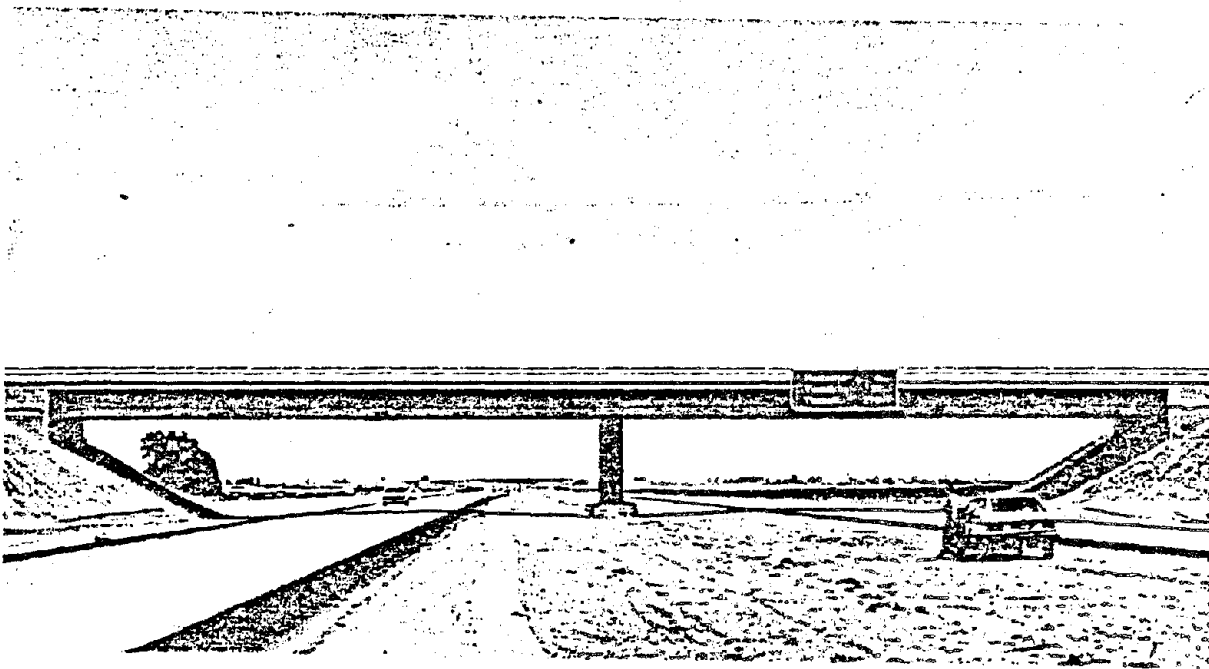


FIGURE 2. VIEW OF MELOLAND ROAD OVERPASS LOOKING EAST

- c. How can information obtained from these strong motion measurements be used to improve procedures for mathematically modeling and dynamically analyzing bridge structures?

PROJECT DESCRIPTION

To evaluate the strong motion data at the Meloland Road Overpass in accordance with above issues, a two-year project was initiated in April 1982, under the sponsorship of the National Science Foundation. This project consists of the following main tasks: (1) evaluation of the basic data, in terms of the information it provides pertaining to the bridge response characteristics; (2) application of state-of-the-art parameter optimization procedures to the data, in order to develop a finite element model of the bridge that "fits" the data to within an acceptable tolerance; and (3) use of this model as a basis for carrying out further dynamic analyses to evaluate the bridge response characteristics in accordance with the project objectives.

This paper describes some initial results obtained from this ongoing project. To do this, it first describes the strong motion instrumentation and data measured at the bridge. Then, it describes how the data were re-digitized and re-processed under this project, in order to provide consistent data from all 26 channels and to overcome effects of periodic stalling of a recorder that contaminated the traces from Channels 1 to 13. The remaining sections summarize new methodologies that have been developed to carry out the parameter optimization for the bridge model development, and to extract normal modes of the bridge from the measured response data.

STRONG MOTION INSTRUMENTATION AND ACCELEROGRAMS

Instrumentation

The instrumentation of the Meloland Road Overpass has been described in some detail by Rojan et al. (1982) and is briefly summarized in this section. This bridge was selected for instrumentation because of its structural characteristics and its close proximity to the Imperial Fault. It was instrumented in November 1978, and the instrumentation is maintained by the California Division of Mines and Geology, Office of Strong Motion Studies.

The instrumentation consists of two 13-channel Kinematics CRA-1 remote-accelerometer central recording systems. It is comprised of FBA-1 (single axis) and FBA-3 (triaxial) accelerometer packages, two 13-channel central recording units interconnected for common timing, and one VS-1 starter. The

recorders and starter are located at the ground level next to the base of the central pier. The FBA accelerometers have a natural frequency of 50 Hz and are designed to measure accelerations up to 1 g over a nominal frequency range of 0 to 50 Hz.

The instrumentation layout is shown in Figure 3. The data recorded at the indicated instrument locations provide measurements of the vertical (flexural), transverse (horizontal), and torsional response of the road deck, the translational response at the two abutments and the base of the central pier, the motions in the embankments adjacent to the abutments, and the free field response. Some typical instrument locations are shown in Figure 4.

Accelerograms

The 26 accelerograms recorded at the Meloland Road Overpass during the 1979 Imperial Valley earthquake are shown in Figure 5. This figure shows that, although each of the 13-channel accelerometer systems operated during the earthquake, the records from one system (involving data from Channels 1 to 13) were contaminated because the recorder film transport stalled periodically during the earthquake. These stalls occurred at approximately 3 sec intervals, and are characterized by a distortion of the acceleration trace and a bulging and shortening of the time trace. Because of these stall effects, special digitization techniques were developed and implemented as part of this project, in order to reconstruct the bridge response in the stalled regions of the trace. These techniques are described subsequently in this paper.

DATA DIGITIZATION AND PROCESSING

Overview

A key aspect of this project to date has been the redigitization and reprocessing of the strong motion data measured at the Meloland Road Overpass. The objectives of this effort were: (1) to reconstruct the motions from Channels 1 to 13 that were distorted by the recorder stalls; and (2) to provide consistent data from all 26 channels that can be used simultaneously to evaluate the bridge response characteristics in accordance with the project objectives. This work was carried out by Trifunac and Lee (1983) at the facilities of the University of Southern California (USC), under a subcontract to this project. The endeavor was aided by the support and cooperation of personnel from the Office of Strong Motion Studies, California Division of Mines and Geology.

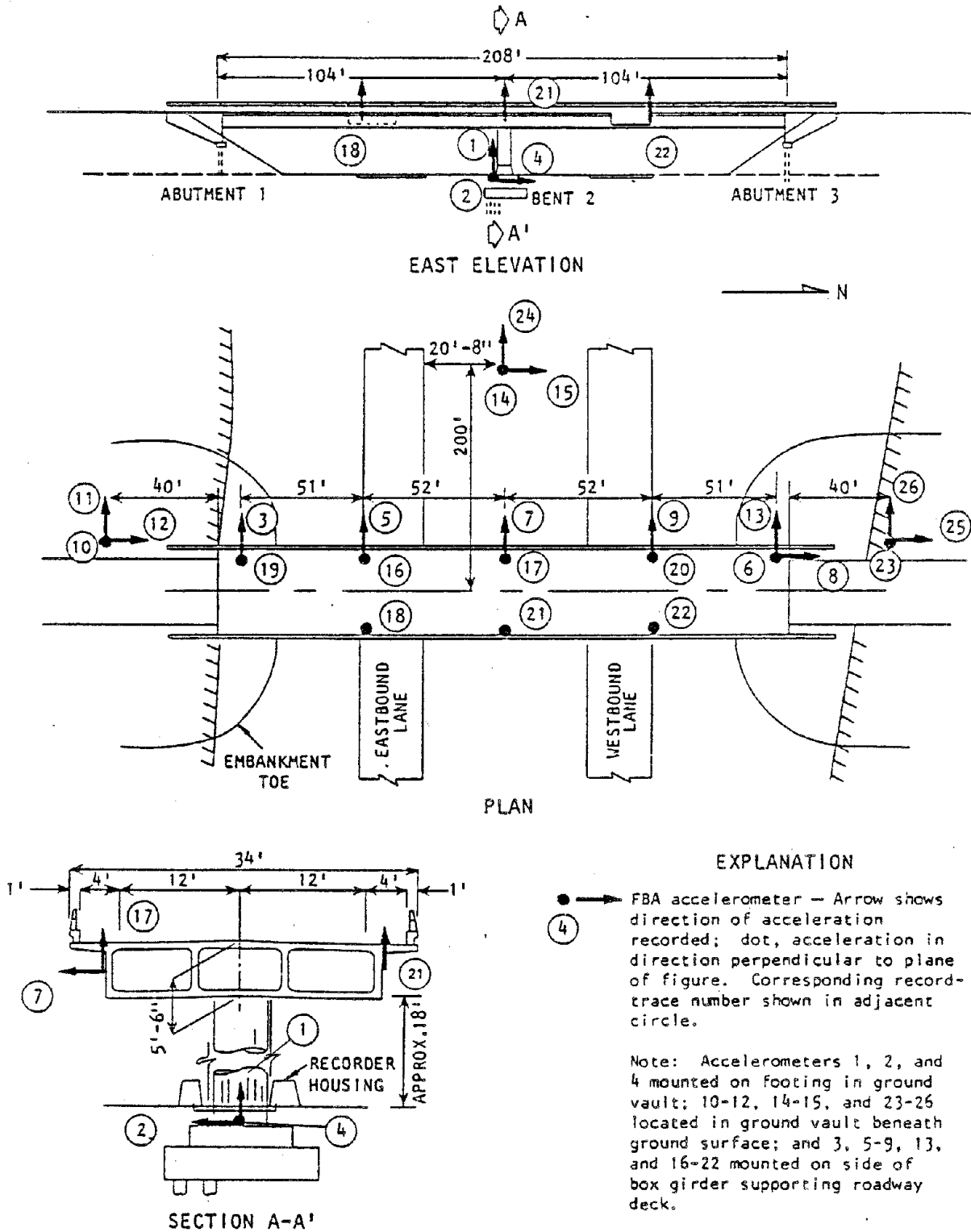
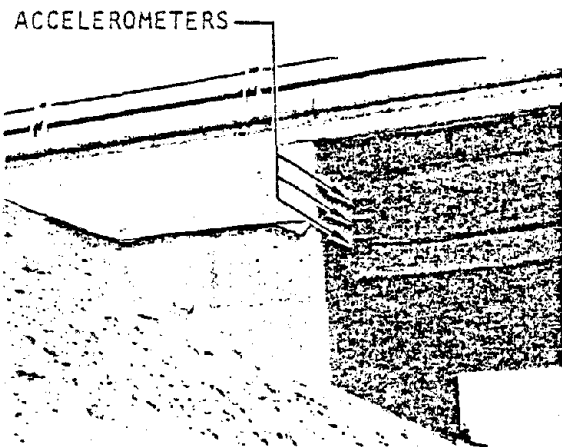
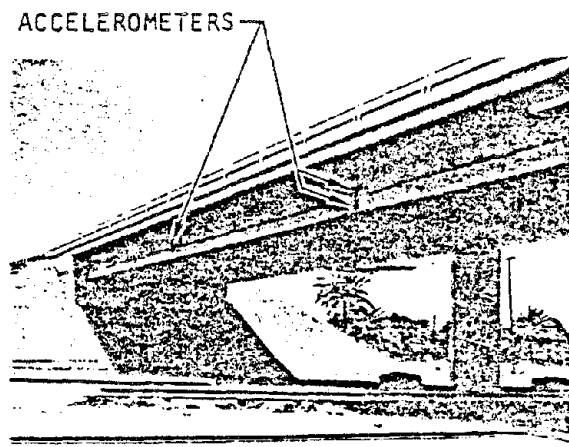


FIGURE 3. STRONG MOTION INSTRUMENTATION LAYOUT AT MELOLAND ROAD OVERPASS (Rojan et al., 1982)



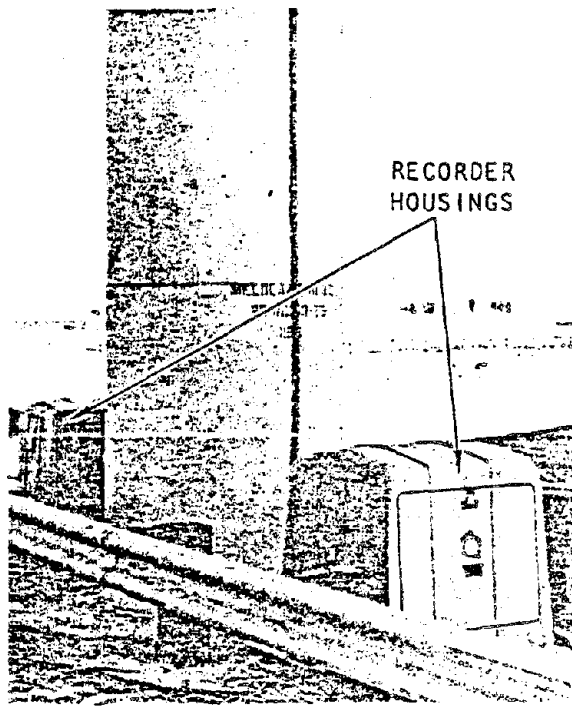
(a) West face of north abutment



(b) West face of road deck



(c) North embankment

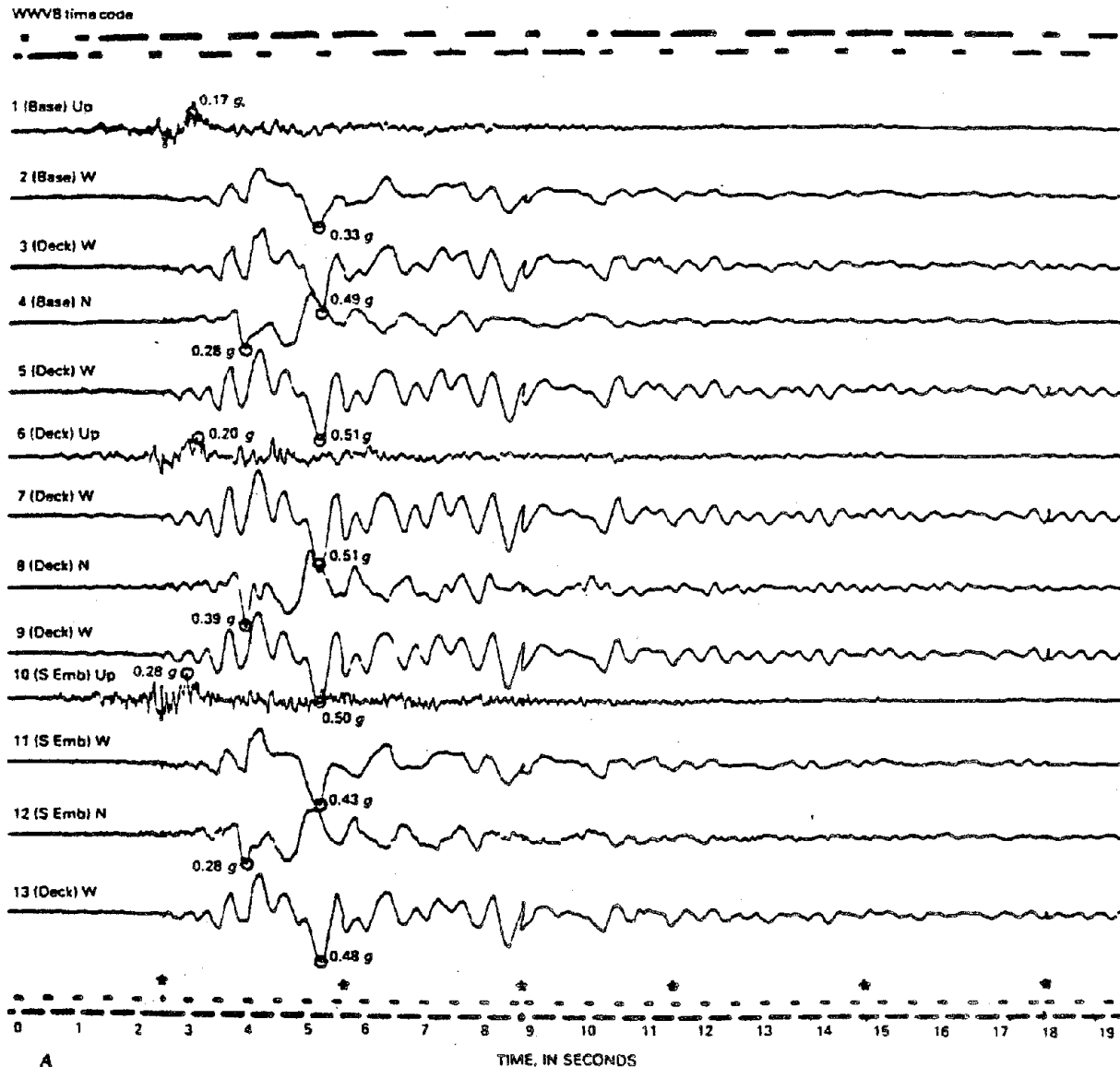


(d) Central recorders

FIGURE 4. INSTRUMENTS ALONG MELOLAND ROAD OVERPASS

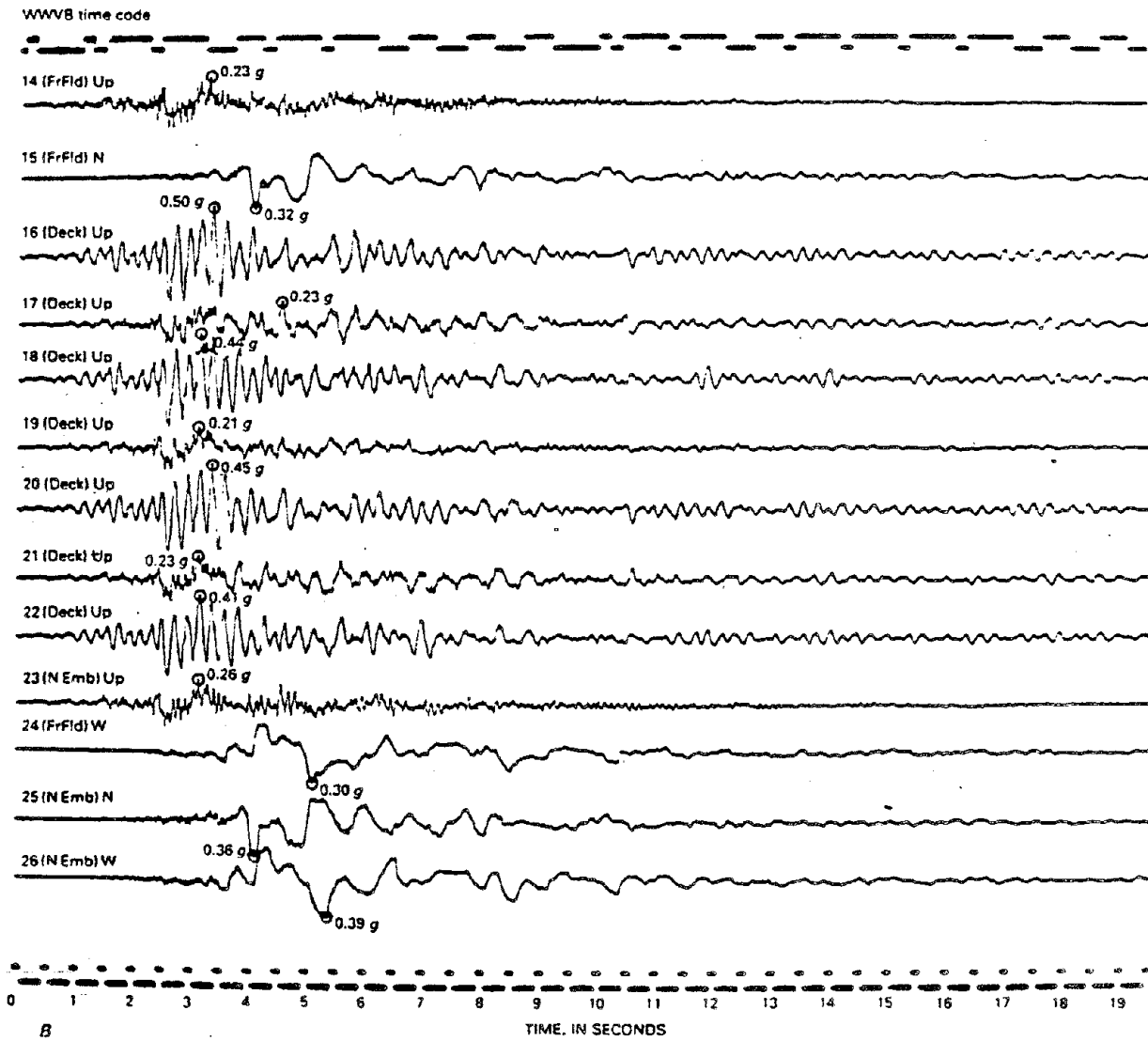
NOTES:

1. Directions in trace identification denote direction of positive acceleration — N (north), W (west), or Up (vertical).
2. Circle denotes peak acceleration for each trace.
3. Asterisks along lower time traces denote approximate times of recorder stalls.



(a) Traces from Channels 1 to 13

FIGURE 5. RAW ACCELEROGRAPH TRACES OBTAINED AT MELOLAND ROAD OVERPASS DURING 1979 IMPERIAL VALLEY EARTHQUAKE



(b) Traces from Channels 14 to 26

FIGURE 5. (CONCLUDED)

The reconstruction of the data at the recorder stalls was carried out using the Automatic Record Digitizing System (ARDS) at USC. This effort involved certain manual operations, together with automatic operations controlled by the ARDS routine software and one additional program developed specifically for this application. Once the data from Channels 1 to 13 was reconstructed, it was then reprocessed using the USC routine data-processing software. Data from Channels 14 to 26 (which were not affected by recorder stalls) were also redigitized and reprocessed so as to assure consistency between records from all channels.

Data Digitization

The basic elements of the ARDS facility are indicated schematically in Figure 6 and are described in detail by Trifunac and Lee (1979). All digitization operations using these elements are controlled through the existing programs FILM, TRACE, TV, and SCRIBE, and through the special purpose program, MAKGAP, written for application to the Meloland Bridge data. The use of these programs in the reconstruction of motions from Channels 1 to 13 is illustrated in Figure 7, and is summarized in the paragraphs that follow. The existing programs were also used in the routine digitization of the traces from Channels 14 to 26.

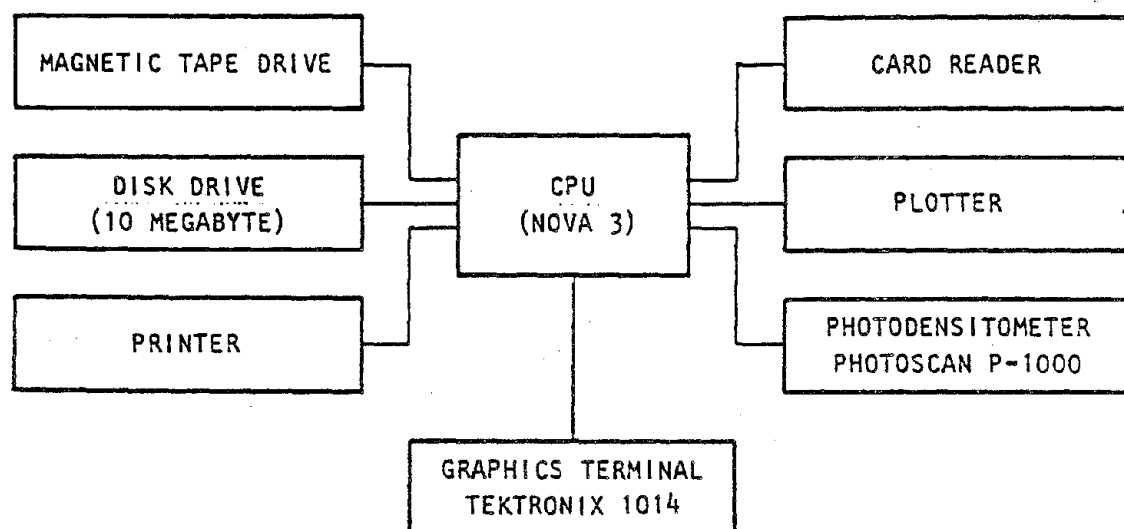


FIGURE 6. HARDWARE COMPONENTS OF USC AUTOMATIC ACCELEROGRAPH RECORD DIGITIZING SYSTEM (Trifunac and Lee, 1979)

Program FILM. The reading of the film negative is performed by the ARDS drum photodensitometer, which is controlled by the program FILM. In this operation, a rotating drum to which the film is attached is scanned by a light source, and

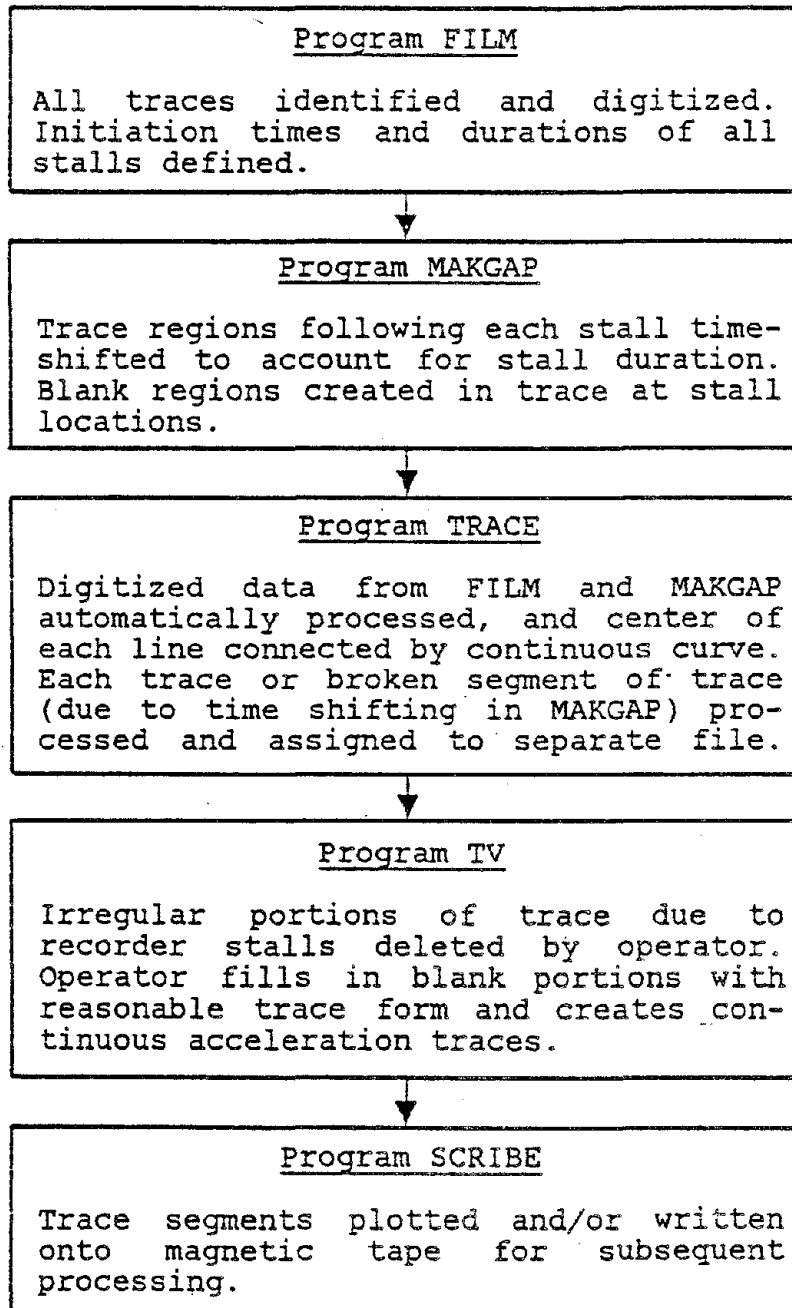


FIGURE 7. PROCESS FOR RECONSTRUCTION OF MOTION AT RECORDER STALLS

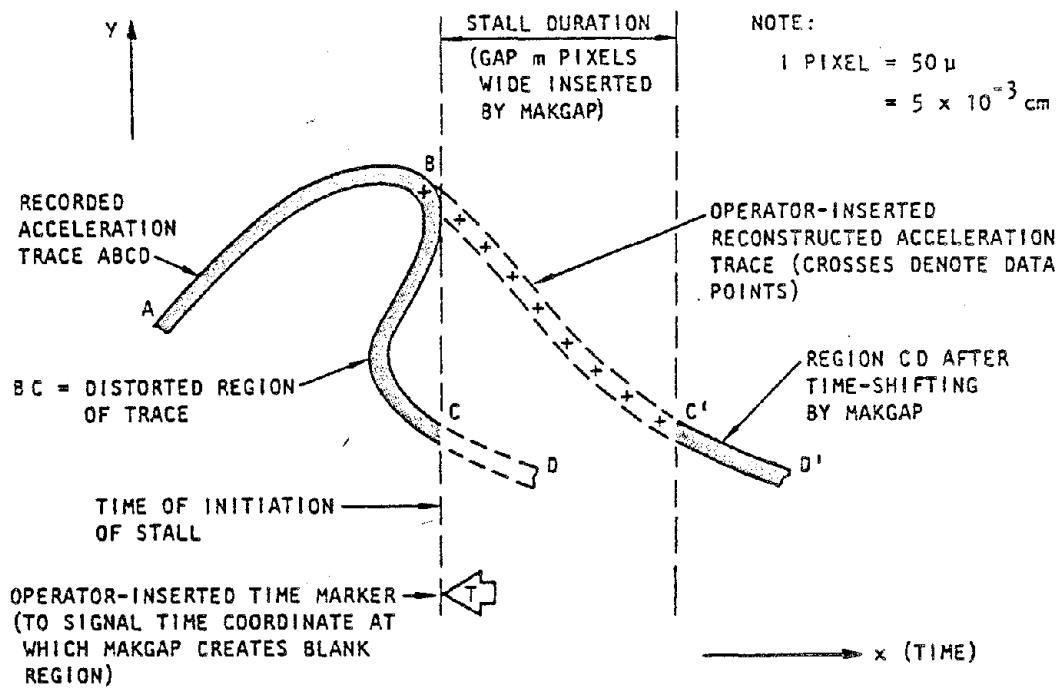
light intensities are measured. This scanning operation proceeds along the vertical axis of the film at 1 pixel (50 micron) intervals, and each light intensity reading greater than a chosen threshold level is stored onto a disk file for future use. After each vertical scan is completed, the light source moves 1 pixel to the right (along the horizontal axis of the film) and the above vertical scanning process is repeated.

This automated scanning operation was applied to the Meloland Bridge data until a region affected by a recorder stall was encountered; as previously noted, such stall effects were evidenced by a localized distortion of the Channel 1 to 13 acceleration traces displayed on the ARDS graphics terminal, and a discernable bulge in the time trace (Figure 8). When this occurred, the automated digitization process was temporarily halted, and the following manual procedures were conducted by the operator: (1) the distorted region of the film trace was enlarged on the graphics terminal; (2) from careful examination of this distorted region, the estimated time of initiation of the stall was defined by manual insertion of a time-marker at the appropriate pixel location along the time axis of the trace (Figure 8a); and (3) the duration of the stall was obtained by measuring (in pixel units) the amount of shortening of the time trace in the stalled region (Figure 8b). This procedure, repeated for each stall in the Channel 1 to 13 records, resulted in the identification of seven stalls with initiation times approximately 3 sec apart and with durations ranging from 0.04 sec to 0.25 sec (Table 1).

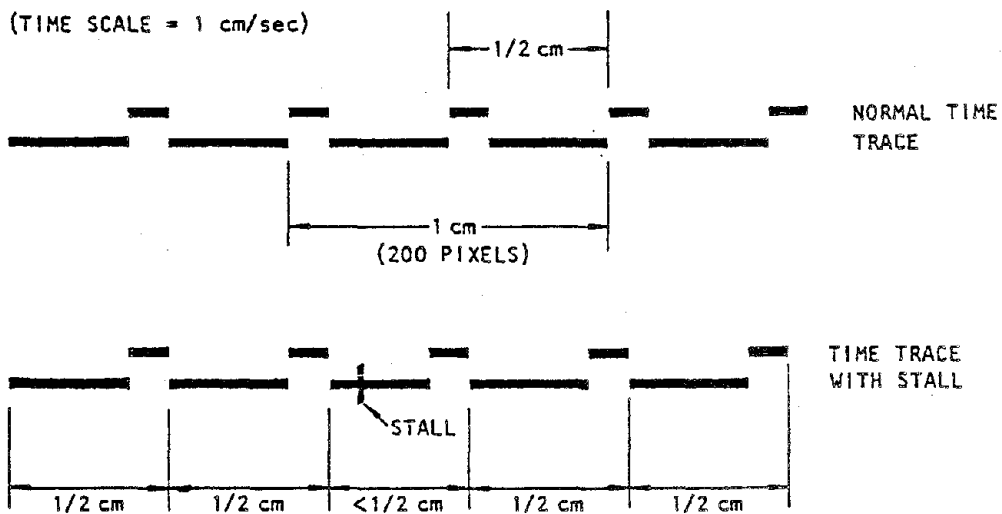
TABLE 1. RECORDER STALLS IN TRACES AT CHANNELS 1 TO 13 OF MELOLAND ROAD OVERPASS RECORDS

Stall Number	Initiation Time After Triggering (sec)	Duration of Stall (sec)	Width of Stall (pixels)
1	2.65	0.13	26
2	5.60	0.04	8
3	8.55	0.25	51
4	11.15	0.05	10
5	14.30	0.04	8
6	17.35	0.22	44
7	20.05	0.19	38

Program MAKGAP. The second part of this process involved the use of MAKGAP which, as indicated previously, was a special program incorporated in the ARDS software to facilitate the reconstruction of the motions that occurred during the recorder



(a) Acceleration trace



(b) Normal vs. stalled time trace

FIGURE 8. RECONSTRUCTION OF MOTION AT RECORDER STALL

stalls. MAKGAP served to correct the time coordinates of each digitized point of the acceleration trace by: (1) reading the data generated by FILM until one of the operator-inserted time-markers denoting the initiation of a stall was encountered; and (2) inserting an appropriate number of blank pixel bands so as to shift the time coordinates of every point beyond the flag, by an amount equal to the duration of the stall (Figure 8a). This operation was carried out for each stall identified in FILM.

Program TRACE. During the third part of this digitization process, the digitized data were automatically analyzed by the program TRACE in the following manner: (1) at each time location, it identified the coordinates of the mid-thickness of each acceleration trace (whose overall thickness was defined in terms of light intensity readings obtained from the vertical scanning process controlled by FILM); and (2) it defined each continuous trace segment on the film negative and assigned it to a particular file. When the traces were broken due to the gaps created by MAKGAP at each stall occurrence, TRACE assigned a new file number to each trace segment.

Program TV. The fourth operation in this digitization process involved editing of the acceleration trace data in the vicinity of the stalls to produce a continuous trace. This operation can be illustrated by referring to Figure 8a, which shows the original recorded accelerograph trace at a stall as curve ABCD, as well as the gap created by MAKGAP over the duration of the stall. The following steps were involved in the editing process indicated in this figure: (1) the operator deleted segment BC, which is the portion of the trace distorted by the recorder stall; and (2) the operator then inserted points to define a reasonable "corrected trace segment" over the duration of the stall, that connected the undistorted trace segments AB and C'D',* and created a continuous trace ABC'D'. This process was repeated at each of the seven gap locations for all acceleration traces (Channels 1 to 13) and for all fixed and other traces present on the film.

Program SCRIBE. In the final operation in this digitization process, the reconstructed accelerograms were plotted and written onto magnetic tape for subsequent data processing.

Data Processing

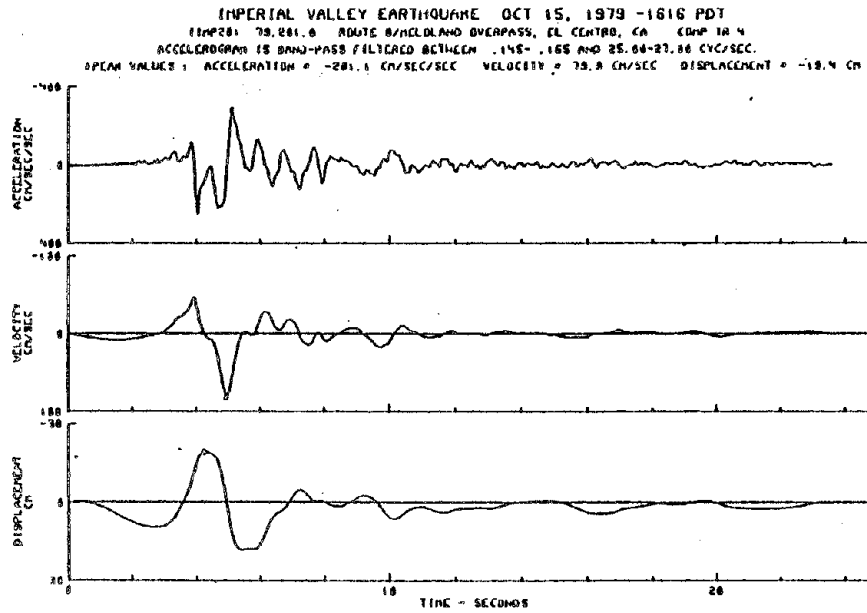
The processing of the data from the Meloland Road Overpass, after correction for the recorder stall effects, was carried out using standard USC software described by Lee and Trifunac (1979). This processing is briefly summarized as follows:

* Note from Figure 8a that segment C'D' corresponds to segment CD of the original acceleration trace, after it was time shifted by MAKGAP to account for the stall duration.

- "Volume 1" Processing. The "Volume 1" processing consists of various smoothing and scaling operations. These operations, however, represent a minimum interference with the basic data, so that the digitized data so obtained may be referred to as "uncorrected."
- "Volume 2" Processing. In this stage of the processing operation, the Volume 1 data are corrected for instrument frequency response and baseline adjustment, as described by Hudson (1979). This results in "corrected" acceleration, velocity, and displacement histories at each channel (Figure 9a). It is noted that the data from each channel of recorded motion at the Meloland Road Overpass was band-pass filtered over the same frequency range, so as to maintain consistency when all of the channels of data are used together in the subsequent modal extraction and parameter optimization tasks under this project.
- "Volume 3" Processing. In this final data processing stage, Fourier amplitude spectra and response spectra for damping ratios of 0, 2, 5, 10, and 20 percent of critical are obtained (Figure 9b).

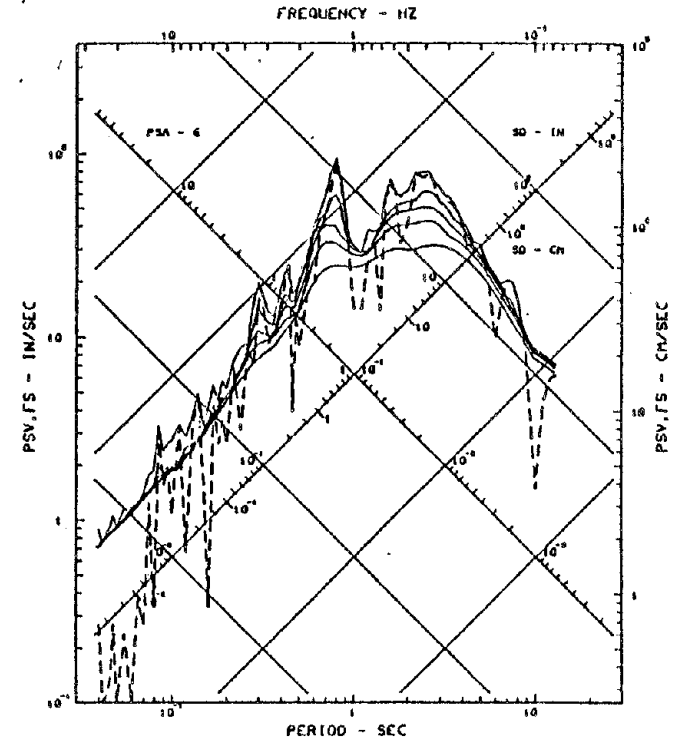
Discussion

The above process for reconstructing the bridge response during the recorder stalls utilizes state-of-the-art digitization hardware and software. Nevertheless, the end results of the process are clearly dependent on the judgment of the operator; i.e., different qualified operators may well interpret the bridge motions within the stalls somewhat differently. However, the relatively short duration of most of the stalls and clearly visible limits of maximum and minimum excursions of recorded acceleration were not difficult to interpret. In view of this, errors in the final digitized data, though certainly present, are believed to be small. This can be seen by comparison of motions reconstructed for stall effects (Channels 1 to 13) vs motions not affected by recorder stalls (Channels 14 to 26) at corresponding locations within the bridge/embankment system (Figure 10). Focusing on the overall displacement patterns and long period ground motions, it is seen that these motions are quite consistent, suggesting that the errors remaining after correction for the recorder stall effects are indeed small. Along these lines, it is fortunate that the stalls were as short



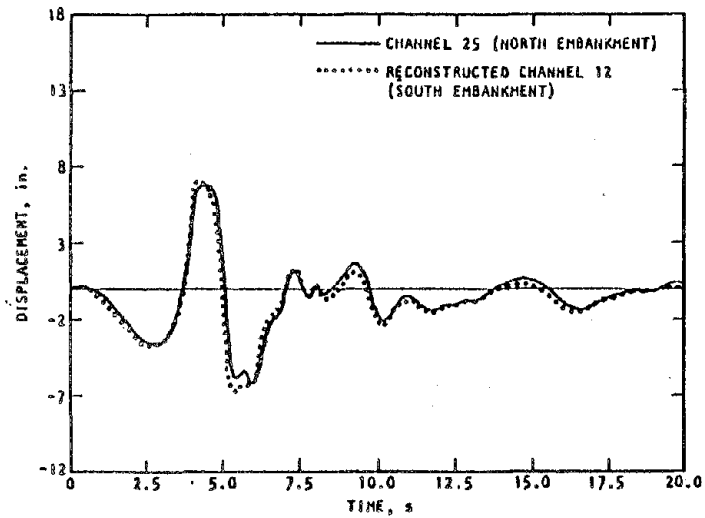
(a) "Volume 2" processing - corrected time histories

RESPONSE AND FOURIER SPECTRA
 IMPERIAL VALLEY EARTHQUAKE OCT 15, 1979 -1616 PDT
 STATION: 79.201.0 COMP TR 4
 ROUTE 8/MELOLAND OVERPASS, EL CENTRO, CA
 ACCELEROGRAM IS BAND-PASS FILTERED BETWEEN .145- .165 AND 25.04-27.06 CYC/SEC.
 DAMPING VALUES ARE 0, 2, 5, 10 & 20 A OF CRITICAL

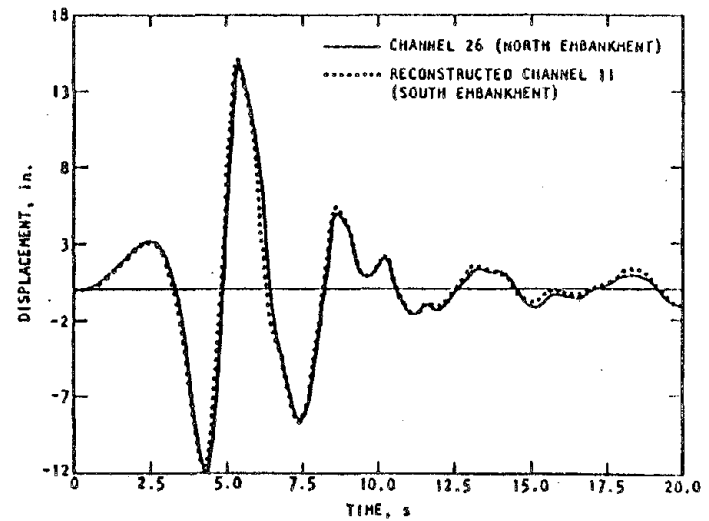


(b) "Volume 3" processing - Fourier and response spectra

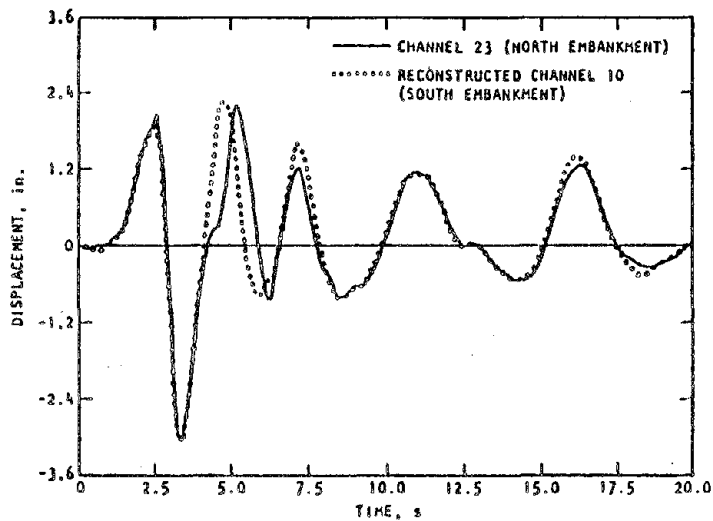
FIGURE 9. DATA PROCESSING OF STRONG MOTION DATA FROM MELOLAND ROAD OVERPASS - 1979 IMPERIAL VALLEY EARTHQUAKE



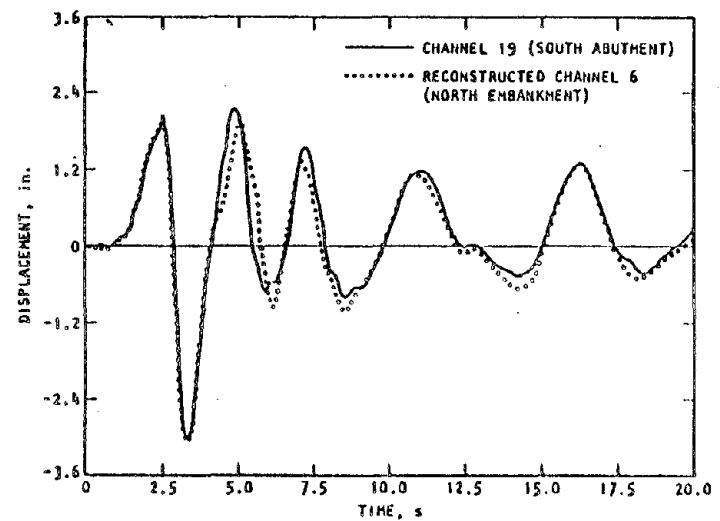
(a) Longitudinal motions - north vs. south embankments



(b) Transverse motions - north vs. south embankments



(c) Vertical motions - north vs. south embankments



(d) Vertical motions - North vs. south abutments

FIGURE 10. COMPARISONS OF RECONSTRUCTED MOTIONS OF MELOLAND ROAD OVERPASS WITH MOTIONS NOT AFFECTED BY RECORDER STALLS

as 0.25 sec or less,* and that the acceleration traces where the stalls occurred did not contain significant high frequency components. This greatly simplified the accelerogram reconstruction process.

PARAMETER OPTIMIZATION

Basic Approach

An important aspect of this research program will be to use parameter optimization methods to fit a finite element model of the Meloland Road Overpass to the measured bridge response. This basic approach to be followed in this effort is illustrated in Figure 11. The approach involves (1) using initial estimates of the bridge parameters in a finite element model, to compute the bridge response to the measured input motions; (2) comparing these computed motions to the measured motions, and quantifying any differences that may exist through the use of an appropriate cost function;† (3) if the differences between measured and computed motions are not sufficiently small, updating the bridge model parameters using state-of-the-art parameter optimization techniques; and (4) repeating Steps 1 to 3 until convergence occurs between measurements and computations.

Methodology

The parameter optimization methodology to be employed in the above process is a mathematical technique for minimizing a function of n variables (in which the function to be minimized corresponds to the cost function, and the variables comprise the structure parameters to be optimized). The coding of this methodology has been carried out and completed under this project, in the form of a program (named IDENT) with the following features:

* From Figure 8b, it is apparent that, if the duration of a stall were longer than 1/2 sec, it would not be possible to determine its actual duration, since a multiple of 1/2 sec could always be added without altering the appearance of the recorded time trace. Fortunately, all stalls encountered in the data from Channels 1 to 13 were less than 1/2 sec, as verified by perusal of the recorded acceleration traces, and by the comparisons shown in Figure 10 with records from Channels 14 to 26 (which were not affected by recorder stalls).

† Cost functions (of which several possible types are available) are typically defined as the root-mean-square difference between the measured and calculated response, summed and weighted over all response locations.

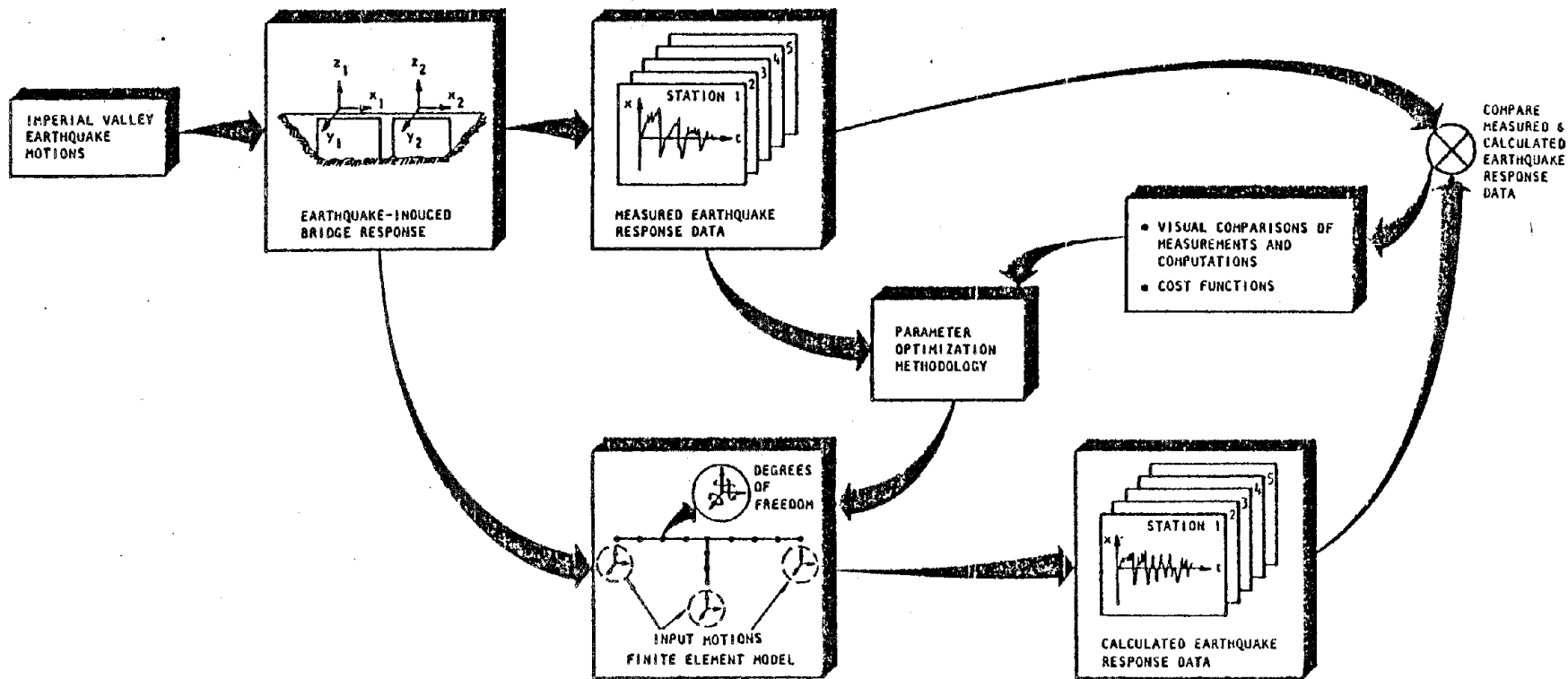


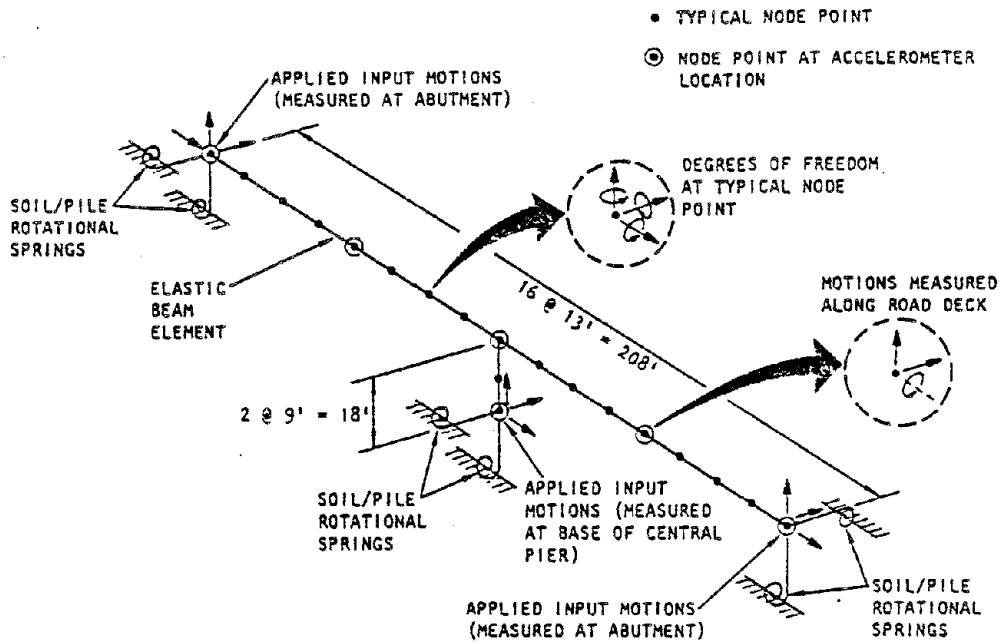
FIGURE 11. FITTING OF FINITE ELEMENT MODEL TO MEASURED RESPONSE DATA

- It is an unconstrained optimization technique, which uses the quasi-Newton optimization approach - an approach that is particularly suitable for handling the type of problems encountered in structural engineering applications.
- It can be coupled with any existing static or dynamic analysis program. (For this particular application, it is coupled with SAP7, an advanced version of the SAP family of structural analysis codes (USC, 1982).)
- It can be used with either linear or nonlinear models of the structural system. (For this particular application, the bridge model is assumed to be linear.)
- It can accommodate any reasonable number of data channels and parameters to be optimized.
- It can optimize according to any desired measure of the structure response (e.g., some measure of the response time history, or normal modes extracted from the structure response measurements).

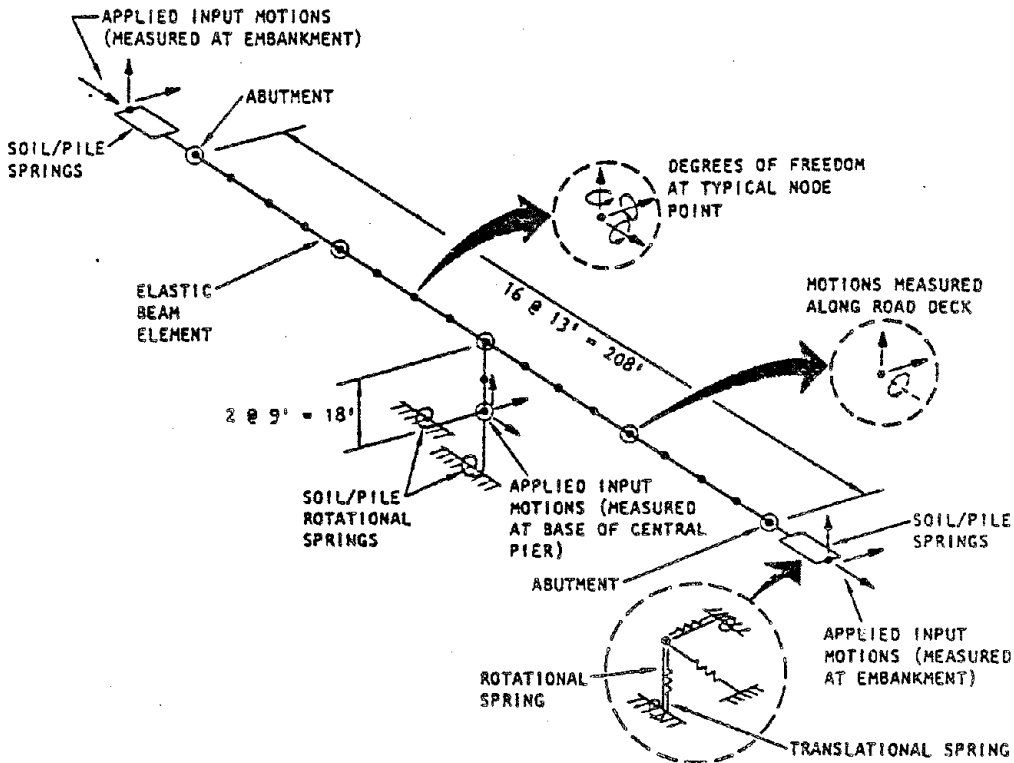
Application in this Project

Two alternative structure models being considered for optimization are shown in Figure 12. Each model is comprised of an assemblage of elastic beam elements to represent the bridge structure, and springs to model the end restraint imposed by the soil and piles at the abutments and at the base of the central pier. The two models differ in the location of the input motions and the particular type of soil/pile restraint imposed at the abutments. One model uses the measured abutment motions as input, in combination with soil/pile rotational springs (Figure 12a); the second model uses measured embankment motions as input, applied to the abutments through a series of translational and rotational springs (Figure 12b). The choice of one model over the other will be based on an assessment of the sensitivity of the bridge response measures to model characteristics.

To aid in the definition of parameters to be optimized, a series of sensitivity studies has been carried out. These sensitivity studies involved a simple model of the bridge (Figure 13a) and the use of SAP7 to extract normal modes of this bridge model. All of the system material properties, section properties, and boundary conditions were systematically varied, and the effects of these parameters on the natural frequencies of the first eight modes of this model were recorded (Figure 13b). From this, the following parameters were identified

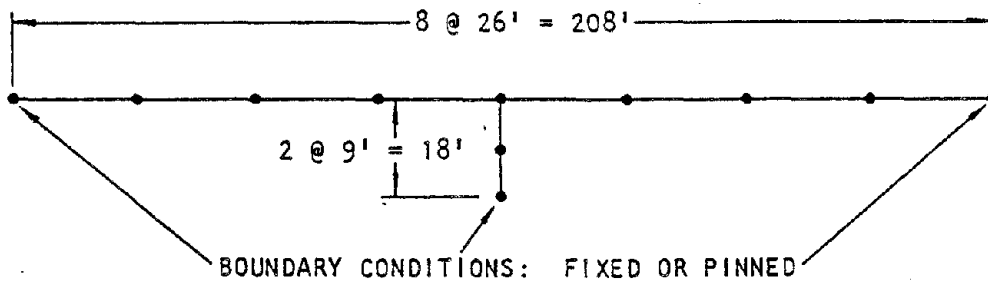


(a) Input motions at abutments and base of central pier

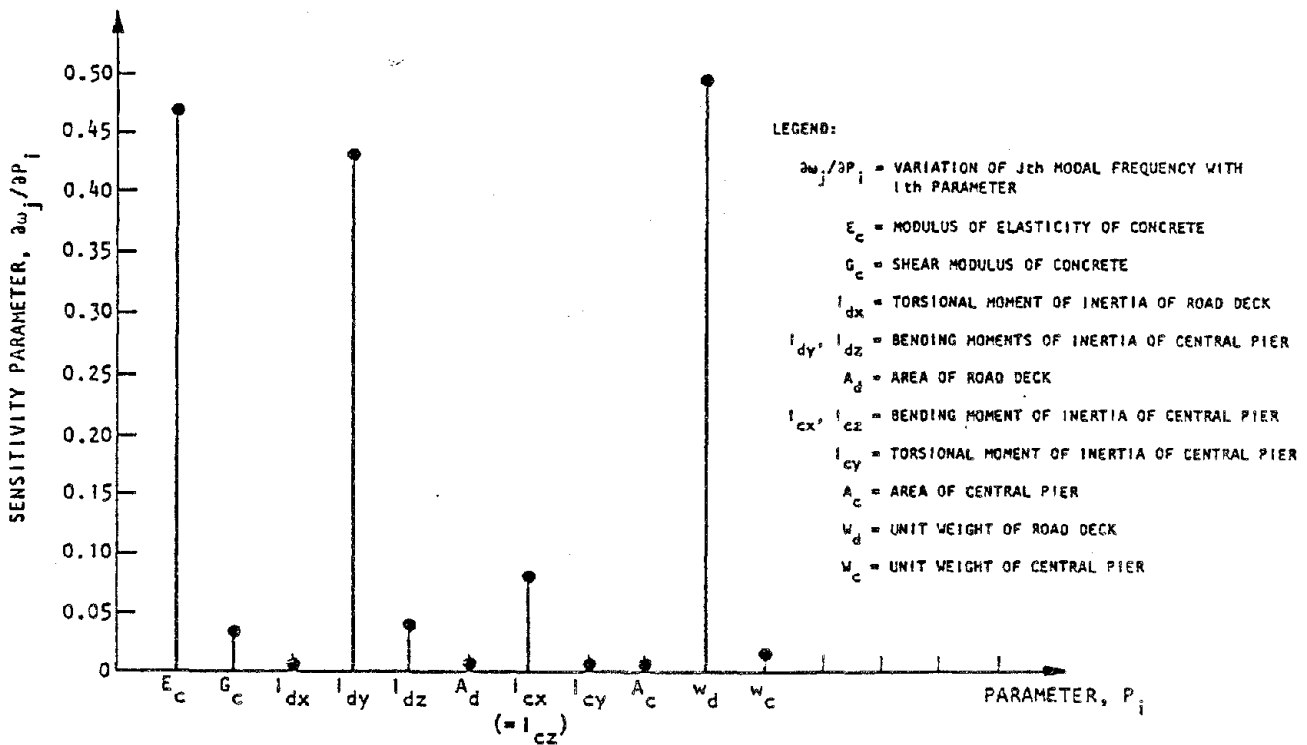


(b) Input motions at embankments and base of central pier

FIGURE 12. ALTERNATIVE FINITE ELEMENT BRIDGE MODELS



(a) Bridge model



(b) Sample results of sensitivity evaluation for first transverse bending mode (fixed-fixed)

FIGURE 13. SENSITIVITY STUDIES

as having a significant effect on the computed modal frequencies: (1) the soil/pile spring constants at the abutments and at the base of the central pier; (2) modulus of elasticity of concrete; (3) moments of inertia of the road deck - for bending in the transverse plane and the vertical plane; (4) shear area of the road deck - for transverse motions; (5) bending moment of inertia of the central pier; and (6) unit weight of road deck.

The final selection of the parameters to be included in the optimization process will be based on the results from the above sensitivity studies and, in addition, on practical considerations associated with limiting the array of parameters to be optimized to a reasonable size. Accordingly, where parameters shown to be important from the sensitivity study can be reasonably well defined from judgment, these parameters will be eliminated from the optimization process.

The optimization of the selected parameters will be directed toward defining a meaningful model of the bridge that will serve as a basis for the subsequent parametric analysis of the bridge response. An important part of the optimization process will involve evaluation of the sensitivity of the results to variations in (1) the form of the bridge response data (i.e., whether normal modes or time-history parameters are used as the basis for the optimization); and (2) the definition of the cost function, including its functional form and the factors used in weighting the parameters in the cost function. This aspect of the project should provide important insights for future optimization efforts pertaining to structural modeling and analysis.

MODAL EXTRACTION

An important means of assessing the seismic response characteristics of the Meloland Road Overpass is to extract its normal modes from the measured response data. The approach to be used for this purpose is a methodology named MODEX, which is an extended version of the Simultaneous Frequency Domain (SFD) technique originally developed by Coppolino (1981). MODEX identifies eigenvalues, eigenvectors, and damping ratios of the modes contained in measured response data for a linear dynamic system. The system can be subjected to a force excitation applied at a single point, and/or to distributed base motion excitations applied at multiple points along the length of the structure. The latter option has recently been incorporated into MODEX for particular application to the data at the Meloland Road Overpass (Coppolino, 1983).

The basic approach used to implement MODEX requires that the user identify specific frequency ranges over which he judges that significant modes may be present. This may be done by examining local peaks and phase shift gradients in the frequency response functions derived from the response measurements, as well as from coherence functions obtained from the measured data. MODEX is then applied separately to extract the modes in each of these frequency ranges.

On this basis, the MODEX procedure is derived through the following steps:

- (1) The system equations of motion in the frequency domain are expressed in terms of the real and imaginary parts of the N response measurements, for each of the frequencies that comprise the frequency range.
- (2) Standard numerical procedures are used to operate on these response measurements, in order to (a) define the number of modes, M , contained in the frequency range; (b) compute corresponding motions for a reduced set of M generalized coordinates; and (c) obtain a transformation matrix $[V]$ that interrelates the motions from the N response measurements and the M generalized coordinates.
- (3) Using the transformation matrix $[V]$, the equations of motion from Step (1) are re-expressed in terms of the computed motions of the M generalized coordinates. Then, the effective damping matrix $[C]$ and stiffness matrix $[K]$ that minimize the residuals of these equations are obtained using least squares fitting techniques.
- (4) A routine procedure for computing complex modes is then applied with $[C]$ and $[K]$ as input, in order to obtain the natural frequencies and damping ratios for the M modes, as well as the mode shapes in terms of the M generalized coordinates.
- (5) The corresponding mode shapes in the expanded coordinate system (i.e., in terms of the motions at the N instrument locations) are obtained by premultiplying the mode shapes computed in Step 4 by the transformation matrix $[V]$, as determined in Step 2.

CONCLUDING REMARKS

This paper has concentrated on various preliminary but vital operations leading up to our forthcoming evaluation of the seismic response characteristics of the Meloland Road Overpass under this project. These operations have included special digitization procedures to correct the recorder stall effects and reconstruct the motions recorded at several of the channels, and the development of state-of-the-art methodologies for modal extraction and parameter optimization. These particular procedures and new methodologies should be valuable, not only in this particular project, but also in future applications involving the interpretation of seismic response measurements.

In the forthcoming months, efforts will be directed toward the application of these methodologies to assess the bridge response characteristics indicated by the measured earthquake data. Detailed evaluations of the basic data, as well as dynamic parameteric analyses using finite element models fitted to the data, should provide important insights for seismic design and for evaluating seismic response characteristics of bridges. Of course, studies of this type would not be possible without the excellent prior planning for the deployment of this system of accelerographs by various agencies, engineers, and scientists marshalled under the California Strong Motion Instrumentation Program. Other bridges within California have also been instrumented as a result of these planning activities, and strong motion data have recently been obtained that should provide valuable supplements to the Meloland Road Overpass measurements (McJunkin and Turpen, 1980; Porter et al., 1983). The value of future planning activities of this type, not only for bridges but for other vital structures as well, cannot be overstated.

ACKNOWLEDGEMENTS

This project is being carried out through support provided by the National Science Foundation (Grant No. CEE-8111964), under the cognizance of J. Scalzi. This support is gratefully acknowledged. AA staff members who have contributed to this effort are S.D. Werner (principal investigator) and M.B. Levine (data and dynamic analysis responsibility). S.F. Masri, Professor of Civil Engineering at USC and part-time AA staff member, developed the parameter optimization methodology IDENT. R.P. Coppolino of Aerospace Corporation formulated and programmed the modal extraction methodology, MODEX.

The data digitization and processing were carried out by M.D. Trifunac and V.W. Lee of USC under a subcontract to this project. N. Kaliakin and J. Ragsdale of the California Division of Mines and Geology provided helpful information and support in this endeavor. J. Gates of CALTRANS provided extensive information, drawings, and data pertaining to the Meloland Road Overpass structure and foundation characteristics.

REFERENCES

- Brady, A.G. (1980) "Current Strong-Motion Ground Record Processing," *Proc. Workshop on Interpretation of Strong-Motion Earthquake Records Obtained in and/or Near Buildings*, UCLA Report No. 8015. Los Angeles: Univ. of California, Apr, pp 23-48.
- Brune, J.N. et al. (1982) "Strong Motion Data Recorded in Mexico During the Main Shock," *The Imperial Valley California Earthquake of October 15, 1979*, Geological Survey Professional Paper 1254, Washington D.C., pp 319-350.
- Coppolino, R.N. (1981) *A Simultaneous Frequency Domain Technique for Estimation of Modal Parameters from Measured Data*, Paper No. 811046, SAE Aerospace Congress and Exposition, Anaheim, CA, Oct.
- Coppolino, R.N. (1983) *User's Manual for MODEX*. El Segundo, CA: Agabian Assoc., in preparation.
- Degenkolb, O.H. and Jurach, P. (1980) "Highway and Bridge Damage, Imperial Valley Earthquake of October 15, 1979," *Reconnaissance Report, Imperial County, California Earthquake, October 15, 1979*, ed. D.J. Leeds. Berkeley, CA: Earthquake Engineering Research Institute, Feb, pp 85-96.
- Hudson, D.E. (1979) *Reading and Interpreting Strong Motion Accelerograms*. Berkeley, CA: Earthquake Eng. Res. Instit.
- Lee, V.W. and Trifunac, M.D. (1979) *Automatic Digitization and Processing of Strong Motion Accelerograms, Part 2: Computer Processing of Accelerograms*, Report No. 79-15 II, Los Angeles: Univ. of Southern California, Dec.
- McJunkin, R.D. and Ragsdale, J.T. (1980) *Compilation of Strong-Motion Records and Preliminary Data from the Imperial Valley Earthquake of October 15, 1979*, Preliminary Report 26. Sacramento: Calif. Div. Mines and Geology, Office of Strong-Motion Studies.
- McJunkin, R.D. and Turpen, C.D. (1980) *Strong-Motion Records Recovered from the Trinidad-Offshore California Earthquake of 8 November 1980*, OMS 80-11.1 (Preliminary Report). Sacramento: Calif. Div. Mines and Geology, Office of Strong-Motion Studies, Nov.
- Porter, L.D. et al. (1983) *Processed Data from the San Juan Bautista 101/56 Separation Bridge and the San Juan Bautista Freefield Records from the Coyote Lake Earthquake, 6 August 1979*, Special Publication 64, Sacramento: Calif. Div. of Mines and Geology, and Menlo Park: U.S. Geological Survey.

- Procella, R.L. et al. (1982) "Strong-Motion Data Recorded in the United States," *The Imperial Valley California Earthquake of October 15, 1979*, Geological Survey Professional Paper 1254, Washington D.C., pp 289-318.
- Rojan, C. et al. (1982) "Main-Shock Strong Motion Records from Meloland Road - Interstate 8 Highway Overcrossing," *The Imperial Valley California Earthquake of October 15, 1979*, Geological Survey Professional Paper 1254, Washington D.C., pp 377-384.
- Trifunac, M.D. and Lee, V.W. (1979) *Automatic Digitization and Processing of Strong Motion Accelerograms, Part 1: Automatic Digitization*, Report No. 79-15 I. Los Angeles: Univ. of Southern California, Dec.
- Trifunac, M.D. and Lee, V.W. (1983) Personal Communication to S.D. Werner, Agbabian Associates, El Segundo, CA, Feb.
- University of Southern California (USC). (1982) *SAP7 User Manual*. Los Angeles: USC, Structural Mechanics Research Laboratory, Jan.

BEHAVIOR OF THE MELOLAND ROAD OVERCROSSING DURING THE
1979-IMPERIAL VALLEY EARTHQUAKEBruce Douglas¹, Gary Norris², Lawrence Dodd³, and James Richardson³INTRODUCTION

The satisfactory characterization of bridge response data obtained for full scale structures from high amplitude or ambient tests does not necessarily mean that such models will correctly describe the earthquake response of these same bridges. Such issues as differences in excitation amplitudes and the legitimacy of using the free field motions as input to bridge models with these very simple foundation models remain open questions. To help deal with these questions, the extensive suite (26 channels) of earthquake response data obtained during the 1979 Imperial Valley earthquake for the Meloland Overcrossing (14) was used in conjunction with system identification methods to identify very simple bridge models which adequately explain the lateral behavior of this bridge during this earthquake. It should be noted that a comprehensive analysis of these data, including a reconstruction of the data lost when one of the recorders stalled, is being conducted by others (19,20). Smith (18) and Lisiecki (11) have also conducted detailed studies the response data obtained from this bridge.

The study of the Meloland Road data indicates that simple models appear quite capable of yielding sufficient accuracy for this earthquake. It should be noted here that this bridge, located within 1/4 mile (0.4km) of the rupturing fault, was subjected to 0.5g peak transverse structural accelerations while the free field ground within 200 feet (61m) experienced about 0.3g peak accelerations in the direction transverse to the bridge (14). Our analysis of this suite of earthquake response data indicates that the rotational stiffness of the pile foundation of the single column (Fig. 3 and 4) to be anomalously low. A careful geotechnical examination of the soils at the site indicates that this anomalously low rotation was most likely associated with the liquefaction or near liquefaction of subsurface sand layers/lenses, and that this foundation very nearly reached a condition of incipient collapse during this earthquake. Given the absence of surficial evidence of liquefaction and observable damage to the bridge, this condition has gone unrecognized until now.

It should also be noted here that the material presented herein is taken from a larger paper (5) submitted for publication to the ASCE.

Description: The Meloland Road Overcrossing (14) is a two span 208 foot (63.4m) long reinforced concrete box girder bridge located within one-quarter mile (.4 Km) of the Imperial Fault (Figs. 1,2,3,4). Twenty-six channels of strong motion data were collected (14) during this earthquake.

¹Professor and Director of the Center for Civil Engineering Research,
²Associate Professor, ³Graduate Research Assistant at the Civil Engineering Department, University of Nevada-Reno, Reno, Nevada, 89557, U.S.A.

The location and sense of all the accelerometers are shown in Figs. 2 and 3 taken from Ref. 14. Only the transverse response of this bridge was treated herein; thus only structural response accelerograms 2, 3, 5, 7, 9, 13, and the free field accelerogram 24 were used in this brief study. A post earthquake study (14) indicated that no structural damage was done, although the structure experienced peak transverse structural accelerations of 50 percent g and a peak ground acceleration in the transverse sense of the bridge of 30 percent g. The soil profile prepared from borings taken at the location of the single column is shown in Fig. 5. The central column is supported on twenty-five forty foot (12.2m) long timber piles spaced in a square grid at three foot (.91m) intervals. The bridge abutments were each built monolithically with the approach fills and supported on seven timber piles extending to about the same tip elevation as the piles of the central pier.

Simple Models and System Identification Results: Two very simple models were constructed to study the lateral responses of the Meloland Overcrossing. Figure 6a shows the simple model used for a phased input analyses of the bridge. It consists of a simple bending beam with 21 lumped mass nodes as shown. Provision was made in the model to accept three distinct out of phase accelerogram inputs indicated by V_1 to V_3 . These correspond to the recorded accelerograms numbered 3, 2, and 13 respectively. Accelerograms 3 and 13 were recorded at the bridge deck over the rigid abutment walls and were thus assumed to accurately represent the input pile cap motions at the abutment foundation. Accelerogram 2 represents the input motion at the base of the single column in the bridge. The springs K_{RA} , taken to be symmetric, represent the rotational soil/structure interaction effect at the abutment where the axis of rotation is vertical to the roadway. The spring K_{LC} represents the equivalent spring made up by combining the transverse structural stiffness of the column in series with the rotational stiffness of the central pile group. Provision to use different phased inputs included in the model (3), precludes the necessity of including additional springs to account for the lateral soil/structure interaction effects of the central pile cap and abutment pile caps for this case.

A second simple bending beam model was constructed to test the validity of using the recorded free field acceleration (record 24) as input to the bridge. In this case the model (Fig. 6b) was taken to be the same as that in Fig. 6a except that an additional node was added to represent the mass of the pier pile cap between spring K_{LC} and K_{LP} . The springs K_{LA} and K_{LP} were added to model the lateral soil/structure interaction effects of the abutments (with symmetry assumed) and the single pier foundation respectively. In this case V_g represents the free field accelerogram 24.

The original uncorrected accelerograms for this bridge contained 13 channels of data with stalls in them due to a recorder malfunction (14). Early stalls occurred at about 2 1/2, 5 1/2 and 8 3/4 seconds. The first stall at 2 1/2 seconds occurred during the initial low amplitude part of the accelerogram and can be seen as the straight line segments in Fig. 7.

The second stall occurred at about 5 1/2 seconds and was short in duration. The uncorrected accelerograms, as supplied by the California Division of Mines and Geology, were repaired by using a simple straight line connect between the missing segment of the record. The stall at 8 3/4 seconds was major and could not be ignored. Since the largest amplitude responses for the entire event occurred during the three to six second interval it was decided to study only the first eight seconds of these traces with the stalled traces repaired by the aforementioned straight lines. Others (36) have a project to reconstruct the stalled records.

A first system identification study was conducted to find the properties of the phased input model (Fig. 6a). Table 1 indicates the variables found in all of the system identification work associated with this study. The phased input model (Fig. 6a) was used to compute the first four variables in column 2 of Table 1. E is the modulus of elasticity of the concrete deck and ζ is the fraction of critical damping applied uniformly to all modes. The phased input system identification was conducted by computing accelerograms 5, 7, and 9 from the three input accelerograms 2, 3 and 13. The criterion function which was minimized, was the total error squared obtained by computing first eight seconds of the three output accelerograms from the three input accelerograms and summing all the error squared terms obtained by comparing the computed versus measured time series on a point by point basis. Minimization of the error squared function led to a very tight, well behaved, system identification solution for the four parameters sought. Fig. 8 shows the computed versus measured accelerograms (record 7) at the center of the bridge. The agreement between the measured and computed trace is excellent over the entire eight seconds of the trace. The accelerograms 5 and 9 exhibit equally good agreement. This excellent fit generated a great deal of confidence in the values obtained for the variables sought. These results will be discussed individually in a later section.

To test the hypothesis of using very simple models in association with the free field input, the free field model (Fig. 6b) driven by acceleration record 24 was used. The first case examined was treated by fixing E , ζ , K_{RA} , K_{LC} , (because they were all so well determined from above) and searching for the remaining three variables, K_{LA} the lateral abutment stiffness spring, K_{LP} the lateral central pier pile group stiffness and ϕ the phase delay (measured in seconds) of the free field time series. From Fig. 7, which compares the recorded bridge accelerograms 2 and 7 with the recorded free field accelerogram 24, it is apparent that there is phase delay in the free field record with respect to the bridge location. This makes sense because the free field station is nominally 200 feet further away from the fault than the bridge. The starting time of the entire free field record was delayed to define this parameter. From early computational runs over the entire eight second record it became apparent that a reasonable correlation would be obtained over the first 5.3 seconds of the record with obvious correlation difficulties being encountered for the remainder of the trace. At this point it was decided to conduct the free field system identification fit over the first 5.3 seconds of the record. Traces 2, 3, 5, 7, 9, and 13 were all computed from the free field trace 24. The criterion function which was minimized consisted of the total error squared produced by comparing the first 5.3 seconds of the

recorded and computed traces 2, 3, 5, 7, 9 and 13 and summing the squared error on a point by point basis.

The solution to this three variable problem in connection with a great deal of experimental data, proved to be non trivial. As opposed to the tight well behaved system identification solution obtained from the phased input model, this free field problem was more difficult to solve. Because of the importance of the problem, and because it was only a three variable problem, it was decided to "force" a solution. This effort included the formal use of the identification algorithm, trial and error, and a good deal of checking. The numerical results for ϕ , K_{LA} and K_{LP} are shown in column 2 of Table 1. Causes for the aforementioned difficulties will be discussed in a subsequent section.

Because the effective damping coefficient was so high relative to the usual damping levels associated with reinforced concrete bridges it was decided to check the result by seeking a different set of variables using the free field model. In this case the stiffness of K_{LC} and K_{LP} in series (this defines K) was taken to be fixed and the intervening nodal mass was taken to be a small nominal value. Then ϕ was fixed at 0.12 seconds and 0.14 seconds in two different trials. In each separate trial E , ζ , K_{RA} and K_{LA} were found by formal use of the system identification algorithm with accelerogram 2 left out of the error comparison leaving only deck level records. These two solutions were well behaved and gave the results indicated in columns 3 and 4 of Table 1. Again damping came in at the high levels, and the lateral stiffness of the abutment K_{LA} was relatively unchanged, but the deck stiffness as indexed by E increased while the abutment rotation spring decreased.

Figure 9 shows the comparison of the measured response at the center of the deck (record 7) and the associated response computed from the "best fit" three variable free field model described above and whose numerical values are listed in column 2 of Table 1. The time series correlations for the three models shown in Table 1 were about the same. The quality of correlation is representative of that simultaneously obtained for records 2, 3, 5, 9, and 13. The correlation is quite reasonable for the first 5.2 seconds of the record with the correlation collapsing at this point for the remainder of the 8 second record. This occurred on all the other traces as well. As will be discussed in more detail in the discussion section, the time at which the correlation stops at 5.2 seconds is the time when the sand lenses at the column in layer C (Fig. 5) may very well have undergone liquefaction in a sequential manner; thus, obviously causing abrupt changes in lateral stiffness which in turn causes the observed lack of correlation in Fig. 9.

Since the simple bending beam models in Fig. 6 were not space frames it was not possible to separate the structural stiffness from the foundation rotational stiffness. The spring K_{LC} contains both the effect of structural column stiffness and pier foundation rotational stiffness. The following hybrid procedure was used to successfully separate the rotational stiffness from the value K_{LC} . The natural frequencies of both the

free field (Fig. 6b) and the phased input model (Fig. 6a) defined by the properties listed in column 2 of Table 1 are given in Table 2 along with the values estimated by others (10) for this earthquake and ambient excitation. The foundation rotational stiffness was determined by constructing two SAP IV space frame models of the bridge corresponding exactly to the models in Figs. 6a and 6b except for an uncertain foundation rotational stiffness. This was found in both cases by adjusting the rotational stiffness in the SAP IV models until "perfect" agreement between the five natural frequencies listed in column 2 and 3 of Table 2 was achieved for each of the SAP IV models. This procedure gave the same value of K_{ROT} (the rotational stiffness of the foundation) from both SAP IV models. Transverse mode shape comparisons between the simple beam and SAP IV models were also made and found to be in superb agreement. This derived value of foundation rotational stiffness shown in Table 1 is an anomalously low value. In fact, it is about fifty times smaller than the smallest rotational stiffness found from field tests for any pile foundation at the Rose Creek bridge (6), and stimulated a serious look at the geotechnical liquefaction potential at this pier foundation.

System Identification Comments: In a previous section it was noted that the three variable free field system identification problem used to search for ϕ , K_{LA} , and K_{LP} was ill-conditioned. Figure 10 illustrates the difficulty, and more importantly it further emphasizes another pitfall which can be encountered when using system identification methods. The three variable free field system identification problem described above which gave the solution for ϕ , K_{LA} , and K_{LP} was used to construct Fig. 10. The variables ϕ and K_{LA} were fixed and the total error squared function vs K_{LP} is plotted with the circles in Fig. 10. The associated natural circular frequency is plotted as the triangles. The actual absolute minimum in error squared (the system identification solution point) is noted by the arrow.

From an examination of the natural frequency plot it can be seen that when K_{LP} is less than about 10^5 lb/ft (14.6×10^5 n/m), K_{LP} is effectively zero as far as the structure is concerned relative to the spring K_{LC} because the natural frequency remains constant. For all values of K_{LP} greater than about 10^7 lb/ft, K_{LP} is effectively rigid in comparison to the spring K_{LC} . The actual absolute minimum occurs well to the right of this value and is a relatively meaningless large number because K_{LP} can be any number greater than 10^7 lb/ft while the criterion function remains essentially unchanged. It is only in the region $10^5 < K_{LP} < 10^7$ that K_{LP} affects the solution and in this region there clearly is no minimum in the error squared criterion function.

If on the other hand, the value of rotational stiffness were not so abnormally low (on the order of a factor of 50), the algorithm would probably be capable of finding a reasonable lateral stiffness of the pile

group from this data set. In this case, it is the large contrast in the relative values of K_{ROT} and K_{LP} , driven by the physical condition of the foundation soils, which causes the system identification to give a misleading result.

Liquefaction Potential and Discussion of Results: The numerical results listed in column 2 of Table 1 labeled the "best fit" values will be discussed in order. The procedure to estimate the effective transverse moment of inertia of the deck of a reinforced concrete box girder bridge indicated in Ref. 9 was used for this bridge. The effective transverse moment of inertia for the Meloland Overcrossing deck was 65 percent of the gross moment of inertia. This was used in the model with the result that the deck concrete had a modulus of 5.43×10^8 lb/ft² or 3.8×10^6 lb/in². This value is consistent with an $f_c = 3900$ psi concrete. This value was obtained by assuming the unit weight of the concrete to be 150 lb/ft³, and is reasonable for a bridge with a specified strength of 3000 psi.

The effective overall damping value of 18 percent is a large number indeed for a conventional reinforced concrete structure operating in the linear range. The explanation for this is that the earthquake waves must arrive at the bridge deck (with a light mass per unit length relative to the mass per unit length of the approach fills) through the approach fills. The monolithic abutments attach the bridge firmly to the approach fills which may be thought of as earth dams or embankments where damping ratios of this magnitude are not uncommon (12). Damping levels of this magnitude, of course, much reduce the earthquake response of this class of bridge (monolithic abutments), and is a partial explanation of why this bridge was undamaged. During the highest amplitude field tests at Rose Creek the damping ratios were much smaller - on the order of three percent of critical (7,8); however, the Rose Creek Bridge did not have monolithic abutments. This extremely important observation needs to be further verified by studies on this type of bridge.

The spring K_{RA} has a very nominal value in relation to the value required to even partially restrain the bridge against this rotational degree of freedom. At this level it would not significantly affect the seismic response of the bridge.

The spring value K_{LP} has previously been discussed and discounted. Its numerical value is too large for any reasonable estimate of the pile group stiffness. The spring K_{LA} , on the other hand, greatly affects the seismic response of the structure. Table 3 indicates that the peak displacement of this spring during the earthquake was 0.46 inches (11.7 mm). Sack (15) also estimates the value of this spring constant from geotechnical considerations. At this same displacement Sack (15), obtains a value for K_{LA} of about half that shown in Table 1. At this point such discrepancy is attributed to an erroneously low estimate of the relatively large contribution of the abutment wingwalls to lateral stiffness. Such contribution should be increased significantly in association with the likely higher strength and stiffness of a desiccated soil crust not considered in the geotechnical analysis.

The spring K_{ROT} is about 50 times smaller than the smallest rotational stiffness observed for the Rose Creek interchange. This is an extremely low value relative to a geotechnical assessment of the rotational stiffness of the pile group with competent subsurface soil conditions. It must be remembered here, that the experimental $K_{ROT} = 8.5 \times 10^7$ lb/ft was derived from the phased input system identification solution which fit the observed responses extremely well (Fig. 8) over the entire eight second record and is thus a reliable experimental estimate.

Two points from the above discussion strongly suggested that a careful examination be made of possible changes in subsurface soil conditions during the course of the earthquake. They are:

1. The rotational stiffness of the central pier foundation derived from a reliable system identification solution is much lower than what might be expected for non-failing soil behavior.

2. The relatively good correlations exemplified by Fig. 9 obtained by using the free field input in a simple model collapse suddenly at about 5.2 seconds into the record, which suggests that some more or less abrupt change in soil behavior took place at this time. These two points in combination with the loose, saturated, silty sand present in the soil profile prompted a closer look.

The ensuing geotechnical analysis resulted in the following plausible explanation for anomalies 1 and 2. Evaluation of liquefaction potential was made following Ref. 17. A strict confirmation of the explanation proposed below will have to await a more detailed subsurface investigation.

The rotational resistance of pile groups derive from the vertical push pull of the piles about a center of rotation. Vertical resistance of the piles derives from skin friction/adhesion along the pile shaft and tip resistance at the point. Layer G (Fig. 5), consists of a clean loose sand interbedded with soft clay which is below the pile tips. The tips are bearing in the middle to lower portion of the liquefaction resistant layer F. Layer G liquefies on the rise side of the first large ground motion pulse at about 4.2 seconds. Treating the pile as losing tip resistance in layer F and shaft resistance in layers E and F due to liquefaction of layer G below, then the fully mobilized shaft resistance that remains relative to soil from the stiff clay layer (layer D) to pile top is about 59^k per pile. This yields a factor of safety of about 1.13 against failure under dead load given that the dead load per pile is about 52 kip (231 N).

Rotational resistance under such conditions is developed with account taken of the following:

1. Differences exist between compressional and axial vertical pile load changes or stiffnesses. Compressional resistance involving plastic strain at ultimate pile compressional capacity is much less than tensional resistance.

2. Corresponding to such differences in response, there is a shifting center of rotation.

3. Rotations occurring between maximum peak to peak horizontal accelerations (4.2 to 5.2 seconds into the record) are associated with a differential vertical displacement of 0.5 inches across the pile group. This corresponds approximately to the value computed from the dynamic response analysis listed in Table 3.

4. Associated with this is an accumulating average permanent downward vertical displacement of the pile group on the order of 3/4 of an inch (19 mm) at 5.2 seconds into the response.

With the foregoing conditions the secant rotational stiffness (peak to peak) is on the order of 6.4×10^9 lb. in = 5.3×10^8 ft lb. (7.2×10^8 n.m) which is about 6 times larger than the experimental system identification value given in Table 1. More importantly, this implies that the real factor of safety against vertical collapse of the pile foundation at the central pier under dead load drops to a value between 1 and 1.13 during the strong shaking phase of the earthquake.

The above accounts for the constant but extremely low value of rotational stiffness over the period four to eight seconds on the record. By contrast a possible explanation of why the correlation stops abruptly at 5.2 seconds into the record (Fig. 9) follows: The lateral resistance of the pile group derives from layers A, B and C near the pile top. Layer C is potentially liquefiable. Free field liquefaction response analysis yields liquefaction at 5.2 seconds where correlation stops in the free field response studies.

The assumption in the above geotechnical analysis is that: the sand interbedded with the clay in layer C is clean and that such sand occurs in strata which are continuous in horizontal extent. A compensating factor relative to such an assumption is that the sand is silty (increases liquefaction resistance) but most likely occurs in lenses rather than strata. Shear stress concentrations present at lens edges increases liquefaction potential. Assuming a lens thickness to be about one to two inches, liquefaction would yield a fluid interlayer that would require shear strains of say 20 percent for there to be a resumption of resistance. This implies a 0.2 to 0.4 inch lateral movement with no resistance. From comparison of measured and computed responses it appears that one lens then another fails and regains strength/stiffness sequentially throughout the record after 5.2 seconds.

It should be pointed out again that it is the sand present in the four foot thick layer G that liquefies such that one cannot count on tip and frictional shaft resistance of layers E and F directly above it. However, the pile loads carried in shaft resistance in layers A through C should be relatively unaffected by the liquefaction of layer G which is well below the base of the intervening stiff clay layer. Pile loads decrease along the length of the pile shaft down to the base of layer G and are differentially distributed outward in a pyramidal fashion.

Note that if the entire layer C were to liquefy all at once at 5.2 seconds as indicated earlier, the pile capacity would have been exceeded and the foundation on this bridge would have failed. This indicates that

the lenses in layer C failed sequentially decreasing resistance slightly but not allowing collapse of the foundation.

As far as the abutments are concerned, the same liquefiable layers under the abutment fills are less likely to liquefy due to the substantially increased overburden pressures associated with the fill; however, away from the fills these layers will behave as above. Furthermore, it may be that liquefaction early on of layer G filters out the high frequency content of the surface motions. The free field acceleration at this site is anomalously devoid of high frequency content as may be seen by comparing accelerograms given by Archuleta (2).

Meloland Ambient Vibration Observations: The ambient level (10) mode shapes and natural frequencies were examined in a crude fashion with the earthquake model (Fig. 6b - column 2 Table 1) for this structure. Without using a formal system identification solution the magnitude of the soil/structure interaction springs at ambient levels were found by scaling the spring values K_{RA} , K_{LA} , K_{LP} , and K_{LC} by a common factor in order to first fit the ambient fundamental frequency of 3.42 hz and then the second natural frequency of 7.32 hz. The factor by which the soil/structure stiffness parameters had to be increased to match the ambient fundamental frequency was 1.8 and 3.1 to match the second ambient natural frequency. A comparison of the mode shapes from these two models with the ambient mode shapes indicated that both the first and second mode shapes tended to fit the experimental ambient level mode shapes better with the higher factor. This indicates that a true system identification solution in the "eigen" domain would be weighted toward the upper value. For the present purposes, the increase in earthquake properties required for the ambient level springs was taken to be the midrange value of 2.5.

The ratio of the fundamental frequencies between ambient and the earthquake levels of excitation is 1.29, which according to the simple oscillator analogy demands a corresponding increase in total stiffness of 1.65. If for the sake of argument, it is again assumed that the soils contribute at least one half of the stiffness at ambient levels, the simple oscillator analogy requires that the increase in stiffness of the soil springs be about a factor of 2.3 which is in relatively good agreement with the above observation. Here again the amplitude dependent (nonlinear) nature of the soil/structure springs is graphically illustrated.

Simple Models For Earthquake Response: For the class of bridge under discussion herein the foregoing results strongly suggest that simple models with adjustable soil/structure interaction springs will give a satisfactory prediction of seismic responses. This will necessitate the use of an iterative displacement compatible solution approach suggested by Douglas and Norris (4) and is a procedure which has been used effectively in soil dynamics (16). This probably isn't too surprising when it is observed that the seismic response of this class of bridge is strongly influenced by soil/structure interaction phenomenon. It appears that the nonlinearities in the problem which arise by virtue of the nonlinear nature of the foundation soils may be treated in this way, but for situations where the structure yields or other substantial structural

nonlinearities are present, a true nonlinear model will be required.

In the single earthquake case discussed here it appears that the free field input can be used with acceptable accuracy with this simple model to predict the seismic response of the system. This has also been observed by Okubo and Iwasaki (13) in connection with studies of the Itajima Bridge in Japan.

Performance Observations: The Meloland Road Overcrossing was undamaged during this earthquake. The reasons for this are noted in this section. Table 3 contains the salient earthquake response results obtained from running various versions of the model. The result in column 2 gives the response results for the model defined in column 2 of Table 1. Column 3 gives the results obtained for a model which would have more reasonable column stiffnesses. In this case K_{ROT} was increased by a factor of 50 and K_{LP} decreased by a factor of 10 relative to the "best fit" case. Column 4 contains the results of the case where K_{LP} alone is reduced by a factor of 100 relative to the "best fit" case. Column 5 gives the results obtained from the "best fit" model using the North-South component of the well-known 1940 El-Centro accelerogram.

The column capacity is about 8000 kip-feet (11000 KN.m) based on the design strengths of the steel and concrete and the axial dead load. This could be ten to fifteen percent higher based on typical overstrengths of steel and concrete. As can be seen from the response results (Table 3), column moments were never near the ultimate capacity for any of the models. It should be noted, that this response result was not very sensitive even to very large changes in foundation stiffness.

On the other hand, the abutments in the models absorb most of the lateral seismic forces. For the models given in Table 3 the pair of abutments receive between 70 and 90 percent of the total lateral seismic load with associated lateral loads on the abutment piles ranging between 44 and 58 kips per pile. This gives rise to shear stresses parallel to the grain at the abutment pile tops in the range of 480 to 630 psi which is well above the allowable shear stresses in wood. Ameliorating circumstances would be the fact that the loads do not all transfer to the piles at the abutments but are shared by the total abutment structure, and factors of safety are relatively high.

On the other hand, it is fortunate that the effective damping level for this structure is as high as it is (18 percent). Had it been five percent, the response results in Table 3 would have to be increased by 50 percent. This would increase the lateral pile loads accordingly, and they are already exceedingly high.

The real threat to this bridge during this earthquake was the substantial loss of vertical pile capacity of the central pile group due to liquefaction of subsurface soils. Had such capacity been exceeded, the central pier could have dropped on the order of feet with obvious deleterious consequences to the bridge.

Phased Input Motions: Finally the sensitivity of the response re-

sults to phased ground motions was investigated. Figure 11 shows the relative maximum acceleration response of the center of the bridge as a function of the phase delay across the bridge. This curve was constructed by delaying accelerogram 13 by the amount shown in the graph with respect to accelerogram 3. Accelerogram 2 was delayed half the amount shown in the figure. The results indicate that absolute acceleration response could vary by about ten percent up or down for phase delays having a magnitude on the order of what was observed at this site. The optimized delay value shown in Table 1 for a 200 foot distance is 0.15 seconds.

This phenomenon needs to be studied in more detail, but it appears that for short stiff structures such as this, the effect of noncoherent (phased input) ground motions will only produce nominal changes in the response relative to that produced by coherent (uniform input) ground motions.

CONCLUSIONS

1. First it should be noted that the seismic response of this bridge during this earthquake and the El Centro record was entirely described by the fundamental mode of vibration. This is further corroboration of the unimodal analysis procedure adopted by the seismic design guidelines (1).

2. The 18 percent effective damping level for this bridge during this earthquake is an extremely important observation. This overall damping ratio substantially reduces the seismic responses. The appropriate damping levels to be used need to be further studied for bridges with monolithic abutments as well as for those without monolithic abutments.

3. A detailed liquefaction analysis of the subsurface soils at the site was conducted to shed light on the anomalously low rotational stiffness of the pier foundation. The results of this investigation indicate that the pier foundation was perilously close to collapse during this earthquake with obvious serious consequences to the bridge deck. Further detailed investigation of the subsurface soils at this site need to be conducted to conclusively establish the liquefaction potential.

4. If the liquefaction potential is born out by a detailed study of this site, this would strongly suggest that boring logs of existing bridges in highly seismic areas be pulled and systematically reexamined.

ACKNOWLEDGEMENTS

Our thanks go to John Ragsdale of the California Division of Mines and Geology for his help in obtaining the Meloland data, and to James Gates of the California Department of Transportation, for his many helpful comments and for extending his ambient vibration survey project to include the Meloland Bridge. Our special thanks go to our colleague Dr. Mehdi Saïdi for his assistance in assessing the capacity of selected reinforced concrete bridge members. This project was supported in part by the National Science Foundation under NSF grant numbers CEE-8245036 and CEE-8206224 and by a subcontract from the Earth Technology Corporation at Long Beach under an FHWA project number DTFH 61-83-C-00138. While these agencies have provided support for the project, the results and conclusion are those of the writers and do not necessarily reflect the views of the sponsors.

REFERENCES

1. Applied Technology Council, "Seismic Design Guidelines for Highway Bridges," Report ATC-6, Applied Technology Council, Berkeley, CA, 1981, 200 pp.
2. Archuleta, R. J., "Analysis of Near-Source Static and Dynamic Measurements from the 1979 Imperial Valley Earthquake," Bull. Seismic Soc. Amer., Vol. 72, Part A, No. 6, 1982, pp. 1927-1956.
3. Clough, R. W., and J. Penzien, Dynamics of Structures, McGraw-Hill Book Company, New York, NY, 1975, pp. 575-578.
4. Douglas, B. M., and G. M. Norris, "Bridge Dynamic Tests: Implications for Seismic Design", Journal of Technical Topics in Civil Engineering, ASCE, Vol. 109, No. 1, April 1983, pp. 1-22.
5. Douglas, B.M., G. Norris, M. Saiidi, L. Dodd, J. Richardson, and W. Reid, "Simple Bridge Models for Earthquakes and Test Data", University of Nevada Center of Civil Engineering Earthquake Research Preprint No. CCEER-1-84, 1984, 55 pp. Submitted for possible publication in the ASCE Journal of Structural Engineering.
6. Douglas, B. M. and J. A. Richardson, "Maximum Amplitude Dynamic Tests of a Highway Bridge," Proceedings of the Eighth World Conference on Earthquake Engineering, July 21-28, 1984 San Francisco, CA 8 pp.
7. Douglas, B. M., M. Saiidi, and J. Richardson, "Dynamic Response of Highway Bridges", Proceedings U.S.-P.R.C. - Bilateral Workshop on Earthquake Engineering, Harbin, China, August 30, 1982, pp. B-7-1 to B-7-15.
8. Douglas, B. M., M. Saiidi, J. Richardson, and J. Hart, "High Amplitude Dynamic Tests and Implications for Seismic Design", Proceedings 15th Joint Meeting of U.S./Japan Panel on Wind and Seismic Effects, UJNR, May 17-28, 1983, 22 pp.
9. Douglas, B. M., and W. H. Reid, "Dynamic Tests and System Identification of Bridges", Journal of the Structural Division, ASCE, Vol. 108, No. ST. 10, October, 1982, pp. 2295-2312.
10. Gates, J. H., and M. Smith, "Verification of Dynamic Modeling Methods by Prototype Excitation", Cal Trans Report, No., 1982, 192 pp.
11. Lisiecki, L. C. "Analysis of the Meloland Road Overcrossing Response to the October 15, 1979 Imperial Valley Earthquake; Master of Science in Engineering Thesis, University of California at Irvine, Irvine, Ca, 1982, 94 pp.
12. Makdisi, F. I. and H. B. Seed, "Simplified Procedure for Evaluating Embankment Response," ASCE JGED, Vol. 105, GT12, 1979, pp. 1427-1434.

13. Okubo, T., and T. Iwasaki, "Summary of Experimental and Analytical Seismic Research Recently Performed on Highway Bridges," Proceedings of a Workshop on Earthquake Resistance of Highway Bridges, the Applied Technology Council, National Science Foundation, January 29-31, 1979, pp. 567-601.
14. Rojahn, C., J. T. Ragsdale, J. D. Ragget, and J. H. Gates, "Main-Shock Strong-Motion Records from the Meloland Road - Interstate Highway 8 Overcrossing The Imperial Valley California, Earthquake of October 15, 1979 Geological Survey Professional Paper 1254, 1982, pp. 337-383.
15. Sack, R. L. "Lateral Stiffness of Pile Groups for Seismic Analysis of Highway Bridges," Master of Science Thesis, Clarkson College of Technology, Potsdam, NY, 1983, 142 pp.
16. Schnabel, P. B., Lysmer, J., and H. B. Seed, "SHAKE--A Computer Program for Earthquake Response Analysis of Horizontally Layered Sites," EERC--Report 72-12, University of California, Berkeley, CA., December 1977.
17. Seed, H. B., I. M. Idriss, and I. Arango, (1983), "Evaluation of Liquefaction Potential Using Field Performance Data," ASCE JGED, Vol. 109, No. 3, 1983, pp. 458-482.
18. Smith, M. J., "The Response of the Meloland Road Overcrossing to the Imperial Valley Earthquake of 1979," Master of Science Thesis, California State University at Sacramento, 1983. 200 pp.
19. Werner, S. and M. Agbabian, "Data Processing and Methodologies for Assessing Seismic Response Characteristics at Meloland Road Overpass," Proceedings of the Fifteenth Joint Meeting of U.S./Japan Panel on Wind and Seismic Effects, UJNR, May 17-28, 1983, 26 pp.
20. Werner, S.D., M. Levine, J. Beck, and S. Masri, "Seismic Response of Meloland Road Overpass", Proceedings of the First USA-Japan Bridge Engineering Workshop, University of Nevada Center for Civil Engineering Earthquake Research Report No. CCEER-84-2, 1984, pp. 140-142.

Table 1. System Identification Properties

Property and Units	Best Fit Values	Variation 1	Variation 2
E (lb/ft ²) *	5.43×10^8	7.27×10^8	7.37×10^8
ζ (%)	17.8	19.3	19.9
K_{RA} (lb·ft)	2.59×10^{10}	1.74×10^{10}	1.31×10^{10}
K_{LC} (lb/ft)	2.58×10^6	-	-
ϕ (sec)	.15	.12	.14
K_{LA} (lb/ft)	9.25×10^6	1.39×10^7	1.07×10^7
K_{LP} (lb/ft)	2.25×10^8	-	-
K (lb/ft)	2.55×10^6	2.5×10^6	2.5×10^6
K_{ROT} (lb·ft)	8.5×10^7	-	-
Metric Equivalents	$1 \text{ lb/ft}^2 = 47.88 \text{ N/m}^2$, $1 \text{ lb/ft} = 14.59 \text{ N/m}$, $1 \text{ lb} \cdot \text{ft} = 1.356 \text{ N} \cdot \text{m}$		

*Note: The effective moment of inertia was taken to be 65 percent of the gross transverse moment of inertia.

Table 2 Natural Frequencies of Simple Models
Shown in Fig. 10 (HZ)

Mode	Phased Input Model Fig. 10a	Free Field Model Fig. 10b	Free Field Model Ref. 6	Ambient Free Field Model Ref. 6
1	4.14	2.66	2.49	3.42
2	13.5	4.60	5.03	7.32
3	26.7	8.54	-	-
4	49.7	18.7	-	-
5	72.6	32.1	-	-

Table 3 Earthquake Response Results For Free Field Model

Column 1	2	3	4	5
Response Parameter	Input Earthquake and Model			
	1979 Imperial Valley; Best Fit Model	1979 Imperial Valley; Stiff Pier Foundation Model	1979 Imperial Valley; Soft Pier Foundation Model	1940 El Centro North; Best Fit Model
Abut. Reaction (Kip)	357	308	407	302
Abut. Disp. (in)	.46	.40	.53	.39
Col. Shear at Bottom (Kip)	153	269	97	133
Pile Cap. Disp. (in)	.0081	.14	.52	.0071
Moment Top Col. (K ft)	2730	2150	1340	2380
Deck Disp. at Centerline (in)	.73	.60	.87	.64
Moment Bot. Co. (K ft)	280	2990	139	244
Vert. Disp. of Outer Pile in Group (in)	.24	.05	.12	.21
Total Lateral Loads (%g)	44%	45%	46%	38%
Natural Frequency (hz)	2.66	2.94	2.49	2.66

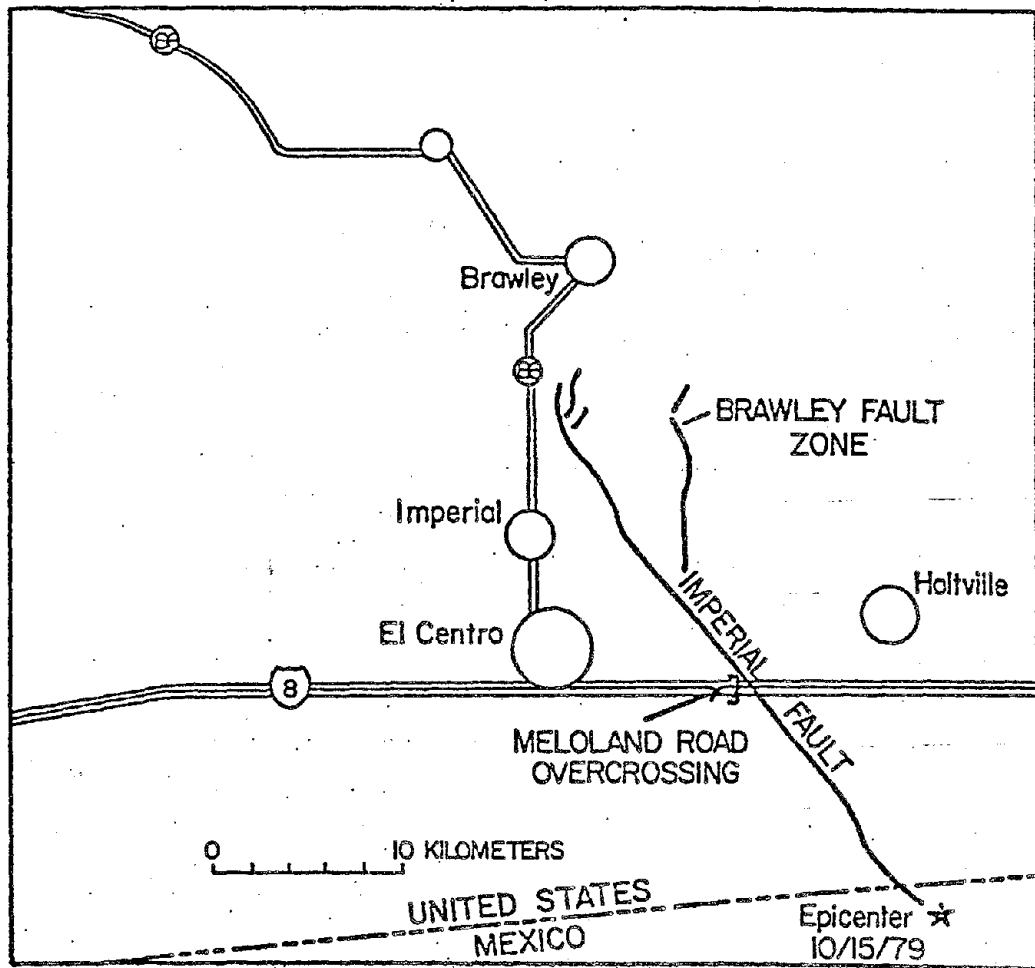


Figure 1 Location map for the Meloland Overcrossing (Ref.14).

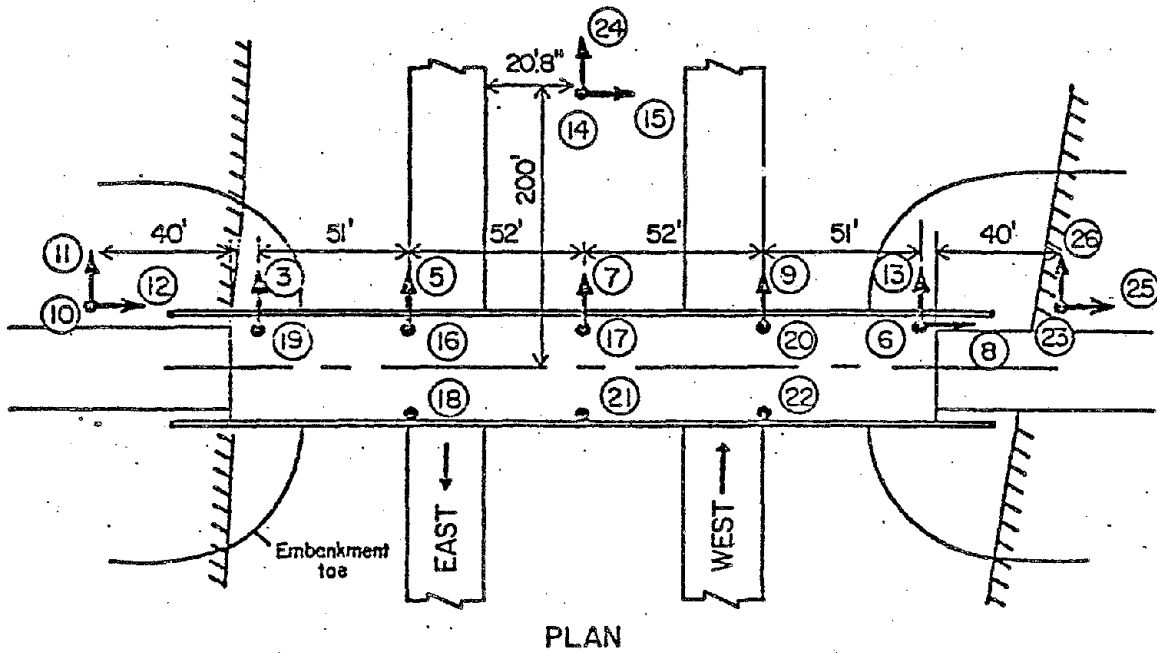


Figure 2 Plan showing the Meloland instrumentation locations (Ref.14).

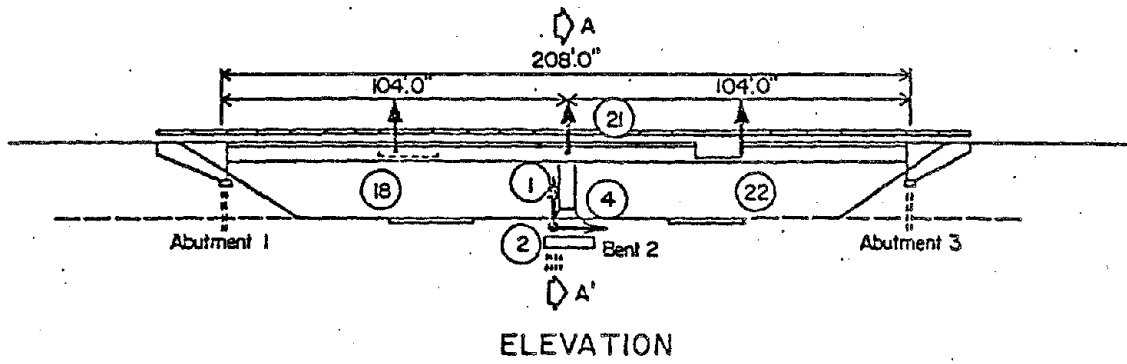


Figure 3 Elevation showing pile foundations (Ref.14').

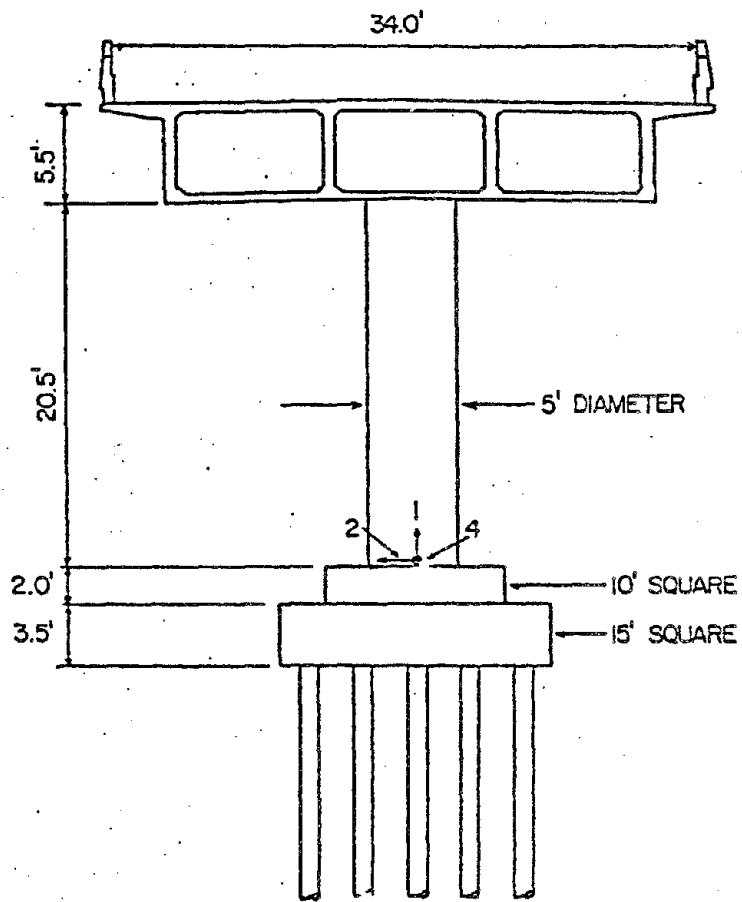
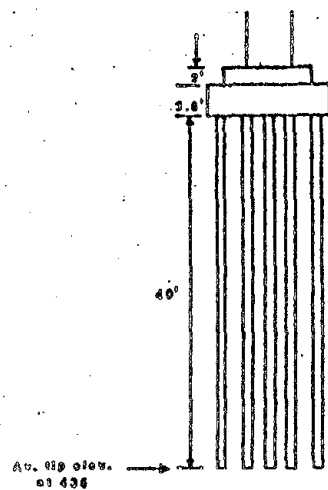


Figure 4 Section AA of Figure 7.



Final (Original Grade)	Layer	Field Recorded SPT Blow Count blows/ft	Stand Corrected Blow Count, N_1 blows/ft	Equivalent Silty Sand Blow Count, $N_1 \times 7.6$ blows/ft
489				
	Soft Sandy Clay			
478	A	8		
474	Compact Fine Silty Sand interbedded with Stiff Silty Clay	31	27	34.6
472 GW				
470	Slightly Compact Fine Silty Sand interbedded with Stiff Silty Clay (Sand 60% Clay 40%)	18	18	33.6
463				
	Stiff Clay	12 _{av} { 11, 13	—	—
448	Slightly Compact Silty Fine Silty Sand interbedded with Thin Stiff Clay Seams	14	13.5	21
440				
	Compact Fine Silty Sand	27	24	31.6
433				
428	Stiff Clay interbedded with Slightly Compact Fine Sand	14	12	—
		38 _{av} { 30, 21, 27		
418				
	Dense Silty Sand	62		

Figure 5 Soil profile at the central pier at Meloland.

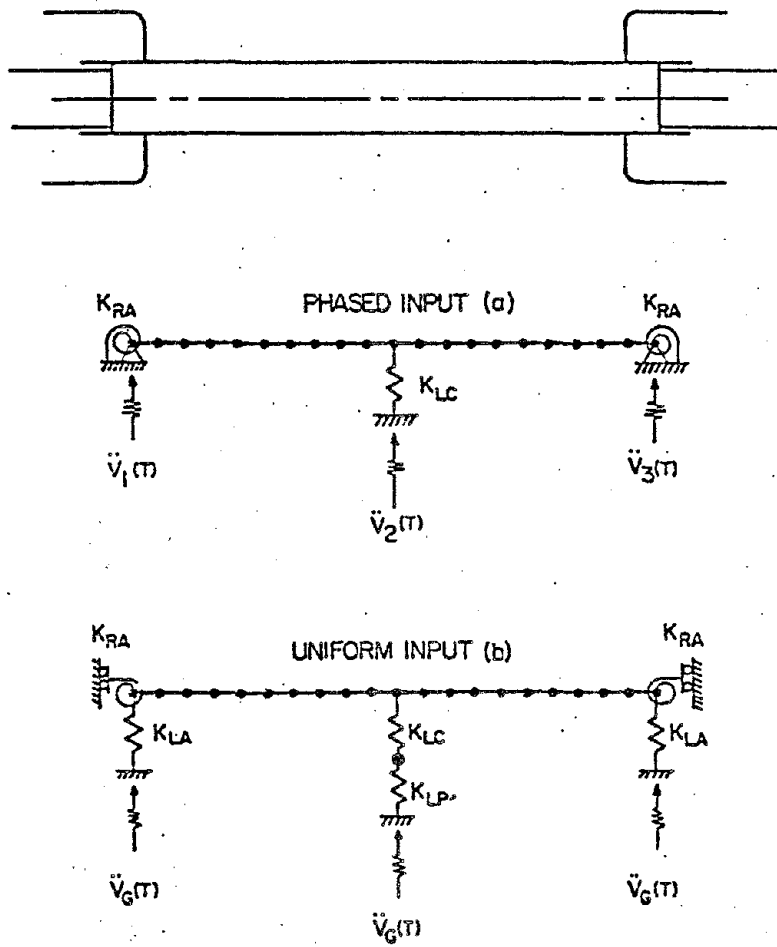


Figure 6 Meloland plan and associated simple beam models.

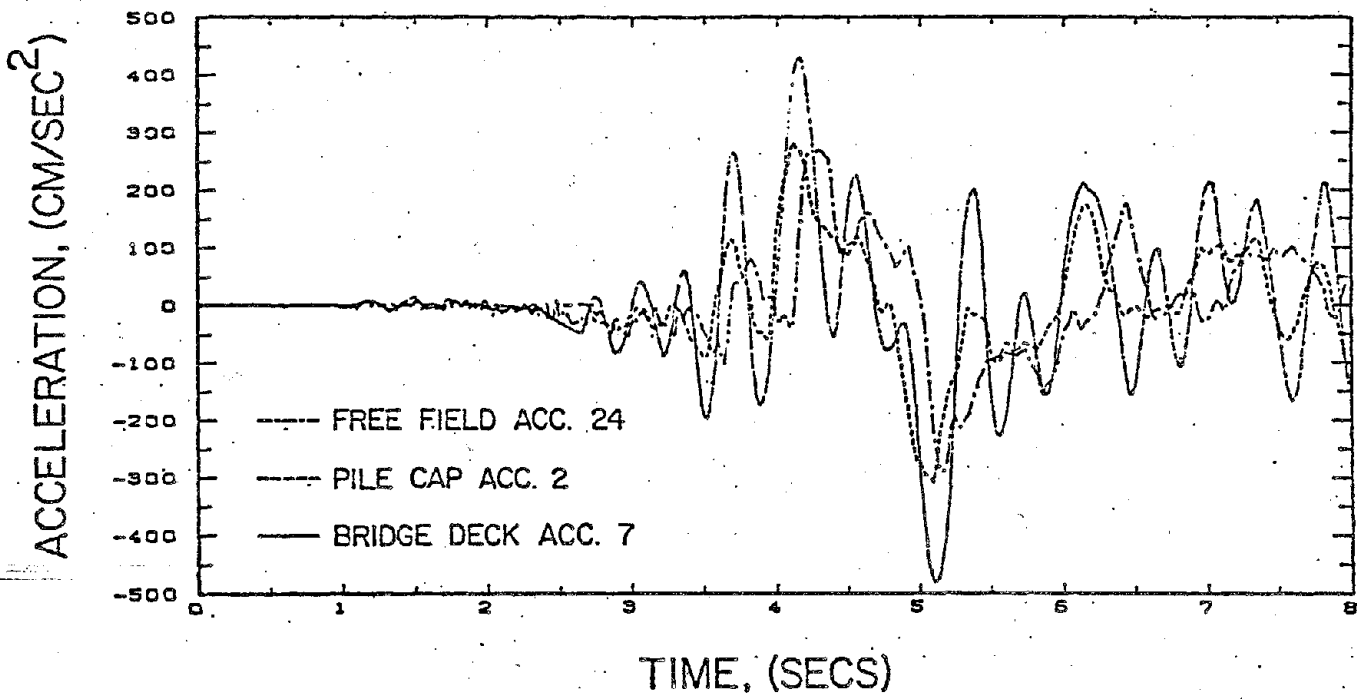


Figure 7 Recorded accelerograms showing phase shift of free field ground motion.

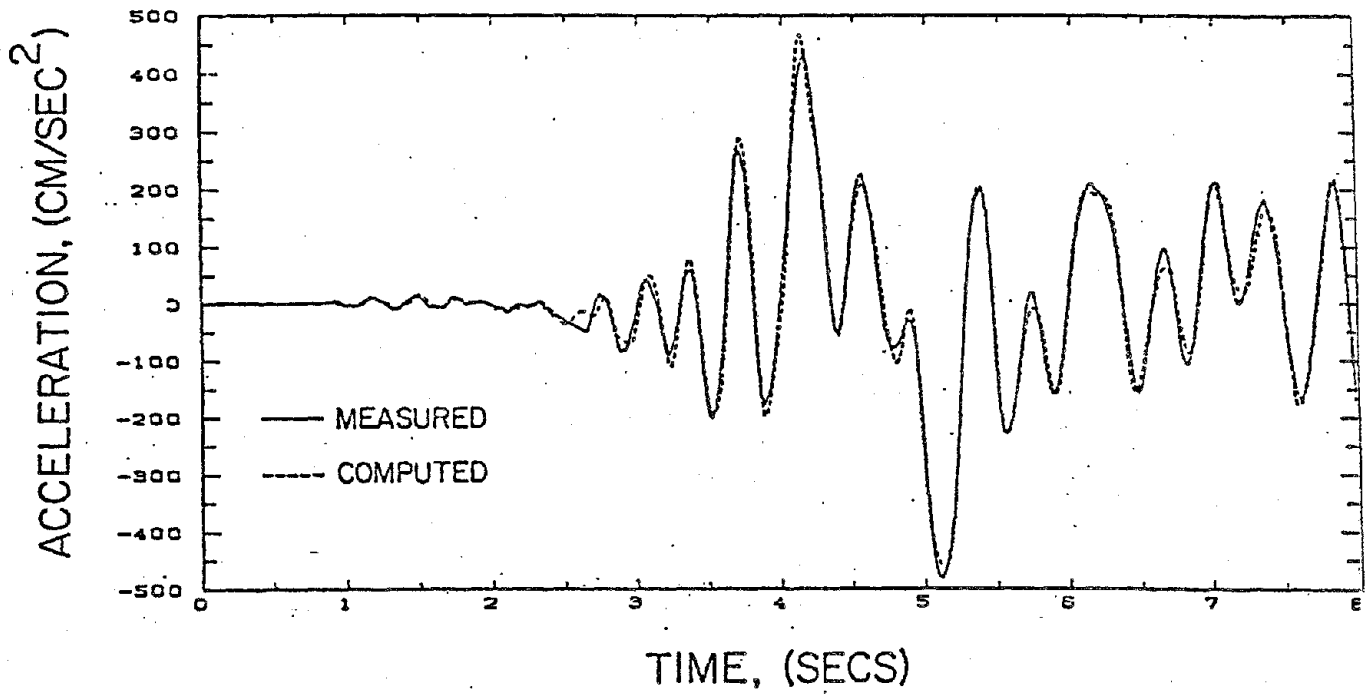


Figure 8 Phased input model computed response compared to the recorded acceleration response of the deck at the centerline.

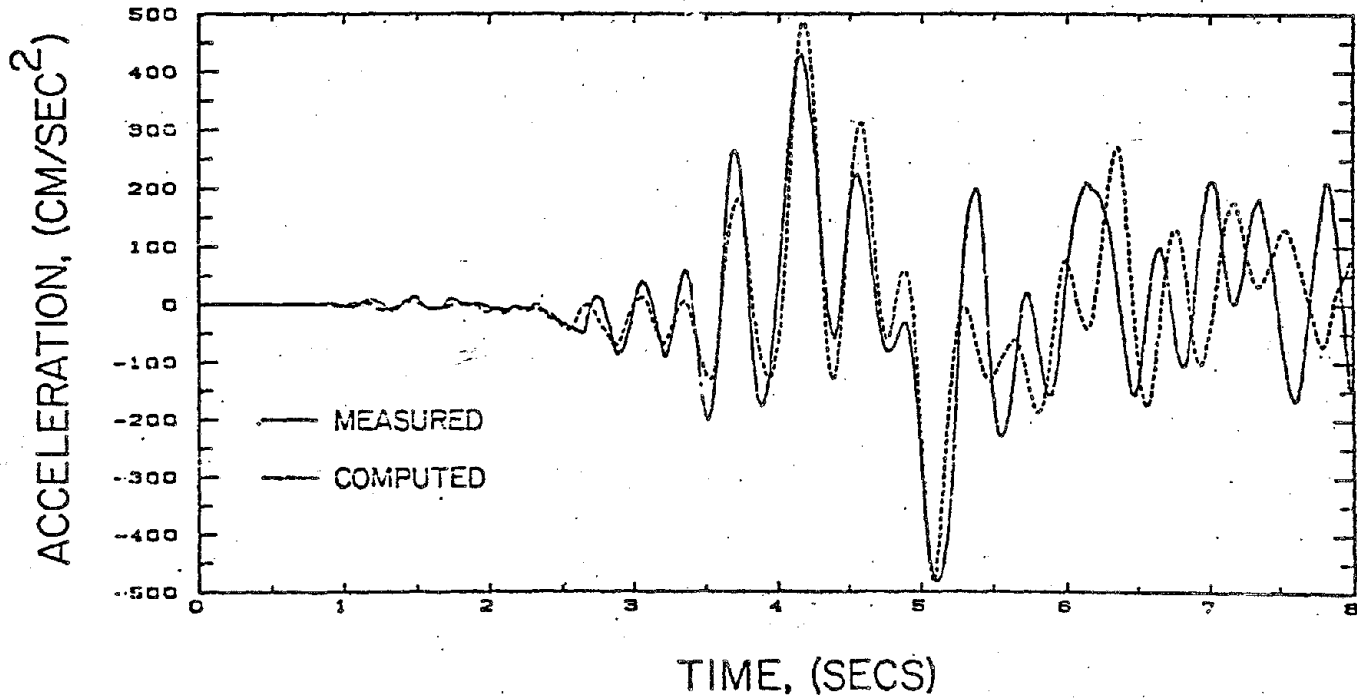


Figure 9 Free field model computed versus measured acceleration response of the deck at the centerline.

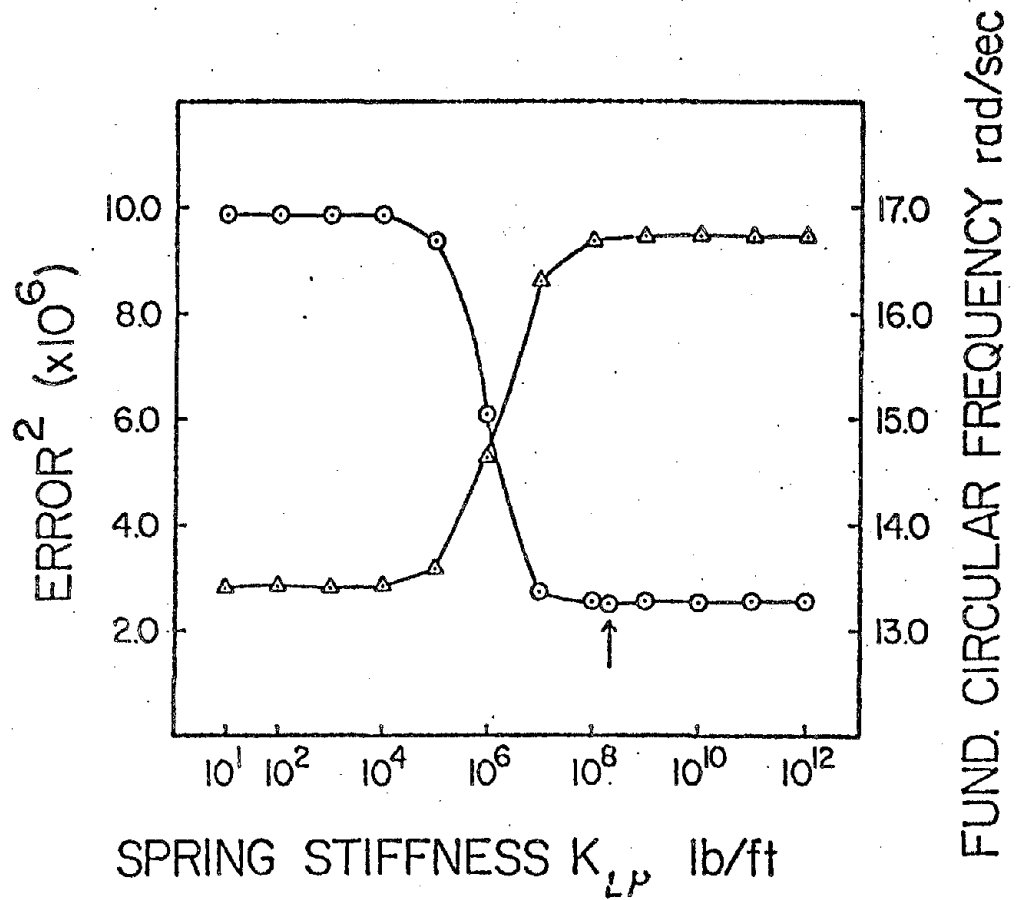


Figure 10 Error squared and circular frequency versus spring stiffness K_{LP} .

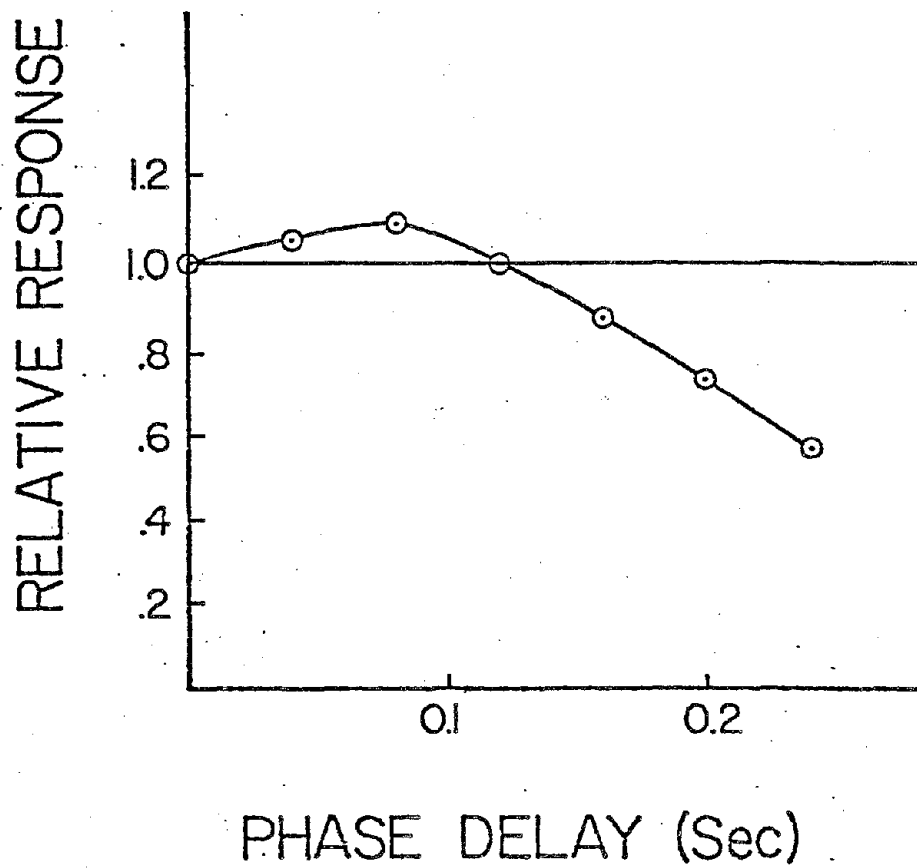


Figure 1] Relative maximum acceleration response versus phase delay (in seconds) for the Meloland Overcrossing.

RESULTS FROM HIGH AMPLITUDE DYNAMIC TESTS AND IMPLICATIONS
FOR SEISMIC DESIGN

by

Bruce Douglas¹, Mehdi Saiidi², James Richardson³, James Hart³

ABSTRACT

A dynamic field experiment to investigate distribution of lateral seismic loads on a 400 foot long reinforced concrete box girder bridge, carried out in May 1982, is described. Four hydraulic rams were used to induce dynamic loads by the quick-release method. The largest release loads used during the dynamic experiments had a magnitude of one and one-half times the design earthquake loads. Preliminary results indicate that damping may be fairly low for bridges of this type, and that the soil-structure interaction phenomenon plays a very significant role in the response of this fairly typical highway bridge.

INTRODUCTION

One of the significant problems bridge designers have when faced with making an assessment of the distribution of seismic loads on bridges is how to deal with the soil structure interaction question. A recent workshop held in New Zealand (1) indicates that this problem, particularly in relation to bridge structures, requires much more attention.

The importance of addressing the soil-structure interaction problem has been recognized by those researchers who have been concerned with the development of analytical models for bridges (11,12). A simple approach for taking account of the soil-structure interaction problem has been to use the extended column concept (2,3,4,16,17,18). Another approach has been to insert boundary element springs at the foundations allowing the appropriate degrees of freedom to approximate the behavior of the foundations (2,3,4,10,13,18). Other more involved foundation models have been used which include the finite element modeling of the soils in approach fills at the abutments (2,3,4) and lumped mass treatments of pile-soil systems (14,15,16). The Itajima bridge in Japan (14) has single caisson-piers for foundations, and this bridge has been instrumented with strong motion accelerographs to obtain the foundation response as well as free-field motions. Several earthquakes have been recorded and by modeling the pier-soil system with a lumped mass model, good agreement has been obtained between the measured seismic response of the pier and the seismic response computed from the model using the free field accelerograms as input. Other studies have included the effects of traveling waves in models where the soil is treated as an elastic half space (19,20). Dynamic tests on full-scale bridge systems have been conducted for the purposes of studying this soil structure interaction problem as well as identifying the salient dynamic properties of the structure (5,6,7,8,9,10).

1. Professor and Chairman, 2. Assistant Professor, 3. Graduate Research Assistant at the Civil Engineering Department, University of Nevada-Reno, Reno, Nevada 89557, USA.

Preceding page blank

Recently (May, 1982), a series of dynamic tests, at high load levels, were carried out on the Rose Creek Interchange at Winnemucca, Nevada. The purpose of this paper is to briefly describe this field experiment, present some of the preliminary results, and to briefly outline some of the analytical and system identification methods and results used to interpret this data.

DESCRIPTION OF THE BRIDGE

This bridge is a 400 foot long symmetrical reinforced concrete box girder bridge (Figs. 1 and 2) which is located on highway I-80 about 10 miles southwest of Winnemucca, Nevada. The piers and abutments are supported on pile foundations because the soil profile consists, in general, of a layer of relatively soft clay over a layer of stiffer clay on sand and gravel. The piles are reinforced concrete in steel shells, and they are about 25 feet long. The deck is supported at each of the abutment foundations by elastomeric bearing pads.

DESCRIPTION OF EXPERIMENT

The basic methodology used to conduct the dynamic tests was the pullback and quick release method (5,9,10). For this experiment, a hydraulic ram (Fig. 3) was used at each of the bridge piers to deform the structure prior to the simultaneous quick-release of the ram hydraulic fluid, which produced the lateral dynamic motions. Lateral forces on the bridge were produced by inclining the rams at a forty-five degree angle to thrust between an auxiliary reinforced concrete reaction foundation and the bridge superstructure. The largest lateral load used during the experiments was one and one-half times the design earthquake load. The AASHTO code under which the bridge was designed required a 6 percent of gravity lateral load to account for earthquakes.

One of the advantages of using this method is that the lateral static response of the bridge could be obtained as a by-product of the dynamic tests. Selected lateral static deformations of the bridge were measured along with the complete suite of dynamic data to observe the in situ dynamic translational and rotational response of pier foundations. The pier foundations were excavated to expose the pile caps of all piers.

The complete dynamic response of the structure including its foundation elements was measured with a four channel system with four force balance accelerometers. The data was recorded on an FM tape recorder for later digitization and analysis. Measurements of all dynamic data were taken at a given release load level using a "fixed" reference accelerometer and a triplet of "moving" accelerometers. Data was recorded at stations 15 feet apart on the bridge deck. In addition, the motions of the bridge abutments were recorded along with the rotation and translation of each pile cap of the pile foundations at the base of each pier. For each different setup of the accelerometers, the bridge was reloaded and the four rams quick-released to produce vibration. A complete set of dynamic data for a given load level required 14 separate loadings and quick-releases to "sweep" over all the required measurement stations.

This bridge structure offered a unique opportunity to study the effect the approach fill produced on the response of the structure. The ends of the bridge are supported on elastomeric bearing pads in such a way that the ends of the bridge deck may be fixed to the bridge abutment by inserting a special device, or left free to move on its elastomeric bearings. Because of this fortunate occurrence, the bridge was made to behave as two separate structures: one with ends floating on its elastomeric pads at the abutment, and the other with ends fixed in the transverse sense. Of course, no attempt was made to block the rotational degree of freedom of the deck with respect to the abutment.

The principal ram release loads and configurations of the structure used during these experiments are summarized in Table 1. Sixteen different load/structure configurations were used during the course of the experiment for the purposes of obtaining structural mode shapes. Each configuration listed in the table required 14 different quick-release excitations to "sweep" the moving accelerometers over the entire structure. In addition, other special purpose data was taken. In all, the bridge was subjected to more than 230 separate quick release excitations during the course of the experiment.

DESCRIPTION OF DATA

Typical accelerograms of the horizontal vibration of the deck obtained during the experiment are shown in Figs. 4 and 5. Fig. 4 shows the accelerogram obtained at the centerline of the deck when the bridge was loaded symmetrically with a total horizontal load equal to one and one-half the design load (Line 13 Table 1). Fig. 5. shows the deck response, obtained 90 feet from the bridge centerline, when subjected to the unsymmetrical loads shown in line 14 of Table 1. The influence of higher modes can be seen more clearly in this figure. Fig. 4 shows that higher mode response dies out very rapidly when the bridge was excited with symmetrical loads, and that the later portion of the accelerogram is almost a pure unimodal response in the fundamental mode.

This unimodal character of a subset of the dynamic data was a fortunate occurrence because it allowed a substantial amount of preliminary interpretation of the data to be made without the use of complex digitization and Fourier transform techniques.

In addition to the dynamic data, selected transverse static displacement measurements of the bridge were made prior to the quick-release excitations. Transverse displacements at the bridge, at the deck centerline and ends of deck at the abutment were made with dial gages. The lateral displacements of the deck at each of the piers were obtained reading a micrometer screw target with a theodolite.

METHODOLOGY OF PRELIMINARY ANALYSIS

As noted above, the unimodal character of the fundamental modal response for the symmetrical loading cases allowed significant interpretation of the data to be made directly from the time series rather than requiring that the data be carefully digitized and analyzed with the aid

of Fourier analysis. Damping was estimated by using the logarithmic decrement approach averaged in a least squares sense over 10 cycles of unimodal response. The fundamental period was also obtained by simply finding the time required for 10 cycles of fundamental modal vibration to take place. Fundamental mode shapes were calculated by computing the peak to peak amplitudes of the last half of the third cycle of vibration in the fundamental mode. All these amplitudes were normalized by those obtained at the reference station near the bridge centerline to generate modal displacements.

RESULTS

a) Damping: A preliminary analysis of the fundamental mode damping ratios of the structure versus ram release load is shown in Fig. 6. The upper curve presents the damping ratios for the fundamental mode of the structure when the abutments were unlocked thus mobilizing the elastomeric bearings. The lower curve gives the damping ratio when the ends of the deck were locked to the abutment in the transverse sense of motion. Each damping value was estimated twice from accelerograms taken at the center of the bridge and the quarter point of the deck for a given excitation. It can be seen that agreement between the elements of each pair of damping determinations is quite good. Additionally, Fig. 6 shows that the damping ratio obtained for the bridge in the locked state is less than that for the free state. This is to be expected since the response of elastomeric pads is hysteretic and this slight additional energy absorption capacity was mobilized in the unlocked state. In addition, Fig. 6 indicates that the damping ratio increases slightly with excitation level. Finally, it should be noted that the magnitude of damping over the entire range of loads up to one and one-half times design is quite small (only about three percent of the critical damping ratio).

(b) Fundamental Period. Figure 7 is a plot of the fundamental period of the structure versus ram release load when the structure was in the unlocked configuration. This figure shows that the fundamental period increases slightly with excitation level. Both Figs. 6 and 7 show that the response of the structure is slightly nonlinear over the range of vibration amplitudes studied.

c) Fundamental Mode Shapes. Fundamental mode shapes were calculated for all the symmetrical loading cases by the procedure indicated above. Fig. 6 contains the mode shape when the ends of the deck were locked to the abutment and all four ram release loads were 56 tons, producing a total lateral load of one and one-half times the design earthquake load. The numbers along the horizontal axis of the graph represent the stations along the deck where transverse acceleration measurements were made. The solid circles represent the modal displacements of the deck, the open circles represent the transverse modal displacements of the foundation elements, and the solid lines between the open circles and solid squares represent the contribution to modal displacement of the deck due to the rotation of the pile caps. The actual modal rotation may be estimated by dividing the modal displacement contribution by 25 feet. The significant result to be observed in this diagram is that the foundation flexibilities at the piers contribute in a

major way to the total flexibility of the structure. From the diagram it is clear that approximately 70 percent of the modal displacement of the deck at piers 1 and 4 is due to foundation flexibility while at piers 2 and 3 about 50 percent of the modal displacement of the deck can be attributed to the flexibility of the foundations. This is a direct measurement of a result which was inferred indirectly from previous quick-release experimental data used in conjunction with system identification techniques (5,10).

d) Static Load Deflection Curves. Figure 9 shows a plot of ram load versus the lateral central deflection of the deck. These curves were developed from data taken before and after dynamic series indicated in Table 1 by LS on May 28, 1982. At this point in the experiment the bridge had been excited by the quick-release method at least 200 times. The curve indicated by the circles was generated before the above dynamic load series and the one indicated by the squares was generated after the 14 excitations required by the dynamic series. The curves through the data points represent second degree regression curves. As it can be seen, the curves are very similar. When these curves are compared to similar static load deflection curves generated at other load levels, no significant difference in slope can be detected. This result suggests that the bridge is exhibiting only slight nonlinear behavior for loads up to one and one-half times the design load and that the cyclic degradation effect upon these curves is minimal.

e) Integration of Accelerograms - One of the major difficulties encountered when attempting to integrate accelerograms twice to calculate displacement time histories is the fact that often the exact initial conditions of motion are unknown. This is not the case with accelerograms generated by the quick-release method of vibration testing (See Figs. 4 and 5). A preliminary analysis of the accelerogram data obtained from the field experiments indicates that it will be possible to estimate the initial static displacements at the time the loads are released to within about 5 percent to 10 percent accuracy by doubly integrating the accelerograms using fairly unsophisticated baseline correction procedures. As this study proceeds, this aspect of the data analysis will be explored in detail. The accuracy of the results obtained by double integration will be assessed by comparing the displacements estimated in this manner to the directly measured static response of the bridge.

NONLINEAR MODELLING

A nonlinear analytical model was developed to compute the static response of the bridge subjected to lateral loads and the free-vibration response of the bridge after the quick-release loading. Unlike buildings where response is usually dominated by structural members, bridges exhibit responses which include significant contribution from the foundation and abutment bearing pads. The analytical model, therefore, included the nonlinear effects due to the foundation and the bearing pads behavior as well as nonlinearity of the piers. An extensive study of the available experimental data on testing of pile-groups and bearing pads and reinforced concrete piers was carried out before appropriate models for these components were developed.

In the analytical model, the superstructure was represented by line elements and the foundation and the abutment pads were idealized by translational and rotational springs. The bridge deck was assumed to remain elastic while the piers were allowed to develop nonlinear deformations only at the base. The former assumption is justified because of the fact that the design of bridge decks is usually controlled by gravity loads which demand relatively large sections. Lateral strength (in terms of cracking and yielding) of these sections are usually very large and are unlikely to be exceeded. The exclusion of nonlinearity of deformation at the top of piers is also reasonable because the horizontal forces and moments are relatively small at pier tops.

The hysteretic behavior of the nonlinear elements was modelled by two hysteresis models: the TQ-hyst and the Ramberg-Osgood models.

IDEALIZATION OF PIER ELEMENTS

The nonlinear deformations of the pier elements were assumed to be concentrated at the base. While this assumption is made for prismatic members in buildings and bridges and has yielded satisfactory results, it is particularly realistic for the Rose Creek Bridge because of the fact that piers were purposely made weaker at the base to prevent build-up of any significant moment with respect to the transverse axis of the bridge. Axial deformation of the piers was ignored. Shear deformations were assumed to remain elastic, and only flexural nonlinearity was taken into account.

The primary moment-rotation relationship was assumed to consist of a trilinear curve, representing pre-cracked, cracked, and post-yielding stages. This curve is determined based on material properties and routine analysis methods. The hysteretic behavior for subsequent unloadings and loadings was idealized by a hysteresis model called Trilinear Q-hyst (Fig. 10) which is a modified version of a simple hysteresis model representative of cracked reinforced concrete elements. The model was modified to include cracking point because the cracking point is known to influence low-amplitude responses. The new hysteresis model incorporates six "rules" to determine stiffness at all loading, unloading, and load-reversal stages.

IDEALIZATION OF PILE FOUNDATIONS

A translational and a rotational spring were assumed at the base of each pier to represent the foundation displacement in the transverse direction of the bridge and foundation rotation with respect to the longitudinal axis. No other rotations or displacements were assumed for the foundation.

Detailed study of experimental data from testing of single piles subjected to horizontal loads indicated the following general characteristics for the lateral stiffness:

- (a) stiffness decreases as load increases. This is correct even at small load amplitudes.

- (b) stiffness increases upon unloading, but decreases as unloading continues.
- (c) when the load is reversed some stiffening occurs followed by a gradual reduction in stiffness.

The available experimental data lack information on two major aspects of the behavior of pile groups, necessary for a realistic modelling of pile foundations. One is about the group effects. While some empirical coefficients are derived and recommended to be used with the data from single piles and arrive at group stiffness, no data are available on pile groups subjected to cyclic loads sufficient to provide significant non-linearity. Another effect generally ignored is the rotation of the pile cap, while in the experimental data obtained for Rose Creek Bridge, pile cap rotation was found to contribute significantly to the deformations of the bridge.

In the absence of the above information, it was assumed that the cyclic behavior of pile groups is similar to that of single piles. It was also assumed that the rotational cyclic behavior of pile groups has the same general characteristics as that of single piles.

To simplify the modelling, the trilinear Q-hyst model was used to idealize the pile foundation stiffness variation in both the lateral and rotational directions (Fig. 10).

IDEALIZATION OF ELASTOMERIC BEARING PADS

Bearing pads can affect the dynamic response of the bridge to a great extent, although in design they are ordinarily ignored and treated as roller supports. Experimental studies on cyclic shear behavior of bearing pads have shown that stiffness varies as the amplitude and frequency of the load vary. While manufacturers of elastomeric pads acknowledge that the stiffness properties are also affected by weathering condition and age, no data on sensitivity of stiffness on these factors are available.

To model the hysteretic behavior of the pads a decision has to be made regarding the primary force-deformation relationship and stiffness variations at unloading, reloading, and load-reversal stages. Based on a study of the overall characteristics of hysteresis loops for bearing pads, the Ramberg-Osgood hysteresis system was adopted for the analytical model (Fig. 11). This model accounts for stiffness variation due to change in load/deformation amplitude. The other parameters, namely load frequency, weathering condition, and age, are to be accounted for in the primary curve.

SEISMIC RESPONSE RESULTS

In order to gain an appreciation of the importance of knowing the foundation stiffnesses when estimating the distribution of seismic loads, a few simple linear seismic response calculations were performed. Five earthquake accelerograms were selected to represent the small to moderate ground shaking for which a linear seismic response analysis would be

appropriate. These accelerograms were selected from the California Institute of Technology series of strong motion accelerograms. The properties of these surface ground shaking records are summarized in Table 2. The name of each accelerogram is listed in row 1 of the table while the Richter magnitude, shortest distance to the causative fault, peak acceleration, peak velocity, and peak displacement of each trace are listed, respectively, in rows 2 to 6.

A relatively simple, symmetric SAP IV analytical model was used for seismic response calculations. The specific properties of the model are described elsewhere (5,10). It has also been shown (10) that this model would be adequate for linear seismic response estimates, and Table 3 summarizes selected peak response results obtained for this model. This table also compares them to the results obtained from the application of the equivalent lateral, static (6% g) load required by the AASHTO code at the time the bridge was designed. From the results presented in the Table 3 it is apparent that the earthquakes selected for analysis cause much larger lateral loads than the design level loads. The Rose Creek interchange was designed prior to the 1971 San Fernando earthquake, which stimulated a great deal of interest in the seismic response of bridges. It should be noted here that the earthquake loads required by the current AASHTO code for bridges are considerably higher than those required when this bridge was designed. Columns 2 and 3 of Table 3 list the peak transverse shear carried to the approach fills through the abutments and the related peak deflection of the ends of the bridge deck. Columns 4 and 5 list the peak shear delivered to the foundation and the related peak pile top displacements at piers 1 and 4. Columns 6 and 7 give the peak shear delivered to the foundation and the peak pile top displacements at piers 2 and 3. The various accelerograms used to calculate the peak response results are indicated in Col. 1.

To illustrate the importance of including the transverse stiffnesses of the pier foundations in the model, a second series of dynamic response calculations were run with a model identical to the one used to calculate the results in Table 3 except that the four pier foundations were taken to be fixed in the transverse directions. This was accomplished by removing the pier foundation springs from the model. This model is referred to as the hard foundation model while the model above with realistic foundation elements is referred to as the basic model. Table 4 compares the peak seismic response results obtained for both the basic model and the hard foundation case as a ratio of the hard foundation case to the basic case. The same response parameters used in Table 3 are also the same ones that are compared in Table 4.

From Table 4, it is immediately evident that the hard foundation model underestimates the seismic loads transferred to the abutments by about a factor of 2 for the 5 accelerograms as well as the equivalent static load. Moreover, it is also clear for the hard foundation model, the shears delivered to the foundations of piers 1 and 4 would be overestimated by a minimum factor of 1.3 to a maximum of 3.8 depending upon the loading. At piers 2 and 3 the hard foundation model would in general underestimate the shears delivered to the foundation. The results indicate that the shears could be underestimated by as much as a factor of 2, but that in the case of the Golden Gate accelerogram they would be overestimated by a factor of 1.9. The Golden Gate accelerogram produces

anomalous results when compared to those produced by the other accelerograms because it is a small, short duration, relatively high frequency record. The point to be made is that failing to account for the significant foundation flexibilities can lead to errors (at least on the order of factors of 2 either way) in the distribution of seismic loads. This conclusion is drawn from the use of a model having specific foundation stiffnesses as opposed to a one which accounts for the variations in foundation stiffness associated with different pile top deflections.

CONCLUSIONS

1. When used with hydraulic ram loading, the quick release method of producing free lateral vibration in highway bridges is a very effective method of dynamic testing.

a) It permits the use of high amplitude dynamic experiments without danger of overloading the structure, which would be more difficult in the case of resonance testing with harmonic shakers.

b) It permits a wide range of useful static response measurements to be made as a by-product of the dynamic testing program.

c) In special cases of bridges where the structure may be deformed statically into the fundamental mode shape, the resulting response will be nearly unimodal. This allows simple complete fundamental mode analysis of the data without resorting to complex computational algorithms.

d) A preliminary study of the accelerogram data suggests that the initial static displacements at the time the rams are quick released may be obtained by doubly integrating the accelerograms. If this is borne out after a much more complete study of the data, this has interesting experimental implications for situations where making static displacement measurements is difficult because a suitable fixed reference is difficult to construct.

2. Damping ratios for reinforced concrete bridge structures of this type may be smaller than expected up to fairly large response amplitudes.

3. From the preliminary analysis of the data obtained from these experiments, it is clear from direct measurements that the soil-structure interaction phenomenon of the pile foundations contribute very significantly to the response of this structure. This agrees with a result obtained previously by more indirect means (16).

4. A preliminary seismic analysis of the Rose Creek Interchange indicates that if the foundation flexibilities are not considered in the model, the distribution of seismic forces could be in error by at least a factor of 2.

5. More carefully conducted dynamic tests of full scale bridges should be performed over the largest deflection range possible. Results from tests such as this would shed experimental light on the deflection

dependent nature of the foundation stiffnesses. Additionally, physical tests of full scale pile groups should be designed specifically to further clarify pile group and cyclic load behavior.

ACKNOWLEDGEMENTS

Our special gratitude goes to our technician T.R. Nielson who designed and fabricated much of the equipment required for the successful completion of the field work. Thanks also go to Frank Cherne who assisted with the electronic aspects of the experiment. Finally, our thanks go to the thirteen undergraduate and graduate students who served as the field crew. A significant portion of this study was supported by a grant from the National Science Foundation, Grant number CEE 8108124; however, the results and conclusions are those of the writers and do not necessarily reflect the views of the sponsor.

TABLE 1

Configuration of Structure and Release Loads		Ram Release Loads (Tons)				Date
		Pier 1	Pier 2	Pier 3	Pier 4	
F	S	9	9	9	9	5-25-82 T
F	U	14	14	0	0	5-25-82
L	S	9	9	9	9	5-25-82
L	U	14	14	0	0	5-25-82
F	S	25	25	25	25	5-26-82 W
F	U	0	0	33	25	5-26-82
L	S	25	25	25	25	5-26-82
L	U	0	0	33	25	5-26-82
F	S	40	40	40	40	5-26-82
F	U	50	50	0	0	5-27-82 Th
L	S	40	40	40	40	5-27-82
L	U	50	50	0	0	5-27-82
F	S	56	56	56	56	5-27-82
F	U	0	0	65	56	5-27-82
L	S	56	56	56	56	5-28-82 F
L	U	0	0	65	56	5-28-82

Note: F = Abutments Free
 L = Abutments Locked
 S = Symmetric Loading
 U = Unsymmetric Loading

TABLE 2 Properties of Earthquake Accelerograms Used for Seismic Analysis

Earthquake Accelerogram	Golden Gate	Hollister	Marengo	Castaic	Taft
Richter Magnitude	5.3	5.6	6.6	6.6	7.7
Distance to Fault (miles)	7	9	20	18	30
A_{max} (g)	0.105	0.18	0.12	0.27	0.18
V_{max} in/sec	1.81	6.73	6.34	10.7	6.96
D_{max} 4.72 (in)	0.31	1.49	4.72	3.66	3.62

Golden Gate = 1957 San Francisco (Golden Gate S80E)

Hollister = 1961 Hollister (City Hall N89W)

Marengo = 1971 San Fernando (1st Floor 1640 Marengo, N38W)

Castaic = 1971 San Fernando (Castaic N69W)

Taft = 1952 Kern County (Taft S69E)

TABLE 3 Maximum Transverse Seismic Response

Load Case	Abutments		Piers 1 and 4		Piers 2 and 3	
	Shear (kip)	Disp. (in)	Shear (kip)	Disp. (in)	Shear (kip)	Disp. (in)
Static 6% g	30.4	.0105	20.9	.0381	66.0	.0404
Golden Gate	72.7	.025	32.8	.0597	129.0	.0790
Hollister	117.0	.0403	133.0	.2424	515.0	.316
Marango	94.6	.0326	102.0	.186	391.0	.239
Castaic	159.0	.0549	148.0	.270	642.0	.393
Taft	99.2	.0342	119.0	.217	474.0	.290

TABLE 4 Ratio of Hard Foundation Model Peak Seismic Response Results Compared to Basic Model Results

Load Case	Abutments	Piers 1 and 4	Piers 2 and 3
Static 6% g	.55	1.85	.92
Golden Gate	.52	3.84	1.91
Hollister	.56	1.26	.54
Marengo	.46	1.45	.86
Castaic	.54	1.57	.64
Taft	.52	1.29	.77

REFERENCES

1. Mayes, Ron, L, and C. Rojohn, "A Comparison of United States and New Zealand Seismic Design Practices for Highway Bridges," Applied Technology Council Report ATC-12, Aug. 1982, 270 pp.
2. Chen, Ma-Chi and J. Penzien, "Analytical Investigations of Seismic Response of Short, Single, or Multiple-Span Highway Bridges," University of California, Berkeley, EERC Report 75-4, Jan., 1975, 164 pp.
3. Chen, Ma-Chi and J. Penzien, "Nonlinear Soil Structure Interaction of Skew Highway Bridges," University of California, Berkeley, EERC Report 77/24, Aug. 1977, 115 pp.
4. Chen, Ma-Chi and J. Penzien, "Soil-Structure Interaction of Short Highway Bridges," Proceedings of a Workshop on Earthquake Resistance of Highway Bridges, Conducted by the Applied Technology Council, sponsored by NSF, Jan 29-31, 1979, pp. 433-466.
5. Douglas, B.M., C.D. Drown, and M. Gordon, "Experimental Dynamics of Highway Bridges," Proceedings of the Second ASCE-EMD Specialty Conference on the Dynamic Response of Structures: Experimentation, Prediction and Control, Jan. 15-16, 1981, Atlanta, GA., pp. 698-712.
6. Douglas, B.M., "Experimental Dynamic Response Investigations of Existing Highway Bridges," Proceedings of a Workshop on Earthquake Resistance of Highway Bridges, Conducted by the Applied Technology Council, sponsored by NSF, Jan. 29-31, 1979, pp. 497-523.
7. Douglas, B.M. and G.M. Norris, "Bridge Dynamic Tests: Implications for Seismic Design," Journal of Technical Topics in Civil Engineering, ASCE, Vol. 109, No. 1, Apr. 1983, pp. 1-22.
8. Douglas, B.M. and G.M. Norris, "Nondestructive Dynamic Tests of Selected Highway Bridges in Nevada and Related Geotechnical Considerations," University of Nevada Engineering Report No. 58, (in preparation).
9. Douglas, B.M., "Quick Release Pullback Testing and Analytical Seismic Analysis of a Six Span Composite Girder Bridge," Report FHWA-RD-76-173, Federal Highway Administration, Offices of Research and Development, Washington, D.C., 1976, 73 pp.
10. Douglas, B.M., and W.H. Reid, "Dynamic Tests and System Identification of Bridges," Journal of the Structural Division, ASCE, Vol. 108, No. ST10., Oct. 1982, pp. 2295-2312.
11. Godden, W.G., R.A. Imbsen, and J. Penzien, "An Investigation of the Effectiveness of Existing Bridge Design Methodology in Providing Adequate Structural Resistance to Seismic Disturbances," Report No. FHWA-RD-79-90, Federal Highway Administration, Offices of Research and Development Structures and Applied Mechanics Division, Washington D.C., 1978, 48 pp.

12. Hall, W.J. and N.M. Newmark, "Seismic Design of Bridges - An Overview of Research Needs," Proceedings of a Workshop on Earthquake Resistance of Highway Bridges, Conducted by the Applied Technology Council, Sponsored by NSF, Jan. 29-31, 1979, pp. 164-181.
13. Imbsen, R.A., "Seismic Design of Highway Bridges - Workshop Manual," Report FHWA-IP-81-2, Sponsored by U.S. Department of Transportation, FHWA, Jan. 1981, 619 pp.
14. Okubo, T., and T. Iwasaki, "Summary of Experimental and Analytical Seismic Research Recently Performed on Highway Bridges," Proceedings of a Workshop on Earthquake Resistance of Highway Bridges, Conducted by the Applied Technology Council, Sponsored by NSF, Jan. 29-31, 1979, pp. 567-601.
15. Penzien, J., "Soil-Pile Foundation Interaction," Earthquake Engineering, R.L. Wiegel, Ed., Prentice Hall, 1979, pp. 349-381.
16. Priestley, M.J.N. and R. Park, "Seismic Resistance of Reinforced Concrete Bridge Columns," Proceedings of a Workshop on Earthquake Resistance of Highway Bridges, Conducted by the Applied Technology Council, Sponsored by NSF, Jan. 29-31, 1979, pp. 254-281.
17. Shepherd, R. and A.W. Charleson, "Experimental Determination of the Dynamic Properties of a Bridge Substructure," Bull. of the Seism. Soc. of Amer., Vol. 61, No. 6, Dec. 1971, pp. 1529-1548.
18. Tseng, W.S. and J. Penzien, "Analytical Investigations of the Seismic Response of Long Multiple Span Highway Bridges," University of California, Berkeley, EERC Report No. 73-12, June, 1973, 200 pp.
19. Werner, S.D. and L.C. Lee, "The Three-Dimensional Response of a Bridge Structure Subjected to Traveling Rayleigh Waves, SV-Waves, and P-Waves," Agabian Associates, El Segundo, CA., Report R-7911-5008, May 1980, 210 pp.
20. Werner, S.D., L.C. Lee, H.L. Wong, and M.D. Trifunac, "An Evaluation of Traveling Seismic Waves on the Three-Dimensional Response of Structures," Agabian Associates, El Segundo, CA., Report R7720-4514, Oct., 1977.

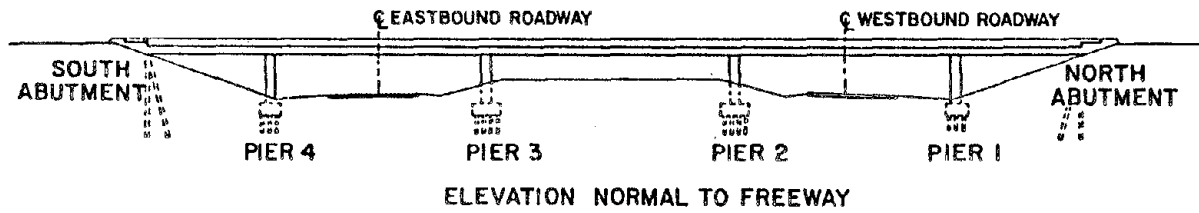
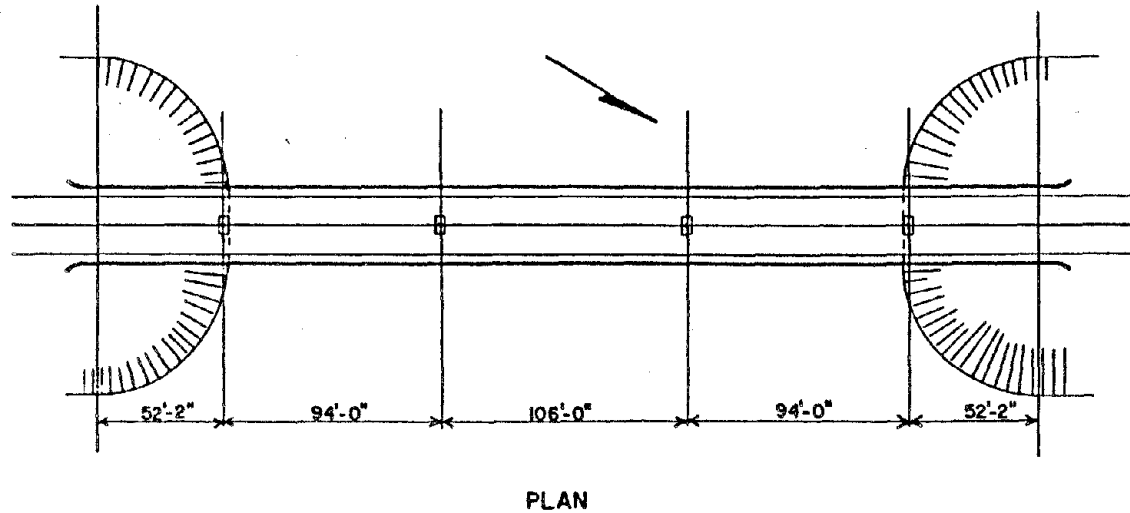


Fig. 1 Plan Elevation of Rose Creek Interchange

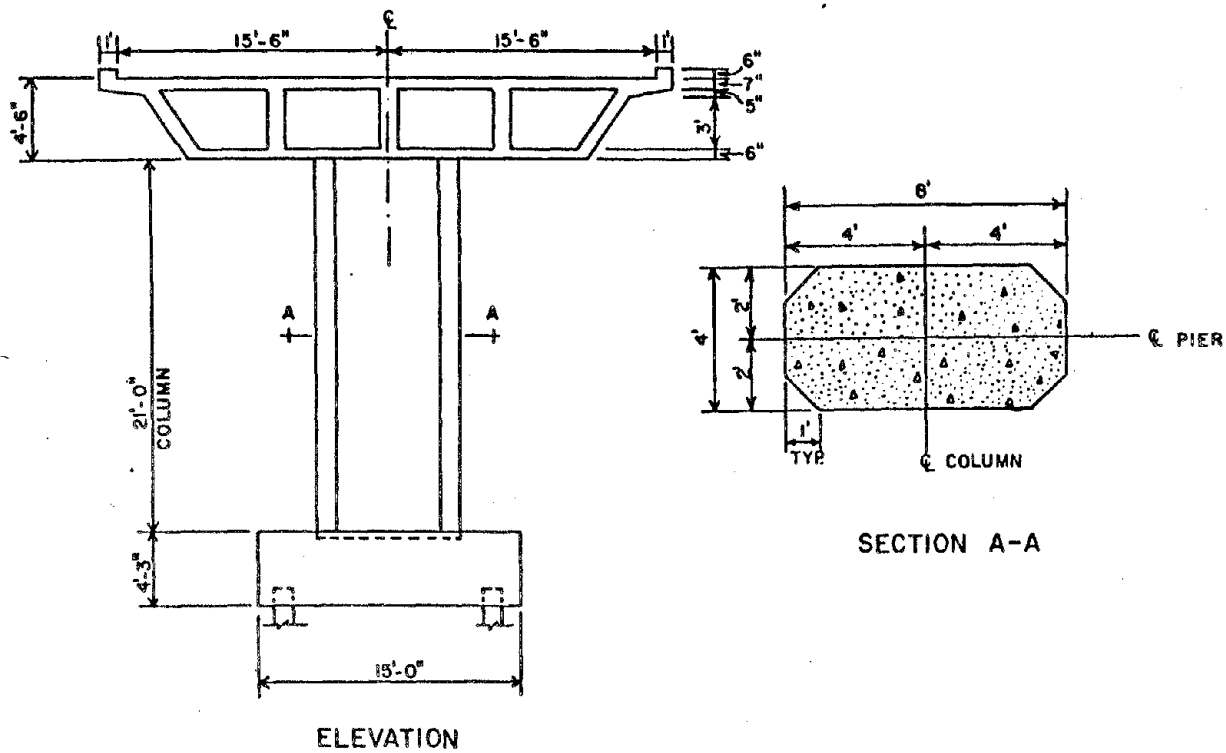


Fig. 2 Section of Rose Creek Interchange

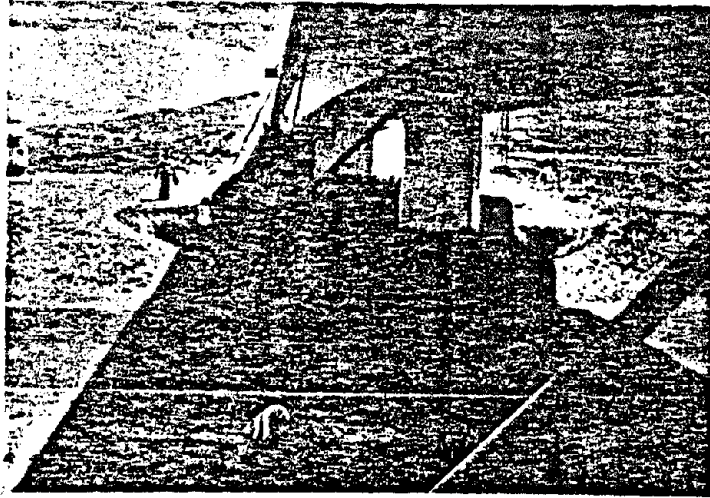


Fig. 3 Hydraulic Rams Used to Load Bridge

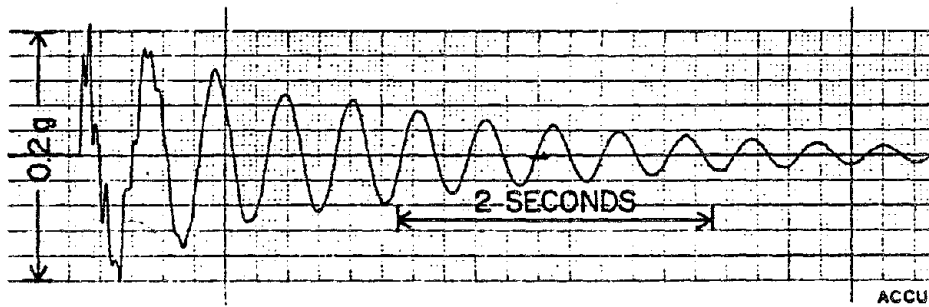


Fig. 4 Accelerogram of Deck Response at Centerline -
Symmetric Loading

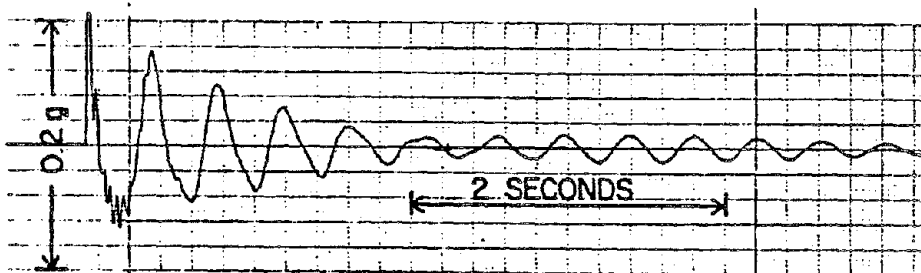


Fig. 5 Accelerogram of Deck Response at Quarter Point -
Unsymmetric Loading

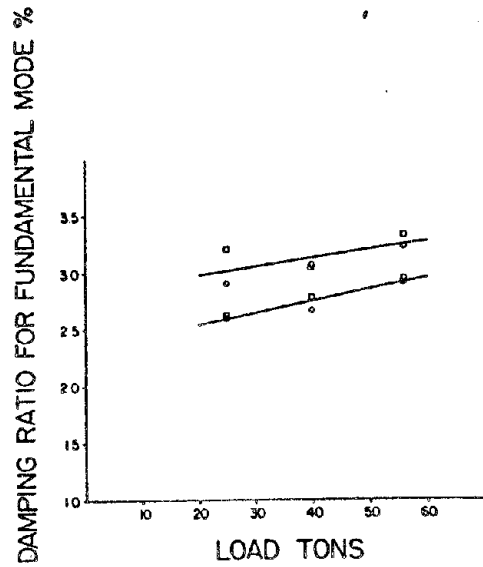


Fig. 6 Fundamental Mode Damping Ratios Versus Amplitude of Loads

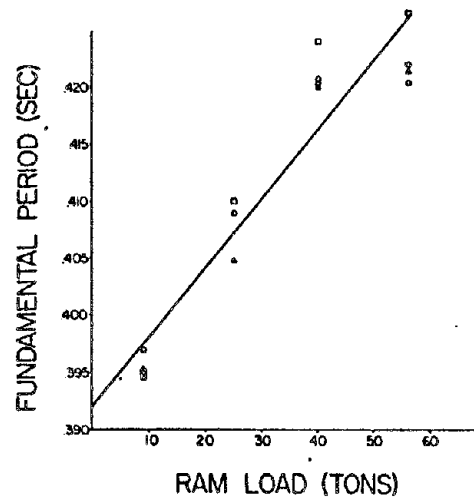


Fig. 7 Fundamental Period Versus Amplitude of Loads - Abutments Free

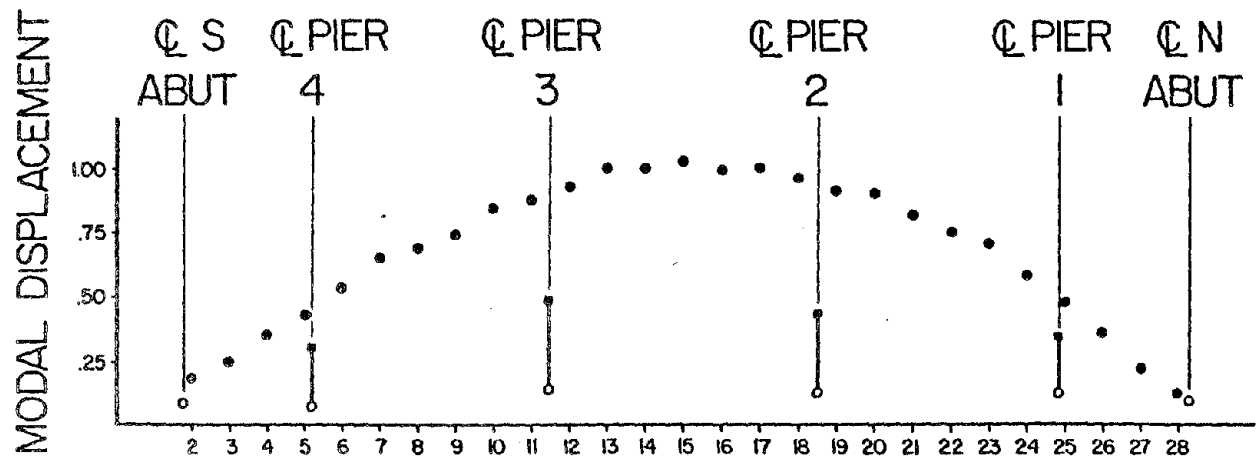


Fig. 8 Fundamental Mode Shape - Abutments Loaded

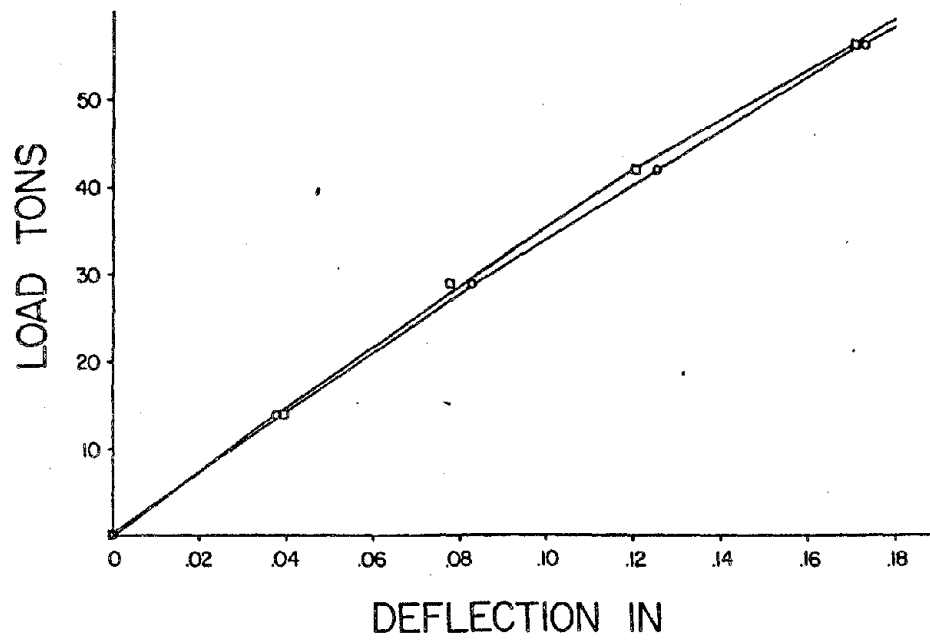


Fig. 9 Ram Load Versus Static Deflection of Deck at Centerline

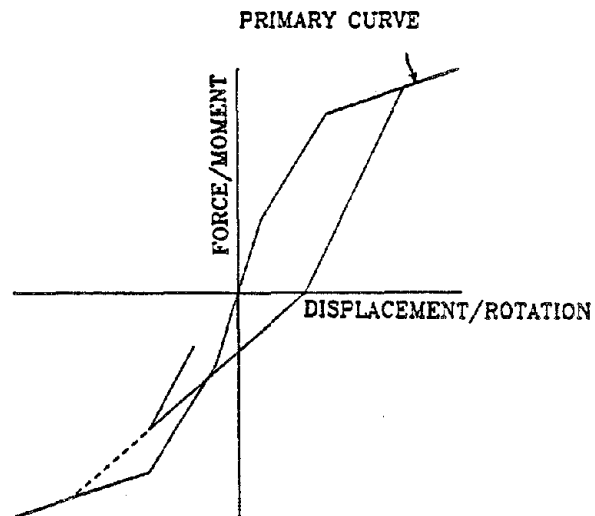


Fig. 10 Trilinear Q-Hyst (TQ-Hyst) Model

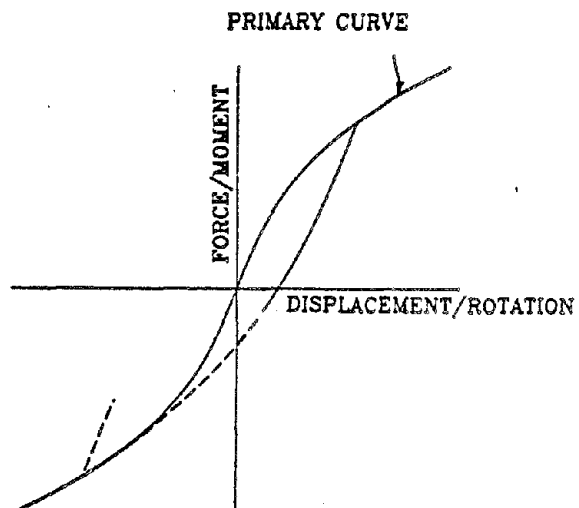


Fig. 11 Ramberg-Osgood Hysteresis Model

VIBRATION TESTS OF BRIDGE MODELS
USING A LARGE SHAKING TABLE

by

Eiichi Kuribayashi^I, Osamu Ueda^{II}, and Ryoji Hagiwara^{III}

ABSTRACT

Results of two vibration tests of bridge models are presented. The subjects of the tests are to study the dynamic response characteristics of Katashina-gawa Bridge in Kan-etsu Expressway and of a continuous girder bridge in Metropolitan Expressway during earthquakes.

Katashina-gawa Bridge is a curved truss bridge with high piers ($R = 2,200$ m, $H_{\max} = 69$ m). Its dynamic response characteristics by longitudinal, transverse, and oblique direction excitations, effects of a curve, and a distribution of stress in its superstructure were investigated by vibration tests of its model. Analytic modeling in the dynamic analysis of Katashina-gawa Bridge was also examined.

The continuous girder bridge has a superstructure connected with piers by hinges through twelve spans. Its dynamic response characteristics by longitudinal and transverse direction excitations were investigated and are compared with those of a simple girder bridge and a continuous girder bridge with dampers by vibration tests of their models. Analytic modeling in the dynamic analysis of the continuous girder bridge was also examined.

1. INTRODUCTION

Several vibration tests have been conducted since June, 1979 by using a large shaking table of Public Works Research Institute, Ministry of Construction. Among them, results of two vibration tests, a vibration test of Katashina-gawa Bridge model and that of a continuous girder bridge model, are presented in this paper. Main specification of performances of the shaking table is shown in Table 1-1.

-
- I) Director, Earthquake Disaster Prevention Department, Public Works Research Institute.
 - II) Head, Earthquake Engineering Division, Earthquake Disaster Prevention Department, Public Works Research Institute.
 - III) Research Engineer, Earthquake Engineering Division, Earthquake Disaster Prevention Department, Public Works Research Institute.

Table 1-1 Main Specification of Performances of the Shaking Table

Items	Performances
(1) Table Size	6m x 8m (1 table)
(2) Maximum Loading Capacity	100 ton
(3) Permissible Overturning Moment	150 ton·m
(4) Maximum Excitation	100 ton
(5) Maximum Stroke	± 75 mm
(6) Maximum Speed	± 60 cm/sec
(7) Maximum Acceleration	No Load : 2.5G 100 ton : 0.7G
(8) Excitation	Horizontal Axis (It is possible to add vertical excitation)
(9) Control of Input Motions	Analog Control and Digital Control
(10) Phase Lag	—
(11) Option of Input Motions	Sinusoidal Motions Triangular Motions Rectangular Motions Arbitrary Motions
(12) Frequency Range	DC - 30 c/s
(13) Automatic Setting of Input Motion	Arbitrary Input displacement, velocity, and acceleration can be kept constant
(14) Exciter	Electro-hydraulic Servo System

2. VIBRATION TEST OF KATASHINA-GAWA BRIDGE MODEL

2.1 Purposes of the Test

Katashina-gawa Bridge shown in Fig. 2-1, slightly curved in plan with 2,200 meter radius, is consisted of three continuous truss bridges (Bridge-A, Bridge-B,

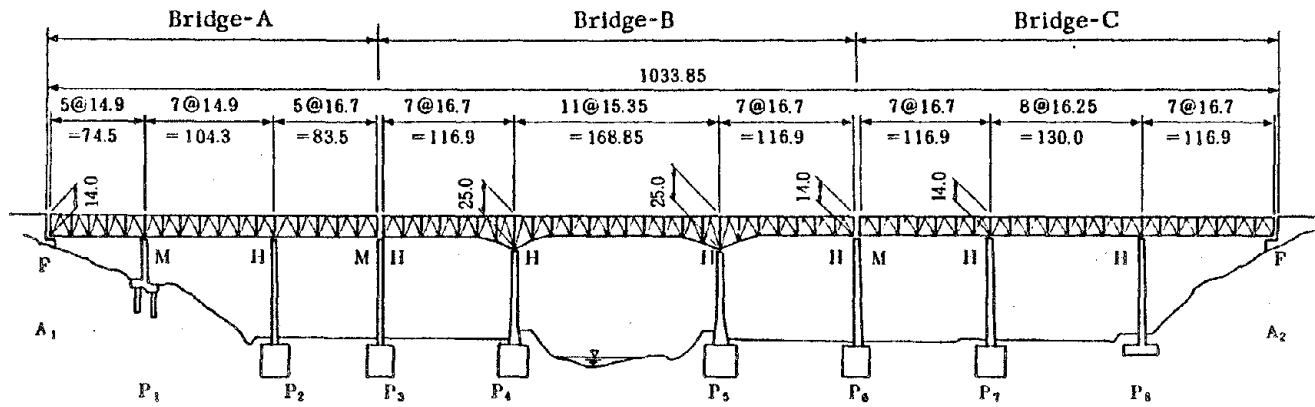


Fig. 2-1 Katashina-gawa Bridge in Kan-etsu Expressway

Bridge-C) with high piers ($H_{\max} = 69\text{ m}$).

Dynamic response characteristics of Katashina-gawa Bridge were examined by a vibration test of its model to introduce its dynamic analysis method and some considerations on its earthquake-resistant design.

2.2 Experimental Model of Katashina-gawa Bridge

The model of Katashina-gawa Bridge used in the test was made of plastics in main. Each base of piers was fixed to the shaking table without a consideration of the deformation of foundations. Scales of the model shown in Table 2-1 were determined considering the followings.

- To measure responses of Bridge-A model and Bridge-B model
- To link simplified Bridge-C model to Bridge-B model
- To consider a half of the stiffness of floor slabs
- To simplify the structures of sway bracings and lateral bracings with satisfying the scale of stiffness in Table 2-1.

Table 2-1 Scales for Katashina-gawa Bridge Model Vibration Test

Items	Scales ($\frac{\text{Model}}{\text{Actual Bridge}}$)
Length	1/100
Elastic Modulus	1/15
Density	100/15
Time	1/10
Acceleration	1
Stiffness EA	$1/(15 \times 10^4)$
Stiffness EI	$1/(15 \times 10^8)$

2.3 Vibration Test

The vibration test of Katashina-gawa Bridge model was conducted as mentioned below (Fig. 2-2 - Fig. 2-5).

- (1) Directions of the excitation
 - 1) Longitudinal direction
 - 2) Transverse direction
 - 3) Oblique direction
- (2) Input waves of the excitation

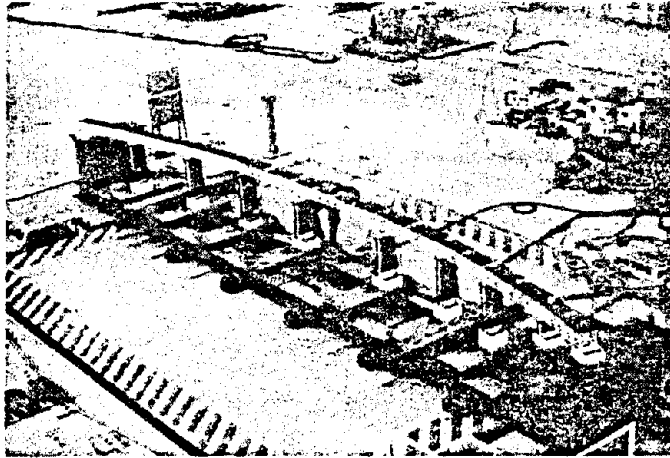


Fig. 2-2 Vibration Test of Katashina-gawa Bridge Model
(Longitudinal Excitation)

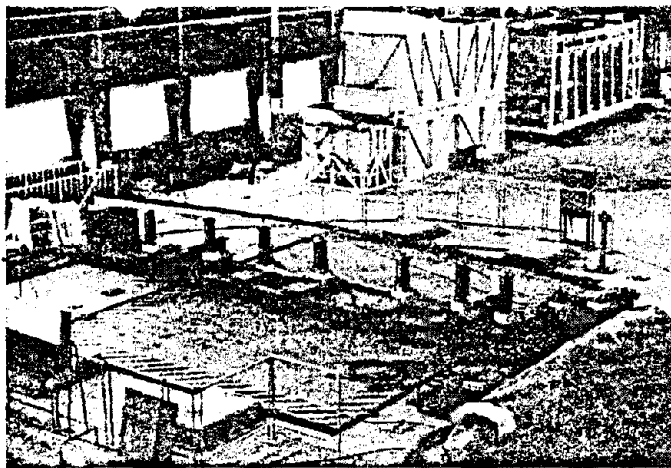


Fig. 2-3 Vibration Test of Katashina-gawa Bridge Model
(Transverse Excitation)

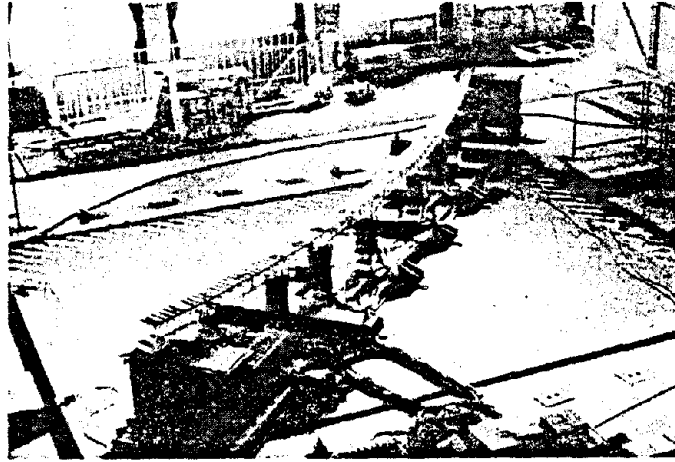


Fig. 2-4 Vibration Test of Katashina-gawa Bridge Model
(Oblique Excitation)

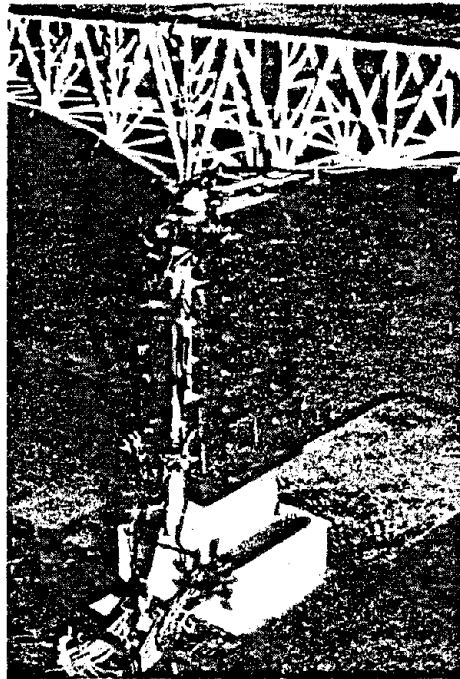


Fig. 2-5 Vibration Test of Katashina-gawa
Bridge Model (Pier P5)

- 1) Sinusoidal wave (input acceleration = 20 gal)
- 2) Earthquake motion recorded at Shizunai (Nemuro-hantoh-oki Earthquake, $M = 7.4$, June 17, 1973)
- 3) Earthquake motion recorded at Horoman (Tokachi-oki Earthquake, $M = 7.9$, May 16, 1968)

Time scale of the earthquake motions was 1/10 as shown in Table 2-1.

2.4 Results of the Vibration Test

Measured damping constants of superstructures and substructures of Katashina-gawa Bridge model were $h = 2-3\%$ and $h = 0.8-0.9\%$ respectively. They are smaller than the assumed damping constant ($h = 5\%$) of Katashina-gawa Bridge. Friction coefficients of shoe models were 0.09 - 0.10, which are a little larger than that of actual shoes.

Measured resonant frequencies and maximum response accelerations by sinusoidal excitation tests are shown in Table 2-2. The resonant vibration of Bridge-B was brought about by the sinusoidal excitation of 8.05 Hz in the longitudinal direction. In the resonant vibration of 9.9 Hz the movable bearings on Pier-P₃ did not seem to be movable and both Bridge-A and Bridge-B were in the resonant vibration. In the resonant vibration of 11.8 Hz Pier-P₂ was vibrating in the transverse direction as well as in the longitudinal direction, which might be the effect of a curve.

The resonant vibration of the superstructure of Bridge-B was brought about by the sinusoidal excitation of 8.4 Hz in the transverse direction. In the resonant vibrations of 12.2 Hz and 13.2 Hz Pier-P₂ was vibrating in the longitudinal direction as well as in the transverse direction:

Most of the resonant vibration modes by sinusoidal excitations in the oblique direction was the same as a mode by an excitation in the longitudinal or transverse direction. When the resonant frequency in the longitudinal direction and that in the transverse direction are fairly close, the vibration modes by the excitations in each direction were combined in the vibration mode by the excitation in the oblique direction like the resonant vibration of 12.9 Hz. The responses by oblique-direction excitations were smaller than those by longitudinal or transverse-direction excitations.

In the case of excitation in the longitudinal direction by sinusoidal waves, vertical vibrations occurred in the superstructure. The vertical vibrations caused stresses in the chords and diagonal members, especially in the chords at the middle

of spans and in the diagonal members over the supports. The stresses caused by the vertical vibrations are not specially considered in the current earthquake-resistant design. When sinusoidal waves were applied in the transverse direction, stresses in the sway bracings and lateral bracings were especially concentrated in the members over the supports. The stress concentration is taken into consideration in the current earthquake-resistant design.

The maximum strains occurred at the base of piers by the first resonant vibration of the piers. The bending strains in the longitudinal and transverse directions occurred at the same time at the bottom of Pier-P₂ by the effect of a curve, but the effect was rather small.

The distribution of response accelerations of Katashina-gawa Bridge model by the earthquake motion excitations are shown in Fig. 2-6 and Fig. 2-7. The distribution of response accelerations in the longitudinal and vertical directions by oblique-direction excitations was similar to that by longitudinal-direction excitations. The distribution of response accelerations in the transverse direction by oblique-direction excitations was similar to that by transverse-direction excitations.

2.5 Dynamic Analysis Model

A few analytic models to estimate the dynamic responses of Katashina-gawa Bridge model were formed, and the results of dynamic analyses by the models were compared with the results of vibration tests to find out adequate analytic models.

The dynamic analysis models are arranged in Table 2-3. Comparisons of the results of the analyses and the tests are shown in Table 2-4. Among the two-dimensional models in the longitudinal direction Case-2 model (masses of superstructures are located at the neutral axis and the supports on Pier-P₁ are movable; Fig. 2-8) provided the best estimations. Only the estimation of 6th mode by Case-3 model (the supports on Pier-P₁ are fixed) was better than that by Case-2 model. As for 6th mode, the supports on Pier-P₁ did not seem to be movable in the vibration test due to the effect of a curve. Among the two-dimensional models in the transverse direction Case-2 model (stiffness of the sway bracings over the supports is considered; Fig. 2-9) provided the best estimations. This agrees to the concentration of stresses in the sway bracings over supports in the vibration test. The results of the analyses by the two-dimensional models also agreed to those by the three-dimensional model except for 6th, 7th, and 8th vibration modes. The vibrations of

Table 2-2 Resonant Frequencies and Maximum Accelerations Measured by the Vibration Test
(Sinusoidal Wave Inputs : 20 gal)

		1st	2nd	3rd	4th	5th	6th	7th	8th	9th	10th	11th	12th	13th	
Longitudinal	Frequency (Hz)	8.05	9.9	11.2	11.8	16.8	20.4	24.5	26.5	-	-	-	-	-	
	Maximum Acceleration (gal)	178	113	216	97	202	390	103	347	-	-	-	-	-	
Transverse	Frequency (Hz)	8.4	10.8	11.6	12.2	13.2	15.6	19.0	21.2	-	-	-	-	-	
	Maximum Acceleration (gal)	542	276	200	239	290	288	149	141	-	-	-	-	-	
Oblique	Frequency (Hz)	8.35	10.0	10.7	11.7	12.9	16.2	16.8	18.0	20.4	21.0	24.2	28.0	29.0	
	xz ^o direction	Maximum Acceleration (gal)	87	77	104	67	103	95	165	90	227	183	78	151	432
	y ^o direction	Maximum Acceleration (gal)	389	107	278	200	153	210	66	131	107	126	99	184	99

Note: x direction: longitudinal direction, y direction: transverse direction, z direction: vertical direction

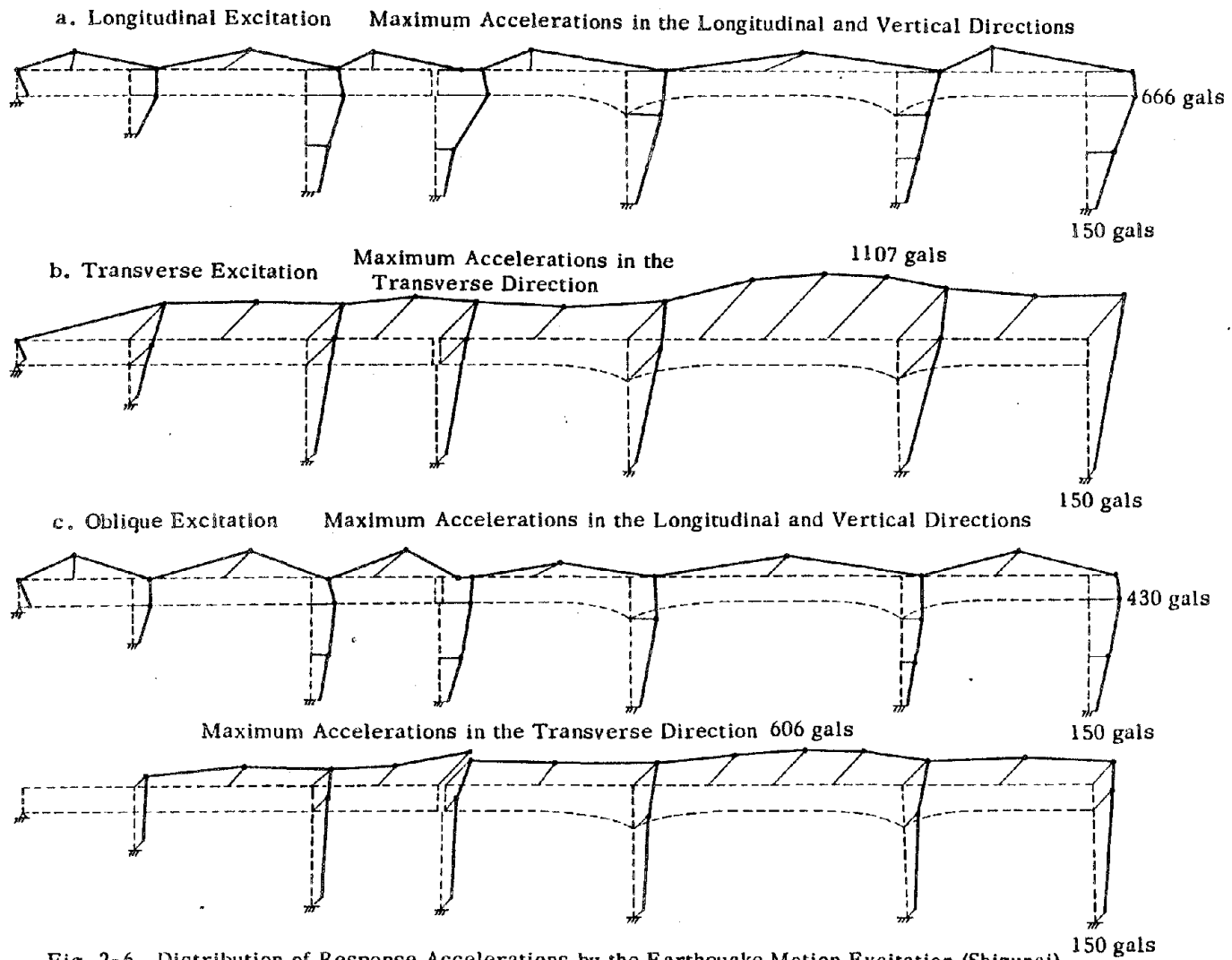


Fig. 2-6 Distribution of Response Accelerations by the Earthquake Motion Excitation (Shizunai)

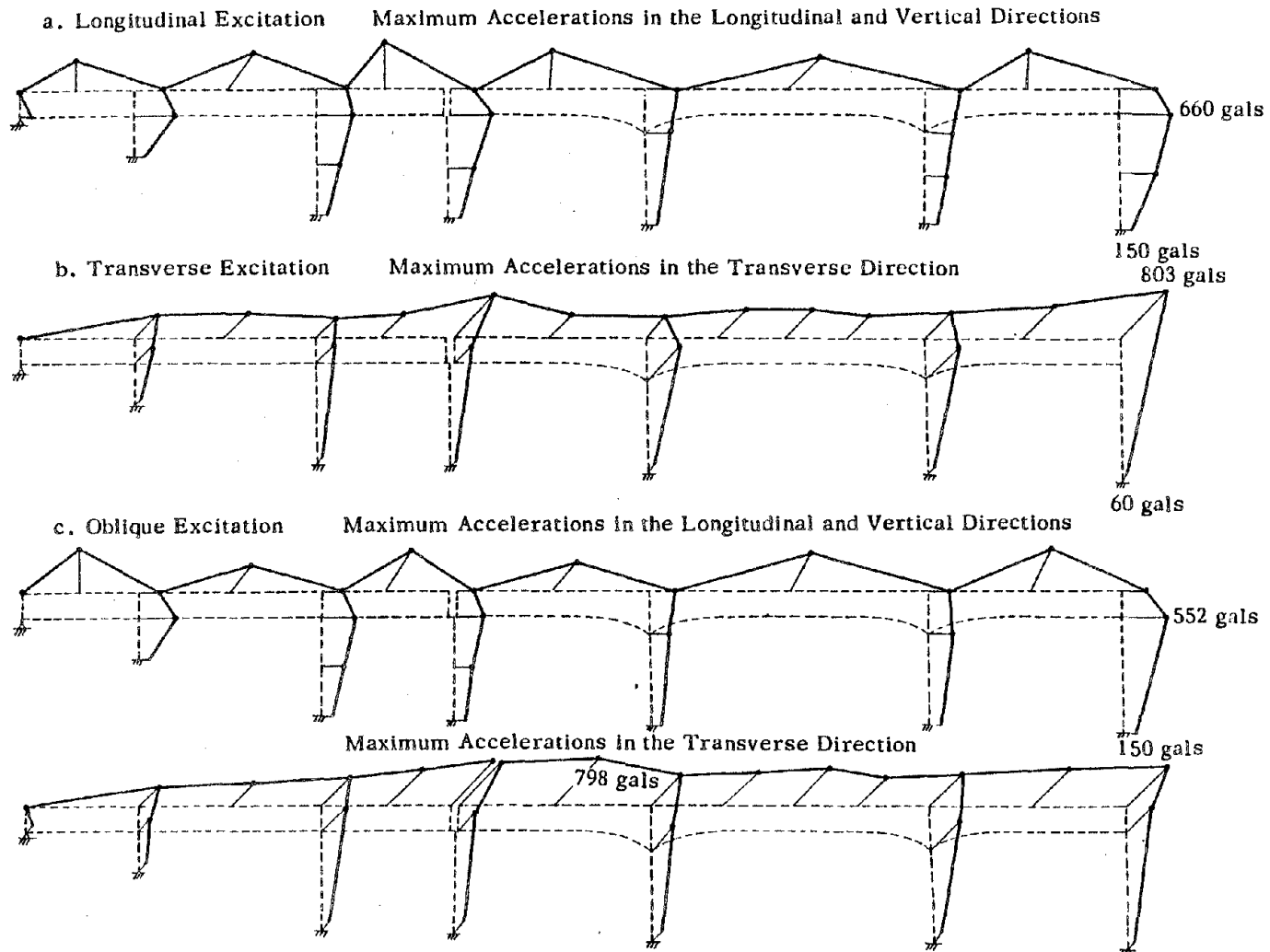


Fig. 2-7 Distribution of Response Accelerations by the Earthquake Motion Excitation (Horoman) 150 gals

Table 2-3 Dynamic Analysis Models

Models		Cases	Mass Location of the Superstructure	Connection between Super and Sub-Structures	Support on Pier-P ₁
Two-Dimensional Model	Longitudinal	Case 1	At the lower chord	—	Movable
		Case 2 (Fig.2-8)	At the neutral axis	Rigid	Movable
		Case 3	At the neutral axis	Rigid	Fixed
	Transverse	Case-1	At the center of gravity	Stiffness of the sway bracings over the supports and their neighboring sway bracings is considered	Fixed
		Case-2 (Fig.2-9)	At the center of gravity	Stiffness of the sway bracings over the supports is considered	Fixed
Three-Dimensional Model	Case-1	At the neutral axis (longitudinal) At the center of gravity (transverse)	Stiffness of the sway bracings over the supports is considered	Movable	

Table 2-4 Calculated Natural Frequencies and Measured Resonant Frequencies

	Calculated Natural Frequencies (Hz)			Measured Resonant Frequencies (Hz)		
	Three-Dimensional Analysis	Two-Dimensional Analysis (Longitudinal, Case-2)	Two-Dimensional Analysis (Transverse, Case-2)	Longitudinal Excitation	Transverse Excitation	Oblique Excitation
1st	7.80	-	7.96	-	8.40	8.35
2nd	7.93	7.93	-	8.05	-	-
3rd	10.46	10.46	-	11.20	-	-
4th	10.67	-	10.56	-	10.8	10.7
5th	11.93	-	11.41	-	-	-
6th	12.50	-	12.47	-	16.6	11.7
7th	12.95	13.43	-	-	-	12.9
8th	13.92	-	13.29	-	12.2	12.9
9th	15.00	-	14.78	-	-	-
10th	15.08	15.10	-	16.8	-	16.8
11th	15.62	15.65	-	-	-	-
12th	17.96	17.99	-	20.4	-	21.0

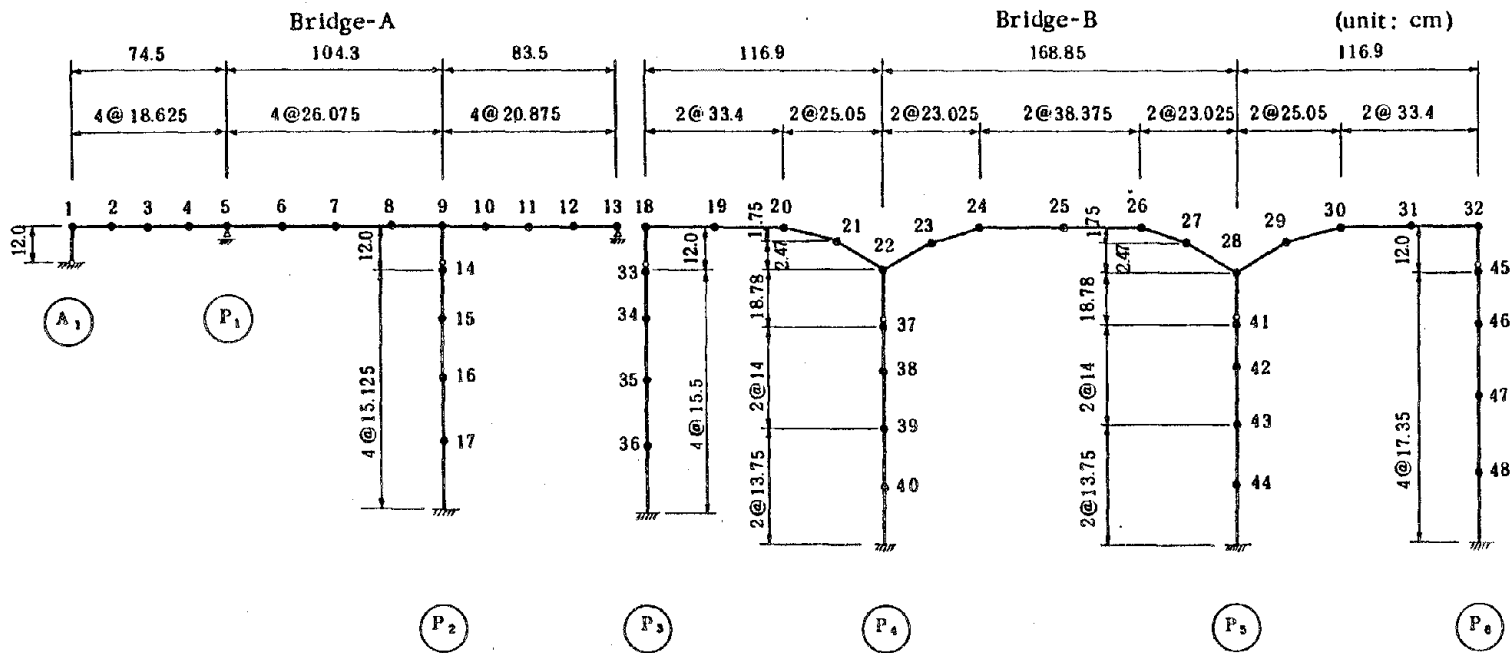


Fig. 2-8 Two-Dimensional Dynamic Analysis Model in the Longitudinal Direction (Case-2)

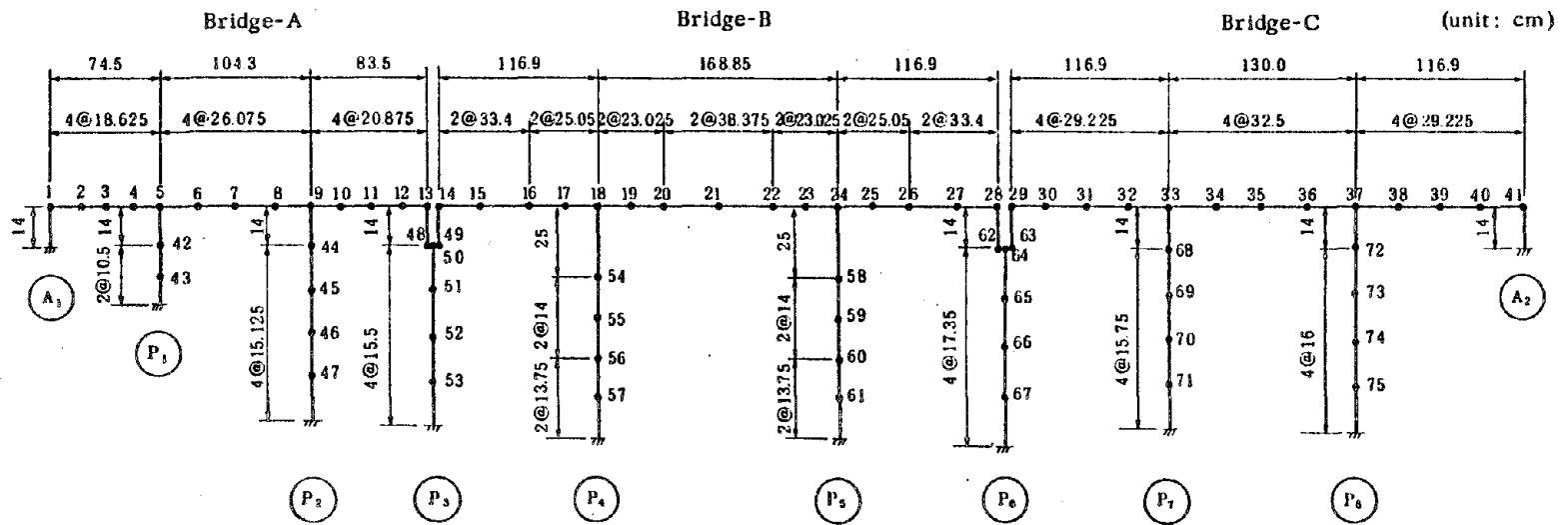


Fig. 2-9 Two-Dimensional Dynamic Analysis Model in the Transverse Direction (Case-2)

6th, 7th, and 8th modes are seem to be affected by the curve of Bridge-A which has the sharpest curve in Katashina-gawa Bridge.

3. VIBRATION TEST OF A CONTINUOUS GIRDER BRIDGE MODEL

3.1 Purposes of the Test

Multi-span continuous girder bridges have been considered as a reasonable type of elevated highway bridges in urban areas to mitigate traffic noise and vibration and give a comfortable drive. The twelve-span continuous girder bridge in Metropolitan Expressway as shown in Fig. 3-1 is one of such bridges. The continuous girder bridge has a superstructure connected by hinges with nine piers of its thirteen piers (mentioned as a hinge-type bridge in the following).

Dynamic response characteristics of the continuous girder bridge were examined by a vibration test of its model. Dynamic response characteristics of a continuous girder bridge which has only movable bearings with dampers installed to it (mentioned as a damper-type bridge in the following) and arrayed simple girder bridges (mentioned as a simple girder-type bridge in the following) were also examined by vibration tests of their models to compare the dynamic response characteristics of each type of the structure.

3.2 Experimental Model of the Continuous Girder Bridge

The models of the bridges used in the test were made of plastics in main. Pile foundations of the bridges were modeled in plate springs. Scales of the models are shown in Table 3-1.

There are three types of models for the hinge-type bridge in the transverse-direction vibration test.

- i) A model without the effect of its neighboring spans nor the stiffness of floor slabs (mentioned as an original-type model).
- ii) A model with rigid-frame piers at the ends of the bridge model to consider the effect of its neighboring spans.
- iii) A model with the stiffness of floor slabs.

There are three types of models for the damper-type bridge in the longitudinal-direction vibration test.

- i) A model without dampers in which horizontal forces by the inertia of the superstructure are transmitted to substructures by the friction at the

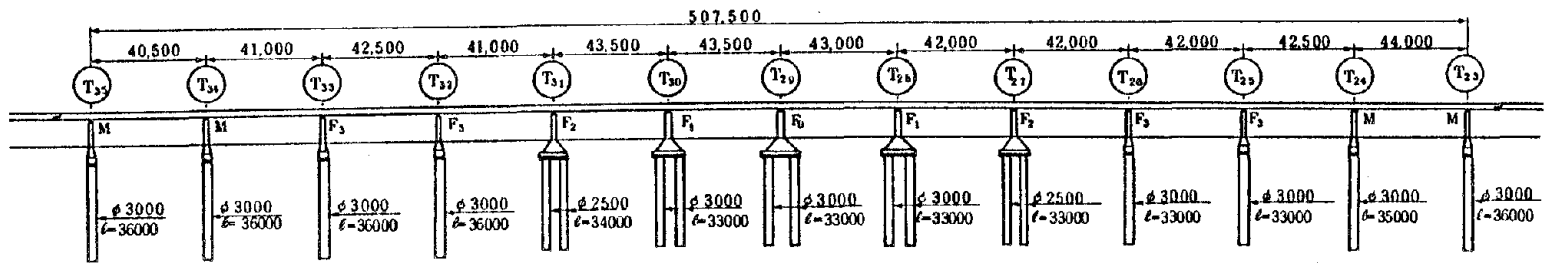


Fig. 3-1 A Continuous Girder Bridge in Metropolitan Expressway

supports.

- ii) A model with dampers of damping coefficient $C = 0.8 \text{ kg} \cdot \text{sec}/\text{cm}$.
- iii) A model with dampers of damping coefficient $C = 1.7 \text{ kg} \cdot \text{sec}/\text{cm}$.

Each stiffness of the piers of the hinge-type bridge model is different, but every stiffness of the piers of the damper-type bridge model and the simple-girder type bridge model is the same except for the stiffness of Pier- P_1 and Pier- P_2 .

3.3 Vibration Test

Vibration tests of the hinge-type bridge model, the damper-type bridge model, and the simple girder-type bridge model are listed in Table 3-2 (Fig. 3-2 - Fig.3-4). Effects of its neighboring spans and the stiffness of floor slabs to the dynamic response characteristics of the hinge-type bridge were examined by the transverse-direction vibration test of its model. Effects of dampers of different damping coefficients to the dynamic response characteristics of the damper-type bridge were examined by the longitudinal-direction vibration test of its model.

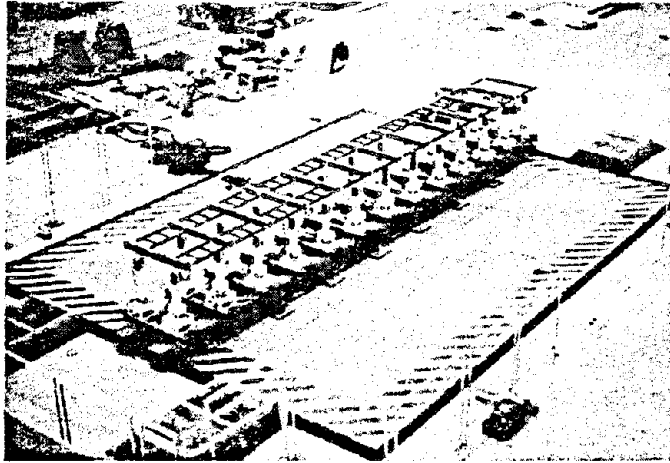
Input waves of the excitation in the vibration tests are:

- (1) Random wave a wave with almost constant power spectra in the frequency domain of 3 - 25 Hz
- (2) Artificial Earthquake motion a wave of the tapered random wave (1) at the beginning and at the end.
- (3) Sinusoidal wave sinusoidal waves of the frequency of 4 - 20 Hz and the amplitude of 50 gals.

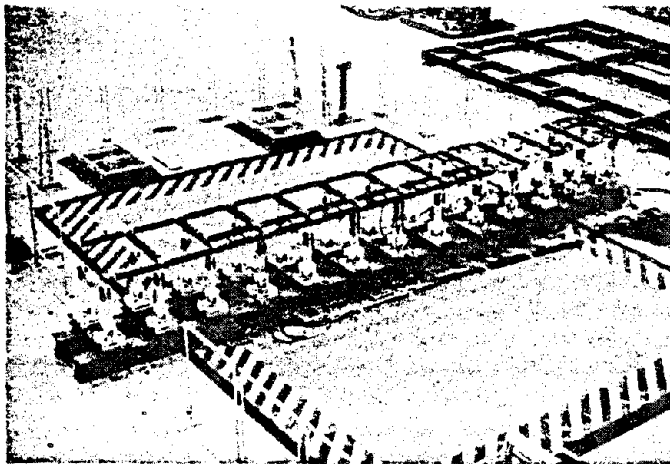
3.4 Results of the Vibration Test

Measured resonant frequencies are shown in Table 3-3. Distributions of maximum response accelerations at the top of piers and maximum bending moments at the base of piers by the random wave input are shown in Fig. 3-5 and Fig. 3-6.

When longitudinal-direction excitations were applied, maximum response accelerations at the top of piers of the simple girder-type bridge model were smaller than those of other type bridge models. The accelerations of piers of the damper-type bridge model and the simple girder-type bridge model were uniformly distributed, but the accelerations of end piers were larger than those of other piers in the hinge-type bridge model. Maximum bending moments at the base of piers by longitudinal-direction excitations were relatively large at the piers located in the middle of the



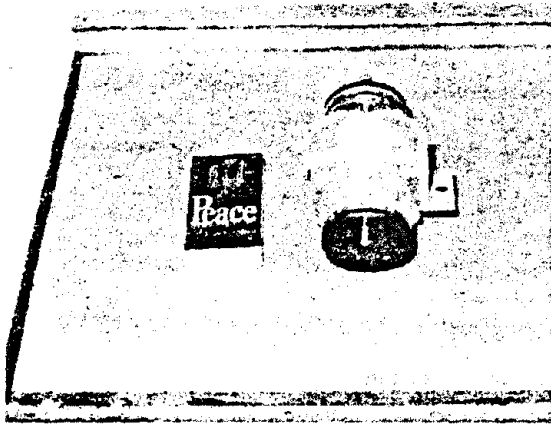
Longitudinal Excitation



Transverse Excitation

Fig. 3-2 Vibration Test of Hinge-Type Bridge Model

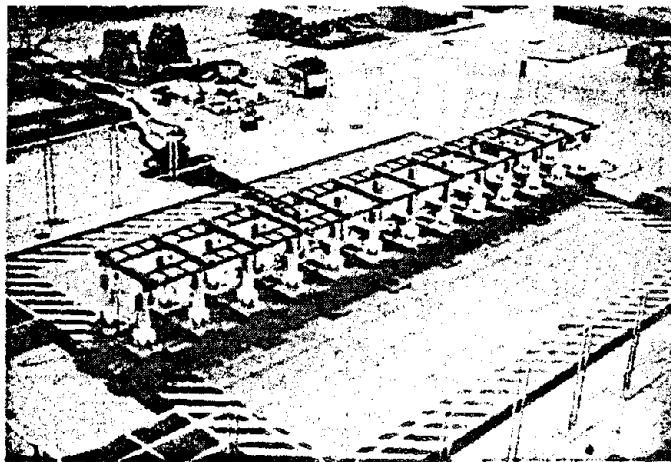
Reproduced from
best available copy.



Oil Damper Model

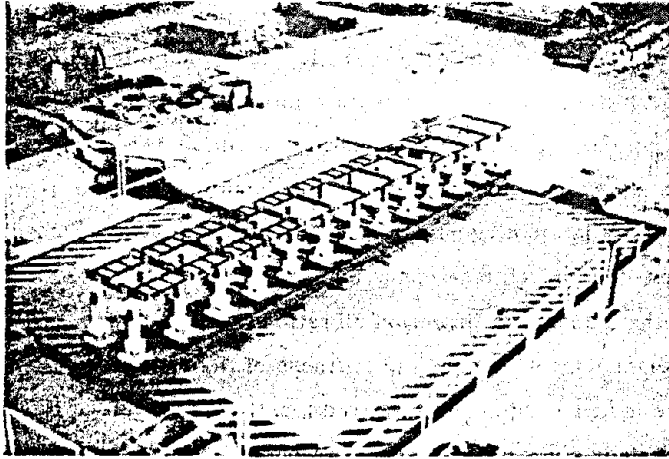


Pier-P7

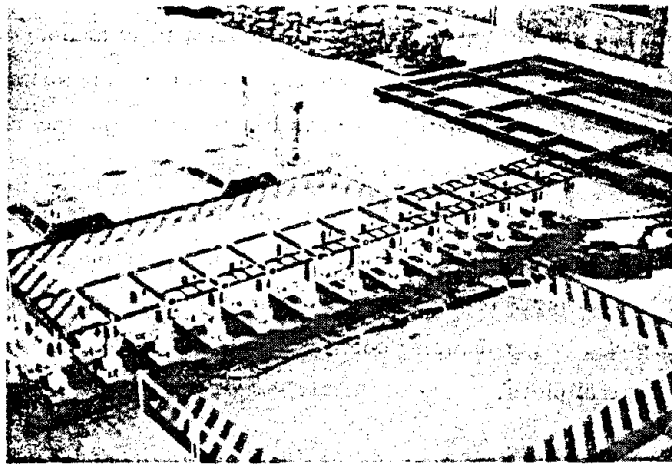


Longitudinal Excitation

Fig. 3-3 Vibration Test of Damper-Type Bridge Model



Longitudinal Excitation



Transverse Excitation

Fig. 3-4 Vibration Test of Simple Girder-Type Bridge Model

bridge model and having larger stiffness than other piers in the hinge-type bridge model, were also a little larger at the piers located in the middle of the bridge model than at other piers in the damper-type bridge model, and were large at the piers located at the both ends of the bridge model in the simple girder-type bridge model.

When transverse-direction excitations were applied, resonant frequencies were dispersed especially in the hinge-type bridge model, and the responses were rather uniformly distributed in each type of the bridge models.

Results of the transverse-direction vibration test of the hinge-type model on the effects of its neighboring spans and the stiffness of floor slabs are shown in Fig. 3-7. The effect of its neighboring spans appeared locally at the ends of the bridge model. The stiffness of floor slabs made resonant frequencies of the bridge model a little higher and its responses slightly smaller.

Results of the longitudinal-direction vibration test of the damper-type model on the effect of dampers are shown in Fig. 3-8. Resonant frequencies of the bridge model became higher by installing dampers to it. The effect of dampers was larger at the piers located in the middle of the bridge model than at other piers. Maximum response accelerations at the top of piers of the model without dampers were larger than those of the models with dampers, and maximum bending moments at the base of piers of the model without dampers were smaller than those of the models with dampers because of different vibrations of the superstructure from the substructure in the model without dampers. When dampers were installed, the inertia forces of the superstructure were transmitted to piers by dampers, and maximum bending moments at the base of piers became large especially in the middle of the bridge model. Dampers of a larger damping coefficient provided larger maximum bending moments at the base of piers.

3.5 Dynamic Analysis Model

Analytic models to estimate the dynamic responses of the bridge models were formed, and results of dynamic analyses by the models were compared with the results of vibration tests by applying the artificial earthquake motion to judge the adequacy of the models. Dynamic analyses were conducted by a time history response analysis method and a response spectrum analysis method. The models for the hinge-type bridge model are shown in Fig. 3-9 and in Fig. 3-10. The model for the damper-type bridge model in the longitudinal direction is shown in Fig. 3-11.

Table 3-1 Scales for the Continuous Girder Bridge Model Vibration Test

Items	Scales ($\frac{\text{Model}}{\text{Actual Bridge}}$)
Length	Height of a pier 1/25 Interval between piers 1/65
Elastic Modulus	1/34.7
Density	1/2
Time	1/6
Acceleration	1/0.694
Stiffness EI	Pier $1/(1.36 \times 10^7)$ Superstructure $1/(2.38 \times 10^8)$
Coefficient of Viscosity	$1/(5.21 \times 10^3)$

Table 3-2 List of the Tests

Structural Types	Direction of the Excitation	Tests
Hinge Type	Longitudinal	Dynamic and static tests of the piers
		Test of the complete bridge
	Transverse	Test of the complete bridge (the effect of its neighboring spans and the stiffness of floor slabs are not considered)
		Test of the complete bridge (the effect of its neighboring spans is considered)
Damper Type	Longitudinal	Test of the complete bridge (the stiffness of floor slabs is considered)
		Dynamic and static tests of the piers
		Test of the complete bridge (without dampers)
		Test of the complete bridge (dampers of $C=0.8 \text{ kg} \cdot \text{sec}/\text{cm}$ are installed)
	Test of the complete bridge (dampers of $C=1.7 \text{ kg} \cdot \text{sec}/\text{cm}$ are installed)	
Transverse	Test of the complete bridge (without dampers)	
Simple-Girder Type	Longitudinal	Dynamic and static tests of the piers
		Test of the complete bridge
	Transverse	Test of the complete bridge

Table 3-3 Resonant Frequencies Measured by the Vibration Test

(unit: Hz)

	Longitudinal						Transverse						
	Hinge Type		Damper Type				Simple-Girder Type		Hinge Type			Damper Type	Simple-Girder Type
	① Pier only	② Complete bridge	① Pier only	② Complete bridge without dampers	③ Complete bridge C=0.8kg·sec/cm	④ Complete bridge C=1.7kg·sec/cm	① Pier only	② Complete bridge	③ Complete bridge (original type)	④ Complete bridge (the effect of its neighboring spans is considered)	⑤ Complete bridge (the stiffness of floor slabs is considered)	③ Complete bridge	④ Complete bridge
P ₄	15.8	7.9	-	-	-	10.1	-	10.8	10.1	10.1	10.1	10.1	11.0
P ₇	-	8.1	-	-	-	9.5	-	-	11.1	11.0	11.1	12.0	10.3
P ₈	-	7.9	-	7.1 (10.1)	9.6	9.4	-	-	17.8	18.0	18.7	8.7	9.8
P ₉	-	7.8	24.4	-	9.6	9.4	-	8.6	11.6	11.8	12.0	7.8	8.2
P ₁₀	-	7.8	-	-	9.6	9.3	-	8.6	9.2	9.3	9.7	7.8	8.1
P ₁₂	15.7	7.8	20.6	9.2 (9.5)	9.4	9.2	-	-	8.6	10.0	8.8	7.3	8.1
P ₁₃	16.0	8.0	23.6	9.5 (10.9)	9.4	9.3	-	8.6	8.5	-	8.6	7.3	7.6

Note: Figures in () of damper type ② are resonant frequencies measured by the vibration test using fixed bearings on Pier-P₈.

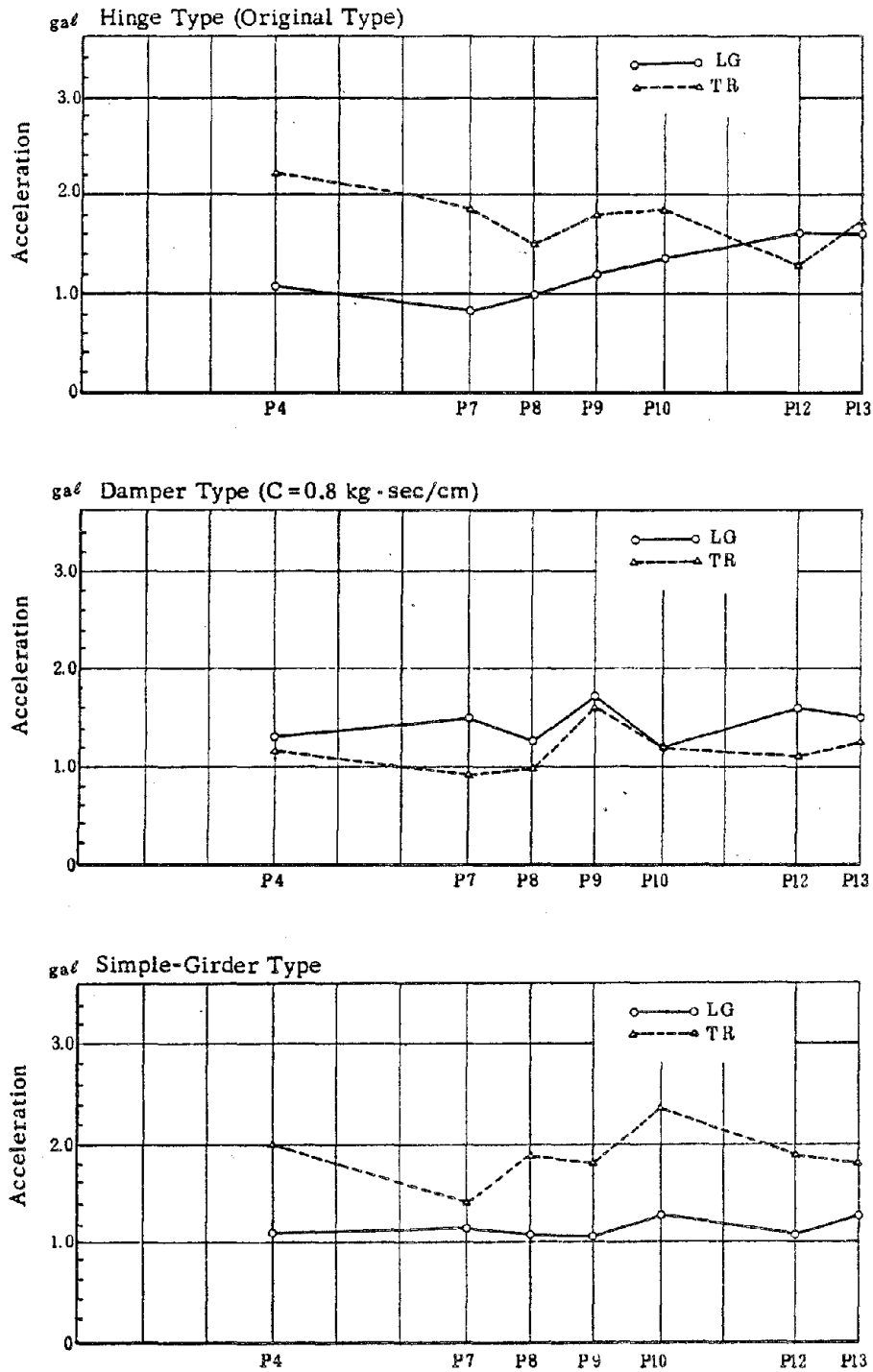


Fig. 3-5 Distribution of Maximum Response Accelerations at the Top of the Piers (Random Wave Input; 1 gal)

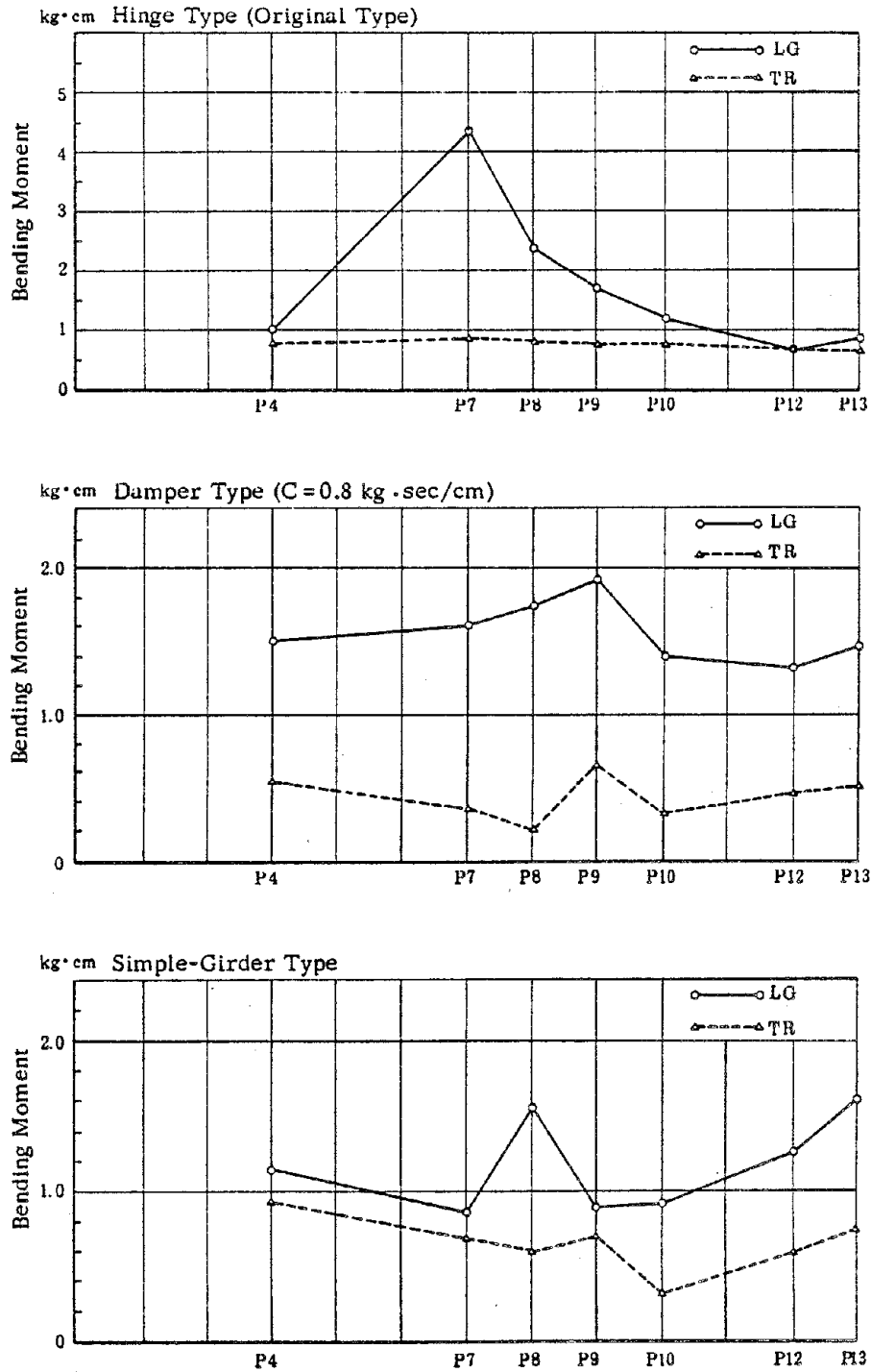


Fig. 3-6 Distribution of Maximum Bending Moments at the Base of the Piers (Random Wave Input; 1 gal)

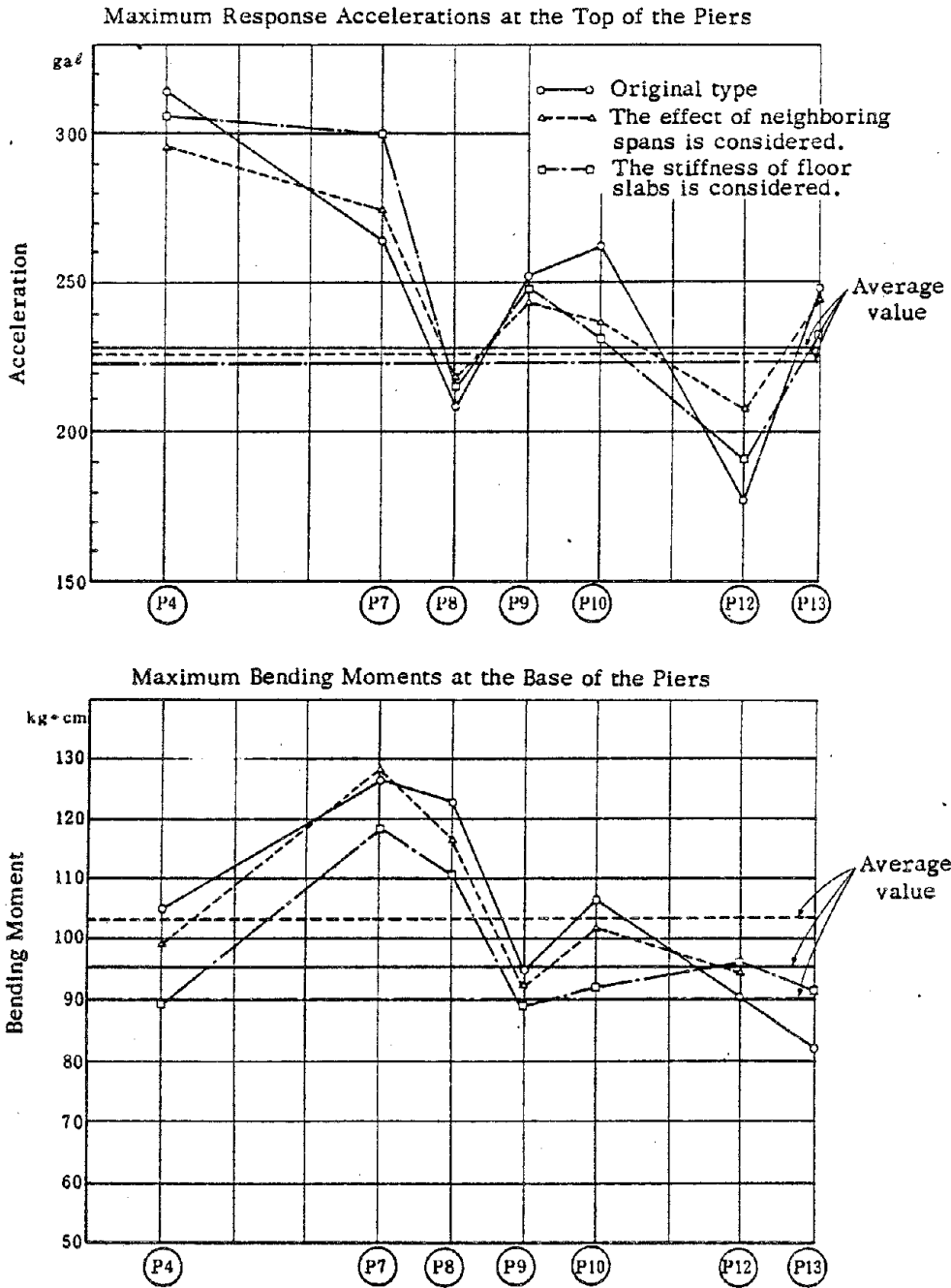


Fig. 3-7 Effects of the Neighboring Spans and the Stiffness of Floor Slabs in the Hinge-Type Bridge Model (Random Wave Excitation in the Transverse Direction; Maximum Input Acceleration; 144 gals)

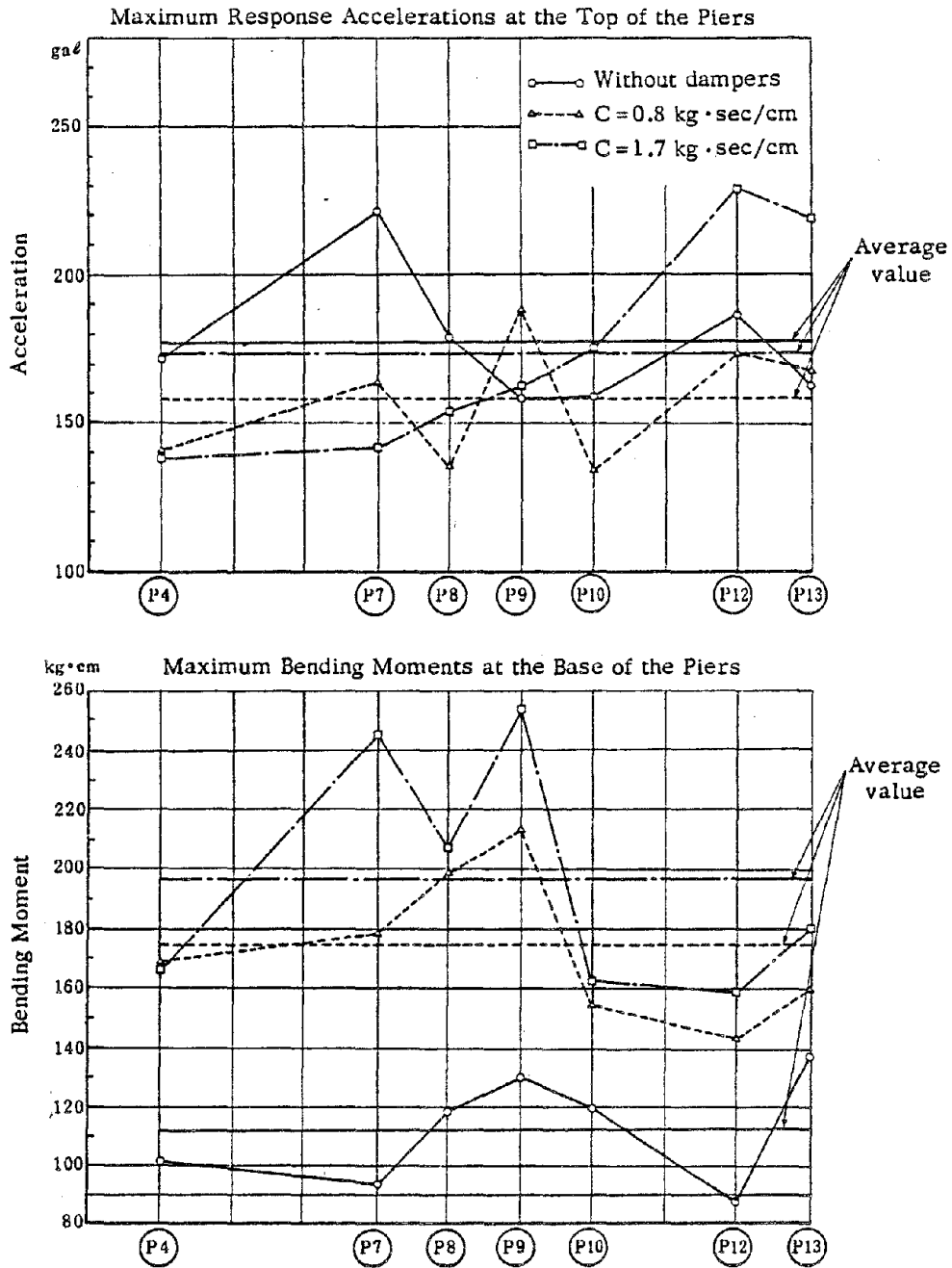


Fig. 3-8 Effects of the Dampers (Random Wave Excitation in the Longitudinal Direction; Maximum Input Acceleration; 144 gals)

The model for the simple girder-type bridge model in the longitudinal direction is separated into every pier and its supporting superstructure. The model for the simple girder-type bridge model in the transverse direction is shown in Fig. 3-10.

Results of the analysis for the hinge-type bridge model are shown in Fig. 3-12 - Fig. 3-15. Results of the time history response analysis agreed well to the results of the vibration tests except for the acceleration at Pier-7 in the transverse direction. The first vibration mode contributed greatly to the total vibration of a hinge-type bridge in the longitudinal direction. Results of the vibration test in the longitudinal direction were similar to the results of the analysis assuming the damping constant as $h=0.05$ in the hinge-type bridge model (refer to Fig. 3-14). Results of the vibration test of the simple girder-type bridge model in the longitudinal direction were similar to the results of the analysis assuming the damping constant as $h=0.10$. This shows that the responses of a simple girder-type bridge are smaller than those of a hinge-type bridge when longitudinal-direction excitations were applied. But results of the analysis for the simple girder-type bridge model in the longitudinal direction did not agree so well as those for the hinge-type bridge model to the results of the vibration tests because of uncertain effects of the friction at the movable bearings. Results of the analysis for the hinge-type bridge model in the transverse direction also agreed better than those for the simple girder-type bridge model to the results of the vibration tests. The dynamic response analysis for the damper-type bridge model in the longitudinal direction was conducted assuming the bridge model as the simple degree of freedom system in Fig. 3-11 and the relationship between the damping constant of the s-d-f system (h) and the damping coefficient of the damper (C) as Eq. (3-1).

$$\left. \begin{array}{l} \frac{mK}{C} = 2 m \omega h \\ \omega = \sqrt{\frac{K}{m}} \end{array} \right\} \longrightarrow h = \frac{\sqrt{mK}}{2C} \quad (3-1)$$

Results of the analysis for the damper-type bridge model are compared with the results of the vibration tests in Fig. 3-16. A larger damping coefficient of the damper provided larger responses in the analysis. Results of the vibration tests agreed to the results of the analysis with a larger damping coefficient than the actual damping coefficient of the damper. Other resistance than the viscous resistance of dampers seems to act against the inertia force of the superstructure and provide

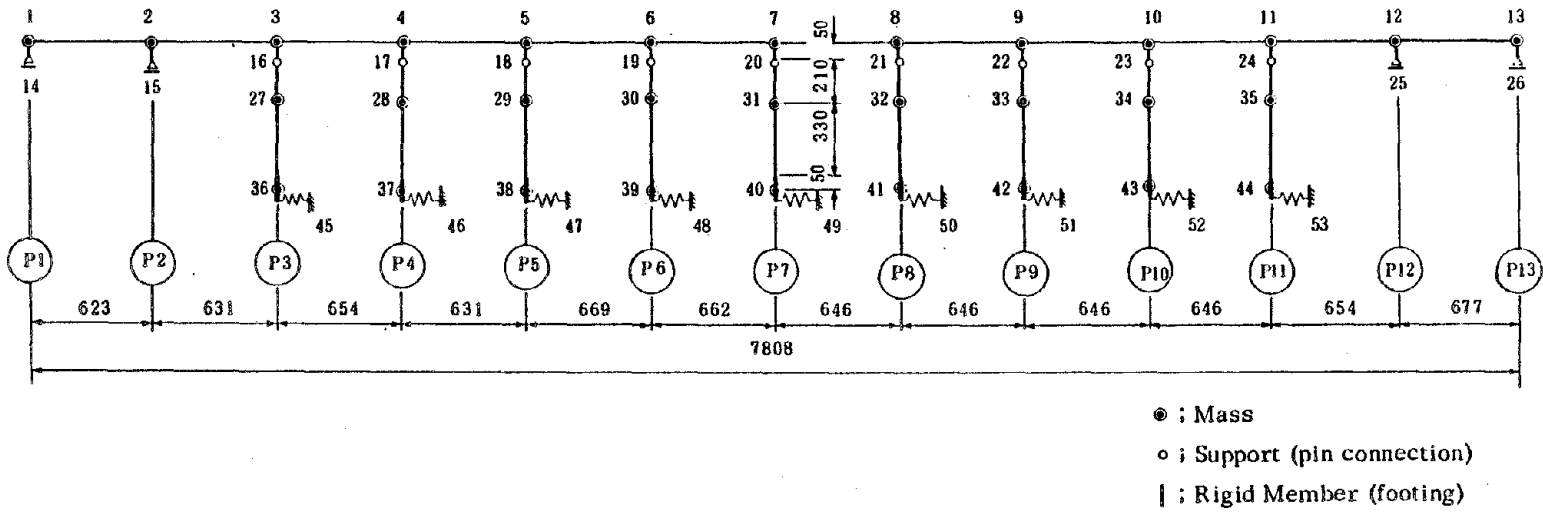


Fig. 3-9 Dynamic Analysis Model of the Hinge-Type Bridge Model in the Longitudinal Direction

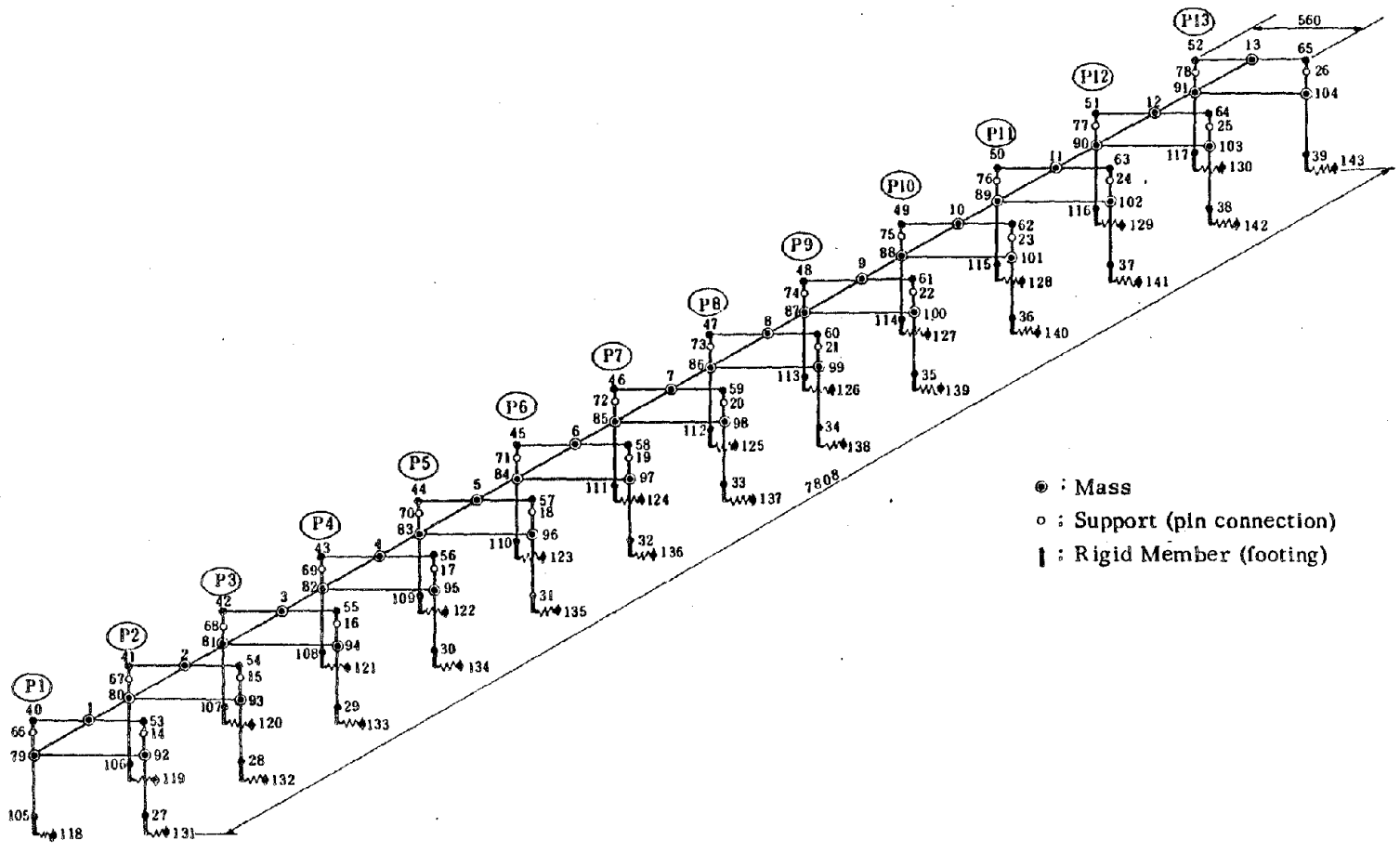


Fig. 3-10 Dynamic Analysis Model of the Hinge-Type Bridge Model and the Simple Girder-Type Bridge Model in the Transverse Direction

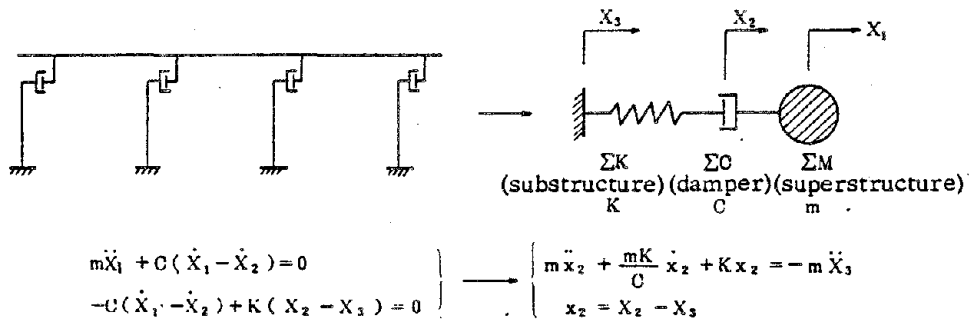


Fig. 3-11 Dynamic Analysis Model of the Damper-Type Bridge Model in the Longitudinal Direction

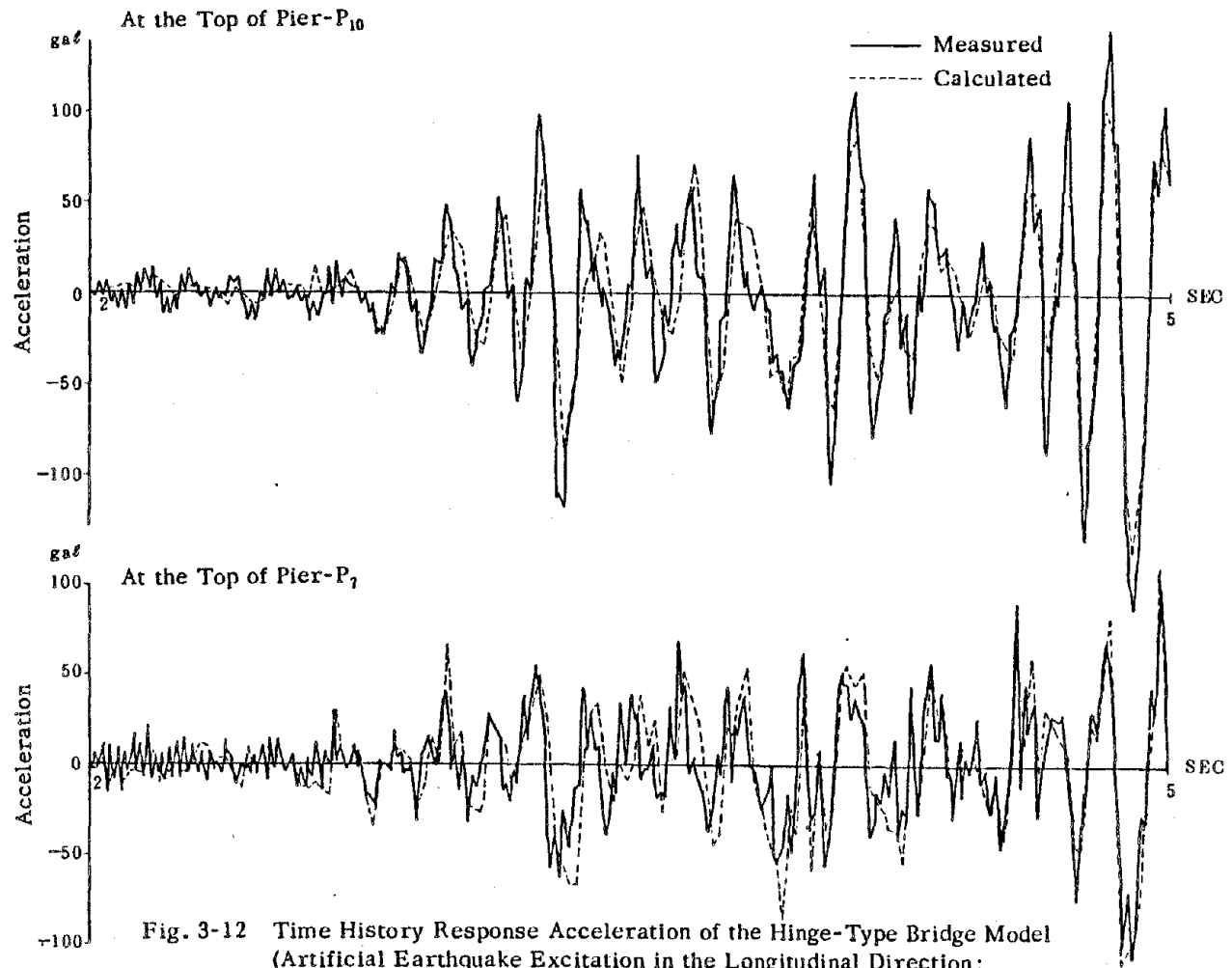


Fig. 3-12 Time History Response Acceleration of the Hinge-Type Bridge Model
 (Artificial Earthquake Excitation in the Longitudinal Direction;
 Maximum Input Acceleration; 90 gals)

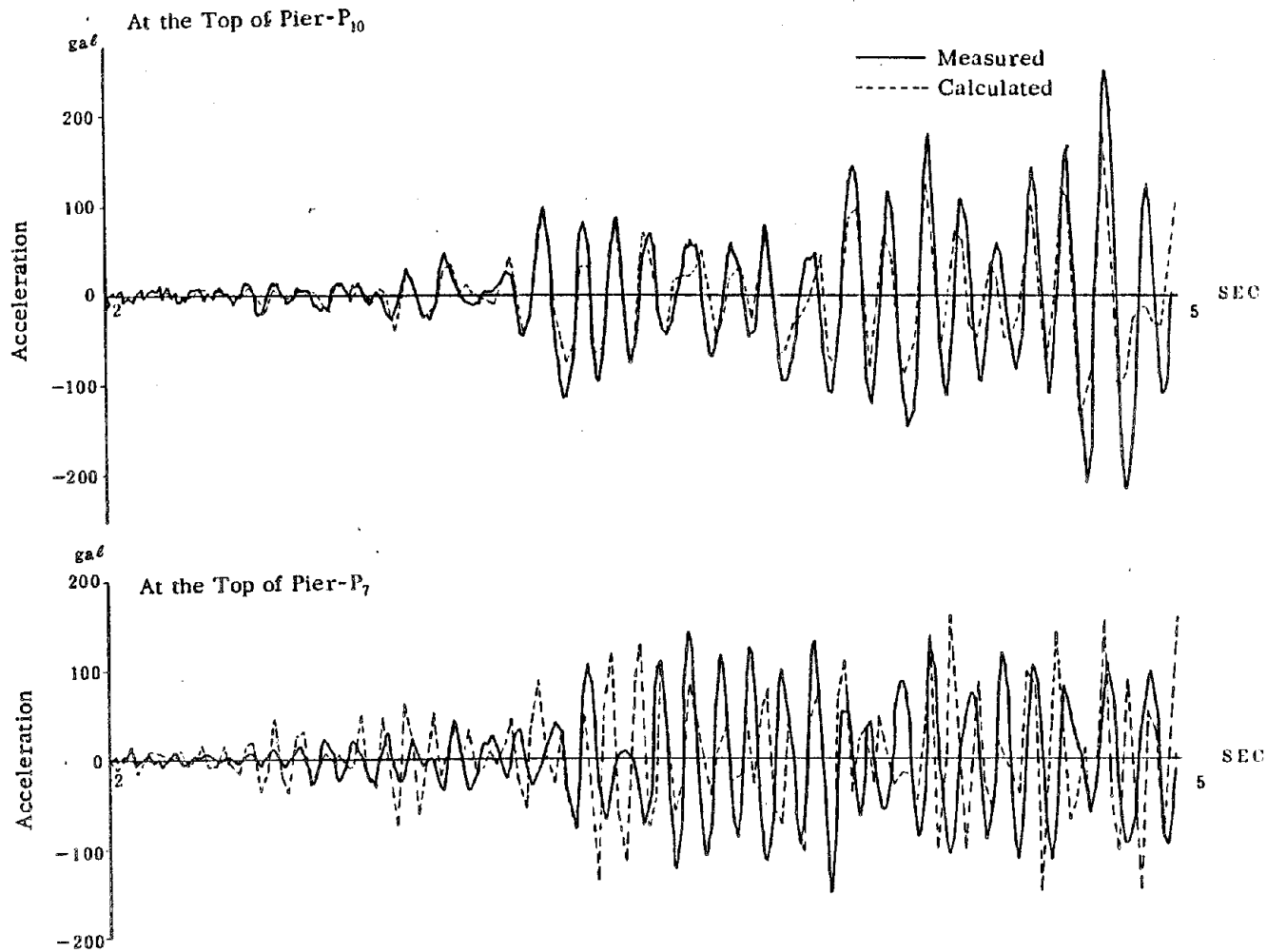


Fig. 3-13 Time History Response Acceleration of the Hinge-Type Bridge Model
 (Artificial Earthquake Excitation in the Transverse Direction:
 Maximum Input Acceleration; 90 gals)

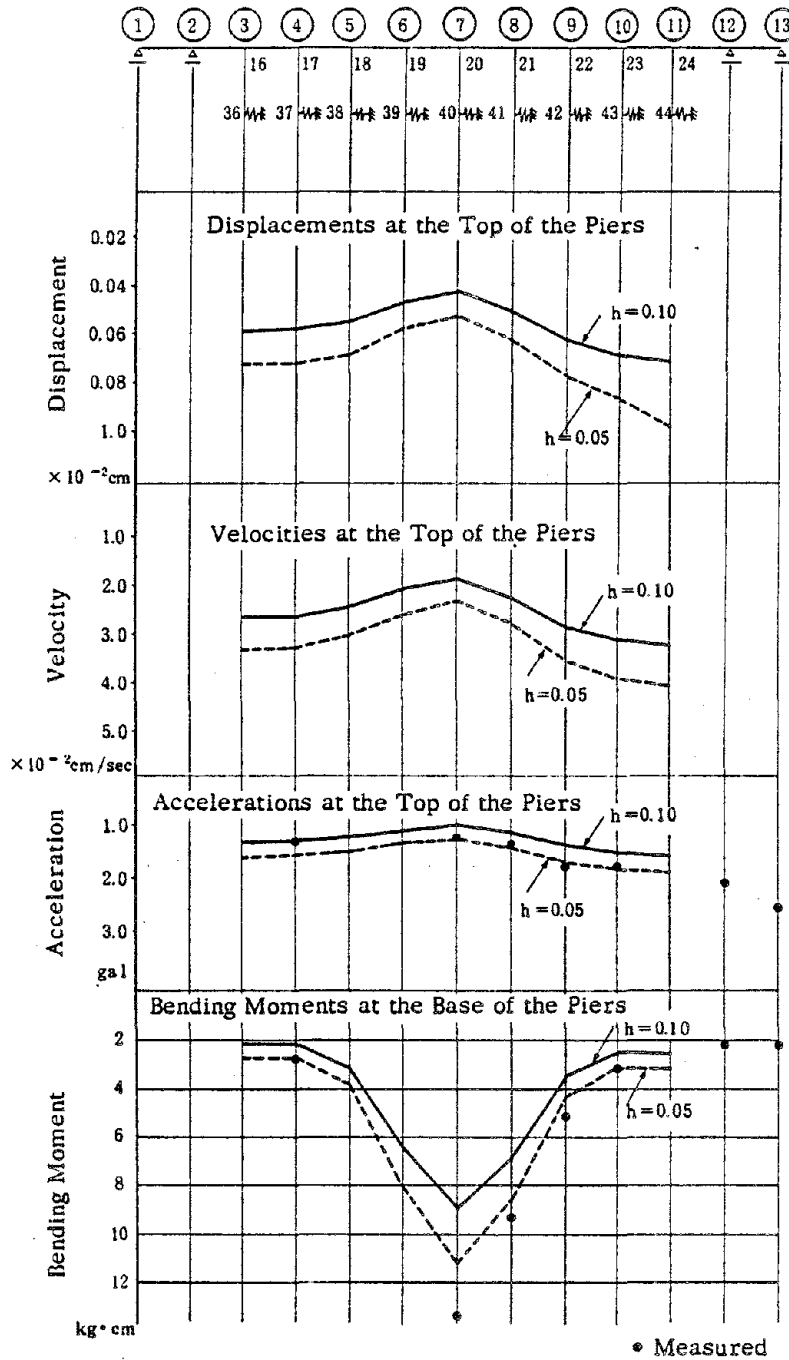


Fig. 3-14 Results of the Dynamic Analysis for the Hinge-Type Bridge Model (Artificial Earthquake Excitation in the Longitudinal Direction: Input Acceleration; 1 gal)

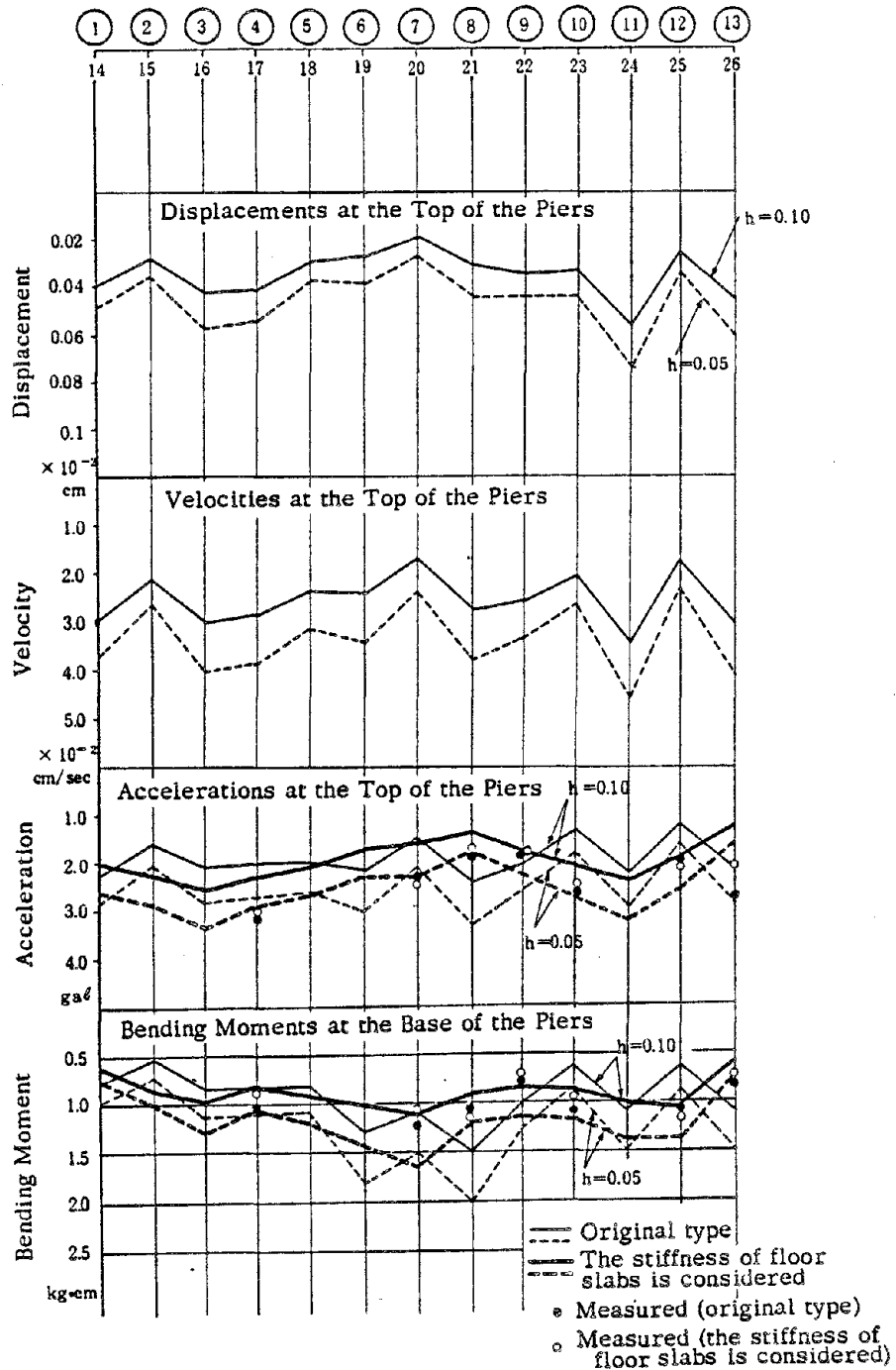


Fig. 3-15 Results of the Dynamic Analysis for the Hinge-Type Bridge Model (Artificial Earthquake Excitation in the Transverse Direction : Input Acceleration; 1 gal)

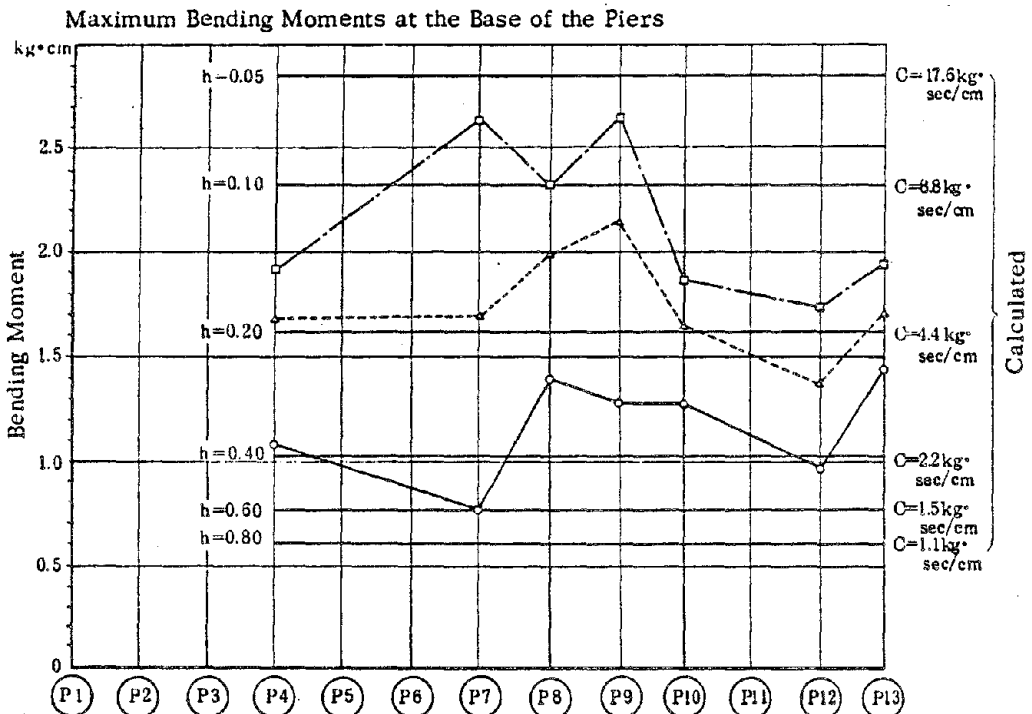
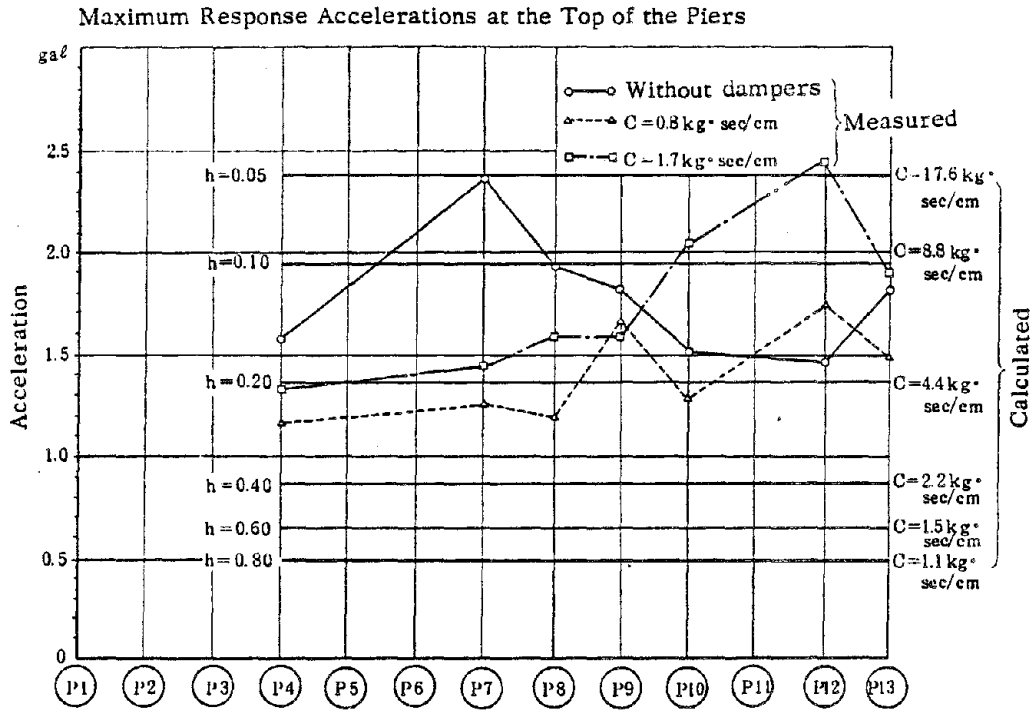


Fig. 3-16 Responses of the Damper-Type Bridge Model Measured by the Vibration Test and Those Calculated by the Dynamic Analysis

the difference between the actual responses and calculated responses by considering only the viscous resistance of dampers.

4. CONCLUSIONS

Based on the results presented, conclusions of the vibration test of Katashina-gawa Bridge model may be deduced:

- (1) Vibration modes of Katashina-gawa Bridge model by oblique direction excitations were the same as the vibration modes by longitudinal or transverse direction excitations or the combined modes of them. Responses by oblique direction excitations were smaller than those by longitudinal or transverse direction excitations. For these reasons the directions of earthquake excitations to be considered in the earthquake-resistant design of Katashina-gawa Bridge are the longitudinal and transverse directions and considerations of the excitations in other directions are not necessary.
- (2) There is an effect of a curve to the vibration modes of Bridge-A. But the effect is small enough to be neglected in the earthquake-resistant design.
- (3) It is necessary to consider the stresses in the chords at the middle of spans and the diagonal members over supports in the vertical vibrations by longitudinal excitations in the earthquake-resistant design.
- (4) Stresses in sway bracings and lateral bracings by transverse excitations are concentrated in the members over supports. The concentrated stresses are considered in the present earthquake-resistant design by the modified seismic coefficient method.
- (5) It is adequate to locate the masses at the neutral axis in the dynamic analysis model of the longitudinal direction (Longitudinal Case-2 in Table 2-3) and to consider the stiffness of the sway bracings over a support in the dynamic analysis model of the transverse direction (Transverse Case-2 in Table 2-3).

Conclusions of the vibration test of the continuous girder bridge model may be deduced:

- (1) Dynamic responses of the continuous girder bridge with hinged connection between super and sub-structures through multiple spans (a hinge-type bridge) are larger than those of the bridge arraying simple girder bridges (a simple girder-type bridge). Dynamic response characteristics of the hinge-type bridge

are not so complicated as those of other type (simple girder-type, damper-type) bridges and their sufficiently precise estimations are possible by the dynamic analysis models of Fig. 3-9 and Fig. 3-10.

(2) Effects of its neighboring spans on the hinge-type bridge during transverse excitations appear locally at the ends of the bridge. It is not necessary to consider the effects, and the hinge-type bridge is able to be considered as an independent structure in its earthquake-resistant design.

(3) Stiffness of floor slabs makes resonant frequencies of the hinge-type bridge higher and its dynamic responses a little smaller during transverse excitations. Effects of the stiffness are slight and not so important in the earthquake-resistant design of the hinge-type bridge.

(4) Inertia forces of the superstructure of the continuous girder bridge (damper-type bridge), which has only movable bearings with dampers installed to it, are not necessarily equally transmitted to each substructure. Effects of the dampers develop much in the middle of the damper-type bridge, and bending moments at the base of piers locating in the middle of the bridge tend to be large. The larger a damping coefficient of the dampers is, the larger bending moments at the base of piers of the damper-type bridge are. Dynamic responses of the damper-type bridge during earthquakes are not able to be precisely estimated by such a dynamic analysis model of Fig. 3-11. Further studies on the dynamic analysis model of the damper-type bridge are necessary.

ACKNOWLEDGEMENTS

The vibration tests of Katashina-gawa Bridge model and the continuous girder bridge model were carried out at the requests of Japan Highway Public Corporation and Metropolitan Expressway Public Corporation. The authors wish to express their deep appreciation for the cooperation of Mr. Enichi Hirakawa, the director of Tokyo Second Construction Bureau, Japan Highway Public Corporation and Mr. Hironobu Nishiyama, the director of Second Construction Department, Metropolitan Expressway Public Corporation in the performance of the tests.

REFERENCES

- 1) Expressway Investigation Committee, "Report of the Investigation and Research on Design and Construction of Large Scale Structures No. 3", March, 1980.
- 2) Expressway Investigation Committee, "Report of the Investigation and Research Committee on New Type Structures of Elevated Bridges in Urban Expressways No. 3", March, 1980.

Increased Seismic Resistance
of Highway Bridges Using
Improved Bearing Design Concepts

ROY A. IMBSEN
Engineering Computer Corporation
Sacramento, California

ABSTRACT

An attempt to increase the survivability of bridges in earthquakes through the use of improved bearing systems is explored. By reviewing the performance of various bearing systems in past earthquakes, the most desirable characteristics are selected and incorporated into new bearing systems. New concepts for fixed and expansion bearings are described. A concept utilizing an elastomeric bearing pad on a sliding friction surface is investigated analytically and found to have some advantages for bridges over other concepts employing isolation. Finally, a potential design procedure for selecting the most cost-effective bearing system is described.

KEYWORDS: Bridges; Bearing systems; Seismic resistance; Isolation; Energy dissipation; Restrainers; Sliding friction; Earthquake damage; Analytical studies; Bearing design.

INTRODUCTION

Experiences in past earthquakes, particularly the 1971 San Fernando earthquake, has demonstrated the vulnerability of bridges to earthquakes. Bridges are vital lifeline links with potentially tremendous demands placed on them for emergency services following an earthquake. Failure of a bridge in a high seismic area where there is little or no redundancy in the lifeline system could have serious effects on emergency operations. Recent federal attention given to emergency preparedness (1) and the improvement of the state of the art of seismic engineering makes it incumbent on the engineer, particularly in the more seismic regions, to pay more attention to the seismic design of structures.

Some recent smaller earthquakes which have occurred since the San Fernando earthquake are providing some insight into the on-set of failures that occur in a bridge prior to total collapse. Inspections following these earthquakes (2-8) indicates that closer attention must be given to the details such as bearings and that survival of a bridge is not contingent just on the presence or absence of ductility. It is becoming more and more apparent that the key factor in the design of a bridge with increased seismic resistance requires consideration of the overall seismic resisting mechanism composed on elastic, ductile and non-ductile components.

BACKGROUND

Bridge bearings have traditionally been used at superstructure/sub-structure interfaces to provide for structural support, relative movements and incompatibility of materials (9). "Fixed" bearings must provide for the transmission of vertical and horizontal forces to the substructure while accommodating the non-compatible rotations of the superstructure with respect to the substructure. Expansion bearings on the other hand are required to accommodate large relative translational movements due to temperature, shrinkage, creep, prestressing, etc., while maintaining their vertical load carrying capabilities. Most bridges in existence today use either sliding plates, rolling devices, linkage or rocking devices, or elastomeric pads as bearings.

In many cases portions of a bridge or even entire bridges have collapsed prior to mobilizing the ductile more energy absorbing components simply because unstable bearings and weak connections at these interfaces were not capable of transmitting the earthquake forces.

Prior to the San Fernando earthquake of 1971, resistance to lateral forces at bridge bearings was provided by shear keys, keepers, or other restraining devices of nominal design. Longitudinal force was transferred to the substructure through fixed bearings at one or more points on the superstructure. In most cases, adjacent superstructure sections were not tied together at the expansion joints which led to several bearing and structural failures during earthquakes.

Within the United States, earthquake resistance at bearings is still provided in the form of shear keys, keepers, cables, etc., which are designed to elastically resist the forces induced during an earthquake (10,11). Restraint of this type represents a cost effective means of mitigating catastrophic failures, but is not effective in absorbing the energy generated by an earthquake. Thus post-elastic behavior of the supporting members must still be relied on for this purpose.

Several improvements in the seismic design methodology have transpired since the San Fernando earthquake (12,13). One such improvement which has a direct effect on the design of bridge bearings and connections is the use of unreduced elastic response spectra for the analysis with subsequent reductions for ductility to only the ductile components (11,14). Bearings, restrainers and shear connections which are now designed to accommodate the unreduced forces are capable of transmitting forces to the ductile energy absorbing components, thus decreasing the possibilities of premature collapse.

Many researchers and innovative engineers have recently been considering a broader role for bearings in bridge earthquake resistance. Most of these efforts are directed toward the use of isolation and/or energy dissipation in the bearings.

Within the United States, the acceptance of bridge bearings as a means of improving earthquake resistance has been slow. In many cases, bearings are an "after thought," selected near the end of the design process when the earthquake resistant mechanism has already been esta-

blished. One reason for this reluctance to use bearings for earthquake resistance is the lack of readily available earthquake resistant bearing systems of proven reliability. Another reason is the lack of reliable, cost-effective analytical tools with which the earthquake resistant qualities of bearings can be assessed. The designer must have the capability to access, at least analytically, the effects of a new device on the overall seismic resistance of structures. It is, therefore, necessary to overcome both of these deterrents if bearings are to play a larger role in the earthquake resistance of structures.

DEVELOPING EFFECTIVE EARTHQUAKE RESISTANT BRIDGE BEARINGS

Evaluation of Existing Bearings

Before developing a more promising earthquake resistant bearing design concept, it is necessary to understand the relative merits of existing bearing types (15).

Rocker bearings have been used in bridges for several years. They are generally made of steel and provide for movement in the direction of expansion by rocking of a steel link which bears on plates imbedded in both the superstructure and the substructure.

During earthquakes, these bearings have not performed very well. They become unstable outside a relatively narrow range of movement and numerous instances of toppled rocker bearings have been reported. A common problem with these bearings during an earthquake is the failure of the transverse keeper plates. This type of failure may increase the energy dissipation potential of these bearings due to subsequent

sliding, but it also increases the likelihood of the bearing becoming unstable.

Roller bearings are also generally made of steel, and provide for movement by rolling of a cylinder.

Under earthquake loading they are much more stable than rockers, since their movement range is generally much larger. Like the rockers, they are difficult to restrain transversely and possess little energy dissipation potential unless sliding occurs. They generally perform satisfactorily during an earthquake, but do not improve the overall dynamic response of the structure.

Sliding bearings range from simple asbestos sheet packing between the substructure and the superstructure for short span bridges to elaborate "pot" bearings with teflon and stainless steel sliding surfaces for structures with large movements. Because of their nature, sliding devices are extremely stable during an earthquake. Although the sliding of two surfaces will dissipate energy, the low friction values used limit the energy dissipation in expansion bearings. Generally, sliding bearings have performed well during past earthquakes.

Elastomeric pads are widely used for bridges and have gained in popularity over the past several years. Most pads are constructed by bonding alternating layers of elastomer and reinforcement (steel or fabric) together. The elastomer consists primarily of either natural rubber or neoprene although other synthetic rubbers have a potential

for bearing applications. In general, these bearings have performed well during past earthquakes although they have been known to "walk-out" if not properly secured.

Although many bearings have suffered damage during earthquakes, it is important to remember that loss of vertical support has resulted in the most spectacular failures. Although qualities of energy dissipation, isolation, and restraint can reduce force levels and/or mitigate structure response, experience has shown that the primary performance characteristic of an earthquake resistant bearing is the maintenance of vertical support. Therefore, any bearing worthy of consideration must possess a high degree of reliability in this area.

Promising New Design Concepts

In exploring potential new bridge bearing design concepts for earthquake resistance, it is convenient to categorize bearings as either "fixed" or "expansion".

Expansion Bearings

There are several concepts for expansion bearings that show promise for improved earthquake resistance. One such concept employs a more or less conventional elastomeric bearing pad. During normal movement and moderate earthquakes, the pad would function exactly as present elastomeric pads. However, during a strong earthquake, one surface would be designed to slide. The coefficient of friction would be selected to

preserve the stability and integrity of the pad itself while limiting the inertia force that could be transferred to the bridge supports. Thus, the pad would limit the forces transferred to portions of the structure which are difficult to inspect following an earthquake. The remaining surface of the pad would be physically attached to the substructure to insure that all movement would take place on the sliding surface and to prevent pad "walk-out". A schematic drawing of this design concept is shown in Figure 1.

Such a system has the following advantages:

1. A history of proven reliability in maintaining vertical support
2. Protection of the supports from loads which could cause excessive damage
3. Potential for significant energy dissipation at high displacement levels
4. Potential for isolation which will tend to limit structural response
5. Compatibility with current production capabilities of bearing manufacturers
6. Designer acceptance of elastomeric bearing pads

A somewhat different concept is to use viscous dampers at the expansion bearings. These devices have force-displacement characteristics that vary with the rate of displacement. At slow rates of displacement, such as temperature movement, very little force is generated. At high rates, such as in an earthquake, more force is required to deform the device. This allows the designer to mobilize all supports to resist

the earthquake load. In addition, energy is dissipated throughout the course of rapid movement. This tends to mitigate the resonant condition that can increase force levels so dramatically during an earthquake.

The Japanese have used this concept extensively for earthquake resistance. To date viscous dampers have been separate devices which are used in conjunction with conventional bearings. These devices have a history of maintenance difficulties due to leaking seals, etc.

To meet the requirements of a self-contained bearing which will be relatively maintenance free and stable under sustained load, a bearing such as the one shown in Figure 2a is proposed. This bearing would consist of a strong, reinforced flexible membrane having a disk-like shape in plan which would contain an incompressible viscoelastic material. Relative movement of the two bearing surfaces would cause the block of viscoelastic material to deform. During an earthquake, this deformation would require more force and therefore the device would behave like a viscous damper.

This type of bearing is, however, susceptible to damage caused by vandalism, fire, or tearing due to excessive relative movement of the bearing surfaces. Any loss of viscoelastic material could result in collapse of the bearing. To prevent damage due to vandalism and fire, a shield could be constructed around the bearing. This shield would be used to induce sliding of the bearing which could prevent the membrane from being torn apart due to excessive movements. A schematic drawing

is shown in Figure 2b.

Another solution is to insert a circular shaped bearing pad as shown in Figure 2c to support the vertical load should the membrane be punctured or damaged. Now the viscoelastic material is confined by the disk shaped membrane and the circular bearing forming a toroidal like shape. The lateral stiffness of the bearing system under slow normal temperature and shrinkage movements is derived from the bearing pad alone. However, during sudden earthquake movements the lateral stiffness will be increased by the effects of the viscoelastic material. The lateral forces increasing until sliding is induced at the friction surface to limit the force level being transmitted to the foundation. During sudden earthquake movements the toroidal shaped viscoelastic material attempting to retain its shape would deform under lateral movements as depicted in Figure 2d. The tendency to deform in the vertical direction would mobilize the vertical dead load effects creating an opposing couple in the direction as shown in the figure. The generated couple will provide an opposing force tending to move the structure back to its original position. Since the bearing is circular shaped in plan, this restoring force would be generated in any horizontal direction depending on the direction of the earthquake force. Mobilizing the dead load will, in addition to creating the resisting couple, dissipate energy as the visco-elastic material is deformed.

A considerable amount of development is required before this flexible membrane concept can be used with confidence in a bridge structure. The membrane must possess unusually high strength, stability, and durability. The viscoelastic material must have suitable force-displacement characteristics over the necessary range of temperatures. These materials must be developed and tested. In addition, these materials must be made to work as a unit. Tests of the assembled bearing system should be conducted to determine performance characteristics during an earthquake. Although a considerable development effort is required, this concept may be the answer to providing reliable, cost-effective viscous damping at bridge bearings.

The restoring mechanism created by bearing system described above couples, to some extent, the horizontal and vertical modes of vibration. This created coupling effect could potentially be utilized to direct some of the energy imparted into the structure during a seismic motion to components which are inherently stronger. For example, bridges designed to resist vertical dead and live loads, are inherently stronger in this direction and can resist large loads elastically. Horizontal earthquakes forces would thus excite the coupled vertical modes and cause additional energy to be dissipated by normal damping effects. Again, this principle would require additional research, but it is practical in that the concept attempts to utilize the characteristics inherent in the structure.

Fixed Bearing

These are in many ways similar to bearings used for buildings or other similar structures. There are essentially two innovative approaches to improving the earthquake resistance of these bearings.

One method of improving earthquake resistance is to provide nominal fixity of a "free" or expansion bearing. Fixity is provided by a "fuse" which will resist lateral loads caused by wind or braking, but will fracture during a strong earthquake. Once the "fuse" has failed, the structure will be isolated from the earthquake ground motion. This will result in very small force levels in the supporting members, but larger relative displacements between the supports and the bridge superstructure. Generally, a restoring force should be provided to return the structure to a neutral position following the earthquake. Several individuals have proposed this type of bearing system.

The second approach to the design of earthquake resistant "fixed" bearings attempts to mitigate the effect of high relative displacements experienced in isolated structures. Although relative movement will be allowed at the bearings under severe lateral loading, the primary mechanism of earthquake resistance is energy dissipation as opposed to isolation. To provide for energy dissipation, several devices have been proposed. In most cases these devices also serve as "fuses" to prevent movement at low force levels.

A currently popular method of providing energy dissipation is through the use of steel devices designed to yield under severe loading. The devices are relatively inexpensive, maintenance free, and if properly designed, reliable through several cycles of yielding. Some of the more popular devices rely on twisting of a torsion bar, bending of a tapered cantilever beam, and bending and rolling of a steel hoop. Another device, which has the advantage of utilizing "off-the-shelf" steel components, is the constant moment simple beam device shown in Figure 3. These devices are very adaptable to bridge use and many of them have been used successfully on bridges in New Zealand (16).

Energy is also dissipated due to the sliding of two surfaces. By selecting the appropriate coefficient of friction, many sliding expansion bearings in use today could be made to function as "fixed" bearings. In this type of installation, attention should be given to preventing sliding of the surfaces caused by vibration of the superstructure under normal loading conditions. A suggested approach to this problem at a typical bridge abutment is shown in Figure 4. In this case, enclosed elastomeric bearings are sloped to keep the structure in a neutral position under normal conditions. During an earthquake, the superstructure would have to be lifted to cause sliding. Because of the sloped surface, the structure would have a biased movement toward the original position.

There is not enough space to discuss in detail the many bearing concepts that have been developed to date. The innovative designer has several reliable bearing systems from which to choose. With continued research in this area, the number of possibilities can only increase.

SEISMIC RESPONSE OF BRIDGE BEARINGS

Analytical Techniques

Faced with a wide choice of bearing types and functions, the designer must be able to select the bearing most appropriate for his bridge. Since many bearings have non-linear force/displacement characteristics, it is difficult for the designer to determine the overall effect of bearing response on the seismic response of his structure. This is primarily due to the lack of a reliable, user-oriented analytical tool for determining the non-linear seismic response of bridge structures. In addition, there has been a limited amount of research into bearing response. Therefore, reliable simplified techniques for determining bearing response from an elastic analysis are also unavailable.

Case Studies

A research oriented computer program was developed at the University of California to study the nonlinear seismic response of bridge structures (17-19). This program was used to study the seismic response of three bridge structures (15) of varying construction types which suffered moderate to severe damage in past earthquakes. Observation of the damage experienced by each of these bridges, along with the nonlinear analysis results, led to the following general conclusions about the

design of bridge bearings:

1. Maintenance of vertical load carrying ability is the most important feature of an earthquake resistant bearing.
2. A discontinuous superstructure on high piers represents a particularly acute seismic risk.
3. Bearing force levels in fixed bearings are extremely high, even in moderate earthquakes.
4. Yielding or even failure of bearing shear capacity is not a serious problem and may even be beneficial to the overall structure performance provided vertical support can be maintained.

Sensitivity Studies

This program was also used to study the potential behavior of the proposed bearing design consisting of an elastomeric pad with a sliding surface. A simple one degree of freedom system was used to study this behavior. Such a system is representative of a continuous bridge structure responding in the longitudinal direction. A schematic diagram of this behavior and the single degree of freedom idealization is shown in Figure 5.

For the purpose of this study, all bearings were assumed to reach the maximum force level simultaneously. In using this earthquake resisting mechanism, the designer is faced with selecting the proper longitudinal stiffness and maximum force level.

In order to investigate the sensitivity of the response to several of the parameters over which the designer has control, the simplified model was analyzed with different values for each of the parameters. A time history of the force and displacement response of each of the simplified models to two different earthquake motions was determined. The maximum responses for each analysis were recorded and plotted on a force vs. displacement graph. This graph is shown in Figure 6. Notice the characteristic shape that these graphs take when bearings of constant lateral stiffness have the coefficient of friction of the sliding surface varied. As can be seen, there is a coefficient of friction at which both displacement and force will be relatively low. This is the type of information the designer must have when selecting the best bearing design for his application.

MINIMUM COST APPROACH

IN SELECTING MOST EARTHQUAKE BEARING SYSTEMS

Once the designer is able to determine the maximum displacement and acceleration response caused by a particular bearing system, must select the most appropriate bearing for his bridge. Criteria has been suggested which seeks to minimize some aspect of structural response, such as acceleration. However, given equal reliability of bearing systems, the most meaningful approach is to minimize cost. A suggested technique for investigating the relative cost of using various bearings systems is illustrated graphically in the following paragraphs.

Consider the maximum force vs. maximum displacement graphs developed in the previous section. Structural displacements of a bridge deck in the longitudinal direction are usually limited by the available seat length and bearing movement capacity at certain supports such as the abutments. When earthquake loading is not considered, these lengths will usually be governed by expansion and contraction of the superstructure and/or minimum detailing standards. In the case of foundation forces, lateral loads other than those created by seismic loadings will require design to a certain capacity. These nominal displacement and force values which do not include the effects of earthquake loading may be plotted on a maximum displacement versus maximum foundation force graph as shown in Figure 7a. Costs associated with increasing the displacement and force capacity are generally the most significant costs in any seismic design.

To assess the economic advantages of a particular design involving a simple structural system such as the one mentioned previously, it is necessary to evaluate the increased displacement or foundation force capacity that can be purchased for a given increase in total structure cost. By plotting the increase in these capacities for incremental increases in cost and by evaluating the various combinations of displacement and force capacities that can be purchased at each level of cost increase, contours of equal incremental cost increases can be plotted on our graph as shown in Figure 7b. With these contours, a means now exists for evaluating the economic merits of a given design approach.

Consider as a hypothetical example the selection of a bearing system for a simple highway bridge. The designer may first wish to consider isolating bearings in which a "fuse" is provided to resist normal wind and braking forces. Once the fuse has failed during an earthquake, the foundation will be isolated from the inertia forces in the superstructure, and foundation forces will remain at a low level. The resulting structural displacements will generally be large, however. The resulting response may be plotted on the graph as shown in Figure 7c.

As a second alternative, the designer might consider a bearing which uses an elastoplastic energy dissipation mechanism. In such a design, the displacement response would be reduced, but at the expense of increased forces. If plotted on the force-displacement graph as shown in Figure 7c, the relative cost can be compared with other alternatives. In this example, the second alternative is more cost effective than isolation. By varying the initial stiffness and yield level of the elasto-plastic energy dissipation mechanism, it may be possible to achieve even better economics. By comparing alternatives based on equal cost contours, the optimum design can be selected. This procedure may be extended to more complicated design problems provided the analytical tools are available to predict structure response.

CONCLUSIONS AND RECOMMENDATIONS

The possibility of improved earthquake resistant bridge design through the effective use of bearings shows great promise. Before this can become a reality, the designer must be convinced that this approach

will produce cost effective bridge designs. This requires that reliable earthquake resistant bearing systems be readily available or easily manufactured. To prove the reliability of new design concepts, laboratory testing is needed. This testing should produce information that is meaningful to the designer and can be used in designing similar bearings.

In addition, the designer must be provided with the analytical tools with which to assess bearing response. Not only should the designer have access to easy-to-use non-linear dynamic analysis computer programs, but he should also have guidelines for using normal elastic analysis techniques to predict bearing behavior.

Once reliable bearings are made available and the designer can analyze their behavior during an earthquake, bridge bearings will begin to achieve their full potential in improving the earthquake resistance of bridge structures.

ACKNOWLEDGEMENTS

The research was sponsored by the Federal Highway Administration with Mr. James Cooper as the Project Manager.

REFERENCES

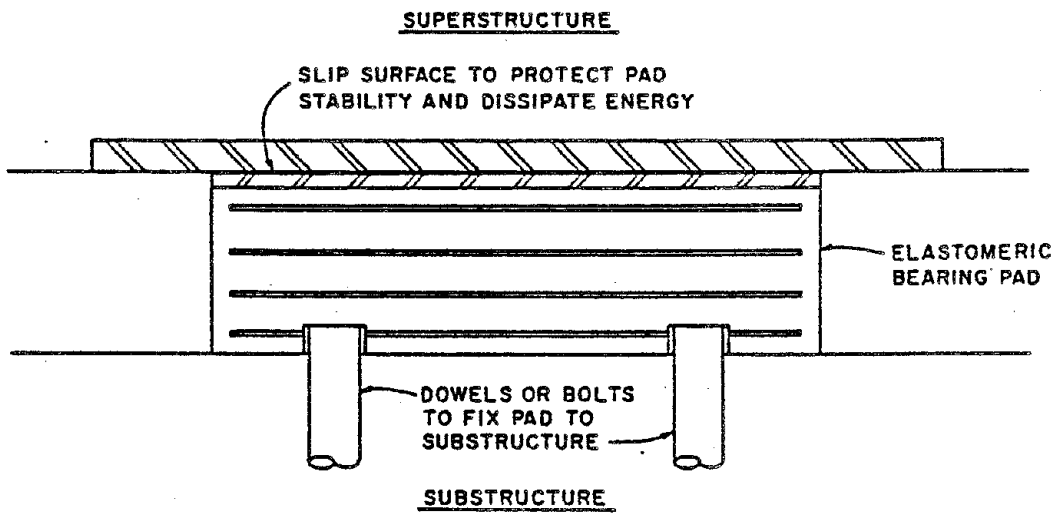
1. Federal Emergency Management Agency, "An Assessment of the Consequences and Preparations for a Catastrophic California Earthquake," November, 1980.

2. Fung, G., LeBeau, R., Klein, E., Belvedere, J., Goldschmidt, A., "Field Investigation of Bridge Damage in the San Fernando Earthquake," State of California, Division of Highways, Bridge Department, 1971.
3. Iwasaki, T., Penzien, J., Clough, R., "Literature Survey-Seismic Effects on Highway Bridges," Report No.EERC 72-11, Earthquake Research Engineering Center, University of California, Berkeley, November, 1972.
4. Cooper, J.D., "Bridge and Highway Damage Resulting from the 1976 Guatemala Earthquake," Report No.FHWA-RD-76-148, Federal Highway Administration, May, 1976.
5. Degenkolb, O.H., "Highway Bridge Damage-Santa Barbara Earthquake of August 13, 1978", Earthquake Engineering Research Institute, Volume 12, No.5, September, 1978, pp.21-24.
6. Jurach, P.J., Storlie, L.N., Miller, G.G., and Imbsen, R.A., "Final Report of the El Centro Earthquake of October 15, 1979," California Department of Transportation, Office of Structures Design, 1979.
7. Imbsen, R.A., "Structural Damage to Bridges in the California Trinidad-Offshore Earthquake of November 8, 1980," Newsletter, Earthquake Engineering Research Institute, Volume 15, No.1, Part B, January, 1981.
8. Seamans, F.M., Zelinski, R., "Final Report of the Eureka (Trinidad-Offshore) Earthquake of November 8, 1980," California Department of Transportation, Office of Structures Design, 1980.
9. "Bridge Bearings," National Cooperative Highway Research Program Synthesis of Highway Practice 41, 1977.

10. American Association of State Highway and Transportation Officials, "Standard Specifications for Highway Bridges," Twelfth Edition, 1977.
11. California Department of Transportation, "Bridge Planning Design Manual," Volume 1, 1977.
12. Gates, J.A., "Factors Considered in the Development of the California Seismic Design Criteria for Bridges," Proceedings of a Workshop on Earthquake Resistance of Highway Bridges, Applied Technology Council, January, 1979, pp.142-162.
13. Degenkolb, O.H., "Retrofitting Highway Structures to Increase Seismic Resistance," Proceedings of the Technical Council on Life Line Earthquake Engineering Specialty Conference, Los Angeles, California, August, 1977.
14. "Guidelines for the Seismic Design of Highway Bridges," ATC-6, Applied Technology Council, 1981.
15. Imbsen, R.A., "Earthquake Resistant Bridge Bearings," Federal Highway Administration, Final Report, Contract No.DOT-FH-11-9527, 1981.
16. Blakeley, R.W.G., Cormack, L.G., and Stockwell, M.J., "Mechanical Energy Dissipating Devices," Bulletin of the New Zealand National Society for Earthquake Engineering, Volume 13, No.3, September, 1980.
17. Tseng, W.S., and Penzien, J., "Analytical Investigation of the Seismic Response of Long Multiple Span Highway Bridges," Report No.EERC-73-12, Earthquake Engineering Research Center, University of California, Berkeley, 1973.
18. Kawashima, K., and Penzien, J., "Correlative Investigation on

Theoretical and Experimental Behavior of a Model Bridge Structure," Report No.EERC 76-26, Earthquake Engineering Research Center, University of California, Berkeley, 1976.

19. Imbsen, R.A., Nutt, R.V., and Penzien, J., "Seismic Response of Bridges-Case Studies," Report No.EERC 78-14, Earthquake Engineering Research Center, University of California, Berkeley, 1978.



EARTHQUAKE RESISTANT BEARING CONCEPT 1E
Elastomeric Pad with Slip Surface

FIGURE 1

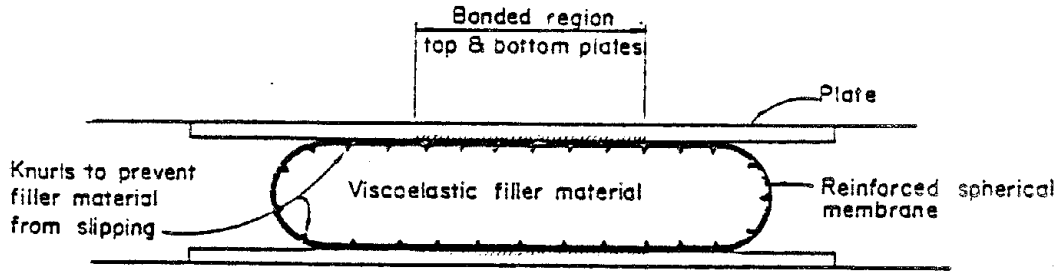


FIGURE 2a

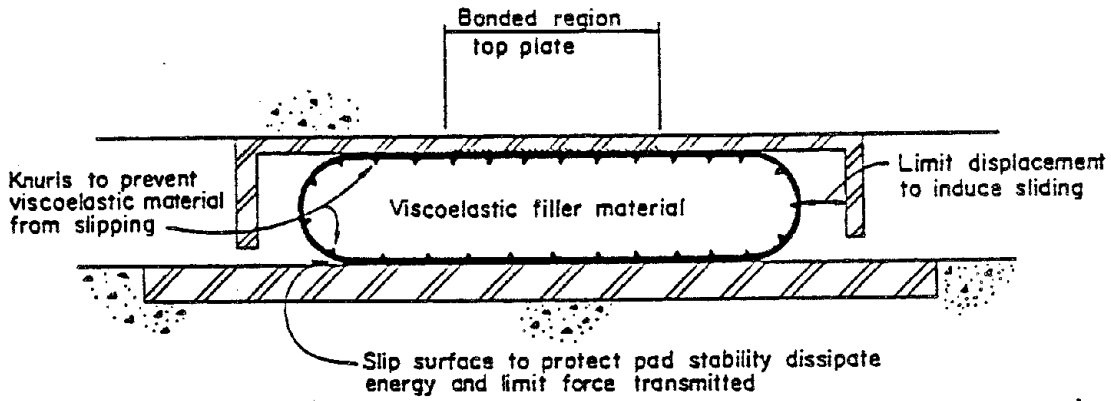


FIGURE 2b

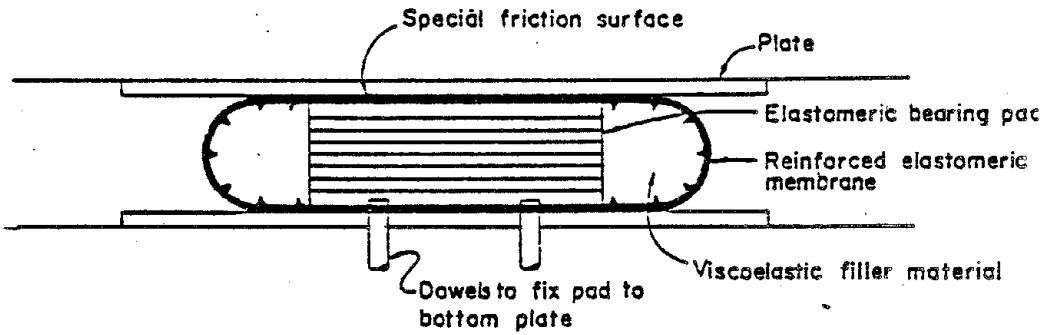


FIGURE 2c

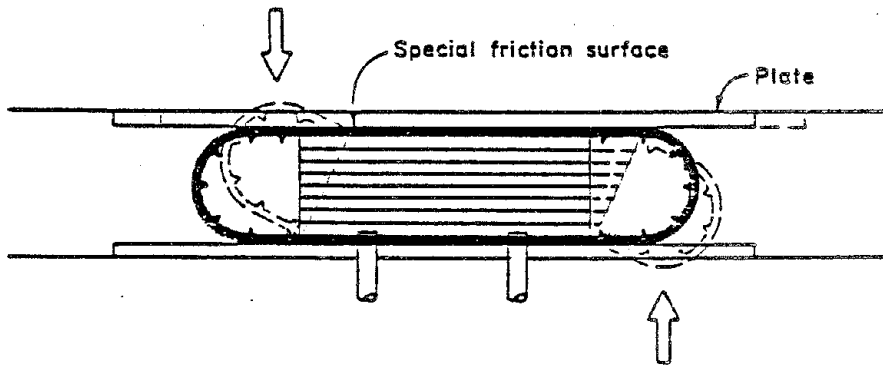
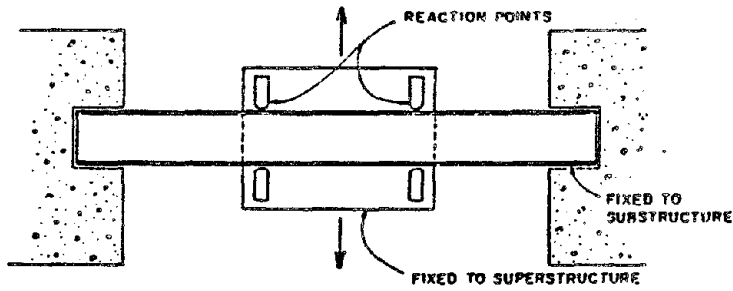


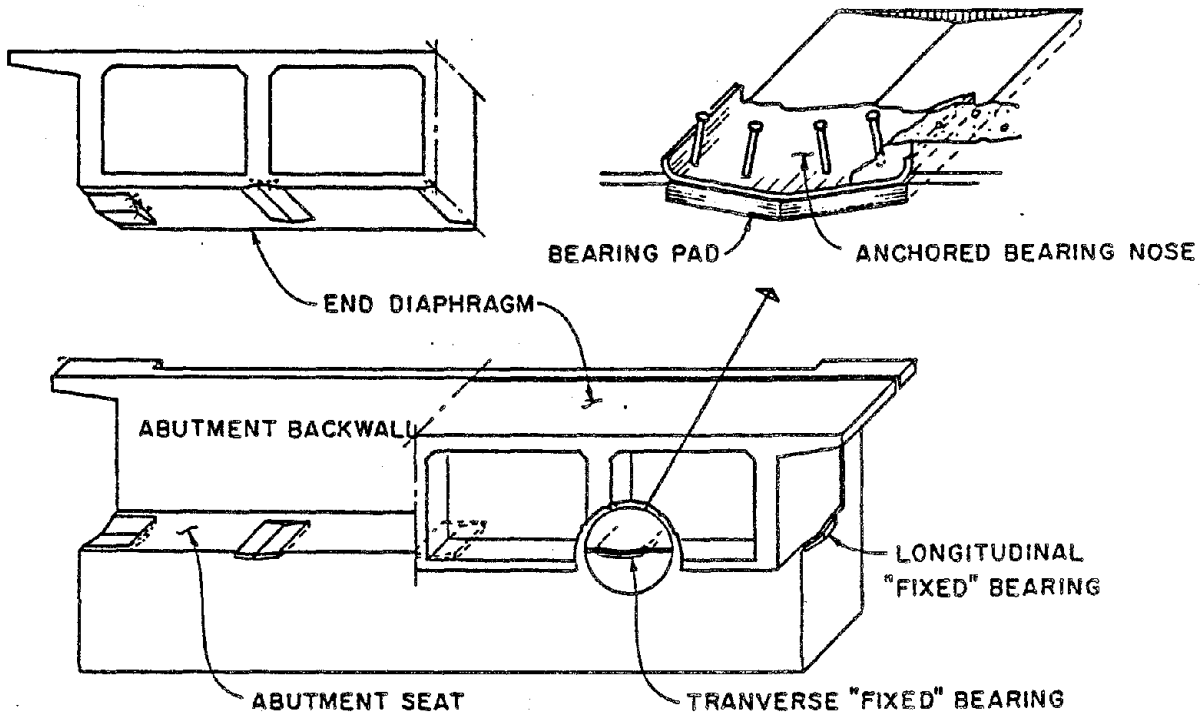
FIGURE 2d

EARTHQUAKE RESISTANT BEARING CONCEPT
Viscoelastic Material Enclosed in a Spherical Membrane



CONSTANT MOMENT SIMPLE BEAM DEVICE

FIGURE 3



SLIDING "FIXED" BEARINGS AT TYPICAL BRIDGE ABUTMENT

FIGURE 4

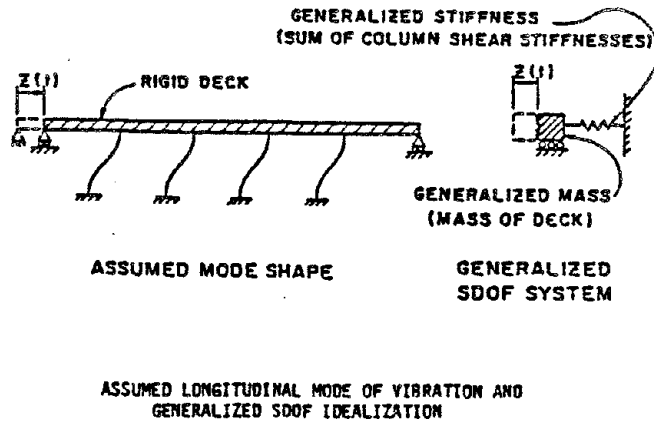
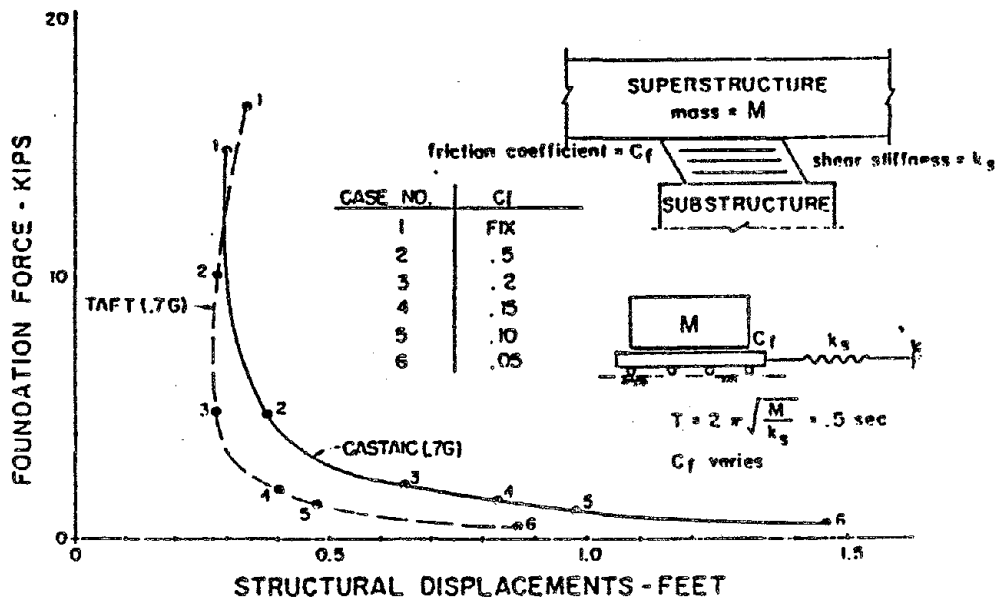


FIGURE 5



MAXIMUM FORCE AND DISPLACEMENTS RESPONSES FOR ELASTOMERIC BEARING PAD SYSTEMS OF PERIOD = .5 SEC & VARIABLE COEFFICIENTS OF SLIDING FRICTION

FIGURE 6

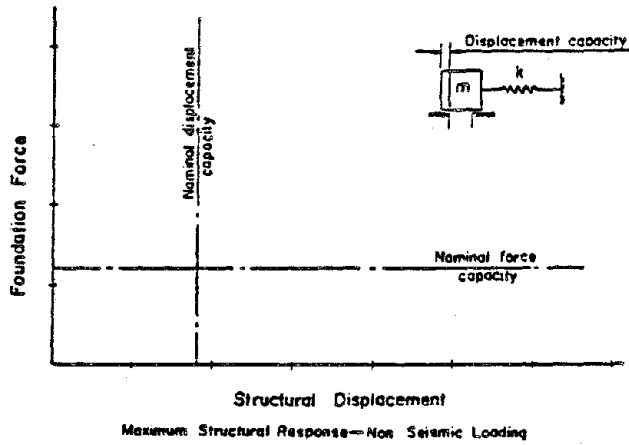


Figure 7a

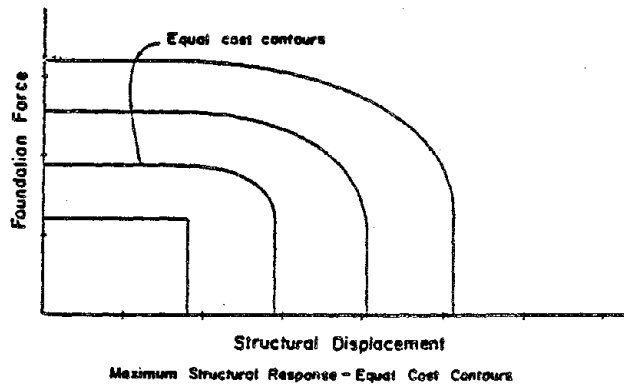


Figure 7b

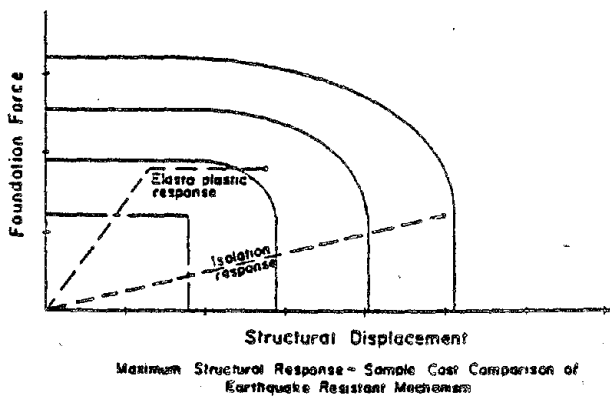


Figure 7c



Studies in the Reinforcement of Bridge Seats against Earthquakes

Y. Shioi^I, Y. Mitsuie^{II}, T. Shimizu^{III}

ABSTRACT

As earthquakes often occur in Japan, the dimensions of the substructures of bridges and their supports mainly depend upon seismic load for their design.

In order to prevent the fall of superstructure or breaking of bridge seat concrete, the 'Substructure Specifications for Highway Bridges' published in 1968 has defined the necessary distance from the edge of a bearing to the edge of a bridge seat in proportion to span length.

Various types of damage to supports resulted from the Miyagiken-oki Earthquake in 1978. In consequence of a detailed investigation, the damage found among substructures designed with the above specifications could be classified into breakage of bearings and anchor bolts, cracking of bridge seat concrete, and slight damage to supports.

The authors have undertaken a series of loading tests on bridge seat concrete to confirm the safety of structures built to present specifications and to examine more effective reinforcements, and have analysed the measured data.

They have thus been able to confirm the validity of the specifications and have been able to propose some effective reinforcements.

-
- I: Head, Foundation Engineering Division, Structure and Bridge Department, Public Works Research Institute, Ministry of Construction.
 - II: Former Researcher, Foundation Engineering Division, ditto. Chief of Bridge, IInd Division of National Highway, Road Bureau, Ministry of Construction.
 - III: Engineer, Foundation Engineering Division, Structure and Bridge Department, Public Works Research Institute, Ministry of Construction.

1. Introduction

As large earthquakes often occur in Japan as shown in Fig. 1.1, the dimensions of the substructures of bridges, including supports, depend mainly upon seismic load for their design.

The substructure specifications for highway bridges have been developed step by step since 1964. The 'Design Guides on Abutments and Piers' published in 1968 describes the details for bridge seats. There were no big earthquake from that time until the Miyagiken-oki Earthquake in 1978.

The Miyagiken-oki Earthquake, which occurred in June 1978, caused damage of some degree to about 100 bridges, and the total damage ran to about 4 billion yen.

There was a total of 662 damaged supports and 77 cracks and breakages at bridge seats, which corresponds to 12% of the total. (see Figs. 1.2, 1.3) Among these, there were 36 supports of broken seats that were not able to withstand the horizontal force to their bottom ribs.

This type of damage is particularly noticeable on fixed supports. Shearing rupture of bridge seats is believed to result from the higher shear stress of the horizontal force of the earthquake compared to the shear strength of the seat concrete.

Factors that may be considered to influence the shear strength of seat concrete are the distance to the edge of the bearing, reinforcement of the concrete and its shape, and the kind and strength of the seat mortar. It is considered that the distance to the edge of the bearing and the reinforcement of the seat concrete are particularly important factors.

However, at present we have not yet established design methods in relation to stress conditions in seat concrete during earthquakes, as there are still several unknown factors.

The authors have undertaken a series of loading tests on models of bridge seats and have studied the behavior, strength and breaking of seat concrete, in particular the following points:

No	Date	Name	M
1	Spet. 1, 1923	Kanto	7.9
2	Dec. 21, 1946	Nankai	8.1
3	Jun. 28, 1948	Fukui	7.3
4	Dec. 26, 1949	Imaichi	6.4
5	Mar. 4, 1952	Tokachi-oki	8.1
6	Apr. 30, 1962	Northern Miyagi	6.5
7	Jun. 16, 1964	Niigata	7.5
8	Feb. 21, 1968	Ebino	6.1
9	May 16, 1968	Tokachi-oki	7.9
10	Jun. 12, 1978	Miyagiken-oki	7.4

(*) Magnitudes are on the Richter scale, after Rika Nenpyo (Annual Report of Science) (1971).

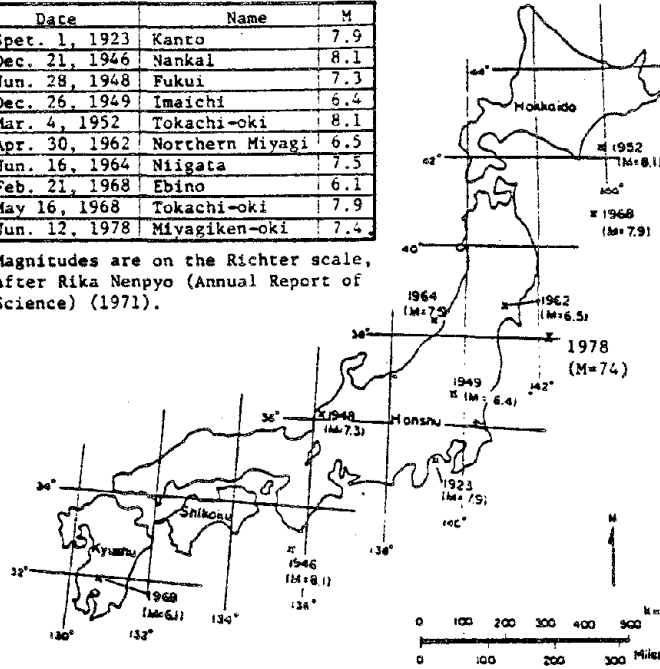


Fig. 1.1 Epicenters of ten earthquakes which caused comparatively severe damage to modern engineering structures in Japan⁸⁾

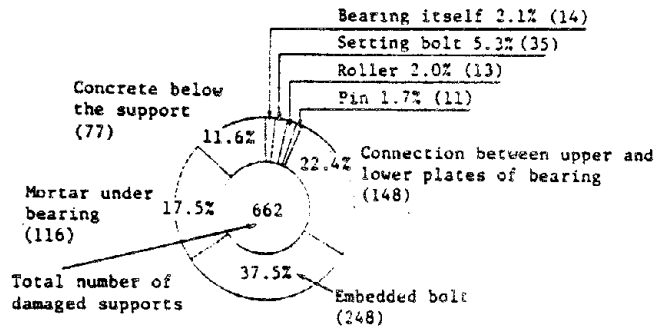


Fig. 1.2 Breakdown of damaged supports⁸⁾

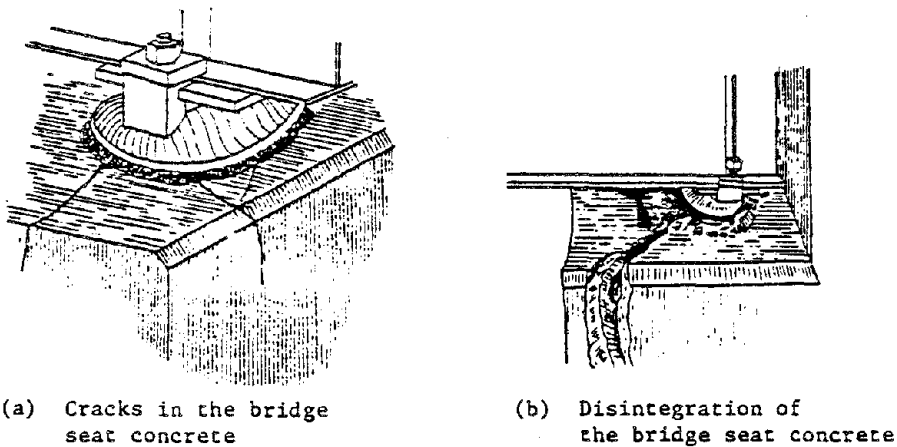


Fig. 1.3 Examples of damage to bridge seat concrete

(1) The causes of damage to bridge seats in the Miyagiken-oki Earthquake and the validity of the current design method for bridge seats.

(2) The effectiveness of the reinforcing seat concrete and the presentation of more rational reinforcements.

2. Test Plan

2.1 Designing the bridge seat portion

To study the causes of damage to the bridge seat concrete and to clarify the problem points in design methods, some studies may be conducted on changes in design methods for the bridge seat portion.

The first regulations concerning methods of designing the seat portion of road bridges were contained in the Design Guide for Highway Bridges: Abutment and Pier⁽²⁾ published in March, 1968, and these regulations are still carried forward unchanged in Part IV (Substructure) of the Specifications for Highway Bridges⁽³⁾.

In this guide, it is considered that shearing damage to the seat portion develops in the surfaces shown in Fig. 2.1.1 and that the

bearing to edge distance S (cm) may be obtained by the following equation.

$$S \geq 20 + 0.5l \quad l \leq 100\text{m}$$

$$S \geq 30 + 0.4l \quad 100 < l \leq 150\text{m}$$

Here, l is the span length (m). Value S of the bearing to edge distance was originally established not only to prevent damage to the bridge seat concrete but also to prevent the girder from falling during an earthquake.

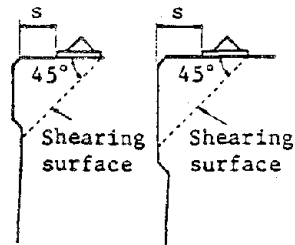


Fig. 2.1.1 Bearing to edge distance

Prior to the guide, there were no basic standards for designing bridge seats; designing was conducted solely on the judgement of the engineer in charge. Therefore, discrepancies in edge distance prior to and after the regulations established in 1968 were generally very great and it is believed that, prior to the application of the 1968 guide the bearing edge distances at many bridges were small. In view of the fact that shearing damage developed during the Miyagiken-oki Earthquake in the bridge seat portion at a comparatively large number of bridges constructed prior to 1968, it may be considered that the influence of the bearing edge distance is great.

As regards the reinforcement of the bridge seat portion with steel bars, the guide provides that cage type steel reinforcements, as shown in Fig. 2.1.3, be installed to prevent the cracking of concrete due to the vertical load transmitted from the seat and also to prevent disintegration of concrete due to the horizontal force or pulling force

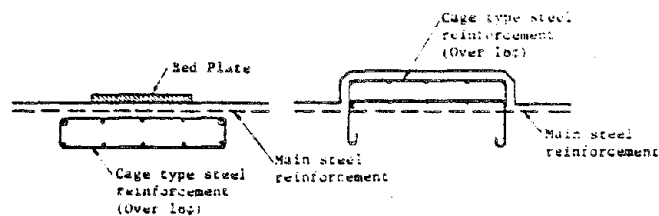


Fig. 2.1.2 Placement of the cage type steel reinforcement

transmitted from the anchor bolt. In many cases, however, similar reinforcements had been used prior to the establishment of the regulations in 1968.

Although the normal method adapted in the past using mortar for the bridge seat was called dry packing in which ordinary mortar was used, nonshrinking mortar has been used in recent years to prevent gaps from developing due to shrinkage and also to increase the reliability of construction. However, as defects due to the strength and application of mortar appear only as damage to the bridge seat mortar, it is believed that these defects cannot be regarded as decisive in the breakage of the bridge seat concrete.

As regards the strength of the bridge seat concrete, the standard designed strength has not changed to any degree from the past, in most cases being $\sigma_{ck} = 210 \sim 270 \text{ kg/cm}^2$.

From the above it may be surmised that the principal reasons for the damage to the bridge seat concrete during the Miyagikenoki Earthquake were: 1) short distance to the bearing edge; and 2) insufficient steel reinforcements.

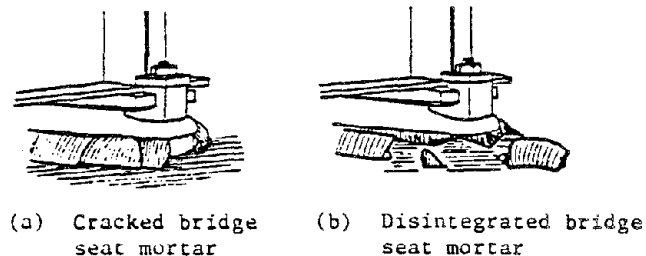


Fig. 2.1.3 Damage to the bridge seat mortar

2.2 Past research

To connect the bearing and the seat concrete, there are the anchor bolt and the lower seat protrusion. In the Highway Bridge Specification⁽⁷⁾, the anchor bolt is designed to take up all of the horizontal force acting on the bearing. In the tests of Japan Highway Public Corporation⁽⁵⁾, however, it is pointed out that the horizontal resistance

of the anchor bolt is become effective after lost of a margin of play between bearing and anchor bolt and that it does not act simultaneously together with the resistance of the lower seat protrusion. In other words, as horizontal force is transmitted to the anchor bolt after considerable displacement of bearing, it is considered that, in the almost of cases, damage to the bridge seat concrete occurs while only the lower protrusion is resisting to the horizontal force.

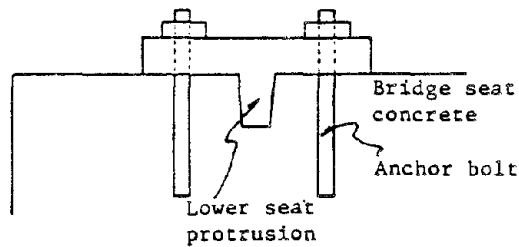


Fig. 2.2.1 Lower seat protrusion and anchor bolts

Furthermore, tests on breakage⁽⁶⁾ due to lower seat protrusion have been carried out on the bridge seat concrete of railroad bridges by the Japan National Railways because the JNR expects the horizontal resistance on the lower protrusion to operate and regulations⁽⁷⁾ have been established concerning methods of reinforcing the bridge seat concrete based on these tests.

2.3 Studies of the primary test factors

The primary test factors in this experiment are the bearing edge distance and the steel reinforcing method of the seat. However, as regulations had been established since 1968 concerning bearing edge distance, we decided to confirm the safety factor of the set value. For this reason, we selected the steel reinforcing method as the main factor in this experiment to study suitable methods of reinforcement by ascertaining the difference in strength with different methods of reinforcement.

As explained in Paragraph 2.1 "Designing the bridge seat portion", although details are provided in the Specifications for Highway Bridges

concerning the method steel reinforcement for the prevention of slitting crack due to vertical loads, there is no explanation of the method of arrangement in relation to horizontal loads.

The amount (A_{SV}) of steel reinforcements required for the prevention of slitting crack may be obtained by the following equation.

$$A_{SV} = \frac{1}{4} \left(1 - \frac{b}{b_c}\right) \frac{R_V}{\sigma_{Sa}}$$

Here, b : Width (cm) of the seat

b_c : Width (cm) of distribution of pier pressure

R_V : Vertical Load (kg)

σ_{Sa} : Permissible tensile stress intensity of the steel reinforcement. (kg/cm²)

Disregarding the resistance of the concrete, the amount of steel reinforcements in relation to horizontal force (A_{SH}) may also be obtained by means of the following equation.

$$A_{SH} = \frac{R_H}{\sigma_{Sa}}$$

Here, R_H : Horizontal load (kg)

σ_{Sa} : Permissible tensile stress intensity of the steel reinforcement. (kg/cm²)

The sum of A_{SV} and A_{SH} shall be the standard amount (A_{S0}) of steel reinforcements.

Carry out studies in relation to strength and behavior by varying the amount of steel reinforcements by the multiple of this A_{S0} of 0, 1, 1.5, and 2.0.

It was also decided to study the results of other special steel reinforcement methods. For details relating to these methods, refer to Paragraph 3.1 "Designing the Test Piece".

Factors other than the amount of reinforcing steel were decided as follows.

(1) To enable carrying out the experiment in the simplest way possible, anchor bolts were not provided and the only provision was the lower seat protrusion.

(2) The bearing edge distance was in accordance with the Highway Bridge Specification IV "Substructure".

(3) Cement based nonshrinking mortar was used for the bridge seat and no mounting was provided.

(4) The strength of the bridge seat concrete was set as $G_{ck} = 210 \text{ kg/cm}^2$.

2.4 Test items

Tests consist of the vertical load test and the inclined load test.

(1) Vertical load test (Fig. 2.4.1)

This test is to study the scale and distribution of slitting crack stress intensity that develops in the bridge seat concrete due to vertical stress.

(2) Inclined load test (Fig. 2.4.2)

This is the main subject in this research and is the test to study the strength and behavior of the bridge seat concrete when it is simultaneously subjected to horizontal and vertical loads.

In this method, the horizontal load may be gradually increased while holding the vertical load at a set value or both the horizontal and vertical loads may be increased while holding their ratio at a set value. In this study, a branched load jig was used as shown in Fig. 2.4.3 to maintain a constant ratio between the vertical and horizontal loads.

This corresponds to the principle of the law of vibration as obtained from the ratio between the horizontal and vertical forces.

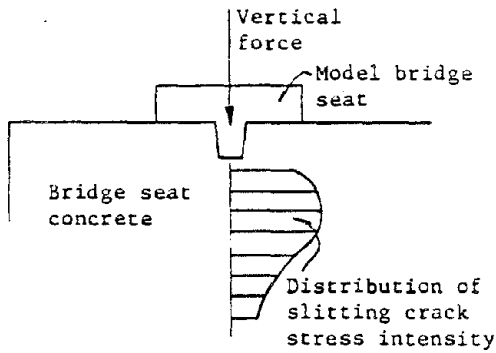


Fig. 2.4.1 Vertical load test

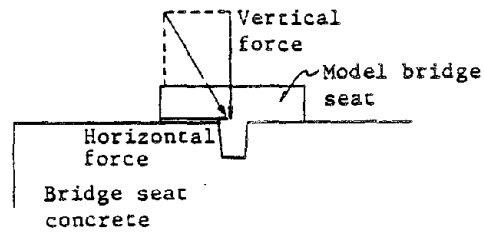


Fig. 2.4.2 Inclined load Test

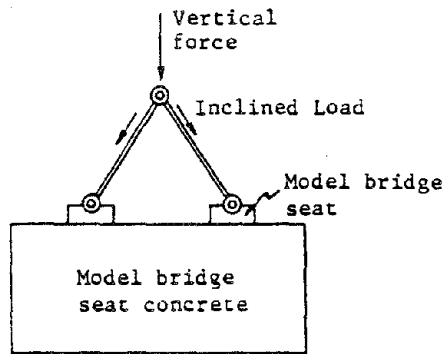


Fig. 2.4.3 Sketch of the branched load jig

3. Test Method

3.1 Designing the test piece

3.1.1 Actual bridge conditions assumed

When studying the test model, the actual bridge conditions assumed should be set as follows from the standard designs of the Ministry of Construction.

Superstructure	—	[Type of Structure	PC T Type Girder Beam Bridge
			Distance between Supports	30 m
			Reaction during Earthquakes	$R_d = 48t, R_H = 24t$ (Intensity 0.25)
Bearing	—	[Type of Structure	Plain Bearing (B.P.)
			Function	Fixed

Substructure: Amount of steel reinforcement comparatively small.
To have wall type abutment or piers

3.1.2 Dimensions and shape of the test piece

Taking into consideration the capacity of the load device and the size of the test piece, the scale used in relation to the actual object was set at 1/3.

The edge distance of the test piece in relation to the assumed edge distance of the actual bridge will be as follows. However, taking into consideration the positioning of the reinforcing steel bars, it was set at 15 cm.

$$\frac{1}{3} (20 + 0.5l) = \frac{1}{3} (20 + 0.5 \times 30) = \frac{1}{3} \times 35 = 11.7 \text{ cm}$$

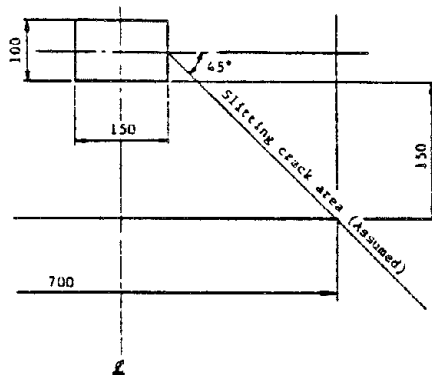


Fig. 3.1.1 Deciding the width of the test piece

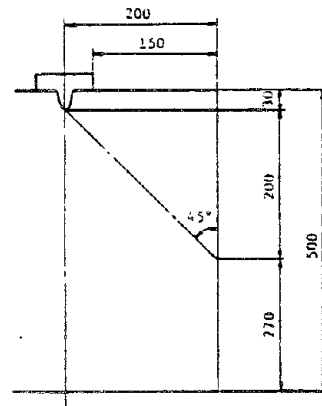


Fig. 3.1.2 Deciding the height of the test piece

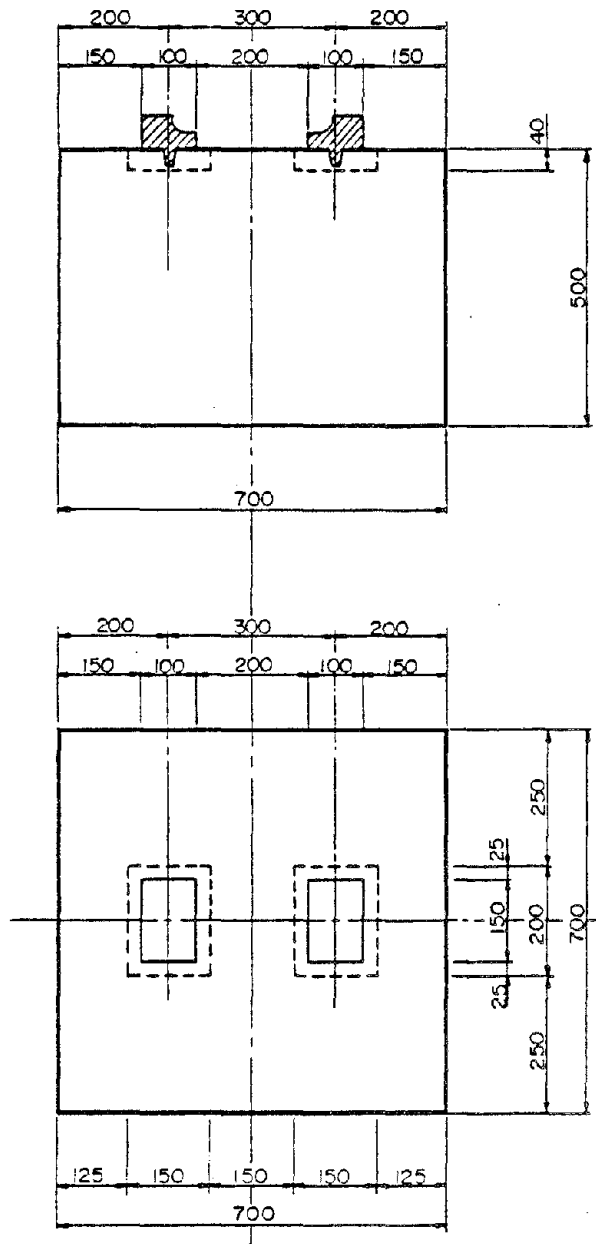


Fig. 3.1.3 General diagram of the test piece

Taking into consideration the breakage area that extends 45° from the center of the bearing, the width of the test piece was set at 70 cm so that the width of the breakage surface would be confined within the width of the test piece. Also, considering that the breakage face on the front surface will be appeared within the height if the breakage occurs at a 45° angle below the protrusion, the height of the test piece was set at 50 cm to incorporate a certain amount of surplus.

Taking into consideration the limitation to the width of the test piece and the installation of the 2-way load jig to apply inclined loads, the model seat was built to a scale of 1/3 of the actual seat. A general diagram of the shape and dimensions of the test piece decided from the foregoing studies is shown in Fig. 3.1.3.

3.1.3 Study of the law of similarity

As the ratio of the material strength of the model and the actual object is 1, in this experiment it will be necessary that the ratio of stress intensity (σ_p/σ_M) generated in the model and the actual object is 1.

To realize this, the load ratio (F_p/F_M) is determined by the following equation.

$$\frac{F_p}{F_M} = \frac{\sigma_p \cdot L_p^2}{\sigma_M \cdot L_M^2} = \frac{\sigma_p}{\sigma_M} \left(\frac{L_p}{L_M} \right)^2 = 1 \cdot R^2 = R^2$$

Here, L_p/L_M : Dimensional Ratio L_p/L_M shall equal R

As $R = 3$ in this experiment, the load ratio will be 9 and, based on this load, if the stress intensity developed in the test piece decided in Paragraph 3.1.2 is compared to that of the actual bridge, it will be as shown in Table 3.1.1. Each stress intensity shows a comparatively good corresponding value.

The slitting crack stress intensity here was calculated based on the standard⁽⁹⁾ calculation method (Fig. 3.1.4) of the Japan National Railways.

Table 3.1.1 Comparison of load and stress intensity

	Test piece	Actual item
Acting vertical force (t)	5.3	48
Acting horizontal force (t)	2.7	24
Average vertical bearing pressure intensity (kg/cm ²)	35.3	28.1
Rib side bearing pressure intensity (kg/cm ²)	60.0	88.9
Slitting crack stress intensity (kg/cm ²)*	2.3	2.1

(*) In accordance with calculation methods in Fig. 3.1.4.

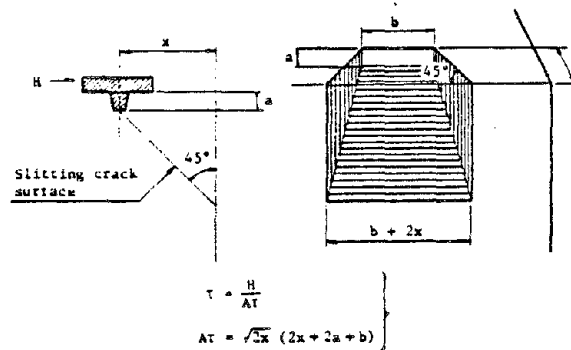


Fig. 3.1.4 Calculation of slitting crack stress intensity according to the Japan National Railway standards

The following law of similarity is proved in relation to the amount of reinforcing steel. As the ratio of strength of the steel reinforcement is 1, the ratio its cross sectional area (A_{SP}/A_{SM}) is expressed by the following.

$$\frac{A_{SP}}{A_{SM}} = \frac{A_{SP} \cdot \sigma_y}{A_{SM} \cdot \sigma_y} = \frac{F_p}{F_M} = R^2$$

The percentage (P_p/P_M) of steel reinforcements when positioned in the cross sectional area of the effective width (l_p, l_M) and the effective height (h_p, h_M) may be expressed by the following equation.

$$\frac{P_P}{P_M} = \frac{A_{SP}/l_p \cdot h_p}{A_{SM}/l_M \cdot h_M} = \frac{A_{SP}}{A_{SM}} \cdot \frac{l_M}{l_p} \cdot \frac{h_M}{h_p} = \frac{A_{SP}}{A_{SM}} \cdot \frac{L_M}{L_p} \cdot \frac{L_M}{L_p} = R^2 \cdot \frac{1}{R} \cdot \frac{1}{R} = 1$$

In other words, the ratio of steel reinforcement will be the same in both the model and the actual item.

3.1.4 Types of test pieces

7 types of test pieces were prepared (Table 3.1.2) according to the different methods of reinforcing with steel. The miscellaneous specifications for these pieces were determined as follows. The standard amount of steel reinforcement was decided by using the method indicated in Paragraph 2.3 "Study of the Test Elements".

$$A_{SH} = \frac{R_H}{\sigma_{Sa}} = \frac{2.7 \times 10^3}{1,800 \times 1.5} = 1.00 \text{ cm}^2$$

$$A_{SV} = \frac{1}{4} \left(1 - \frac{b_1}{b_c}\right) \frac{R_V}{\sigma_{Sa}} = \frac{1}{4} \left(1 - \frac{10}{35}\right) \frac{5.3 \times 10^3}{1,800} = 0.53 \text{ cm}^2$$

$$A_{SH} + A_{SV} = 1.00 + 0.53 = 1.53 \text{ cm}^2 (\phi 6 @ 60)$$

This amount of steel reinforcement is equivalent to D13 @90 in the actual object.

This spacing between the reinforcing bars is decreased ($\phi 60 @ 40$) to cope with the 1.5 times of steel reinforcement of A_{S0} . For double the steel reinforcement of A_{S0} , the standard amount of steel bars may be double-decked (2 - $\phi 6 @ 60$) or a larger diameter ($\phi 9 @ 60$, $2.3A_{S0}$) may be used.

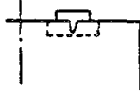


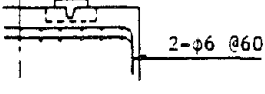

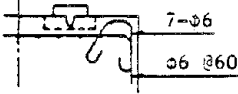

The foregoing arrangement shall hereafter be called reinforcing work^(I).

Separate from the foregoing reinforcing work^(I), steel reinforcements with high shear resistance (hereafter called shear resistance work^(II)) were provided in addition to A_{S0} (See Fig. 3.1.5). The amount of this reinforcement may be calculated from the following equation.

$$A_{ST} = \frac{R_H}{\tau_{Sa}} = \frac{2.7 \times 10^3}{800 \times 1.5} = 2.25 \text{ cm}^2 (\phi 6 \times 7 \text{ each})$$

Here, τ_{Sa} : Allowable shear stress intensity of the steel reinforcement (kg/cm^2)

Table 3.1.2 Relation between the test elements and the types of test pieces

	Reinforcement		Structural Diagram	Remarks
	Reinforcing (I)	Other reinforcements (II) or (III)		
①	None	None	 Bottom and sides reinforced	
②	φ6 @60 (= AS0)	None	 φ6 @60	Standard test pieces equivalent to D13 @90 of the actual item
③	φ6 @40 (= AS3)	None	 φ6 @40	$\frac{AS3}{AS0} = \frac{1.5}{1}$
④	2-φ6 @60 (= AS4)	None	 2-φ6 @60	$\frac{AS4}{AS0} = \frac{2.0}{1}$
⑤	φ9 @60 (= AS5)	None	 φ9 @60	$\frac{AS5}{AS0} = \frac{2.3}{1}$
⑥	φ6 @60 (= AS0)	7 × φ6 Slitting crack reinforcement (II)	 7-φ6 φ6 @60	
⑦	φ6 @60 (= AS0)	Tensile reinforcement φ9 @50 (III)	 φ9 @50 φ6 @60	

This amount of steel reinforcement will be equivalent to D13 × 16 each in the actual item.

Studies were also made in relation to wrapping the seating (Fig. 3.1.6) with steel banding

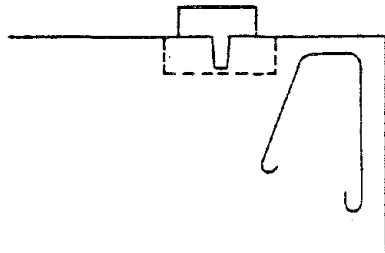


Fig. 3.1.5 Reinforcement for shear stress (II)

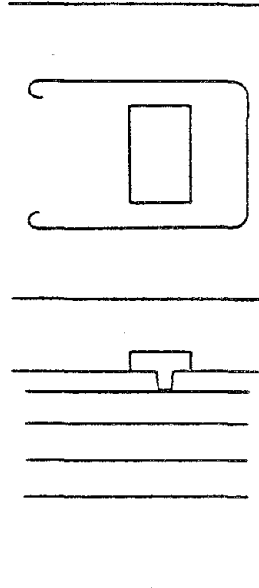


Fig. 3.1.6 Reinforcing work (III) by wrapping the seat with steel banding

(hereafter called tensile reinforcement work^(III)). In this reinforcement work, $\phi 9$ steel bars were arranged at 50 mm intervals. This is equivalent to $\phi 22$ bars placed at 100 mm intervals in the actual item.

3.2 Material used

(1) Concrete

Concrete was used with the mixture ratio shown in Table 3.2.1 with the purpose of obtaining a standard design strength of 210 kg/cm^2 as this was the most common construction material. When measured at time of laying, slump was 13.5 cm, air content was 4.6% and the temperature of the concrete was 25°C .

Table 3.2.2 shows the compression strength of a test piece ($\phi 15 \times 30 \text{ cm}$) and Fig. 3.2.1 shows the relations of the Young's Modulus and the Poisson's Ratio. However, test pieces in Table 3.2.2 that are 48 days old (at time of test) shall be taken by core borings of test piece ① after the load test.

Table 3.2.1 Concrete mixture

C (kg/m ³)	W (kg/m ³)	W/C (%)	S (kg/m ³)	G (kg/m ³)	S/A (%)	NO-5L (kg/m ³)
273	162	59.0	829	1,052	44.1	0.683

Table 3.2.2 Strength of the concrete (kg/cm²)

Age (Days)	Standard curing		Site curing		
7	A	189	Average 186	177	Average 173
	B	190		169	
	C	181		175	
18	A	252	252	247	243
	B	248		239	
	C	256		243	
28	A	288	277	262	261
	B	284		261	
	C	271		260	
48 (At time of test)	A			291	253
	B			225	
	C			243	

(2) Bridge seat mortar

With the purpose of obtaining a design strength of 450 kg/cm², a premixed type hi-early strength cement based nonshrinking grout material (NL-870GHE) was used as the bridge seat mortar. This is a market item containing various admixtures, sand and cement in premixed form. The method of mixing used was to add 4.2 liters of water to 1 bag (25 kg) of the premixture and churning for 2 minutes in an NMB Type hand mixer. The consistency of the mixture at this time was 9 seconds (Flowing time by funnel J).

The bridge seat mortar compression strength according to the test piece (φ15 × 30 cm) was an average 536 kg/cm².

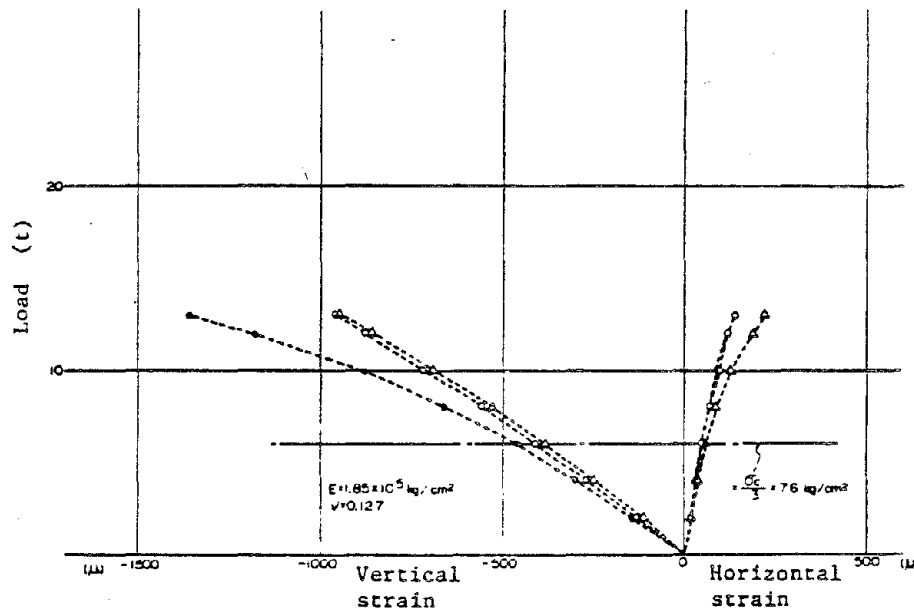


Fig. 3.2.1 Load - Strain curve (Concrete aged 28 days)

(3) Reinforcing steel bars

The reinforcing bars used were 6 mm and 9 mm and both standardized with SR24 material. However, as may be noted by the results of the tensile strength as shown in Table 3.2.3, there is a considerable difference in strength. As it will be difficult to use both as the same material, it was decided to consider this effect in the results of the experiment.

Table 3.2.3 Tensile test results of
the reinforcing steel bars

(kg/cm²)

		Yield strength		Tensile strength			
φ9	A	1.90	2,286	Average 2,967	2.70	4,244	4,338
	B	1.93	3,034		2.93	4,605	
	C	1.87	2,939		2.70	4,244	
	D	1.85	2,908		2.71	4,260	
φ6	A	1.54	5,447	5,580	1.86	6,579	6,677
	B	1.64	5,801		1.94	6,862	
	C	1.52	5,377		1.84	6,509	
	D	1.61	5,695		1.91	6,756	

The cross sectional area was set at φ9: 0.6362 cm²,
φ6: 0.2827 cm².

3.3 Method of loading

(1) Vertical load test

To study the slitting crack stress on bridge seats when vertical load only acts on the bearing, the vertical load test was carried out on test pieces ② and ③ as shown in Fig. 3.3.1 prior to applying incline loads.

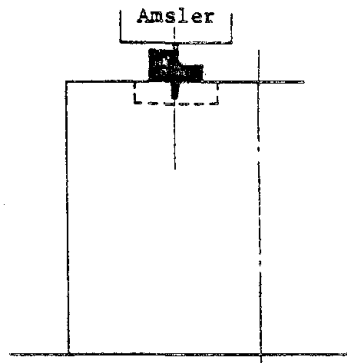


Fig. 3.3.1 Vertical loading test

(2) Inclined load test

As shown in Fig. 3.3.2, the inclined load test was carried out by converting the vertical load from the loading unit to inclined loads by means of a loading jig. In this instance, the load acting on the top of one of the bearings will be a vertical force of 0.5p and a horizontal force of 0.289p in relation to load (P) from the loading unit.

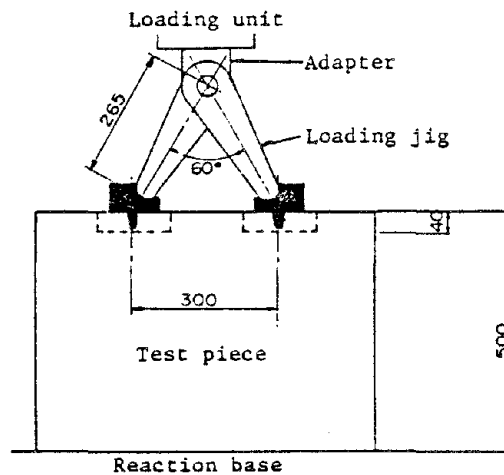


Fig. 3.3.2 Inclined load test

3.4 Method of measuring

In the experiment carried out at this time, prime importance was placed on the load and the breakage conditions during breakage and measurements were taken principally of the relative displacement of the load, concrete and seat. The places of measurement are shown in Figs. 3.4.1 and 3.4.2.

(1) Measurement of displacement

Using a strain conversion type displacement meter, measurements were taken of the relative displacement in the horizontal direction of the concrete and bearing on both sides of the bearing.

Points Measured: 4 Points per piece.

(2) Measurement of strain

(a) Measurements of slitting crack strain due to vertical force were carried out on test pieces ② and ③ by means of an imbedded gauge.

Points Measure : 3 Points per piece.

(b) Tensile strain measurements were made on the top edge of the concrete adjacent to the bearing on all test pieces.

Points Measured: 4 Points per piece

(c) Strain measurements were taken of the steel bars in the reinforcing steel bars and other reinforcing material (shear reinforcement and tensile reinforcements).

Points Measured: ② - ⑤ Reinforcing bars (4 Points vertically and 2 points horizontally) per piece.
⑥, ⑦ (4 Points on the reinforcing steel in the vertical direction and 2 points horizontally) per piece.

(d) To study the distribution properties in the surface of the concrete, a rosette gauge was affixed to test pieces ② and ③ and strain conditions prior to development of cracks were measured with a digital meter.

Points Measured: 20 Points × 3 Axis per piece.

(e) Tensile strain in the horizontal direction on the front surface of the test piece was measured by means of a strain gauge. Measurements were taken on test pieces ②, ④, ⑤, ⑥ and ⑦.

Points Measured: 2 Points per piece.

(3) Measurement of cracks

When cracks on the top surface were visually confirmed, these were attributed to cracking loads.

The width of the cracks in the top surface particularly in the direction of stress was measured by means of a displacement gauge near the bearing.

Points Measured: 2 Points per piece.

(4) Load measurements

The method used in the measurement of static load (digital measurement) was to take direct readings and recording of the load indicated on the Amsler. Also, in measurement of continuous loads (analog measurement), pulse waves of each loading stage were recorded on magnetic tapes in the data recorder.

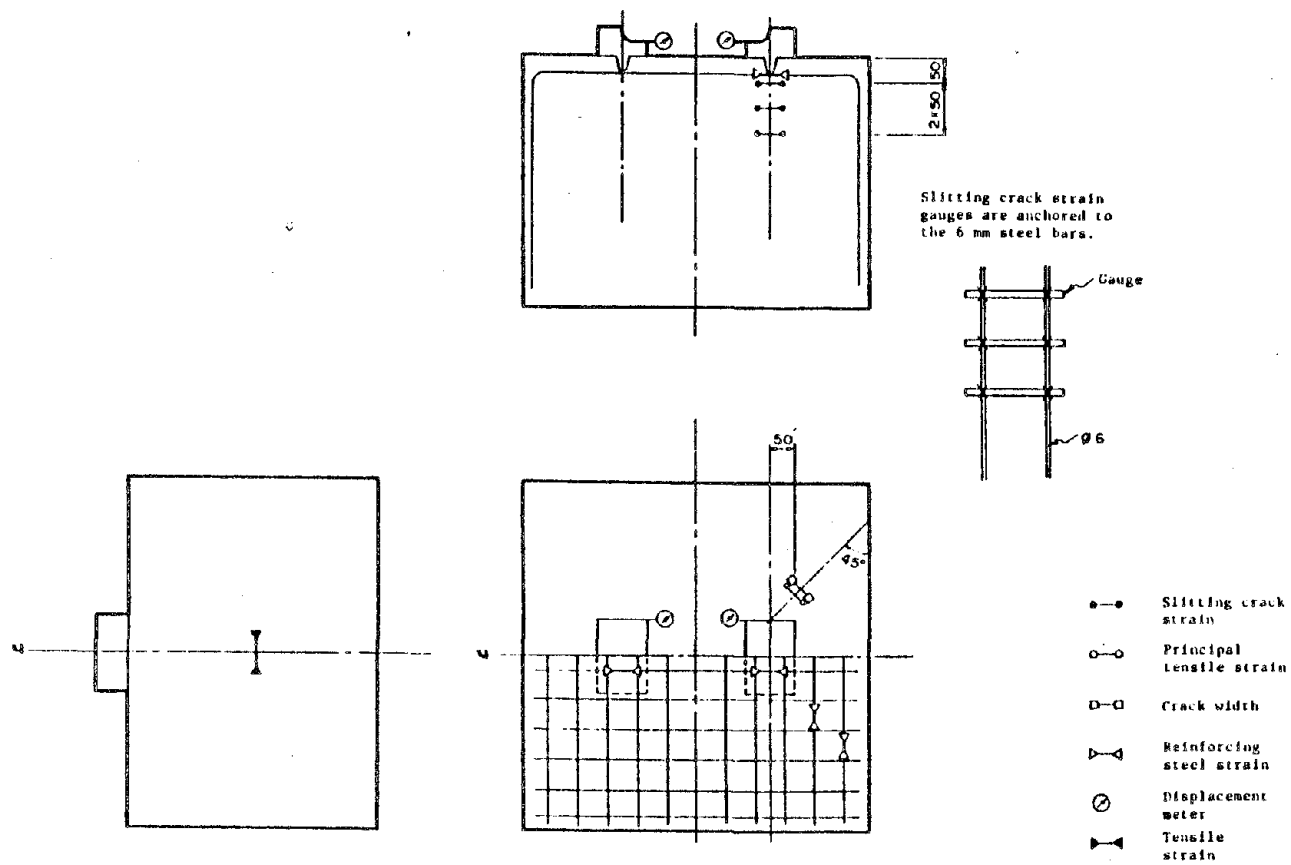


Fig. 3.4.1 Position of the measuring instruments

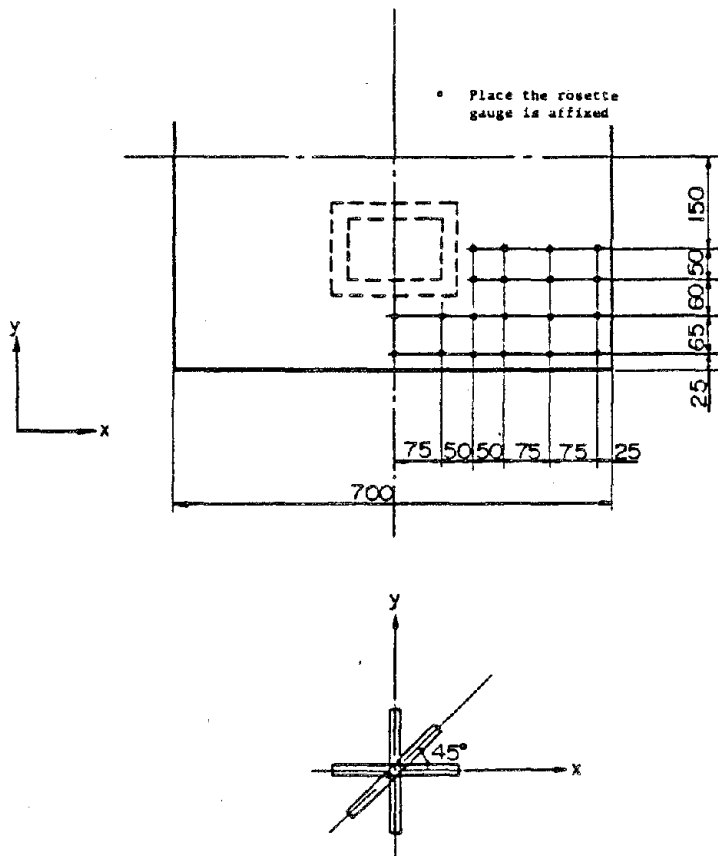


Fig. 3.4.2 Affixing position of the Rosette gauge
(Test peces ② and ③)

4. Vertical Loading Test Results and Considerations

Results of measurements of tensile stress generated by vertical loads (hereafter called cleavage stress) are shown in Fig. 4.1. If we make comparison of test pieces ② and ③ in relation to these results, it will be noted that the distribution properties of stress are exactly opposite. However, we cannot arrive at a final conclusion in relation to the shape of stress distribution in that measurements were made on only 2 test pieces and as the number of points measured were only 3 points per piece.

However, as the degree of slitting crack stress intensity is about 4 kg/cm^2 maximum under designed load conditions ($R_v = 5.3t$) and may be considered to be below the permissible tensile stress intensity (approx. $1/30$ of σ_{ck} . About 7 kg/cm^2 in this case) of concrete. In this instance, it is believed that the amount and positioning of the steel bars as shown in Fig. 2.1.2 and stipulated in the Substructure Design Guide⁽²⁾ will be sufficient to cope with slitting crack stress.

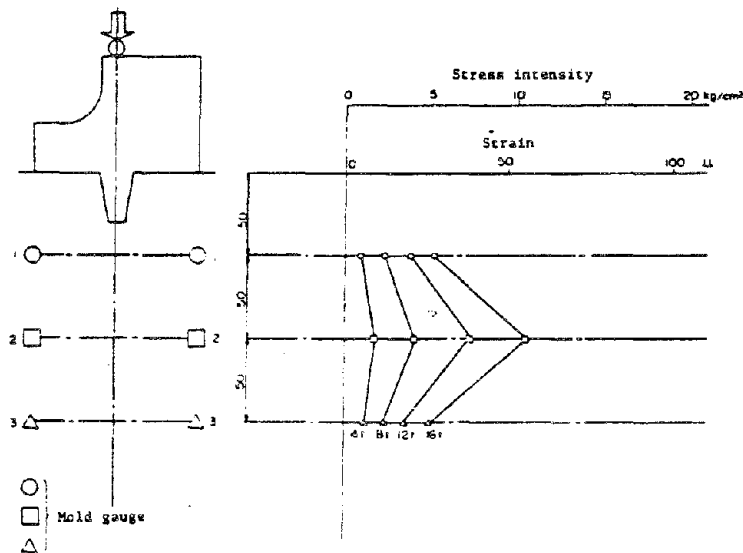


Fig. 4.1(1) Stress and strain intensity distribution diagram of concrete Test piece ②

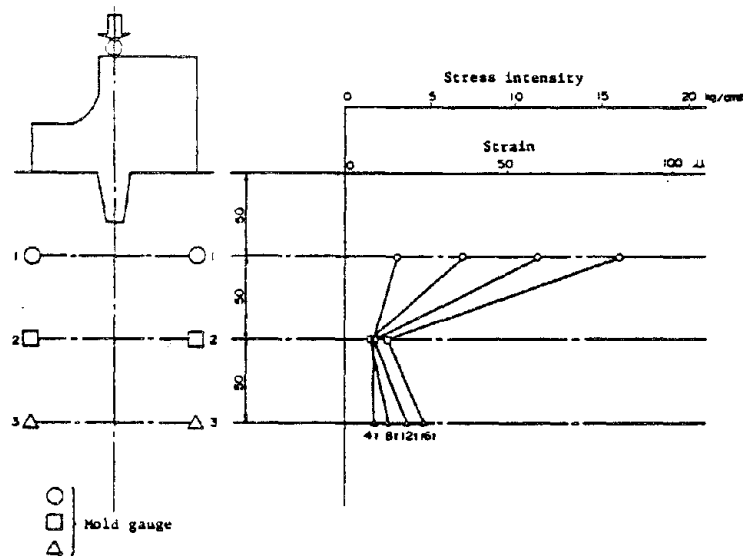


Fig. 4.1(2) Stress and strain intensity distribution diagram of concrete Test piece ③

5. Inclined Loading Test Results

5.1 Breakage properties and strength

(1) Breakage pattern

Conditions after cracks appeared in the test piece until breakage occurred progressed as indicated below in all of the test pieces.

First Stage: Cracks appeared on the top of test piece between 2 of the bearings at right angles to the horizontal load direction. Although widening of the cracks could be noted in accordance with the load (Vertical load P of 80 tons applied from an amsler), they did not lead to breakage.

Second Stage: Cracks developed on the front of the test piece in the vertical direction and cracks soon developed on the corner surface of the concrete in front of the bearing and at a 45° angle. ($P = 80$ to 100τ)

Third Stage: The increasing load stops but displacement continues to increase and the angled crack in front of the bearing widens rapidly and breakage occurs.

Breakage conditions are shown in the expansion diagram in Fig. 5.1.1 and it was noted that the breakage area on some of the test pieces extended to the bottom. In comparing conditions of breakage in each test piece, it was noted that the greater the amount of reinforcing steel the greater the tendency towards restraining sharp slitting cracks and that toughness was therefore improved with the usage of reinforcing steel bars. Fig. 5.1.2 shows the broken portion open on each test piece with an expanded view of the broken surface. The broken surfaces are practically the same in test pieces ① ~ ⑥. The broken surface of test piece ⑦ is different from the other surfaces due to the binding effect of the reinforcing steel.

(2) Breakage strength

In accordance with Table 3.1.1, the designed load for the test pieces is a vertical force R_v of 5.3 tons for each bridge seat. If this is expressed by the vertical force applied by an amsler with a capacity of applying the combined force for 2 bridge seats, and assuming a safety factor of 3, one criterion for the breakage load will be $5.3 \times 3 \times 2 = 32$ tons.

In Table 5.1 we have shown the load (P_{cr}) when the angled crack developed in front of the bearing and also the maximum load (P_{max}) when breakage occurred.

In relation to strength after development of cracks, although the breakage load will be attained immediately upon development of the crack when no reinforcing steel is used such as in test piece ①, where reinforcing steel is used, it was noted that strength increased after cracks developed.

Table 5.1 Experimental results

Test piece	Cracking load	Breaking load
1	85	85
2	80	113
3	89	121.4
4	140	165
5	106	117
6	118	131.8
7	90	164

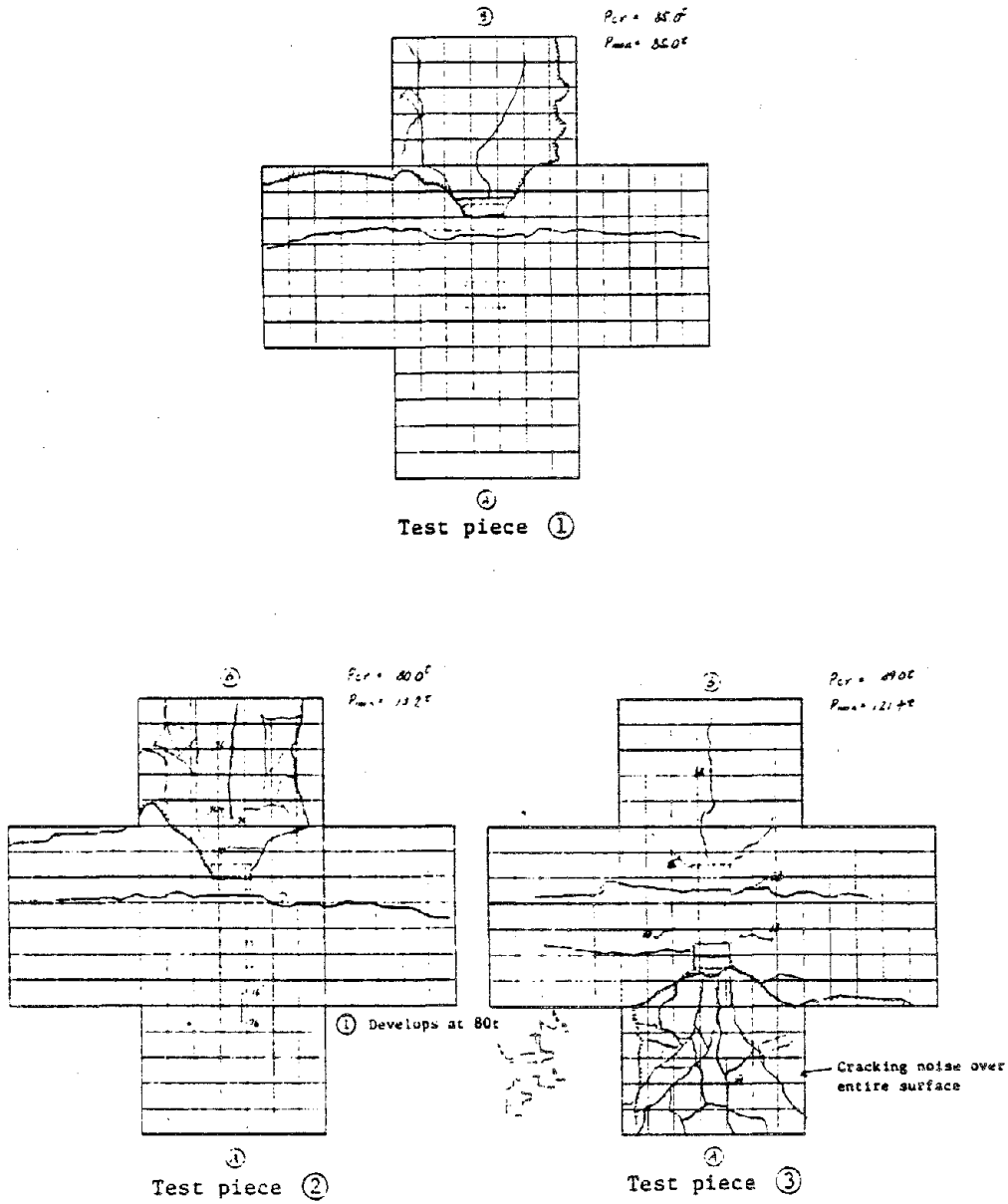


Fig. 5.1.1(1) Expanded view of breakage conditions

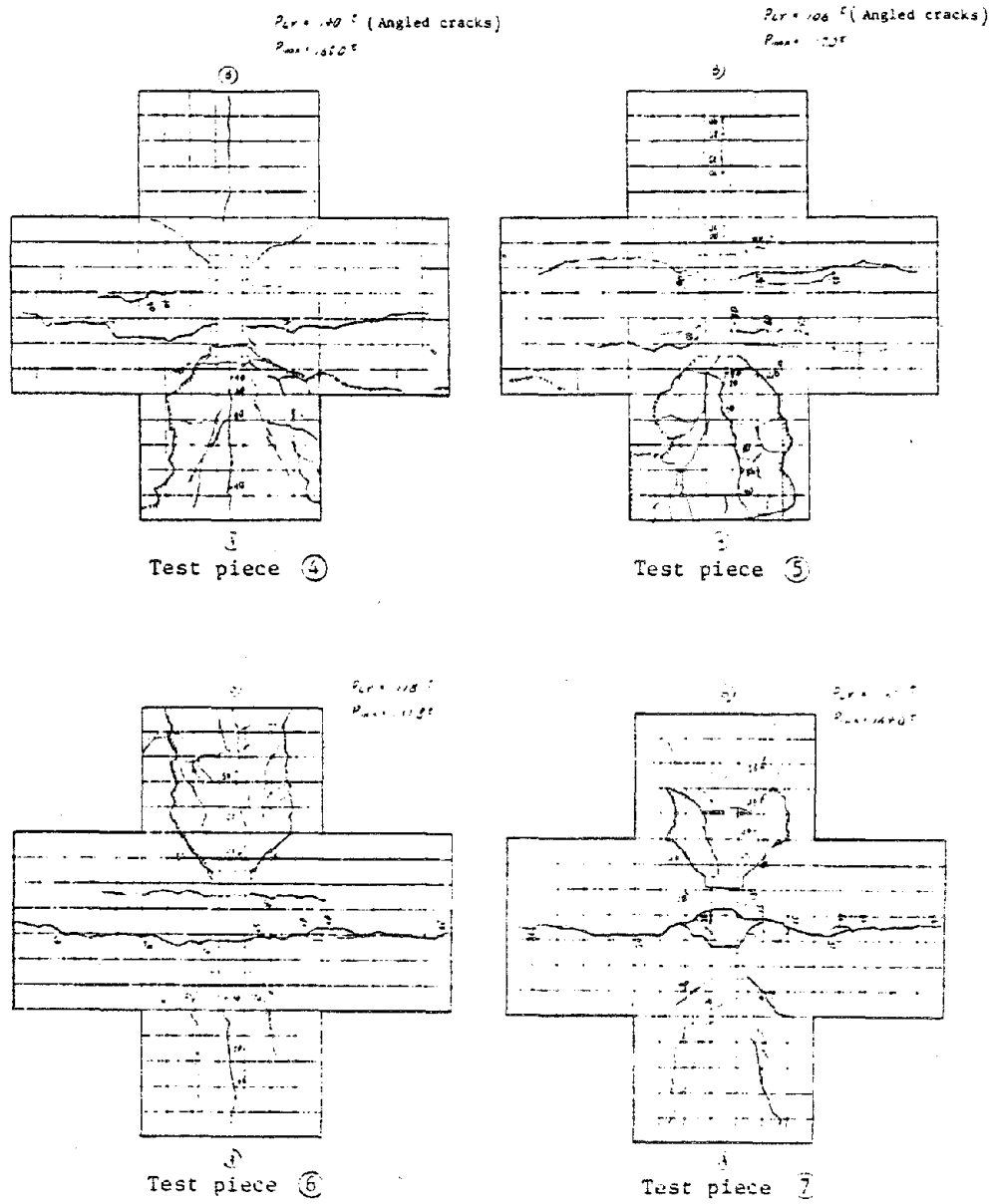


Fig. 5.1.1(2) Expanded view of breakage conditions

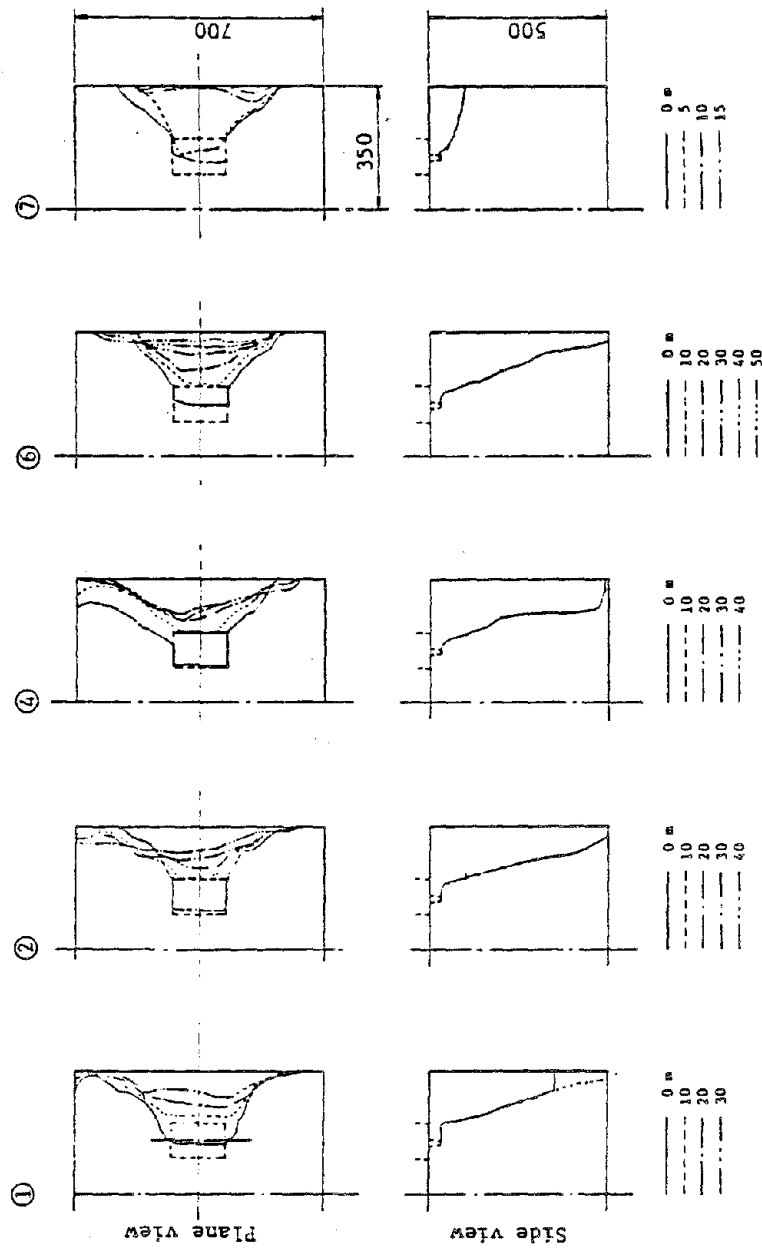


Fig. 5.1.1.2 View of the broken surface

5.2 Load-strain relations

(1) Strain in the concrete (Figs. 5.2.1, 5.2.2)

Measurements were taken on the top and front surfaces of the concrete in relation to strain. The amount of increase in strain in the top surface was small during low loads but increased sharply as the cracking load of 80t was approached. Cracks developed when it reached approximately 1,000 μ . Although strain in the front surface increased from a much lower load than that compared to the top surface, there was no sharp increase in any of the test pieces up to about 50t.

(2) Strain in the reinforcing steel bars (Fig. 5.2.3)

Measurements of strain in the reinforcing steel bars were carried out in the longitudinal and horizontal directions. Strain measurements were also carried out on other types of reinforcing steel material. Results of the measurements indicated the same tendency of increasing strain as in concrete and strain increased sharply simultaneously with cracking of the concrete.

5.3 Load-displacement relations

An example of the relative displacement of the seat and the concrete is shown in Fig. 5.3.1. Displacement was extremely small up to the cracking load of 80 tons but increased sharply simultaneously with development of the crack.

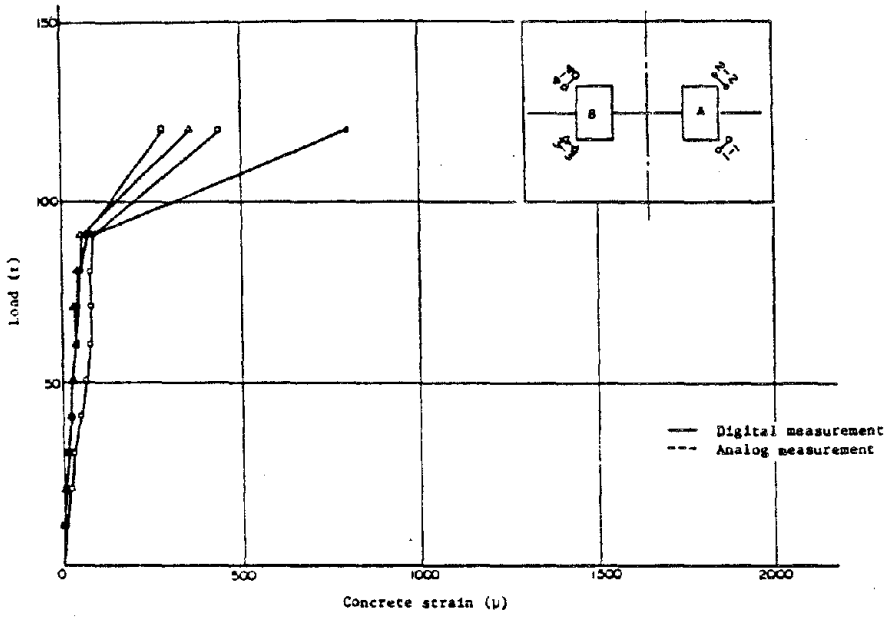


Fig. 5.2.1 Load-concrete strain (Main tensile strain)
Test piece ④

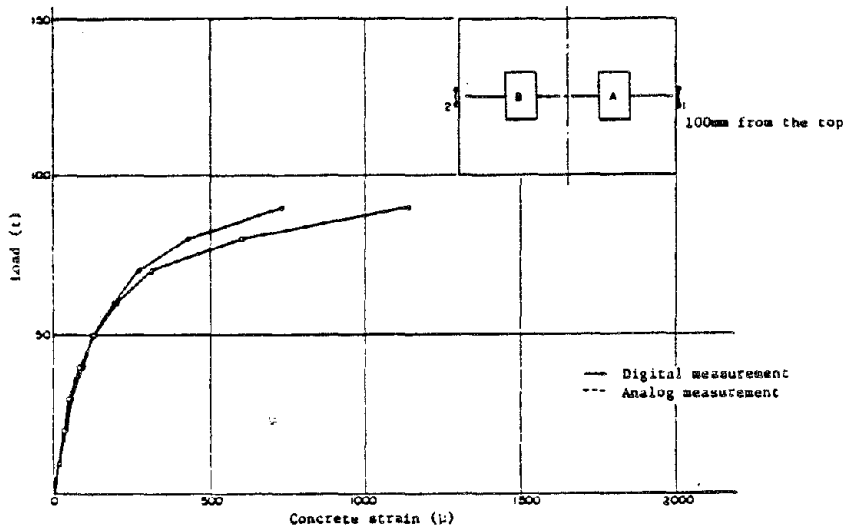


Fig. 5.2.2 Load-concrete strain Test piece ④

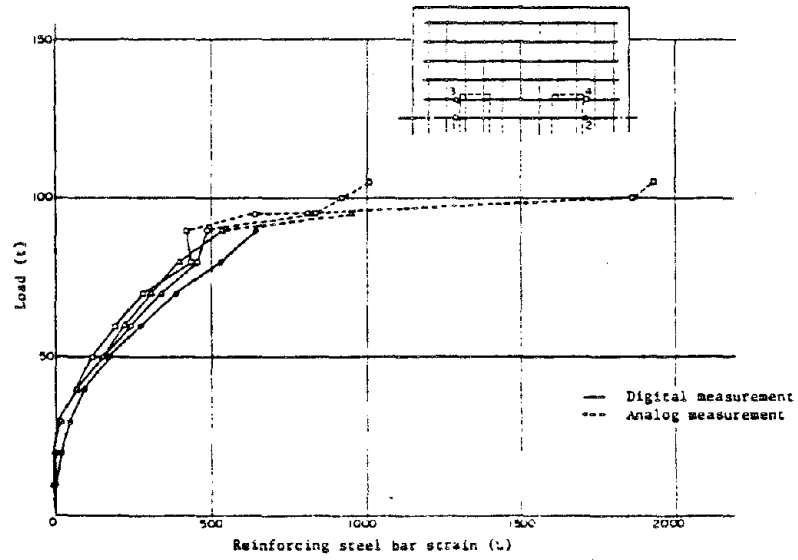


Fig. 5.2.3 Load-reinforcing steel strain
(Longitudinal direction of steel bars)
Test piece ⑤

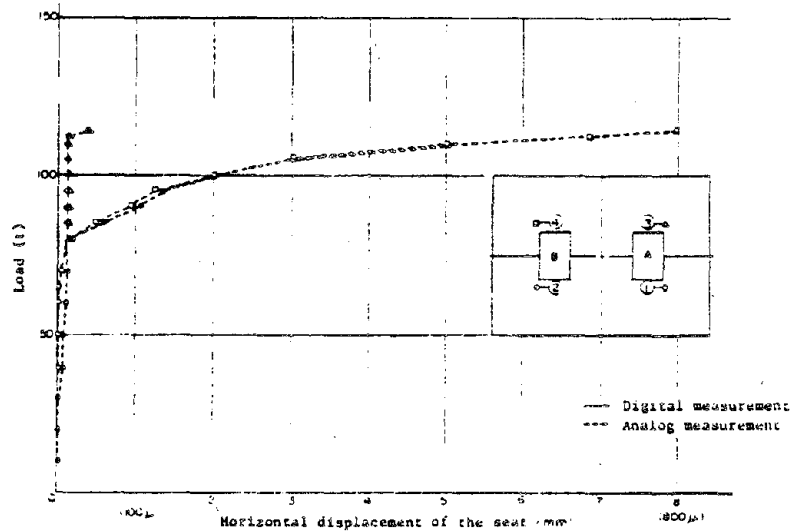


Fig. 5.3.1 Horizontal displacement of the load and seat
Test piece ②

5.4 Rosette gauge

On test pieces ②, ③, measurement of strain prior to cracking was carried out by affixing rosette gauges to the test pieces. The gauge used was a right angle 3 axis type and was affixed in the direction shown in Fig. 5.4.1

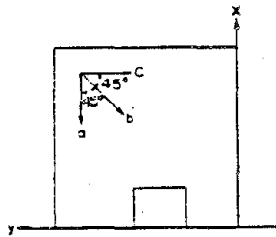


Fig. 5.4.1 Direction of the gauge

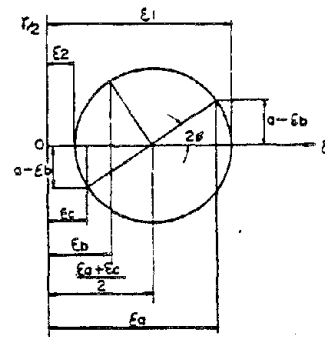


Fig. 5.4.2 Mohr's strain circle

The following equations may be obtained from the strain directions in Fig. 5.4.2.

$$a = \frac{\epsilon_a + \epsilon_c}{2} \quad \tan 2\phi = \frac{a - \epsilon_b}{a - \epsilon_c}$$

$$r = \frac{\sqrt{2}}{2} \sqrt{(\epsilon_a - \epsilon_b)^2 + (\epsilon_b - \epsilon_c)^2}$$

If we interchange $\epsilon_a \rightarrow \epsilon_x$, and $\epsilon_c \rightarrow \epsilon_y$, it can be substituted in the following stress-strain equation.

$$\sigma_x = \frac{E}{1 - \nu^2} (\epsilon_x + \nu \epsilon_y)$$

$$\sigma_y = \frac{E}{1 - \nu^2} (\epsilon_y + \nu \epsilon_x) \quad \nu : \text{Poisson's ratio}$$

$$\tau_{xy} = \frac{\sigma_x - \sigma_y}{2} \tan 2\phi$$

Principal stress will be determined as follows from the axial force.

$$\sigma_1 = \sigma_{\max} = \frac{1}{2} (\sigma_x + \sigma_y) + \frac{1}{2} \sqrt{(\sigma_x - \sigma_y)^2 + 4\tau_{xy}^2}$$

$$\sigma_2 = \sigma_{\min} = \frac{1}{2} (\sigma_x + \sigma_y) - \frac{1}{2} \sqrt{(\sigma_x - \sigma_y)^2 + 4\tau_{xy}^2}$$

$$\tau_1 = \tau_{\max} = \frac{1}{2} \sqrt{(\sigma_x - \sigma_y)^2 + 4\tau_{xy}^2}$$

The plane of principal stress will be $\tan 2\phi_n = \frac{2\tau_{xy}}{\sigma_x - \sigma_y}$

The principal stress obtained by substituting the results of the measurements taken with the Rosette gauge in the above equation is shown in Figs. 5.4.3 and 5.4.4. The actual slitting crack line and a straight line drawn at an angle of 45° from the bearing (assumed slitting crack line) are shown in the diagram. As may be discerned from the diagram, the slitting crack develops along the principal tensile stress surface and approximately matches the 45° line.

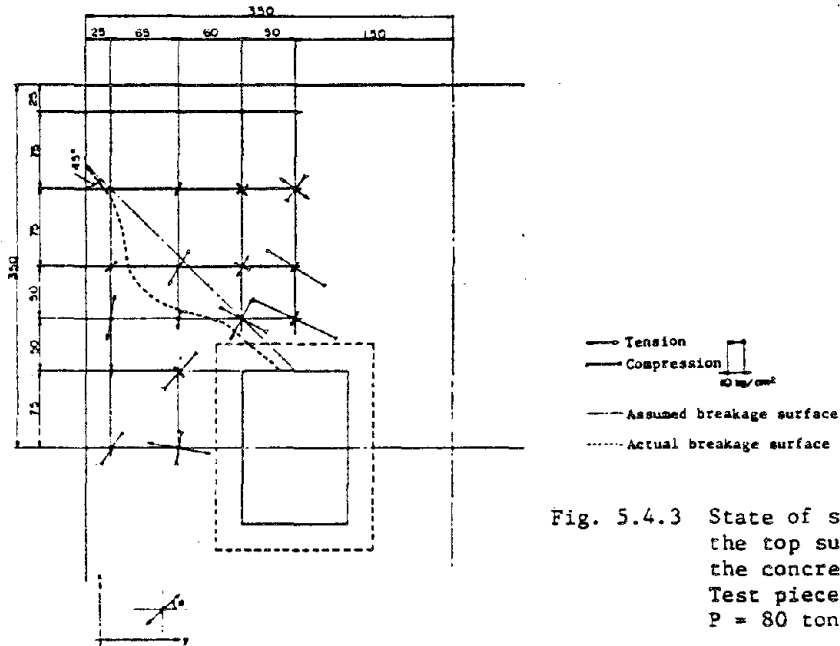


Fig. 5.4.3 State of stress on the top surface of the concrete
 Test piece ②
 P = 80 tons

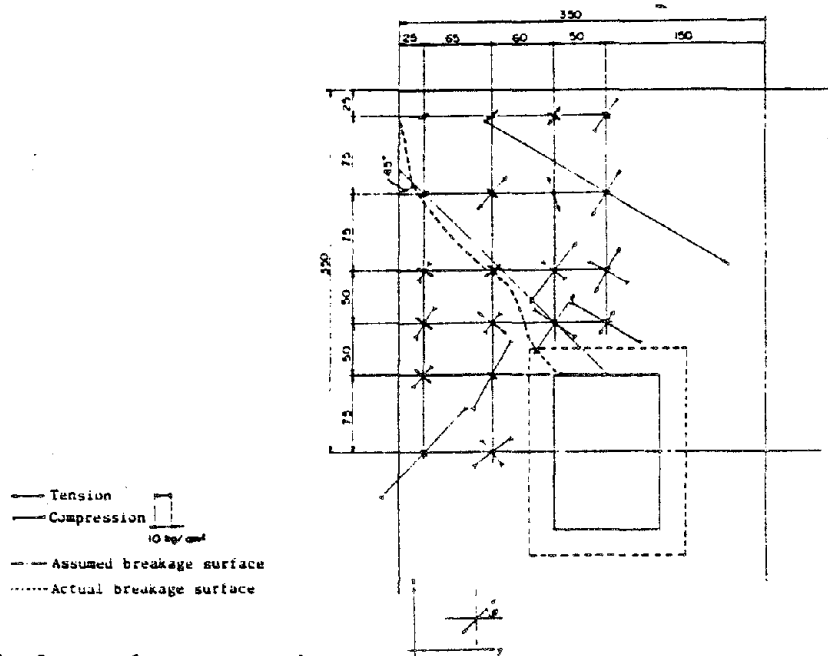


Fig. 5.4.4 State of stress on the top surface of the concrete
 Test piece ③ P = 90 tons

6. Analysis with F.E.M.

6.1 Analytic model

In relation to the experimental analysis, an analysis of stress properties was carried out by means of F.E.M. (Finite Elemental Method) as the theoretical analysis. Taking into consideration the symmetry of the loads and the test pieces, plane analysis of a half model of the test piece was used as the analytic model as shown in Fig. 6.

Number of reinforcing points	245
Number of elements	214
Thickness of the elements	1 cm

Supporting conditions:

Lower Surface	"x" Direction Free, "y" Direction Fixed
Center	"x" Direction Fixed, "y" Direction Free

Furthermore, the values for Young's Modulus and Poisson's Ratio in the diagram are those obtained from material tests. Load was applied from a horizontal and 60° direction (same as in the experiment).

6.2 Analytic results

An example of analytic results of the F.E.M. method is shown in diagrammatical form in Fig. 6.

Fig. 6.(1) shows displacements of the reinforcing points and indicates the displacement trends of the test piece which are approximately the same as those surmised.

Fig. 6.(2) is a diagram of the principal stress and from this diagram it may be discerned that tensile stress has developed in the concrete from the bearing towards the center of the test piece. In the actual test piece, resistance is offered by the reinforcing steel bars.

If we observe the direction of principal stress on the front side of the bearing under study in this experiment it may be noted that direction of maximum compression stress is inclined near the bearing but faces in the vertical direction the further away it is from the bearing. If we assume that the concrete breaks due to the tensile

stress intensity, the envelope of the direction of the maximum compression stress becomes the breakage surface. If this is compared to the breakage surface in the experiment shown in Fig. 5.1.2, it may be noted that this envelope is very close in shape.

From this study, it is considered that there will be little chance of breakage actually developing in a 45° angle when subjected to inclined loads.

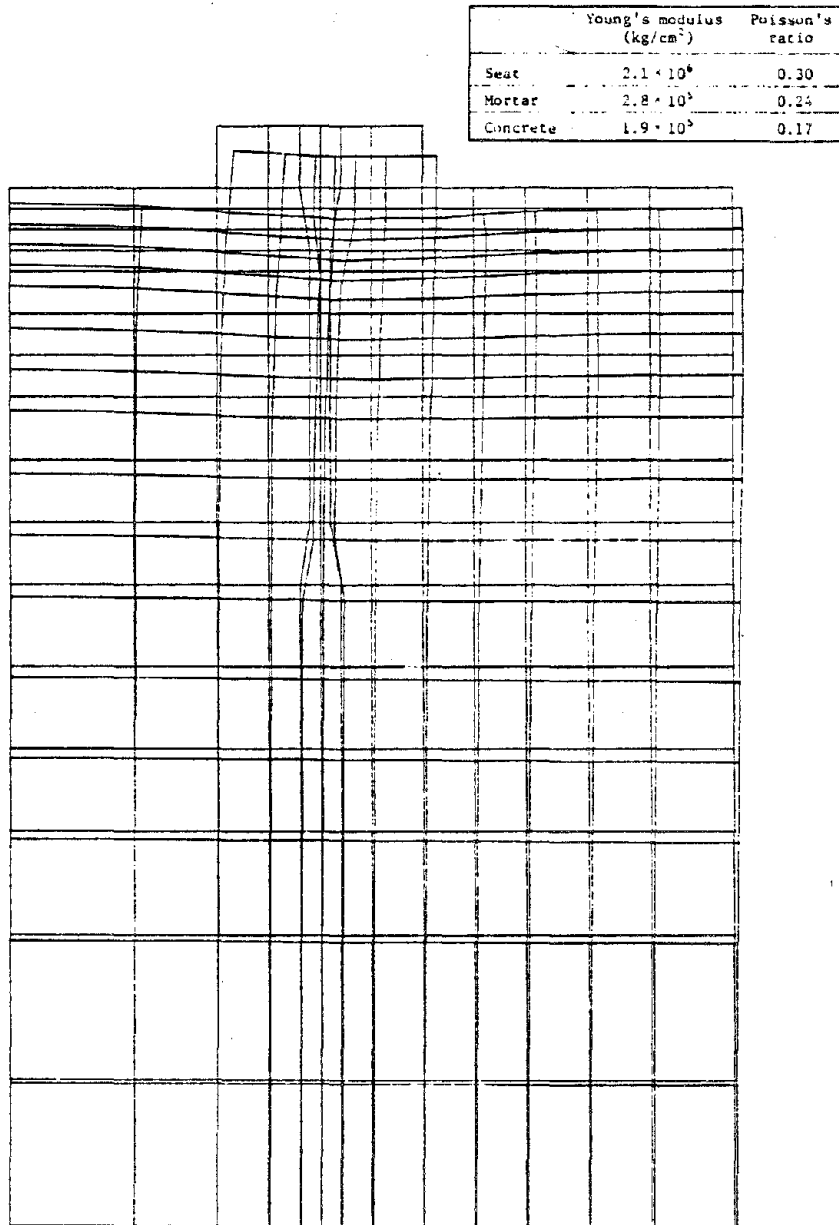


Fig. 6.(1) Model analysis, displacement of reinforcing point
when $N = 1.0t$ and $H = 0.5St$

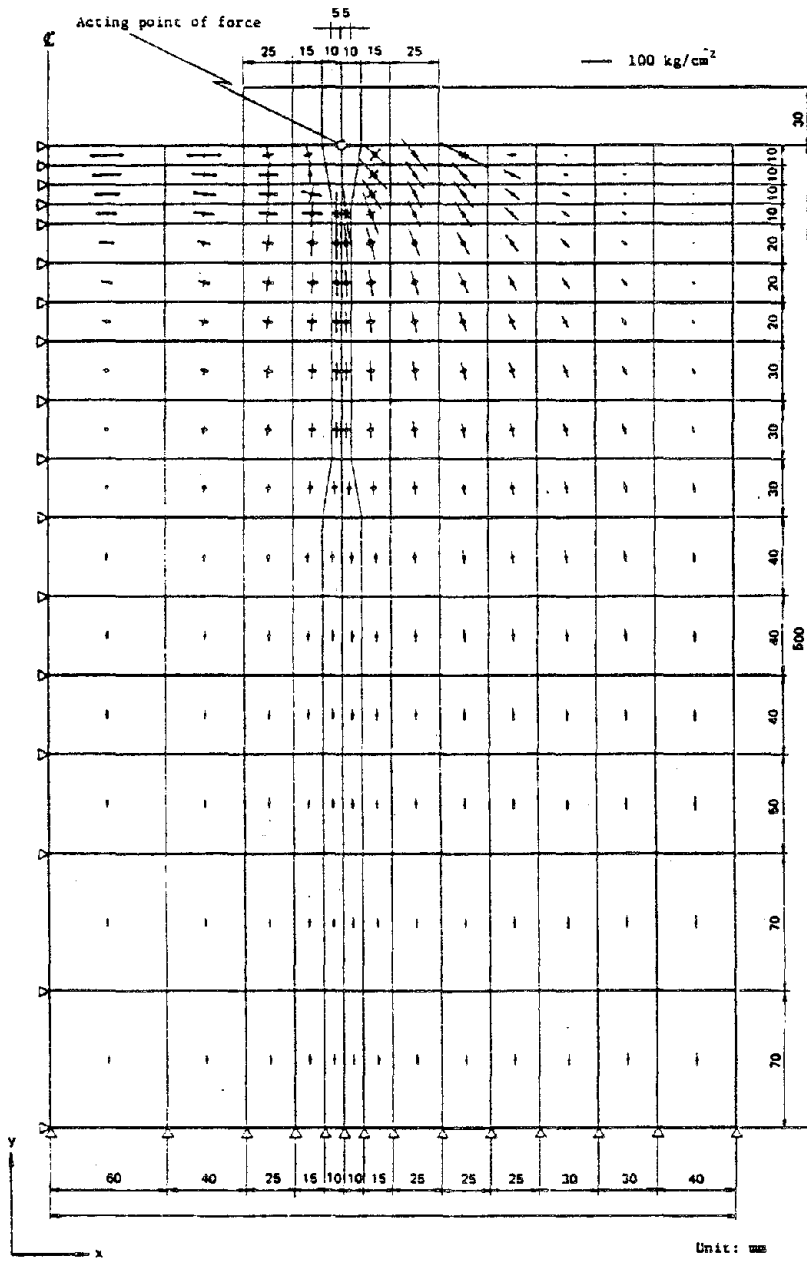


Fig. 6.(2) Model analysis, principal stress
when $N = 1.0t$ and $H = 0.58t$

7. Studies in Relation to Bridge Seat Concrete Designing Methods

7.1 Studies of safety factor in relation to current design methods

We shall study the safety factors in the current design methods in relation to bridge seat concrete based on the strength of the concrete obtained by experiments.

In the studies carried out in Section 5.1 "Breakage properties and Strength", it was discovered that shearing of the surface was not on a horizontal plane and a 45° angle but was inclined at a much greater angle (See Fig. 5.1.2). If the load is from the horizontal direction only, it is believed that there is high possibility that shearing will develop in the direction forecasted. However, it is also believed that the shearing angle will be greater than 45° with the addition of a vertical force.

It will therefore be necessary to carry out studies in relation to past breakages of bridge seat concretes by comparing the combined force of inclined loads and the surface actually broken. However, from a practical standpoint it will be desirable that the analytical process be as simple as possible. For example, when the ratio of the vertical load and horizontal load on a regular simple fixed bearing is approximately the same, even if calculations are carried out on the assumption that the broken surface is of a simple form and considering the load to be a horizontal load only, it is believed sufficient from the viewpoint of safety as long as conditions for the actual bridge and the model are the same.

(1) Strength in the experiment

In the experiment, the ratio of the vertical load and the horizontal load is $\sqrt{3} : 1$. On one hand, the ratio of the vertical force and horizontal force applied to the fixed bridge seat in the axial direction of the bridge during an earthquake will be $1 : 2 \cdot K_H$ in the case of simple girder bridges if the horizontal vibration is K_H . As $2 \cdot K_H$ equals $1/\sqrt{3}$, in the current experiment it will be equivalent to carrying out the experiment with K_H at approximately 0.3.

Although a certain amount of reinforcement will be provided in the current design to prevent vertical slitting crack in the bearing, no special reinforcement was provided to offer resistance to horizontal loads. That is, it may be considered that the bridge seat had practically no reinforcements. For this reason, the strength of test piece ① may be used as the criterion to check its safety factor. Horizontal force S acting on the bridge seat may be calculated from the following equation from breaking load P .

$$S = P/2\sqrt{3} = 85/2\sqrt{3} = 24.3 \times 10^3 \text{ kg}$$

If the breakage surface is assumed to expand in a 45° angle as indicated in Fig. 3.1.5, its area A_T may be obtained with the following equation.

$$A_T = \sqrt{2}x(2x + 2a + b) = \sqrt{2} \cdot 20(2 \cdot 20 + 2.3 + 15) = 1,725 \text{ cm}^2$$

Here, x : Distance from the edge of the concrete to the bottom projection of the bridge seat.

a : Height of the bottom projection of the bridge seat.

b : Width of the bottom projection of the bridge seat.

The ultimate stress intensity due to horizontal force may be obtained with the following equation.

$$\tau_{\max} = S/A_T = 24.3 \times 10^3 / 1,725 = 14.1 \text{ kg/cm}^2$$

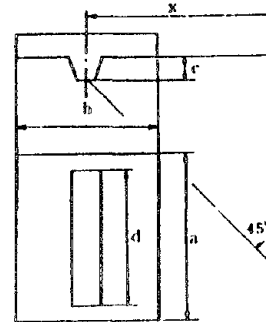
(2) Study of stress intensity in actual bridges

Studies will be carried out in relation to the degree of stress intensity that has developed in the bridge seat concrete in actual bridges. In this instance, the calculation model selected will be as standard as possible.

A simple PC pier construction was considered for the above structure and span lengths between 23 to 40 meters were employed from the standard designs of the Ministry of Construction. The bridge seat was selected from standard designs as shown in Fig. 7.1.1 based on horizontal forces acting on a fixed bridge seat when vibration $K_H = 0.3$. When the bearing edge distance is determined from the span length and

Table 7.1.1 Studies of shearing force from current guide lines

Model No.	Span ℓ (m)	Dead-load reaction per seat DL(kg)	Horizontal pressure (kg) when $R_H = 0.3$ $R_H = DL \times 2 \times 0.3$	Dimensions of standard seats a, b * c, d (cm)	Bearing edge distance x (cm)	Edge distance x (cm) from lip	Shearing area A_T (cm ²)	Stress Intensity τ (kg/cm ²)
1	23.0	34,700	20,800	a = 69.0	31.5	50.5	11,525	1.80
2	24.0	36,500	21,900	b = 38.0	32.0	51.0	11,713	1.87
3	25.0	38,700	23,200	c = 6.0	32.5	51.5	11,899	1.95
4	27.5	43,000	25,800	d = 48.4	33.75	52.75	12,376	2.08
5	30.0	46,000	27,600	a = 78.0	35.0	54.0	12,860	2.15
6	32.5	52,800	31,700	b = 43.0	36.25	57.5	14,946	2.12
7	35.0	58,000	34,800	c = 7.0	37.5	59.0	15,478	2.25
8	40.0	71,000	42,600	d = 53.5 a = 84.0, b = 48.0 c = 8.0, d = 57.0	40.0	64.0	18,192	2.34



the shape of the bottom projection of the seat is determined from the type of seat, the cross sectional area of the concrete sufficient to withstand shearing may be obtained by the same method as in (1). The shearing stress intensity that develops here may then be calculated as shown in Table 7.1.1.

(3) Studies of safety factors

As stress intensity in this type of bridge is a maximum of about 2.4 kg/cm^2 , a safety factor of about 6 times is used as compared to the strength in the experiment. We believe this safety factor will be sufficiently high even considering the following conditions.

(i) Strength tends to become high due to the precision work in this experiment.

(ii) Strength in relation to repeated loads such as earthquakes is weaker than that in relation to static loads.

(iii) As all bridge seats will not function uniformly in actual bridges, there will be a possibility of load concentration occurring.

In the design of bridge bearing seat concrete of simple girder type bridges it will therefore be safe as long as the bearing edge distance is determined according to current design methods, and it may be said that there will be no necessity of using any special reinforcing bars in the bridge seat concrete.

However, in the case of bridge seats where particularly great horizontal forces are believed to exist such as fixed bearings in multidiameter continuous pier bridges, there will be cases where reinforcing will be necessary with steel bars. Thorough consideration will be required in these instances.

7.2 Method of reinforcing bridge seats with steel bars

7.2.1 Steel bar reinforcing and breaking load

The relation between reinforcing steel bars and breaking load is shown in Fig. 7.2.1. With $b+2x$ (See Fig. 3.1.5) as the effective

width, the amount of steel reinforcements A_s in the diagram is the cross sectional area of the steel reinforcements that is included in this width.

(a) Although the diagram shows the relation between the breaking strength and the amount of reinforcing steel, certain irregularities were found to exist. This is believed to be due to the fact that the material strength of the steel bars used at this time differed as $\phi 6$ and $\phi 9$ were used. Fig. (b) shows the horizontal axis as the product of the amount of reinforcing steel and the yield strength. Compared to Fig. (a), it is clear that it has excellent corresponding characteristics.

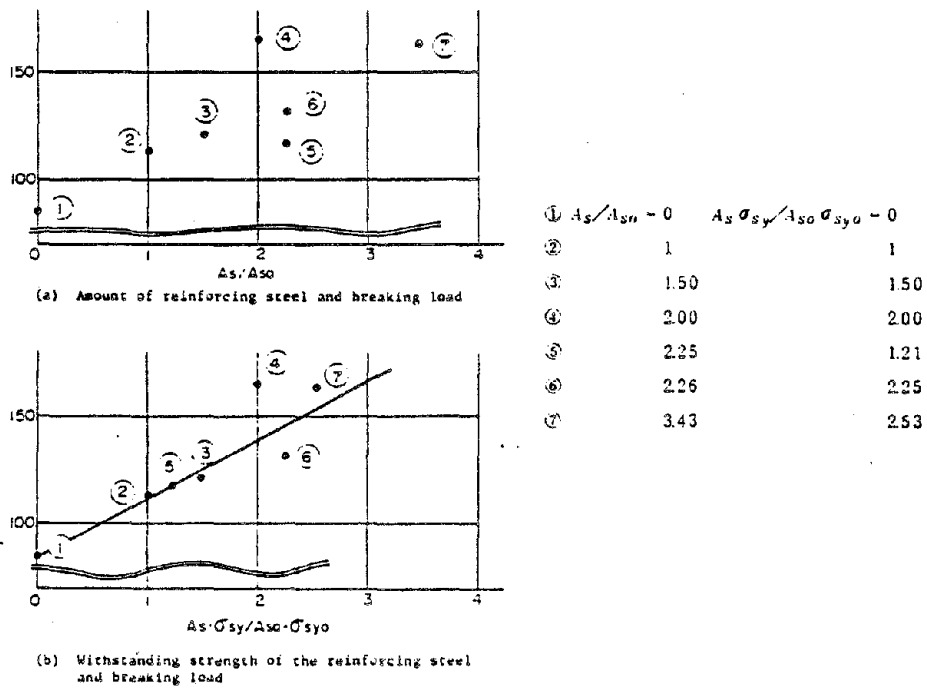


Fig. 7.2.1 Reinforcing steel bars and breaking load

In other words, the breaking strength increases in an almost linear state with increases in strength of the reinforcing steel. Test piece ④ in the diagram was provided with 2 layers of reinforcing steel and, as may be noted, has greater strength compared to the other cases.

Table 7.2.1 shows these relations in the form of efficiencies of reinforcing steel bars. This table shows the comparisons between the sum N_s of the tensile strengths of the steel bars in each test piece and the strength ΔS_u in relation to the increased horizontal force as a result of the steel bars, and also indicates the percentage of the strength of the steel bars that is working effectively. When this ratio is 1, it will mean that the strength of the bridge seat is indicated by the sum of the strength of the concrete and the strength of the steel bars. Although this efficiency is approximately 0.5 - 0.8 in the table, it may be noted that efficiency is high in test piece ④ where 2 layers of steel reinforcing bars are used and in test piece ⑦ which uses reinforcing steel bands.

In general, when designing reinforced concrete, the steel bars are designed to sustain all of the tensile force and the tensile strength of the concrete is disregarded. However, as far as this experiment was concerned, it was noted that there were certain elements in the resistive force of the concrete that could not be disregarded. It is therefore believed that, from the viewpoint of economic design methods it will be desirable that the bridge seat be designed in such a manner that the reinforcing steel bars do not bear all of the horizontal force and that the concrete bears a certain amount of the force in common with the steel bars. Also, when the degree of contribution of concrete strength is great, it indicates that, in bearings with large horizontal force, it will be more effective to increase the bearing edge distance rather than simply providing steel reinforcements.

Furthermore, no consideration whatsoever was given to the reinforcing steel already provided in the substructure in this study. However, in substructures having a large amount of reinforcing steel, it is believed that they may be considered a portion of the reinforcement in the bridge seat.

Table 7.2.1 Effectiveness of steel reinforcements

No.	Area of reinforcing steel (cm ²)	Strength N _s of steel bars	Breaking strength P _u	Increased strength Portion ΔP _u	Increased portion of horizontal force ΔS _u	ΔS _u /N _s
1	0	0	85	0	0	0
2	φ6 × 9 = 2.54	14.2	113	28	8.08	0.57
3	6 × 13 = 3.68	20.5	121	36	10.3	0.50
4	6 × 18 = 5.09	28.4	165	80	23.1	0.81
5	9 × 9 = 5.73	16.9	117	32	9.23	0.55
6	φ6×9+φ6×7 = 4.51	25.2	131	46	13.2	0.52
7	φ6×9+φ9×10 = 8.90	33.0	164	79	22.8	0.69

7.2.2 Workability of the reinforcing steel bars

If reinforcement of the test piece is evaluated from the standpoint of workability, it will be as follows.

1 Layer of Reinforcing Steel: No special problems. Withstanding strength is practically assured with this method.

2 Layer of Reinforcing Steel: No special problem when the amount of reinforcing steel in the substructure. However, installation is practically impossible where the amount of reinforcing steel bars is great such as in overhang or rigid frame type construction.

Reinforcing steel (I) + slitting crack reinforcing steel bars (II): Although installation is possible, the reinforcing effect is small compared to the amount of work involved.

Reinforcing steel (I) + tensile reinforcing steel (III): Work is simple and effect is great even when the amount of reinforcing steel in the substructure is great.

7.3 Plan in relation to a bridge seat concrete designing method

The following is a plan in relation to a designing method for a bridge seat concrete based on the foregoing studies.

(1) If the bridge is a simple girder type bridge of normal size, there will be no need for special steel reinforcements as long as the prevailing bearing edge distance and detailed specifications for reinforcing steel bars are adhered to.

(2) Even in simple girder bridges, when the horizontal force is extremely great, or in cases of fixed bearings in continuous girder bridges, current designing methods are satisfactory as long as the product of the acting horizontal force and the area of the assumed breakage surface (45° surface) does not exceed a slitting crack stress intensity τ_{aI} including a certain safety factor. When the value exceeds τ_{aI} , the stress intensity should be brought within τ_{aI} by increasing the bearing edge distance. When it is not possible to increase the bearing edge distance, it will be necessary to provide reinforcing steel. In this instance, the reinforcing steel should not be made to bear all of the horizontal force but a portion S_c to be borne by the concrete should be set and reinforcing steel be installed so it will bear the entire horizontal force less S_c . For method of reinforcement, reference may be made to test pieces ②, ④ and ⑦. Also, when the main reinforcing steel bars in the substructure are within the assumed breakage surface, their effect must be included in the calculation.

A problem in this plan is what value to use for τ_{aI} and S_c . Although it will be necessary to continue to carry out closer studies in this relation, the following may be considered from this experiment.

$$\tau_{aI} = 5 \text{ kg/cm}^2$$

$$S_c = \frac{1}{2} \tau_{aI} \cdot A_T$$

A_T : Assumed breakage surface of 45°.

Examples of widening reinforcement of existing abutments and bridge pier seats for collapse prevention also are shown in Fig. 7.3.1 and 7.3.2.

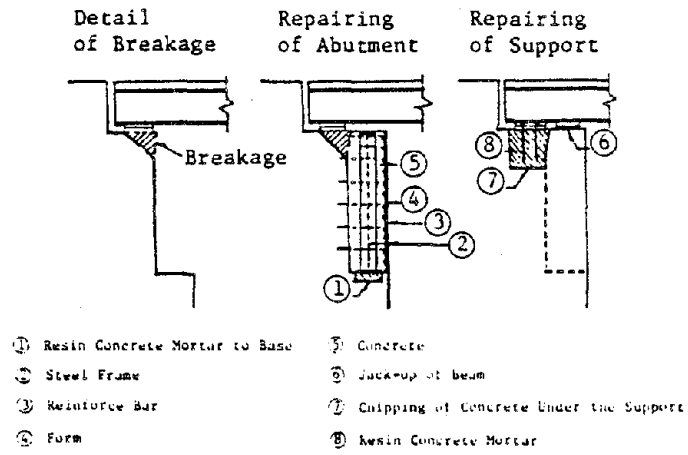


Fig. 7.3.1 A exsample of repairing and retrofitting of support⁸⁾

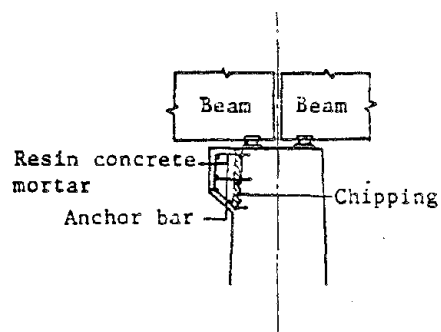


Fig. 7.3.2 Widening of coping⁸⁾

8. Conclusion

The following items were principally confirmed as a result of this study.

(1) Slitting crack stress intensity due to vertical force is of a level that may be completely ignored.

(2) Horizontal displacement of the bearing due to inclined loads commenced immediately prior to breakage and reached the breaking point immediately after displacement developed. Therefore, when we consider the difference (approx. 5mm) between the diameter of the anchor bolt and the hole diameter in the lower seat of actual bearings, it may be considered that breakage will be considerably advanced when the horizontal force acts on the anchor bolt.

(3) Although breakage occurred simultaneously with development of slanted cracks in front of the bridge seat when no reinforcing steel bars were provided, when reinforcing steel bars were used, load increased even after cracks developed and it was noted that toughness increased with the usage of steel reinforcements.

(4) As a result of the studies carried out in relation to reinforcing with steel bars, it was learned that the breakage strength of the bridge seat concrete increased in an almost linear state in relation to increases in strength of the reinforcing steel bars. Disparity in effectivity due to different methods of reinforcement was also noted.

(5) The share of the overall strength occupied by the strength of the concrete is great even in bridge seat concrete with reinforcing steel bars.

(6) Results of comparisons made of the ultimate strength of the concrete obtained from the breakage strength of the test piece with no reinforcement and the stress intensity generated in actual bridges disclosed that concrete strength alone provided a high

safety factor in normal simple girder bridges. This indicates that, in normal bridges, it is safe even without reinforcing bars as long as bearing edge distance is maintained in the current design methods and work is carried out completely. The safety factor was therefore confirmed in the current design method.

(7) It is not possible to always ensure sufficient safety factor with the current design in relation to footing concrete of bearings subjected to particularly large horizontal forces during earthquakes such as fixed bearings in continuous girder bridges. A plan of a design method for footing concrete was prepared for cases of this nature based on the results of this experiment.

The general outline of this plan is to cope with horizontal forces by increasing the bearing edge distance and when this is not possible, to also use concrete and reinforcing bars to cope with these forces. (See Fig. 7.3)

Lastly, I wish to express my appreciation to Mr. Tadashi Oshitari and Mr. Koji Wada of Oriental Consultants Co., Ltd. for their cooperation in making this study possible.

Reference Literature

- (1) The Miyagiken-oki Earthquake Highway Bridge Disaster Research Committee, Japan Road Association: "Research Report in Relation to the Miyagiken-oki Highway Bridge Disasters and Earthquake Resistance of Bearings", Japan Road Association, July, 1980.
- (2) Japan Road Association: "Guide to Design of Highway Bridge Substructures, Abutment and Bridge Pier Designs", March, 1968.
- (3) Japan Road Association: "Highway Bridge Specifications IV, Substructures", May, 1980.
- (4) Japan Road Association: "Highway Bridge Specifications I, Common Structures", February, 1980, PP 76 - 77
- (5) N. Arakawa: "Withstanding Tests of Anchor Bolts", Japan Highway Public Corporation Test Laboratory Report.
- (6) S. Yanagida and Others: "Research on Bridge Pier Seating", Technical Railroad Laboratory Report No. 597. July, 1967.
- (7) Japan Society of Civil Engineers: "National Railways Standard Manual of Structural Designs, Reinforced Concrete Structural Material and Non-reinforced Concrete Structural Material", November, 1976, PP 191 - 197.
- (8) T. Asama, Y. Shioi, T. Tazaki and H. Asanuma: "Repair and Retrofit Works for Existing Highway Bridges", Public Works Research Institute, Ministry of Construction, May, 1980.

REPAIR AND RETROFIT WORKS FOR EXISTING HIGHWAY BRIDGES

Tatsuo Asama, Yukitake Shioi,
Tadayuki Tazaki and Hideya Asanuma

Public Works Research Institute
Ministry of Construction

I. Introduction

Japan has an extensive road network consisting of 40,000 km of national highways and 130,000 km of prefectural roads; they account for 87% of the total domestic transport volume in tonnage, or 37% of the total ton-km.

If a major earthquake occurs, these roads may be damaged along with other structures, hampering evacuation, rescue and repair activities in the stricken area. Past cases show, however, that where the function of the road was maintained the disaster was kept at a minimum.

Bridges are important structures to cross over obstacles; but they are liable to be affected by earthquakes. Such damage as the fall of the superstructure results in the loss of the function of the road and is difficult to repair. If the damage is not as severe as the fall of the superstructure, temporary repairs may be made so that the bridge may be open to emergency traffic; it may be used semi-permanently, depending on the repair method.

There are 33,000 bridges on the national highways and prefectural roads with a total length of 22,000 km, and they vary in age, type, specifications, materials, etc. In order to ensure a certain level of safety for these bridges against earthquakes, it is necessary to devise appropriate methods of repair and retrofit and equipment.

Though complete regulations cannot be provided under the present circumstances, some measures have been taken for several important bridges and a repair manual has been prepared. This paper is intended to introduce a part of the manual together with some cases of repairs actually carried out.

II. Damage to Highway Bridges by the Past Earthquakes

The damage to the bridge was often extensive when the magnitude of the earthquake was relatively large. Let us review below the damage to the highway bridges caused by such big earthquakes as to have influenced the earthquake-resistant design for highway bridges (see Fig. 1).

Table 1 shows the number of bridges damaged by the Great Kanto Earthquake of 1923 ($M = 7.9$); Tables 2 and 3 give the breakdown of the damage in Tokyo and Yokohama. The damage caused by ground vibration was predominant in Yokohama as the city was close to the epicenter; but it decreased with distance from the epicenter.

The Fukui Earthquake ($M = 7.3$) of 1948 was a typical short-distance earthquake. The number of damaged bridges is given by Table 4. It is not possible to give the damage ratio here as the total number of bridges in the area at that time is not available.

The Niigata Earthquake ($M = 7.5$) of 1964 damaged many structures due to large scale liquefaction on the saturated alluvium sandy ground. It was characteristic of the earthquake that the damage was mostly related to the problem of stability: settlement, tilting and sliding. The extent of the damage is shown by Table 5. Table 6 is intended to show the relationship between the damage and types of superstructure and of foundation with respect to the bridges within the 60 km radius of the city. Tables 7, 8 and 9 give the breakdown of the damage.

The Tokachi-oki Earthquake ($M = 7.9$) of 1968 causes extensive damage to roads, mainly to earth banks; but the damage to bridges was relatively small. Table 10 shows the extent of damage to bridges; Table 11 gives the breakdown of the damage.

The Miyagiken-oki Earthquake ($M = 7.4$) of 1978 caused damage mainly to structures. The damage was characterized by the fact that while many of those structures with their foundations on comparatively good bearing strata were damaged, the damage relating to stability, e.g., overturning and sliding, was small. Fairly extensive damage was caused to bridges, as shown by Table 12. Table 13, Figs. 3 and 4 give the breakdown of the damage into superstructure, support and substructure.

Table 14 gives the number of bridges which suffered severe damage such as the fall of the superstructure in the past.

III. Methods of Repair and Retrofit for Highway Bridges

There is no prescribed method of repairing bridges damaged by earthquakes and of retrofitting existing bridges against earthquakes. But the Manual of Repair Work for Highway Bridges, published by the Japan Road Association in 1979, serves as a very useful guide.

As the damage to bridges takes various forms, repairs are usually carried out on a case by case basis. The procedure of repairing may be explained with a flow chart shown as Fig. 5.

The procedure begins with inspection of the bridge concerned. It is necessary to inspect the structural dimensions, age, specifications, etc., as well as the extent of the damage. In this case it will be convenient if a check list is prepared prior to inspection.

Upon discovering a damaged section, the extent and the form of the damage are to be ascertained in detail, e.g., failure, deformation, tilting, etc., in the light of the volume of emergency traffic and of future traffic. Before deciding as to whether the bridge can sustain the load of emergency traffic immediately after the disaster, it is necessary to ascertain if the bridge can be open to traffic with or without repairs or if it should be closed.

After order has been restored in the stricken area, the method of reconstruction will be selected. Depending on the durability, repair cost, future plan, etc. of the remaining structure, construction of a new bridge may be required.

After the method of retrofit for future earthquakes as well as that of repair has been selected, works at the site may commence. Effects of repairs and retrofit are to be examined upon completion of the works.

Among the existing bridges, there are many which were constructed to old specifications. The problem with roads is that the closing at one point of a route often leads to the loss of the function of the entire route.

Therefore, even in the case of an old bridge, it is necessary to take such measures as to ensure a certain level of safety against earthquakes corresponding to that of a new bridge. Past experience shows that unless the superstructure falls it is possible to make temporary repairs so that emergency traffic may not be obstructed. Accordingly, it was decided to take two of the three measures given below for all bridges located on trunk routes and they are now in progress.

- (1) Minimum length of overlapping of girder and coping at support.

The minimum length S in Fig. 6 may be prescribed as:

$$\begin{aligned} S &= 70 + 0.5\ell \quad (\ell \leq 100) \\ &= 80 + 0.4\ell \quad (\ell > 100) \end{aligned}$$

where S : minimum length (cm)

ℓ : span length (m)

- (2) Devices for preventing dislodgement

The types of devices are shown in Fig. 7.

- (3) Connecting devices for neighboring superstructures

The types of devices are shown in Fig. 8.

IV. Examples of Repairs and Retrofit

There have been many examples of repairing bridges damaged by earthquakes. But the old methods are not applicable to the present bridges. So some examples and methods of repairing damages caused by recent earthquakes are given below.

Those parts of bridges damaged by earthquakes can be classified into superstructure, support and substructure as mentioned before.

As the damage to the superstructure is concentrated in expansion joint, handrail, buckling of sway bracing, it is easy to replace them. The buckling of web plate can be reinforced with stiffener. As a special case, repairing works on the side span of the Bandai Bridge in Niigata Earthquake are illustrated in Fig. 9.

The main damage to the support is shown in Fig. 2. In many cases, they are repaired by jacking up the superstructure as shown in Fig. 10. If jacking is difficult, another temporary support, serving to secure the length of overlapping of girder and coping, shall be prepared as shown in Fig. 11.

The damage to the substructure can be divided into two types. One is related to stability, e.g., as settlement, tilting, sliding and so on. Another concerns safety of structures, e.g., failure, breakage, crack and so on.

For the former case, there are several methods such as underpinning, filling up, etc. However in most cases the cost is so high that reconstruction is advantageous.

For the latter, such method as wrapping with reinforced concrete as shown in Fig. 12, is common. Besides, there are many cases where partial repairs are sufficient to keep the bridges open. But in the case of the structural damage, it is dangerous

even for emergency traffic, some emergency measures are taken as in Fig. 13. In Fig. 14 typical examples of the cases requiring either emergency measures or permanent repairs.

Recently, projects to give retrofit to old bridges against earthquakes are in progress in Japan. Most of them are works to expand the length of overlapping on the support conforming to current specifications, to install devices to prevent dislodgement and to attach the connecting devices between neighboring beams.

The latter two are relatively easy works as shown in Figs. 7 and 8. For the former some methods as Figs. 15 and 16 are used.

Sometimes the retrofitting of the substructure of old bridges against earthquake is adopted because they have not been designed according to earthquake resistant regulations. In Fig. 17 one example of the retrofitting of an abutment is explained. The increment of pile is planned in a curious shape depending on a narrow space around the existing bridge. Fig. 18 is one example of the retrofitting of a pier.

In Japan, the foundations are often exposed because of the lowered riverbed due to the heavy demand for gravel. Accordingly, these foundations have become dangerous in earthquakes because of decreased lateral ground resistance. As a countermeasure, one example of the stabilization of riverbed is shown in Fig. 19.

A cast in site diaphragms wall method used in Fig. 19 and explained in Fig. 20 is recently becoming one of the most effective methods for retrofitting.

V. Discussion

So far the authors have introduced the current methods of repairing and retrofitting against earthquakes in Japan. But they are not methodical and not systematical. So we must apply them on a case by case basis. However, it is very difficult to evaluate the damage and to decide on the repair method during the confusion following an earthquake. Therefore, an appropriate guide is desirable.

On the other hand, the planning of retrofitting for old bridges to give some resistance against earthquakes is also difficult because in many cases their figures and records of calculation have been not kept. Therefore some regulated methods are required.

In this connection, the subjects to be studied in future may be listed as below.

(Repairing)

Method for survey and inspection

- Composition of a check list for inspection
- Evaluation method of load carrying
- Capacity for damaged structure
- Manual for the selection of repair method
- Inspection method for repaired structure

(Retrofitting)

Method for survey

- Evaluation method for earthquake resistance of existing structures
- Estimation of durability for existing structures
- Manual for the selection of retrofitting method
- Evaluation method for effects of retrofitting

Table 1 Total number of bridges damaged in the Kanto earthquake of 1923¹⁾

Prefectures or Cities	Total Number of Bridges Surveyed	Number of Bridges Damaged due to Vibration and/or Fires	Percentages of Damage	Remarks
Tokyo	3,338	230	6.9%	Except city of Tokyo
City of Tokyo	675	358	53.0%	
Kanagawa	1,253	893	71.3%	Except city of Yokohama
City of Yokohama	108	91	84.2%	
Shizuoka	358	100	27.9%	Inside the affected area (Numazu or northern area)
Saitama	1,313	27	2.1%	Only wooden bridges suffered inside the affected area
Yamanashi	245	21	8.6%	
Chiba	690	65	9.4%	
Total	7,980	1,785	22.4%	

Table 2 Damage characteristics in the City of Tokyo¹⁾

Type of Bridges	Total Number of Bridges Surveyed	Number of Bridges Damaged and Percentages		
		Caused by Vibration	Caused by Fires	Total
Wooden	420	6(1.4%)	276(65.7%)	282(67.1%)
Steel	60	6(10.0%)	49(81.7%)	55(91.7%)
Masonry	144	2(1.4%)	5(3.5%)	7(4.9%)
Plain concrete	4	4(100%)	0(0%)	4(100%)
Reinforced concrete	47	0(0%)	10(21.3%)	10(21.3%)
Total	675	18(2.7%)	340(50.3%)	358(53.0%)

Table 3 Damage characteristics in the City of Yokohama¹⁾

Type of Bridges	Total Number of Bridges Surveyed	Number of Bridges Damaged and Percentages			
		Caused by			Total
		Vibration + Fires	Vibration Only	Fires Only	
Wooden	75	26(34.6%)	25(33.4%)	8(10.7%)	59(78.7%)
Steel	31	11(35.5%)	16(51.6%)	3(9.7%)	30(96.8%)
Reinforced concrete	2	0(0%)	2(100%)	0(0%)	2(100%)
Total	108	37(35.2%)	43(39.8%)	11(10.2%)	91(84.2%)

Table 4 Statistics on damage to highway bridges due to the Fukui earthquake of 1948¹⁾

Prefectures	Bridge Damage		Highway Damage Except Bridges	
	Number of Bridges	Repairing Cost	Number of Sites	Repairing Cost
Fukui	180	Thousand Yen 189,869	475	Thousand Yen. 205,945
Ishikawa	63	17,782	155	41,463
Total	243	207,651	630	247,408

(Note) Amount of loss was evaluated at the value at the time of the earthquake.

Table 5 Statistics on damage to highway bridges (except wooden bridges) due to the Niigata earthquake of 1964¹⁾

Prefectures	Number of Damaged Bridges	Number of Severely Damaged Bridges	Number of Fallen Bridges	Approximate Epicentral Distance
Akita	7	0	0	140 - 160 km
Fukushima	5	0	0	120 - 150 km
Niigata	74	8	3	30 - 100 km
Yamagata	12	0	0	60 - 100 km
Total	98	8	3	

Table 6 Damage percentages of individual portions of highway bridges within 60 km from the center of Niigata City¹⁾

Structural Classification	Type of Structures	Number of Structures Surveyed	Damaged Structures		
			Number of Structures	Percentages	
Super-structures	Steel Girders	168 spans	19 spans	11.3 %	
	Reinforced Concrete Girders	222 spans	33 spans	14.9 %	
	Prestressed Concrete Girders	132 spans	11 spans	8.3 %	
	Wooden Girders	8 spans	8 spans	100 %	
	Total	530 spans	71 spans	13.4 %	
Substructures	Abutments	With Spread Footings	24	4	16.7 %
		With Pile Foundations	99	19	19.2 %
		With Caisson Foundations	29	7	24.0 %
		Sub-Total	152	30	19.7 %
	Piers	With Spread Footings	40	0	0 %
		With Pile Foundations	214	21	9.8 %
		With Caisson Foundations	180	15	8.3 %
		Sub-Total	444	36	8.1 %
	Total	596	66	11.1 %	

Table 7 Type and number of damages of superstructure in Niigata earthquake⁴⁾

Part \ Damage	Peeling	Crack	Yield	Failure	Buckling	Deformation	Crash	Shear	Displacement	Slip out	Breakage	Fall
1. Pavement	14	15										
2. Handrail	7	14		6	1	2	1		4	2	4	
3. Expansion Joint		1							9			
4. Slab	2	5					2		2			
5. Floor System		1										
6. Sway and Lateral					1	2			2			
7. Main Structure	3	12	2				1		11	1		6
8. Sole Plate								4	2			
9. Bearing								5	2			
10. Mortar under Bearing	10	10					1		2			
11. Embedded Bolt									2	5		

Table 8 Type and number of damages of substructure in Niigata earthquake⁴⁾

Part \ Damage	Peeling	Crack	Yield	Failure	Buckling	Deformation	Displacement	Breakage	Tilting	Sliding	Overturning	Settlement
1. Support	1					2		5	26	13	2	32
2. Coping	10	16		4		1						
3. Body		9		1	3	4		5	26	13	2	32
4. Footing												
5. Foundation												

* Tilting, sliding, overturning and settlement are to be considered in terms of the whole substructure.

Table 9 Type and number of damaged of approach road in Niigata earthquake⁴⁾

Part \ Damage	Peeling	Crack	Yield	Failure	Buckling	Deformation	Displacement	Breakage	Tilting	Sliding	Overturning	Settlement
6. Approach Portion		10		1			1	2		4		22
7. Bank		4					1			2		14
8. Retaining Wall	2	8				8	1		18	23		22
9. Wing	4	16				6	4		5	16	1	14

Table 10 Statistics on damage to highways and highway bridges due to the Tokachi-oki earthquake of 1968

Administrative Agency		Highways		Highway Bridges		Total		Remarks
		Number of Sites	Loss	Number of Bridges	Loss	Number	Loss	
Ministry of Construction		111	Thousand Yen 969,604	-	-	111	Thousand Yen 969,604	Mostly to National Highways in Aomori Prefecture
Prefectural Governments	Hokkaido	63	319,359	30	Thousand Yen 206,176	93	525,535	
	Aomori	818	1,167,060	64	187,770	882	1,354,830	
	Iwate	41	34,178	3	19,000	44	53,178	
	Miyagi	-	-	3	5,100	3	5,100	
	Akita	4	4,600	1	3,000	5	7,600	
Total		1,037	2,494,801	101	421,046	1,138	2,915,847	

Note) Amounts of loss were estimated at the value as of June, 1968.

Table 11 Type and number of damages in Tokachi-oki earthquake of 1968⁵⁾

Damage		Failure	Move- ment	Deform- ation	Settle- ment	Incli- nation	Buckl- ing	Crack	Fall of covering of RC
Damages to Super- structures	Main girder		7	1			2	2	1
	Pavement							2	
	Handrail	2	1	1					
	Shoe and its fixed mortar	4	7					4	3
Damages to Sub- structures	Abutment	6	6		4			14	4
	Pier				3	1		3	3
	Foundation								
	Ground				1			1	
Damages to Approaches	Embankment in contact with abutment	2	3		2			2	
	Embankment	1	4		3			1	
	Retaining wall and revetment	3	11	1				11	

Table 12 Whole bridges and damaged bridges in Miyagiken-oki earthquake³⁾

	Number of Whole Bridges	Number of Damaged Bridges			
		Super-structure	Bearing	Sub-structure	Total Number of Damaged Bridge
Under the Government	55	2	21	35	42
Under the Governor of Miyagi	400	13	43	72	95
Under the Governor of Iwate	170	6	18	8	20
Under the Governor of Fukushima	4	1	2	0	2
Under the Japan Highway Corp.	269	0	40	18	47
Total	898	22	124	133	203

Table 13 Damages of superstructure in Miyagiken-oki earthquake³⁾

Steel

Name of Bridge	Type	In augu- lation	Damage
1 Kinnoh	Cantilever Girder (Gerber)	1956	Fall of Suspended Girder
2 Yanaizu	Continuous Truss	1975	Buckling of Web Plate on Fixed Support
3 Maiya	Cantilever Truss (Gerber)	1928	Breakage of Upper Chord of Truss
4 Date	Continuous Truss	1965	Buckling of Web Plate on Fixed Support
5 Sin Eai	Continuous Girder	1974	Buckling of Sway Bracing on Support
6 Fukuda	Cantilever Girder (Gerber)	1955	Buckling of Sway and Lateral Bracings Near Support, Failure of Rivets.
7 Fuji	Continuous Girder	1971	Buckling of Sway Bracing on Support
8 Sakunose	Langer Girder	1962	Deformation of Portal and Lateral Bracing on Support
9 Iwaigawa	Continuous Girder	1977	Buckling of Sway Bracing on Support
10 Wagagawa	ditto	1969	ditto

Concrete

11 Yuriage	PS Beam	1972	Crack of Beam on Support
12 Dohdono, 10 others	RC Beam and RC Cantilever Beam	-	Crack of Beam on Support

Table 14 Number of bridges fallen and burned by earthquakes after Kanto earthquake

Name of Earthquake	Year	Fallen	Burned
Kanto	1923	8	9
Nankai	1946	1	0
Fukui	1948	7	0
Niigata	1964	3	0
Miyagiken-oki	1978	1	0
Total		20	9

No	Date	Name	M
1	Spet. 1, 1923	Kanto	7.9
2	Dec. 21, 1946	Nankai	8.1
3	Jun. 28, 1948	Fukui	7.3
4	Dec. 26, 1949	Imaichi	6.4
5	Mar. 4, 1952	Tokachi-oki	8.1
6	Apr. 30, 1962	Northern Miyagi	6.5
7	Jun. 16, 1964	Niigata	7.5
8	Feb. 21, 1968	Ebino	6.1
9	May 16, 1968	Tokachi-oki	7.9
10	Jun. 12, 1978	Miyagiken-oki	7.4

(*) Magnitudes are on the Richter scale, after Rika Nenpyo (Annual Report of Science) (1971).

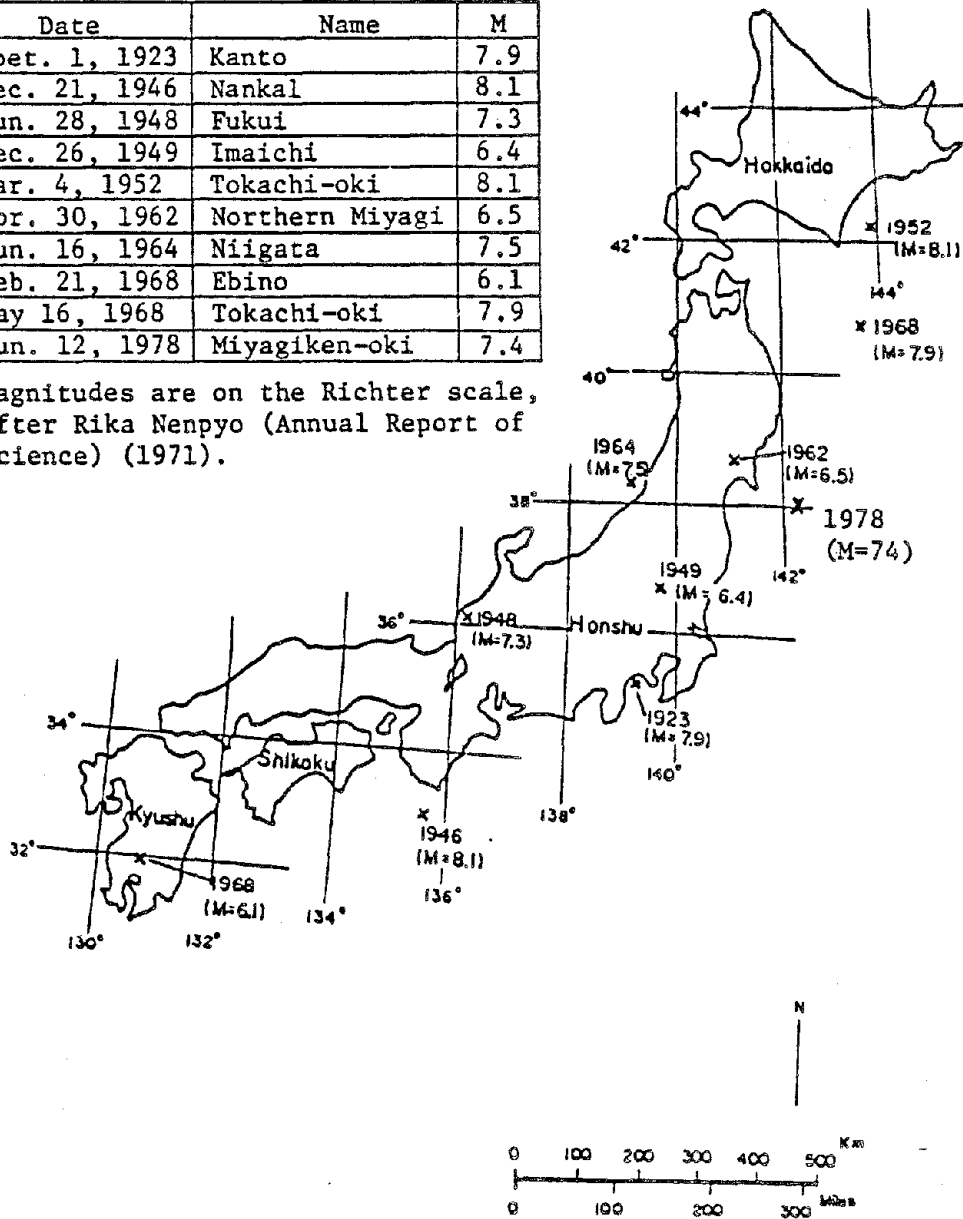


Fig. 1 Epicenters of ten earthquakes which caused comparatively severe damage to modern engineering structures in Japan¹⁾

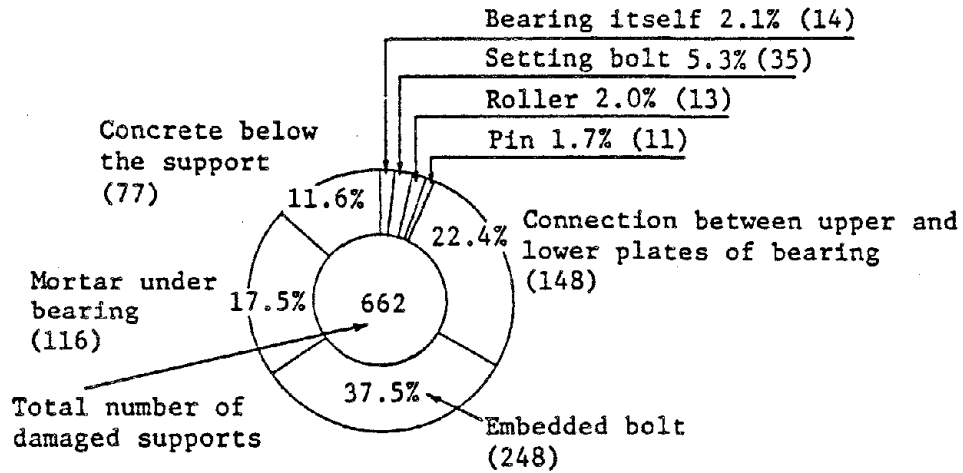


Fig. 2 Breakdown of damaged supports³⁾

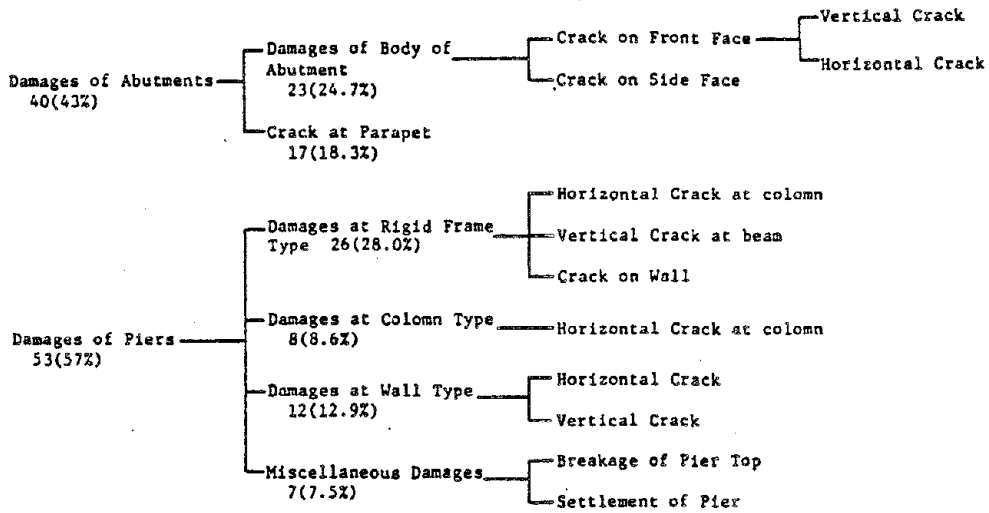
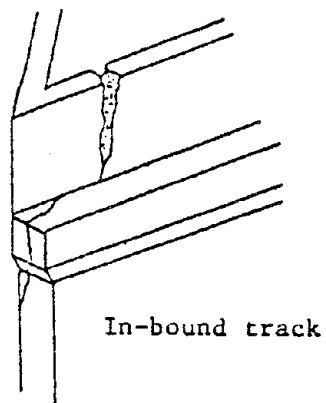
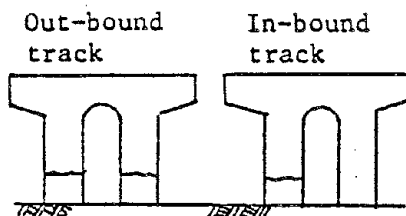


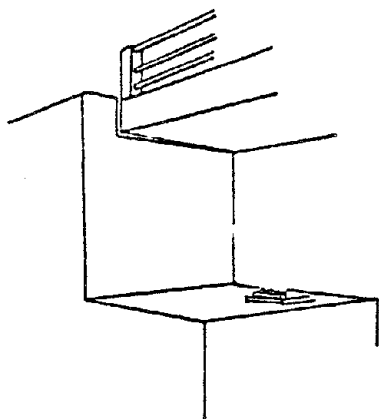
Fig. 3 Classification of damages of substructures³⁾



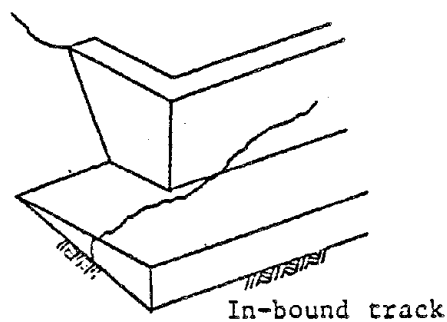
1. Nagamachi Overpass (A₁)



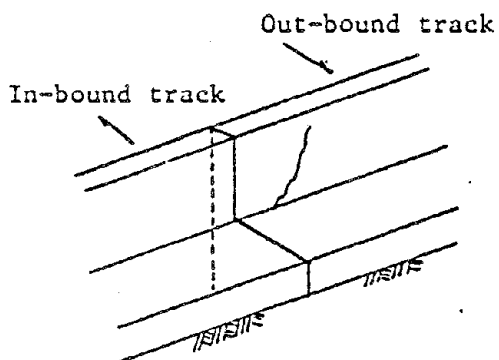
2. Umedagawa Br. (P₁)



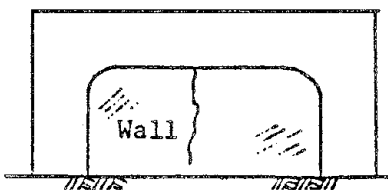
3. Umedagawa Br. (A₂)



4. Izumi Br. (A₁)

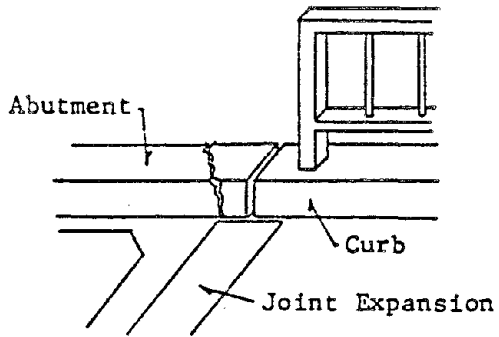


5. Izumi Br. (A₁)

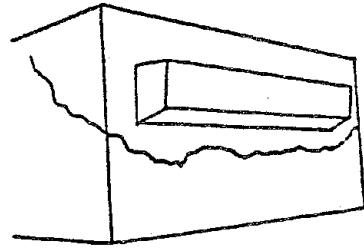


6. Tadagawa Br. (P₁)

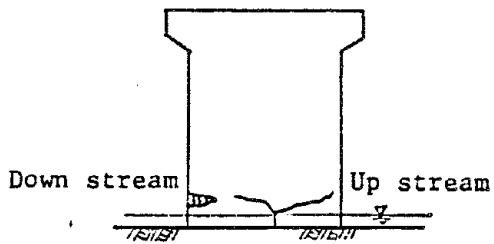
Fig. 4 Damages of abutments and piers in Miyagiken-oki earthquake (1/11)



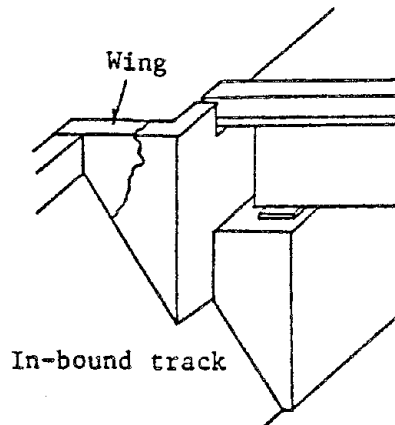
7. Tadagawa Pedestrian Br. (A₂)



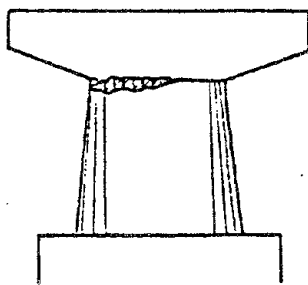
8. Sin Eai Br. (A₁)



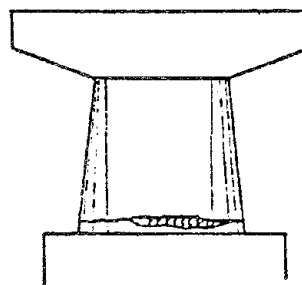
9. Sin Eai Br. (P₃)



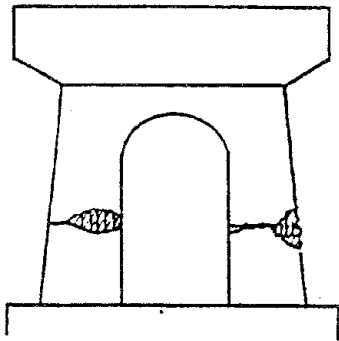
10. Arase Br. (A₁)



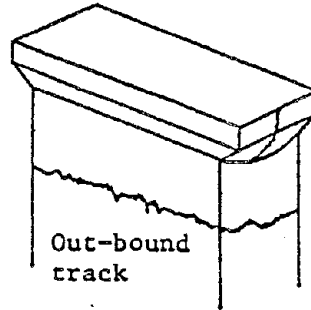
11. Sendai Br. (P₅ ~ P₈)



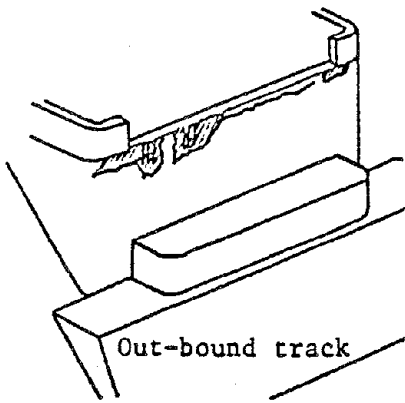
12. Sendai Br. (P₁ ~ P₄, P₇)



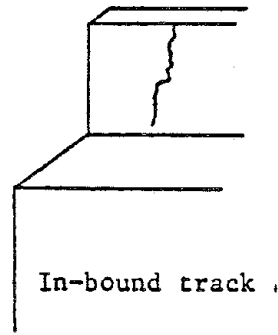
13. Abukuma Br. (P₂ ~ P₉)



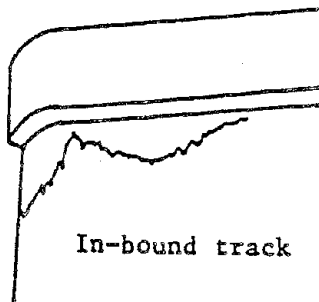
14. Fukuda Br. (P₂)



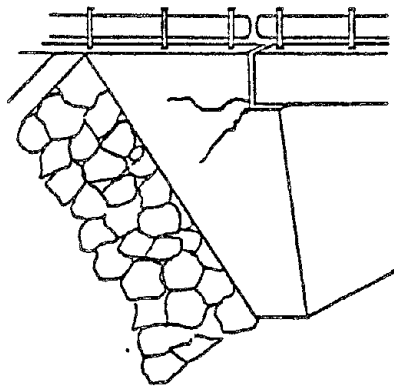
15. Fukuda Br. (A₂)



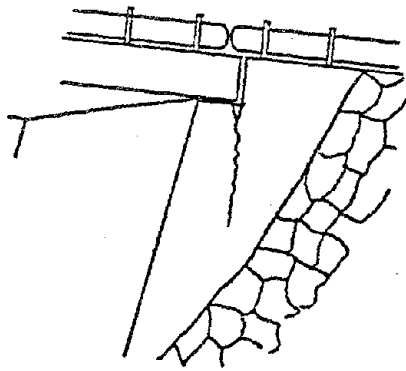
16. Fukuda Br. (A)



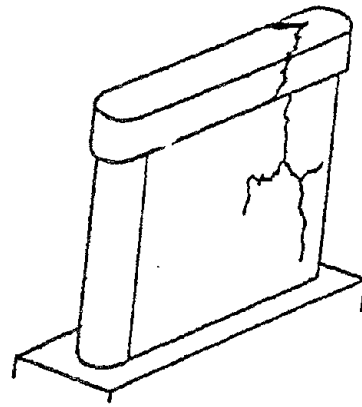
17. Fukuda (P₃)



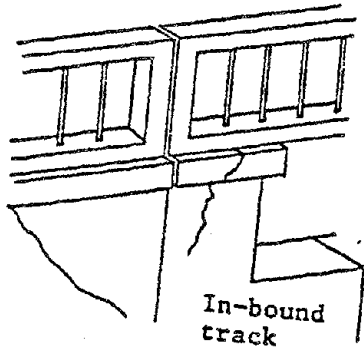
18. Hebita Overpass (A₁)



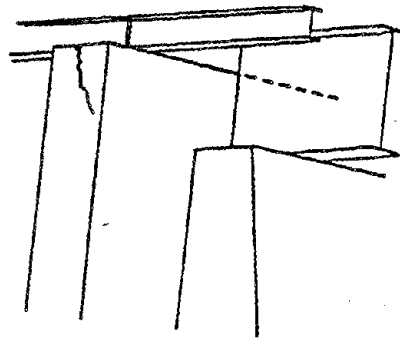
19. Hebita Overpass (A₂)



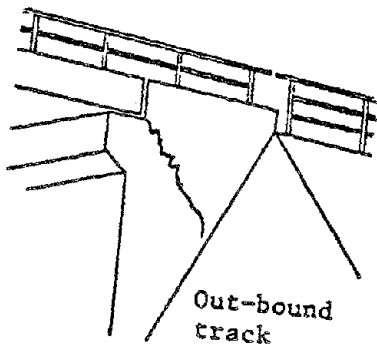
20. Tenno Br. (P₁)



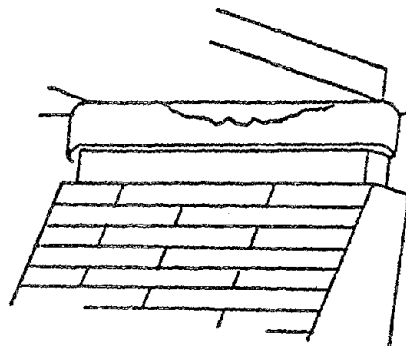
21. Iwadeyama Br. (A₁)



22. Kawawatari Pedestrian Br. (A₂)

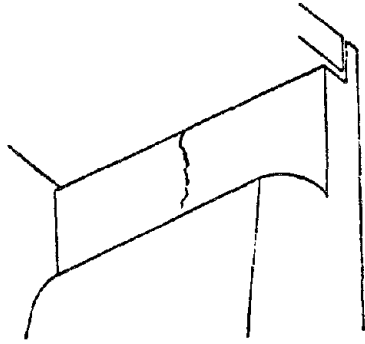


23. Ayashi Overpass (A₁)

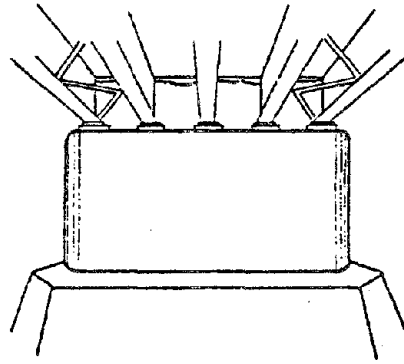


24. Takakuragawa Br. (A₂)

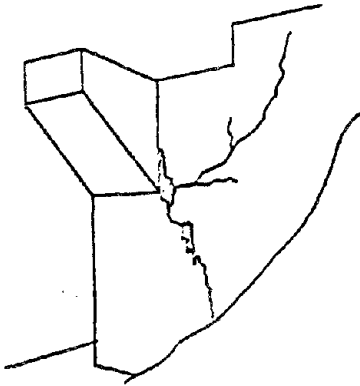
Fig. 4 (4/11)



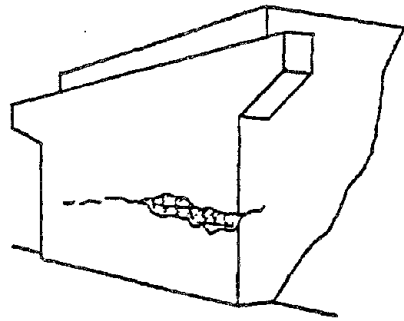
25. Natori II Br. (AR)



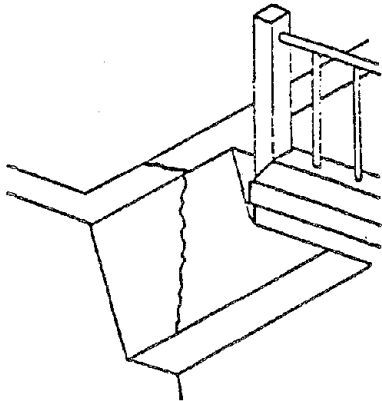
26. Ochiai Br. (AL)



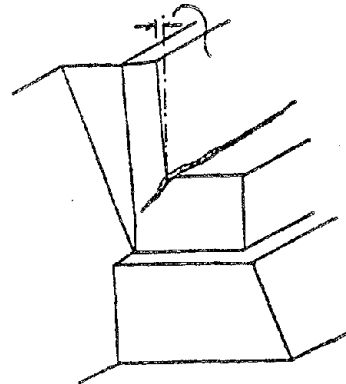
27. Nanakitada Br. (AL,AR)



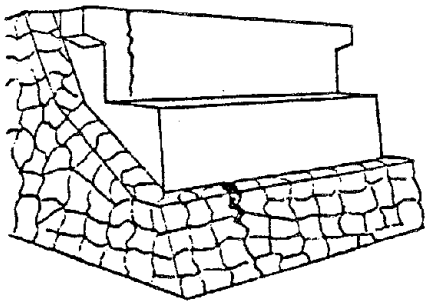
28. Nanakitada Br. (AR)



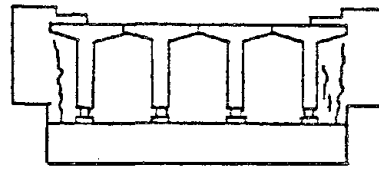
29. Sin Abumikawa Br. (AL,AR)



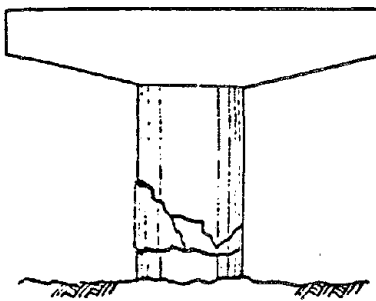
30. Yaotome Br. (AL,AR)



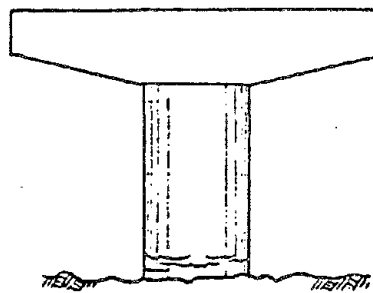
31. Shinainuma Br. (AR)



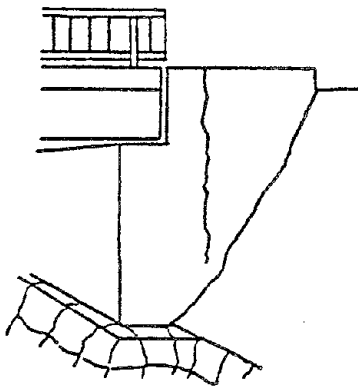
32. Yuriage Br. (AL)



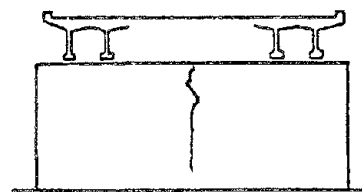
33. Yuriage Br. (P₁)



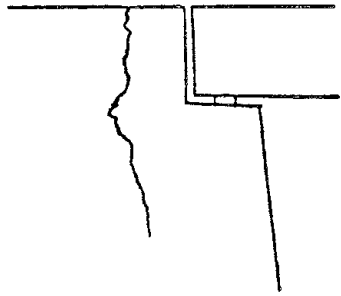
34. Yuriage Br. (P₃~P₉)



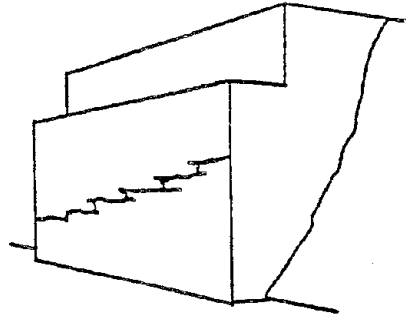
35. Takasago Br. (AL)



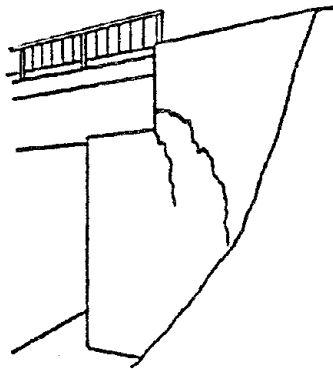
36. Nakanoshima Br. (AR)



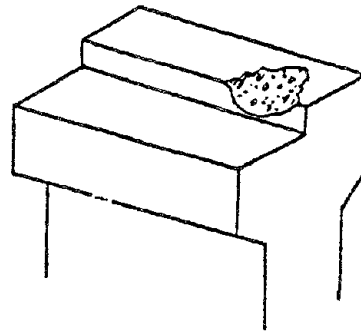
37. Ohshiro Br. (AL)



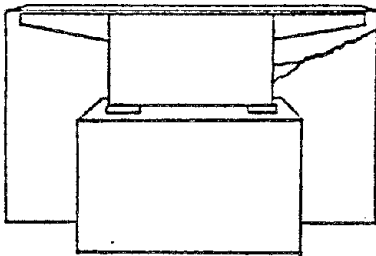
38. Shimo Tsuruta Br. (AL)



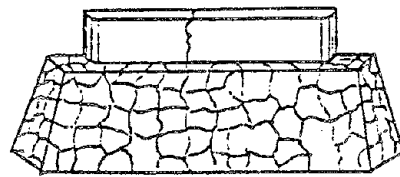
39. Shimo Tsuruta Br. (AL)



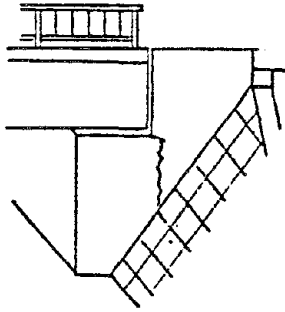
40. Shimo Tsuruta Br. (P1)



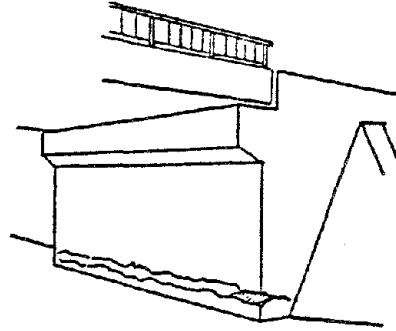
41. Kaihoku Br. (AL)



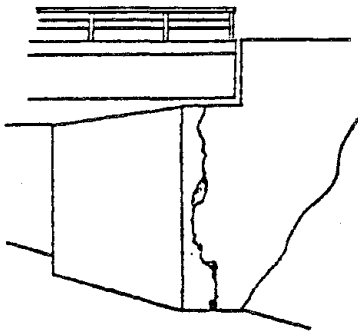
42. Tsujido Br. (AL)



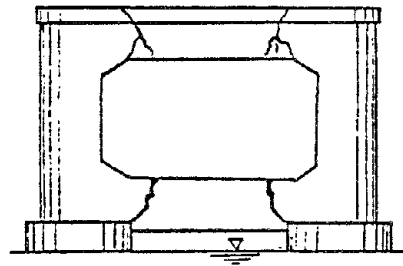
43. Ohwada Br. (A_L)



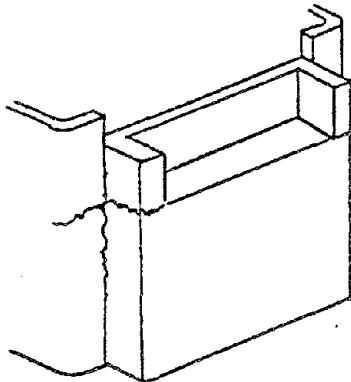
44. Tamachi Br. (A_L)



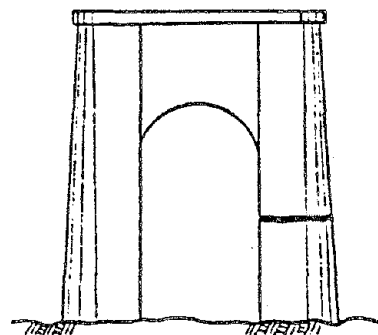
45. Takakawa Br. (A_L, AR)



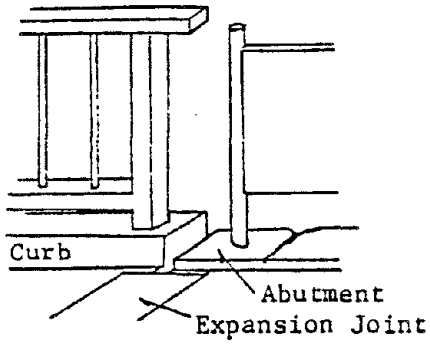
46. Eaigawa Br. (P₁ ~ P₈)



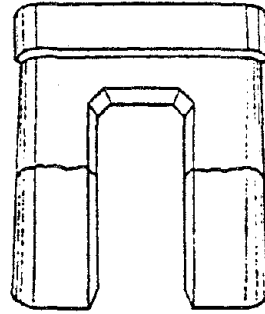
47. Eaigawa Br. (A_L)



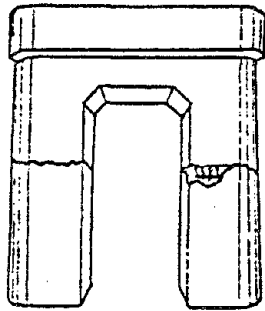
48. Noda Br. (P₃)



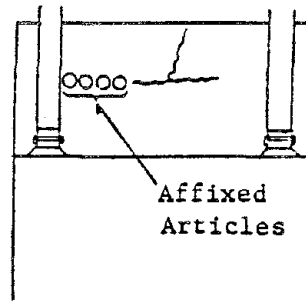
49. Shikitama Br. (AR)



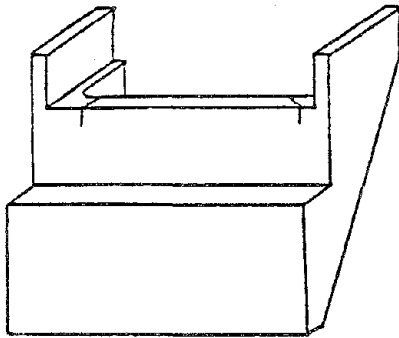
50. Shida Br. (P₃, P₆)



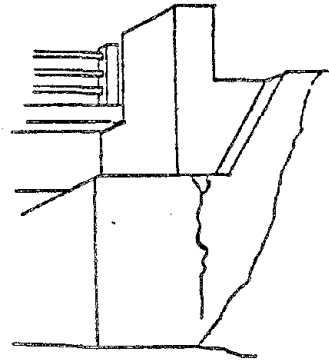
51. Shida Br. (P₄)



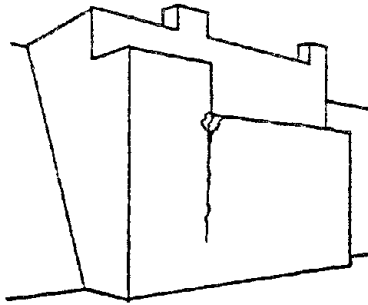
52. Sakuranome Br. (AR)



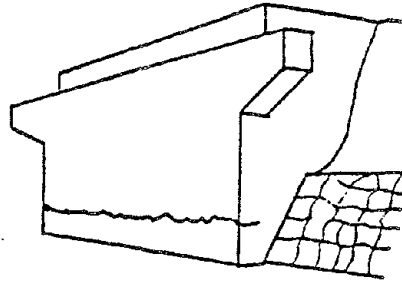
53. Fujiya Overpass (A)



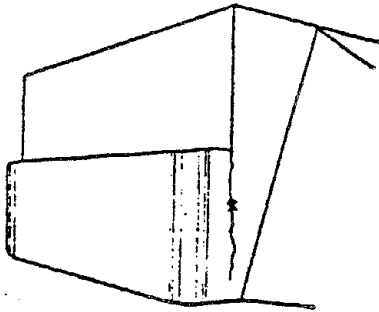
54. Daiji Br. (AL)



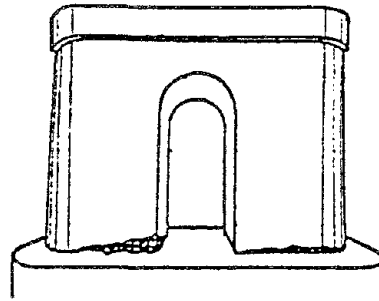
55. Daiji Br. (A_L)



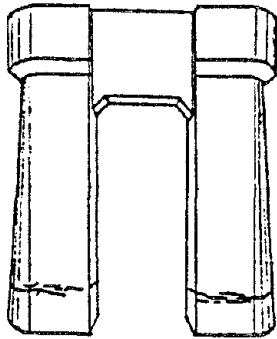
56. Wakayanagi Br. (A_L)



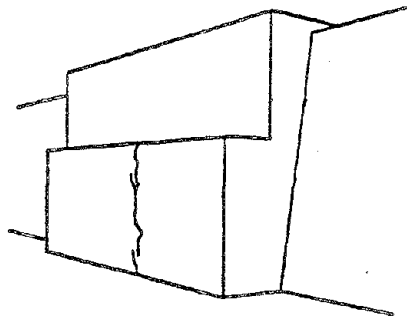
57. Shimoda Br. (A_R)



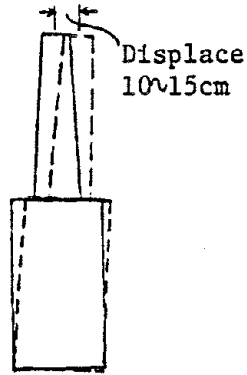
58. Tome Br. (P₁₂)



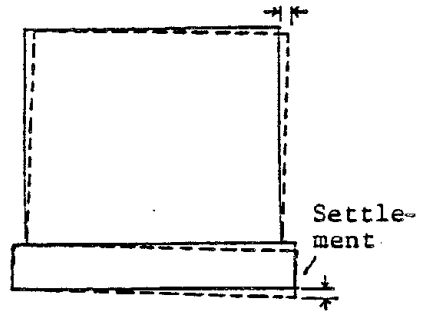
59. Kinnoh Br. (P_W)



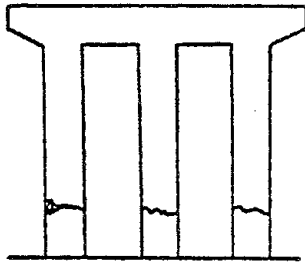
60. Namiita Br. (A_L)



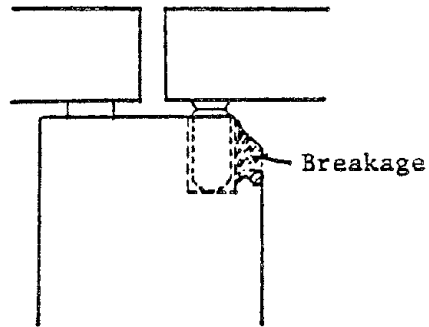
61. Kitakamigawa Br. (P₁)



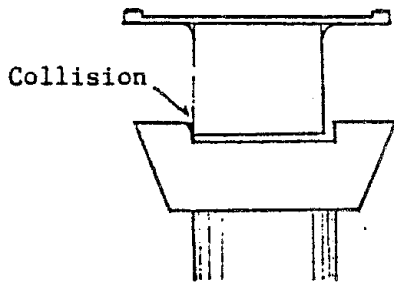
62. Ipponsugi Br. (P₁)



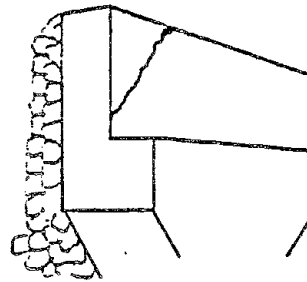
63. Konai Overpass (P)



64. Shinonome Br. (P₄, P₆)



65. Kunimi Br.



66. Sakunose Br. (AR)

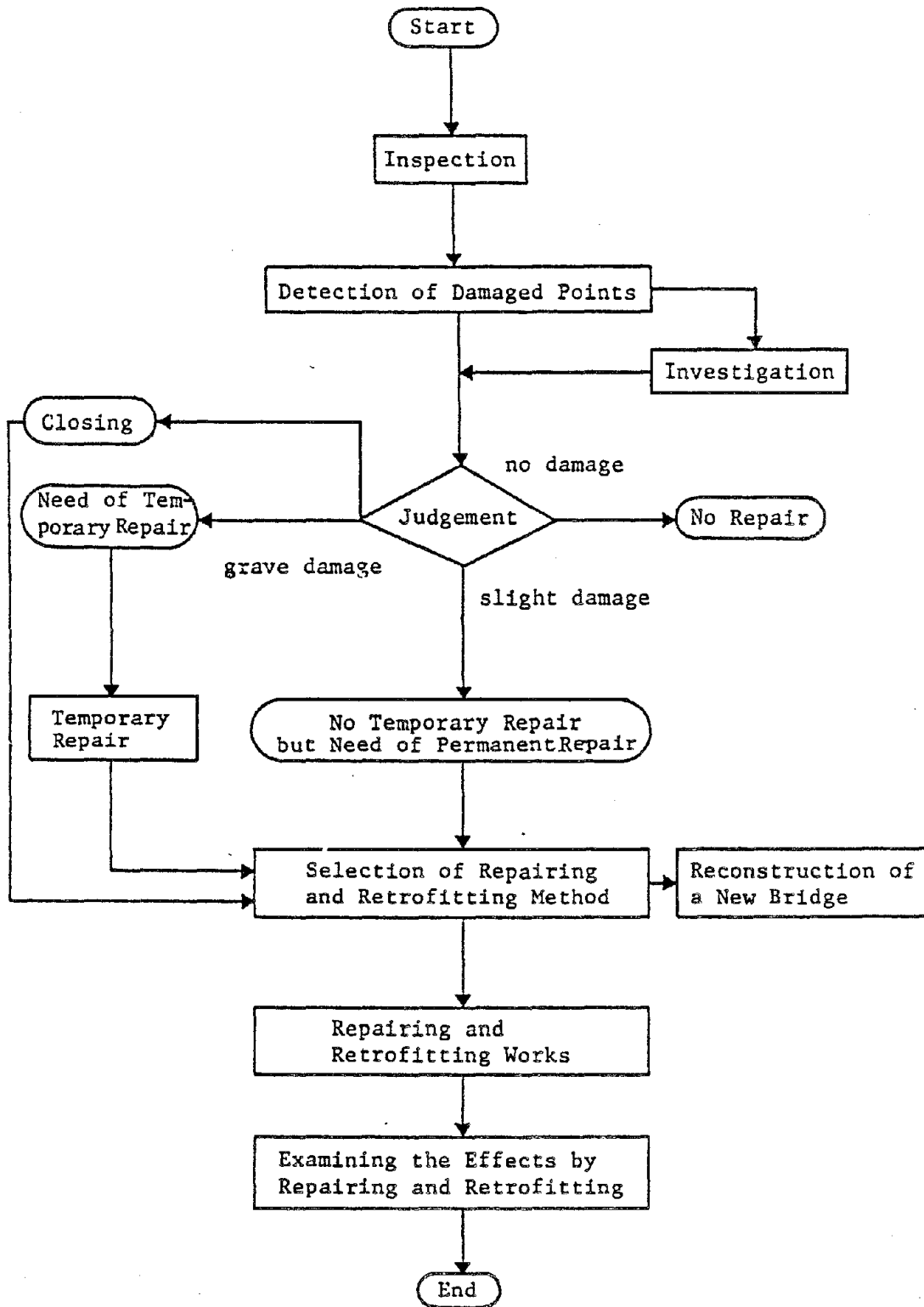


Fig. 5 Flow of repair and retrofit for bridge

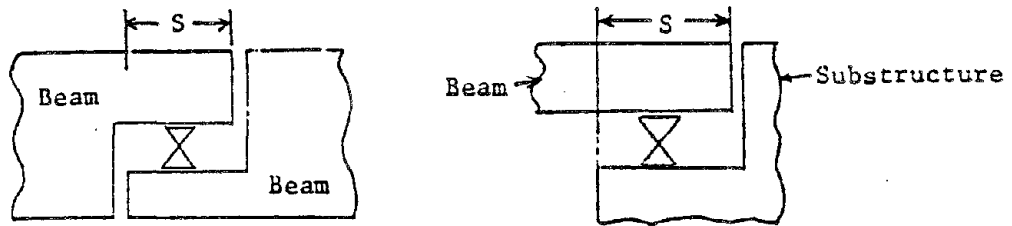


Fig. 6 Length of overlap on support

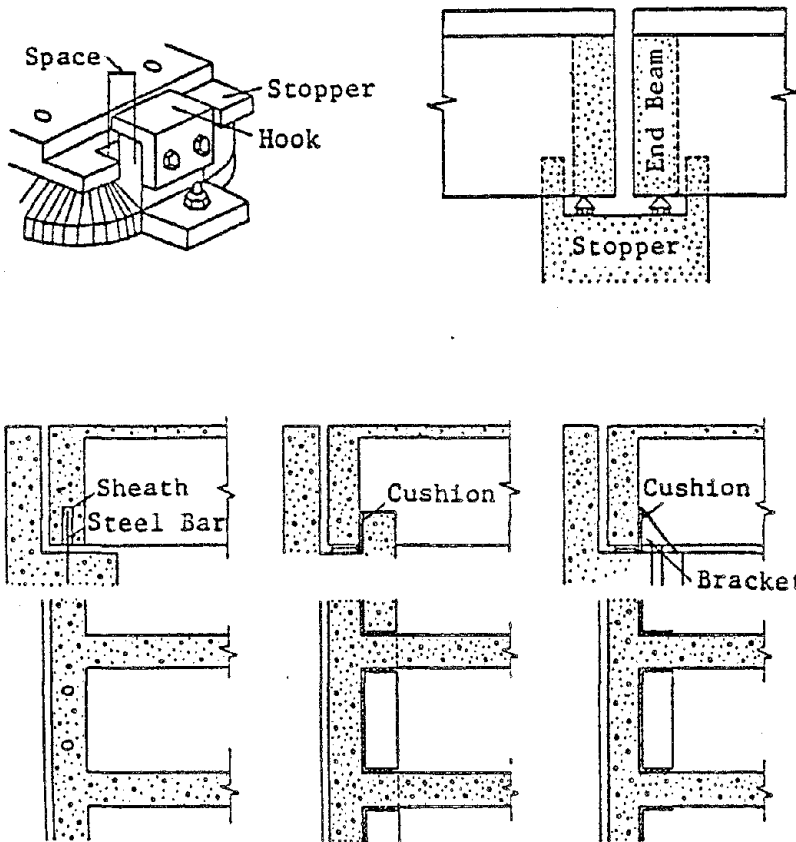


Fig. 7 Devices preventing dislodgement²⁾

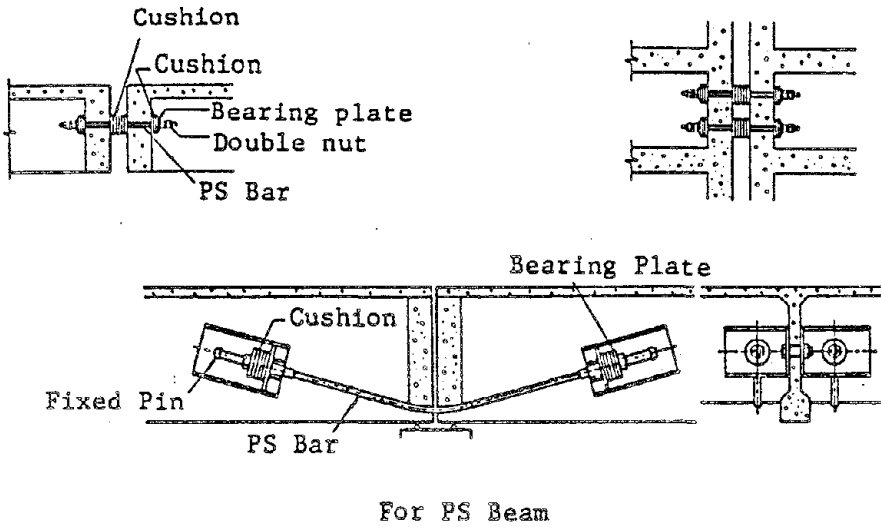
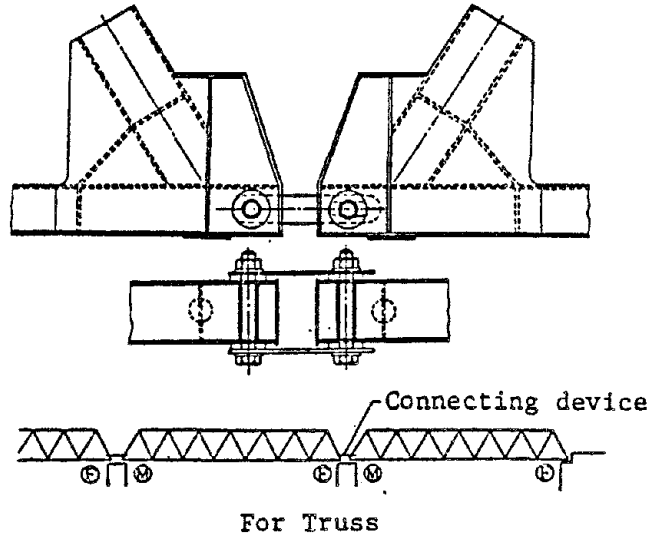
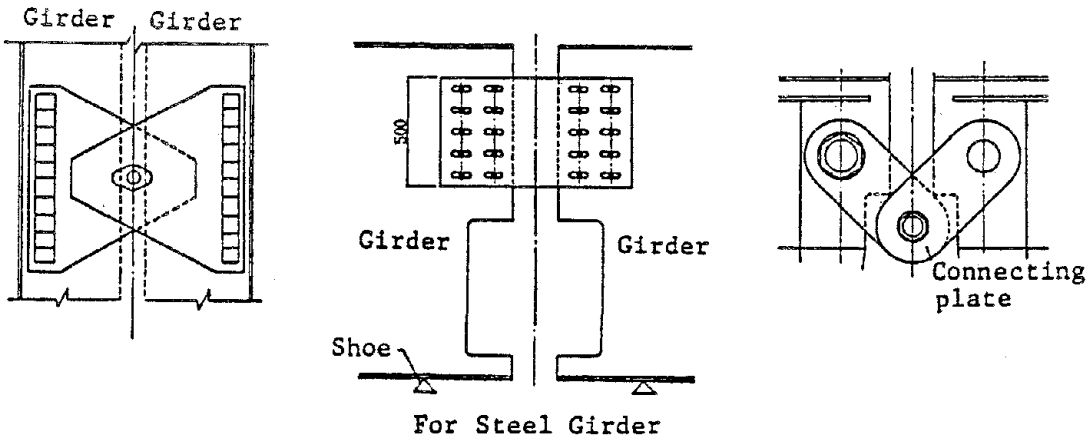
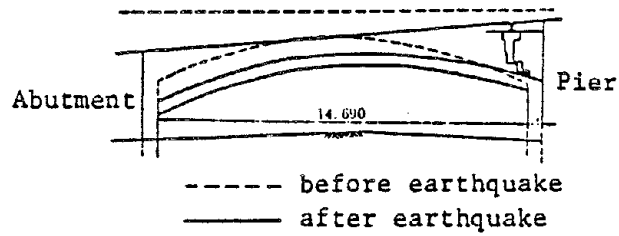
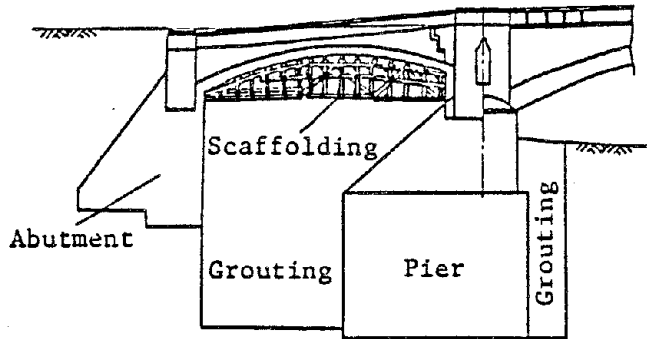


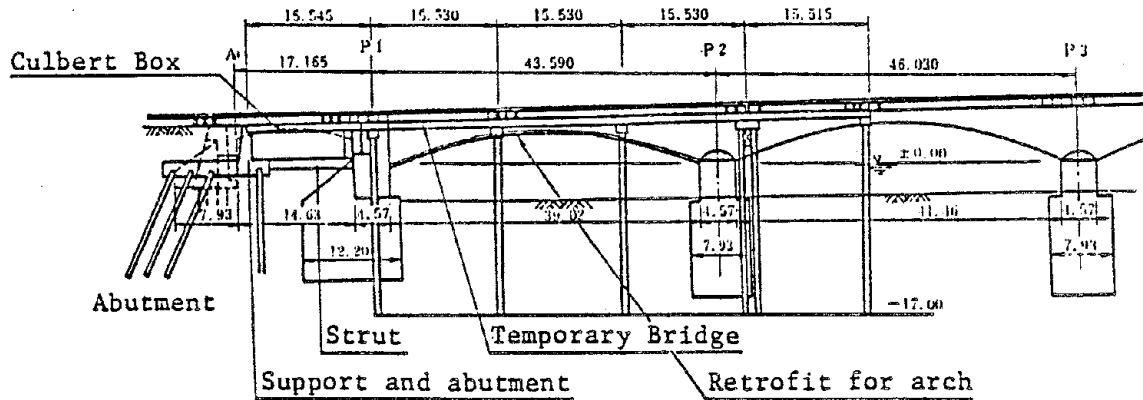
Fig. 8 Connecting devices²⁾



Damage at end span



Urgent Step



Real repairing & retrofitting

Fig. 9 Repairing for Bandai bridge in Niigata 8)

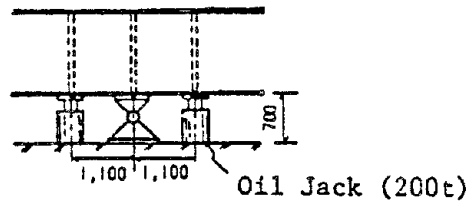


Fig. 10 Jacking up ⁶⁾

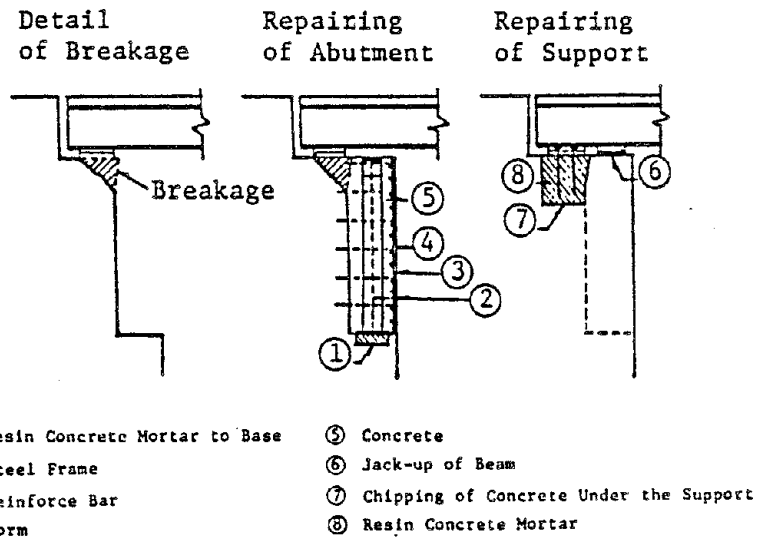


Fig. 11 A example of repairing and retrofitting of support ¹⁰⁾

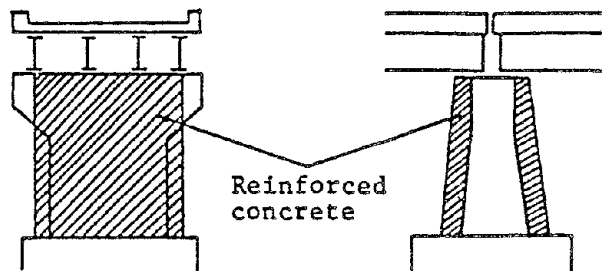


Fig. 12 Wrapping with Reinforced concrete ⁷⁾

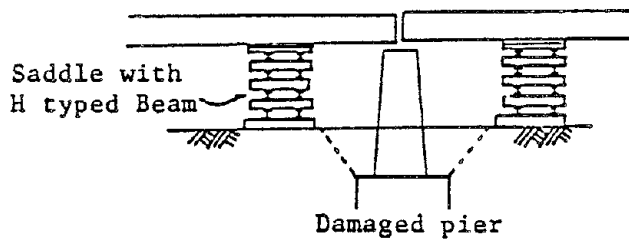
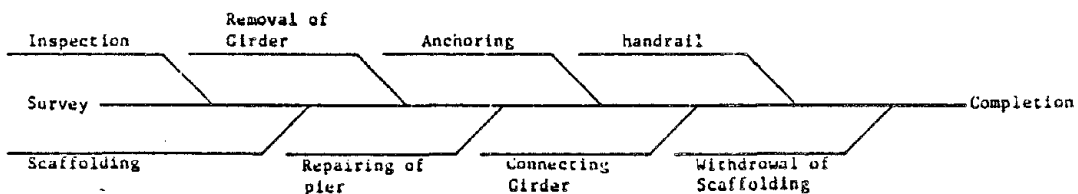


Fig. 13 Temporary Support⁷⁾

Temporary (Stoppgap) Repair



Parmanent Repair

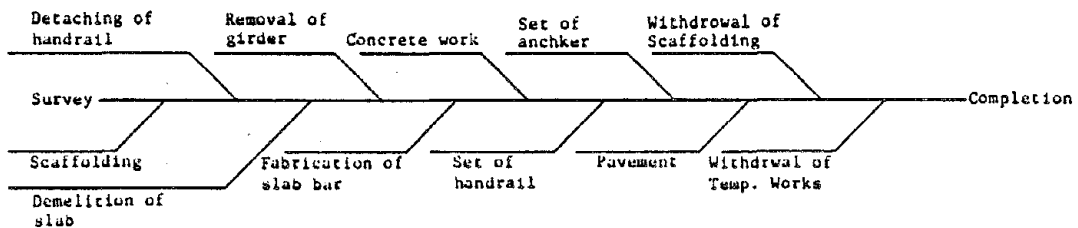


Fig. 14 One example of repairing procedure⁶⁾

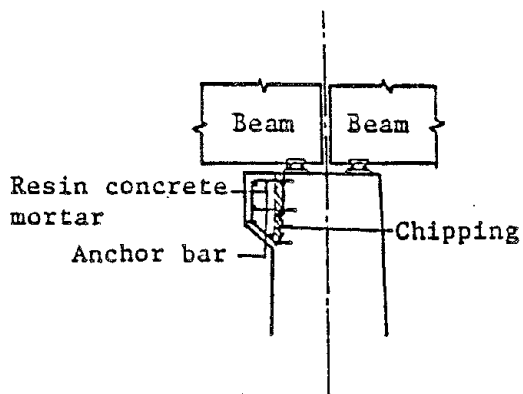


Fig. 15 Widening of coping¹⁰⁾

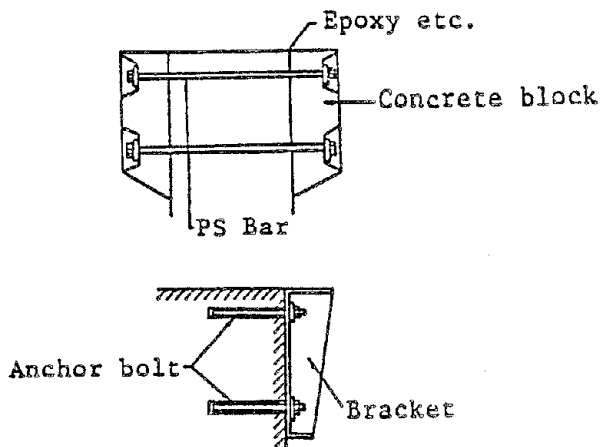
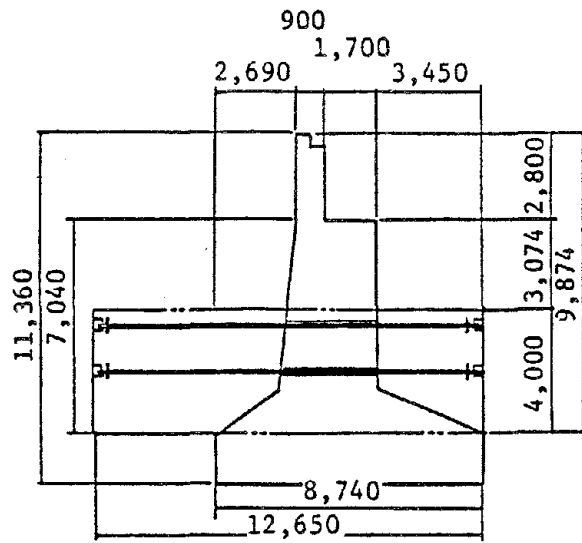
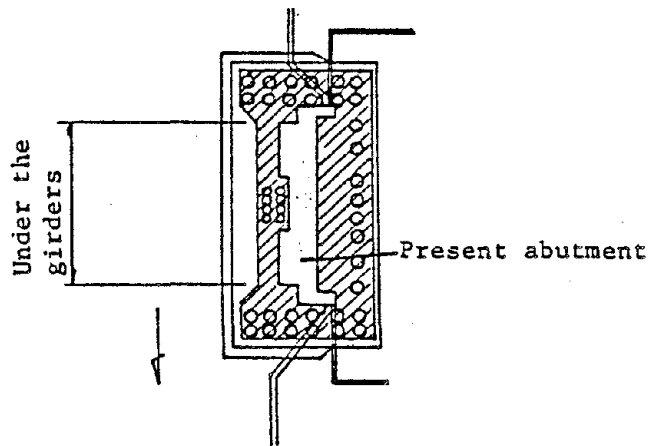


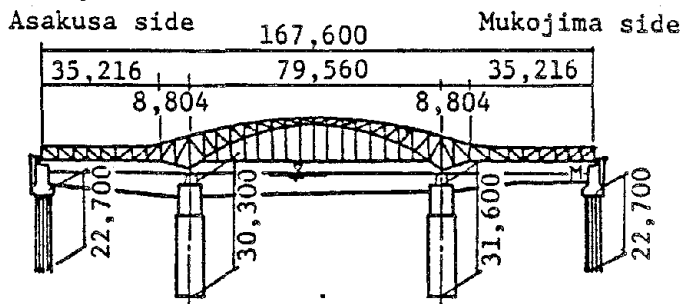
Fig. 16 Special method for widening of coping



Widening of footing

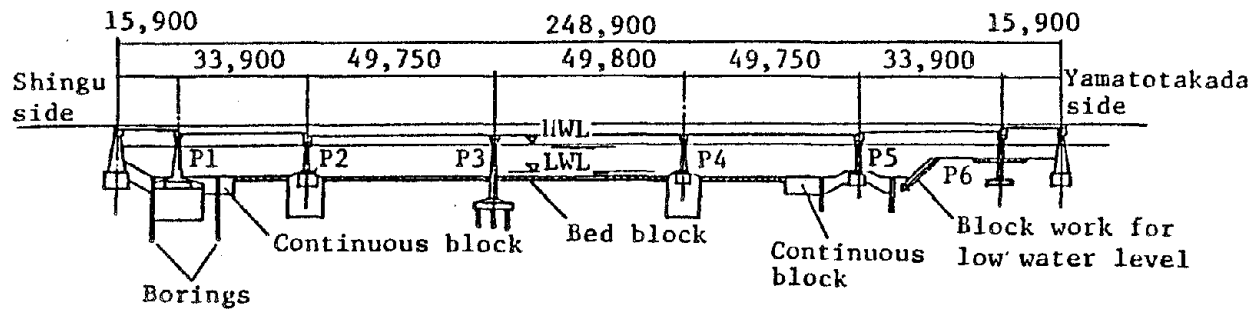
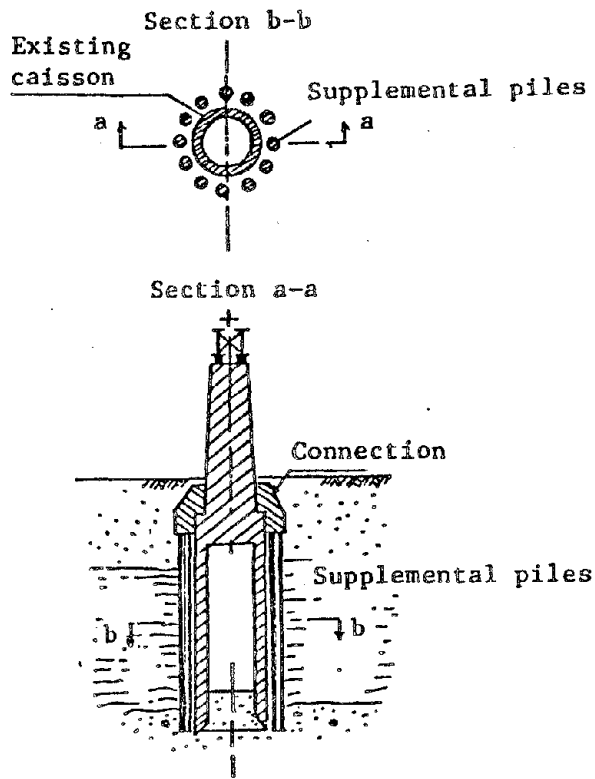


Increment of piles

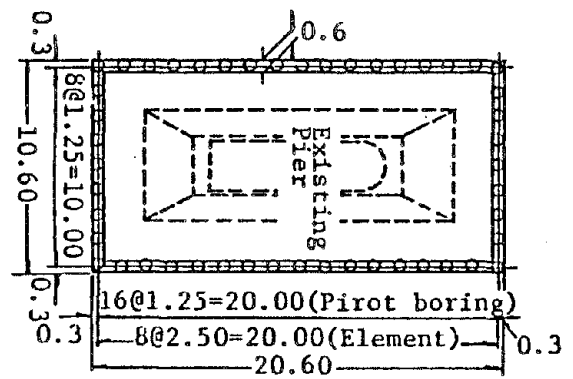


Retrofit for abutments

Fig. 17 Retröfitting of abutment for earthquake¹⁰⁾



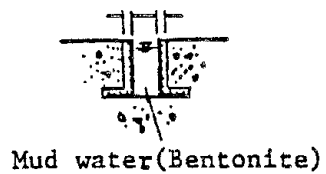
Stabilization of river bed



Sealing of foundation

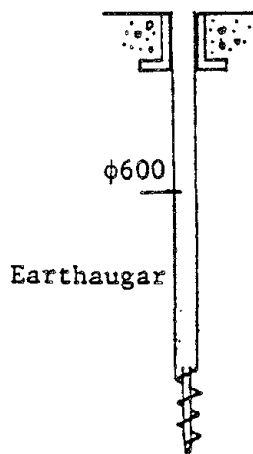
Fig. 18 Retrofit for insufficient bearing capacity¹⁰⁾

Fig. 19 Retrofitting for scouring to keep lateral resistance of foundation¹⁰⁾



Mud water (Bentonite)

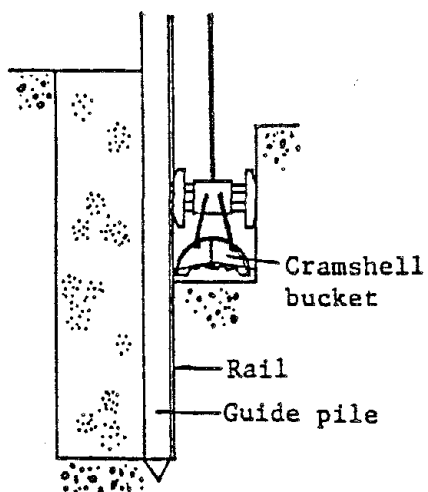
(1) Set of guidewall



$\phi 600$

Earthauger

(2) Pilot boring

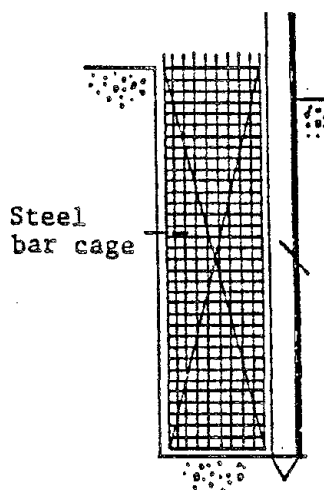


Cramshell bucket

Rail

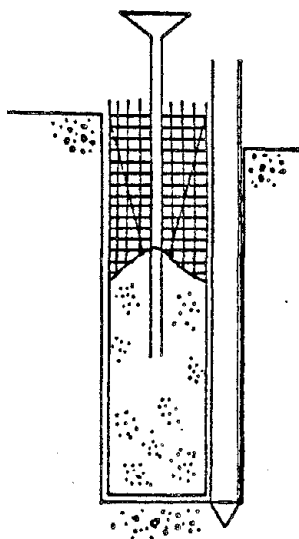
Guide pile

(3) Excavation with cramshell



Steel bar cage

(4) Hang down of steel bar



(5) Concrete works with tremie pipe

Reference

1. T. Iwasaki, Earthquake-Resistant Design of Bridges in Japan, Bulletin of Public Works Research Institute, Vol. 29, May 1973
2. Manual of Repair Method for Highway Bridges, Japan Road Association, February 1979
3. Draft Report on Survey of the Damage to Highway Bridges and Resistance of Support in Miyagiken-oki Earthquake (in Japanese)
4. Survey on Disaster due to Niigata Earthquake 1964, Bulletin of P.W.R.I. Vol. 125, June 1965 (in Japanese)
5. Survey on Disaster due to Tokachi-oki Earthquake 1968, Bulletin of P.W.R.I. Vol. 141, June 1971 (in Japanese)
6. Survey on Disaster due to Miyagiken-oki Earthquake 1978, Report from Tohoku Regional Bureau, Ministry of Construction, November 1979 (in Japanese)
7. Outline of the Disaster caused by Miyagiken-oki Earthquake 1978, Report from Miyagi Prefecture, December 1978 (in Japanese)
8. S. Katayama, Repairs of the Bandai Bridge damaged by Niigata Earthquake, Kisoko. Vol. 6, No. 11, November 1978 (in Japanese)
9. E. Kusubayashi & T. Iwasaki, Progress Report of Research Works in Bridge Earthquake Engineering at P.W.R.I. Japan, 7th World Conference on Earthquake Engineering, September 8-13, 1980
10. Y. Shioi, Maintenance and Repair of Substructure of Bridge, Lecture Note on Bridge Seminar, October 5, 1979
11. Specifications for Highway Bridges, Part I Common Specifications, Part II Steel Bridges, Part III Concrete Bridges, Part IV Substructures, Part V Earthquake Resistant Design, Japan Road Association

EXAMPLES OF REPAIR AND RETROFIT WORK
ON ROAD BRIDGE SUBSTRUCTURES

by

Hideya Asanuma
Public Works Research Institute
Ministry of Construction

1. INTRODUCTION

Japan has a network of some 1,110,000 km public roads covering all the territory including remote islands, and administrates as many as 580,000 bridges ranging a 2m-long culvert to a long suspension bridge.

These bridges subjected to severe natural conditions, heavy traffic loads and sometimes strong motion of earthquakes are liable to sustain injuries and harm in years after their construction.

Repairing and retrofitting damaged bridges against further harm is a work of great importance from the socio-economical point of view amid a low-growth economic circumstance of the country.

Here, the author introduce general concepts of repair and retrofit works on road bridge substructures with an emphasis on concrete structures, and then show some examples of the works.

2. DAMAGE TO BRIDGE SUBSTRUCTURES

Damages which concrete piers and abutments are apt to sustain are confined to some categories by portion of their location. Most liable cases are

- (1) Damage around a support
- (2) Crack and fracture of a column, wall and beam
- (3) Damage to a foundation including a footing

Among the above items, the third one is very hard to be found or detected and also very difficult to be repaired or retrofitted because they exist under ground level. So, this problem would be omitted from the following discussions. Causes which bring damage are,

- (1) Deterioration of the materials due to weathering
- (2) Unequal settlement or consolidation of the ground
- (3) Experience of an unexpected strong force like what hit by an earthquake.

3. GENERAL CONCEPT OF REPAIR AND RETROFIT

1. Support-related Damage

(1) Appearance of Damage

Most damages concerning supports are concentrated to those of shoes; breakage of a slide confining device, dislodgement or fall-down of rollers, fracture of a lower shoe, fracture of a pin or rollers, rusting of a sliding surface or rolling surface, erosion of shoe members and so forth. However, here we will deal with only concrete structures beneath shoes, and also exclude anchorbolts.

Fig. 1 shows an example of fracture of mortar filled between a shoe and its bed. In a case of slight damage, the fracture degree is low and only cracks develop, while the mortar apparently breaks in a severer case.

Fig. 2 shows how a crest of pier or abutment breaks.

This type of fracture often takes place around a movable shoe. The reason would be that a stronger force than expected is liable to be transmitted through a movable shoe because of greater friction due to rusting of its sliding surface or rollers.

(2) Repair and Retrofit

Against cracking or a fracture of shoe mortar, such measures of filling up with fresh mortar as shown in Fig. 3 are effective. (a) is a likeliest case of filling with fresh mortar, but should be paid much attention to make sure if the mortar is filled up sufficiently. (b) shows an example of grouting in case a gap between a sole plate and its bed is narrow. And, (c) is an additional case of using pre-packed concrete as a filler.

Measures against a break incurred to shoe bed concrete should be chosen in compliance with the seriousness as well as the cause of break.

Common methods for repair or retrofit would be

- 1) wrapping the pier top by steel plates to strengthen a damaged portion as shown in Fig. 4
- 2) placing fresh concrete with reinforcing steel bars at the breakage. Fig. 5 is one example of this method.
- 3) attaching steel frames with anchors embedded into the column or abutment as shown in Fig. 6

In Japan, the Specifications for Highway Bridges provides that any pier or abutment should have sufficient length of overlapping with a corresponding superstructure so that even in the worst case a superstructure could escape falling down, unless it has a special device to prevent dislodgement or even falling-down of a beam.

However, bridges constructed before these provisions were established have not necessarily enough overlapping length. In order to enhance the safety of these relatively old bridges, such retrofit works were required as enlarging the crest of a sub-structure and having it overlapped sufficiently.

Fig. 7 shows some examples of the works done for this purpose.

2. Damage to Columns or Walls

(1) Appearance of Damage

Columns and walls are generally made as reinforced concrete structures except steel piers of elevated bridges constructed in a downtown. These structures are exposed to drying, humidity, frost and melt, as well as salty water, acid, alkali, heat, industrial drainage and so on. These factors cause concrete structures gradually deteriorate and lose their strength year by year. This effect is known as weathering.

However, damage due to weathering is very slight if compared with that due to an earthquake. So, here we lay emphasis on quake-related damages.

The damage sustained by sub-structures due to strong motion can be classified into following degrees from the lightest to the heaviest.

1) Cracking of concrete

Vertical cracking as seen in Fig. 8 and horizontal cracking as seen in Fig. 9.

2) Flaking of concrete and exposure of steel bars as seen in Fig. 10.

3) Complete destruction of concrete and buckling of steel bars as seen in Fig. 11.

Typical features of the damage are illustrated in Fig. 8 through Fig. 11.

The cause of damage can be considered as

- 1) excessive tensile stress induced in concrete due to bending moment, which causes tensile cracks on a surface of the structure.
- 2) buckling of reinforcing steel bars due to an excessive alternate force. As the case may be, the buckling causes flaking-off of the concrete outside the steel bars.
- 3) shear failure of concrete. Since a concrete member is brittle against shear failure, this type of collapse is mostly destructive and fatal.

(2) Repair and Retrofit

1) Measures against cracks

As regards repair of cracks, grouting or injection of such adhesive materials as cement mortar, resin mortar, epoxy resin etc. is effective. When cracking is not so profound, surface treatment or grouting of mortar as illustrated in Fig. 11 are sufficient. Against extensive and deep cracking, grout should be infiltrated under some pressure up to about 3kgf/cm^2 . Fig. 12 is one of most progressed methods of this type. Another measure is to introduce prestressing across the cracks through PC steel bars or wires as seen in Fig. 13.

2) Measures against breakage

Heavier damages to a column or wall than cracking are flaking of surface concrete, exposure or even buckling of steel bars, and finally complete collapse of the structure. In the worst case of collapse, reconstruction of a new structure will become easier and more economical.

These breaks not only reduce a cross sectional area of the structure, but cause rust of steel bar. Therefore, we should make up for the reduced section and reinforce strength of the members. For this purpose it is common to wrap the column or wall with some materials.

Fig. 14 indicates an example of wrapping with steel plates or fiber reinforced plastic plates. Void between the plates and the concrete surface is filled with resin mortar or epoxy resin.

Fig. 15 shows how to thicken a faulty column by placing concrete with reinforcement and anchorage into the original column.

When durability against future strong motion is estimated insufficient, construction of a new member for additional support or reinforcement of the existing structure becomes of course necessary, even if there is no substantial damage on it.

4. EXAMPLES OF REPAIR AND RETROFIT WORKS

1. The Sendai Bridge

The Sendai Bridge, completed in 1965, is located in south part of Sendai City, and is crossing over the Hirose River as a part of the National Highway No. 4. The general side view is shown in Fig. 16. Superstructures are 9-span simply supported composite steel-plate girders, with span length of $9 \times 33.840\text{m}$, total length of 310m , and width of 19m . Substructures are T-shape columns (6.1m high) founded on rigid well foundations (9 to 18m deep)

embedded into rather stiff sands. Bearing supports are of type of line bearings. Since this highway connecting Kanto and Tohoku regions is an important one, Sendai Bridge carries very heavy traffic (54,000 cars daily).

Due to the earthquake (the epicentral distance to the bridge is $\Delta=120\text{km}$), all of the nine pier columns sustained damage. Piers 1 through 4 cracked horizontally at the column bases and surface concrete pieces separated heavily from the columns near the bases. Piers 5 through 8 had similar damage near the haunches which connect columns and beams. Pier 6 which has the lowest free height sustained the severest cracking at both sides (see Fig. 17). Concrete pieces separated at the haunch and reinforcing bars buckled. Near the haunch volume of reinforcing bars as well as concrete sectional area change rapidly. It is estimated that relative displacements between adjacent girders were 1 to 2.5 cm on the pier caps and that displacements at the pier caps of Piers 1, 2 and 6 were 11 to 18 cm.

Fig. 18 shows temporary frame works supporting the girders near Pier 6. Since the bridge is very important, damaged piers were repaired without stopping traffic even for a short time. Fig. 19 illustrates an example of permanent repairing work at Pier 6. The thickness of added concrete was 50 to 70 cm, and vertical reinforcing bars were fixed by epoxy adhesive into the well foundation and lateral bars were fixed to the columns. Moreover, chemical resin was placed into small cracks. It took only one month to completely repair the damage to this bridge.

2. The Abukuma Bridge

The Abukuma Bridge, constructed in 1932 and annexed a sidewalk in 1967, is spanning the Abukuma River on National Highway No. 6.

The general plan is shown in Fig. 20. The bridge had beared heavy traffic over 46 years and the possibility of replacement was just studied so that it might be accommodated to modern and heavy road traffic.

The Miyagi-ken-oki Earthquake hit this bridge and 8 of 16 piers, which all supported trusses, suffered cracking, separation of concrete and exposure of steel bars.

Fig. 22 shows how these piers were repaired. The piers of slight damage with only hair cracks underwent the repair of epoxy resin injection. Since design data of this bridge was missing and not available, the repair work was designed to stand on as safe side as possible; it means enough reinforcement and sufficient cross sectional area. Concrete with reinforcement was newly placed surrounding the existing piers after chipping their surfaces and taking anchorages into them.

Additionally, the crests of piers were widened to keep enough overlapping length with the corresponding girders for future safety.

3. The Ten-noh Bridge

The Ten-noh Bridge is spanning the Kitakami River with 367.7 m length and 8.0 m width, completed in 1959 and annexed a sidewalk in 1975. A main structure is a Langer-type arch with simple supported side spans.

A pier which supports the arch sustained heavy damage. Many cracks propagated outward from the shoe positions and a long vertical cracking occurred at the center of the pier as seen in Fig. 24.

From the viewpoint of importance for regional traffic and the degree of damage, the bridge was opened to public traffic under some restrictions. Taking such a situation into consideration, the bridge was temporarily supported by H-shape steel frames, resting on the footing, with some stiffening members.

Therefore, as a permanent repair, the pier was designed to be enclosed by a new reinforced concrete structure with stiffening H-shape steels and afterward tied with the original pier by tie-rods.

In this case, the surface of the footing was under water table and a measure to prevent water from infiltration was needed. Fig. 26 shows the construction of a cut-off wall on the footing.

Table - I Present Status of Roads in Japan as of April 1, 1980

	Classification			Length of road, bridge, tunnel and ferry						
	Total (km)	Improved roads (km)	Un-improved roads (km)	Length of roads (km)	Bridges		Tunnels		Ferries	
					Number	Length (km)	Number	Length (km)	Number	Length (km)
National expressways (Urban expressways)	2,579 (253)	2,579 (253)	-	2,225	2,941	288	97	66	-	-
Sub-total	2,322	2,322								
National highways	40,212	35,299	4,914	33,666	36,206	1,053	1,720	483	3	41
Principal local roads	43,906	32,287	11,619	43,026	36,113	722	372	159	5	3
Prefectural roads	86,930	45,530	41,250	35,517	65,662	1,278	982	135	29	11
Municipal roads	939,760	252,327	686,933	935,880	440,058	3,752	1,410	129	140	126
Sub-total	1,110,306	356,093	744,715	1,103,089	578,139	6,809	4,894	911	182	181
Total	1,112,328	363,672	744,715	1,105,314	581,080	7,097	4,981	977	182	181

Note: 1. Referred to the Annuals of Road Statistics 1981.
 2. The length of urban expressways is included in either principal local roads or prefectural roads.

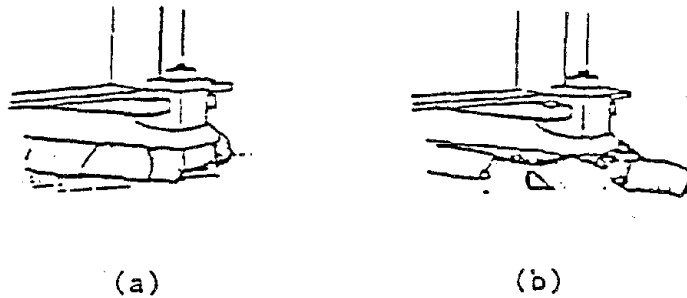


Fig-1 Fracture of shoe mortar

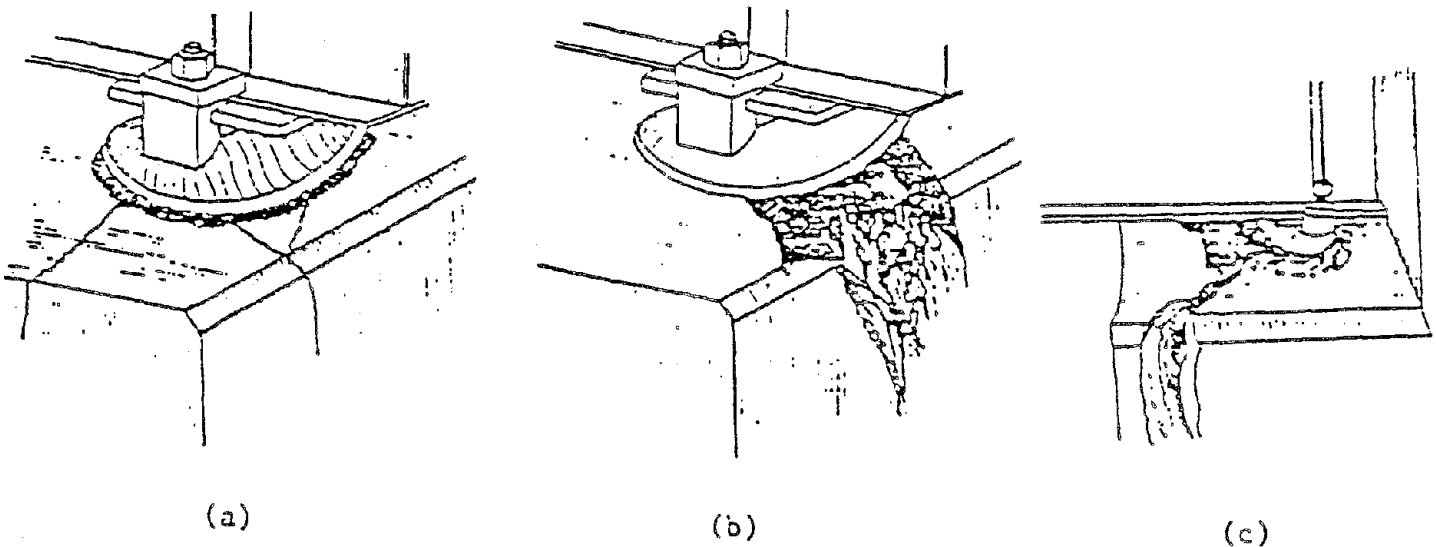


Fig-2 Fracture of shoe bed concrete

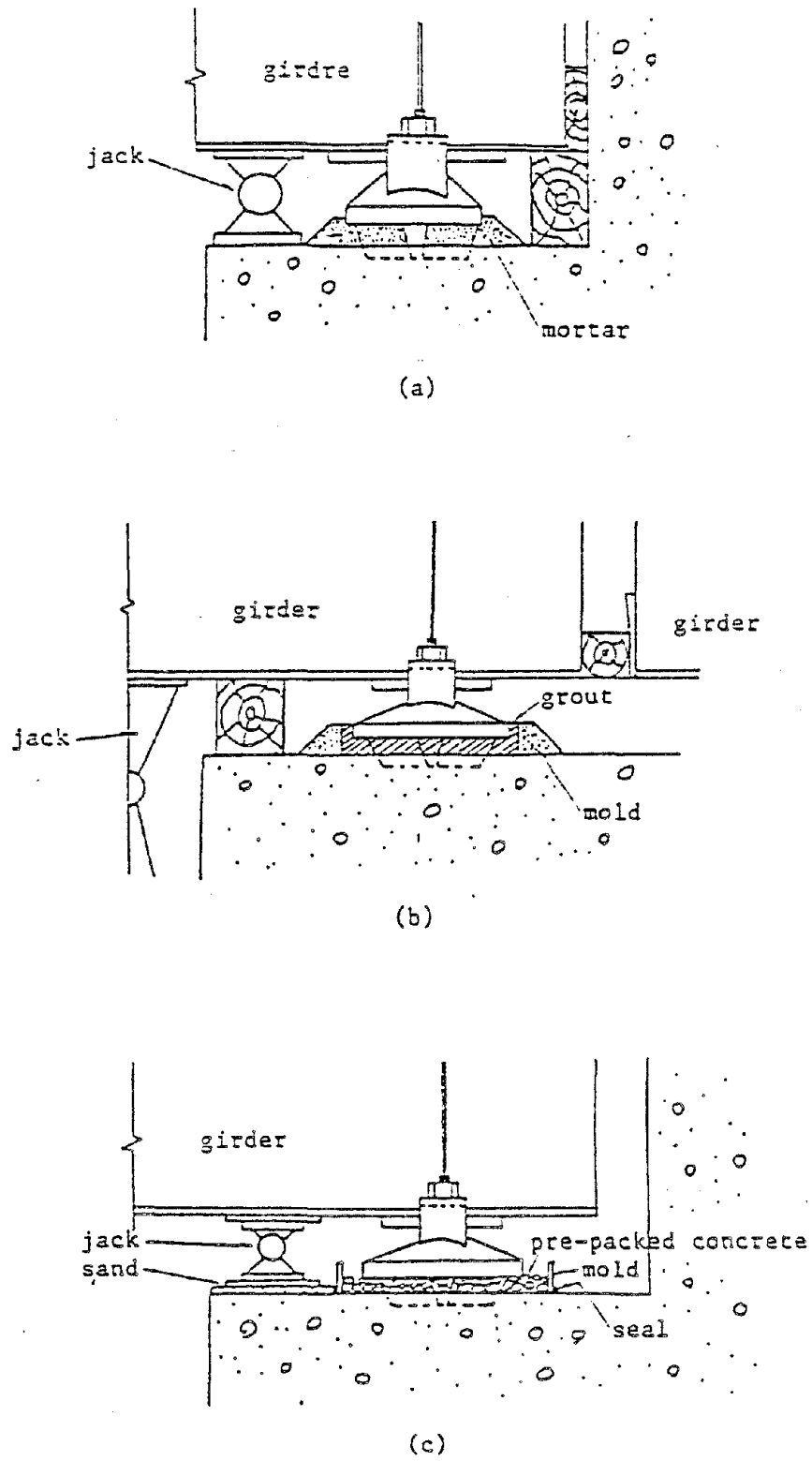
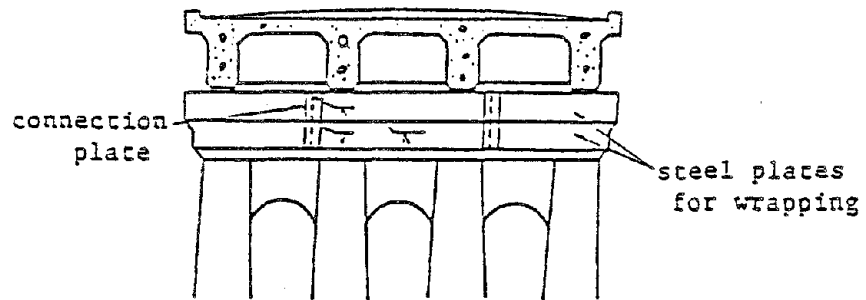
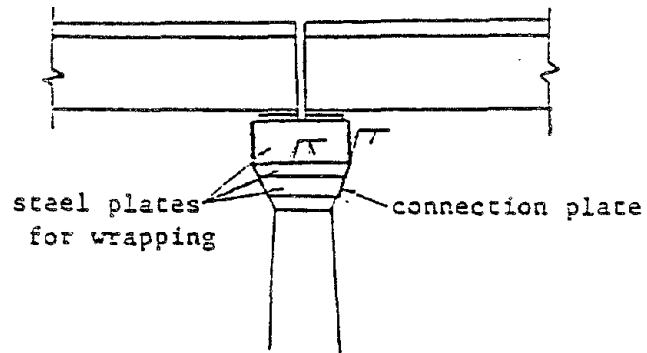


Fig-3 Methods of repair for shoe mortar

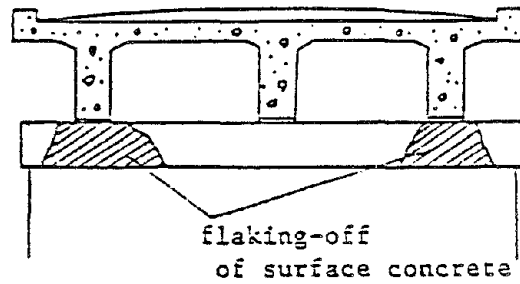


(a) Front view

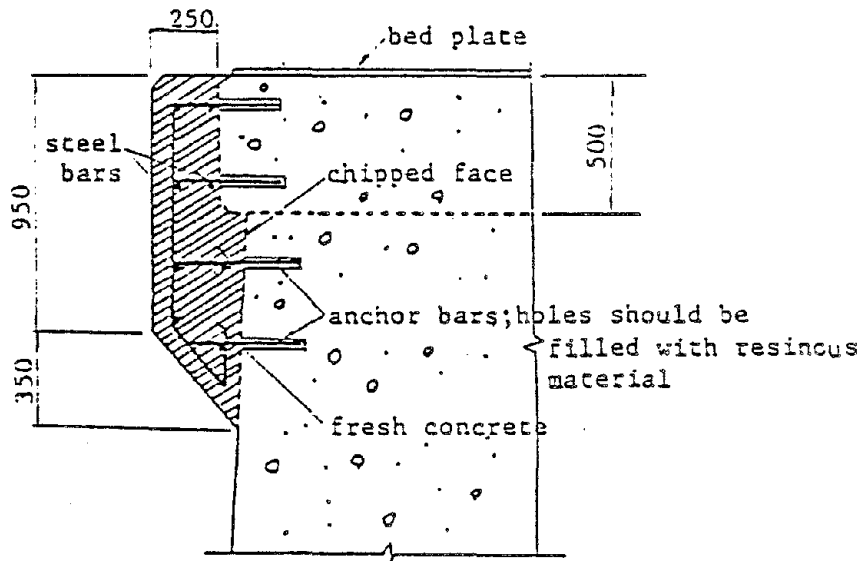


(b) side view

Fig-4 Wrapping with steel plates



(a) General view of damaged portion



(b) Detail of the repair

Fig-5 Reinforcing by new concrete

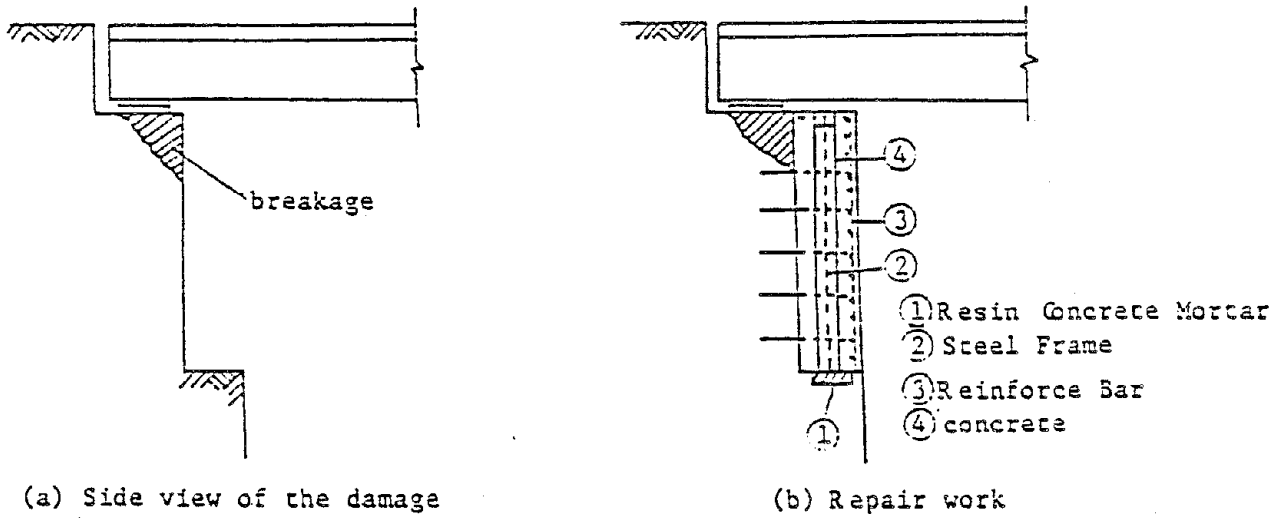


Fig-6 Reinforcing by steel frames

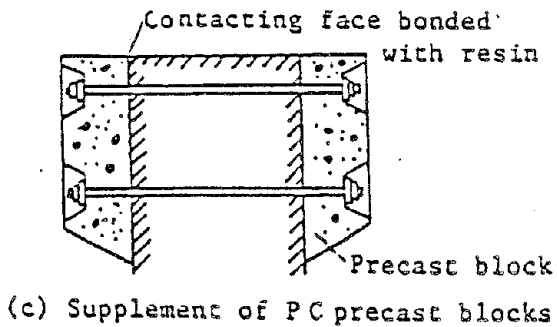
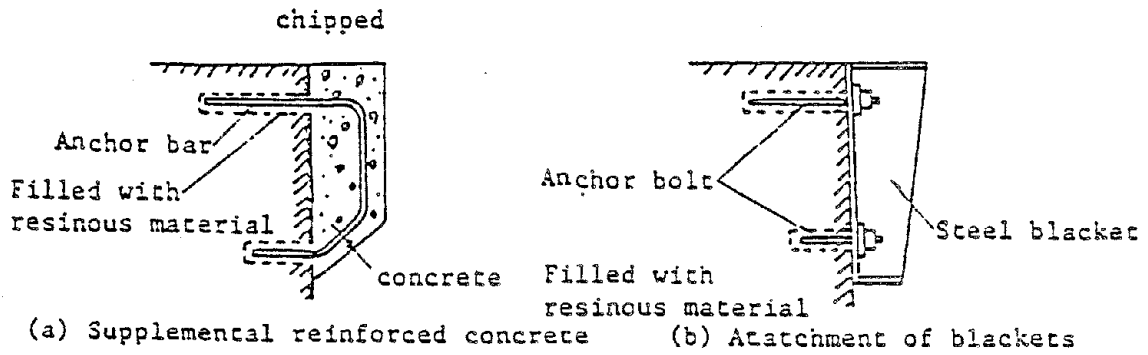


Fig-7 Enlargement of the Crest of a Substructure

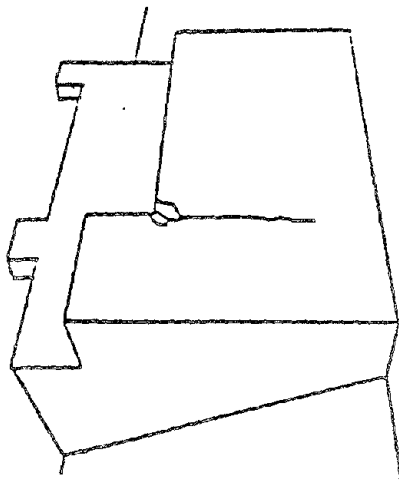
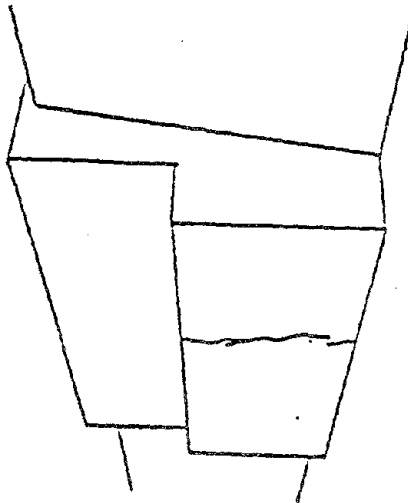
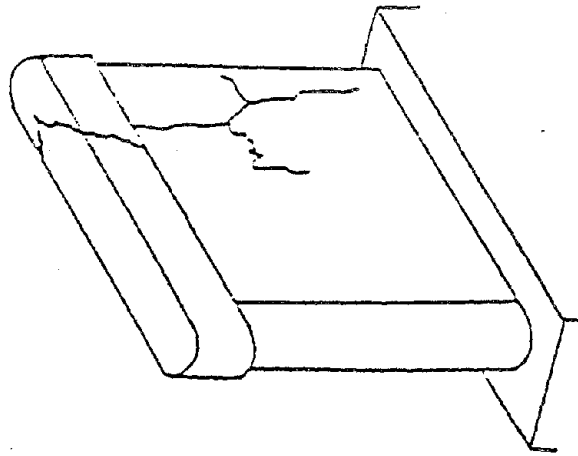


Fig-8 Vertical cracking

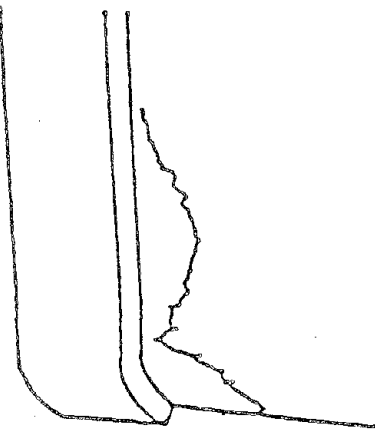
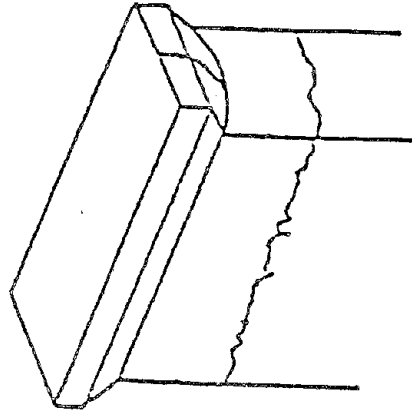
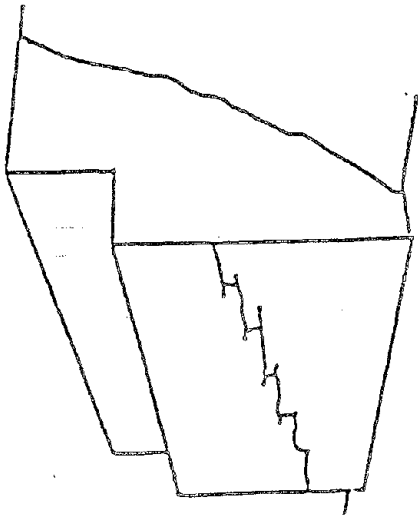
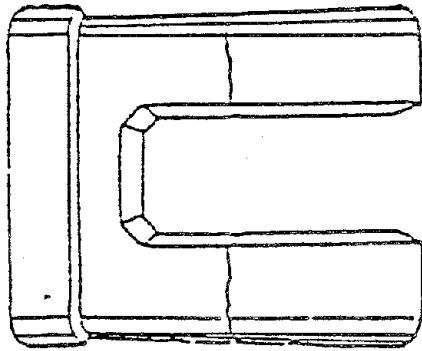
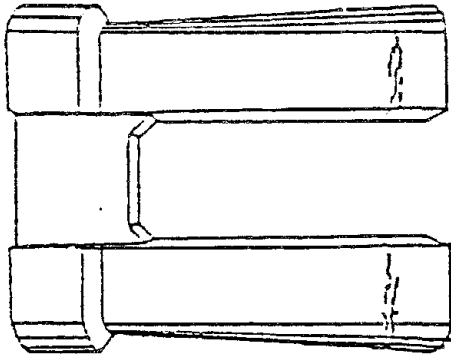


Fig-9 Horizontal cracking

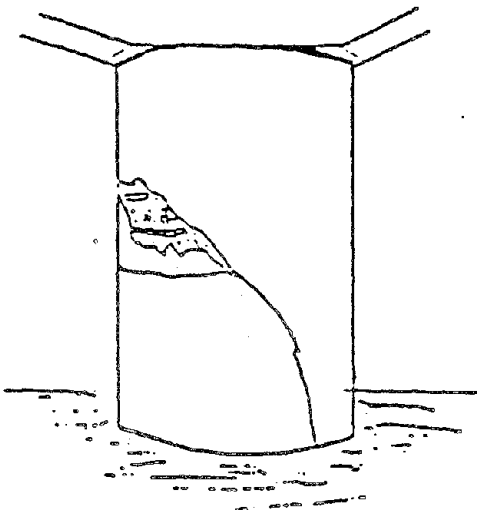
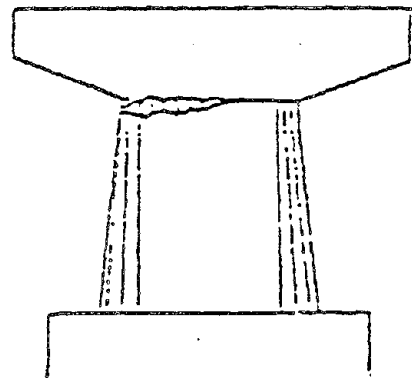
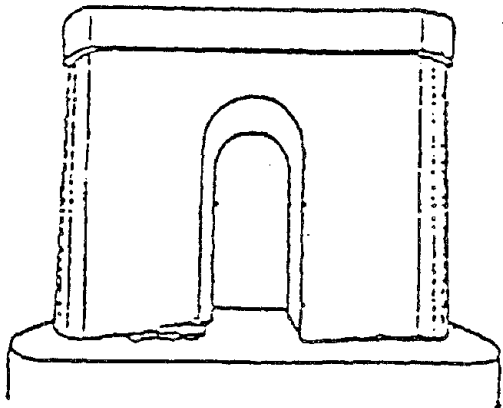
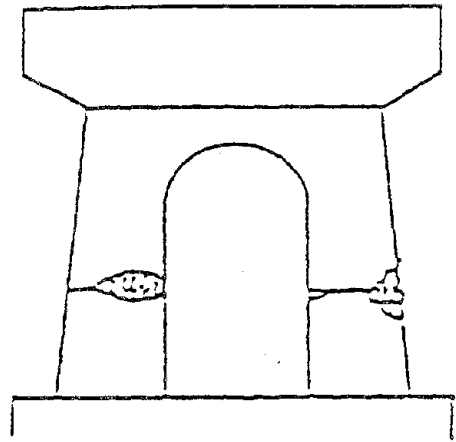
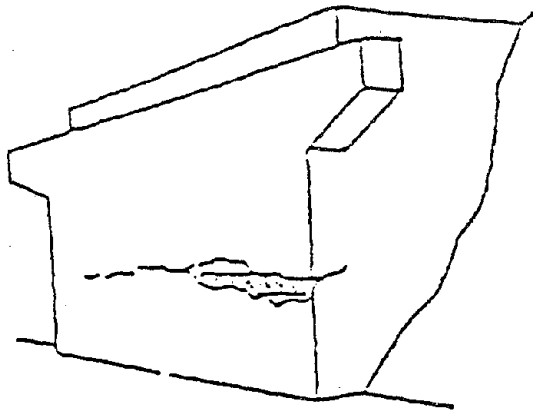


Fig-10 Flaking off of concrete
and exposure of steel bars

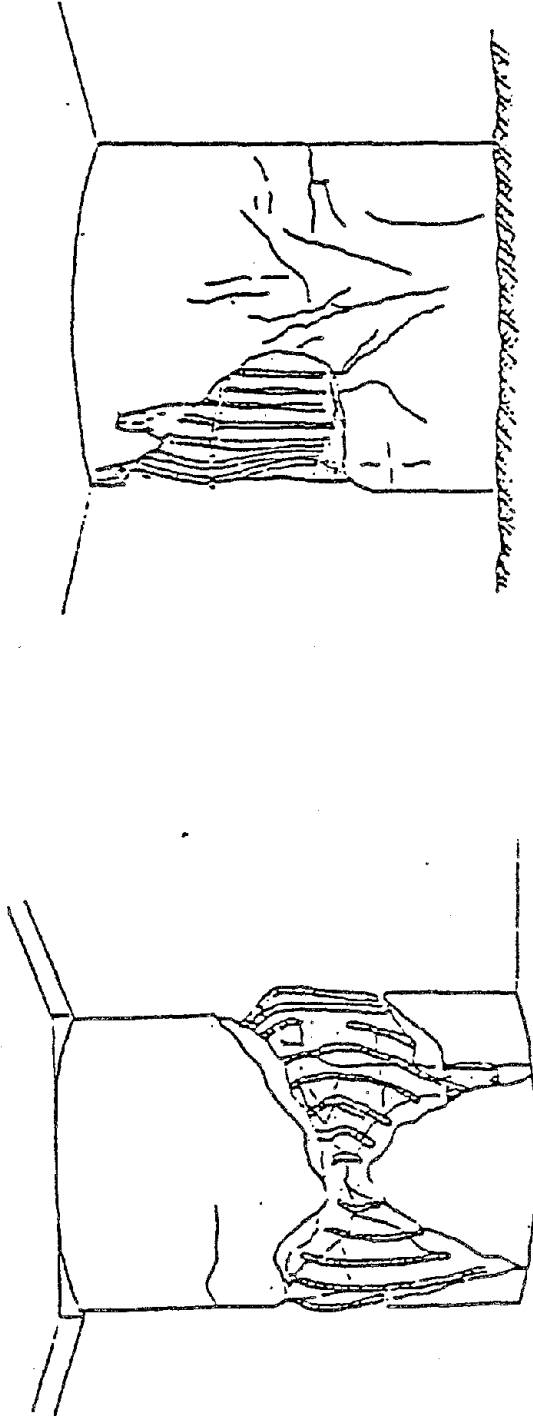
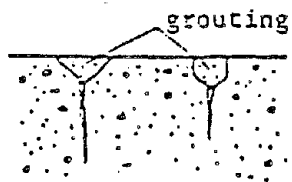
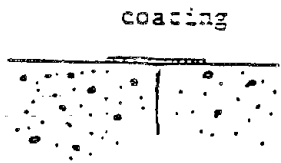
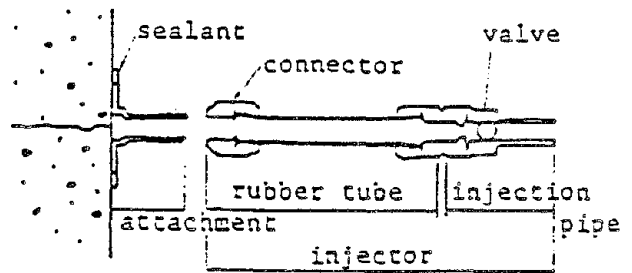


Fig-11 Complete destruction



(a) Surface treatment



(b) Pressured injection

Fig-12 Grouting

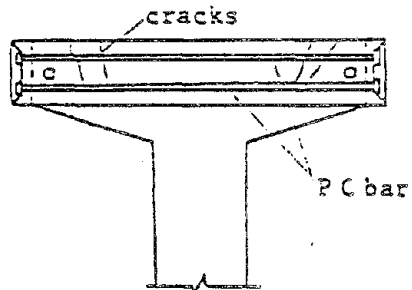
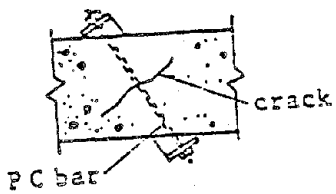
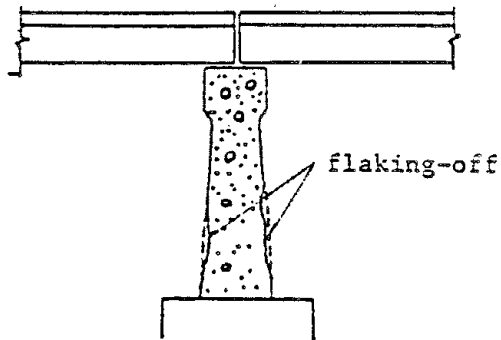
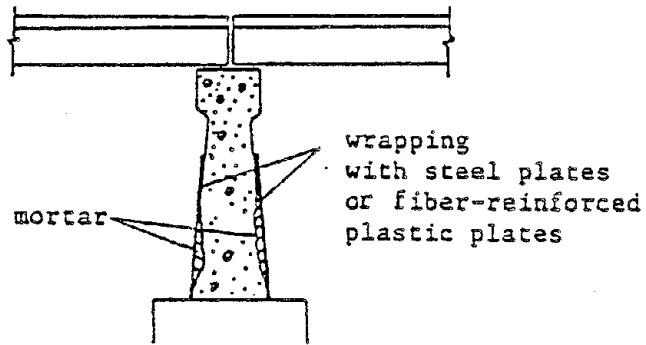


Fig-13 Prestressing

(b)



(a) damaged state



(b) repair work

Fig-14 Wrapping

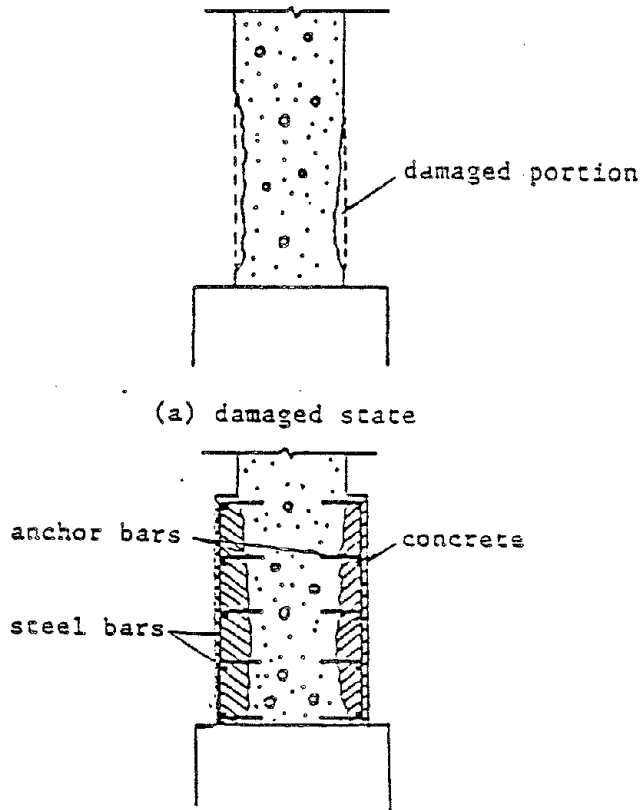


Fig-15 Supplemental reinforced concrete

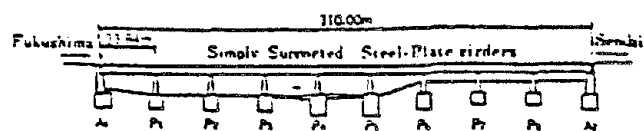


Fig. 16 General View of the Sendai Bridge.



Fig. 17 Failure of Pier 6, the Sendai Bridge.



Fig. 18 Temporary Frames Supporting Girders near Pier 6, the Sendai Bridge.

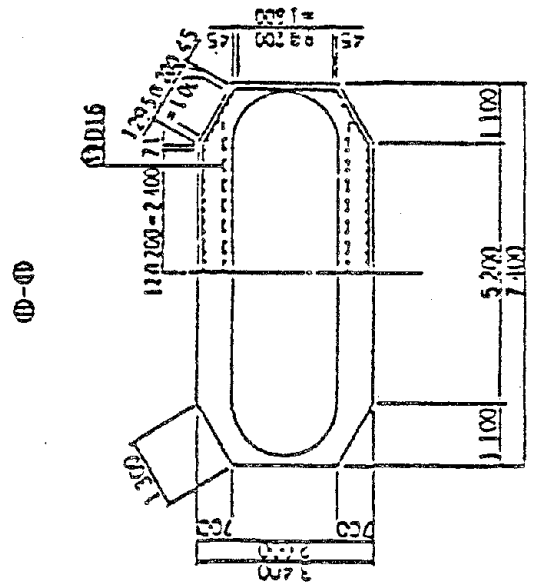
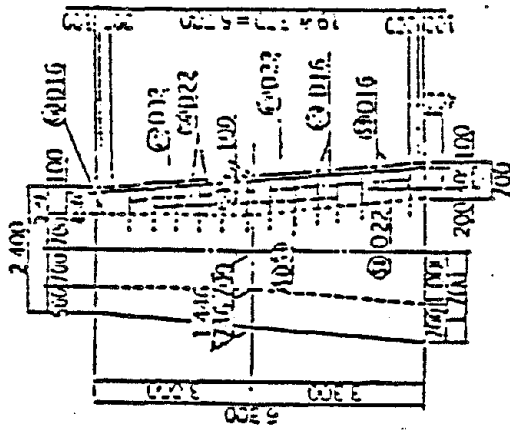
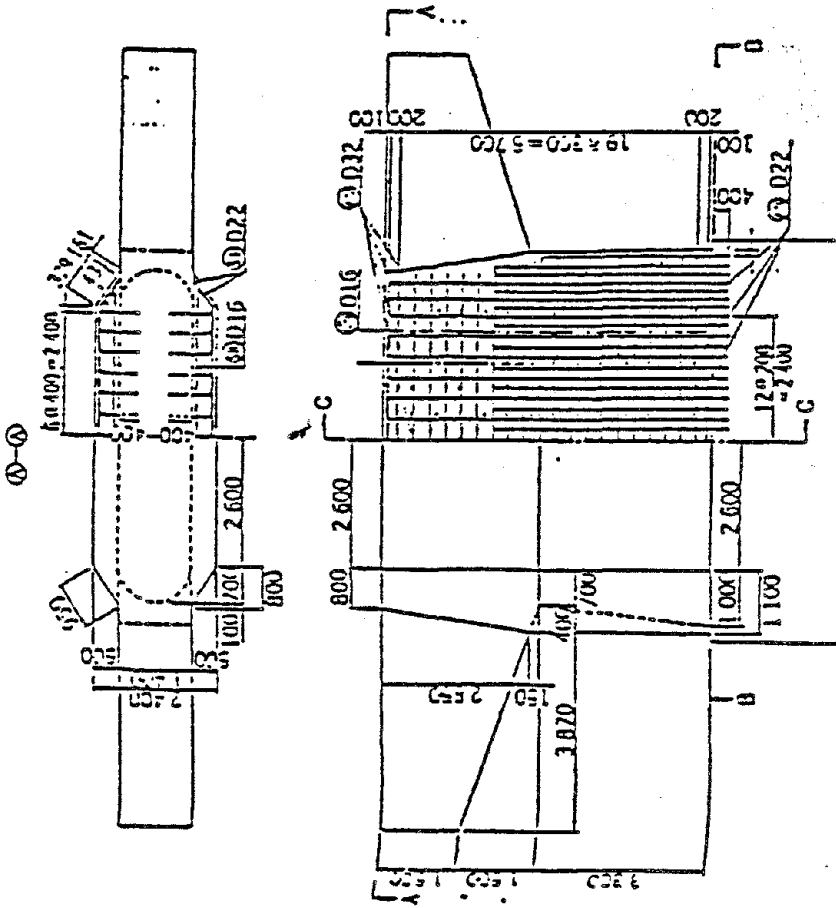


Fig-19 Repair Work of Pier 6, the Sendai Bridge


 Reproduced from best available copy.

852
855

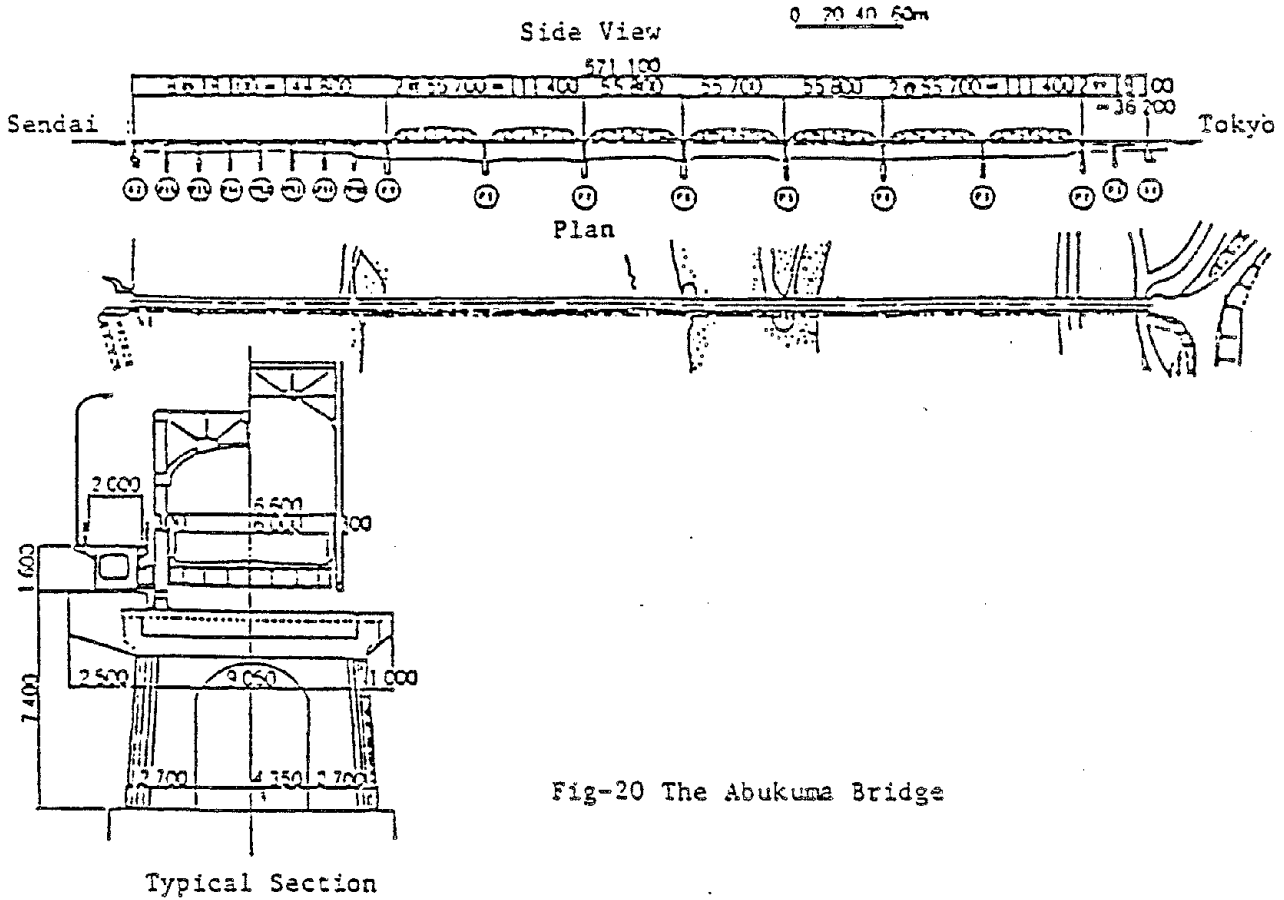


Fig-20 The Abukuma Bridge

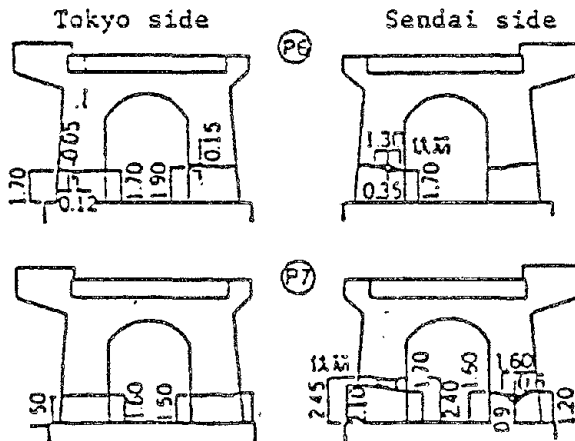


Fig-21 Damage to the Abukuma Bridge

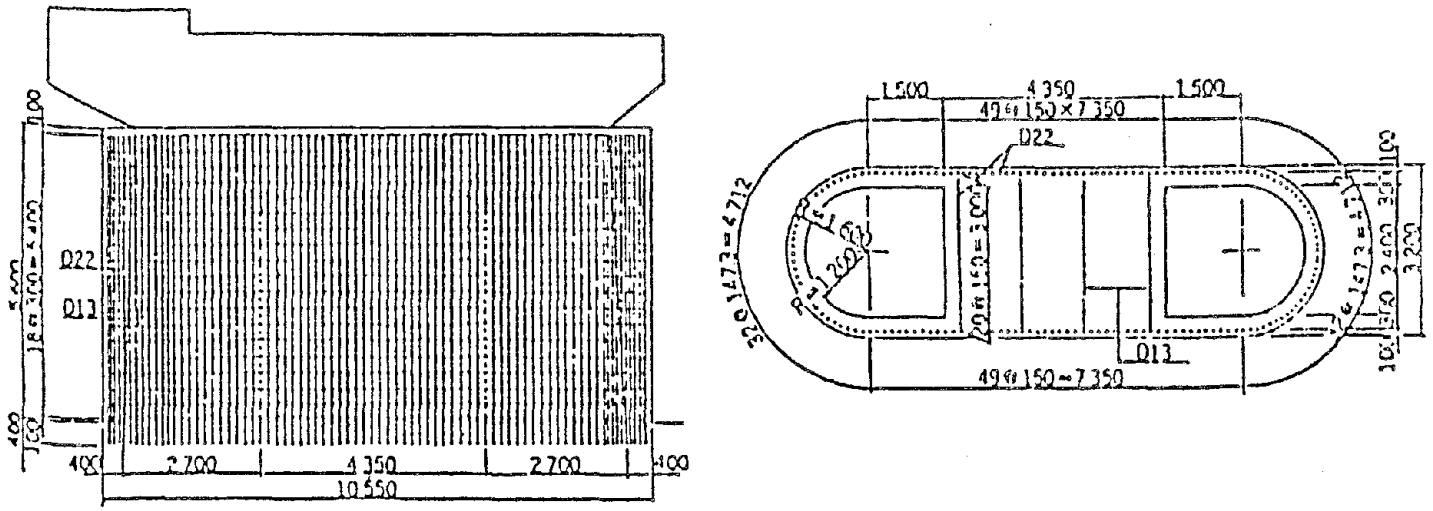


Fig-22 Repair Work of Pier 6 and 7, the Abukuma Bridge

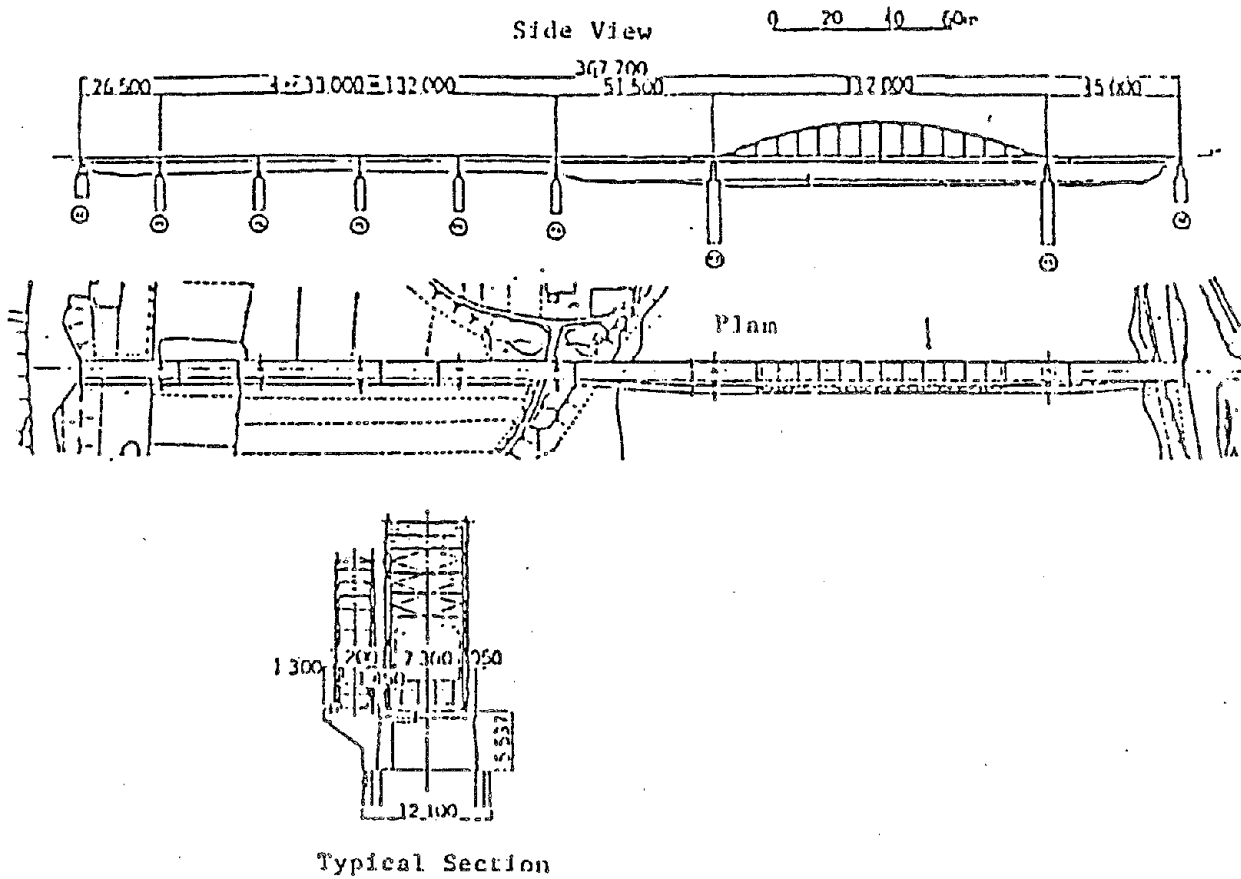
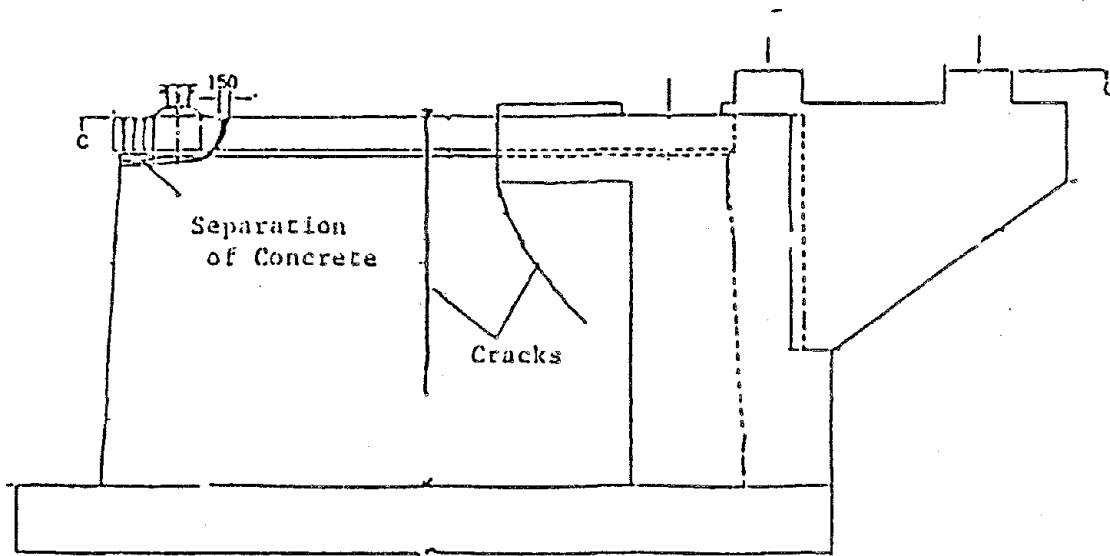


Fig-23 General View of the Ten-noh Bridge



C-C Section

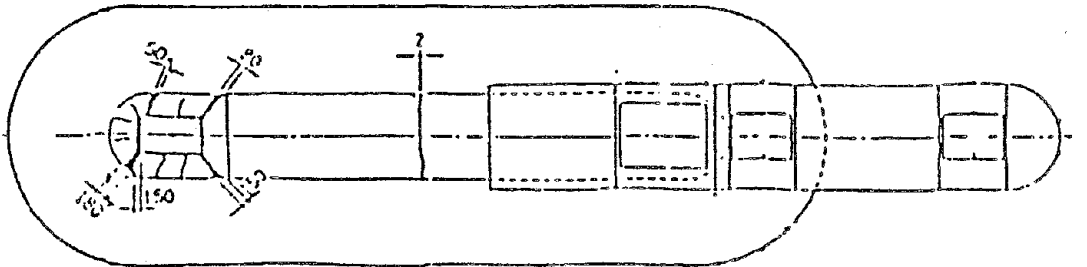


Fig-24 Damage to Pier P-1, the Ten-noh Bridge

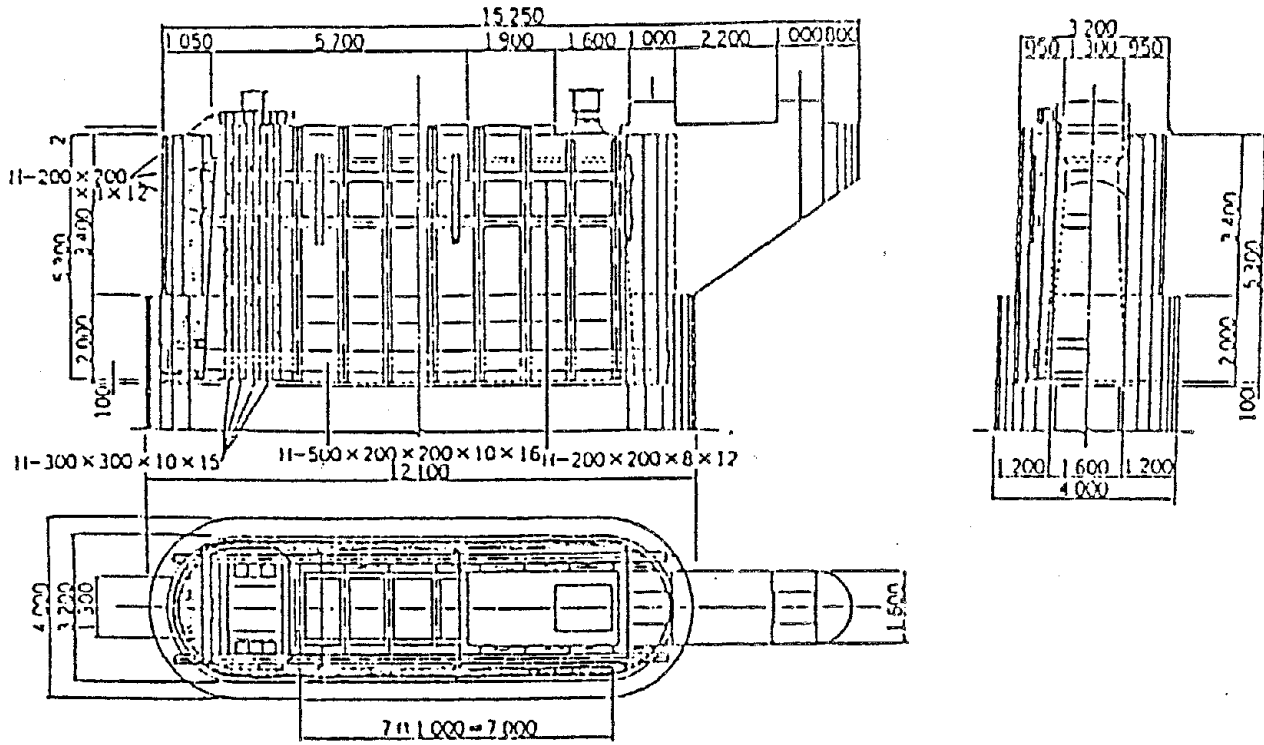


Fig-25 Repair Work of P1, The Sendai Bridge.

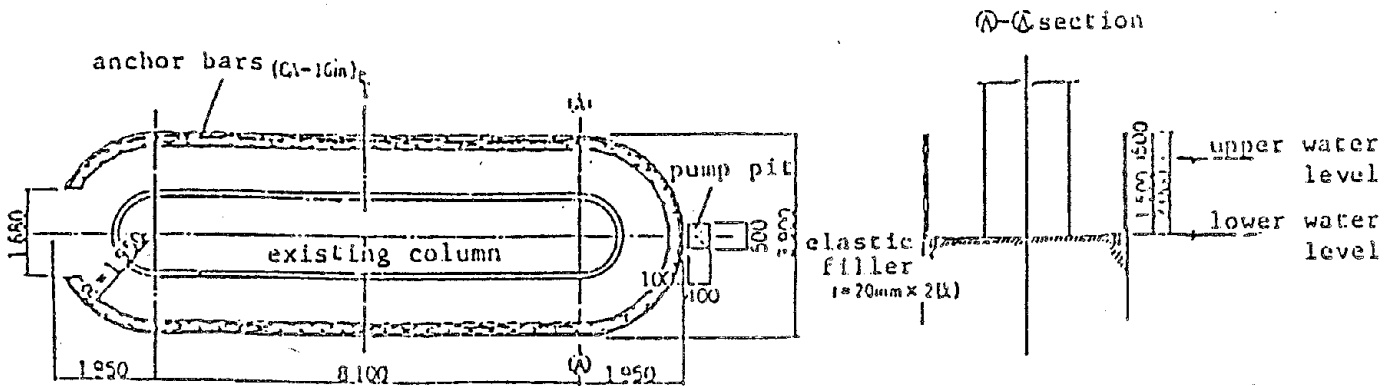


Fig-26 Detail of cut off wall

REHABILITATION OF ROAD TRANSPORTATION NETWORKS
DAMAGED BY EARTHQUAKES

By

Toshio Iwasaki*, Takeo Nakajima**, and Katsushi Goto***

* Dr. Eng., Head, Earthquake Engineering Division, Earthquake Disaster Prevention Department, Public Works Research Institute, Ministry of Construction, Tsukuba, Ibaraki, Japan

** Senior Research Engineer, do

*** Assistant Research Engineer, do

ABSTRACT

The damage to highway facilities followed by large earthquakes causes consequential socio-economic damage, since the damage spoils transportation systems. From this point of view, the repair of damaged highway facilities would be one of the most important factors for the social rehabilitation after earthquakes. In conducting countermeasure such as aseismic design, highway planning, and road administration, it is also important to consider the indirect effects of damage to highway facilities.

This report discusses the problems on rehabilitation of highway networks after earthquakes. And, some precedents for the damage to highway networks after earthquakes are surveyed minutely. Data from the Niigata Earthquake of 1964, the Izu-Ohshima kinkai Earthquake of 1978, the Miyagiken oki Earthquake of 1978, and the Urakawa oki Earthquake of 1982, are presented.

From the study, a concept of countermeasures of rehabilitating highway networks with view of seismic damage, a definition of periods after the outbreak of an earthquake, and characteristics of highway traffic from each period, are clarified.

1. INTRODUCTION

Highways support almost all socio-economic activities as a fundamental facilities in the present time. If highways lose their transportation function followed by earthquake damage, the indirect effect on others will be large; e.g. delay of social activities, stagnation of productive activities or confusion of our daily life. Because of this, damage to highway facilities should be understood as socio-economic damage as well as physical damage. On the way to restore or to reconstruct, it would be important wheter the transportation function will be secure or not. So highways should be restore according to the state of rehabilitation of the damaged district in order to keep the social order.

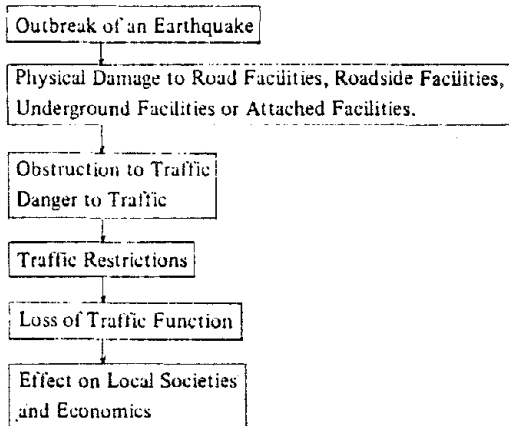
In the countermeasure planning, thoughtful consideration is recommended in relation to the socio-economic effect which is caused by earthquake damage to highway facilities. For example, the importance factor should be considered in aseismic design, the redundancy of

network should be considered in the highway network planning, or the system of road administration after earthquakes should be established in advance.

This report surveys some historical earthquakes in Japan, arranges the conditions of transportation after earthquakes, and discusses the rehabilitation of highway networks in some stages after an earthquake.

2. HIGHWAY DAMAGE AND TRAFFIC CONTROL

The spread of earthquake damage to highway facilities is shown as follows.



The damage to highway facilities followed by an earthquake causes obstruction or danger to passing through. In the circumstances, traffic is controlled strictly and the transportation function, such as moving people or carrying commodities, is lost. As a result, daily social activities such as commutation or business are obstructed, and economic activities such as circulation are affected. Increasing required time due to detour and the congestion cause social confusion. In the worst case stagnation of productive activities would be occurred. The repair of water supply, electric power or gas facilities are also affected by the delay of restoration of highway systems.

In the restoration or the reconstruction period, the more the repair advances, the more the traffic control becomes relaxed. The functional disorder becomes stored to normal, so that the normal transportation comes back again.

The duration of rehabilitation depends on state and severity of damage, and the indirect effect depends on rehabilitation time. The longer the rehabilitation lasts, the bigger the effect of functional disorder will be. The effect of functional disorder is also influenced by the character of local area.

The examples of damage to highway facilities and restoration period are shown in table 1, so as to clarify the damage to highways. The damage patterns are classified two large catego-

ries. One is damage to road, i.e. failure of earthstructures, that of bridges and that of attached facilities. The other is after kind of damage which affects the functional disorder of highways, including inundation, big fire, evacuation or cars on the road.

Among them, the damage to pedestrian bridges and underpasses are not seen in historical earthquakes. Judging from the past aseismic test on pedestrian bridges or underpasses, their damage never causes the functional disorder of highway transportation. So their damage can be neglected in the discussing the transportation function after earthquakes. Leaving cars on the road are also not seen in historical earthquakes. According to the removing cars test, it would take for several days to clean up them.

In the Niigata and the Miyagiken oki Earthquakes, which hit the urban area in the plain, a lot of severe damage to bridges was seen, and it took a long time to repair them. On the contrary, in the Izu-Ohshima kinkai Earthquake, which hit the mountain area, the damage caused by landslide and falling rocks and earth was seen here and there. These kind of damage need not much time to repair each site in comparison with damage to bridge structions. However, as these kind of damage ocured many sites even in a line, the restoration couldn't advance simultaneously. As a result it took a lot of time to finish the emergency restoration. At the site where landslide ocured and the road was venished with basic earth, it was impossible to complete the restoration. Because of this, a new route was planned apart from damaged site.

The examples of traffic control are shown in table 2. Although the worst case is road blocked and any vehicles can't be permitted passing through, the traffic control becomes lightened after the emergency restoration. The examples are shown in table 3. In the case of falling rocks and earth the lane restrictions are taken, and in the case of damage to bridges the car size restrictions are taken.

3. EXPERIENCED EARTHQUAKES

3-1 Niigata Earthquake (June 16, 1964, Wed., 1:02pm, M=7.5)

In the Niitata Earthquake, three bridges over the Shinano river, which are situated in the central district of Niigata city, were closed due to damage to bridges. The bridges are Mantai, Yachiyo and Showa bridges. Because of this the urban area splitted into two parts. And just after the earthquake, the traffic which got across the Shinano river had to detour Taishaku bridge which are situated some 15 KM upstream from the central district.

Almost all roads are cut in pieces here and there in the urban area, owing to crack, rising and subsidence of road, and inundation. As a result the traffic inside the city had got into a terrible mess.

There was much traffic demand of the emergency and the relief activities, especially fire-fighting, because of great fire to huge plants for petroleum caused by the shake. Fire companies from the Tokyo metropolitan fire department and other neighbouring cities partici-

pated.

The following days a lot of cars, whose purpose was inquiring after sufere and carrying various kind of commodities, concentrated on city area. The confusion of traffic became intensified.

Leaving such confusion would have obstructed the emergency, relief and restoration activities. From July 17 wide scope traffic control was taken so as to restrict cars entering urban area except urgent vehicles. This control lasted for 11 days until July 27. At the Mantai bridge, which was one of the damaged bridges over the Shinano river, two of four lanes had become reopened the following day.

And then, eastern and western parts of city were connected to earth other by two bridges, they are Taishaku and Mantai bridges. The traffic was controlled by circulation one way system, i.e. using Taishaku bridge from east to west and Mantai bridge from west to east.

Yachiyo bridge reopened one lane on July 2. At last, the emergency restoration was finished except Showa bridge which was fallen down, and the circulation one way control was abandoned. As a result the traffic inside urban area was smoothed after 16 days from outbreak of earthquake.

The traffic volume at Mantai bridge was 32,019 cars/12 hr before the earthquake (Oct. 1962) and was 32,334 cars/12 hr after the earthquake (Sept. 1964). Judging from them, the volume would be about 40,000 cars/day at the time, and the National highway route No. 7 is understood as a main trunk. The effect of the obstruction upon the local society was expected very large. The peak traffic volume (AM9 – AM10) was 3,057 cars/hour by the observation done on October 1962. From the peak traffic volume after the earthquake, as shown in Fig. 2, the traffic had recovered normal daily one until July 6, after twenty days from the outbreak of the earthquake.

3-2 Izu-Ohshima Kinkai Earthquake (January 14, 1978, Sat., 12:24pm, M=7.0)

In the Izu-Ohshima kinkai Earthquake, the highway through mountain area was blocked in 27 places by landslide and falling rocks and earth. An the transportation between areas was almost impossible, so that Shimoda city was isolated just after the earthquake (Fig. 2).

As the urgent traffic, rescue activities were originated because of many casualties. At a landslide site, where houses were buried in the earth and 7 people passed away, fire fightings plice, self defence forces and contractors did rescue activities, and 13,408 man days and a lot of construction machines were thrown into there.

Water supply was one of big problems in the transportation of daily necessities. 15,000 man days were supplied water by the emergency water supply tanks. And in the isolated area, water was supplied by warship belong to self defence forces.

The restoration of highway was focussed on that the urgent vehicles could reach isolated area as soon as possible. Especially connecting outer region with Shimoda city, where is the

center of Izu peninsula, was given first priority. In this case, one lane was secured for the urgent and the construction vehicles at first. As a result, national highway route number 136, which is located in the western coastal of Izu peninsula, was reopened on January 16, as it was relatively, small damaged. Higashi Izu toll road (R.135), which is located in the eastern coast, was reopened on January 17 only for urgent vehicle.

A principal local road Shuzenji-Shimoda line, which is another trunk road reaching to Shimoda city, was rather heavy condition. The highway facilities were damaged in 86 sites, and repair couldn't help being done one by one from both side of this route. It took two months to repair and the vehicles not more than two tons became permitted passing through on March 14. And on July 18, 6 months after the earthquake, the emergency restoration of all route finally had been done and all vehicles became permitted. This long time was necessitated, because of new slope failures due to rainfalls after the occurrence of the earthquake.

The purpose of traffic in Izu peninsula is mainly sightseeing and the volume is not so much except on tourist seasons. Besides this, the number of tourists was decreased, the demand of traffic itself was diminished, and almost all demand was relief and restoration. So that the quantitative problem such as congestion was not occurred.

From the data of the traffic observation, during the restoration of Shuzenji-Shimoda line, the traffic volume at Higashi-Izu toll road was increasing by 20% to the same month of the previous year. But the daily traffic volume on May 1978 was only 5,700 cars/day (May 1977; 4,800 cars/day), so that the increasing of volume was not so important. The estimation of daily traffic volume at Nawaji of R.135 in the entrance of Shimoda city was being decreased until March, compared with the data of previous year (Fig. 4).

3-3 Miyagiken-oki Earthquake (June 12, 1978, Mon., 5:14pm, M=7.4)

The Miyagiken-oki Earthquake becomes the focus of attention as the Earthquake hit the large city, who has more than 500 thousand inhabitants. It was the first time after the Kanto earthquake of 1923. However, damage to highway facilities were not so seriously as the cases of Niigata and the Izu-Oshima Kinkai Earthquakes were.

The transportation of relief commodities and restoration materials and machines was originated for one week after the earthquake. The estimated traffic volume was some 3,000 cars/day (Table 4), and it was only 2% of freight cars originated in Sendai. The traffic volume was not causing any serious problems.

The features of the Miyagiken-oki Earthquake as seen from traffic were shown as follows:

a) Traffic Congestion Due to Stoppage of Traffic Signals

The stoppage of traffic signals due to suspension of electric power (occurred on June 12) affected severely the urban traffic. The outbreak of the earthquake was just the time of coming back home from work, and the cars to suburbs were distinguished. The traffic in urban area was congested for a while. And it took about twice as much time as usual, to move from the city center to the outskirts of the city by cars as shown in Table 5. The rehabilitation of functional disorder of traffic signal was almost done until 9 AM of June 13 by the emergency power supply using storage batteries. This congestion affected the activities of fire fighting and

ambulance.

b) Diminution of Traffic Volume in Central District

The traffic volume at 7 intersections in central district of Sendai city has been surveyed using the data of traffic counters for one week after the earthquake as shown in Fig. 5. This shows that the traffic volume in front of Sendai station is decreased remarkably. It is understood that the passengers would have been decreased because of the delay in rehabilitation of the National Railway.

At the other 6 intersections, the traffic volume is fewer than that of previous week for a few days after the earthquake.

The urban traffic has such features that the rate of large sized cars is small, that of private cars is large and not a few cars move only inside the city. On the one hand, the purpose of daily activities such as shopping, or attending work and school became decreased just after the earthquake. Under the influence of these, the demand of traffic in the central district was less than usual.

c) Increasing of Traffic Volume in National Highway Route Numbers 4 and 6

The traffic volume was increased in national highway route numbers 4 and 6, which are the main trunk roads coming into Sendai City, as shown in Figs. 6 and 7. It shows that increasing traffic volume in R.6 is 3,000 cars/day on June 12 and 2,000 cars/day on June 13, and that in R.4 is 2,000 cars/day on June 13.

Though Sendai bridge in route number 4 and Abukuma bridge in route number 6 were damaged to their pier columns, traffic control was not done. This was mainly due to the efforts of Sendai Construction Office, MOC which is charge of the maintenance. On the contrary, in the Tohoku Expressway was closed its lumps between Fukushima-Iizaka and Tsukitate, 126.3 km, from June 12 to 14. As a result, drivers made use of national highway instead of expressway.

This also shows that the demand of traffic between Sendai and external zone was not changed so remarkably. In the main trunk highway between large cities, the rate of large sized cars is high (20–25%) and transporting daily necessities or industrial commodities is occupied large parts of their purpose. As the demand of such kind of commodities in this earthquake was the same as usual, the total traffic volume was not decreased in the main trunk road.

d) Traffic Volume in Tohoku Expressway

The traffic volume for a week after the earthquake in southern part of Tohoku Expressway has been compared to that of previous and following weeks. The examples of two sites in which roads were not closed are shown in Figs. 8 and 9.

Judging from the data, the traffic volume, leading to Sendai on June 13, shows increase of 1,000 or 2,000 cars/day all along the line south of Fukushima. This is understood that the effect of closing the Tohoku and Jhoban railway line, which connect with Tokyo and Sendai. The Passengers changed their means from train to cars.

On the contrary, the traffic volume, leading to Tokyo was not so fluctuated as former

one. But the volume on the day outbreak of the earthquake shows decrease of 500 or 1,000 cars/day. It is understood that originating traffic volume from the damaged area north of Fukushima was diminished.

e) Traffic Across the Kitakami River

All bridges over the Kitakami river, which located in the north-eastern Miyagi prefecture, were damaged to some extent. Some of them are blocked. And then the transportation in this district got confused, but it never caused the worst case such as Kesen-numa city was isolated. Kesen-numa city is the biggest city situated in north-eastern Miyagi prefecture and has 69 thousand inhabitants.

This is because the network in this district has more redundancy than that of Niigata city in the case of the Niigata Earthquake of 1964.

The concrete reasons on this are as follows.

- Only one bridge of eight damaged bridges was closed due to fall down. The one was Kin-no bridge. And the others were permitted to pass through by small cars at least.
- Yanaizu and Shin-Inogawa bridges were permitted large sized cars passing through.
- The traffic volume across the Kitakami was some 16,000 cars/day, and the rate of large sized cars was about 15%. The cars forced to detour were some 2,400 cars/day by a rough estimate. They were not so much.
- Detour routes were easily secured.

3-4 Urakawa-Oki Earthquake (February 21, 1982, Sun., 11:32am, M=7.1)

In Urakawa-oki Earthquake the only trunk road national highway route number 235, which runs along the seashore in Hidaka district of Hokkaido, was closed due to the damage to bridge piers of Shizunai bridge.

The traffic except pedestrians and bicycles was banned at Shizunai bridge after the earthquake. The prefectural road which included 7 km rough road was used as the detour route, and it was 24.9 km against 9.2 km of national highway.

On April 15, 25 days after outbreak of the earthquake, the bridge was reopened under the traffic control. The control was 5 tons as a weight limit, 2.5 m as a width limit and a height limit respectively, 30 KM/H as a speed limit and mutual traffic using one lane. The steel gate was set on the approach road to bridge and small sized cars could be used since then.

However the steel gate brought about a big social problem, because Hidaka district is the well known area as a famous racer breeding area in Japan. Those cars carrying more for breeding are very frequently passing to and fro on this route. But the roofs of the cars for them are remodeled higher. As they were higher than the gate, those cars were forced to detour.

Because of this the owners of ranches required that the restriction to those cars should be abandoned. And then Shizunai bridge became available for those cars in daytime on account of stationing guards for operating at the gates.

The restoration of Shizunai bridge had been done during September, and the control was wholly relaxed from October 1, after 194 days restriction.

The traffic volume of Shizunai bridge is some 8,500 cars/day usually. In the restoration time the detour trip was estimated 7,500 cars/day until April 15, and after then it was done 1,500 cars/day. From these data the total detour trip reached 440 thousand car-days.

The network across the Kitakami rivers in the case of the Miyagiken-oki Earthquake is the typical example of redundant one. In comparison with this, Shizunai bridge is the typical example of vulnerable one. It shows the vulnerability of the area in which almost all local activities depend on the unique trunk road.

In this case, the traffic volume was not so much. But the only detour route was in the distance and long, and the duration of restriction was long. Because of this the effect of the damage to the bridge was not neglected. Especially the indirect economic effect on buses seemed to be big. e.g. the increase in fuel rate and personnel expenses, and decrease in bus fare income.

4. REHABILITATION OF TRANSPORTATION AFTER EARTHQUAKES

The state of transportation after a earthquake is varied owing to the characteristic of the local or the extent of damage. The feature of transportation in each earthquake is shown in Table-7.

The state of damage to the area and the quality and the quantity of originating traffic should be considered, when the transportation is rehabilitated. And the functional level of highway facilities to secure varies as the restoration is advanced. In the rehabilitation process, the necessary function in compliance with the rehabilitated level should be satisfied.

The concept of rehabilitation of traffic according to the state of damage is arranged as follows, with reference to the historical earthquakes.

a) In the case of highway is blocked everywhere, the rehabilitation should focus on dissolving the isolated area. So that the most important subject in such case is to secure the connection between areas.

b) In the case of the damage to the area that needs a lot of restoration and relief commodities, the main subject in rehabilitation should focus on carrying these commodities surely as soon as possible.

c) In the case of relatively slight damage, a lot of daily traffic originated as usual. So that to satisfy these demand is focused primarily just after the earthquake. It is necessarily to control a lot of traffic and to secure their safety.

And then the rehabilitation process of transportation systems after earthquake is shown in Table 8. In the table, the process after the earthquake is divided 4 periods as follows.

- 1) Emergency activities
- 2) Removal cars and carrying material for the relief
- 3) Emergency restoration and carrying restoration commodities
- 4) Restoration and reconstruction and carrying daily necessities

The characteristics of each period are represented as follows.

1) Stage of Emergency Activities

In this stage, the urgent movement such as fire fighting or ambulance is to secure primarily. The volume of them are limited, the region of activity is relatively small, and the urgent cars are operated by the men who know the local very well. But this period is also the time of confusion just after an earthquake. It is very difficult to secure the functional order of transportation, because of the leaving cars on the road or congestion of the road by other reasons. Therefore the activities on this period depend upon the calm judgment of responsible persons on the spot, and also the orderly command systems.

2) Stage of Removal Cars and Carrying Materials for the Relief

In this stage the principal purpose of transportation is to secure carrying indispensable goods to our life. The region of those activities are almost limited inside the municipality. Because of this it is most important to dissolve the isolated area and to supply necessary services to everybody. In process of removing waste matters or cars on the road, the connection with areas and raising the mobility of the activities should be taken into account. On the earthquake countermeasure programs, it would be recommended that the appropriate stationing of necessary materials and machines or the arrangement of countermeasure in which the early stage of rehabilitation is considered.

3) Stage of Emergency Restoration and Carrying Restoration Commodities

In this stage a lot of trips, whose purposes are mainly moving workers or carrying necessities for restoration activities, are originated. The trips for introducing commodities from outer area are increasing and traffic become complicated. But in the majority of cases the purposes and the destinations of trips are clear and accurate, and the traffic concentrates some important sites. So that in the restoration process, the important sites should be connected each other and it is necessary to lessen the time length and to enlarge the traffic capacity between them.

And also it is very important to secure the labors' conveyance, because they play important role in the various kind of restoration activities in this stage. The labors are the valuable generating power for rehabilitation. The public transportation for attending work is so important that bus lanes are primarily secured.

4) Stage of Restoration and Reconstruction

In this stage, the restoration and the reconstruction activities became more actively, and the traffic demand is increasing. Because of this, the serviceability of highway transportation would required the level as usual.

The traffic in this period is originated in large quantity and has various kind of purpose. So that the traffic is complicated and the trip length is not unified, and long and short distance trips are mixed in confusion. Because of this, it is important to maintain the mass traffic and to secure the safety of traffic.

Especially, on the trunk roads, safety countermeasure should be considered as well as plural lanes are secured. On the other hand, on the collector roads, local services should be

expected to be unified to the stretch of urban area, and it is necessary to compensate for the lack of functional disorder of trunk roads.

5. CONCLUSION

This report discusses on the problems for rehabilitation of transportation networks, through surveying historical earthquakes and the state of transportation after the earthquakes. As a result the concepts of countermeasures on traffic according to damage level, the rehabilitation process, and the characteristic of traffic on each stage are formed. The simulation model for the transportation after an earthquake will be made in the future. The model should be taken into account of the damage state and the restrict conditions of materials and machines. Some case study will be applied to the existing transportation network, and the local problem to be resolved will be deduced.

The results of this study will be useful for organizing road administration systems after earthquakes, and stationing plan of materials and machines for the restoration. And it will be also applied to the highway planning with disaste prevention. It is useful for the road administrator to exercise on the desk in advance using the model, because a trial experience is said to make them active when the real earthquake will occur. It is one of the most important subjects to decide the importance factor in aseismic design, considering the effect of earthquake damage to highway facilities upon the local society and economics. The effect of rehabilitation period should be also considered in the seismic design.

In conducting the survey described in the above, extensive informations were given from the Tohoku Regional Construction Bureau, (MOC), the Hokuriku Regional Construction Bureau (MOC), the Miyagi Prefectural Government, the Niigata Prefectural Government, and the Shizuoka Prefectural Government. An analysis of the available data was conducted by the Mitsubishi Institute. The authors express their sincere appreciations to the staff members of the above organizations.

References (All in Japanese)

- 1) Niigata Prefecture: The Records of the Niigata Earthquake; June, 1965.
- 2) Hokuriku Regional Construction Bureau. M.O.C.: Damaged to National Highway Caused by the Niigata Earthquake; Nov., 1964.
- 3) Japan Road Association: Highway Damage Caused by the Izu-Ohshima-Kinkai Earthquake of 1978; March, 1979.
- 4) P.W.R.I., M.O.C.: Survey on Relief and Restoration in the Izu-Ohshima-Kinkai Earthquake of 1978; Technical Memorandum of P.W.R.I., No. 1343, Feb., 1978.
- 5) P.W.R.I., M.O.D.: Report on Damages due to the Izu-Ohshima-Kinkai Earthquake of 1978, of 1978, Report of P.W.R.I., No. 158, March, 1982.
- 6) P.W.R.I., M.O.C.: Functional Damage and Rehabilitation of Lifeline in the Miyagi-ken-Oki Earthquake of 1978, Technical Memorandum of P.W.R.I., No. 1437, Dec., 1978.

- 7) Tohoku Office of Japanese Civil Engineering Society: Report on the Miyagike-Oki Earthquake of 1978; 1980.
- 8) Tokyo Regional Disaster Prevention Organization: Tokyo Metropolitan Regional Disaster Prevention Program; 1980.
- 9) Japan Urban Center: Transition of Urban Area and Disaster Prevention System; 1976.
- 10) P.W.R.I., M.O.D.: Rehabilitation of Transportation after Past Earthquakes; Technical Memorandum of P.W.R.I., No. 1854, July, 1982.

Table 1. Damage to Highway Facilities and Restoration Period.

	Damage	Time		Restoration period						Examples		
		Types		3hr.	1d.	3d.	1w.	1m.	3m.		1y.	
Road facilities	Earth structures	1	Landslide								Izu-Ohshima Kinkai Eq.	
		2	Crack, Subsidence and Rising of earth structures									Miyagiken-oki Eq.
		3	Falling rock or earth									Izu-Ohshima-oki Eq. Miyagiken-oki Eq.
	Bridges	4	Falling, Moving or inclining of girders									Niigata Showa Br. Miyagiken-oki Eq. Kin-no Bri.
		5	Failure of bearing supports									Miyagiken-oki Ten-no Bri.
		6	Crack of pier columns or abutments, Failure of foundation									Miyagiken-oki Eq. Yuriage Bri. Urakawa-oki Eq. Shizunai Bri.
		7	Sinking of the earth behind abutments									Miyagiken-oki Eq.
		8	Gap in approaching roads									Niigata Eq. Miyagiken-oki Eq.
	Attached facilities	9	Failure of pedestrian bridges									
		10	Failure of underpasses									
		11	Stoppage of traffic signal									Miyagiken-oki Eq.
Others	Facilities along the road	12	Failure of underground pipes									Miyagiken-oki Eq. Shiraishishi, Furukawashi
		13	Collapse of building									Miyagiken-oki Eq. R. 346
		14	Falling down of fences or stone-walls									Miyagiken-oki Eq.
		15	Inclining or falling down of poles or trees									Miyagiken-oki Eq. Miyagicho-sakunami
	Others	16	Inundation									Niigata Eq.
		17	Great fire									Kanto Eq.
		18	Evacuation									Kanto Eq.
		19	Leaving cars on the road									From removal trial

Table 3. Relaxation of Traffic Control after Earthquakes as the Emergency Restriction Progressed.

Earthquakes	Routes	Damage	Traffic Restrictions	Duration
Izu-Ohshima kinkai Eq.	Shuzenji-Shimoda Line	Falling earth and rock	Blocked Weight limit (2 tons)	Jan. 14, '78 - Mar. 14, '78 Mar. 14, '78 - Jul. 18, '78
Miyagiken-oki Eq.	National Highway R. 45 Ono Bridge	Movement of all girders	Blocked Weight limit (1 ton) Blocked (Repair work)	Jun. 12, '78 - Jun. 17, '78 Jun. 17, '78 - Oct. 18, '78 Oct. 18, '78 - Feb. 28, '79
DO	National Highway R. 286	Falling rock	Blocked One lane	Jun. 12, '78 - Jun. 20, '78 Jan. 20, '79 - Nov. 14, '78
DO	Okumatsushima-Matsushima park Line	Subsidence	Blocked One lane	Jun. 12, '78 - Jun. 13, '78 Jun. 13, '78 - Apr. 27, '79
DO	Shiogama-Watari Line Yuriage Bridge	Crack at the pier columns	Blocked Weight limit	Jun. 12, '78 - Jun. 21, '78 Jun. 21, '78 - Sep. 30, '79
DO	Ishinomaki-Ayukawa Line Mangoku Bridge	DO	Blocked One lane	Jun. 12, '78 - Jun. 29, '78 Jun. 29, '78 - Apr. 5, '79
DO	Sadayoshi-Sendai Line	Falling rock	Blocked One lane Blocked at nighttime	Jun. 12, '78 - Jun. 28, '78 Jun. 28, '78 - Jul. 19, '78 Jul. 19, '78 - Jul. 29, '78
DO	Kitakami-Kakoku Line	Crack on the pavement	Blocked Weight limit	Jun. 12, '78 - Jun. 17, '78 Jun. 17, '78 - Jun. 5, '78
Urakawa-oki Eq.	National Highway R. 235 Shizunai Bridge	Break of pier columns	Blocked Weight limit (4 tons) Height limit (2.5M) Width limit (2.5M) Speed limit One lane	Mar. 21, '82 - Apr. 15, '82 Apr. 15, '82 - Oct. 1, '82

Table 4. The Estimation of Originating Traffic Volume Caused by Emergency Restoration Activities after the Miyagiken-oki Earthquake of 1978.

	Facilities	Restoration time (days)	Workers (man)	Emergency cars (cars)	mans/day cars/day
Daily necessities	Emergency watersupply	11	394		
	Dispatch of Self Defence Army	6	356		
	Repair of dwellings	20	3,140		
Public assets	Highways				
	M.O.C.	5	1,065		
	Miyagi Prefectural Office	10			
	Japan Road Corporation	3			
	River				
	M.O.C.	15			
	Miyagi Prefectural Office	15			
	Water supply	10			
	Sewage	3			
	Electric power	6			
	Gas	27			
	Communication	4			
	J.N.R.	10			
Port	2				
	TOTAL				

Table 5. Commutation Time by Cars in the Miyagiken-oki Earthquake of 1978.

	From	To	Distance (KM)	Starting time (PM)	Time required (Mins)	Speed (KM/H)	Usual commutation time (Mins)
1	Municipal Office	Kamiyashi	24.0	5:30	60	24.0	30
2	DO	Yoshioka	23.0	5:30	120	11.5	60
3	DO	Ishigakicho	4.0	5:15	75	3.2	20
4	DO	Matsumori	10.5	5:25	45	14.0	30
5	DO	Nankohdai	16.2	5:00	120	8.1	30
6	DO	Gamou	17.0	5:30	90	11.3	30
7	DO	Matsushima	27.0	5:30	60	27.0	50
8	DO	Keitsuen	5.5	5:30	20	16.5	20
9	DO	Kagitori	8.0	5:00	45	10.7	30
10	DO	Mukoyama	2.5	5:00	55	2.7	15
11	DO	Kasuminome	7.5	5:15	90	5.0	30
12	DO	Shiroumaru	14.0	5:05	105	8.0	60
	Average		13.2		74	11.8	34

Table 6. Damage to Bridges over the Kitakami River in the Miyagiken-oki Earthquake of 1978.

		Con- structed	Route	Length (M)	Width (M)	Damage	Traffic Restrictions
A	Kin-no Bri.	1956	National Highway R. 346	575.5	6.0	Fall of a girder	Closed until Nov. 1
B	Maya Bri.	1928	Principal Local Road Yuzawa- Tsukidate- Shizugawa Line	181.4	5.5	Break of upper chord	The Weight limit 2 tons a car until Jan. 12, 1982
C	Tome Bri.	1945	National Highway R. 342	306.0	5.3	Failure of a girder, Pier and Bearing supports	The weight limit 2 tons a car until Jul. 1, 1979
D	Yanaizu Bri.	1975	Prefectural Road Kanan-Tsuyama Line	450.0	10.5	Crack and buckling at lower truss chord	
E	Toyosato Bri.	1967	Principal Local Road Kanan- Yoneyama Line	349.0	8.0	Failure of bear- ing supports	One lane
F	Kamitori Bri.	1965	Principal Local Road Kanan - Yoneyama Line	287.0	6.0	Failure of bear- ing supports	
G	Sin-inogawa Bri.	1974	National Highway R. 45	441.5	10.0	Failure of bear- ing supports	Blocked while repair
H	Ten-no Bri.	1959	National Highway R. 45	367.7	6.0	Crack at stop of pier column	The weight limit 1 ton a car One lane until Aug. 12

Table 7. Traffic Features after Earthquakes

Earthquakes	Niigata June 16, 1964 (M=7.5)	Izu-Ohshima Kinkai January 14, 1978 (M=7.0)	Miyagiken-oki June 12, 1978 (M=7.4)	Urakawa-oki March 21, 1982 (M=7.1)
Damage to Highways	Divided into two urban areas by damage to bridges over the Shinano river. Feeder roads blocked everywhere in urban area.	Trunk roads blocked. City and towns isolated	A lot of damage to highways but little isolated area. Stoppage of traffic signals.	Single trunk road blocked.
Qualitative Feature	Many trips for condolence and movement of restoration commodities.	The purpose totally changed from sightseeing to rescue and restoration.	Ordinally trips	All local activities depended on the trunk road. Trucks for more with colt.
Quantitative Feature	Great confusion for a time because of extraordinarily trips.	Not so much traffic volume	Roads conected everywhere because of commuter trips just after the earthquake.	Traffic volume as usual. Detour duration prolonged and the number of detour cars reaching large quantity.

Table 8. Rehabilitation Process of Transportation after Earthquakes and Originating Traffic.

Rehabilitation process of transportation	Necessary function to secure	Originating traffic
1st stage Emergency activities (within 3 hours)	<ul style="list-style-type: none"> • Fire fighting • Rescue • Information • Road 	<ul style="list-style-type: none"> • Fire fighting, Fire Engine • Rescue and carrying sufferer, Ambulance • Gathering and communicating information on damage and evacuation. • Securing minimum transportation facilities.
2nd stage Removal cars on the road Carrying materials for the relief (within 3 days)	<ul style="list-style-type: none"> • Fire fighting • Flood defense • Rescue • Relief • Guard • Road • Inspection 	<ul style="list-style-type: none"> • Fire fighting against great fire or oil tank. • Defense against Tsunami or inundation • Rescue the wounded • Moving doctors, nurses and medicine. • Carrying water tank, food, clothes and mechanical power. Moving workers. • Removal cars on the road, Inspecting and judging damage to road facilities. • Inspecting damage to public assets or buildings.
3rd stage Emergency restoration Carrying restoration commodities (within 1 week)	<ul style="list-style-type: none"> • Fire fighting • Flood defense • Medical care • Relief • Remains • Guard • Emergency restoration • Waste disposal • Daily traffic 	<ul style="list-style-type: none"> • Remaining fire • Repair of embankment to prepare the blood. • Moving doctors, nurses and medicine. • Traveling clinic, Disinfection • Supplying water, food and clothes. • Carrying daily necessities, building materials for temporary house, Moving workers. • Gathering dead bodies • Patrolling • Carrying materials and machines for emergency restoration, Moving workers. • Disposal of waste matters, Carrying machines for disposal, Moving workers • Public traffic (Bus, Taxi)
4th stage Restoration and Reconstruction Carrying daily necessities	<ul style="list-style-type: none"> • Medical care • Relief • Restoration • Waste disposal • Daily traffic • Reconstruction • Daily traffic 	<ul style="list-style-type: none"> • Disinfection • Supplying water, food, clothes and other daily necessities. • Carrying materials and machines for restoration, Moving workers. • Disposal of waste matters and collapsed matter, Carrying machines for disposal moving workers • Public traffic (Bus, Taxi) • Private traffic (Commutation, Business) • Carrying materials and machines for reconstruction • All kind of traffic purpose with every traffic means (including shopping, recreation, etc.)

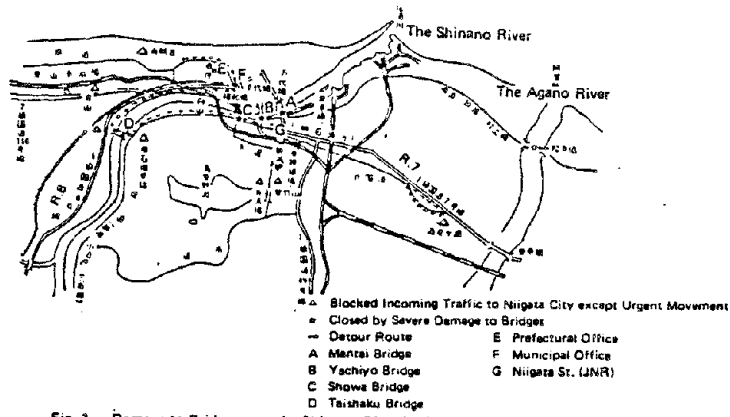


Fig. 1 Damage to Bridges over the Shinano River in the Niigata earthquake of 1964.

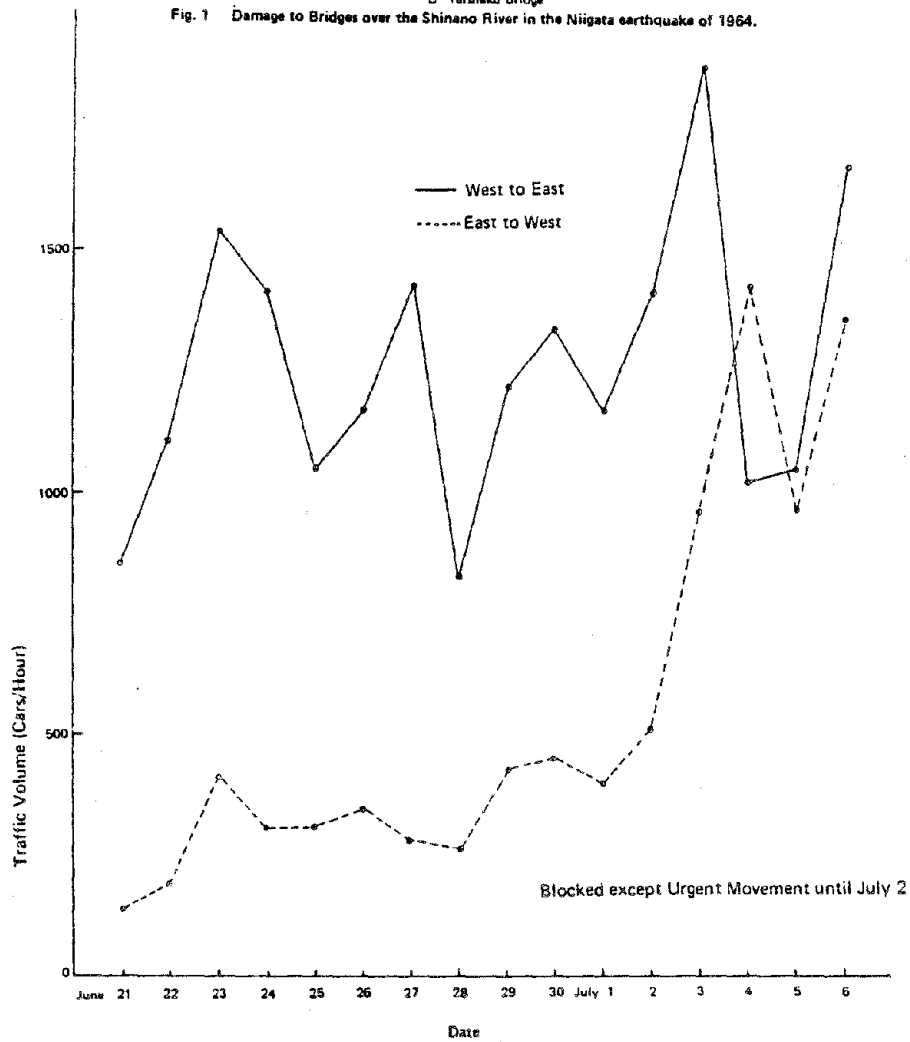


Fig. 2 Transition of Traffic Volume in Peak Hour.

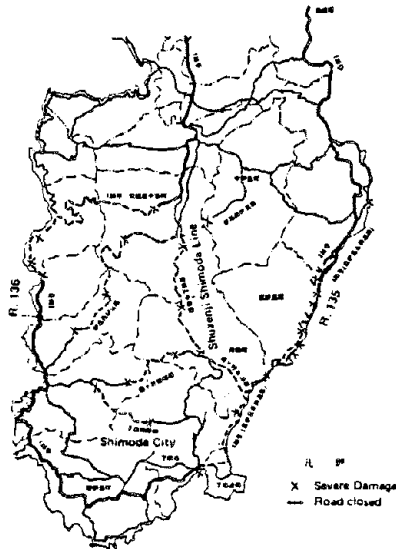


Fig. 3 Damage to the Highways in Izu-Peninsula in the Izu-Oshima Kinkai Earthquake of 1978. (as of January 15, 1978)

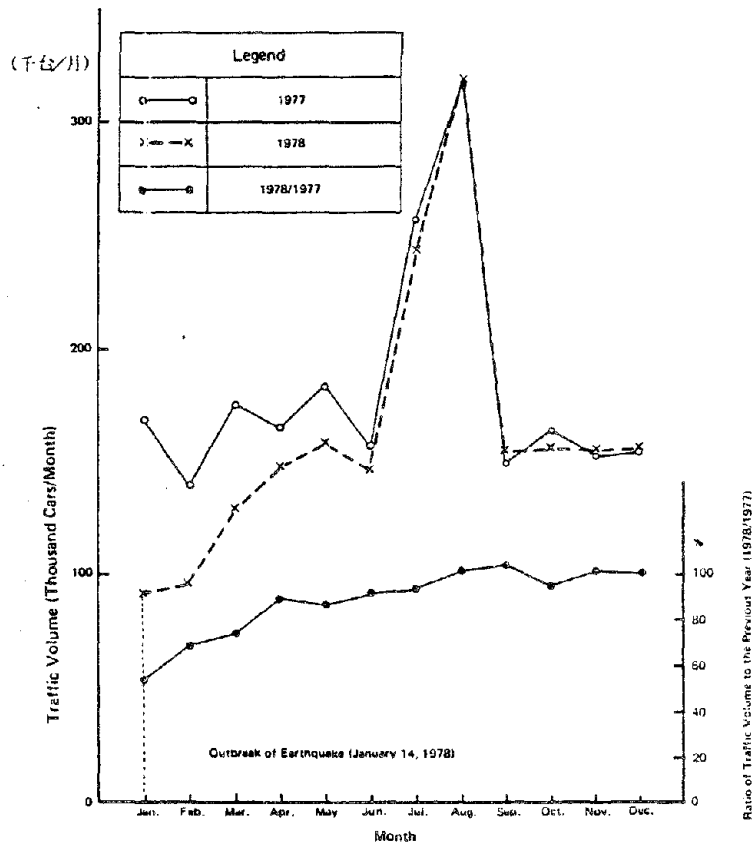


Fig. 6 Transition of the Traffic Volume at Nawaji of Shimoda Toll Road in the Izu-Oshima Kinkai Earthquake of 1978.

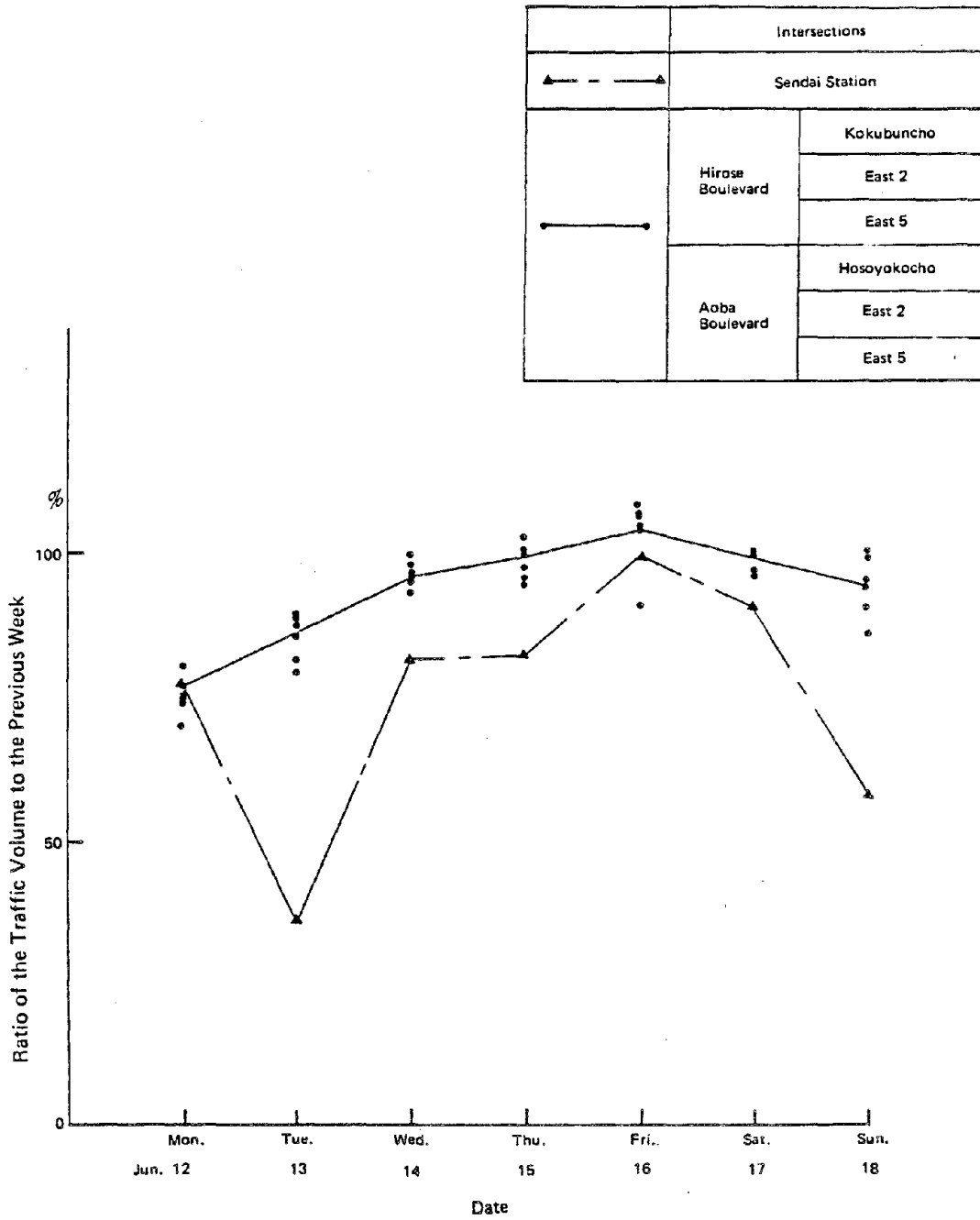


Fig. 5 Transition of the Traffic Volume at Intersections in the Central District of Sendai City in the Miyagiken-oki Earthquake of 1978.

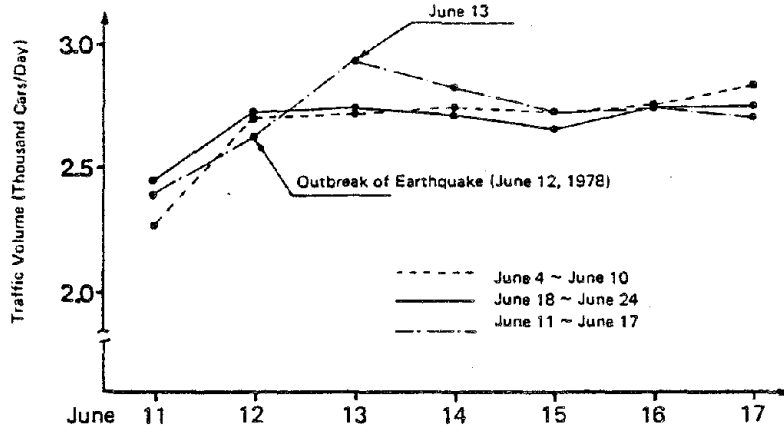


Fig. 6 Transition of the Traffic Volume at Iwanuma of National Highway Route No. 4 in the Miyakiken-oki Earthquake of 1978.

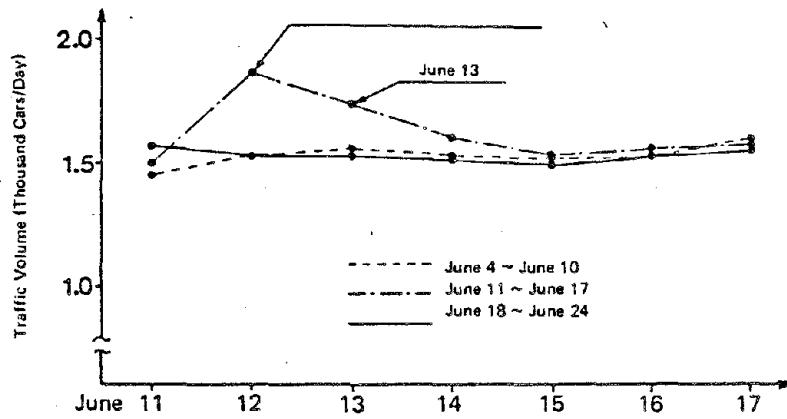


Fig. 7 Transition of the Traffic Volume at Watari of National Highway Route No. 6 in the Miyakiken-oki Earthquake of 1978.

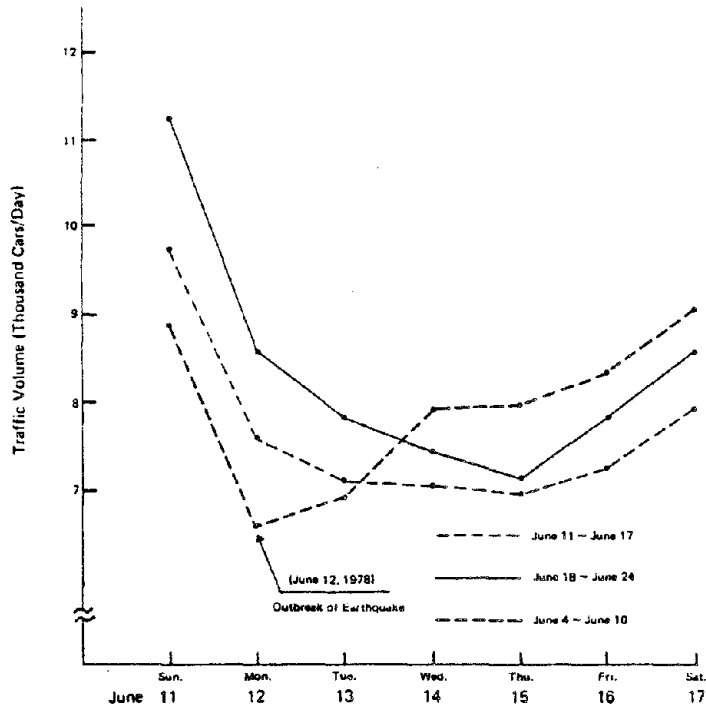


Fig. 8 Transition of Traffic Volume Leading to Sendai in Tohoku Expressway between Sukagawa and Koriyama in the Miyagiken-oki Earthquake of 1978.

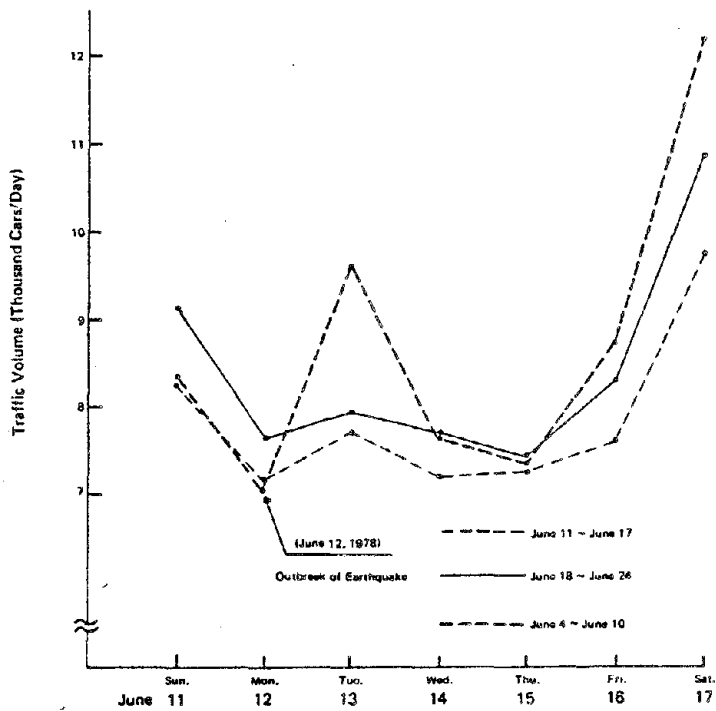
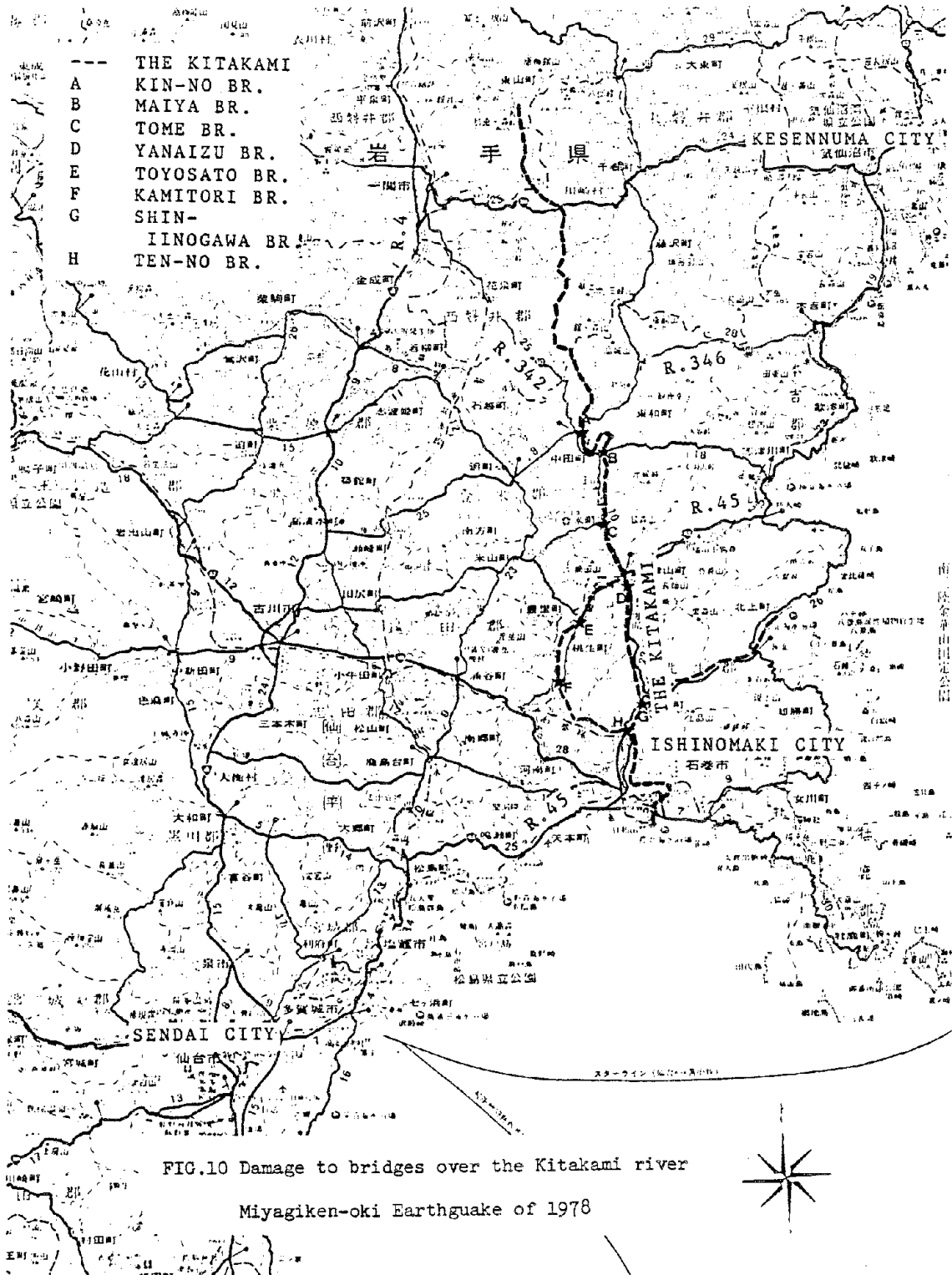


Fig. 9 Transition of Traffic Volume Leading to Tokyo in Tohoku Expressway between Sukagawa and Koriyama in the Miyagiken-oki Earthquake of 1978.



Reproduced from
 best available copy.



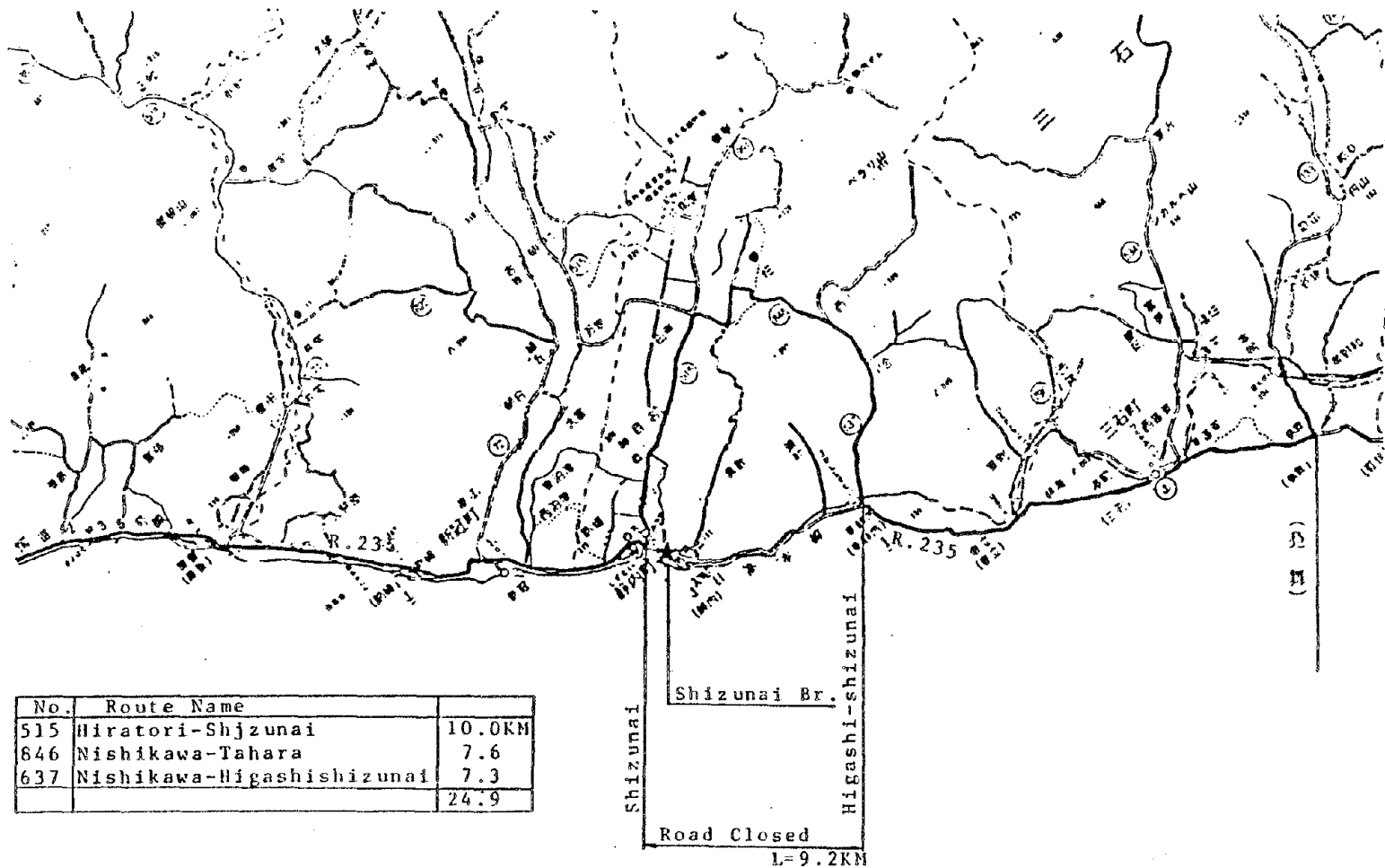


FIG.11 Detour Route in Urakawaoki Earthquake of 1982

DEVELOPMENT OF SEISMIC REPAIR TECHNIQUES FOR
REINFORCED CONCRETE MEMBERS

by

Masaya Hiroosawa^I, Shinsuke Nakata^I, Tetsuo Goto^I,
Manabu Yoshimura^I, Toshio Shiga^{II}
Akenori Shibata^{II} and Hiroshi Imai^{III}

ABSTRACT

In order to inspect and define the grade of damage, seismic loading tests for reinforced concrete columns and shear walls were carried out. Both full-scale and half-scale test specimens were constructed for columns in order to check the scale effects on the grade of damage. The column specimens were designed for three type of modes. The shear wall specimens were designed for flexural failure type. After repairing these members by injecting epoxy resin into cracks and setting epoxy mortar at the exfoliated portions of concrete, the seismic loading tests were again executed in order to evaluate the effectiveness of the repair.

The data of measured crack widths after the seismic loading became effective materials for evaluating the damage grade of reinforced concrete members. Generally, the initial stiffness after repair was a little less than the one before repair. The shear capacity of each specimen of columns and shear walls after repair increased compared with the corresponding value before repair. Consequently, column specimens that failed in shear before repair failed in flexural after repair. The specimen designed for flexural shear failure also had bond splitting failure before repair. After repair work, it did not show such bond splitting. Thus, the epoxy resin improved the bond characteristics.

1. INTRODUCTION

An extensive five-year research project entitled "Post-Earthquake Measures for Buildings and Structures Damaged by Earthquakes" was started from April, 1981 by the Ministry of Construction, Japan. The objective of this project is to develop guidelines for a measuring and inspection method of damaged structures for repair and strengthening methods and for selecting optimum repair and strengthening methods.

In this report, the following items are discussed with respect to the loading tests of each member: the inspection of damage and the evaluation of repair effects by epoxy material on the reinforced concrete columns (half-scale and full-scale) and scale model shear walls. During the initial seismic loading test for each specimen, the damages and the damage situation,

I: Building Research Institute, Ministry of Construction
II: Tohoku University
III: Tsukuba University

the crack patterns and the crack widths were inspected. This inspection was done in each damage grade of the test specimen; slight damage, medium damage and severe damage. After the initial tests, all of the test specimens were repaired by epoxy resin and epoxy mortar. Then the repaired test specimens were retested in the same loading sequence as before repair.

2. EXPERIMENTAL STUDY OF COLUMN ON REPAIR EFFECT

2.1 Outline of the Tests

The details of the test specimens are shown in Fig. 2.1. Three full-scale columns and three half-scale ones were tested. The ratios of shear span, longitudinal reinforcement and shear reinforcement were similar between each full-scale specimen and corresponding half-scale one for three types of failure modes. The dimensions of the half-scale columns are given below. The column section for flexural failure type had dimension of 0.25m x 0.25m and its height is 1.0m. Tensile longitudinal reinforcement ratio ρ_t was 0.64%. The shear reinforcement was 0.26%. The calculated shear capacity P_{mu} at flexural yield was 8.11ton and the value Q_{su} at shear failure was 9.79t. The specimen for flexural shear failure type was a half-scale model of the column of Izumi Senior High School which was damaged by Miyagiken-oki earthquake in 1978. The dimensions of the column are as follows: section, 0.25m x 0.20m; height, 0.825m, shear span ratio a/D , 1.65; tensile reinforcement ratio ρ_t , 0.94%; and shear reinforcement ratio ρ_w , 0.32%. The design shear force P_{mu} at flexural failure was almost the same as the shear failure capacity which is based upon the empirical equation. The dimensions of the shear failure type specimen were as follows: section, 0.25m x 0.25m; height, 0.5m; shear span ratio a/D , 1.0; tensile reinforcement ratio, $\rho_t = 0.64\%$; and shear reinforcement ratio, $\rho_w = 0.26\%$. The calculated shear failure capacity was 89% of the calculated flexural failure capacity.

The compressive strength of concrete which was tested from the concrete cylinder was 210kg f/cm^2 which is higher by 17% than the design strength.

Reinforcing bars (5.5 ϕ , D10 and D13) were tested in accordance with Japan Industrial Standards, similar to ASTM in the U.S.

The yield stresses of 5.5 ϕ (No.2), D10 (No.3) and D13 (No.4) were 4.3ton/ cm^2 (62.4ksi), 4.10ton/ cm^2 (59.5ksi), and 3.2ton/ cm^2 (46.4ksi) respectively. D10 and D13 reinforcing bars showed clear yield plateaus, and 5.5 ϕ bars yielded gradually. The loading apparatus is shown in Fig.2.2. Constant axial load was applied to the column, simulating the gravity load corresponding to the working load condition in the full-scale structure.

The level of axial stress was 20.0kg/cm^2 (290psi) in each specimen.

A 100-ton capacity actuator with $\pm 10\text{cm}$ stroke was used to apply the constant axial load in the column. The load was measured by a 100-ton load cell. An electrical pump with automatic control was used to apply hydraulic pressure in the 100-ton actuator. A 50-ton capacity actuator ($\pm 20\text{cm}$ stroke) were used to displace the columns.

The loading program is also schematically shown in Fig. 2.2. This is controlled by story deformation angle, R which is defined as the measured story displacement, δ_{story} , divided by the inter-story height h .

$$R = \delta_{\text{story}}/h$$

The loading cycle orders before repair are as follows:

$$R = \pm 1/1,000, \pm 1/500, \pm 1/200, \pm 1/100 \text{ and } \pm 1/50$$

After this test program, the remaining story deformation was shifted to zero. Then repair works by epoxy resin were done and the loading program were again conducted which is the same as those before repair adding $R=1/30$.

2.2 Test Results

a) Damage Situation Before Repair

Both full-scale and half scale test specimens showed the following damage situation. In the column top and bottom which were designed for flexural failure, the flexural yield hinges were formed and the concrete crushing occurred.

The specimens designed for shear failure showed many shear cracks and finally exfoliated concrete covering at the center of columns.

The specimen designed for shear flexural failure showed flexural cracks and shear cracks in the first stage. However, the bond cracks along the longitudinal reinforcements has gradually developed, and the bond splitting failure occurred.

b) Test Results After Repair Works

Fig.2.3 shows the damage comparison of full-scale and half-scale columns between the situation before and after repair. Fig.2.4 shows the hysteresis loops of horizontal displacements in each specimen. The solid lines of these loops show before repair and the broken lines show after repair. In the specimens for flexural failure type, the initial stiffness after repair was smaller than those before repair. However, the test value of the flexural yielding strength after repair is eight percent larger than those before repair. These tendencies are shown in both full-scale and half-scale columns.

In the flexural-shear-failure-type columns, the characteristics on stiffness and strength was the same as that of the flexural failure type. The rising ratio of shear capacity after repair was about thirty percent in full-scale and half-scale specimens.

After repair work the columns designed for shear failure did not cause shear collapse, and showed enough ductility. However such a recovery after repair has some differences between full-scale and half-scale specimens.

Fig.2.5 illustrates the rising ratios of shear capacities after repair works in half-scale three test specimens. The specimen designed for shear failure showed the highest rising ratio after repair and the next one is the specimen designed for the flexural shear failure. The flexural failure type specimen showed the smallest rising ratio.

3. EXPERIMENT ON REPAIR EFFECT FOR THE DAMAGED SHEAR WALL

3.1 Outline of the Test Process

In order to discuss repair effects of the shear wall which was designed for flexural failure, cyclic loading tests of scale-model shear walls were conducted. Three test specimens were constructed in the same parameter combinations, and each specimen was tested for each damage grade, i.e. slight, medium and severe damage. After these loading tests they were repaired according to the damage grades. Then the loading tests were again conducted in order to check the repair effects. Test specimens were half-scale models derived from prototype medium rise structures (6 - 8 story).

Fig.3.1 shows the details of the dimensions and arrangements of reinforcements. In order to distribute uniform shear stress into the top beam that was subjected to lateral load by the oil jack, the section of the top beam was designed as a larger section than the prototype section. One face of the shear wall was covered with finishing surface so that the crack width would be measured in the real situation. The design compressive strength (F_c) was planned to be 210 kgf/cm^2 . Test results of concrete material are shown in Table 3.1. Finishing mortar was applied to one face of the shear wall. It was 8mm thick and this work was separated in two steps. In each step the thickness was 4mm. The physical properties of steel reinforcements are listed in Table 3.2. The loading system is shown in Fig.3.2. Two columns connected to the shear wall were subjected to uniform axial force ($F_c/6.0$) through the test by oil jack actuators. Horizontal force was applied at the second floor beam. The shear span ratio of this system is 0.95. Through the loading cycles, a small deviation of the axial forces

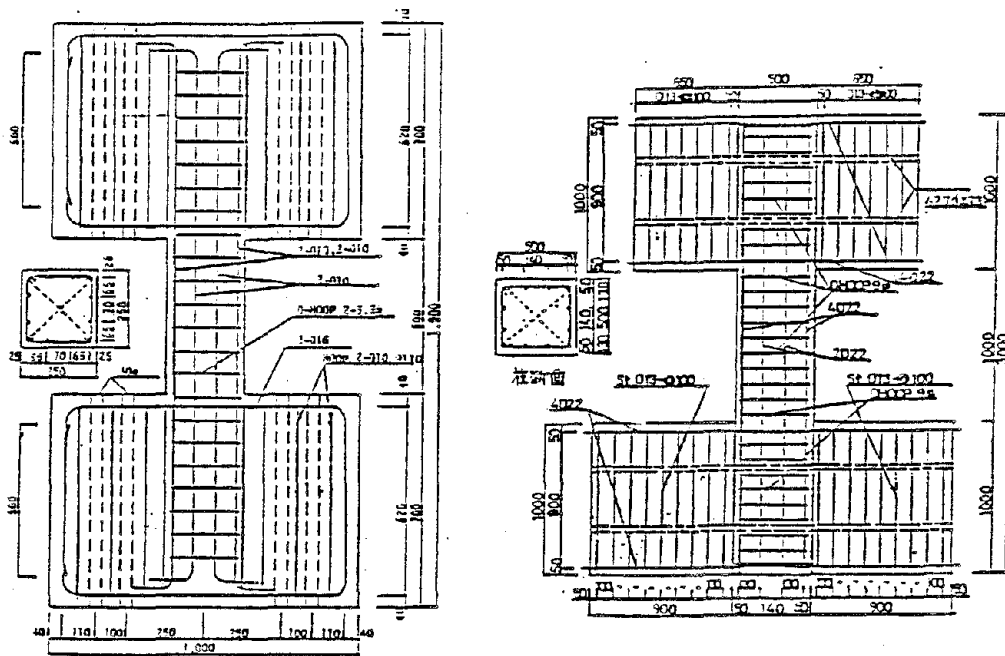
occurred. However it was not controlled. The axial force became thirty percent higher than the designed value at the story drift angle, $R=18/1000$ (first floor). Three specimens were damaged by loading tests to three levels; slight, medium and severe. After repair works for these test specimens, again the cyclic loading tests were conducted. The loading program for each specimen is shown in Fig.3.3. The loading was controlled by the horizontal displacements at the first story.

3.2 Test Results After Repair Works

Fig.3.4 shows the damage comparison between the situation before and after repair. All test specimens showed flexural cracks at first and next shear cracks. Finally flexural yield occurred at the base for each specimen. Cracks were concentrated at the first story. Cracks which occurred after repair works, appeared at uncracked portions before repair. The shear resistance after flexural yield went up about ten percent, however, the numbers of cracks did not change compared to the situation before repair. In the specimen SP-10, the finishing mortar was spalled at the first story drift angle $R_1=8/1000$ rad. In the base of connecting column, the spalling of concrete occurred and the longitudinal reinforcement buckled for its compressive failure at $R_1=10/1000$ rad. Fig.3.5 shows the hysteresis loops of the first story drift for each specimen. The shapes of the hysteresis loops after repair were almost the same as those before repair. The test values of flexural yield strength and maximum strength are a little larger than the calculated values because of the axial force increasing during the test. However, the initial stiffnesses after repair decreased to about 60% to 80% of those before repair. It was considered that such stiffness reduction was based upon the epoxy resin which Young's modulus is one tenth of the value of concrete. Fig. 3.6 shows the envelope curves of positive side story drift. This figure contains the original loading data (before repair) and those after repair. The original curves show the clear point where the stiffness changes magnificently. Those curves after repair do not show such a point, and the stiffness changes gradually. After releasing the load attachment, free vibration tests were conducted. The measured natural period of the original specimen were two to four times longer than the one before damage. It's value after repair work remained two times that of the natural period of the virgin test specimen.

3.3 Conclusion

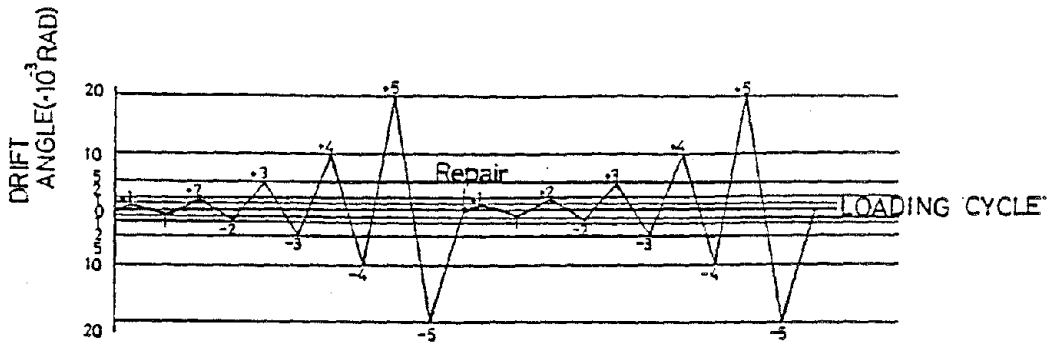
Through these experimental studies, the following basic data were summarized: Hysteresis loops of flexural-failure-type shear walls, judgement of damage criteria and guidelines for repair design. Even if structures are damaged severely due to earthquakes, their strength, stiffness and deformability can be recovered by epoxy resin repair work.



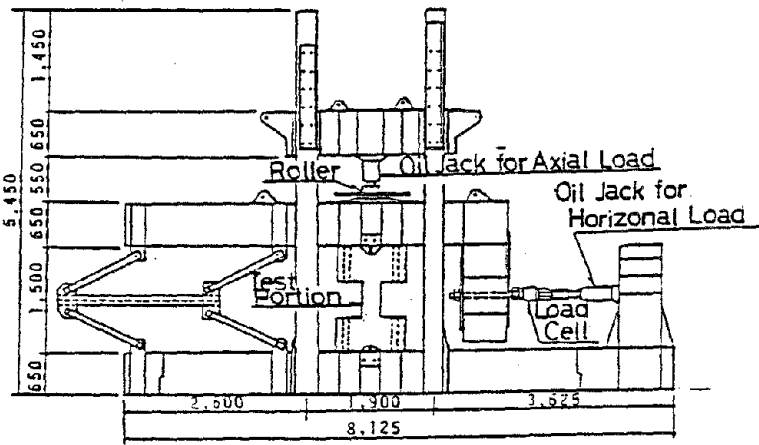
Dimensions of Test Specimens

	UNITS	B-SPECIMEN	BS-SPECIMEN	S-SPECIMEN	
$b = D$	cm × cm	25 × 25	20 × 25	25 × 25	
A	cm ²	625	500	625	
h	cm	100	82.5	50	
Longitudinal Reinforcement		4-Ø13, 3-Ø10	8-Ø13, 5-Ø10	4-Ø13, 3-Ø10	
	A_g	cm ²	10.78	14.44	10.78
	P_g	%	1.72	2.39	1.72
Longitudinal Reinforcement for Tension		2-Ø13, 2-Ø10	2-Ø13, 3-Ø10	2-Ø13, 2-Ø10	
	A_t	cm ²	3.97	4.68	3.97
	P_t	%	0.64	0.94	0.64
Hoop		2-5.5 @ Ø75	2-5.5 @ Ø75	2-5.5 @ Ø75	
	A_w	cm ²	0.48	0.48	0.48
	P_w	%	0.256	0.32	0.256
Axial Force	kg	12500	10000	12500	

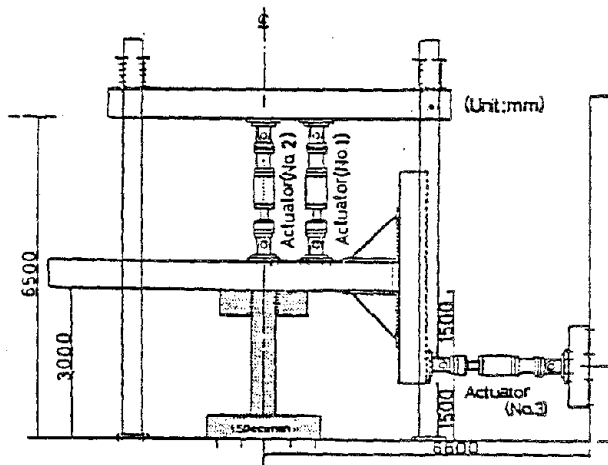
Fig.2.1 Details of Test Specimens



Loading Program



LOADING APPARATUS FOR HALF SCALE SPECIMEN



LOADING APPARATUS FOR FULL SCALE SPECIMEN

Fig.2.2 Loading System and Loading Program

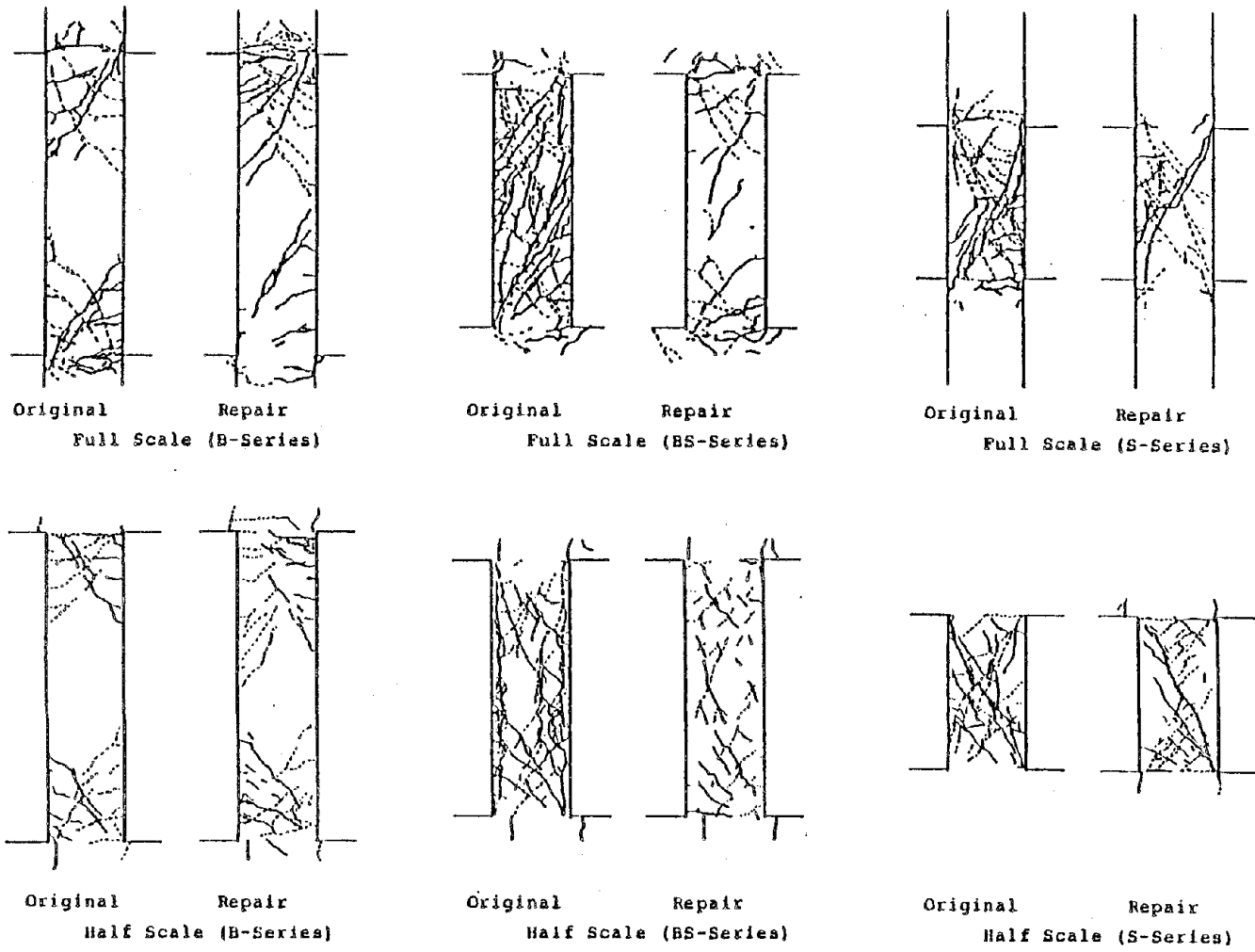


Fig.2.3 Comparison of Damage Situation

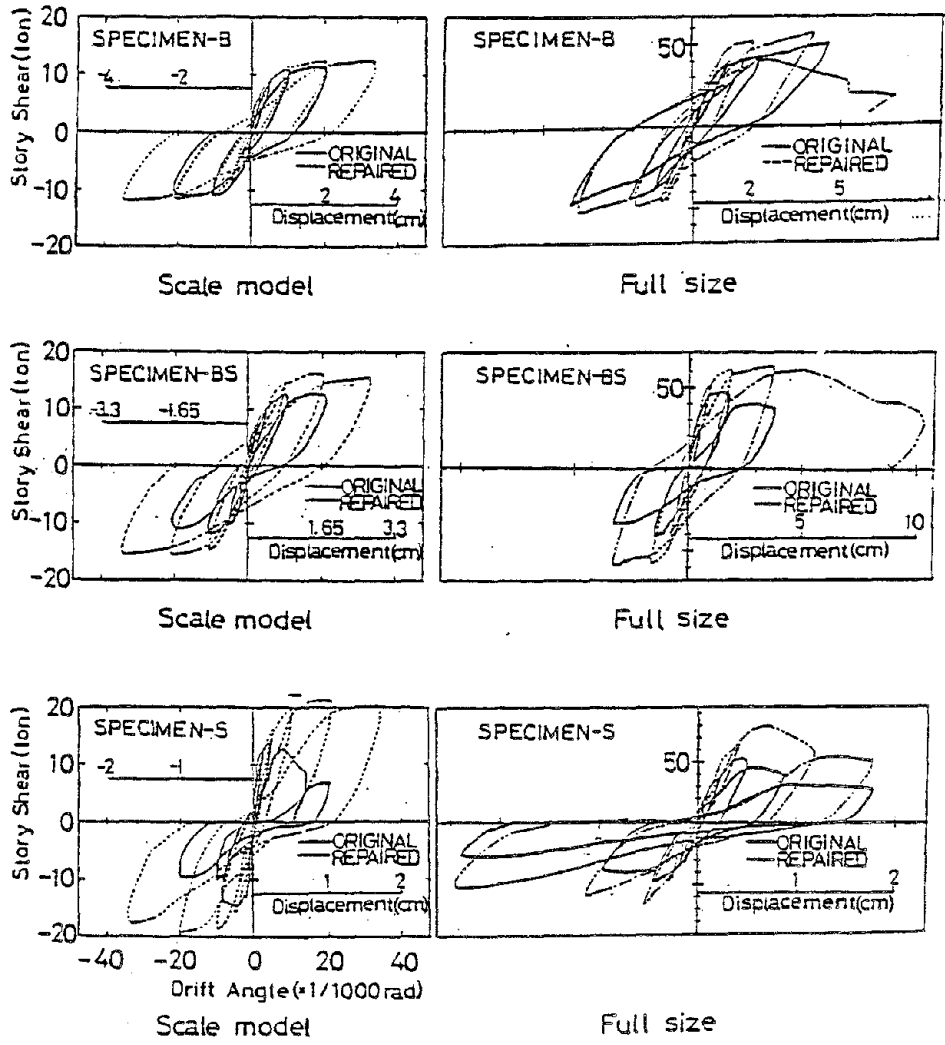


Fig.2.4 Hysteresis Loops of Story Displacements

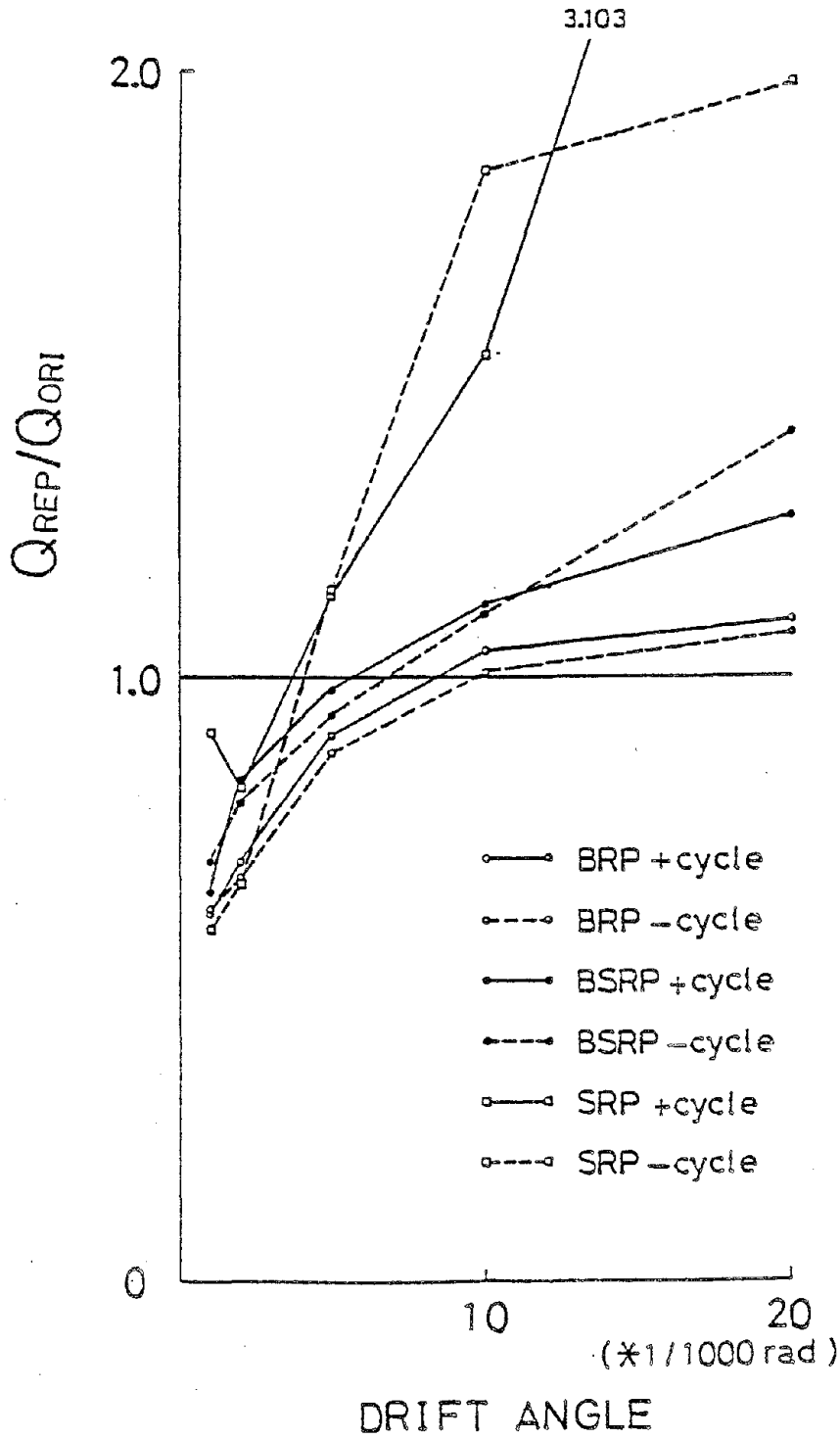
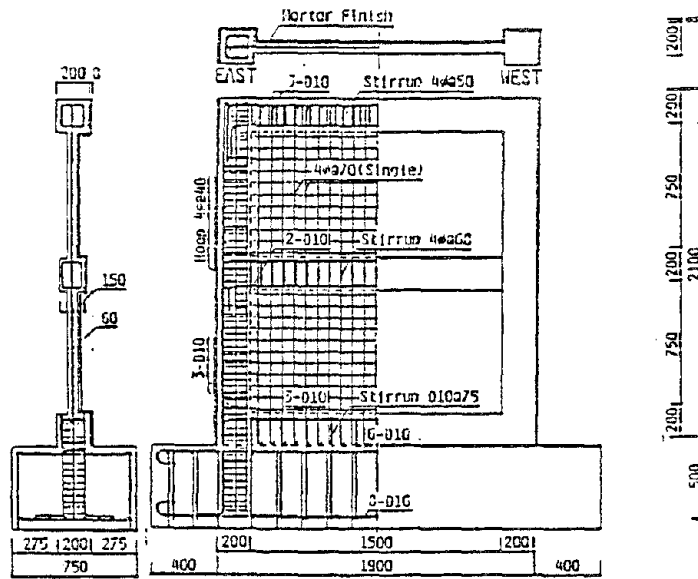


Fig.2.5 Strength Rising Ratio (After Repair/Before Repair)



Classification	Arrangement	Reinforcement Ratio (%)	
Column	8-D10	1.43	
Beam	1st Story	4-D10	0.95
	2nd Story	5-D10	1.09
Roop	4#440	0.31	
Str.	1st Story	4#468	0.24
	2nd Story	4#450	0.25
Wall	4#470	0.30	

Fig. 3.1 Details of Test Specimens

Table 3.1 Physical Properties of Concrete

Specimen	F_c (kg/cm ²)	F_{sp} (kg/cm ²)	$E_{1/3}$ (x10 ⁵ kg/cm ²)
SP-1	189	14.8	—
SP-2	201	14.9	1.96
SP-3	196	16.4	2.10
Ave.	195	15.4	2.03

 F_c : Compressive Strength F_{sp} : Splitting Strength $E_{1/3}$: Secant Modulus at One-third Compressive Strength

Table 3.2 Physical Properties of Reinforcements

Specimen	Sectional Area (cm ²)	Yield Stress (kg/cm ²)	Maximum Stress (kg/cm ²)	Elongation (%)
D10	0.71	3747	5408	26.4
4φ	0.13	1976	3109	45.3

Standard of Reinforcing Bar : D10 - SD30

4φ - Annealing Steel Bar
(corresponding to SR24)

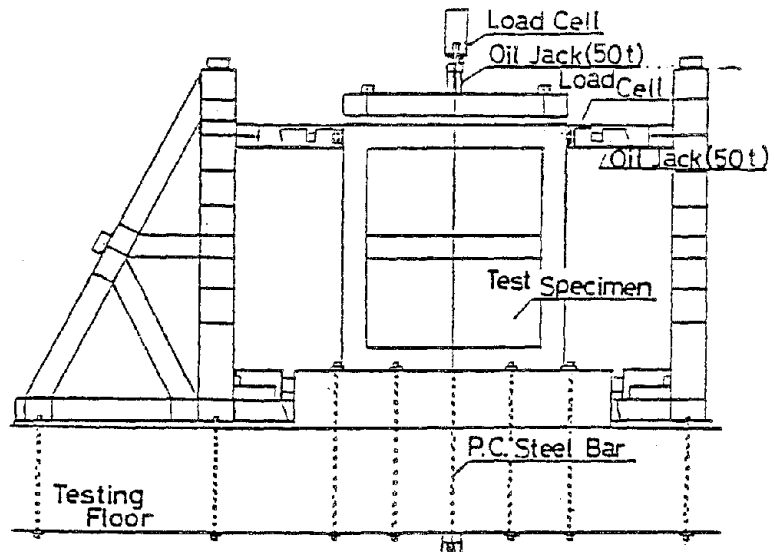


Fig.3.2 Loading System

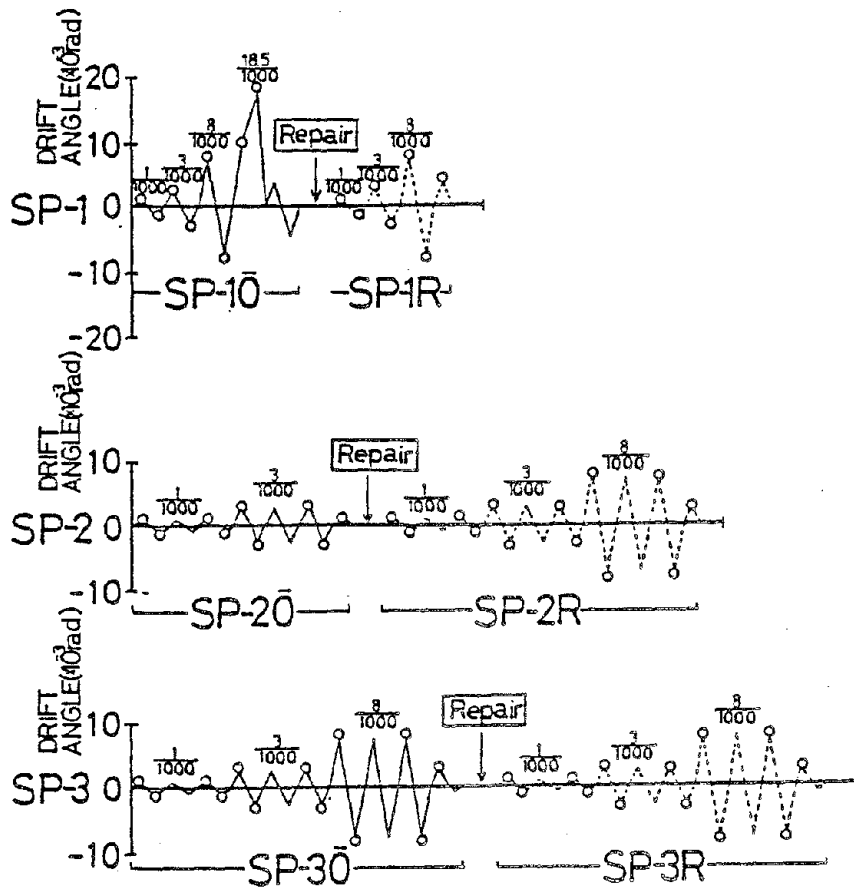


Fig.3.3 Loading Program

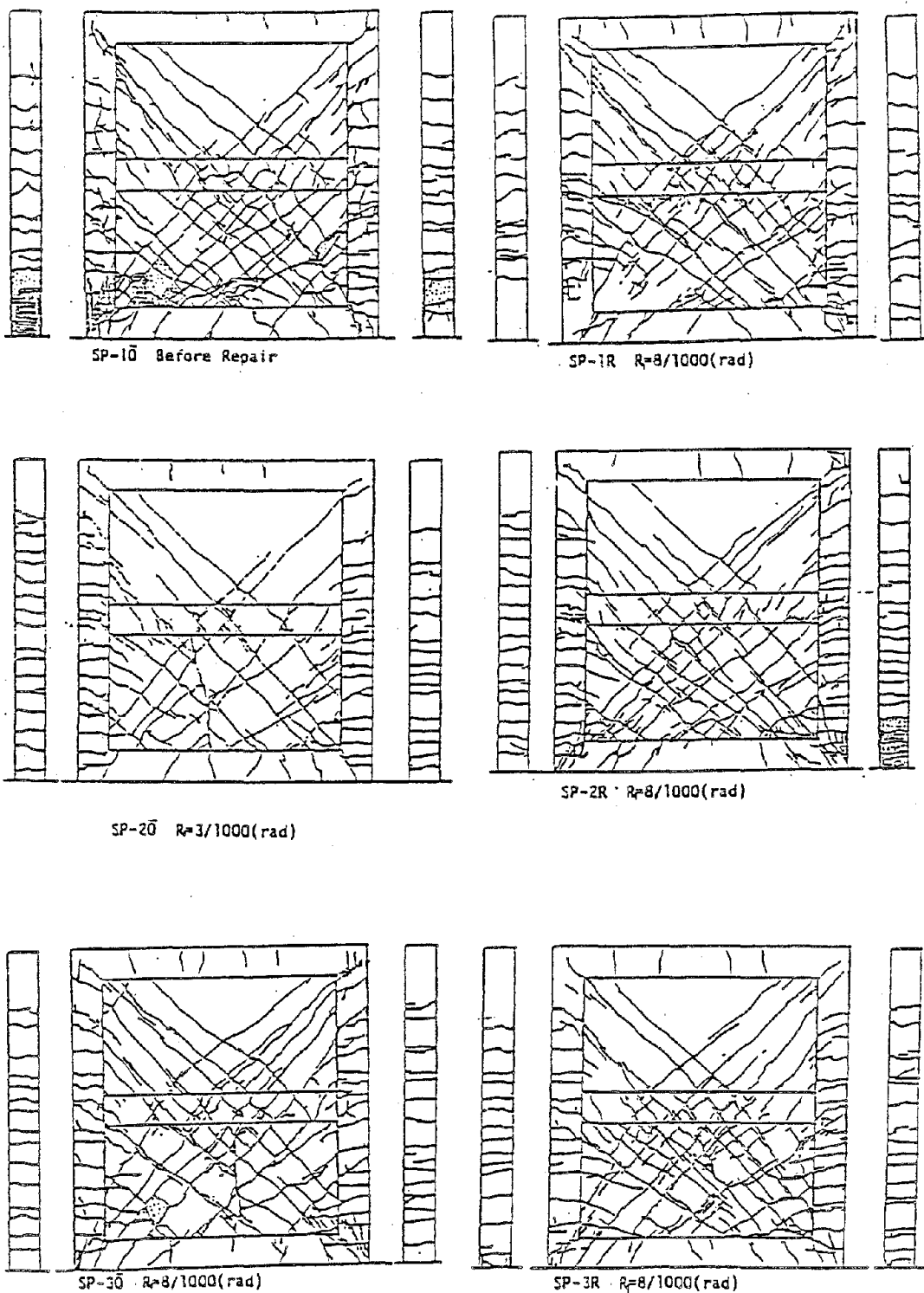


Fig. 3.4 Crack Patterns of Test Specimens

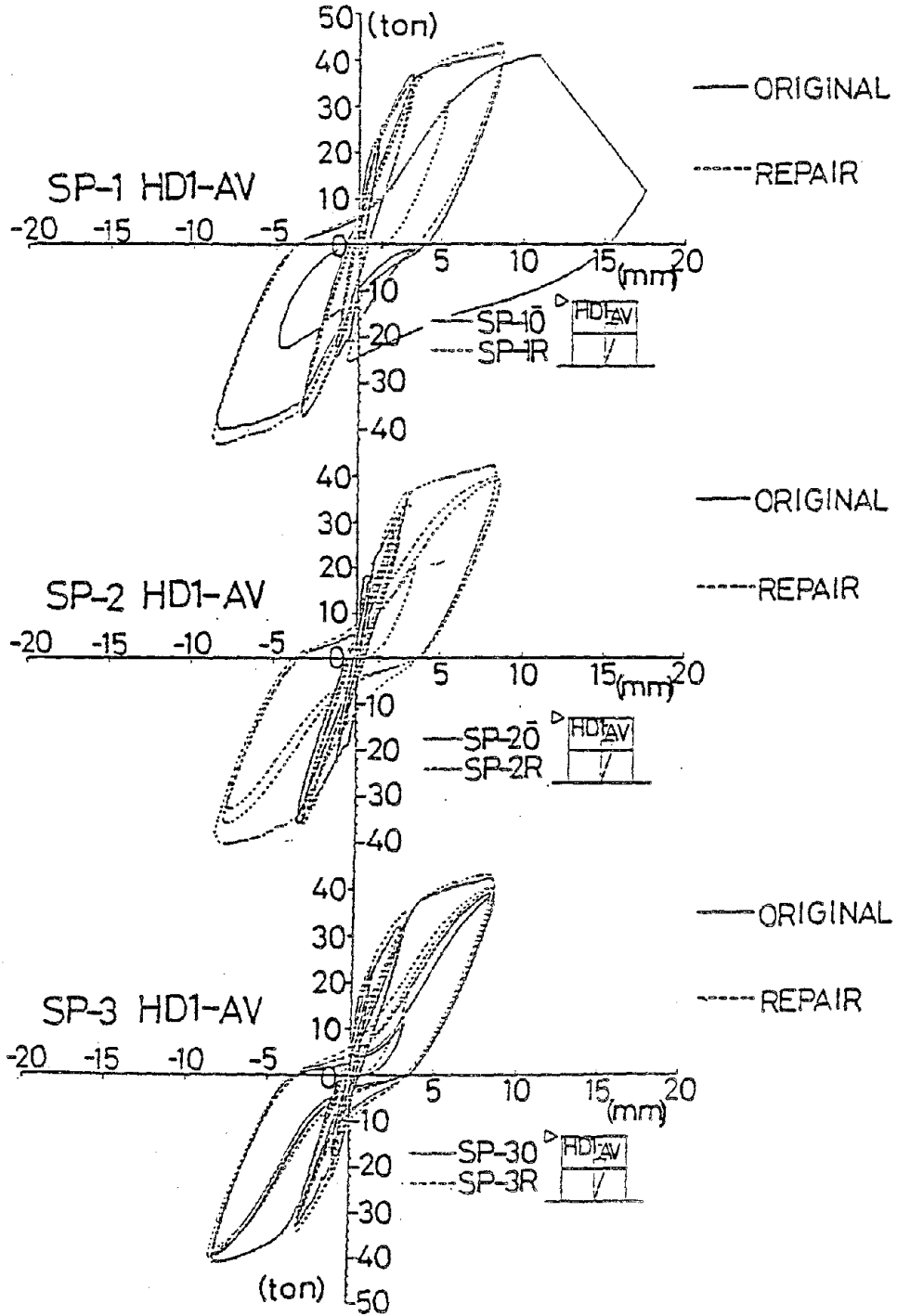


Fig.3.5 Load-Deflection Curves at First Story

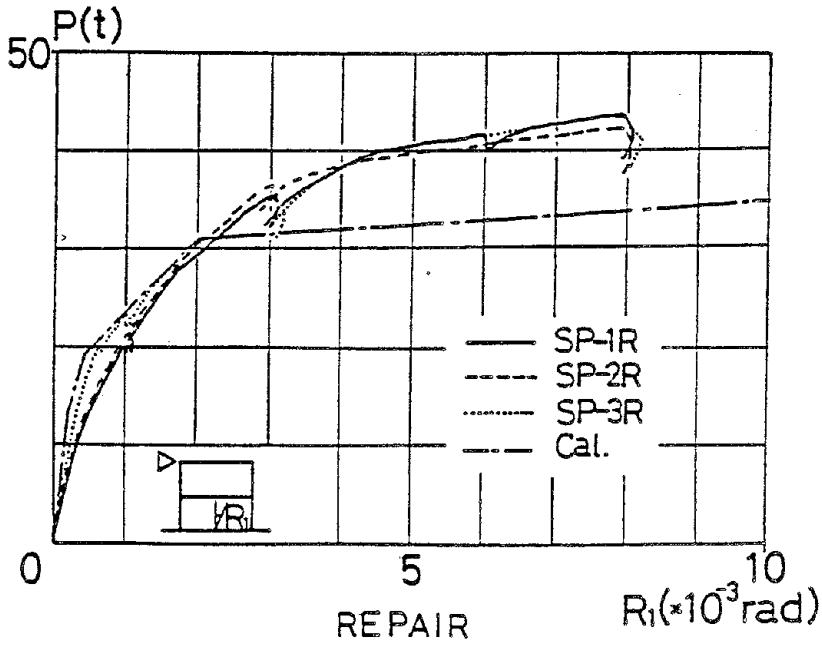
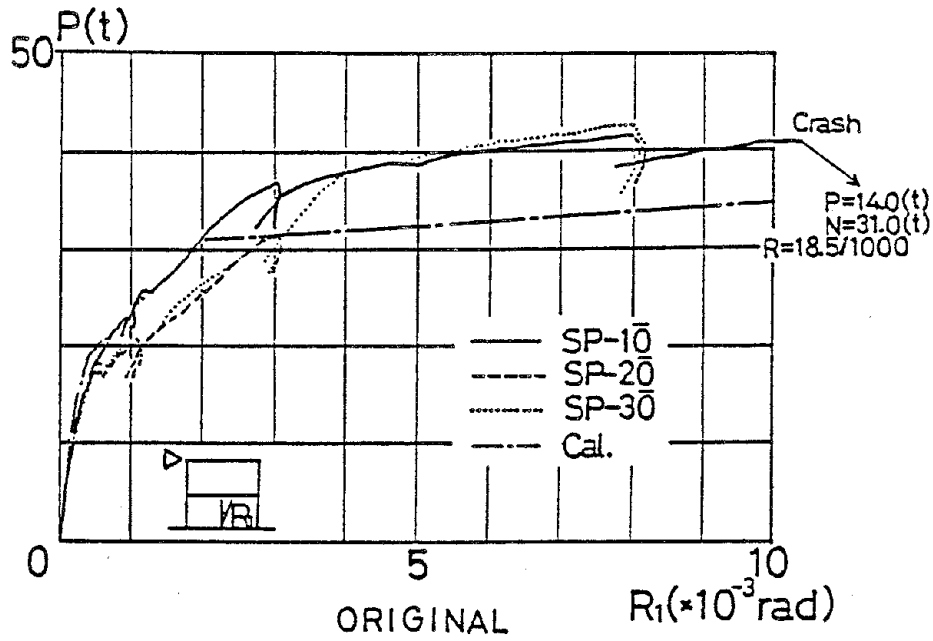


Fig.3.6 Envelope Curves of Horizontal Displacements

DEVELOPMENT OF RETROFIT GUIDELINES
FOR HIGHWAY BRIDGES

James D. Cooper
Federal Highway Administration
Washington, D. C.

Richard V. Nutt
Ronald L. Mayes
Applied Technology Council
Berkeley, California

ABSTRACT

Much recent attention has been given to the development of seismic design guidelines for highway bridges. Unfortunately most existing bridges in the United States have not been designed to resist potentially devastating earthquake induced ground motion. Those existing bridges designed by then state-of-the-art seismic design methods have weaknesses which may require strengthening or retrofitting to reduce the susceptibility to seismically induced damage. Although limited retrofit information is available in the literature, a concerted effort is being made to develop general retrofit guidelines applicable for use in the United States.

This paper highlights vulnerable details associated with existing bridges and presents general retrofit concepts developed to date. A summary of retrofit philosophies developed by several organizations is presented. Finally, issues which must be resolved and will form the basis for the development of retrofit guidelines for existing highway bridges are discussed.

INTRODUCTION

Significant earthquake engineering research has been initiated by many organizations during the past three decades. Structural analyses, designs, building codes, and specifications have been refined and updated to provide the engineer with the necessary tools to design and construct modern buildings to resist the forces developed during periods of strong earthquakes. While research had been conducted to better understand building performance, little research had been conducted in the United States prior to the 1971 San Fernando earthquake to insure the satisfactory seismic performance of highway structures. Since 1971, researchers have focused their attention on the conduct of studies to improve the seismic resistance of both new and existing highway bridges.

The highway network is a vast, sprawling, existing system which forms necessary and vital links between cities and towns across the country. The interstate system of roads extends approximately 41,000 miles and has about 47,000 bridges in the network. Added to that is another 89,000 bridges on the primary system. With very few exceptions, existing highway bridges in the United States have not been designed to resist motions and forces that may be generated by the occurrence of earthquakes in the surrounding areas. As a result, many bridges may be expected to fail in some major way during their remaining life if subjected to strong motion seismic loads. Obviously, the exposure of the network of roads and bridges to seismic hazards varies greatly across the country. Specifically, bridges form the critical links in the road network and are most susceptible to seismic induced damage. They also represent the greatest economic risk if destroyed or damaged.

Two approaches can be taken to improve the seismic resistance of the highway network. One approach requires an investment of time to upgrade seismic resistance while the other requires large sums of money. First, design standards can be upgraded as more knowledge is gained about the response of these specialized transportation structures to seismic activity. New standards can be applied as older bridges are removed from service because they are either structurally unsound or functionally obsolete. This approach, although time consuming, is economically feasible and should be pursued.

The second approach involves identifying those existing bridges which are important to the network and are susceptible to significant damage or collapse in the event of an earthquake. Those structures could be strengthened or retrofit to enhance their response to seismic activity. This approach might prove quite costly and consequently economically infeasible.

What is required is a balanced approach to harden the highway system against seismic attack. This can be accomplished by upgrading those structures which form critically vital links in the network and are vulnerable to damage while at the same time imposing new seismic design standards on bridges which are being replaced.

Specifically this summary paper is intended to focus on the proposed development of a set of retrofit guidelines for use on highway bridges. Vulnerable bridge details are identified. Retrofit concepts previously developed are highlighted and are available in other reports and publications listed in the references. Published retrofit philosophies developed and used by several organizations and countries are summarized.

VULNERABLE DETAILS

Site investigation following earthquakes which cause structural damage and failure has become a necessity to gain insight into failure modes of highway bridges. Based on past earthquake damage investigation and analysis, rational retrofit procedures have and can be developed to insure the structural integrity of the highway system during periods of ground motion. Investigation of numerous earthquakes has pointed to the following general types of damage that most often occur to bridges during seismic attack.

- . displacement and tilting of piers
- . displacement, cracking and dislodging of superstructure girders
- . displacement, settlement and tilting of abutments
- . concrete crushing at the supports
- . bearing anchor bolt pullout or shearing deformations
- . settlement, sliding and tilting of wingwalls
- . bearing instability and failure
- . expansion joint damage
- . settlement of approach slabs

The general types of damage to conventional bridges to be expected in future earthquakes can be grouped into two categories which lead to bridge failure. They are substructure failures (column, pier, or abutment) which lead to loss of support capacity, and superstructure collapse due to excessive relative motion at supports. Both types of failure result from the types of damage documented above. Structural failure and damage to bridges may also be caused by inadequate foundation strength or load-bearing degradation during the course of seismic loading. Soil liquefaction is an example of this failure mode.

Specific retrofit details have been developed based on the observed failure modes mentioned above. Specific details are available in other reports but general concepts developed to date are presented below.

RETROFIT CONCEPTS

Specific retrofit concepts must be based on feasibility and practicality. It is important to emphasize that seismic and structural considerations are not the only ones that need to be considered in the overall bridge retrofit decision process. Other decision factors entering the process are the importance of the bridge to the given locality based on the type of highway, traffic volume and accessibility of other crossings, and replacement or repair costs based on estimated damage including lost time.

A brief summary of some retrofit measures are given below.

Restrict longitudinal, vertical, and lateral relative displacements of the superstructure at expansion joints and bearing seats, by means of cables, tie bars, shear keys, extra anchor bolts, or metal stoppers.

Restrict rigid body motion of the superstructure by connecting it with high strength steel cables to a supporting or an adjacent foundation or pier cap, enlarging bearing areas, or placing stoppers at edges of bearing areas.

Reduce induced vibrations by installation of energy absorbing devices such as elastomeric bearing pads at bearing seats, or adaptation of a "shock absorber" type of damper which allows slow movement such as displacement due to creep, shrinkage, and temperature change with negligible resistance but develops a large resistance in the event of a rapid displacement.

Strengthen substructure elements such as increasing the strength of an existing column by adding longitudinal and spiral reinforcement to the exterior of the columns, then bonding the added reinforcement with a new layer of high strength concrete using pressure grouting procedures and/or gunite. The added longitudinal reinforcement could also be extended into the cap and the footing thus increasing the flexural strength of the column-to-cap and column-to-footing connections. There are many variations in detail when actually implementing the retrofit concepts identified above. The designer must be given general guidelines to adapt the concepts to the specific structure in question.

SUMMARY OF

BRIDGE SEISMIC RETROFIT PHILOSOPHIES AND EXPERIENCE

There is a very limited amount of published material available that is directed specifically toward the problem of seismic retrofitting of bridges. The California Department of Transportation (CalTrans) has been a leader in the area of bridge retrofitting and is the only State to carry out an extensive construction program. The IIT Research Institute has conducted research on bridge retrofitting for the Federal Highway Administration and two countries, Japan and New Zealand, have published material describing their approaches to the retrofit problem. The following paragraphs summarize the philosophies of each of these four organizations and countries.

California Department of Transportation

Following the 1971 San Fernando earthquake, CalTrans undertook a program to strengthen seismically deficient bridges. Many structures were deficient and it was not economically feasible to strengthen all of them to new design standards. Efforts were directed toward the most cost effective retrofit concepts. These retrofit concepts consisted of elastic restrainers designed to prevent separation of the sections of a bridge structure at the expansion joints. These restrainers were relatively inexpensive and prevented failure by reducing the chances of support loss at the expansion joints and by distributing forces more uniformly to the columns.

In selecting bridges for retrofitting, a prioritizing system was developed, but final retrofitting decisions relied heavily on engineering judgment. Initially structures on major lifeline routes within densely populated areas were strengthened. Second to be retrofit were those less critical structures located within the same densely populated areas. Finally, those seismically deficient bridges in less populated areas will be retrofitted.

Restrainers are designed to resist a minimum force level based on the weight of the lightest member being restrained. Higher force levels are used if predicted by a dynamic analysis. In many cases several dynamic analyses are performed with different parameters and the results tempered with judgment to obtain the correct design forces. Physical tests were performed to determine the capacity of the restrainers most commonly used by CalTrans.

Column retrofitting to increase available ductility is being considered by CalTrans although no construction has taken place. The schemes under consideration are designed to increase concrete confinement in the area of plastic hinges. Inadequate bond length of main reinforcement is also a problem with some CalTrans structures. Details have been developed but have not been implemented.

IIT RESEARCH INSTITUTE

The Illinois Institute of Technology Research Institute conducted a study on bridge retrofitting for the Federal Highway Administration. In this study three steps of the bridge retrofit decision process were identified and studied. These steps include:

1. A determination of the susceptibility of the existing bridge to a critical failure resulting from an earthquake loading.
2. A determination of the level of importance of the bridge to the given locality.
3. A determination of the type of retrofit measures to employ.

To determine the relative degree of vulnerability of a bridge to failure, preliminary assessment of critical structural factors is proposed. Bridges

which have a predetermined structural factor value require further analysis to more accurately establish their vulnerability. A simplified analysis method was developed and subsequently modified during the course of the project. This method reduces a bridge to an equivalent single degree of freedom system. Limit states are defined which represent catastrophic failure so that the results of this analysis can be systematically interpreted to establish the vulnerability of the structure.

A method was developed for establishing the criticality or importance of a bridge. A numerical value is assigned to each bridge to reflect its relative importance in terms of administration/transportation systems effects; social/survival effects; security/defense effects; and economic/personal effects. The criticality of a bridge is compared with its structural integrity to determine if the bridge warrants retrofitting.

In determining the type of retrofit measures to be used, the type of failure modes and damage experienced by highway bridges in previous earthquakes was considered. Failures are categorized as either loss of substructure strength and/or stability of excessive relative movement at the bearings. Eight retrofit measures were identified. The analytical determination of forces to be used in the design of these retrofit measures was not covered in the study. In an actual design it was proposed that these forces be determined from a seismic analysis.

JAPAN

The Japanese propose a probabilistic approach to the design of retrofit measures. Bridges are selected for retrofitting based on physical and socio-economic conditions relating to the bridge. It is proposed that these bridges be strengthened to have a reasonably small probability of failure but not to the extent that costs become excessive.

To determine the probability of failure the structural resistance is assumed to be totally deterministic (i.e. there is no variation in dimension or material properties that could cause a probable distribution of resistance levels). Resistance is assumed to deteriorate at a known rate with the increased age of the structure. Therefore, at any point in time, the probability of failure depends only on the probability of a seismic loading that will exceed the resistance level.

Excessive costs will result if retrofit design is based on force levels and failure probability used for new bridges. Therefore, it is proposed to use force levels which will result in a probability of failure consistent with the remaining service life of the structure.

NEW ZEALAND

The draft New Zealand Seismic Design Code for Bridges has a section on the strengthening of existing bridges for seismic loads. This section states that the need for seismic retrofitting should be established by comparing the seismic risk with other risks by any one of several techniques such as a cost-benefit analysis.

The importance of a bridge is established and retrofitting priorities set by considering several socio/economic factors relating to the bridge. New Zealand design force levels are described elsewhere in the code and are dependent on an earthquake return period based on the structure life and importance. The design force levels for retrofitting existing bridges are determined in the same manner as for new bridges except that the remaining economic life is used in place of the new structure life.

Design for smaller force levels are allowed if it is not cost effective to strengthen the structure to the full force level. Designers are cautioned to be aware of the overall behavior of the structure during an earthquake and the effect strengthening measures might have.

Retrofit measures should conform to the same principles of capacity design used for new structures. Design details are not specified, but the designer is instructed to select appropriate details after an adequate site inspection, review of the design calculations and construction drawings, and an analysis. Certain methods used to retrofit bridges are summarized.

DEVELOPMENT OF RETROFIT GUIDELINES

The existing highway system has many bridges which either have not been designed to resist earthquake induced ground motion or have been designed by older, inadequate seismic design standards. Thus it is necessary to focus attention on the seismic protection of those existing structures which are known to be vulnerable to seismic attack. To accomplish that objective, the Federal Highway Administration awarded a contract to the Applied Technology

Council (ATC) to develop seismic retrofitting guidelines for highway bridges. Representative segments of the bridge design and construction profession form a Project Engineering Panel (PEP), Appendix A, and are participating in the development of the guidelines.

Seven issues have been raised by the ATC staff and are to be considered by the PEP to define the scope and general format of the proposed retrofit guidelines. Summaries of the seven issues follow. They include a question followed by a brief discussion of the issue. Answers to the questions have not been finalized and are presented herein for the purpose of stimulating additional thought and discussion. Undoubtedly additional issues will be raised throughout the development of the guidelines.

ISSUE 1 - What aspects of the bridge retrofit problem should be addressed by the guidelines?

The bridge retrofitting problem can be divided into two major areas of concern. The first deals with the evaluation of the seismic resistance of existing bridges and the selection of bridges to be retrofitted. Since it may not be economically feasible to retrofit all seismically deficient bridges to provide earthquake resistance equivalent to new bridges, the selection process is important if the best use of resources is to be realized. The second major area of concern is the design of improvements to increase the seismic resistance of bridges. Because many possible methods of retrofitting are unproven or excessively expensive, partial strengthening should be considered. Selection of the appropriate levels of seismic performance for partially strengthened bridges may depend on the evaluation of the existing bridge. Therefore, it may be difficult to write guidelines that adequately address the design of retrofit measures without including some method of bridge seismic evaluation.

ISSUE 2 - What should be included in the guidelines in relation to the evaluation of existing bridges?

The proper evaluation of the seismic resistance of a bridge depends on the availability of accurate information about the characteristics of the bridge, its location, and seismic exposure. Certain information will be required if a specific evaluation system is to be used. It would be appropriate if the guidelines were to specify the type of information required.

Because a large number of bridges exist in the highway systems of some jurisdictions, it is impractical to perform a thorough investigation, including dynamic analysis, of all bridges in that system. A preliminary screening method is needed to select only the bridges which have the highest potential for failure during an earthquake. A method of performing preliminary screening has been used by CalTrans in their retrofit program. An alternate approach has also been recommended by IIT Research Institute as a part of their investigation of the bridge retrofit problem. A method of utilizing concepts developed by ATC to accomplish the preliminary screening could use the seismic performance category of the bridge to establish importance and seismicity plus the characteristics of structural deficiency developed by CalTrans or IIT Research Institute.

A method of quantitatively rating the seismic hazard of existing bridges could be used as the basis for a benefit to cost analysis for establishing final retrofit priorities or for determining the merits of retrofitting a given bridge to various levels of seismic resistance. In addition, the rating system could provide a method for considering the remaining life of a bridge. One possible rating system would first require an analysis to be performed to determine the effective peak acceleration of a damaging earthquake. The probability of an earthquake of this magnitude occurring at the bridge site within the remaining life of the structure could be obtained from peak acceleration maps and probabilistic relationships already developed. The importance of the bridge would be established in terms of a lifeline classification taken from a table similar to a method used to establish the occupancy potential of existing buildings in ATC-3-06 (Tentative Provisions for the Development of Seismic Regulations for Buildings). By multiplying the probability of a damaging earthquake by the lifeline classification, the relative seismic hazard rating of the bridge is obtained. This rating can then be used to make retrofitting decisions.

ISSUE 3 - What type of retrofit concepts should be addressed by the guidelines?

Although many retrofit concepts have been presented in the literature, virtually all retrofit construction to date has dealt with providing elastic restraint at bearings to prevent instability or loss of support. Such restraint also tends to distribute seismic forces in the columns more uniformly, and can thus prevent column failures. Restraint of this type can be a cost-effective method of retrofitting.

Column retrofitting requires complicated details, involves difficult construction procedures, and the relative effectiveness of various retrofit concepts has not been demonstrated by physical testing. Small-scale physical tests of a column retrofit concept using steel banding to increase concrete confinement has demonstrated an increased available ductility but may prove less effective on full-scale bridge columns. Increasing column yield levels for moment may overload the foundation or cause serious column shear failures thus resulting in more harm than good. It would appear that not enough is known at this time to gauge the effectiveness of column retrofitting concepts.

Special energy dissipating bearings and other similar devices have been used extensively in New Zealand and Japan but are virtually nonexistent in the United States. One of the primary reasons for this is the lack of availability of analytical tools to determine the response of structures fitted with these devices. If the analytical tools are made available, the use of these special devices could open up a whole new area in seismic resistant bridge design.

ISSUE 4 - What type of analysis procedures should be used for evaluation and/or design?

To date, retrofitting of existing bridges has consisted mostly of fitting expansion joints with elastic restrainers to prevent separation and loss of support at these joints. The primary modes of vibration that can cause this type of failure are longitudinal and include both in-phase and out-of-phase vibration of adjacent sections of the bridge. The analysis procedures do not consider different ground motions at various supports or the rotation of the columns due to surface wave effects. Little research information is currently available at this time, but approximate analyses are available.

The use of special energy-dissipating and isolating bearings has great potential in the retrofitting of deficient bridges. These devices, in many cases, rely on their nonlinear behavior to modify the forces and displacements in the bridge. Many of these effects may be difficult to determine with an elastic analysis. Nonlinear analysis computer programs are available, but are difficult and expensive to use. To overcome the need for nonlinear analysis the New Zealand Ministry of Works and Development has developed design charts.

ISSUE 5 - What method of design and evaluation should be specified in the retrofit guidelines?

Seismic design guidelines developed by ATC allow both load factor and working stress methods for design. In evaluating existing structures, however, the ultimate strength of the structure is the principal concern. By using an ultimate strength approach, a more reliable evaluation of the relative danger of structural collapse can be made.

In evaluating existing structures it will be necessary to define the limit states which will represent loss of support or serious structural damage. In the case of structures with substandard confinement in the columns, for example, it will be necessary to account for the reduced available ductility. At bearings, where excessive movement can result in loss of support, a method of accounting for effects such as nonuniform support motion that are not considered in the analysis should be included. The newly developed ATC guidelines use a minimum support length concept based on superstructure length and column height to account for unknown displacement effects. This concept may be inappropriate for evaluating existing bridges. The use of special analysis methods or response modification factors to account for increased displacements and reduced available ductilities may be the best way to approach the problem.

ISSUE 6 - How shall the guidelines address the design of specific seismic strengthening measures?

The design of retrofit measures has problems similar to the design of any type of modification to an existing structure. The designer is restricted in what he can economically accomplish by the characteristics of the existing bridge. In addition, he must be aware of the effect any construction will have on the normal operation of the bridge. To a certain degree, each retrofitting design is unique. Standardization of details can be accomplished only to the extent that the original structural details are standardized. Some standardization has been possible in California, for example, in the design of retrofit measures for intermediate expansion joints in concrete bridges.

Presentation of details, whether standardized or not, is useful since it provides the bridge designer concepts to which simple modifications may be possible.

It is necessary that the designer be given criteria on which to base his design. In the case of expansion joint restrainers, for example, there may be a trade-off between force in the restrainer and displacement of the joint. Allowable capacities should be specified in the guidelines. Since the design of certain retrofit measures may involve a trial-and-error solution, a preliminary design procedure would also be helpful to obtain a realistic first try.

ISSUE 7 - What force levels should be used for the design of retrofit measures?

Based on seismic design guidelines developed by ATC, new structures are designed to resist force levels that have a 10% chance of occurring in 50 years, the assumed economic life of the new structure. Retrofit measures could be designed to resist the same force levels as new structures, but if the remaining useful life of the existing structure is less than 50 years, then the probability of the structure being subjected to these loads is less than that of a new structure. To design the retrofit measures based on equal probability of failure requires that a reduced force level be used for structures with remaining lives of less than 50 years.

From an economic point of view, designing to a specified force level may not be cost effective. For example, in the case of expansion joint restrainers, very little additional cost may be required to increase the capacity of the restrainers to new design standards. On the other hand, there may be a practical limit as to how much additional earthquake resistance expansion joint restrainers can provide. To require design to standards for new structures, or even to a force level based on an equivalent probability of failure may require column strengthening which can have a much smaller benefit-to-cost ratio than joint restrainers. Therefore, it may be justifiable to strengthen several structures to resist smaller force levels than to spend an equivalent amount to strengthen one structure to new standards.

Once the above issues have been resolved, an initial draft of retrofit guidelines will be prepared. They will be refined and updated as more information becomes available and will eventually form a supplement to the seismic design guidelines for new bridge construction developed by ATC.

REFERENCES

1. Degenkolb, Oris H., "Retrofitting of Existing Highway Bridges Subject to Seismic Loading - Practical Considerations," Proceedings of A Workshop on Earthquake Resistance of Highway Bridges, Applied Technology Council, January 29-31, 1979, pp. 343-359.
2. Longinow, A., Robinson, R. R., and Chu, K. H., "Retrofitting of Existing Highway Bridges Subject to Seismic Loading - Analytical Considerations," Proceedings of A Workshop on Earthquake Resistance of Highway Bridges, Applied Technology Council, January 29-31, 1979, pp. 362-389.
3. Longinow, A., Robinson, R. R., and Chu, K. H., "Seismic Retrofit Measures for Highway Bridges - Training Course Materials," IITRI Report J6364, Illinois Institute of Technology Research Institute, June 1977.
4. Longinow, A., Robinson, R. R., and Chu, K. H., "Seismic Retrofit Measures for Highway Bridges - Design Reference Manual for Retrofitting Bridge to Withstand Earthquakes," IITRI Report J6364, Illinois Institute, June 1977.
5. Mayes, R. L. and Sharpe, R. L., "Design Guidelines for Highway Bridges," FHWA Report FHWA/RD-81/081, June 1981.
6. McGuire, J. F., Fisher, R. W., Stanford, P. R., and North, P. J., "Seismic Design of Bridges - Section 12 - Strengthening of Bridges for Seismic Loads," New Zealand Ministry of Works and Development - Advance Copy, August 1980.
7. Ohashi, M., Fujii, T., Kuribayashi, E., and Tazaki, T., "Inspection and Retrofitting of Earthquake Resistance Vulnerability of Highway Bridges - Japanese Approach," Proceedings of A Workshop on Earthquake Resistance of Highway Bridges, Applied Technology Council, January 29-31, 1979, pp. 391-407.
8. Robinson, R. R., Privitzer, E., Longinow, A., and Chu, K. H., "Structural Analysis and Retrofitting of Existing Highway Bridges Subjected to Strong Motion Seismic Loading," FHWA, Washington, D. C., Report No. FHWA-RD-75-94, May 1975.

ATC Project Engineering Panel

Prof. Helmut Krawinkle
Board Representative
Applied Technology Council
Berkeley, California

Dr. Ronald L. Mayes
Executive Director
Applied Technology Council
Berkeley, California

Mr. Oris H. Degenkolb
California Dept. of Transportation
Sacramento, California

Mr. Gerard Fox
Howard, Needles, Tammen and
Bergendoff
New York, New York

Mr. James H. Gates
California Dept. of Transportation
Sacramento, California

Mr. Veldo M. Goins
Oklahoma Dept. of Transportation
Oklahoma City, Oklahoma

Mr. Robert C. Wood
Federal Highway Administration
Washington, D. C.

Mr. James D. Cooper
Federal Highway Administration
Washington, D. C.

Mr. Richard V. Nutt
Associate Director
Applied Technology Council
Berkeley, California

Mr. Roland L. Sharpe
Managing Director
Applied Technology Council
Berkeley, California

Mr. Robert Kealey
Modjeski and Masters
Mechanicsburg, Pennsylvania

Mr. Felix Kulka
T. Y. Lin International
San Francisco, California

Dr. Art Longinow
IIT Research Institute
Chicago, Illinois

Dr. Walt Podolny
Federal Highway Administration
Washington, D. C.

Prof. Alex Scordelis
University of California
Berkeley, California



RETROFITTING BRIDGES TO INCREASE THEIR SEISMIC RESISTANCE

Oris H. Degenkolb

The 1971 San Fernando, California earthquake was a major milestone in the seismic design of bridges. It was the first earthquake that shook modern type bridges and caused major damage to bridges in the contiguous forty-eight states. That event pointed out a number of deficiencies in bridge design specifications and practices that were in use at that time. Consequently, it was realized that a great number of existing bridges could be severely damaged or collapsed if subjected to earthquakes that could possibly occur during the life of the bridge. Severe damage or collapse of these bridges could be hazardous and cause serious disruptions to lifelines and badly needed transportation routes at a time when they are urgently needed.

One of the major seismic deficiencies of pre-1971 bridges is that superstructure units were not adequately connected at hinges and bearings. Severe shaking could cause spans to drop off of their supports, as illustrated in Figure 1.

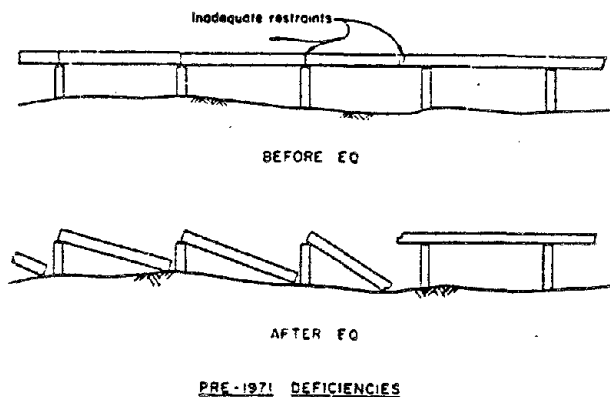


Figure 1

Figure 2(a) shows a number of other common structural seismic deficiencies that were responsible for the bridge failures in the 1971 San Fernando earthquake. Figure 2(b) notes the changes that were made in bridge design practice to make new bridges more seismically resistant. It is obvious that all of these improvements cannot be made to existing bridges and it is generally not practical to increase the seismic resistance of older bridges to the level achieved with new construction.

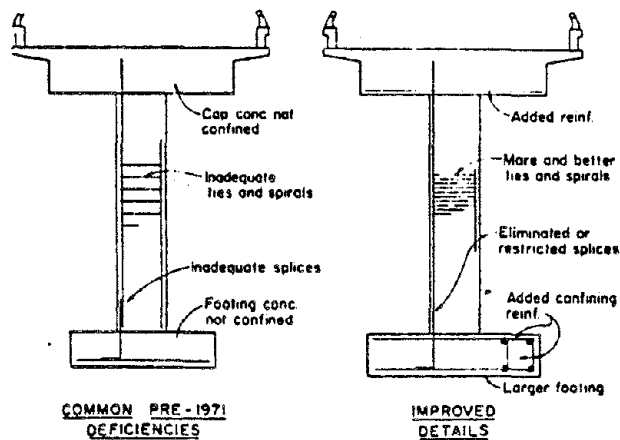
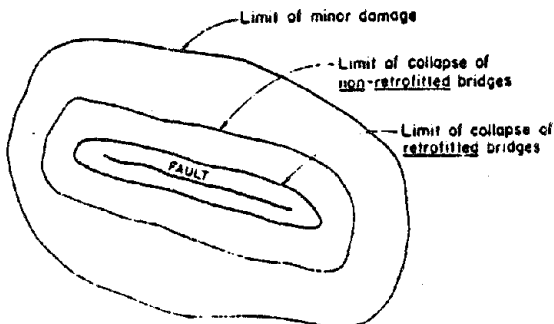


Figure 2

Fortunately, connecting segments of a structure together to alleviate the deficiency illustrated in Figure 1 is the least costly but the most effective method of retrofitting older bridges. This is generally accomplished by connecting the bridge segments together with restrainers consisting of steel cables or rods. Although this strengthening will not overcome all of the other deficiencies it will, in many instances, minimize them to some extent.

A certain amount of damage can be expected in seismically shaken bridges regardless of whether or not they have been retrofitted with hinge and bearing restrainers. This type of damage will usually consist of cracked abutment wing-walls; damage to girder bearings and grout pads; crushed ends of railings, curbs and sidewalks at joints; spalling of decks at joints; minor lateral displacement of decks at joints (especially in skewed spans); and spalling of concrete columns. This damage will occur because restrainers must permit some movement required for normal functioning of the bridge and, when acting during an earthquake, will permit additional differential movement of the structural units.

As illustrated in Figure 3, the area surrounding the fault within which bridges might collapse should be diminished considerably if the bridges are retrofitted with hinge and bearing restrainers.



EXTENT OF BRIDGE DAMAGE CAUSED BY A MAJOR EARTHQUAKE

Figure 3

Many older bridges provide very little or no restraint for keeping the superstructure seated on the abutments. Figures 4(a) and (b) show how superstructures can be shaken off of their supports if bearings, shear keys, or columns fail or permit excessive movements.

One of the more common seismic deficiencies is shown in Figure 4(c). Joints at the ends of simple spans and intermediate expansion joints in long continuous bridges permit the bridge to act as a number of individual units when shaken by an earthquake. Even moderate earthquakes may damage the bearings and joints in the decks, curbs, and railings of these structures. More severe or longer duration earthquakes can fail bearings and cause excessive forces and deflections in the columns, leading to collapse. If these

joints could be connected to make them act as single units, column forces and deflections would be reduced considerably -- increasing the level of seismic resistance of the entire bridge. Unfortunately, restrainers at these joints must usually be left with enough slack in them to accommodate normal daily and seasonal movements.

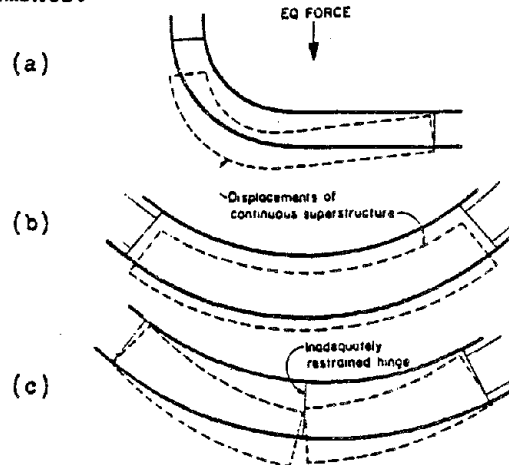
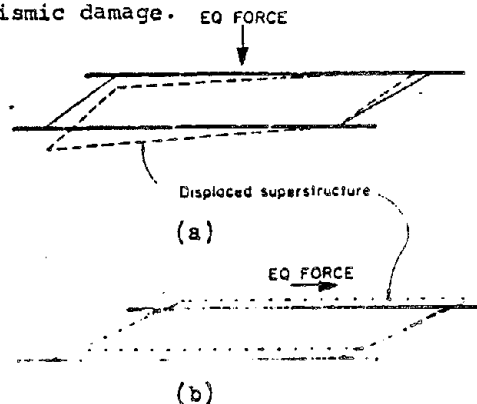


Figure 4

EFFECT OF EQ FORCES ON CURVED BRIDGES

Skewed bridges are generally much more susceptible to earthquake damage than a similar size and type square bridge. Figures 5(a) and (b) illustrate the additional actions involved. In addition to the general lack of adequate transverse restraint provided at the abutments of older bridges, skews complicate the details and increase the structure's vulnerability to seismic damage. EQ FORCE



EFFECT OF EQ FORCES ON SKEWED BRIDGES

Figure 5

The two most commonly used materials for hinge and bearing restrainers in California are 3/4" 4x19 steel cable (Federal Spec. RR-W-410c) and 1 1/2" Ø high strength steel bars (ASTM A-722 with supplementary requirements).

Figure 6 shows the results of tests in which cables and bars were tensioned from near zero stress to specified minimum yield stress (assumed to be $0.85 F_u$ for cables) for 14 cycles and then pulled to failure. Figure 7 shows the results of tests in which cables and bars were stretched to failure but the loads were reduced to nearly zero at approximately one inch increments of elongation. The gage length of all specimens was 114 inches.

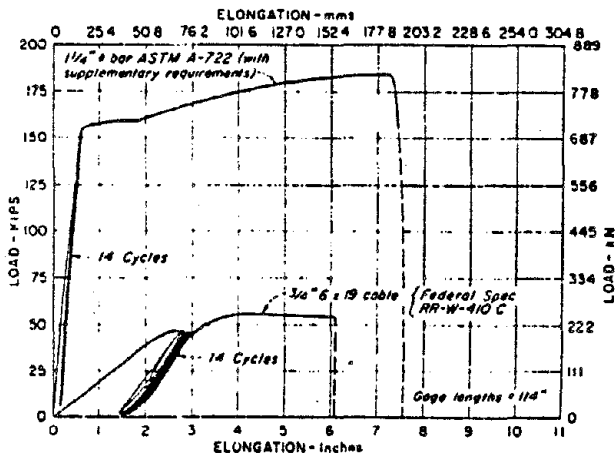


Figure 6

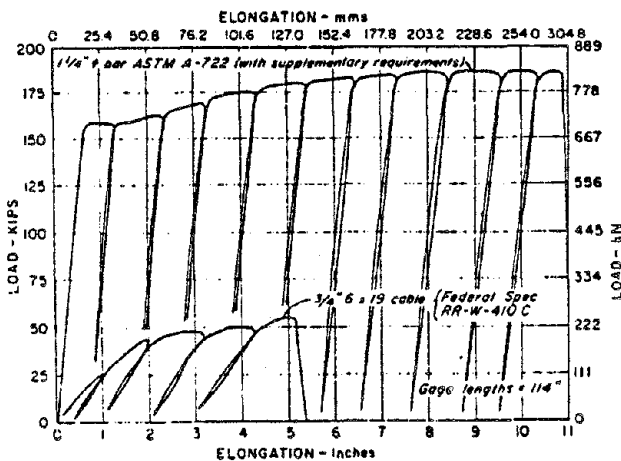


Figure 7

Cycling $3/4$ " cables within the elastic range requires more than twice the amount of energy than cycling an equivalent number of $1/4$ " $\bar{\sigma}$ bars of the same length for the same number of cycles. This is due to the fact that bars have a greater modulus of elasticity and the elongation within the elastic limit is less than for cables. Within this range the cables and bars store energy but do not dissipate any significant amount.

When stretched beyond their elastic limits, bars dissipate approximately 3 times as much energy as the equivalent number of the same length cables.

If restrainers are permitted to yield, greater joint openings and column deflections will be realized. Once either type restrainer is stretched beyond its elastic limit it obviously will not assist in closing the joint to its normal position. Although bars will dissipate more energy than cables when failure occurs, the elongation will also be much greater. This could be an extra factor of safety in some structures but could be disastrous for structures with relatively short, stiff columns. When a restrainer is stretched to its ultimate limit, however, the structure is vulnerable to any additional shocks.

Considering the impreciseness of predicting a bridge's response to a possible future earthquake, it is generally not prudent to depend on restrainers acting beyond their elastic limit.

Restrainers should be capable of developing a minimum force equal to 25% of the weight of the lighter segment of superstructure connected, if Working Strength Design methods are used. When using Load Factor Design methods and the yield strength of the restrainer material, almost identical results are obtained by using 33% of the Dead Load. Column shears should be ignored in either case. Larger restrainer capabilities should be provided whenever required by dynamic analysis. A minimum of two restrainers are used at each bent or hinge -- one as close as possible to each edge of the superstructure. Restrainers are adjusted to permit normal movements of the joint and to start acting as soon as maximum normal open joint width is exceeded.

Assumptions concerning the interaction between the bridge and earth at the abutments is one of the greatest uncertainties in making a dynamic analysis. For this reason the minimum amount of restraining force may be satisfactory for many relatively short square bridges with only one hinge or joint. However, geological conditions, seismicity of the site and structural features may require that greater restraining forces be provided. Dynamic analyses will generally indicate whether cables or rods are preferred for any particular installation.

Slightly different assumptions for restrainer arrangements, foundation conditions, column stiffnesses, abutment restraints linear or non-linear action of the restrainers and columns, etc. can make drastic differences in the results of a dynamic analysis. In some cases the computer has given forces in restrainers that

were so low, or movements of joints so little, that they did not appear to be consistant with observed actions of structures.

Considering all of the uncertainties and assumptions that are made in making a dynamic analysis, it is realized that the seismic design of a bridge is a developing art rather than an exact science. A number of analyses should be made and the results tempered with judgement.

The ideal restrainer should absorb and dissipate energy, keep joint movements within a safe range, and force the structure back to its pre-earthquake position. For practical reasons, the most suitable devices for new construction are not necessarily the best for retrofitting existing bridges. Most of our restrainers to date have used steel cables or rods which act as tension members only.

These devices may not be ideal from a strictly theoretical point of view and they may not prevent as much damage as other types of restrainers that have been considered but, reviewing all of the factors involved, they are hard to beat. They will raise the level of seismic resistance of a bridge, they are relatively easy to install and they are economical.

One of the problems of adding restrainers to existing bridges is attaching to existing members. Existing construction often is not strong enough to develop the required anchorage forces. In these cases, existing features may have to be strengthened in order to prevent premature failures. Another problem is that restrainer forces, if fully developed, may fail the columns or other portions of the bridge. In spite of these problems, restrainers by themselves can decrease a bridge's vulnerability to damage more than any other retrofiting system. The most seismic protection can be obtained for the least money by retrofitting existing bridges with restrainers. In the meantime, studies are being made for possibly retrofitting columns and footings of selected structures sometime in the future.

Figure 8.

Detail for restraining hinges of T-Beam bridges.

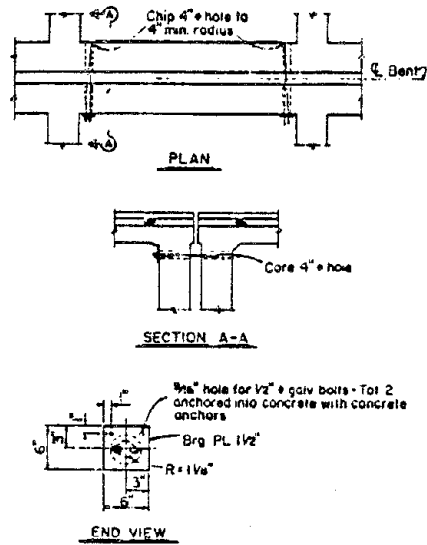


Figure 9.

Most commonly used detail for retrofitting concrete box girder bridges. Concrete bolsters prevent cable anchorages from destroying existing diaphragms.

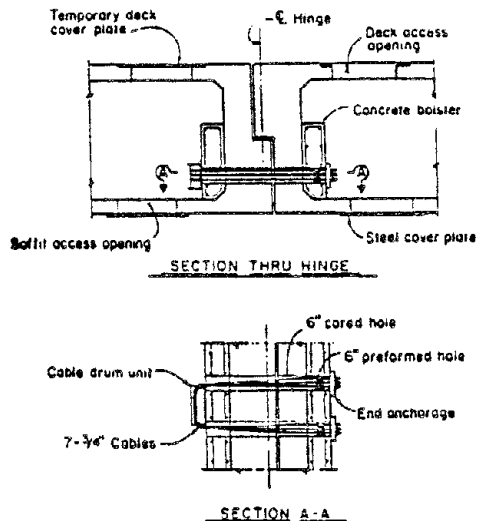


Figure 10.

Seven cables passed through a hinge joint three times to give the restraining force of 21 cables.

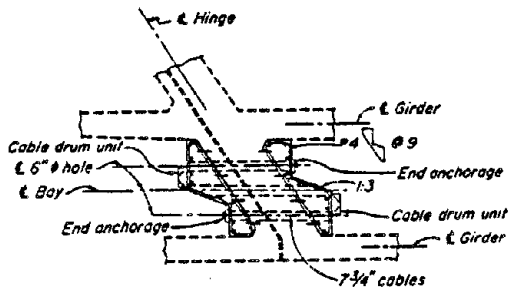


Figure 13.

Plan view of steel rod restrainers similar to Figure 11. Bolsters used to compensate for skew and strengthen hinge diaphragm.

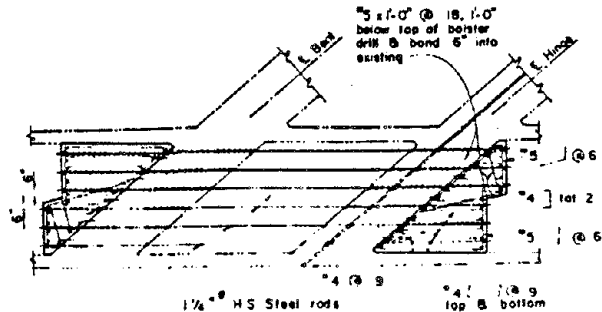
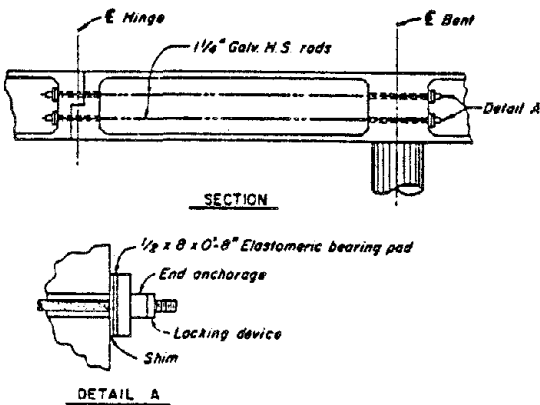


Figure 11.

High strength steel rods used to limit hinge movements. Long rods are used to absorb energy.



HIGH STRENGTH ROD RESTRAINER

Figure 14.

Simple restrainer for precast - prestressed I girder spans at inverted T-bent.

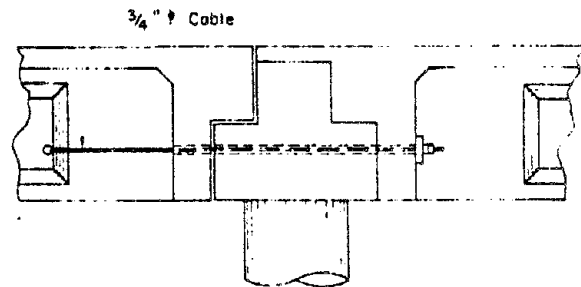
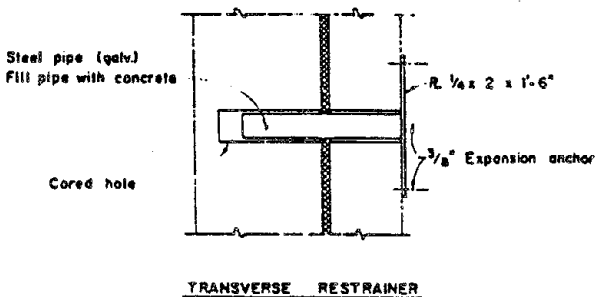


Figure 12

Detail of transverse restrainer used in conjunction with high strength steel rod restrainers to limit differential transverse movements of hinges.



TRANSVERSE RESTRAINER

Figure 15.

Restrainers for short drop-in spans. Longer spans require more cables in order to limit amount of hinge movements.

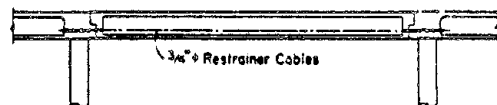


Figure 16.

Restrainer for limiting hinge movement of suspended slab span.

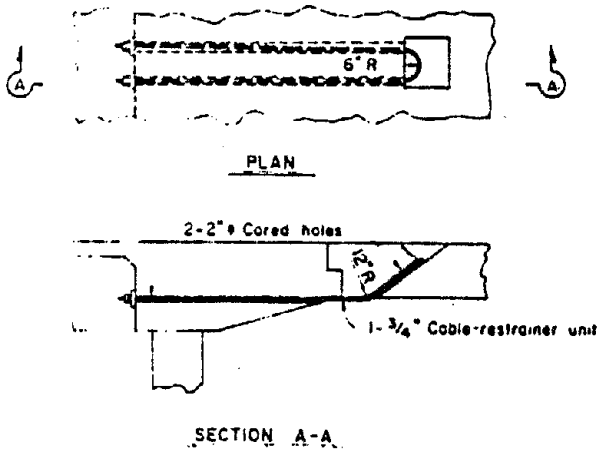


Figure 18.

3/4\"/>

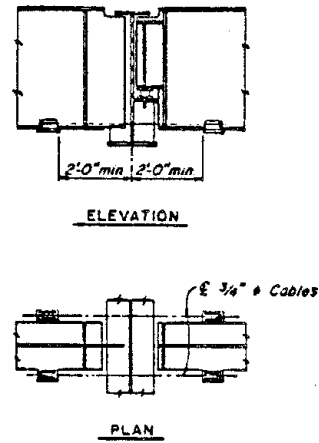


Figure 17.

Typical restrainers for connecting steel girders to concrete bent caps.

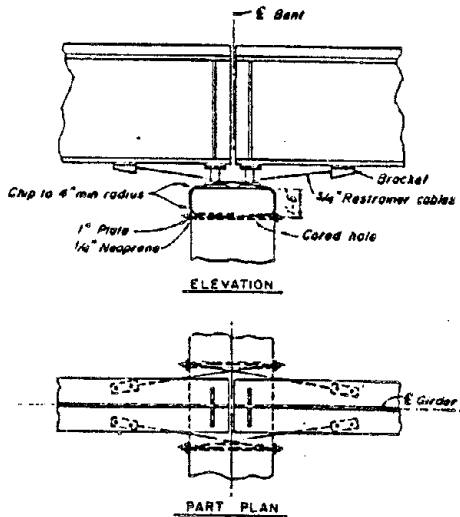
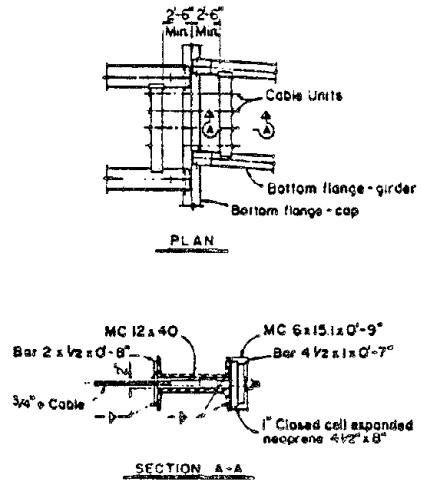


Figure 19.

Typical restrainers for steel girders supported on steel bent caps where girders in adjacent spans are offset.



CONSIDERATIONS FOR RETROFITTING BRIDGES

Oris H. Degenkolb

May 1981

Introduction

The San Fernando earthquake of February 9, 1981 was the only event to cause any significant amount of damage to any of California's bridges. The total amount of earthquake damage to bridges experienced before that time was minor and was generally ignored. Five small earthquakes since 1971 have caused some minor damage and the collapse of two spans of one four span bridge. The knowledge gained by studying that damage gives an insight into how structures react to seismic shaking and what can be done to mitigate the damage expected from the larger earthquakes that are certain to occur in the future.

Studying the damage from minor earthquakes is valuable because it demonstrates the stages of failure and it is not necessary to speculate on the sequence of events as might be done when conducting a post-mortem on a completely collapsed structure. Although there is a wide variety of bridge details used in California and in other countries, there is a consistency in the seismic damage experienced.

Even though bridges can be retrofitted to increase their resistance to total collapse in the event of a major earthquake, they will still experience minor damage from smaller seismic events.

Most of the retrofitting done to date has consisted of tying units of the superstructure together and to their supports. Although this directly solves only the problem of the spans dropping off of their supports, it partially alleviates some of the other seismic deficiencies.

The California bridge most seriously damaged since the 1971 earthquake would have sustained relatively minor damage rather than losing two spans if it had been retrofitted with restrainers.

Retrofitting Philosophy

The goal of retrofitting is to increase the seismic resistance of a bridge to minimize the probability of total collapse.

Retrofitting should eliminate or reduce the hazard to human life as much as possible.

If practical, critical bridges should be able to carry emergency vehicles after being damaged.

It is not practical or economically feasible to retrofit a bridge so that it will have the same seismic resistance as a new structure designed to current specifications.

Retrofitting is generally not recommended if the only expected deformation is a small probable maximum vertical displacement ($\leq 6''$) and some traffic can be accommodated by ramping the vertical offset with dirt or other readily available material until permanent repairs can be made.

Main spans of Pedestrian Overcrossings that could drop on vehicular traffic should be retrofitted. Other spans need not be retrofitted unless they can be done at a low cost when the main spans are done or unless there is a considerable amount of school or other high volume pedestrian traffic that could be injured.

Considerations for Retrofitting

It is not possible to formulate simple rules to determine whether or not a structure requires retrofitting to improve its performance during an earthquake or, if so, what type of retrofitting it requires. In addition to the geological and seismological conditions at a particular site, any one of a combination of two or more of the following physical features of a bridge could determine whether or not retrofitting is advisable.

- . Type of construction
- . Physical condition of the bridge
- . Length
- . Width
- . Ratio of length to width
- . Skew
- . Curvature
- . Number and location of joints
- . Type of bearings and hinges
- . Abutment type and height
- . Bent type and height
- . Number of spans
- . Restraining devices (shear blocks, curtain walls, etc.)
- . Type and degree of failure anticipated if not retrofitted.
- . Column reinforcement details
- . Lifeline requirements
- . Sociological considerations
- . Utilities carried

The following figures illustrate some of the different conditions that should be considered in determining whether or not a bridge should be retrofitted and the type of retrofitting that is required. It should be remembered that adverse geological conditions may complicate many of these situations.

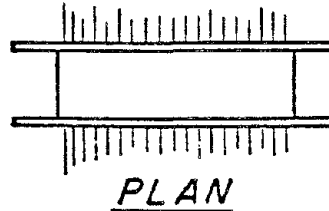
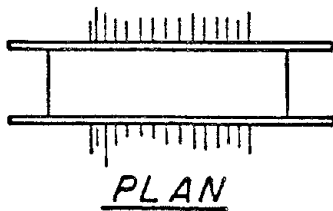
ELEVATION

Figure 1

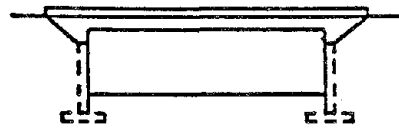
ELEVATION

Figure 2

Figures 1 & 2 As a rule, single span square structures should not require retrofitting. Although they may sustain some damage, they should be serviceable unless they cross a fault. If they do cross a fault, it is not likely that retrofitting will be effective.

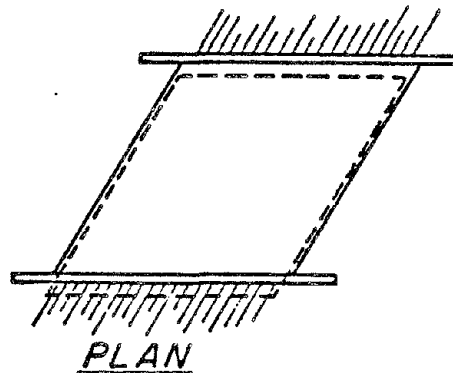
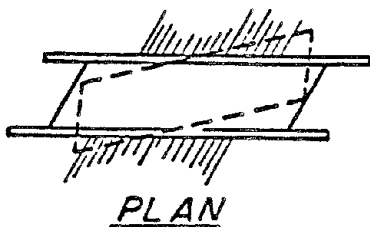
ELEVATION

Figure 3

ELEVATION

Figure 4

Figure 3 Skewed bridge spans have a natural tendency to rotate even when not shaken. Longitudinal seismic shaking produces transverse components of force which tend to rotate the span each time it moves back and forth. Transverse seismic forces cause one end of the span to bear against one abutment while the opposite end tends to swing free -- in the natural direction of rotation. If the bearings, curtain walls or other means of restraining rotation fail, the span can rotate excessively. In some cases the span may drop only a few inches and the bridge can be used with minor inconvenience and easily restored to its pre-seismic condition. If the supporting seats are very narrow, the span can drop and the bridge will be a total loss.

Figure 4 If a bridge is very wide in relation to its length, it may be locked between its abutments so that the rotation described in Figure 3 is negligible. Longitudinal shaking may cause insignificant damage. Transverse shaking may damage the bearings, shear keys or curtain walls, but there is much less probability for the more serious damage that might be expected with a longer, narrower structure.

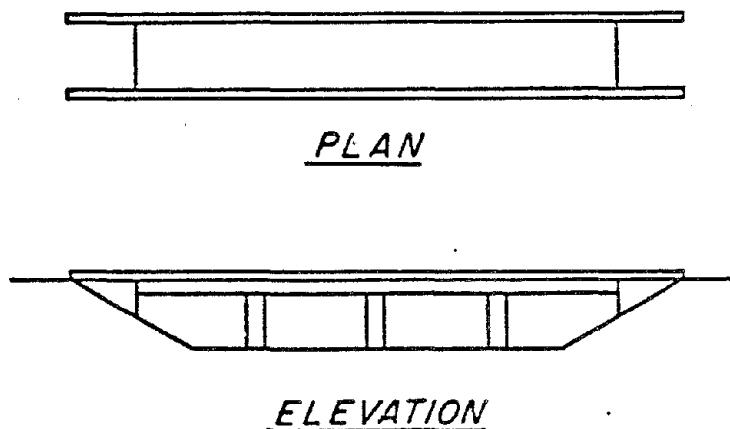


Figure 5

Figure 5 Long, non-skewed, continuous bridges with diaphragm type abutments and without intermediate hinges or joints need not be retrofitted. Bridges with bearings at the abutments may require transverse restrainers at the abutments if it is determined that there is insufficient restraint provided by bearings, curtain walls, shear keys or other restraining features.

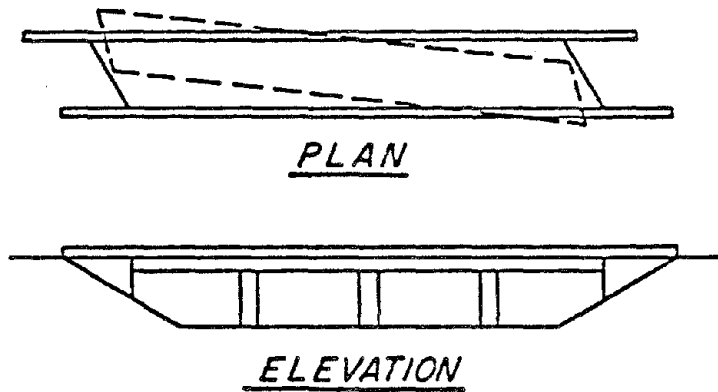


Figure 6

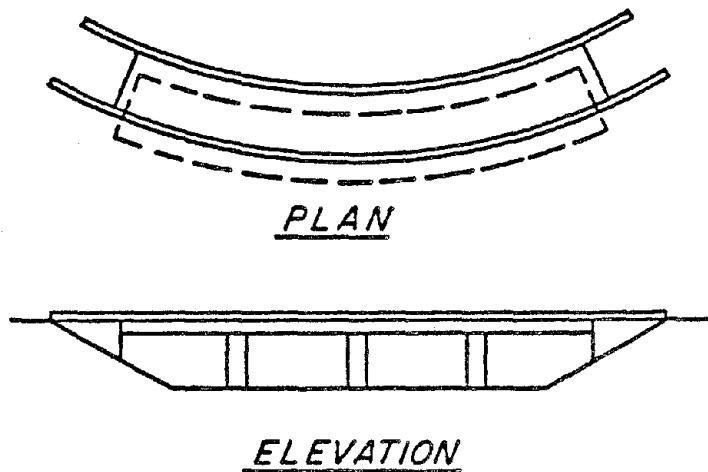
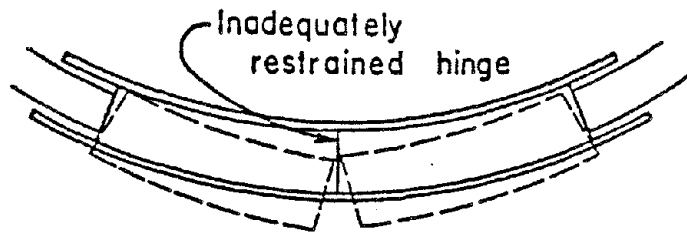


Figure 7

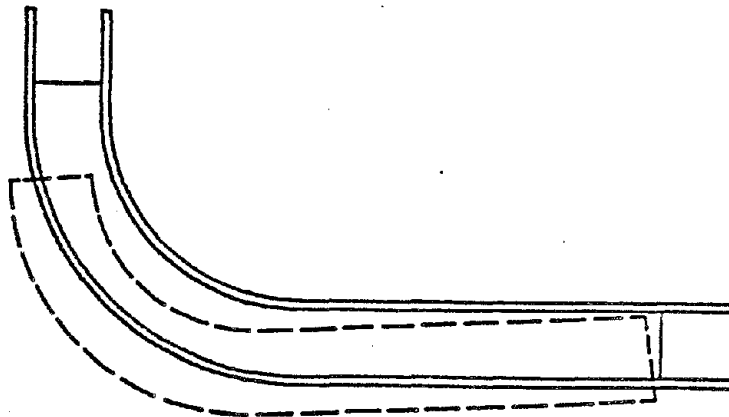
Figures 6 & 7 Long, continuous, skewed or curved bridges without intermediate hinges or joints are more prone to seismic damage than similar square bridges. Due to the nature of the details, they will probably require additional transverse restraint at the abutments for a lower seismic level of shaking than a similar square bridge.



PLAN

Figure 8

Figure 8 Segments of a superstructure which aren't adequately restrained act independently and may tend to fly apart when shaken. If the bearings or other means of transverse restraint fail, longitudinal restrainers (if installed) may act as tension members in a large horizontal beam. Restrainers should generally be placed as close to the edge of the structure as possible so they can offer the maximum amount of resistance for this condition.



PLAN

Figure 9

Figure 9 Sharply curved bridges which have seismically inadequate bearings at an abutment and very flexible or seismically deficient columns may require additional restraint at the abutments. Abutment restraint, in cases such as this, may alleviate some column weaknesses. One common problem, however, is that the abutments may not be capable of resisting the anticipated forces. Many abutments are very light-weight and the shear resistance of the soil or piles may be insufficient

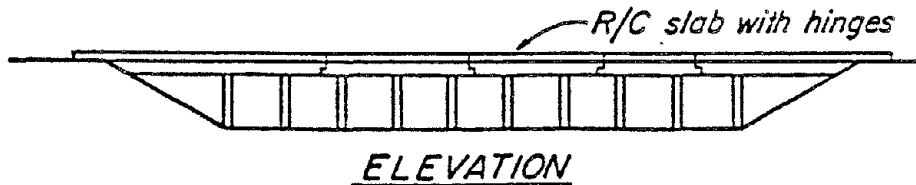


Figure 10

Figure 10 Long continuous reinforced concrete slab bridges, as a general rule, need not be retrofitted with hinge restrainers. This is based on the assumption that if the suspended span becomes unseated, the dead load of the resulting cantilever will not be sufficient to make it fail. Long span non-standard slabs should be checked for this criteria. Retrofitting should be required if there are two hinges in the same span or if the unseating of any hinge will lead to a dropping of any or all spans with dead load only. It is assumed that those unsupported ends will be quickly recognized and resealed, temporarily strutted, or traffic barricaded from using the bridge before any serious accident occurs.

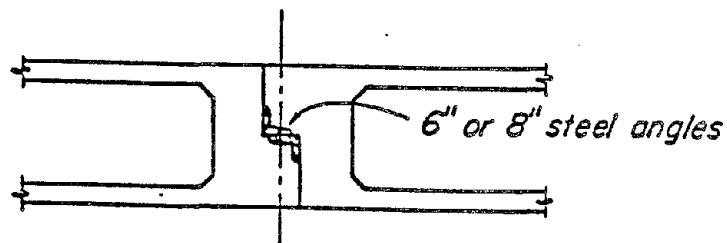


Figure 11

Figure 11 Any bridge with 6" or 8" steel angle hinges, or equivalent, should be retrofitted regardless of what seismic area it is in. Due to shrinkage, seasonal variations, and other factors, many of these hinges have marginal seating length under even normal conditions. Any seismic shaking could cause them to become unseated.

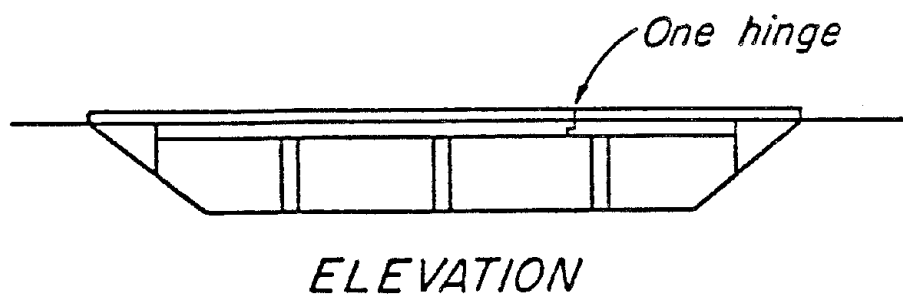


Figure 12

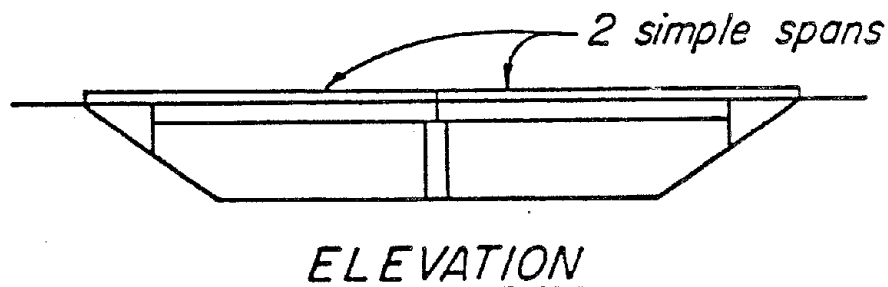


Figure 13

Figures 12 & 13 A non-skewed, straight, continuous bridge with only one hinge or a non-skewed straight bridge with two simple spans may be designed for the minimum of 25% (33% for LFD) of the dead load of the lighter segment of superstructure connected. This would be consistent with the rough assumptions made for the resistance and action of the earth behind the abutments.

The influence of the earth behind abutments becomes relatively less important if the superstructure is curved or skewed. The equivalent static force method or dynamic analysis should be used for designing restrainers for these structures if they are skewed or curved.

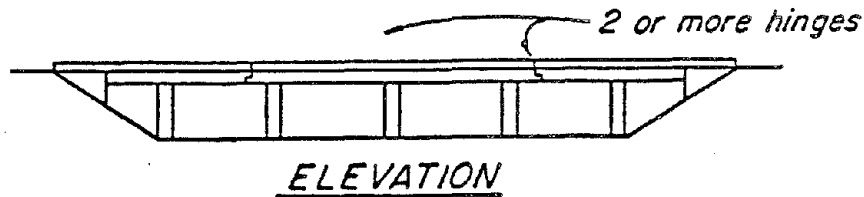


Figure 14

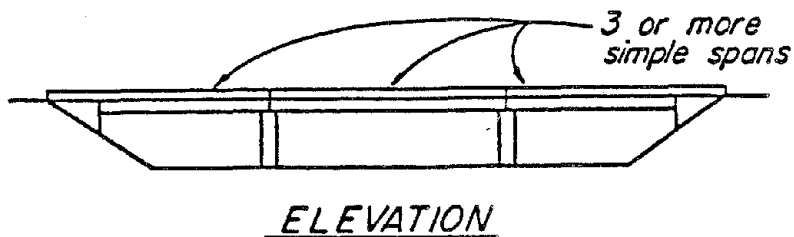


Figure 15

Figure 14 & 15 A dynamic analysis should be made for any bridge with two or more hinges or three or more simple spans.

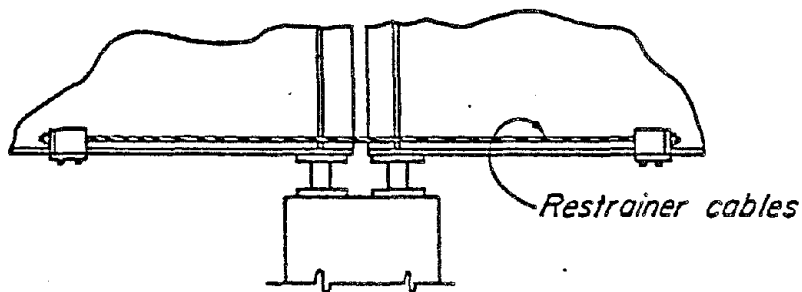


Figure 16

Figure 16 Connecting the ends of girders together in adjacent spans may be satisfactory for short structures with only a few spans and wide bent caps where it seems certain that the ends of girders won't drop off the bents. This detail can also be used where it is considered that the additional longitudinal forces produced by connecting the girders to the bent caps (see Figure 17) may fail the columns. Although the bearings will probably fail, the superstructure will not fall very far and the bridge will not be completely out of service.

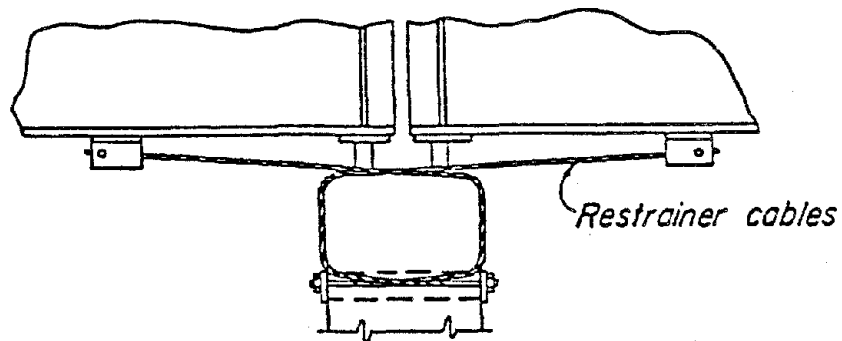


Figure 17

Figure 17 This detail is generally preferred to the one illustrated in Figure 16 with the spans butting against each other. The restrainers must be able to resist the force produced by both spans supported on that pier and possibly adjacent spans as well. Vertical clearances under the structure should be considered.

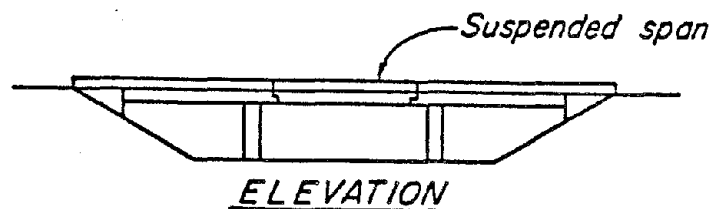


Figure 18

Figure 18 Suspended spans are particularly vulnerable to seismic shaking. Curved and skewed alignments greatly increase their vulnerability.

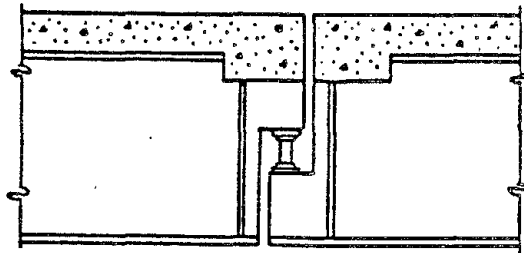


Figure 19

Figure 19 It can generally be assumed that any seat type hinge used with steel girders will need additional transverse, longitudinal, and vertical restraint in even moderately severe seismic areas.

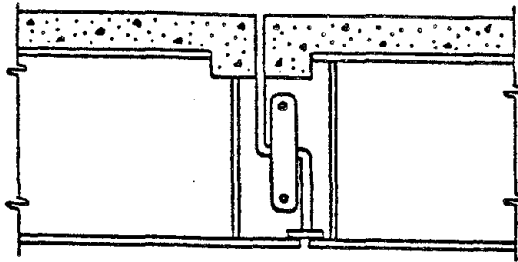


Figure 20

Figure 20 Hanger type hinges generally have more seismic resistance than the seat type shown in Figure 19, but are still subject to seismic damage. These hinges often have steel bars or angles that bear against the opposite web, or lugs attached to the flanges, which were designed to keep the girders aligned transversely for wind forces. Those devices are usually structurally inadequate and are too short to be effective with even moderate seismic shaking. Consideration should be given to replacing them or adding supplemental transverse restrainers.

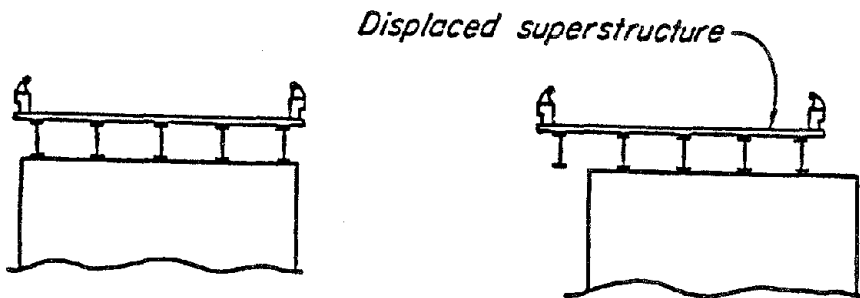


Figure 21

Figure 21 Very few older bridges have bearings that will not fail in a moderate or greater earthquake. It should be anticipated that a bridge superstructure can be displaced transversely. If the exterior girder of a multi-girder bridge is moved beyond the end of a bent, it is likely that that side of the bridge may be severely damaged and the use of a shoulder or lane will be lost, but traffic can be routed over a portion of the bridge with few or no emergency repairs. This is considered to be an acceptable risk.

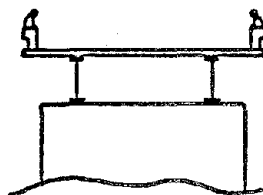


Figure 22

Figure 22 If the superstructure of a two or three girder bridge is displaced transversely so that one line of girders loses its support, the entire bridge may collapse. Adequate transverse restraint should be provided.

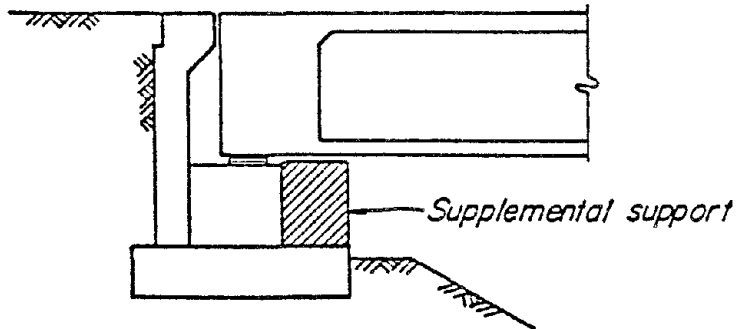


Figure 23

Figure 23 In most locations it is generally not practical to restrain longitudinally the superstructure at an abutment. Supplemental supports can be provided to prevent the superstructure from dropping excessively. This same principle may also be applied at bents in certain circumstances.

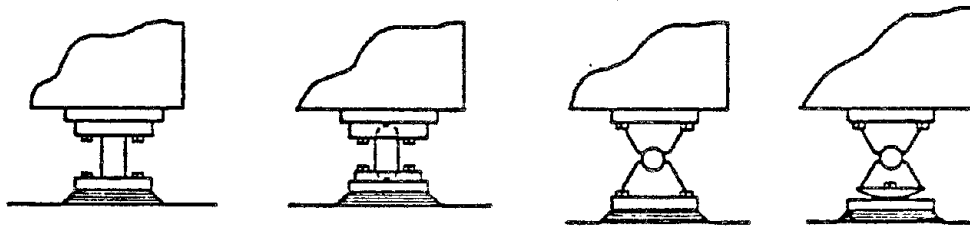


Figure 24

Figure 24 Numerous types of steel bearings used on various types of steel and concrete bridges have been damaged by relatively minor seismic shaking. It should be assumed that they will fail in areas where the maximum credible bedrock acceleration is $0.3g$ or greater. If the failure of any type of bearing will result in the superstructure dropping 6" or more without falling off of the pier or abutment, consider replacing the bearings with a modern type or adding bolsters that will minimize the drop.

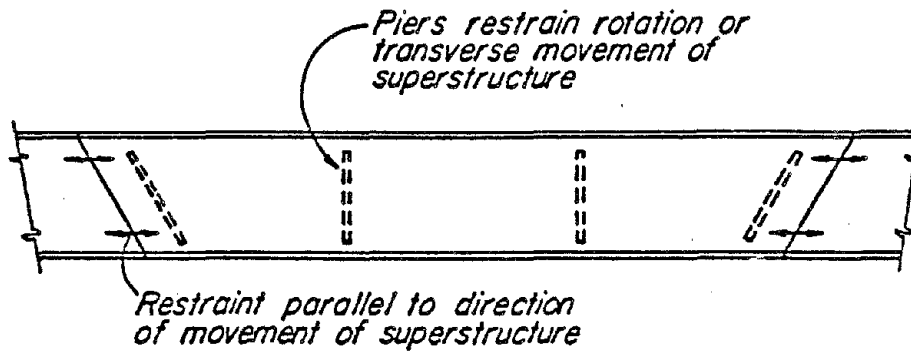
PLAN

Figure 25

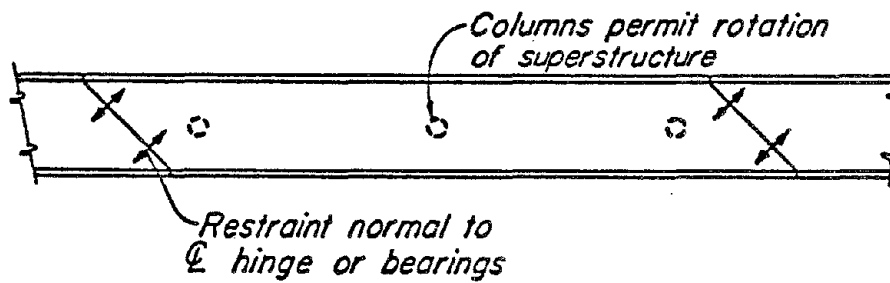
PLAN

Figure 26

Figures 25 & 26 The rigidity of piers and bents can control the direction of movement of a structure. Restrainers will be more effective if they are oriented in the principal direction of movement.

Restrainer Requirements

Hinge and bearing restrainers should have redundancy. There is always a chance that a single unit has a defect (due to faulty material, fabrication, installation, adjustment, maintenance, etc.) and will fail sooner than expected. Additional units or other devices should be capable of doing their share of the job if one unit fails prematurely.

Restrainers should fail in a ductile rather than brittle manner when subjected to ultimate loading. They should not fail before the structure as a whole fails.

Restrainer brackets and connections should be at least 25% stronger than the cables, rods or primary restraining devices. They should be designed so that they will not fail or cause failure of the portion of structure they are attached to if some component part or parts of the unit are misadjusted or fail prematurely.

The following ultimate strengths should be assumed for designing connections and determining the adequacy of supporting members:

3/4" cables (6x19 Federal Spec. RR-w-410c)

$$F_u = 53 \text{ kips}$$

1 1/4" H.S. rods (ASTM A-722 with Supplemental Requirements)

$$F_u = 188 \text{ kips}$$

(use $53 \times 1.25 = 66.2$ kips and
 $188 \times 1.25 = 235.0$ kips per cable
 and rod, respectively)

Bolted Connections shall be designed as a bearing type:

H.S. Bolts (A325)	Allowable Shear ($F_v = 0.6 F_u \phi A_r$)	Allowable Tension ($F_t = \phi F_u$)
3/4"	20.1 kips	34.1 kips
7/8"	27.7	47.1
1"	36.3	61.8
1 1/8"	45.8	68.1

Combined Tension and Shear:

$$F_{vc} = \sqrt{(F_v)^2 - (0.6 f_t)^2}$$

Where: F_{vc} = Allowable shear per bolt for combined shear and tension

ϕ = Reduction Factor = 0.85

F_v = Allowable shear per bolt (kips)

f_t = Applied tension per bolt (kips)

A_r = Area of bolt with threads in shear plane

F_y = Ultimate tensile strength (kips)

The following allowable stresses should be used for designing ASTM A-36 steel brackets for ultimate conditions:

Tens. or Comp. = 36,000 psi
 Shear = 22,000 psi

Bearing $\frac{L F_u}{1.18 d}$ or $3.0 F_u$ whichever is smaller
 $F_u = 58,000$ psi

L = Distance in inches measured in the line of force from the centerline of bolt to the nearest edge of the hole for an adjacent bolt or to the end of the connected part toward which the force is directed.

d = Diameter of bolt in inches.

F_u = The lowest specified minimum tensile strength of the connected parts.

L/d shall not be less than 1.5

Groove welds = 36,000 psi

Fillet welds = 26,000 psi

Bearings:

One of the primary seismic weaknesses of older bridges is that the spans are not connected to each other or to the bents and abutments. Bearings usually provide the only connection between these units. Experience has shown that the seismic resistance of bearings is often overrated and they are damaged by relatively minor shaking.

When seismic shaking becomes more severe or prolonged, damaged bearings offer no restraint and allow the spans to fall off their supports.

As a general rule, a designer should be very cautious about assuming that bridge bearing anchor bolts, keeper bar bolts or welds and similar details have any significant effect in keeping a bridge superstructure on its supports during a major earthquake. The following shortcomings of bridge bearings should be considered:

1. All of the bearings at the end of a span probably are not subjected to identical forces simultaneously. Because keepers or other devices are not set with exactly the same clearances, only one half, or fewer than one half, of the bearings will initially resist a horizontal force in one direction. Rotation of a span in a horizontal plane puts unequal loads on the bearings. It is not uncommon for bearings at one end of a span to be damaged to varying degrees by an earthquake.
2. Grout pads under bearing masonry plates have traditionally given trouble during and after construction and have been one of the main sources of trouble in minor quakes. Failure of a grout pad will allow the bearing assembly to move and subject the anchor bolts to combined bending and shear.
3. The common detail of a girder seated on an elastomeric pad will subject anchor bolts to combined bending and shear.
4. Anchor bolts are frequently threaded below the top surface of the pier or abutment seat. This gives a reduced area for shear and minimal resistance to bending before failure occurs due to notch sensitiveness at the root of thread.

5. Although it is less common, some anchor bolts are too close to the edge of the bearing seat, have inadequate reinforcement around the bolts, and will spall off the concrete when subjected to horizontal loads.
6. Keeper bars allow movement between the sole plate and bearing bar or rocker. Sliding takes place on this surface. Sliding obviously does not start until the horizontal force exceeds the vertical load times the coefficient of friction. When this happens, does it result in an impact on the keeper bar and anchor bolts? If so, it can increase the calculated force considerably.
7. Bridge bearings may not be what they are represented to be on "As Built" plans or maintenance records. Adjustments to keepers or other details are occasionally made after construction is completed and the details or workmanship may be inferior to the original.

Earthquake restrainers should be considered if the strength of the bearings is less than twice the calculated seismic force on them, after taking due consideration of the above deficiencies and uncertainties.

Columns

Many older bridges have seismically deficient columns as well as inadequate bearings. The deficiencies may be due to an insufficient amount of longitudinal reinforcement; too few, too small or improperly detailed ties or spirals; improperly located lap splices; or inadequate anchorage or confinement of longitudinal steel in footing or caps. These deficiencies are much more critical for structures with single columns than those with multi-column bents. The problem is so extensive and costly to correct that most structures with seismically deficient columns (especially those with multi-column bents) will never have those deficiencies corrected. In some of those cases the calculated forces required for hinge restrainers may be greater than the columns can resist. If it is obvious that deficient columns will not be retrofitted, consideration should be given to limiting bearing restrainer forces to approximately 25 percent greater than what is required to fail the columns.

BRIDGE RETROFITTING DETAILS

Oris H. Degenkolb

INTRODUCTION

The 1971 San Fernando, California earthquake disclosed the fact that many existing bridges had serious seismic deficiencies. The State of California initiated a survey of all its bridges and determined that approximately 1220 could have their seismic resistance increased by retrofitting them to keep the structural segments from separating when shaken by an earthquake. The total program is estimated to cost approximately \$50 million and is now slightly more than half completed.

DESIGN METHODS

California's criteria for designing restraining devices have changed a number of times since the retrofitting program was initiated in 1971. The first criteria was very simple and consisted of providing a restraining force equal to 25% of the dead load of the lighter segment of superstructure connected. An effort was made to use ductile materials.

Bridge seismic design specifications have been revised radically since that time, bridge designers are now able to take advantage of the advancements made in the field of computers and structural dynamics, and Load Factor Design methods have superseded the Working Strength Design method.

Restrainers are now basically designed in accordance with the American Association of Highway and Transportation Officials Standard Specifications for Highway Bridges. The equivalent Static Force Method may be used for designing restrainers for bridges with well balanced spans and supporting bents or piers of equal stiffness, but the Response Spectrum Method applied to the structure as a whole is generally preferred for more unusual structures and where contributing dead loads may come from beyond the immediate spans or frames.

Unless there are other limiting factors, such as the ability of a structure to accommodate the restraining forces, restrainers should be designed to resist forces equal to the acceleration, expressed as a percentage of the gravitational force, times the contributing dead load, but not less than 0.35 times the contributing dead load.

The dynamic analysis utilizes a modal analysis based on the application of the response spectrum of ground acceleration to a lumped sum mass space frame of the structure. This method considers the relationship of the site to active faults, the seismic response of soils at the site, and the dynamic response characteristics of the whole bridge.

Dynamic analyses sometime appear to give what seem to be erratic results. Minimum, or less than minimum, restrainers may be determined to be satisfactory, but more restrainer capability at the same location may be calculated as being insufficient. This apparent inconsistency is due to the fact that a stiffer element in a system will "attract" more force. In specific instances where this phenomena has been observed, restrainers with minimum or greater than minimum capacities have been considered to be the more appropriate. Considering the fact that different methods of analysis give drastically different results, none of which may represent what may happen when a structure is shaken by an actual earthquake, it should be realized that a designer must use a considerable amount of judgment.

RESTRAINER DETAILS

Many compromises must be made in designing seismic restrainers. Ideally, restrainers should:

- Be effective in an earthquake.
- Be economical.
- Dissipate energy.
- Keep units of a structure in their initial relative locations.
- Require no maintenance.
- Be accessible for inspection and repair.
- Be repaired or replaced by ordinary maintenance workers.
- Use ordinary tools for repair or replacement.
- Use commonly available parts which don't become obsolete.
- Not use liquids which can leak out or evaporate.
- Be foolproof.

The basic restrainer materials used for retrofitting California's bridges are $3/4"$ 6x19 cable (Federal Spec. RR-W-410C) and $1\frac{1}{4}"$ ϕ bars (ASTM A-722 with supplementary requirements). The end anchorages for the $3/4"$ cables (Figure 1) develop the full strength of the cable. Cables have a minimum breaking strength of 46 kips, are assumed to have a yield strength of 39.1 kips, and frequently test to 53 kips ultimate.

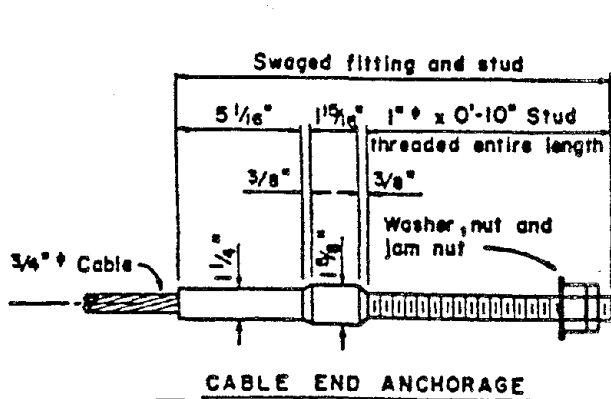


Figure 1

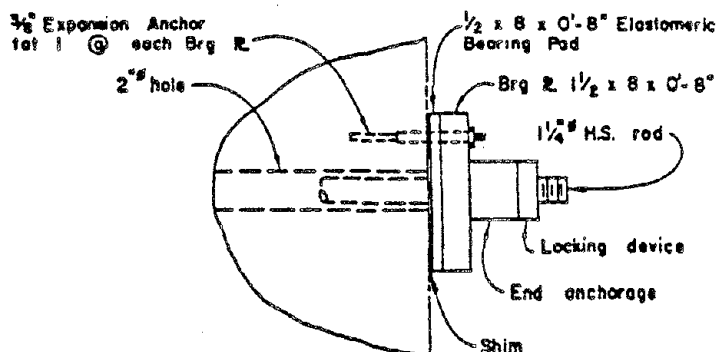


Figure 2

1½" dia. high strength steel rods are required to have a minimum ultimate strength of 150 kips. The supplementary requirements of ASTM A 722 assure greater ductility. The 1½ dia. size is readily available competitively, whereas the supply of other sizes may be somewhat limited. The design yield strength is 120 kips and two types of bars are commonly used: Dywidag threadbars, which have a continuous rolled-in pattern of threadlike deformations along their entire lengths, and smooth rods which are cut to length and have machine threaded ends. Although they frequently develop the full strength of the rod, couplers and anchorage devices are required to develop not less than 95% of the specified ultimate tensile strength of the rod. Figure 2 is a diagrammatic sketch of a typical end anchorage for high strength steel rods.

Transverse restraining devices in the hinges of older concrete bridges are often considered to be inadequate for keeping the adjacent sections of superstructure aligned during an earthquake. Differential movement between the two sides of a hinge would shear high strength steel rod restrainers. Transverse restrainers (Figure 3) are added when required, to assist in keeping the two sides of a hinge in alignment. The concrete filled pipe transverse restrainers are placed in the direction of normal hinge movements.

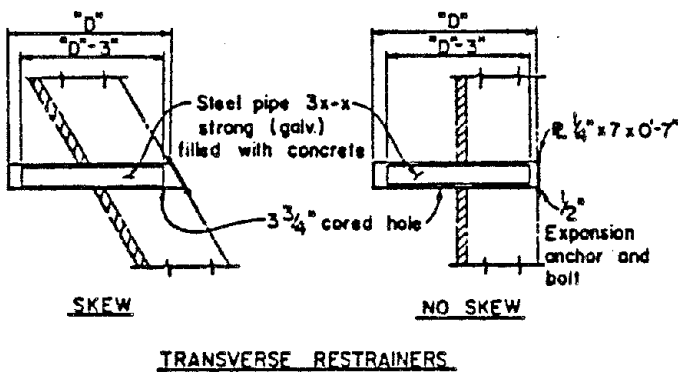


Figure 3

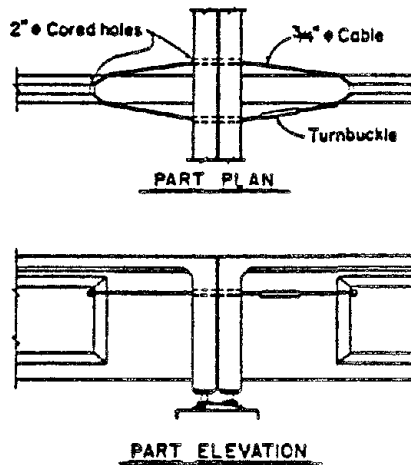


Figure 4

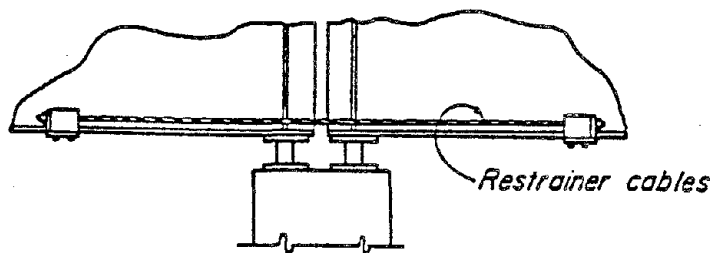


Figure 5

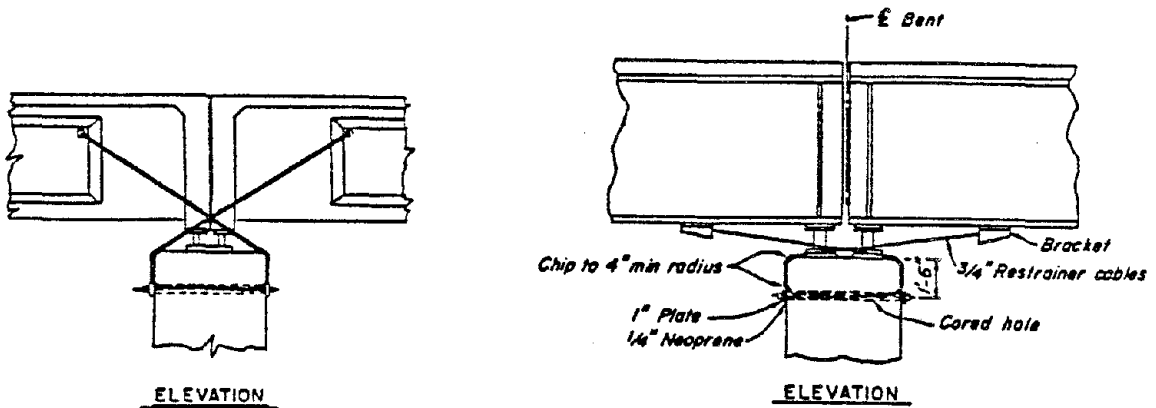
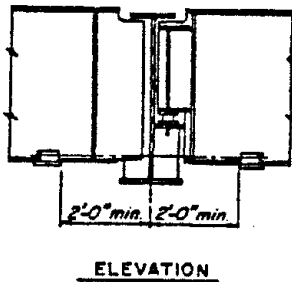
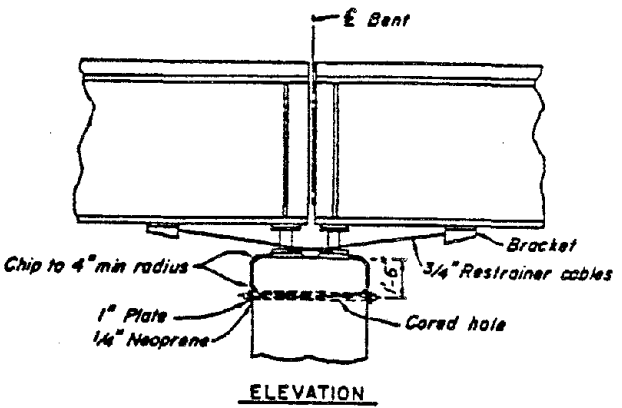


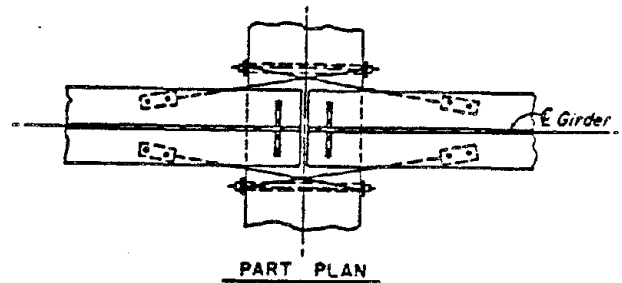
Figure 6



ELEVATION

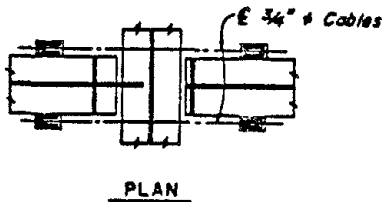


ELEVATION



PART PLAN

Figure 7



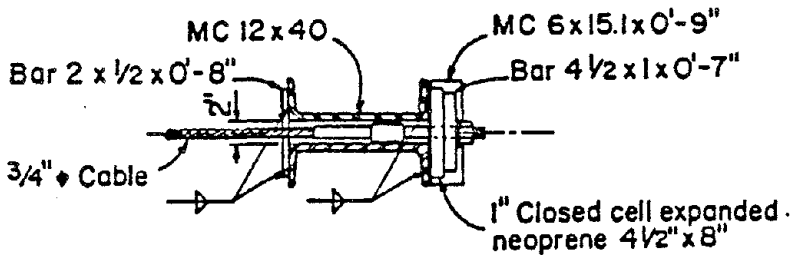
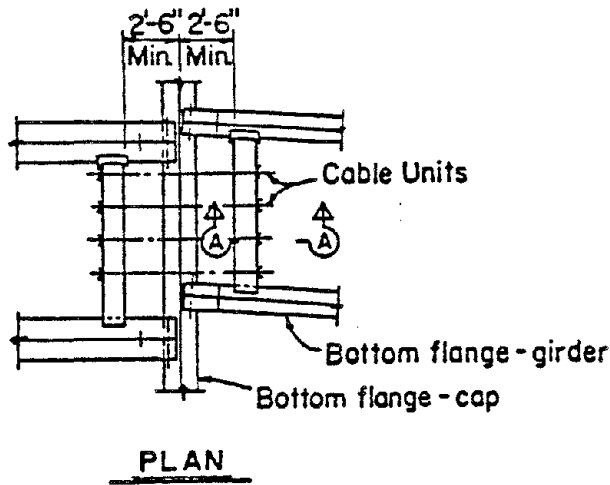
PLAN

Figure 8

Figures 4 and 5 have been used for connecting segments of superstructures together and are suitable for relatively short structures with wide supports.

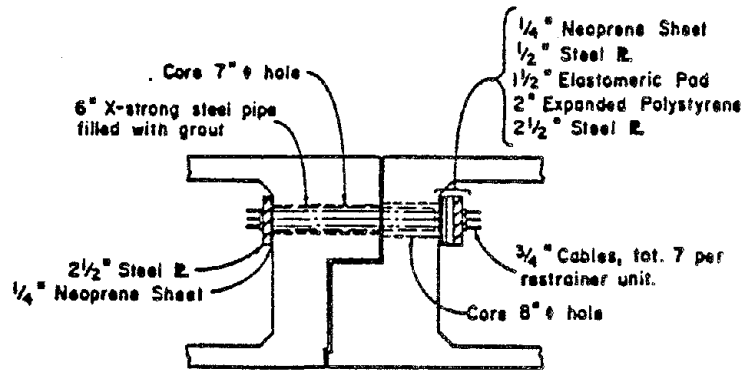
Figures 6 and 7 show methods of connecting precast-prestressed and steel girders to bent caps. Although these details are especially suited to long multi-span structures, they are also preferred for shorter structures with few spans. The detail illustrated in Figure 7 may not be suitable in some instances where vertical clearance underneath the structure is critical.

Figure 8 illustrates a method used for connecting steel girders which are supported on a steel girder cap where the girders are in line with each other. In cases where girders cannot be connected directly, because of curved or flared roadways, cable restrainers are attached to beams made up of steel channels which are connected to the bottom girder flanges as shown in Figure 9.



SECTION A-A

Figure 9



TYPE H-1A HINGE RESTRAINERS

Figure 10

An early type restrainer which was used in box girder hinges is shown in Figure 10. It had the advantage of providing a considerable amount of transverse and vertical, as well as longitudinal, restraint. Its use is limited, however, because many hinge diaphragms don't have the strength to resist the punching-out effect of the restrainer cable anchorages. Another disadvantage is that the grout, which is placed in the pipe to increase the transverse and vertical shearing capacity, reduces the stretching capacity (ductility) of the cables.

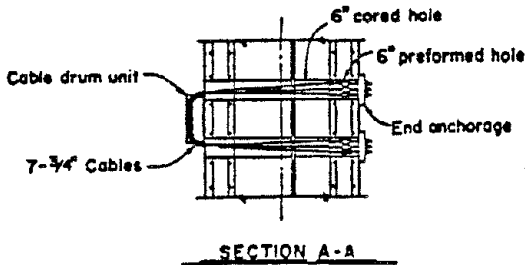
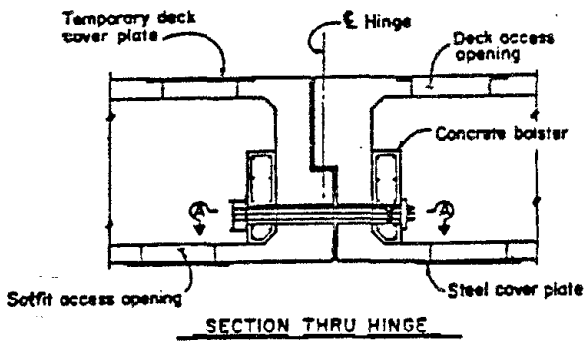


Figure 11

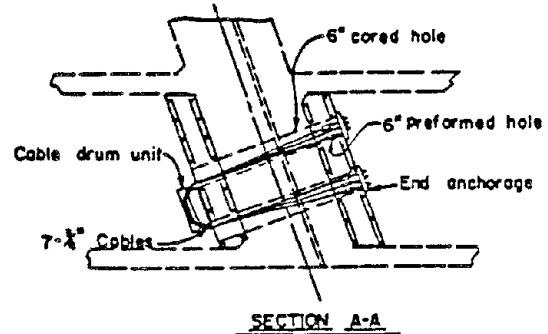
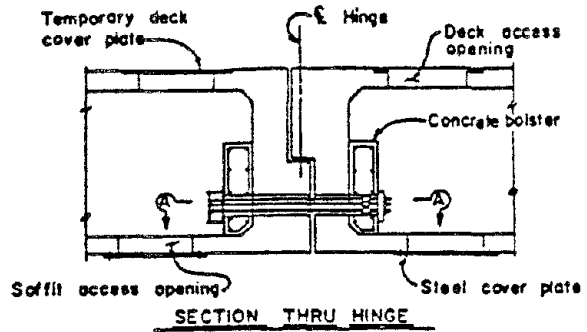


Figure 12

The most commonly used retrofitting detail in California is shown in Figure 11 because of the predominance of concrete box girder bridges. Reinforced concrete bolsters are used to spread out the anchorage forces which would otherwise destroy the hinge diaphragms. Figure 12 is a similar detail which aids in preventing rotation of superstructure segments caused by the skewed ends. The seven cables which are passed twice through the joint give the restraint of 14 cables. Seven cables passing through the hinge three times give the effect of 21 cables, as shown in Figure 13.

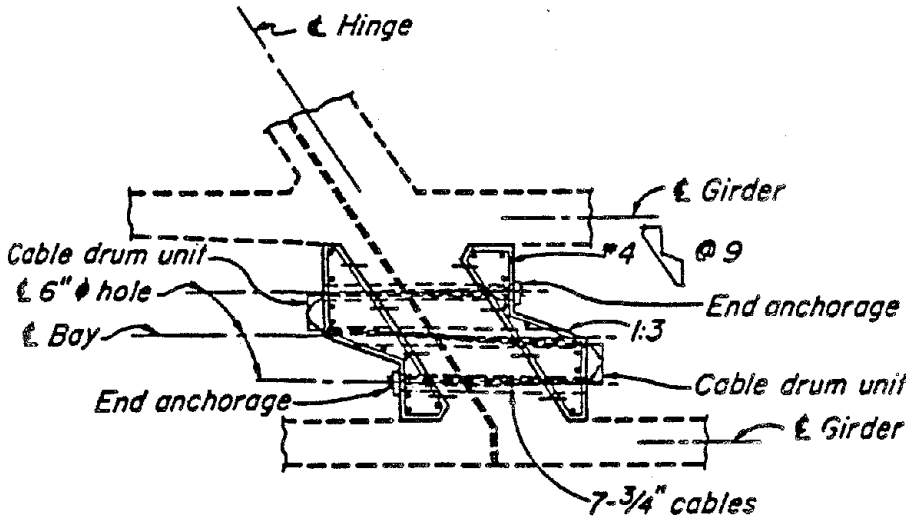
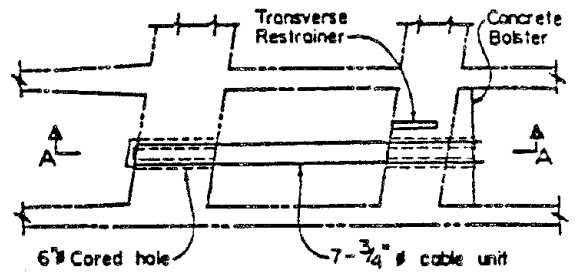
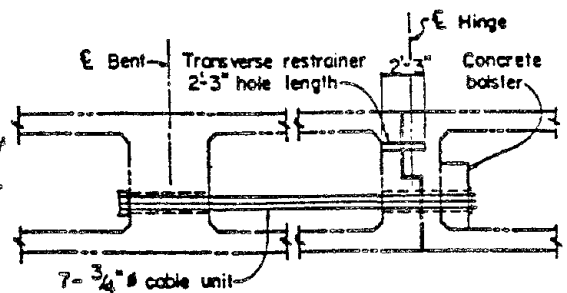


Figure 13



PLAN



SECTION A-A

Figure 14

Hinges in box girder bridges are usually located about one-fifth of the span length from a bent. In cases where it is desirable for cables to stretch more than allowed in the previous details, cables are passed all the way through the cantilever end of the span and around the bent cap as shown in Figure 14. This same scheme is also used with rod restrainers. Rods must be longer than an equivalent cable restrainer which provides the same amount of restraint, because of the greater modulus of elasticity. A plan view of rods connecting a hinge to the bent cap of a skewed bridge is shown in Figure 15.

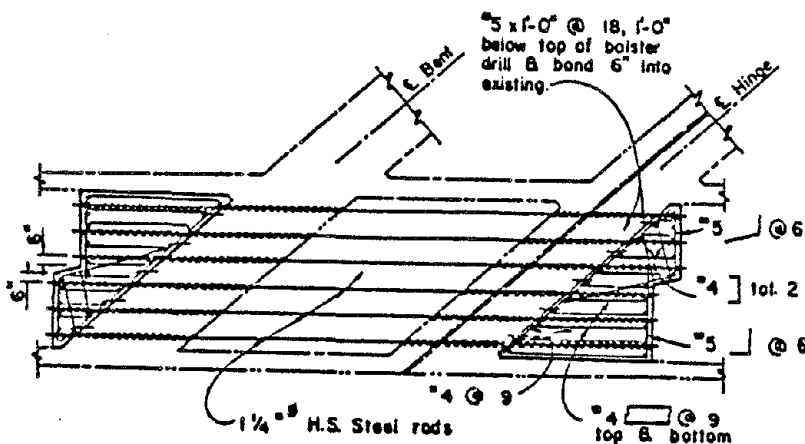
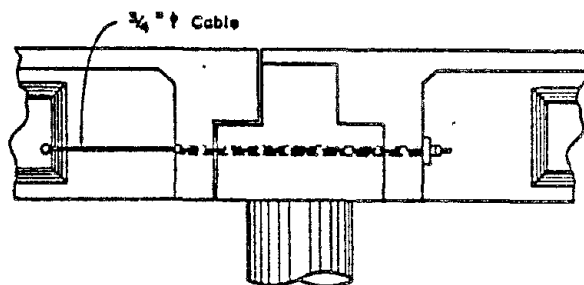


Figure 15



ELEVATION

Figure 16

Although access holes have been made in all three cells, in some contracts, some contractors have found it more economical to omit the access opening in the cantilever cell. They have been successful in aligning the holes through the cap and diaphragm and threading the restrainers through the cantilever cell from the first and third cells. Minor obstructions, caused by supports for the deck forms, can generally be pushed out of the way. Access to the cantilever cells is now optional and at the contractor's expense, if he prefers to use them.

Precast-prestressed girders supported on an "inverted T" cap can be restrained as shown in Figure 16. Coring holes near the ends of prestressed girders present no special problems if the girders are prestressed with strands or wires. Severing a few small tendons will have a negligible effect on the strength of a girder. If girders are tensioned with large rods, precautions should be taken to avoid damaging them.

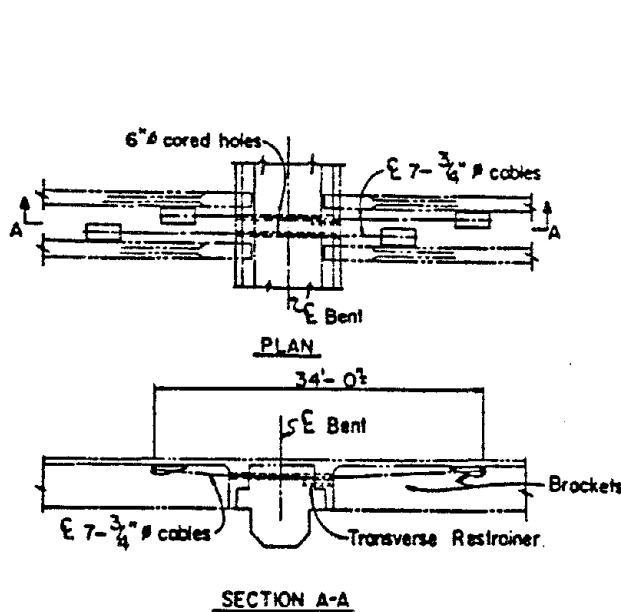


Figure 17

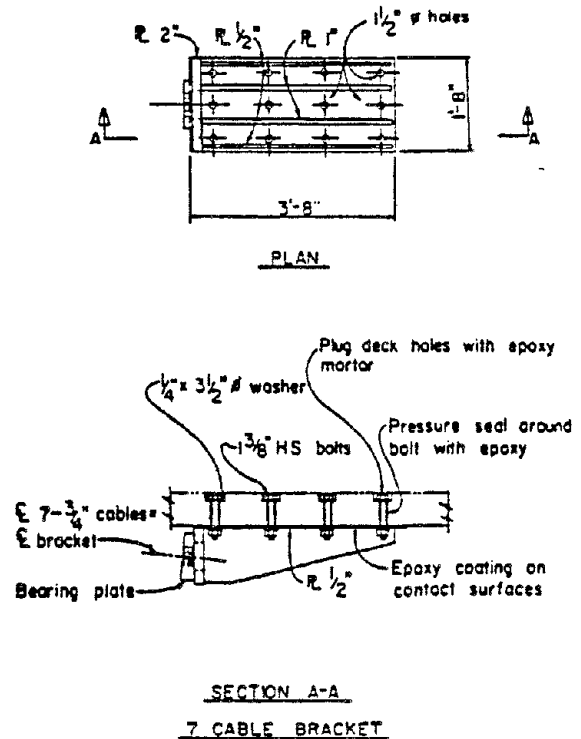


Figure 18

Figures 17 and 18 illustrate a method of restraining precast-prestressed girders at a bent by attaching cable anchorages to the underside of the deck and passing the cables through holes cored through the bent cap where it was considered impractical to attach the anchorages to the girders. Similar schemes have been used using rods in lieu of cables. Care must be taken to avoid damaging main cap reinforcement and not bending restraining rods excessively. Figure 19 shows the same general scheme where it was not practical to attach restrainers to the girders or inadequately reinforced diaphragms.

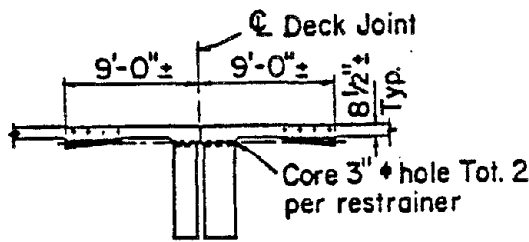
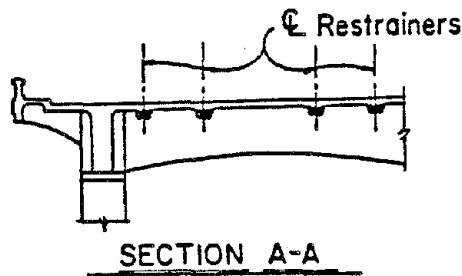
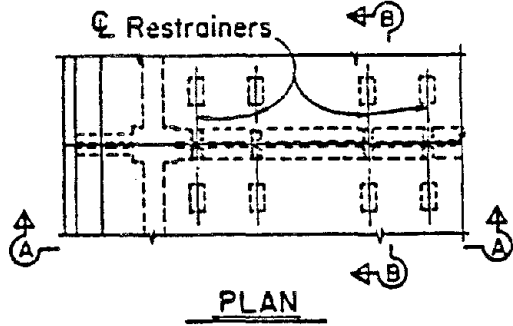


Figure 19

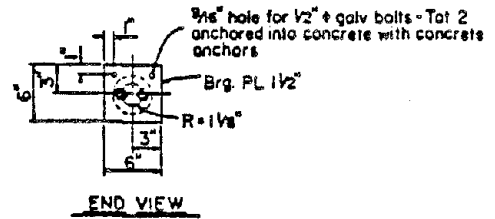
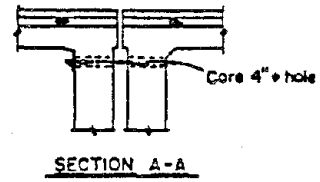
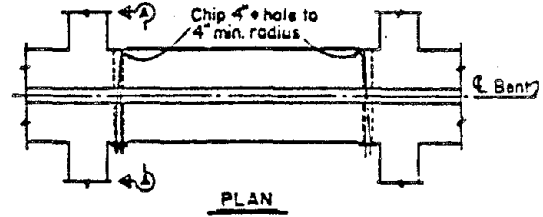


Figure 20

Figure 20 shows a typical restrainer for small T-beam bridges which have only a few spans with wide supports. An identical detail has been used for T-beam bridges with very narrow hinge seats.

Figure 21 is commonly used for T-beam bridges with diaphragms too lightly reinforced to safely resist the required restrainer forces.

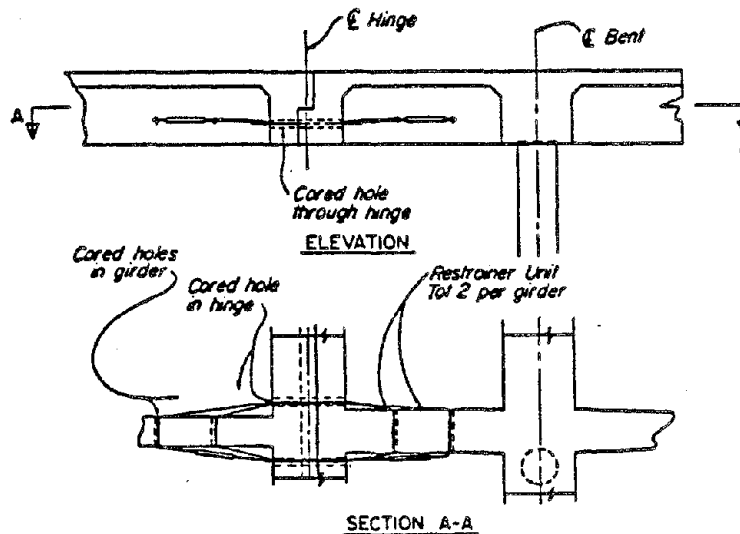


Figure 21

Continuous longitudinally reinforced concrete bridges with hinges are seldom retrofitted because the spans, if unseated in an earthquake, will not fall down under the influence of their own dead load. It is presumed that the problem will be recognized and temporary shoring placed or other remedial action taken before any serious problems occur. Simple spans, drop-in spans, and some specially designed slab bridges which are certain to drop if they become unseated, have been retrofitted.

Figure 22 shows the detail used for restraining a drop-in slab adjacent to a T-beam span. Hinges of special slab bridges have been restrained in an almost identical manner with diagonal holes being cored on both sides of the hinge (similar to the right hand side of Figure 22). The cable ends in those cases were either anchored in the deck or connected with a turnbuckle underneath the deck.

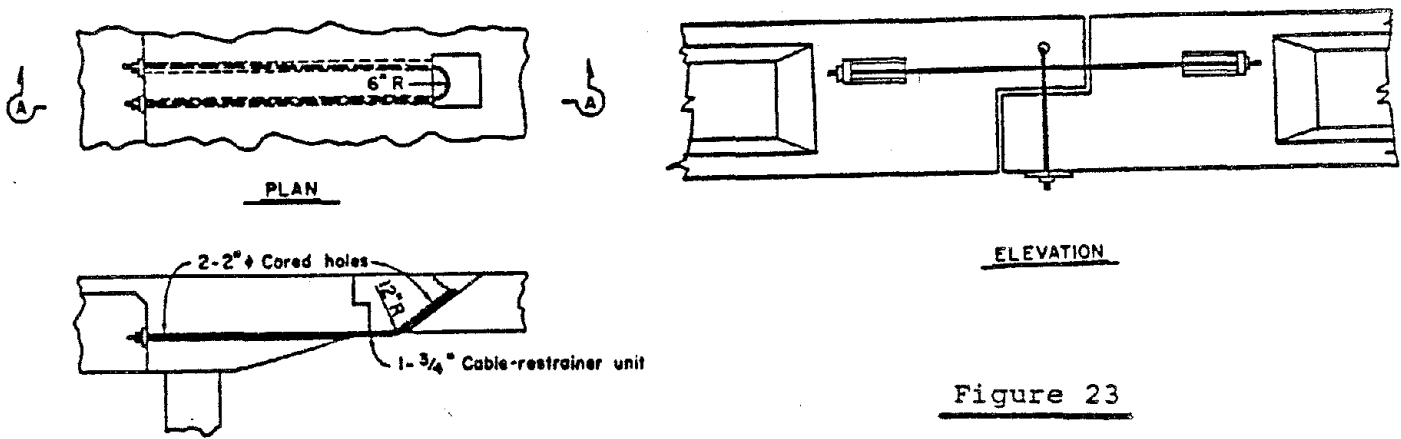
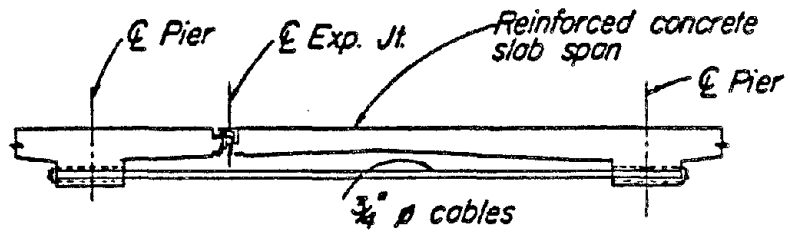


Figure 23

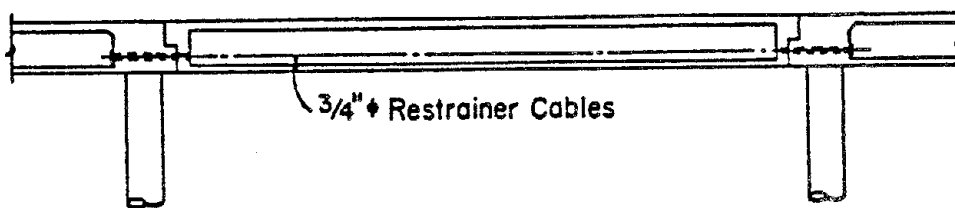
SECTION A-A
Figure 22



LONGITUDINAL SECTION
Figure 24

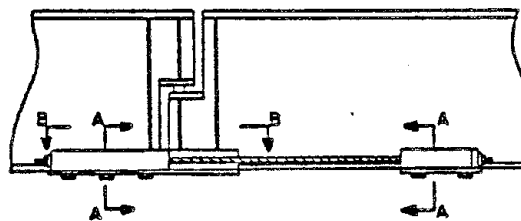
Precast-prestressed girder hinges have been restrained longitudinally and vertically as shown in Figure 23. The possibility of differential lateral movement should be considered also -- especially if the spans are skewed.

Hinges in relatively short spans or short drop-in spans can be restrained by connecting the adjacent piers with restrainers as shown in Figures 24 and 25. One of the main problems with this scheme may be excessive stretching of the tendons if the span is rather long. More tendons can be used to overcome that problem, but that also increases the cost.

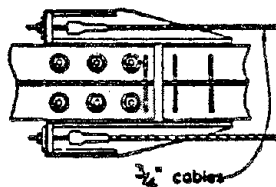


ELEVATION

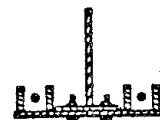
Figure 25



ELEVATION



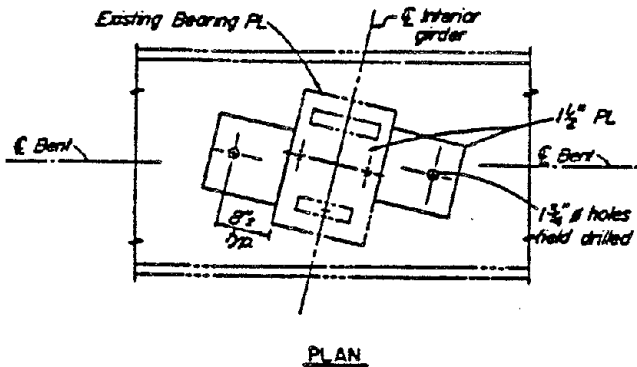
SECTION B-B



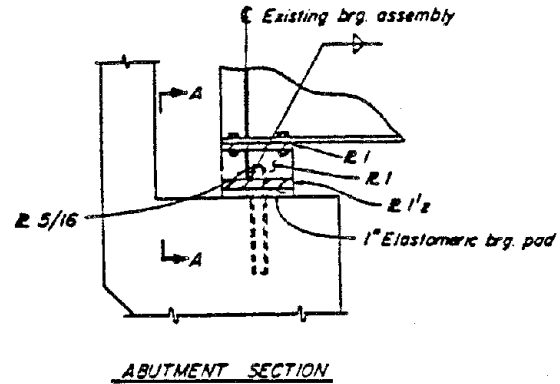
SECTION A-A

Figure 26

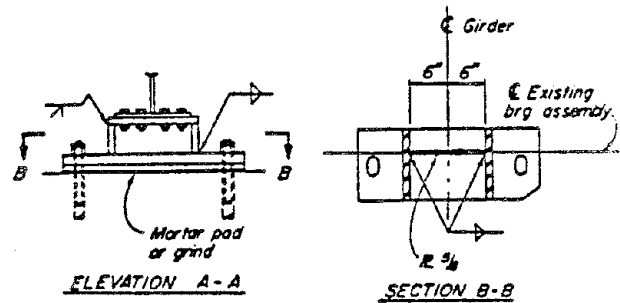
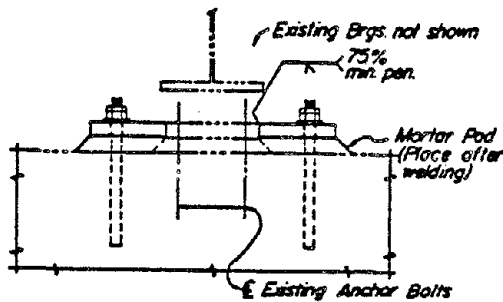
Figure 26 shows a detail for restraining a commonly used steel girder hinge. The welded plate assembly bolted to the bottom flange of the suspended side restrainers excessive transverse and vertical movement. The cables connecting that assembly and a bracket attached to the bottom flange of the cantilever limit the longitudinal opening of the hinge.



ELEVATION
Figure 27



REPLACEMENT BEARING
Figure 28



Masonry plate anchor bolts are one of the most seismically vulnerable details. Additional horizontal support has been given to some masonry plates by welding steel plate extensions with additional anchor bolts to existing bearing assemblies, as shown on Figure 27. Other portions of the bearings should be investigated and additional corrective action taken, if necessary, to make certain that there are no equally vulnerable deficiencies remaining. Steel bearings and anchor bolts should be designed to resist at least twice the calculated force that they may be subjected to.

It is sometimes advisable to replace existing steel bearings -- especially if they might allow the bridge to drop more than 6 inches or lead to other failures. This has been done as shown in Figures 28 and 29. Figure 28 shows a steel rocker bearing that was replaced with a welded steel pedestal and elastomeric bearing pad. It may also be necessary to provide additional longitudinal and/or transverse restraint in addition to this detail. Figure 29 illustrates how steel rocker bearings have been replaced by using elastomeric pads for new bearings and reinforced concrete to support the pad and provide transverse restraint. Longitudinal restrainers may also be required in addition to this detail.

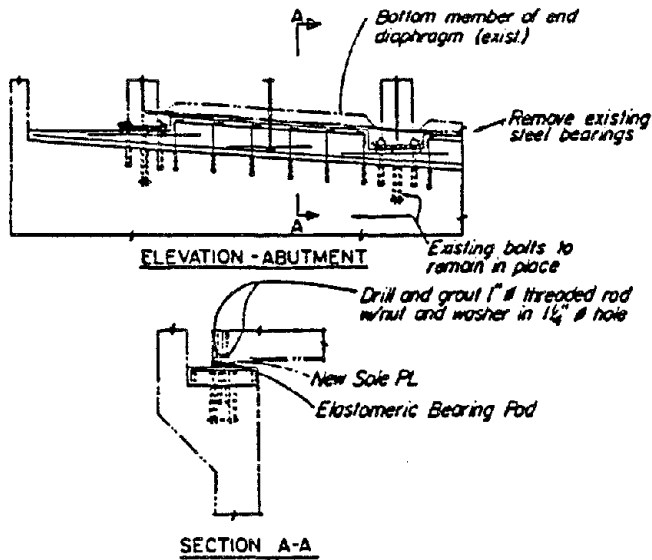


Figure 29

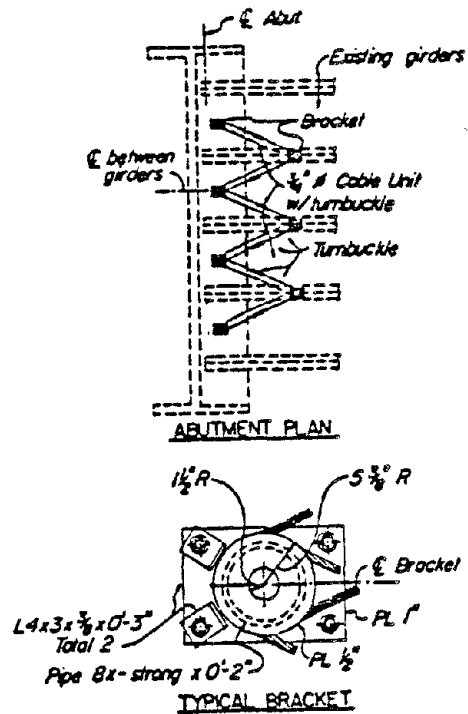


Figure 30

Figure 30 shows how steel girders can be given additional longitudinal and transverse restraint at an abutment. A method used for restraining steel girders transversely is shown in Figure 31.

The solid steel pin shown on Figure 32 will provide transverse and longitudinal restraint at an abutment. One of the main limiting factors for this detail is the strength of the abutment seat and end diaphragm. It is also a good detail for new construction where the concrete can be reinforced to develop the forces imposed by the steel pin. Although this scheme can also be used at intermediate supports there may be large amounts of negative reinforcement in bent caps that would be cut or damaged by coring the vertical holes.

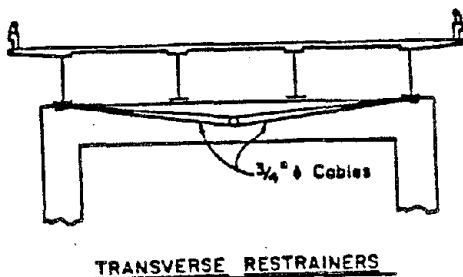
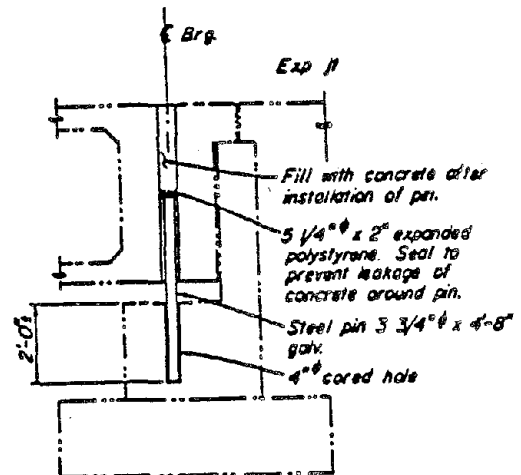
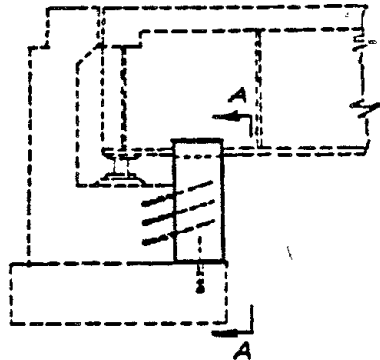


Figure 31

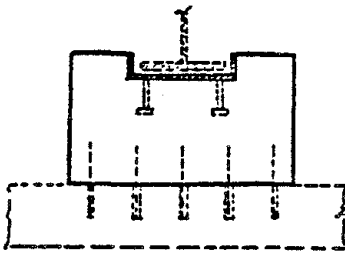


ABUTMENT SECTION

Figure 32



ABUTMENT SECTION



SECTION A-A
Figure 33

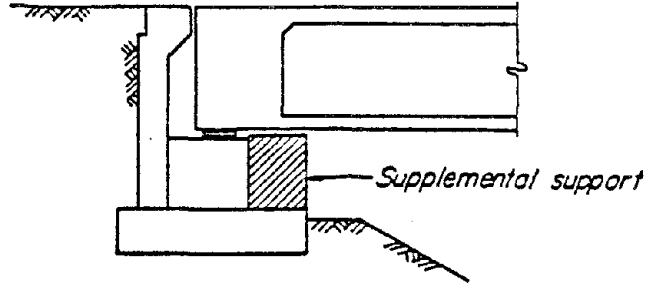
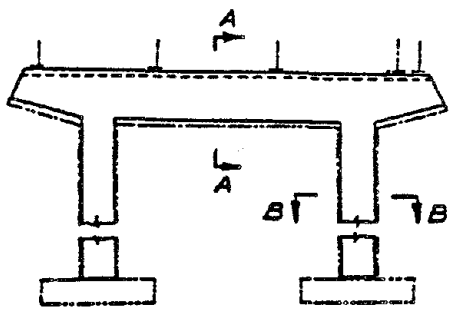
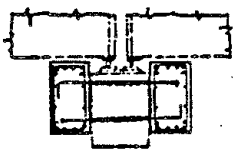


Figure 34

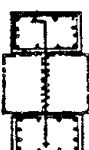
Figures 33 and 34 illustrate methods used for providing supplemental support under the ends of steel or concrete box girders, respectively, when longitudinal movements might exceed the capacity of the bearings.



ELEVATION

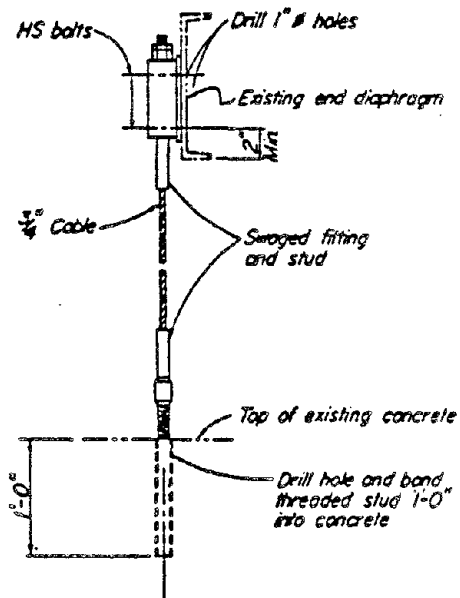


SECTION A-A



SECTION B-B

Figure 35



VERTICAL RESTRAINER

Figure 36

The support width of one bent in the center of a long viaduct was increased as shown in Figure 35. Based on the results of a dynamic analysis, it was felt that it would be advantageous to permit the viaduct to work as two short structures rather than one long one, with provisions for extra movement taken at this bent. Extensions were made on both faces of the cap and two columns to make the bent architecturally compatible with the rest of the structure.

Figure 36 shows a type of vertical restrainer commonly used in steel girder bridges. The upper end is attached to the end diaphragm and the lower end grouted into the top of the bent cap. Care should be taken to avoid the negative reinforcement in the bent cap.

CONCLUSIONS

The wide variety of bridges constructed over a period of many years in a large and varied area such as California makes it virtually impossible to use a few standard details for accomplishing an extensive retrofitting program. The details described in this paper are not necessarily complete in themselves. It is frequently necessary to use more than one detail to restrain a segment of a structure adequately. The combination of different construction materials, span lengths, skews, alignment, framing, vulnerable details, etc., makes it necessary to examine every structure as a unique problem.

INSPECTION AND RETROFITTING FOR EARTHQUAKE RESISTANCE
VULNERABILITY OF HIGHWAY BRIDGES IN JAPAN

by Eiichi Kuribayashi
Osamu Ueda, Tadayuki Tazaki
Public Works Research Institute

SUMMARY

All highway bridges in Japan are supervised technologically through the authorized specifications by the Ministry of Construction. The ministry has conducted the inspection of highway bridges three times (i.e. 1971, 1976 and 1979). The first one in 1971 was to point out the deteriorated bridges liable to be damaged in earthquakes. The second in 1976 was to check the items being closely related with the possibility of damage. The third inspection in 1979 was to classify bridges according to their earthquake resistances. This paper introduces the procedure of the latest inspection and its retrofitting in 1979.

INTRODUCTION

It is necessary in earthquake disaster mitigation planning to extract structures liable to be damaged in earthquakes. Two methods exist for the extraction. The one is to point out the structures liable to be damaged when they have the vulnerably structural factors according to the experiences of past earthquakes. The other is to analyse structures and to judge their safety.

The inspection of highway bridges conducted by the Ministry of Construction, Japan, in 1979 sequentially applied both of the methods. Possibly vulnerable bridges were extracted by the former method. The vulnerable factors considered were;

- (1) the design based on the old specifications,
- (2) deteriorated materials, and
- (3) vulnerable types of structures according to the damage in past earthquakes.

The extracted bridges were inspected by the latter method.

The priority of retrofitting was determined by the importance of bridges.

PROCEDURE OF THE INSPECTION

The inspection of highway bridges conducted in 1979 consists of four steps. The first step is to select the routes to be inspected, which are indispensable in emergency.

The second step is to extract the possibly vulnerable bridges. Referring the reports of past earthquakes, damage of bridges is more affected by the vulnerable subgrounds and substructures than superstructures, so that the formers are emphatically inspected.

The bridges extracted by the second step are to proceed to the third step. It is to inspect the stability of subgrounds and foundations, and

1) Senior Research Engineer, Earthquake Engineering Division, Public Works Research Institute, Ministry of Construction, Tsukuba Science City 305, JAPAN

the section moduli of piers.

The fourth step is to analyse structures dynamically if required.

The retrofitting method for each type of vulnerability identified is lastly proposed. The priority of retrofitting is to be determined by the availability of substitutive routes and the easiness of traffic resumption in emergency.

The procedure of the inspection is shown in Fig. - 1. This paper mainly describes the second and third steps.

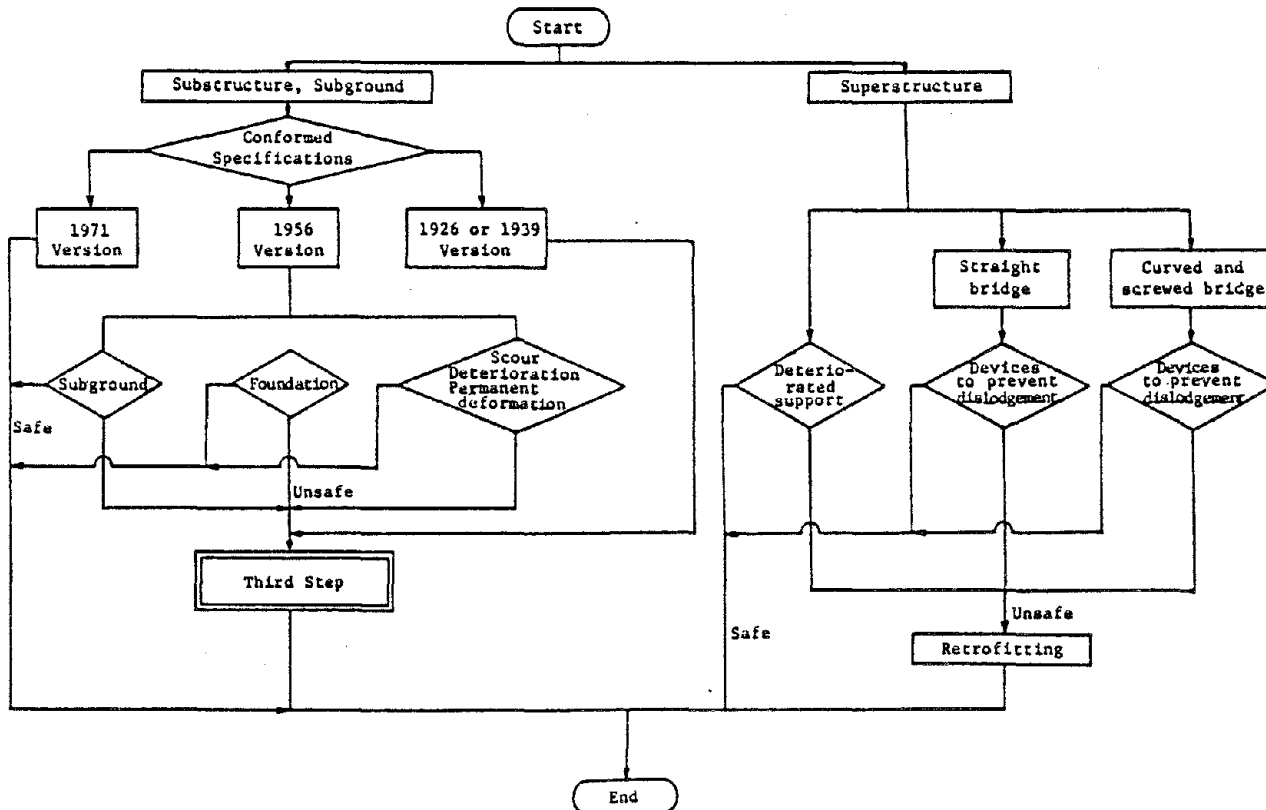


Fig. 1 Flow Chart of Inspection in the Second Step

Possibly Vulnerable Bridges (Second Step)

The second step is to extract the possibly vulnerable bridges which should proceed to the more detailed inspection in the third step. The vulnerable factors considered are as follows:

(1) Specifications Conformed

Owing to the progress of earthquake engineering, specifications have been revised several times.

At least the structures conformed with the latest specifications of 1971 were considered to have enough safety. The structures before the 1956 specifications were considered to be possibly unsafe. Those between 1956 and 1971 were judged depending on the subground, foundation and deterioration of the substructure.

For instance of the improvement of the specifications no attention had been paid to liquefaction before the specifications of 1971 were issued.

(2) Subground

a. Loose and Saturated Sand

Loose and saturated sand is liable to liquefy in earthquakes. Sandy layers which were less than 10 m deep and whose N-values were less than or equal 10, or the sites where historical liquefaction was reported were extracted.

b. Poor Subsoil

Peat layers or the sites where adjacent dikes and embankments settled were extracted.

(3) Substructure

a. Lack of Enough Rigidity

The substructure as shown in Fig. 2 suffered damage in Miyagiken-oki earthquake of 1978. The damage would have been attributable to the independent two caissons and insufficient rigidity of the tying members.

The pile bent substructure as shown in Fig. 3 experienced damage in Niigata earthquake of 1964.

Both types of the foregoing substructures have insufficient rigidity. Therefore the substructures without enough rigidity were extracted.

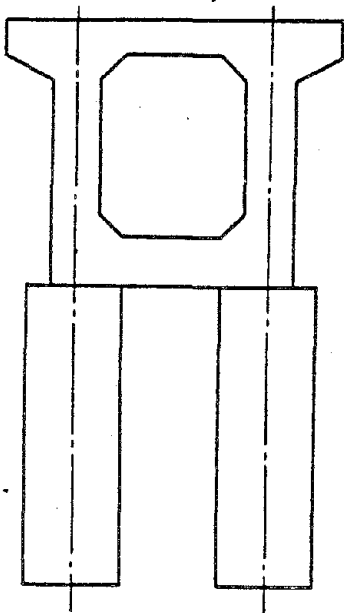


Fig. 2 Independent Caisson Foundation

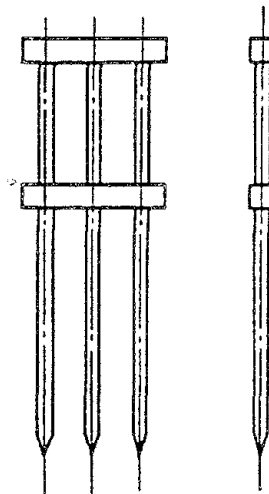


Fig. 3 Pile-bent Foundation

b. Brittle Materials

Substructures made of plain concrete, brick and masonry were extracted.

c. Settlement and Inclination

The substructures which settled or inclined were extracted.

(4) Superstructure

a. Curved Bridge

A curved bridge acts rather different in an earthquake from what is expected in conventional design. In conventional design a bridge was designed in longitudinal and transverse directions.

However a curved bridge bears not only the forgoing loadings but also torsional loading. The curved bridges without considerations of torsional loading and whose radius were less than 100 m were extracted.

b. Skew Bridge

By the similar reason as curved bridges, skew bridges of less than 60° of angles were extracted.

c. Deteriorated Supports

The supports of deteriorated anchor bolts, deteriorated bearings and over-dislodged supports were extracted.

d. Lack of Devices to Prevent Dislodgement

The supports without devices to prevent dislodgements which were specified by the specifications of 1971 were extracted.

Classifying Bridges by their Resistance (Third Step)

The bridges extracted by the second step were to be inspected in the third step. Here only subgrounds and substructures were inspected, because superstructures do not affect the damage according to the experiences of past earthquakes as far as they passed the second step inspection.

(1) Subground

a. Liquefaction Resistance Factor

Liquefaction resistance factor, F_L is defined as the ratio of the resistance index of soil elements to dynamic loads R , and the shearing stress loads index to soil elements induced by earthquake motions L . The procedures to calculate R and L are shown in Reference [2]. Subground having the total thickness of the layers of greater than 10 m whose F_L were less than 0.6 was judged to be liquefied in earthquakes.

b. Bearing Capacities

In the relationship between the overturning moment and the bearing capacity of foundation three zones were defined as safe (A), slightly unsafe (B) and unsafe (C) in Fig. 4.

(2) Substructure

a. Section Modulus of Pier

Aged piers possibly have the insufficient section moduli compared to the current specifications. The section moduli of inspected piers were compared with those of the Standard Design issued by the Ministry of Construction and other institutions, which were designed based on the current specifications. The checking charts are shown in Figs. 5 - 7. Fig. 5, Fig. 6 and Fig. 7 correspond to wall pier, column pier and rigid frame pier

respectively. The line dividing zones A and B was drawn by enveloping the dimensions designed by the Standard Design. The line dividing B and C was drawn by multiplying by 1.1 (reserve strength of reinforcement) of the line between A and B. Zone C was determined to be preferentially retrofitted.

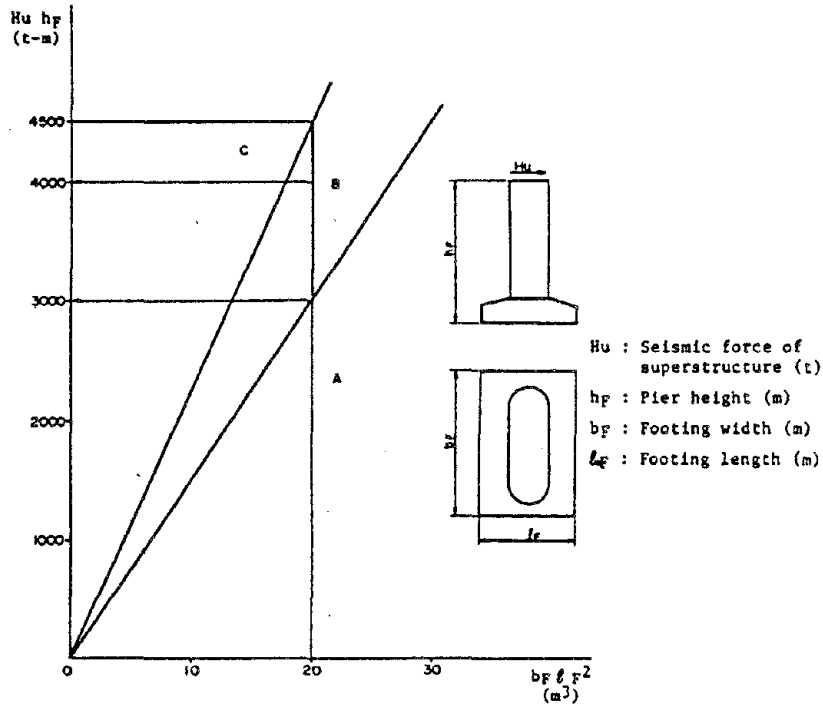


Fig. 4 Checking Chart for Bearing Capacity

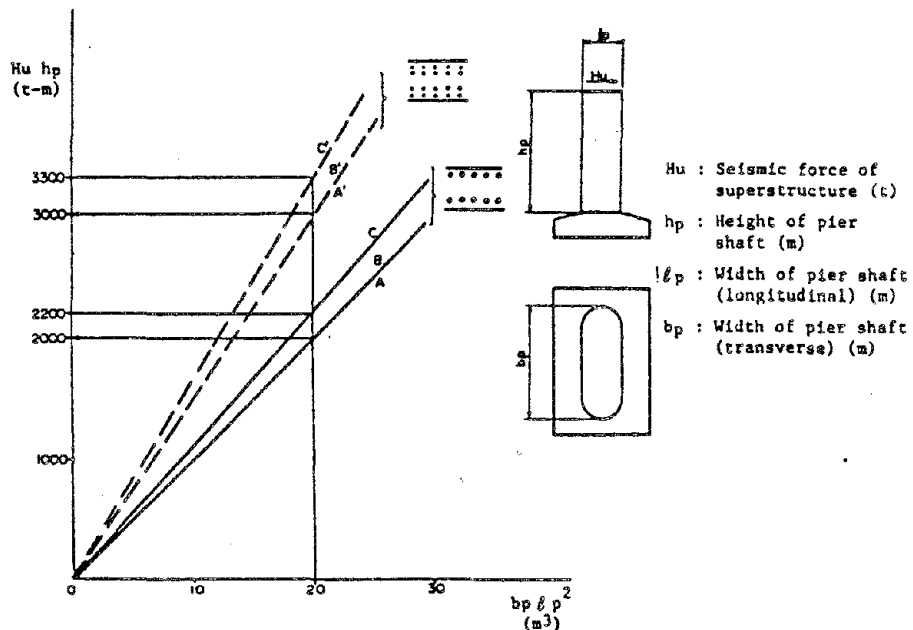


Fig. 5 Checking Chart for Wall Pier

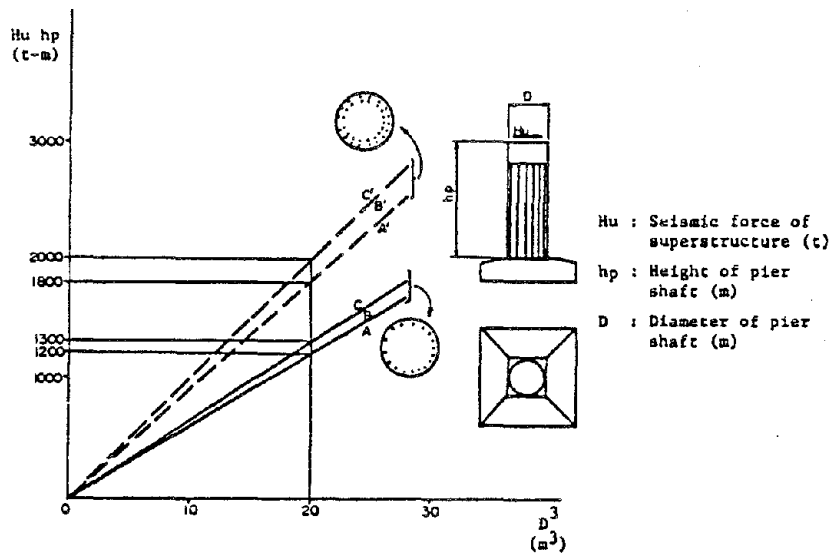


Fig. 6 Checking Chart for Column Pier

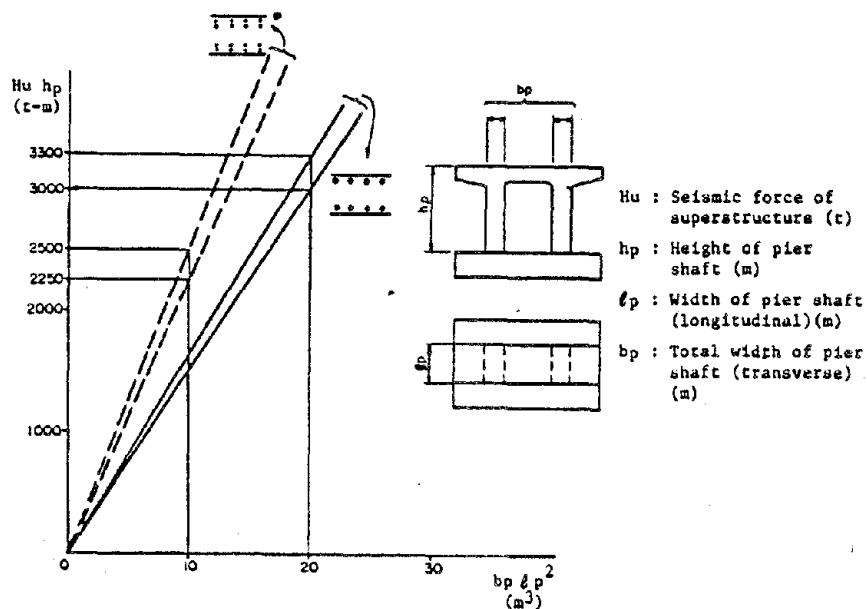


Fig. 7 Checking Chart for Rigid Frame Pier

b. Safety Factor of Pile Foundation

Aged pile foundations are liable to be damaged than other types of foundations according to the experiences of past earthquakes. The reason for this would be that there did not exist capable pile drivers in old days. Additionally most piles before 1950 were made of timber. Therefore pile foundation was exceptionally inspected by calculating the safety factor SF as follows.

$$SF = \frac{R_u}{V_1}$$

R_u : Ultimate bearing capacity of a pile (t)

- V_i : Vertical reaction of pile i (t) = $\frac{V}{n} + \frac{Ve}{X_i^2} X_i$
 V : Vertical load (t)
 n : Number of piles
 e : Eccentricity (m)
 X_i : X coordinate of i -th pile (m)

Dynamic Analysis

The bridges extracted by the above step were inspected by applying the the dynamic analysis, if required.

Determining the Method of Retrofitting

The retrofitting method for each type of vulnerability identified is shown in Table 1.

Table 1. Proposed Method of Retrofitting

Classification	Vulnerable Factor	Method of Retrofitting
Subground		Surrounding by sheet piles Pile driving behind abutments Driving additional piles Sand compaction piles
Substructure	Scour Lack of enough rigidity Section modulus of pier Section modulus of footing Safety factor of pile foundation	Consolidation of foundation Additional rigidity Additional section Expansion of footing Additional piles
Superstructure	Curved bridge Screw bridge Deteriorated support Lack of devices to prevent dislodgement	Devices to prevent dislodgement Enlargement of bridge seat Connecting devices of adjoining girders Exchange of support Installing devices

DISCUSSIONS

About 37000 bridges were inspected in which 42% were judged to be retrofitted.

It is necessary to get a reasonable level of retrofitting from an economic point of view. Because of the low recurrence of damaging earthquakes, the retrofitting investment is obliged to be at a lower level, when the direct effects of retrofitting are only considered. However the retrofitting also has the indirect effects, such as the traffic and transportation, regional economy and opportunity loss for repair and reconstruction. When such indirect effects are considered, more retrofittings are rationalized.

ACKNOWLEDGEMENTS

The author wishes to express his gratitude for the suggestions and supports of Messrs. Tatsuya Fujii and Yoshihiko Enami of Ministry of Construction, Japan.

REFERENCES

- 1) Specifications for Earthquake Resistant Design of Highway Bridges, Japan Road Association, 1971
- 2) T. Iwasaki, et al : A Practical Method for Assessing Soil Liquefaction Potential Based on Case Studies at Various Sites in Japan, Second International Conference on Microzonation, San Francisco, 1978
- 3) A. Longinow, et al : Bridge Retrofitting Selection of Critical Bridges in a Road Network, Technical Council on Lifeline Earthquake Engineering Specialty Conference, Los Angeles, August 1977

INTRODUCTION TO AN EARTHQUAKE EVALUATION TEST FOR EFFECTS
TO RETROFIT OF REINFORCED CONCRETE BRIDGE PIER ELEMENTS

by

Eiichi Kuribayashi
and
Shigetoshi Kobayashi

Public Works Research Institute
Ministry of Construction

1. Introduction

This paper briefly describes an evaluation test for effects to retrofit of reinforced concrete bridge pier elements conducted at the Public Works Research Institute in the past.

In order to increase strengthes of the existing concrete structures there are many kinds of methods in the design and construction procedures as follows,

- 1). Strengthening using steel plates
 - 2). Strengthening employing Prestress Forces
 - 3). Strengthening casting additional sectional area of reinforced concrete
- and
- 4). Strengthening using additional members of reinforced concrete

In this paper authors introduce an example which evaluated the method 1. and method 3. of the above.

2. Experimental Study

2.1 Specimen Details

Five kinds of test specimens were designed to meet the objectives of this program. Table-1. and Fig.1 show the details and dimensions of the specimens.

Specimen R is 30cm wide, 30cm deep and 2m high original reinforced column member.

Specimens RR-1,RR-2,RR-3 and RS are retrofitted members.

The method to strengthen for RR's is additional casting of 10cm deep reinforced concrete on both tension and compression sides of the original member R. The differences among RR-1,RR-2, and RR-3 are the method of the pretreatment on the surface to which additional concrete is casted. Details are shown in Table-1.

The strengthening method used for RS is to adhere 6mm thick steel plates on both the tension and compression sides of the original member.

2.2 Material Properties

Material properties used for the specimens were as follows.

Concrete: Ready mixed concrete with high-early portland cement, crashed rock coarse aggregate 20mm in maximum size and river sand was used. The mix proportion of the concrete is shown in Table-2.

The strength of concrete is shown in Table-3.

Steel: Deformed bars used for reinforcement were SD30 (JIS Designation) of 13mm nominal diameter.

Steel plates used for strengthening RS are SS41 (JIS Designation) of 6mm thick.

Adhesive agent: Epoxy resin was used for sticking steel plates, for fixing anchor bars and for spreading on the joint surface of RR-2 and RR-3. Mechanical properties of the resin is shown in Table-5.

2.3 Casting of Specimens

Original column: 10 original columns were fabricated. Concrete was casted continuously being compacted with inner vibrators.

Retrofit 8 columns of original ones were retrofitted with the methods shown in Table-1 and Fig.1.

2.4 Testing Procedure

For giving both the axial force and the bending moment eccentric longitudinal loads were applied by a 1000t compression test machine. The distance of the eccentricity is shown in Table-6.

The load was not increased monotoniously but repeated loading and unloading several times as shown in Table-8 until it reached at the ultimate state. The loading speed was 10t/min.(for R) or 20t/min. (for others). Strains of concrete, reinforcement and steel plates, and the deformation of each specimen were measured during the test.

3. Test Results

3.1 Load-Strain Relations

The relation between the applied load and observed strain of each specimen is shown in Fig.2 and Fig.3. Calculated values in the figures are given by the elastic design method assuming that the ratio of Young's modulus of steel to concrete and the cross sectional area of members are as shown in Table-7.

The relationship between loads and strains of the specimen which was strengthen by additional casting of reinforced concrete is similar to the calculated value when the strength of the load is around the level as usually allowed. In other words the concrete member which casted later is working as a part of the member.

The difference of the treatment of the joint surface selected in this program scarcely affected to the strength of the retrofitted member.

The load-strain relation of the specimen strengthened with steel plates is also similar to the elastically calculated value when the load is such low as the stress of concrete is around the allowable stress which is 100kg/cm^2 in this case. But when the load exceeds the value, strains of the specimen exceed gradually to the calculated value and they approach to the values which were calculated neglecting the strength of compression of the steel plate.

3.2 Failure Pattern

Typical examples of failure are shown in Fig.4. In the case of RR type, tension cracks appeared first to the tension side, then vertical cracks were observed in the additional concrete subjected to tensile stresses and lastly a long crack extended along the joint of the compression side.

In the case of RS type, the steel plate on compression side was partly separated from the surface by buckling when the compressive stress of the steel plate reached to around 1300kg/cm^2 . When the load reached a level at 120t, suspected shear cracks appeared at the end of the steel plate subjected to tensile stresses. The load decreased after the compressive failure was observed, when the load reached 140t.

3.3 Bearing Capacities of Loads

The comparison of the observed bearing capacity with calculated one is shown in Table-8. Calc. A is given by the working stress method. Calc. B is given by the ultimate strength method. In case of RS, the strength of the compressive steel was neglected as it had buckled before the maximum load was applied.

The reason that the observed strengths of case RR's were lower than calculated ultimate strengths is that the calculation of strength was carried out assuming that concrete was homogeneous and the strength of the original concrete was assumed as the same strength to additional one although the strength of the original concrete was weaker than the post casted one.

4. Conclusions

Conclusions through the tests and analysis are given as follows.

- 1). The concrete column member retrofitted by additional casting of reinforced concrete behaves like as a composite structure and its effect is seemed to be reliable.
- 2). For evaluating the effect of the retrofit by above method, the working stress method can be comprehensively, used.
- 3). There was little difference on the effect of pretreating of the joint surface among the three methods selected in this program.
- 4). The retrofiting method to adhere steel plates may cause buckling of the compression steel plate if the compressive stress is subjected. Then,
- 5). It is recommended to neglect the effect of steel plates as the compression member.

Those tests were carried out under the one directional static load. It is recommendable that the necessity to do more other tests which apply the reversible load for examining whether the conclusions are reliable or not to the bridge pier which would be subjected to such strong reversible load as earthquakes.

5. Acknowledgments

The authors sincerely express their thanks for the cooperation of Prof. M.Ohta, Kanazawa Institute of Technology, former head of Concrete Division, the Public Works Research Institute.

Table-1 Specimens

Specimen Type	Retrofitting Method	Steel		Concrete Strength			Space of tie bar (cm)	Number
		Orig.	Ret.	Origin.		Ret.		
				No.1	No.2			
R	Original Member.	SD30 D13	-	384	273	-	15	2
RR-1	Chipping. Anchor bar. Additional cast of R.C.	SD30 D13	SD30 D13	384	273	458	15	2
RR-2	Chipping & resin spread. Anchor bar. Add.cast of R.C.	SD30 D13	SD30 D13	384	273	458	15	2
RR-3	Grinding & resin spread. Anchor bar. Additional cast of R.C.	SD30 D13	SD30 D13	384	273	458	15	2
RS	Grind. & resin spread. Sticking steel plates.	SD30 D13	SS41	384	273	-	15	2

Table-2 Mix Proportion of Concrete

Max. Agg. Size (mm)	Slump (cm)	W/C (%)	S/a (%)	Amount in $1m^3$ (kg)			
				W	C	S	G
20	8±2	62	44	175	282	841	1091

Table-3 Strength and Young's Modulus of Concrete

		Comp. Strength (kg/cm ²)	Young's Modulus (kg/cm ²)
Original Concrete	No.1	384	2.6×10^5
	No.2	273	2.1×10^5
Addition. Concrete:		458	2.9×10^5

Table-4 Mechanical Properties of Steel

Steel	Yield. Streng. kg/cm ²	Ultimate ₂ Streng. kg/cm ²	Elongation %
SD-30 D13	3460	5160	25
SS41	3060	4770	25

Table-5 Mechanical Properties of Epoxy Resin

Use for Factor	Spreading on Joint	Fixing Anchor bar	Sticking Steel Plate
Specific Grav.	1.29	1.22	1.17
Flex. Strength kg/cm ²	523	-	780
Comp. Strength kg/cm ²	1219	1031	1946
Young's Modul. kg/cm ²	24900	26500	27800
Tensile Streng. kg/cm ²	266	-	473

Table-6 Loading Process

Specimens	Eccentricity cm	Stress kg/cm ²	Load t	Repetition n
R	12	≈ 100	40	1
		" 150	60	1
		" 300	80	3
RR	15	≈ 100	60	1
		" 150	150	4
		" 200	210	5
RS	12	≈ 100	60	1
		" 200	80	6
		" 300	120	4

Table-7 Assumptions for Calculation

Specimens	Young's Mod. Ratio	Assumption
R	9.0	
RR	7.0	Strengthes of the concrete are equal to the additional concrete.
RS	9.0	Caluc.1 Compressive strength of steel plate is effective. Caluc.2 Compressive strength of steel plate is ineffective.

Table-8 Bearing Capacities

Specimen		Observed t	Calcu. A t	Calc. B t
R	No.1	110*	99	124
	No.2	97	71	95
RR-1	No.1	268	247	295
	No.2	250		
RR-2	No.1	210*		
	NO.2	260		
RR-3	No.1	260		
	NO.2	260		
RS	No.1	140	123	149
	No.2	140	88	113

A.: The Working Stress Method.

B.: The Ultimate Strength Method.

* : Locally failed at the loading point.

In all of the cases, the compressive side yielded first.

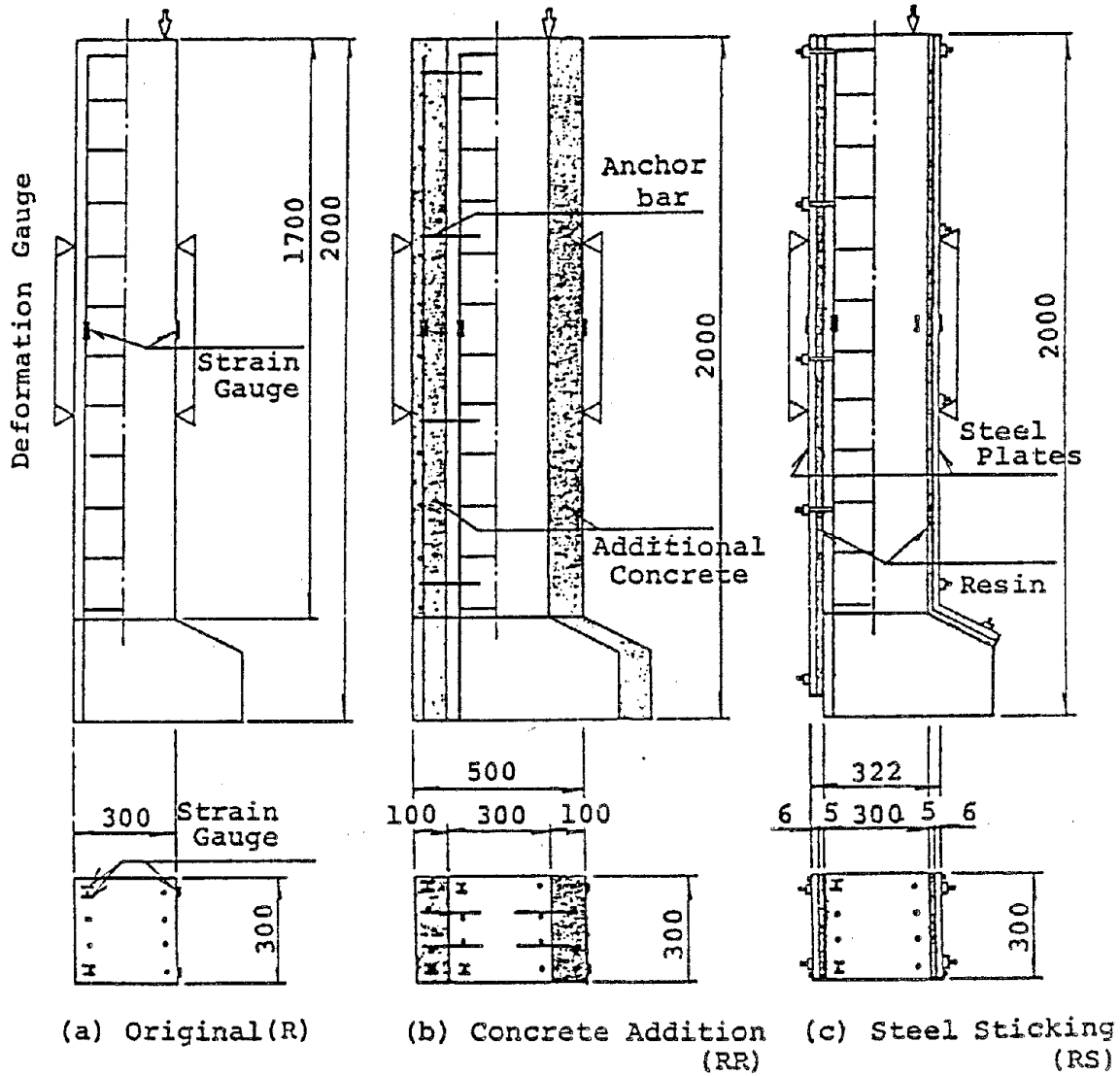


Fig.1 Dimensions of Specimens

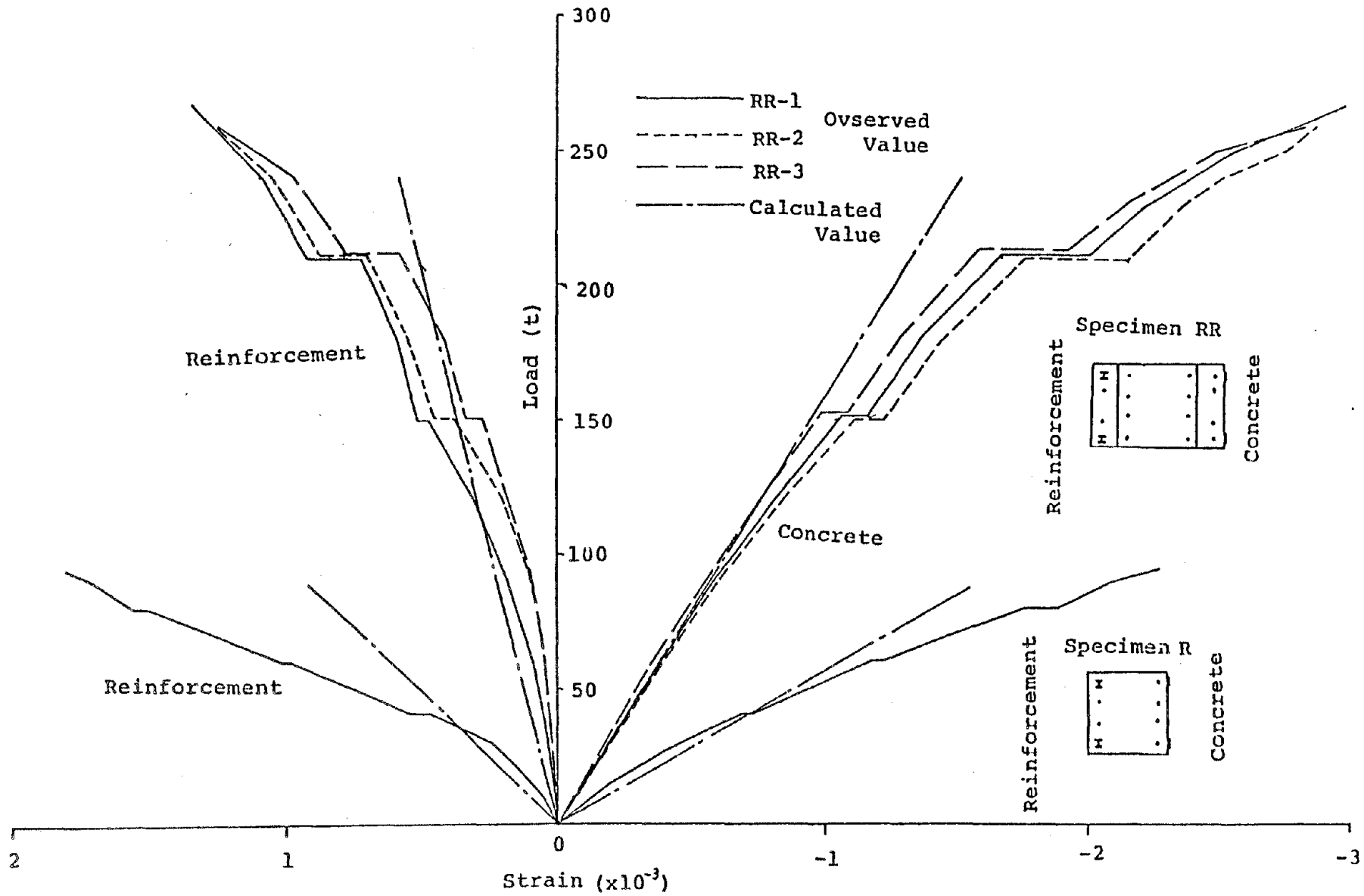


Fig.2 Load-Strain of R & RR

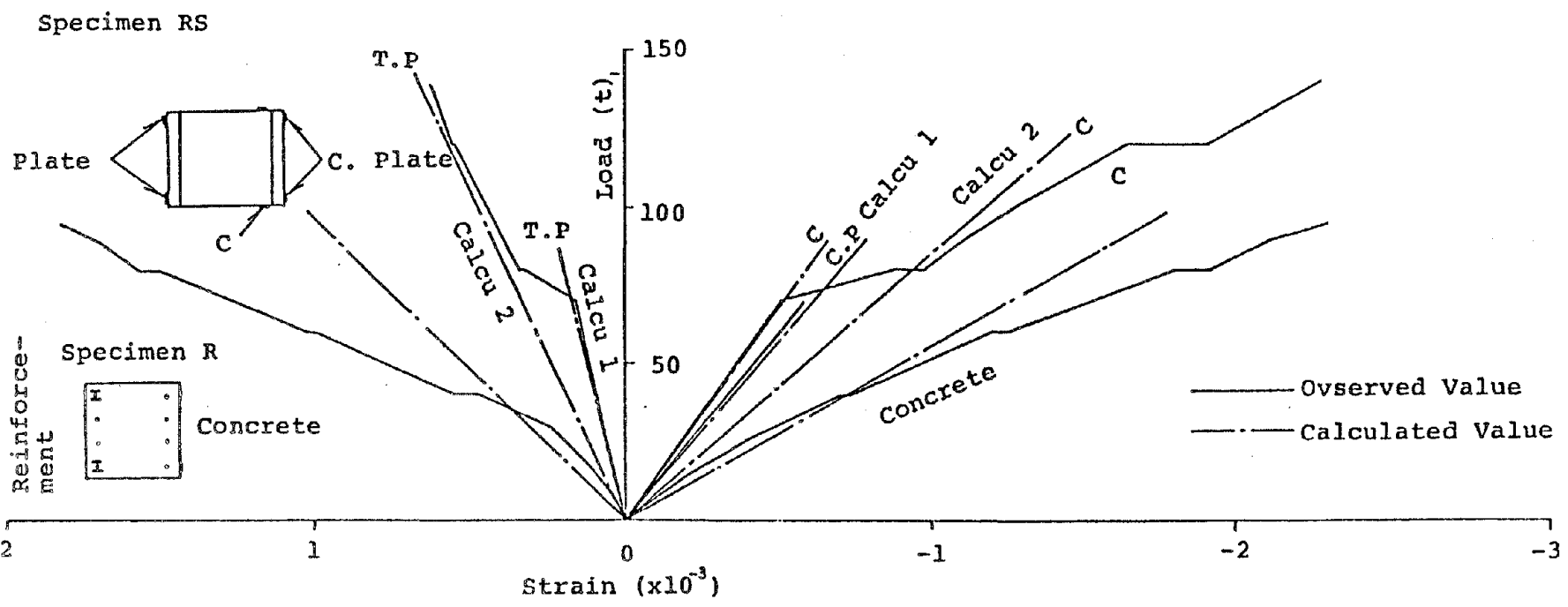


Fig.3 Load-Strain of R & RS

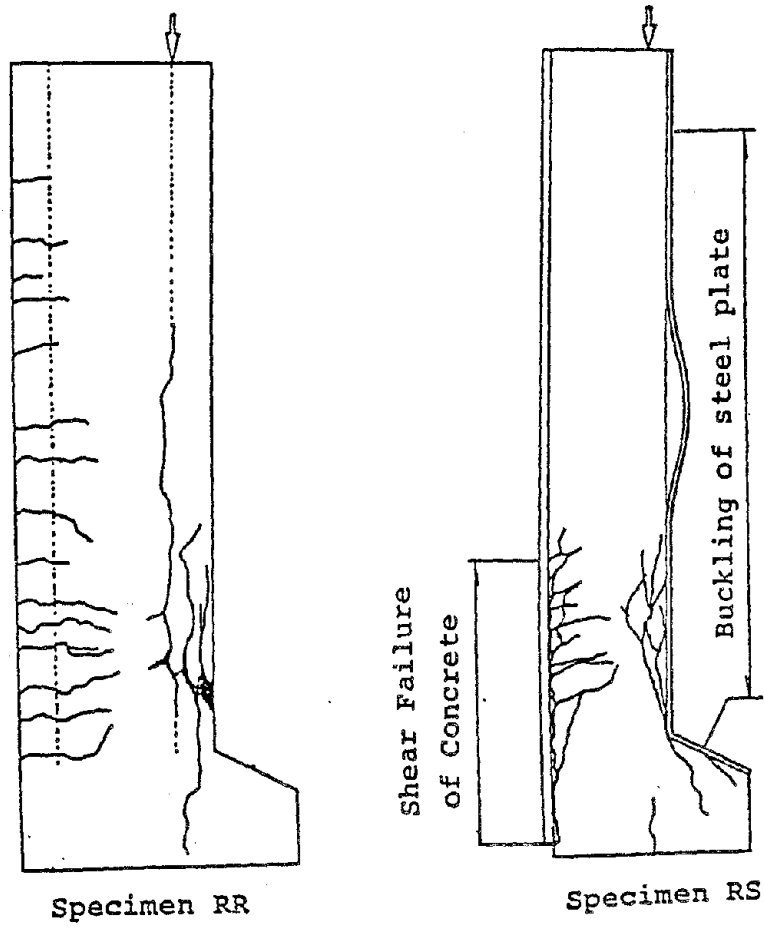


Fig.4 Failure Mode of RR & RS